



Friedrich-Schiller-Universität Jena

Tailored polymeric nanoparticles for gene delivery and diagnostic

Dissertation

zur Erlangung des akademischen Grades

doctor rerum naturalium (Dr. rer. nat.)

vorgelegt dem Rat der Chemisch-Geowissenschaftlichen

Fakultät der Friedrich-Schiller-Universität Jena

von Diplom-Chemikerin Antje Vollrath

geboren am 12.07.1984 in Weimar

Gutachter:

1. _____

2. _____

Tag der öffentlichen Verteidigung: _____

Für meine Familie

“Be the change that you wish to see in the world.”

Mahatma Gandhi

Table of contents

Documentation of authorship	4
1. Introduction	8
2. Nanoparticles for diagnostic	10
3. Nanoprecipitation for tailored nanoparticle preparation	14
4. Advanced characterization of nanoparticles	19
5. Targeting of polymeric nanoparticles for cell internalization studies	24
6. Nanoparticles for gene delivery	30
7. Summary	37
8. Zusammenfassung	40
9. References	43
Supplementary information	46
List of abbreviations	48
Curriculum vitae	49
Publication list	50
Acknowledgement / Danksagung	54
Declaration of authorship / Selbstständigkeitserklärung	57
Publications P1 – P9	59

Documentation of authorship

This section contains a list of the individual authors' contribution to the publications reprinted in this thesis.

- P1) A. Vollrath, S. Schubert, U. S. Schubert, "Fluorescence imaging of cancer tissue based on metal-free polymeric nanoparticles – Review", *J. Mater. Chem. B* **2013**, accepted.

A. Vollrath: preparation of the manuscript, conceptual development
S. Schubert, U. S. Schubert: correction of the manuscript, supervision

- P2) I. Y. Perevyazko, A. Vollrath, S. Schubert, G. M. Pavlov, U. S. Schubert, "Characterization of poly(methyl methacrylate) nanoparticles prepared by nanoprecipitation using analytical ultracentrifugation, dynamic light scattering, and scanning electron microscopy", *J. Polym. Sci., Part A: Polym. Chem.* **2010**, *48*, 3924–3931.

I. Y. Perevyazko: nanoparticle preparation and characterization,
conceptual development, preparation of the manuscript
A. Vollrath: nanoparticle preparation and characterization,
conceptual development, preparation of the manuscript
G. M. Pavlov: correction of the manuscript, supervision I. Y. Perevyazko
S. Schubert, U. S. Schubert: correction of the manuscript, supervision

- P3) I. Y. Perevyazko, J. T. Jr. Delaney, A. Vollrath, G. M. Pavlov, S. Schubert, U. S. Schubert, "Examination and optimization of the self-assembly of biocompatible, polymeric nanoparticles by high-throughput nanoprecipitation", *Soft Matter* **2011**, *7*, 5030–5035.

I. Y. Perevyazko: nanoparticle preparation and characterization,
conceptual development, preparation of the manuscript
J. T. Jr. Delaney: conceptual development, preparation of the manuscript
A. Vollrath: nanoparticle preparation and characterization,
preparation of the manuscript
G. M. Pavlov: correction of the manuscript, supervision I. Y. Perevyazko
S. Schubert, U. S. Schubert: correction of the manuscript, supervision

- P4) I. Y. Perevyazko, A. Vollrath, C. Pietsch, S. Schubert, G. M. Pavlov, U. S. Schubert, "Nanoprecipitation of poly(methyl methacrylate)-based nanoparticles: Effect of the molar mass and polymer behavior", *J. Polym. Sci., Part A: Polym. Chem.* **2012**, *50*, 2906–2913.

I. Y. Perevyazko: nanoparticle preparation and characterization, conceptual development, preparation of the manuscript
A. Vollrath: nanoparticle preparation and characterization, preparation of the manuscript
C. Pietsch: polymer synthesis and characterization
G. M. Pavlov: correction of the manuscript, supervision I. Y. Perevyazko
S. Schubert, U. S. Schubert: correction of the manuscript, supervision

- P5) A. Vollrath, D. Pretzel, C. Pietsch, I. Y. Perevyazko, R. Menzel, S. Schubert, G. M. Pavlov D. Weiß, R. Beckert, U. S. Schubert, "Preparation, cellular internalization, and biocompatibility of highly fluorescent PMMA nanoparticles", *Macromol. Rapid Commun.* **2012**, *33*, 1791–1797.

A. Vollrath: nanoparticle preparation and characterization, conceptual development, preparation of the manuscript
D. Pretzel: biological studies, preparation of the manuscript
C. Pietsch: polymer synthesis and characterization, contribution to the manuscript
I. Y. Perevyazko: PUC studies, contribution to the manuscript
R. Menzel: synthesis and characterization of fluorescent dye
G. M. Pavlov: supervision I. Y. Perevyazko
D. Weiß, R. Beckert: supervision R. Menzel
S. Schubert, U. S. Schubert: correction of the manuscript, supervision

- P6) A. Vollrath, A. Schallon, C. Pietsch, S. Schubert, T. Nomoto, Y. Matsumoto, K. Kataoka, U. S. Schubert, "A toolbox of differently sized and labeled PMMA nanoparticles for cellular uptake investigations", *Soft Matter* **2013**, *9*, 99–108.

A. Vollrath: polymer labeling, nanoparticle preparation and characterization, conceptual development, preparation of the manuscript
A. Schallon: biological studies, conceptual contribution, preparation of the manuscript
C. Pietsch: polymer synthesis and characterization
T. Nomoto, Y. Matsumoto: cell studies (fluorescence microscopy), correction of manuscript
K. Kataoka: correction of the manuscript, supervision
S. Schubert, U. S. Schubert: correction of the manuscript, supervision

- P7) K. Babiuch, D. Pretzel, T. Tolstik, A. Vollrath, S. Stanca, F. Foertsch, C. R. Becer, M. Gottschaldt, C. Biskup, U. S. Schubert, "Uptake of well-defined, highly-glycosylated, pentafluorostyrene-based polymers and nanoparticles by human-heptocellular carcinoma cells", *Macromol. Biosci.* **2012**, *12*, 1190–1199.

K. Babiuch: synthesis, characterization, conceptual development, preparation of the manuscript
D. Pretzel: biological studies, preparation of the manuscript
T. Tolstik: cell studies (flow cytometer)
A. Vollrath: nanoparticle preparation and characterization
S. Stanca, F. Foertsch: cell studies (fluorescence microscopy)
C. R. Becer, M. Gottschaldt: correction of the manuscript, supervision K. Babiuch
C. Biskup: cell studies (fluorescence microscopy), supervision
F. Foertsch
U. S. Schubert: correction of the manuscript, supervision

- P8) S. Ochrimenko,# A. Vollrath,# K. Kempe, L. Tauhardt, S. Schubert, U. S. Schubert, D. Fischer, "Dextran-*graft*-linear poly(ethylene imine) for gene delivery – influence of linker strategies on the phyicochemical and biological properties", *Bioconjug. Chem.* **2013**, submitted.

S. Ochrimenko: biological studies, conceptual development, preparation of the manuscript
 A. Vollrath: polymer synthesis and characterization, conceptual development, preparation of the manuscript
 K. Kempe: synthesis and characterization of pEtOx
 L. Tauhardt: synthesis and characterization of IPEI
 S. Schubert, U. S. Schubert: correction of manuscript, supervision
 D. Fischer: correction of manuscript, supervision S. Ochrimenko

- P9) A. C. Rinkenauer,# A. Vollrath,# A. Schallon, L. Tauhardt, K. Kempe, S. Schubert, D. Fischer, U. S. Schubert, "Parallel high-throughput screening of polymer vectors for non-viral gene delivery: Evaluation of structure-property-relationships of transfection", *ACS Comb. Sci.* **2013**, submitted.

A. C. Rinkenauer: biological and stability studies of polyplexes, conceptual development, preparation of the manuscript
 A. Vollrath: polyplex preparation and DLS measurements, conceptual contribution, preparation of the manuscript
 A. Schallon: conceptual development, preparation of the manuscript
 L. Tauhardt: synthesis and characterization of IPEI
 K. Kempe: synthesis and characterization of pEtOx
 D. Fischer: conceptual contribution, correction of the manuscript
 S. Schubert, U. S. Schubert: correction of manuscript, supervision

Jena, 25.02.2013 _____

Equal contribution

1. Introduction

Nanomedicine is one of the most promising fields within the area of nanotechnology and may be the answer to many intractable medical challenges. Nowadays, it benefits already from novel nanotechnologies in detection, imaging, treatment and prevention of diseases, such as cancer.^[1,2] Due to the increased surface-to-volume ratio, small nanoscale objects possess unique physicochemical characteristics. They reveal a different behavior in suspension compared to their bulk material and can pass fine capillaries as well as internalize into cells. Thus, nanocarriers are able to resolve important limitations accompanied with conventional diagnostic and therapeutic devices, such as lack of water solubility, non-specific biodistribution and low therapeutic indices. With the development of “theragnostic” nanoparticles that combine diagnostic and therapy *via* integration of drug and dye molecules, the medical effectiveness was even more improved.^[3]

Nanoparticles can consist of various inorganic and organic materials, whereby polymer based formulations have gained significant attention owing to their good biocompatibility, structural diversity and excellent adjustability of their resulting properties.^[4,5] Synthetic polymers, like poly(lactide-*co*-glycolide) (PLGA) and poly(ϵ -caprolactone) (PCL), but also biopolymers, like dextran and chitosan, were found to be perfectly suitable matrix materials.^[6-9] By utilization of top-down or bottom-up engineering, nanoparticle systems can be systematically designed with well-tuned size, shape and cargo loading.^[10,11] New generations of nanoparticles are furthermore functionalized on the surface with targeting and “stealth” moieties to reduce or to exclude adverse effects. By utilization of the sophisticated concept of a specific surface modification an enhanced blood circulation time of the nanoparticles as well as a highly-efficient delivery of drugs and diagnostic agents can be realized.^[12,13]

But despite the wide field of possible polymeric systems, preparation methods and surface modifications, until now only a few targeted polymeric nanoparticles have progressed to clinical trials demonstrating the challenges that come along with their development.^[3] Limiting factors of capital importance are the controlled and reproducible production and the still existing insufficient understanding of the particle interactions and distributions *in vitro* and *in vivo*. Innumerable studies can be found in literature that investigated the characteristics and tissue interactions of nanoparticles. However, these studies are based on different materials and basically non-defined surfaces due to the use of surfactants. No final conclusion can thus be drawn about the optimal particle design for safe and efficient administration.^[14-16]

In order to gain deeper insights into vital characteristics of nanoparticles, this thesis addresses the preparation of various polymeric particles in the nanoscale without using surfactants and includes their characterization as well as the biological evaluation. An overview about polymer-based nanoparticles applied for cancer detection is presented (see Chapter 2), whereby important parameters and possibilities for the design of nanocarriers for improved diagnostic applications are discussed. The formulation of several polymers

into nanoscaled objects by nanoprecipitation is investigated in Chapter 3, whereby an automatic high-throughput (HT) approach using pipetting robots is described that enables a systematical analysis of versatile materials and formulation process parameters. For the development of optimized particle formulations, a detailed physicochemical characterization of the nanoparticles represents a central prerequisite. In particular, parameters like the size are known to significantly influence the biodistribution and clearance of the nanoparticles; therefore, the size values should always be evaluated with great care.^[17] Though many techniques are available for their characterization, the particle sizes and size distribution are frequently poorly described using mainly only one analysis technique, mostly dynamic light scattering (DLS).^[18] For a sufficient characterization and detailed insight into the nanoparticle properties, orthogonal analysis methods, such as DLS, scanning electron microscopy and analytical ultracentrifugation are utilized and compared amongst each other (see Chapter 4). Admittedly, such a comprehensive investigation of the nanoparticle size is not feasible for a HT-approach, but with the application of a HT-DLS plater reader device for the fast analysis of all nanoparticles and a subsequent review of selective samples by other methods, deeper insights into various nanosystems could be achieved.

However, many issues in the field of nanomedicine which come along with the application of polymeric nanoparticles, like long-time consequences or unexpected side effects, are still precarious and need to be considered carefully. To study their interactions with biological tissue more in detail, various polymeric nanoparticles with defined sizes and surfaces were prepared and utilized for cellular internalization and biocompatibility studies (Chapter 5). Furthermore, nanoparticles were targeted with different sugar molecules and investigated with regard to their specific cellular uptake. Finally, since the polymer itself plays an important role for the effective design of nanocarriers useful for diagnostic and drug delivery applications, it is of high importance to understand fundamental structure-property relationships. Hence, a range of cationic polymeric vectors useful for gene delivery were synthesized applying different linker strategies, complexed into nanoscale assemblies with negatively charged DNA and evaluated with regard to their physicochemical and biological properties (Chapter 6). Moreover, a HT-workflow for an automatic and parallel evaluation of gene vectors is presented.

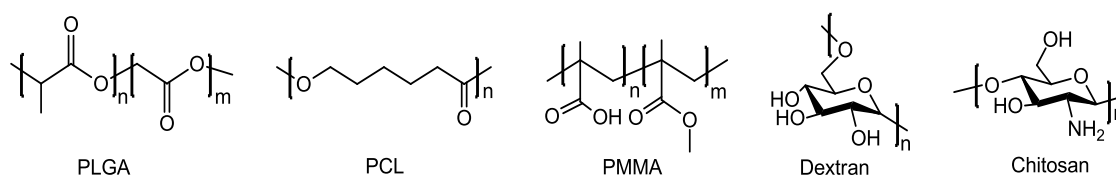
2. Nanoparticles for diagnostic

Parts of this chapter will be published: **P1**) A. Vollrath, S. Schubert, U.S. Schubert, *J. Mater. Chem. B* **2013**, accepted.

The area of medicine and biological diagnostic is a research field of great magnitude as it enables the detection of manifold processes inside the body and forms the major basis for the understanding of disfunctionalities and the subsequent occurrence of diseases. In particular for cancer treatment, an early diagnosis is of vital importance and decides about the success of the therapy. Since the development of nanoparticle-based technologies has revolutionized the diagnostic area, tremendous effort was set on the investigation of new, suitable nanomaterials and detection systems.^[2] A diagnostic technique that utilizes nanoimaging agents is fluorescence imaging. It is easy applicable and provides high spatial and temporal resolution, superb sensitivity as well as good selectivity.^[19,20] This imaging technique allows insights into living organisms with high sensitivity without the need of dissection, e.g., by usage of endoscopes.^[21,22] The examinations of vascular networks and sentinel lymph node mapping are only two examples of the successful application of fluorescence imaging.^[23] Besides an early detection, the surgical removal of the tumor is mostly efficient for cancer therapy, but it is a demanding task for the surgeon to remove the tumor tissue completely without damaging healthy tissue. In order to visualize tumors while surgery and to improve its radical resection, new systems were developed that enable the intraoperative identification of tumors. It was preclinically validated that by using specific fluorescent nanoagents and image guided surgery, tumors can be detected and removed very efficiently with reduced complications.^[24] At the moment, fluorescence image guided surgery is in the transit to clinical practice.^[3,20] However, in order to enable a fast clinical realization, new fluorescence probes need to be established and approved for *in vivo* application. The use of dye containing polymeric nanoparticles represents an excellent opportunity since the concept to incorporate fluorophores into a polymer shell provides a protection of the dye against external influences. Further benefits associated with the usage of fluorescent nanoparticles are: (1) Enhanced fluorescence intensities owing to a potential multiple loading of fluorophores into the particle, (2) increased surface area of the nanoparticle, which is perfectly suited for the attachment of targeting moieties or stealth polymers and (3) enhanced *in vivo* distribution as well as prolonged blood circulation time of the nanoagents compared to single dye molecules. Moreover, if two or more different chromophores are embedded in the polymer, it is also possible to obtain systems with switchable emission and/or stimuli-responsive fluorescent nanoparticles.^[25] Nevertheless, for a realistic *in vivo* application of fluorescent nanoparticles the agents have to fulfill a couple of prerequisites: (1) Fluorescent nanoparticles have to exhibit high purity and must be non-toxic to ensure a safe administration; (2) superior colloidal stability must be given in biological systems in order to avoid degradation or agglomeration and to prolong the blood circulation time, (3) carriers should be targetable for a controlled imaging, (4) complete

clearance from biological systems must be warranted after the imaging process is completed and (5) dye containing nanoparticles should possess a high and stable fluorescence to ensure the long-term imaging as well as a good signal-to-noise ratio. In order to realize the development of nanocarriers that fulfill all prerequisites mentioned above, the polymers used as matrix material should offer excellent biocompatibility, low or non-toxicity and the ability to form stable particles that persist over a long time also in biological environments.

To this end, a significant amount of effort was devoted to the synthesis and characterization of biocompatible polymers as matrix material. By utilizing living and controlled polymerization techniques, the architecture, composition and constitution as well as molar mass of the polymer can be easily adjusted resulting in defined chemical and physical properties. Polymers such as poly(lactide-*co*-glycolide) (PLGA) and poly(ϵ -caprolactone) (PCL) and poly(methyl methacrylate) (PMMA) derivatives are often used (Scheme 2.1).^[26] PLGA is thereby most extensively investigated as matrix material for nanoparticle based diagnostic and drug delivery owing to its outstanding characteristics, such as excellent biocompatibility, biodegradability into metabolizable moieties, and good manufacturing abilities.^[27] PCL represents a good alternative that shows comparable properties and is also widely applied for particle-based drug delivery and imaging application.^[28] Although nanoparticles consisting of PMMA are not biodegradable, their proven biocompatibility and high stability *in vitro* and *in vivo* declare them suitable for *in vivo* applications.^[29,30] PMMA is a FDA approved polymer for some *in vivo* applications (contact and intraocular lenses, filler for bone cavities) and can be combined with versatile polymers to obtain functional copolymers with fine-tuned properties.^[29,30] Beside the synthetic compounds, which can be tailored with regard to their desired properties, biopolymers are well-suited for nanoparticle preparation as they offer excellent biocompatibility, good biodegradability as well as multiple functional groups for conjugation with dyes or drugs. Important representatives amongst others are polysaccharides, such as dextran and chitosan.^[8,31]



Scheme 2.1. Schematic representation of synthetic and natural polymers applied for the synthesis of nanoparticles.

To prepare fluorescent nanoparticles, two different techniques can be applied to embed the fluorophore in a polymer matrix. The non-covalent procedure is characterized by physical entrapment of the dye molecules in the matrix material, either by encapsulation during the particle formation or by diffusion of the dye molecules into the nanoparticle core. The physical inclusion method has the advantage that changes in the optical properties evoked by the attachment of the dye to the polymer backbone do not occur. Additionally, the

manner of possible dyes is much less limited as no functionality on the chromophore is required for a chemical attachment. However, the dye may leak out of the nanoparticle shell. Such a leakage can be prevented by covalent attachment of the dye to the polymer scaffold. Several techniques can be utilized for the preparation of fluorescent nanoparticles. In detail, *in situ* polymerization of monomers in an emulsion polymerization can be performed.^[32] In addition, particles are fabricated by forcing the polymer material into nanostructures. Therefore, single or double emulsification, solvent-displacement/ nanoprecipitation, electro spraying, salting out, supercritical- and microfluidic processes as well as the inkjet printing of nanoparticles were developed.^[10,11]

In order to predict the particles fate *in vivo*, their physicochemical characteristics as well as target unit should be adjusted very carefully with regard to the final application (Figure 2.1). By implementation of passive (size, shape, charge) and active (targeting moieties) targeting concepts, nanoparticles can be directed to desired active sites (tumors) without adverse effects such as fast blood clearance by the macrophagocytotic system or accumulation in healthy tissue.^[3,12] For an improved diagnostic application, it is essential that the fluorescent particles accumulate, but to a great extent only in the target site to avoid interferences and will achieve high signal-to-background ratios for, e.g., refined tumor detection. The most important passive targeting parameter of the nanoparticles is their size. In literature, controversial size specifications are found to be used for *in vitro* and *in vivo* applications.^[17] Although the data range thereby from small particles below 10 nm up to a size of 500 nm, the optimal particle diameter is expected to be in the range of 30 nm to 200 nm, since nanoparticles in that size range benefit from the enhanced permeation and retention (EPR) effect.^[33] The influence of the shape was also determined to be considerable. In detail, rod-like nanoparticles with high aspect-ratios were internalized faster into cells in comparison to spherical ones with similar volume.^[13] Furthermore, it was predicted that prolate ellipsoids and discoidal shapes possess prolonged blood circulation times in comparison to spherical nanoparticles and are internalized most effectively into cells.^[34] Likewise controversially discussed as the size, the surface charge has an explicit impact on the particle stability and their interactions in suspension with cells and proteins. *In vitro* studies suggest that positively charged particles reveal a high cellular uptake through endocytosis because of the attraction for the negatively charged cell membrane (due to the presence of phospholipid groups and proteins).^[17,35] But as a result of this sticking, they display also highly non-specific internalization rates. Contrary, it was remarked that strong negatively charged nanoparticles exhibited lower cellular uptake efficiencies, but also decreased plasma protein absorption as well as non-specific interactions.^[35] For *in vivo* applications, a neutral charge was found to be more beneficial due to the fact that charged nanoparticles are recognized by the macrophagocytotic system and rapidly cleared from the body.^[35] To this end, the nanocarriers are often surface-functionalized with non-charged hydrophilic polymers, such as poly(ethylene glycol) (PEG), in order to minimize nonspecific protein binding and to enable prolonged blood circulation.^[36,37]

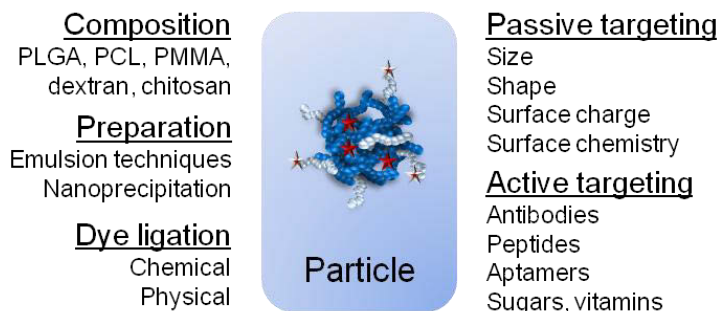


Figure 2.1. Important parameters for the design of polymeric nanoparticles.

Moreover, for *in vivo* applications an active targeting strategy of the nanoparticles is beneficial to ensure a controlled accumulation in the desired tissue.^[38] The idea is to conjugate ligands, such as antibodies, peptides, nucleic acids and other small molecules to the nanoparticle surface, which bind specifically to antigens or receptors that are only expressed on the target cells.^[39] Manifold studies demonstrated that the attachment of targeting units, in particular in combination with a PEG surface modification, significantly increased the accumulation of the nanoparticles in the tumor tissue.^[40,41] The undesired accumulation in healthy organs, such as liver, spleen, heart and lung was thereby decreased, which is beneficial in terms of enhanced cancer detection and unknown long-time consequences that might be accompanied with the application of fluorescent nanoparticles.

In the past few years a great progress in the development of polymer based nanoscale agents could be observed and many promising studies demonstrated the large potential of targeted fluorescent particles for selective imaging. However, in order to realize the usage of polymeric nanoparticles in clinical applications it is certainly required to gain deeper knowledge about their production and design, *in vivo* stability, circulation behavior and their interactions with blood, proteins and cells as well as their definite faith.

3. Nanoprecipitation for tailored nanoparticle preparation

Parts of this chapter have been published: **P2**) I. Y. Perevyazko, A. Vollrath, S. Schubert, G. M. Pavlov, U. S. Schubert, *J. Polym. Sci., Part A: Polym. Chem.* **2010**, *48*, 3924-3931. **P3**) I. Y. Perevyazko, J. T. Jr. Delaney, A. Vollrath, G. M. Pavlov, S. Schubert, U. S. Schubert, *Soft Matter* **2011**, *7*, 5030-5035. **P4**) I. Y. Perevyazko, A. Vollrath, C. Pietsch, S. Schubert, G. M. Pavlov, U. S. Schubert, *J. Polym. Sci., Part A: Polym. Chem.* **2012**, *50*, 2906-2913.

As mentioned in the last chapter, nanoparticles were investigated with great effort in the last years as a result of their enormous potential in diagnostic and therapy, but their controlled and reproducible production and their specific design still remain a demanding process. One straightforward methodology that gained significant attention for the construction of nanoparticles, by both industry and academia, is nanoprecipitation.^[42-44] This method describes the formation of nanoparticles if a dissolved polymer is exposed to a non-solvent and is known as a facile and time efficient as well as inexpensive preparation technique. Nanoprecipitation offers a remarkable and unique advantage over alternative techniques, meaning no surfactants are required, which is of high relevance for biological studies. Furthermore, since for preparation of the nanoparticles no washing step is necessary, the concentration of the polymeric particles in the suspensions remains constant and must not be determined in subsequent time-consuming lyophilization and weighing procedures. The term nanoprecipitation encompasses the dialysis and the dropping technique (Figure 3.1a, b). Dialysis describes the exchange of the solvent against the non-solvent molecules through membranes, while the dropping technique specifies the dropwise addition of a polymer solution to the non-solvent while stirring (or *vice versa*).

Both methods allow the manipulation of the nanoparticle sizes by alteration of the initial polymer concentration, while the dropping technique additionally convinces with low costs (non-necessity of a membrane) and the ability to fine-tune the size and shape of the nanoparticles by the way of dropping (Figure 3.1c). While the dropwise addition of the polymer solution into water yields small but irregularly formed nanoparticles as a results of the rapid replacement of the solvent to the non-solvent, the addition of water into the polymer solution tends to result in more defined, spherical nanoparticles due to the stepwise change of the solvent environment (Figure 3.1d).

Due to the great applicability of the nanoprecipitation methodology for manifold materials, versatile synthetic polymers were tested with regard to their potential to form nanoparticles. To this end, the polymers were dissolved in suitable solvents, e.g., acetone or tetrahydrofuran (THF), with a concentration of 1 to 10 mg · mL⁻¹ and added dropwise into water or water was added to the polymer solutions, respectively. It could be shown that almost all polymers were able to form stable particles on the nanoscale by applying nanoprecipitation for particle formulation (Table S.1 and Figure S.1, supporting information).

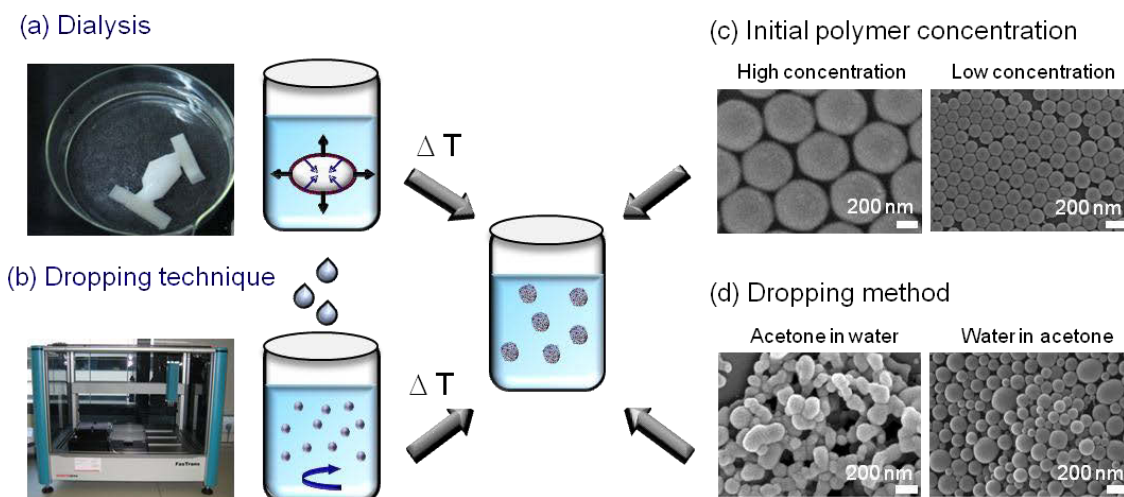


Figure 3.1. Left: Overview about the nanoprecipitation methods (a) of dialysis and (b) dropping technique. Right: Tuning possibilities of the size and shape of the nanoparticles by variation of (c) initial polymer concentration and (d) dropping method.

Stimulated by the successful application of nanoprecipitation for various synthetic polymers, the dropping technique was accomplished in a high-throughput (HT) manner *via* utilization of pipetting robots, in order to facilitate a faster, reproducible, and more in-depth exploration of process-property relationships of the materials. In particular, for the development of improved particle formulations for drug delivery or systematic biotechnological studies, the HT-nanoprecipitation represents a highly suitable tool. In a first set of experiments, the biocompatible polymers poly(methyl methacrylate-*stat*-methylacrylic acid) (p(MMA-*stat*-MAA)_{0.66:0.33}), poly(lactide-*co*-glycolide)_{0.5:0.5} (PLGA) and acetal-derivatized dextran (ac-dex) were chosen to be processed *via* HT-nanoprecipitation (Figure 3.2a). The interplay of the manufacture process and the resulting characteristics of the nanoparticles was thereby investigated by alteration of the initial polymer concentration and the solvent-to-non-solvent ratio (Figure 3.2b). For this purpose, a dilution series of the respective polymer solution with concentrations ranging from 1 mg · mL⁻¹ up to 12 mg · mL⁻¹ was created and combined with different proportions of water, in a way that the solvent (acetone) to non-solvent (water) ratios varied from 0.1 to 0.5 (v/v). After each polymer solution was added dropwise into water, the net result was an array of 96 different formulations, which exhibits a visually observable trend in appearance, following the changes made in the nanoprecipitation process (Figure 3.2b).

The fabricated plates of the different nanoparticle formulations were subsequently characterized with regard to their particle size distribution in an automated manner using a high-throughput dynamic light scattering (HT-DLS) device (Figure 3.2c). The HT-DLS measurements confirmed the dependency of the final average particle sizes on the polymer concentration (Figure 3.3a-c). At diluted polymer concentrations, the nanoprecipitation process yielded small nanoparticle sizes below 100 nm with monomodal and narrow size distributions for all polymers. But with rising concentration, the particle diameters

increased, which was indicated before by the increased turbidity of the suspensions. In detail, 60 nm to 290 nm sized nanoparticles were obtained by nanoprecipitation of the $p(\text{MMA-}i\text{stat-MAA})_{0.66:0.33}$ polymer within a concentration range from $1 \text{ mg} \cdot \text{mL}^{-1}$ to $12 \text{ mg} \cdot \text{mL}^{-1}$ (Figure 3.3a). The sizes of the PLGA nanoparticles varied from 40 nm for $1 \text{ mg} \cdot \text{mL}^{-1}$ to 170 nm for $10 \text{ mg} \cdot \text{mL}^{-1}$, while ac-dex particles revealed increasing sizes from 80 nm to 140 nm for the same range of concentrations (Figure 3.2b,c).

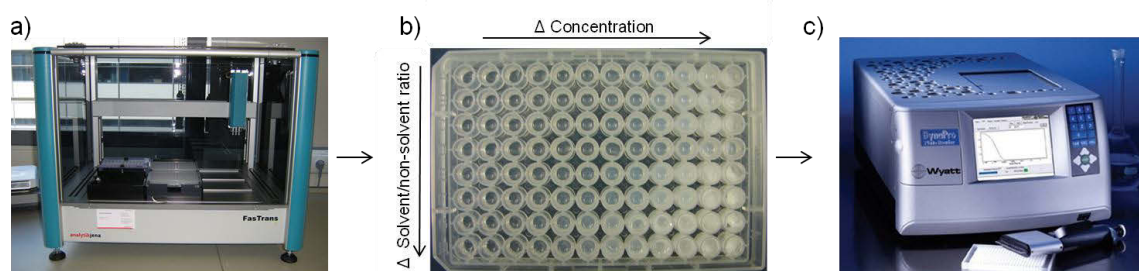


Figure 3.2. HT-experimental set-up: (a) HT-nanoprecipitation of polymers a pipetting robot. (b) Layout of a 96 well plate after nanoprecipitation. The concentration of the polymer is varied along the x-axis and the ratio of solvent/non-solvent solution along the y-axis. (c) The final well plates of different nanoparticle formulations were characterized using HT-DLS.

For all examined polymers the tendency of a growth of the mean particle diameter as a function of initial polymer concentration was detected. This effect was expected since with higher concentration of the polymer in the organic phase more polymer molecules per unit volume of solvent are present. A comparatively small effect on the nanoparticle sizes exhibited the solvent to non-solvent ratio in the studied region. Merely a slight decline in the mean nanoparticle diameter with increasing solvent/non-solvent ratio was observed. Furthermore, the polymer characteristics itself revealed a high impact on the nanoparticle size as well. Regarding to its hydrophobicity and molar mass, a difference in the particle formation for the different polymers is the consequence. By HT-DLS investigations, an exponential growing in the particle size was observed for the $p(\text{MMA-}i\text{stat-MAA})_{0.66:0.33}$ copolymer, while the sizes of the ac-dex particles increase less considerably, and the concentration dependence tends to play a minor role (Figure 3.3d). The tendency obtained for PLGA-nanoparticles is located between the $p(\text{MMA-}i\text{stat-MAA})_{0.66:0.33}$ and ac-dex, and it also tends to show a linear correlation between concentration and size, contrary to the exponential one of the $p(\text{MMA-}i\text{stat-MAA})_{0.66:0.33}$ copolymer. To evaluate the influence of the polymers and the manufacturing parameters on the resulting surface charge of the nanoparticles, zeta potential (ζ) measurements were performed of selected samples. As mentioned in Chapter 2, the zeta potential provides vital information about the nanoparticle stability and affects the cellular internalization as well as the biodistribution *in vivo*.^[17,45] $p(\text{MMA-}i\text{stat-MAA})_{0.66:0.33}$ particles revealed values between $\zeta = -17$ to -65 mV, while a lower surface charge of $\zeta = -14$ to -22 mV was obtained for ac-dex and PLGA particles. A correlation of the zeta potential and particle size was evident due to the fact that the surface charge was increasing with higher polymer concentrations, whereas with varying solvent/non-solvent ratio the measured zeta potential remained unchanged.

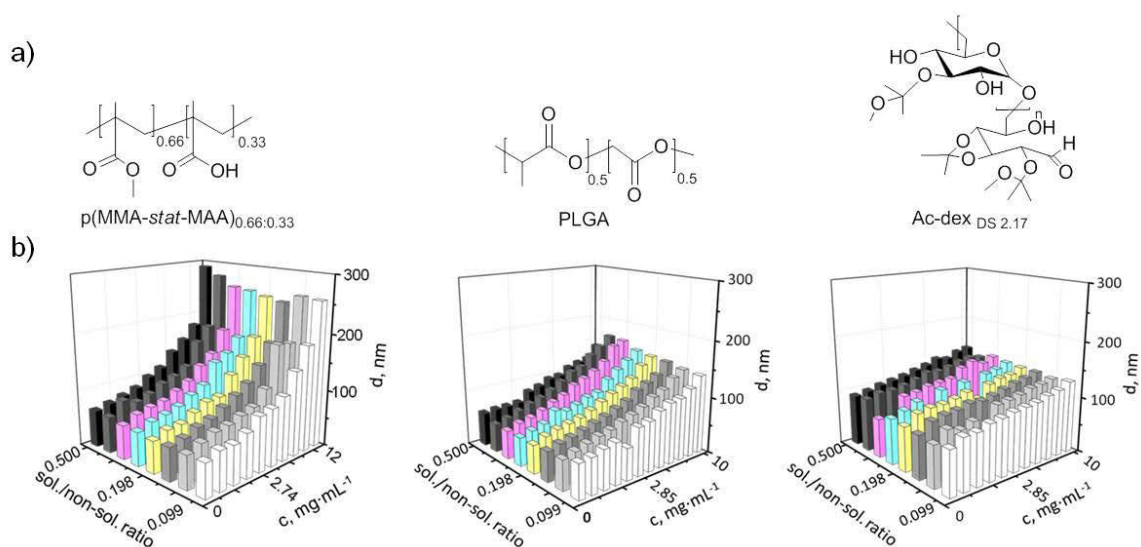


Figure 3.3. (a) $P(\text{MMA-}stat\text{-MAA})_{0.66:0.33}$, PLGA, and ac-dex applied for HT-nanoprecipitation and (b) corresponding 3-D representation of the size distribution obtained by HT-DLS as a function of initial polymer concentration and solvent to non-solvent ratio. The particle suspensions were prepared by dropping the polymer acetone solution into water.

Additional studies were addressed to extend the understanding of the effect of the molar mass of the polymer on the nanoparticle formation. For this purpose, a homologous series of a poly(methyl methacrylate) (PMMA) polymer with molar masses ranging from $3,000 \text{ g}\cdot\text{mol}^{-1}$ to $278,000 \text{ g}\cdot\text{mol}^{-1}$ was applied for the HT-nanoprecipitation process. In first studies identical to previous experiments, the polymer concentration and the solvent to non-solvent ratio were altered. HT-DLS measurements revealed that with increasing molar mass of the PMMA polymer the range of particle sizes was rising as well, while the critical polymer concentration for aggregation was decreased (Figure 3.4). For instance, PMMA with a molar mass of $38,000 \text{ g}\cdot\text{mol}^{-1}$ showed an aggregation of the particles already at an initial concentration above $10 \text{ mg}\cdot\text{mL}^{-1}$, whereas PMMA with a molar mass of $6,000 \text{ g}\cdot\text{mol}^{-1}$ formed stable nanoparticles up to a concentration of $c = 30 \text{ mg}\cdot\text{mL}^{-1}$.

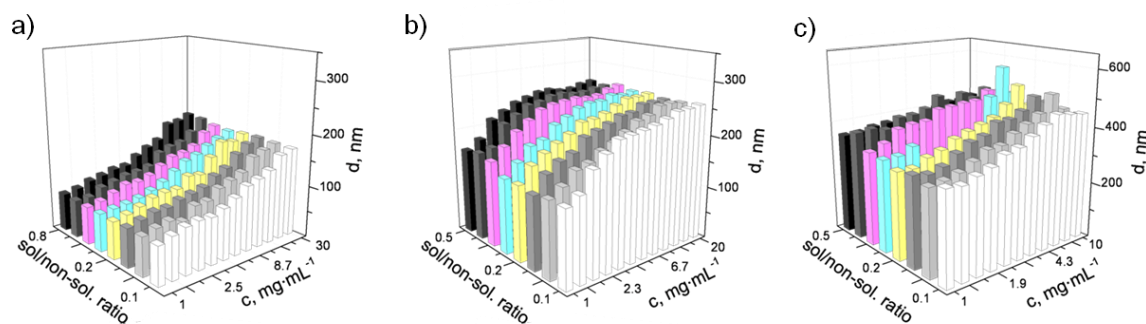


Figure 3.4. 3D-Representation of a size distribution obtained by DLS of PMMA polymers with different molar masses: (a) $M_w = 6,000 \text{ g}\cdot\text{mol}^{-1}$, (b) $M_w = 18,000 \text{ g}\cdot\text{mol}^{-1}$, and (c) $M_w = 38,000 \text{ g}\cdot\text{mol}^{-1}$. The particles were prepared by dropping polymer acetone solution in water.

However, to allow a reliable conclusion about the influence of the molar mass of the polymer it is crucial to maintain the same initial conditions for each nanoprecipitation process. But since polymers with various molar mass will occupy different volumes owing to the altered length of a polymer chain, the equality of the initial polymer concentration will not reflect the same conditions for the nanoprecipitation process. Thus, an approximation of the volume fraction of the macromolecular coils in the solution represented by the product of the polymer concentration (c) and the intrinsic viscosity $[\eta]$, the so-called Debye parameter ($c \cdot [\eta]$) was introduced. If $c \cdot [\eta] \ll 1$, the polymer solution can be considered as diluted and overlapping of the macromolecular coils can be excluded. Therefore, in further HT-experiments the nanoparticle suspensions of the different PMMA polymers were prepared with a degree of dilution ranging from $0.004 < c \cdot [\eta] < 0.12$. As expected, the particle size increased with increasing Debye parameter. The detected growth of the particle size was thereby more rapidly for higher molar mass polymers and reached a plateau. Furthermore, it was investigated that generally stable nanosuspensions were only observed when $c \cdot [\eta] < 0.1$ was applied. For $c \cdot [\eta] > 0.1$ the nanoparticle suspensions were found to be highly polydisperse with diameters larger than 500 nm. Thus, it could be proven that not only the polymer concentration, but rather the volume fraction occupied by the polymer macromolecular coil and, related to this, the molar mass, are key factors for the production of well-defined particles on the basis of a certain polymer.

In conclusion, it was demonstrated that nanoprecipitation represents a well-suitable methodology for the preparation of polymeric nanoparticles with desired size and polydispersity. In order to allow the preparation of particle suspensions in large numbers in an automated, reproducible manner, a HT-nanoprecipitation technology was developed for a highly efficient particle formulation screening. With the assistance of the HT-nanoprecipitation set-up, it was verified that the properties of polymeric nanoparticles primarily depend on the initial polymer characteristics and concentration used for nanoprecipitation process.

4. Advanced characterization of nanoparticles

Parts of this chapter have been published: **P2**) I. Y. Perevyazko, A. Vollrath, S. Schubert, G. M. Pavlov, U. S. Schubert, *J. Polym. Sci., Part A: Polym. Chem.* **2010**, *48*, 3924–3931. **P5**) A. Vollrath, D. Pretzel, C. Pietsch, I. Y. Perevyazko, R. Menzel, S. Schubert, G. M. Pavlov, D. Weiß, R. Beckert, U. S. Schubert, *Macromol. Rapid Commun.* **2012**, *33*, 1791–1797.

For future applications of nanoparticle dispersions in biomedical fields the tailoring of the main particle parameters like mean size, size distribution and shape is extremely important.^[13,17,18] To optimize nanosuspensions and to prevent undesired side effects like aggregation (e.g., of drug-containing particles in the blood stream), a detailed analysis of the nanoparticle characteristics with regard to their preparation procedure must be ensured. A frequently used technique to characterize nanoparticles is dynamic light scattering (DLS).^[46,47] Based on the detection of the fluctuation of scattered light caused by the Brownian motion of particles in the sub micron region, the translational diffusion coefficient (D) is determined and used to calculate the average hydrodynamic diameter (d_h , Z average) *via* the Einstein-Stokes equation (4.1) and the polydispersity.^[48,49] The calculated particle size is thereby assumed to be the size of a sphere that reveals the same diffusion coefficient as the scatterer.

$$D = \frac{k_B T}{3 \pi \eta_0 d_h} \quad (4.1)$$

In general, DLS is a rapid, facile and well adapted method for routine measurements of nanoparticles. However, for very polydisperse samples or high concentrated suspensions the accurate data analysis and interpretation becomes demanding due to the occurrence of multi scattering.^[50] Multiangle DLS analysis offers here more detailed insights into the nanoparticle size and provides further information about the shape. But accordingly the measurement time and data analysis becomes more complex and time-consuming. Adversely, DLS is very sensitive against the presence of small amounts of aggregates, larger particles or dust.^[18] Hence, the intensity distribution can be somewhat misleading (e.g., due to an enormous increase in mean calculated size) since the scattering intensity of spherical particles is proportional to the power of six of the diameter or the square of the molar mass ($I \sim d^6 \sim M^2$). Although the intensity weighted distribution can be transformed into volume and number weighted distributions based on the Mie theory, all results obtained by DLS investigations should be advisedly evaluated.^[49] In addition, a couple of parameters like viscosity of the medium, refractive index and concentration of the suspension as well as temperature may also affect the data and should be considered very carefully. Thus, for a reliable conclusion about the particle size and size distribution the application of additional analysis methods such as scanning electron microscopy (SEM) or analytical ultracentrifugation (AUC) are required.^[51,52]

SEM offers the advantage that an image of the particles is obtained, and, hence, also detailed information about the nanoparticle shape and surface (roughness) can be achieved. In comparison to DLS, the particles are investigated in a dried status. This is beneficial because once the sample is prepared it is less sensitive against measurement artifacts. But during the drying process particle shrinking appears, which frequently results in underestimated particle sizes.^[52,53] However, resolution problems may arise with particles well below 100 nm, depending on the instrument. The sample preparation, measurement and analysis are additionally more elaborating for the microscopy method than for the DLS investigations. Furthermore, SEM images provide only information about a small fraction of nanoparticles, whereas DLS enables a more statistical size analysis of many nanoparticles in the suspension.^[52,53]

Likewise DLS, AUC measurements are performed in solution and no further sample preparation is necessary. AUC detects the sedimentation of objects in solution during the centrifugation with different optical systems and provides information about size, size distribution, shape and molar mass of nanoparticles in a range of 1 nm to 100 μm .^[54,55] Although providing many information about the nanoparticle suspension, AUC requires a complex and time-intensive data analysis and various parameters, such as viscosity and density of the solvent as well as density of the particles, need to be considered. Consequently, in order to obtain an all-embracing insight into the particle size and size distributions for a reliable conclusion, all polymeric nanoparticles fabricated by nanoprecipitation were investigated by at least two of the before mentioned analysis methods.

In a first study, different poly(methyl methacrylate) (PMMA) copolymers, like a poly(methyl methacrylate)-*stat*-(methacrylic acid) (p(MMA-*stat*-MAA)_{0.66:0.33}) and a fluorescence labeled poly(methyl methacrylate)-*stat*-(pyrene-methacrylic acid) (p(MMA-*stat*-PyMAA)_{0.95:0.05}) polymer were precipitated by dialysis and the dropping method, and the nanoparticles obtained were characterized by DLS, SEM and AUC (Table 4.1).

Table 4.1. Weight average diameters of p(MMA-*stat*-PyMAA)_{0.95:0.05} and p(MMA-*stat*-MAA)_{0.66:0.33} nanoparticles determined by DLS, SEM and AUC.

Polymer	Nanoprecipitation method	d_{DLS} [nm]	PDI_p	d_{SEM} [nm]	d_{AUC} [nm]
p(MMA- <i>stat</i> -PyMAA) _{0.95:0.05}	Dialysis	480	0.35	280	570
	Dropping AW	100	0.23	75	65
	Dropping WA	680	0.32	490	380
p(MMA- <i>stat</i> -MAA) _{0.66:0.33}	Dialysis	46	0.31	36	28
	Dropping AW	41	0.30	43	35
	Dropping WA	190	0.13	110	104

AW = polymer acetone solution was dropped into water, WA = water was dropped into polymer acetone solution.

For a facile comparison of the size distribution measured by SEM with the values obtained by DLS and AUC, the weight average diameters were calculated from the SEM images, whereby the number of individual particles N considered in the calculations varied between 100 and 300. A satisfactorily good agreement of the three analysis techniques was identified for small nanoparticles below 100 nm (Table 4.1). But with rising diameters of the nanoparticles, the sizes obtained by the different techniques vary incremental. Often DLS revealed the largest values, which was expected due to the before mentioned sensitivity against the presence of aggregates and dust as well as the overrepresentation of larger particles. In return, SEM provided in most cases the smallest size values, which was likewise expected due to the “dried state” investigation. For a closer look, the size distributions for $p(\text{MMA-}i\text{stat-MAA})_{0.66:0.33}$ particles measured by DLS, SEM, and AUC are shown as a typical example in Figure 4.1. The shapes of the distributions obtained from the different techniques had a similar appearance (i.e., similar modalities of distribution). But the DLS size distribution clearly exceeded the sizes obtained by AUC and SEM, which were found to be in a good agreement. The observed considerable discrepancies in the sizes and size distributions proved the necessity of different characterization techniques for a final conclusion about the nanoparticle size.

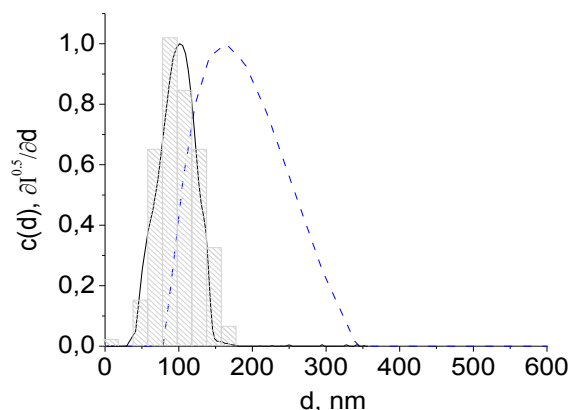


Figure 4.1. Size distribution of nanoparticles (prepared from an acetone solution of $p(\text{MMA-}i\text{stat-MAA})_{0.66:0.33}$ by dropping water into it) as analyzed by SEM (in bars), AUC (—) and DLS (---).

In another study, a PMMA copolymer that contained methacrylate units functionalized with a thiazole chromophore (MA^y) ($p(\text{MMA-}i\text{stat-MA}^y)_{0.97:0.03}$) was utilized. Differently sized nanoparticles were prepared by nanoprecipitation and separated using the preparative ultracentrifugation (PUC). PUC is a technique that can be used to fractionate nanoparticles and provides another degree of physical control of the size distribution of particles on the nanoscale compared to nanoprecipitation.^[56-60] In the following, the particles were characterized by DLS, SEM and AUC to evaluate the dimensions of the nanoprecipitation method as well as of the characterization techniques. However, by means of the two techniques a small (**S**) and a large (**L**) nanoparticle batch was prepared, respectively, whereby **S1** and **L1** were produced by the dropping method and **S2** and **L2** were obtained by PUC fractionation of an initially polydisperse sample. The resulting diameters observed by DLS, SEM and AUC are displayed in Table 4.2.

Table 4.2. Summary of the size distributions of the nanoparticles based on $p(\text{MMA-}i\text{stat-MA}^y)_{0.97:0.03}$.

Sample	Preparation method	d_{DLS} [nm]	PDI _p	d_{SEM} [nm]	d_{AUC} [nm]
S1	Nanoprecipitation	118	0.10	111	120
L1	Nanoprecipitation	488	0.03	696	503
S2	PUC fractionation	120	0.26	131	97
L2	PUC fractionation	597	0.19	502	381

It was explored that the small $p(\text{MMA-}i\text{stat-MA}^y)_{0.97:0.03}$ particle batches (**S1** and **S2**) revealed similar average sizes and size distributions proving the superior qualification of the nanoprecipitation to prepare narrow, defined nanoparticles in a straightforward manner. Contrary, for the larger particles (**L1** and **L2**) diverging sizes were obtained ranging from 400 up to 600 nm, depending on the characterization method applied. Although no remarkable discrepancy in the size plots of the differently prepared particle suspensions could be observed by DLS (Figure 4.2a), the distributions obtained by AUC already illustrate broader size distribution for the samples prepared by nanoprecipitation (Figure 4.2b). This was further confirmed by a detailed analysis of the SEM images, in which the fractionated samples were obviously more uniform in their size than the initial, non-fractionated samples (Figure 4.2c). Yet, it is difficult to predict if a fractionation process by PUC is actually more efficient than using a defined nanoprecipitation process. The precipitation method convinces due to its fast and easy applicability. Furthermore, it already led to monomodal and narrow size distributions for the small nanoparticles. In contrast, for the large particles prepared by nanoprecipitation a broader size distribution was observed (as revealed by AUC and SEM measurements) indicating that the effort to use PUC for more distinct size distribution might be profitable.

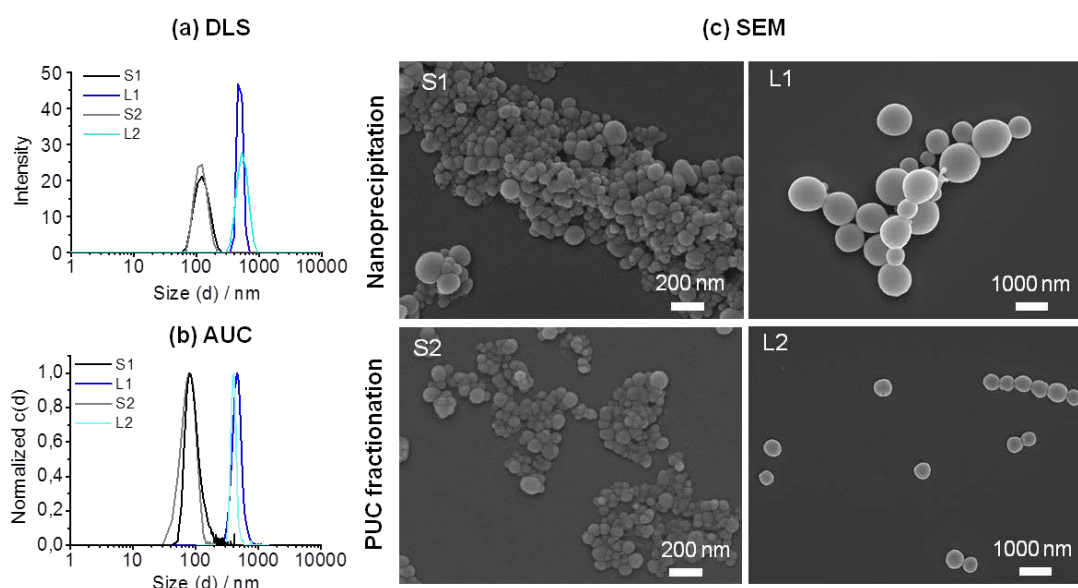


Figure 4.2. Characterization of small and large nanoparticles of $p(\text{MMA-}i\text{stat-MA}^y)_{0.97:0.03}$ prepared by nanoprecipitation and fractionation *via* PUC. Size distributions of the particles in water determined by DLS (a) and AUC (b) as well as SEM images of the particle suspensions (c).

In conclusion, for a detailed characterization of nanoparticles orthogonal analysis techniques are required. Certainly, all mentioned characterization methods have their advantages as well as their limitations and none of the techniques provides ultimate information about the size and shape as well as flow behavior of nanoparticle systems. Only a combination of these techniques can lead to satisfying characterization results. Therefore, all prepared suspensions were characterized with at least two analysis techniques, mostly DLS and SEM.

5. Targeting of polymeric nanoparticles for cell internalization studies

Parts of this chapter have been published: **P5)** A. Vollrath, D. Pretzel, C. Pietsch, I. Y. Perevyazko, R. Menzel, S. Schubert, G. M. Pavlov, D. Weiß, R. Beckert, U. S. Schubert, *Macromol. Rapid Commun.* **2012**, *33*, 1791–1797. **P6)** A. Vollrath, A. Schallon, C. Pietsch, S. Schubert, T. Nomoto, Y. Matsumoto, K. Kataoka, U. S. Schubert, *Soft Matter* **2013**, *9*, 99–108. **P7)** K. Babiuch, D. Pretzel, T. Tolstik, A. Vollrath, S. Stanca, F. Foertsch, C. R. Becer, M. Gottschaldt, C. Biskup, U. S. Schubert, *Macromol. Biosci.* **2012**, *12*, 1190–1199.

For an efficient utilization of nanoparticles in diagnostic and therapy with low or non-adverse side effects, it is crucial to address them specifically to the target side of action. Nowadays, different strategies for a controlled nanoparticle application are available, encompassing passive and active targeting concepts.

5.1 Passive targeting

As already discussed in Chapter 1, the most important passive targeting parameter is the size since it certainly influences the biodistribution and cellular internalization of nanoparticles significantly.^[13,17] While for large particles up to the range of 10 μm a cellular uptake *via* phagocytosis and macropinocytosis is assumed, smaller particles below 300 nm most likely internalize into cells by clathrin- and caveolin-dependent endocytosis.^[61-64] Although plenty of investigations focused on the understanding of the cellular internalization process of nanoparticles, no final conclusion regarding the size dependency can be drawn, due to the fact that the studies are based on different materials and cells.^[14,17] Furthermore, the nanoparticles were frequently prepared by techniques that require the use of surfactants, which were found to influence the cellular uptake as well.^[65]

To achieve well-defined nanoparticles with different sizes for cellular uptake studies in the absence of any surfactants, poly(methyl methacrylate) (PMMA) copolymers were formulated into nanoparticles *via* the nanoprecipitation method. The intracellular detection of the particles was thereby enabled by incorporation of various fluorescent dyes into the copolymers used as matrix material. The fluorophores were either covalently introduced during the polymerization reaction or chemically attached in a post-modification reaction to the polymer. A thiazole chromophore functionalized poly(methyl methacrylate)-*stat*-(methacrylic acid) (p(MMA-*stat*-MA^y)_{0.97:0.03}) copolymer was applied for nanoprecipitation, whereby small particles were obtained by dropping the polymer acetone solution with a concentration of 4 mg · mL⁻¹ into water. Larger particles were achieved if water was added to a polymer acetone solution with a concentration of 3 mg · mL⁻¹. In addition, small and large particles were furthermore prepared by fractionation of a polydisperse nanosuspension *via* preparative ultracentrifugation (PUC). The comprehensive characterization of the prepared nanoparticles *via* orthogonal analytical techniques, such as dynamic light scattering (DLS), scanning electron microscopy (SEM) and analytical ultracentrifugation (AUC), was already discussed in Chapter 4. All suspensions revealed

monomodal particle size distributions in the range of 120 nm (small) or 500 nm (large), respectively.

In order to ensure that the nanoparticles would be applicable for biological studies, the occurrence of adverse side effects, e.g., bulk precipitation and Ostwald ripening during storage or at subsequent manufacturing processes, such as autoclavation and lyophilization, must be excluded. For this purpose, stability studies of the nanoparticles were performed. In detail, samples of the initial nanosuspensions were analyzed by DLS and SEM after storage for 6 months at 5 °C, incubation with cell culture media (DMEM), centrifugation at 24.650 *g* for 20 minutes, autoclavation and lyophilization with subsequent resuspension. Since no signs of instability in terms of agglomeration or creaming up and no changes in the size distributions were observed, the nanoparticles were declared as highly stable and well-suitable for *in vitro* studies.

To investigate the biocompatibility and cell internalization of the nanoparticles, mouse fibroblasts L929 cells were incubated with the suspensions. The particles revealed excellent biocompatibility, since no cytotoxicity, hemolytic activity and no red blood cell aggregation was observed. Furthermore, a concentration dependent internalization of the particles was proven by CLSM, whereby a clear discrimination of small and large particles was possible regarding the amount of cells with internalized nanoparticles (Figure 5.1). Next to the size and the concentration, the preparation method exhibited a significant influence on the resulting nanoparticle-cell interaction. The particles prepared by fractionation *via* PUC were internalized to a much higher degree compared to the suspensions prepared by simple nanoprecipitation. This unexpected difference is presumably caused by the presence of sugar molecules on the surface of the fractionated nanoparticles since sucrose was used as concentration gradient during the PUC treatment.^[45] Even after purification by extensive dialysis, some sucrose moieties might still be attached on the particle surface leading to enhanced cellular recognition and internalization.^[66-68]

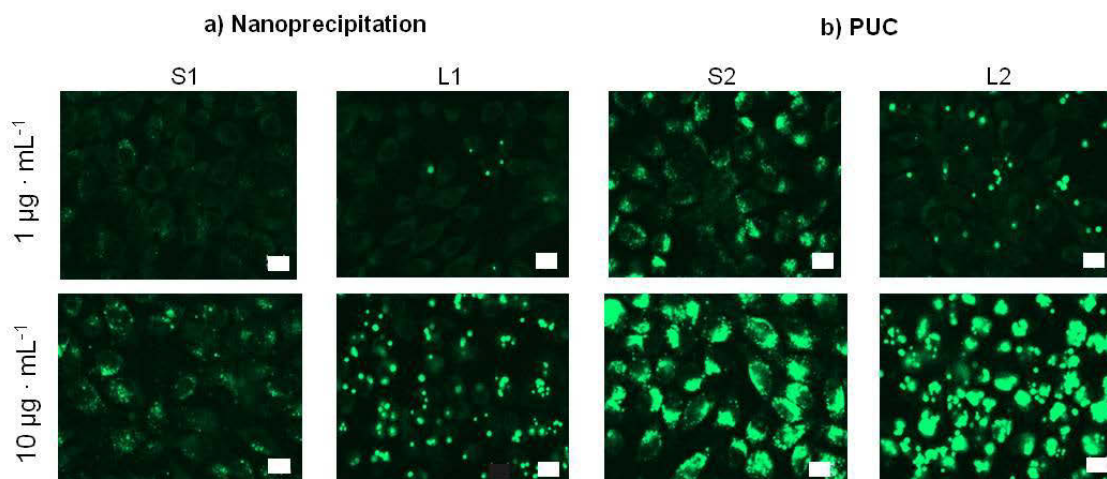
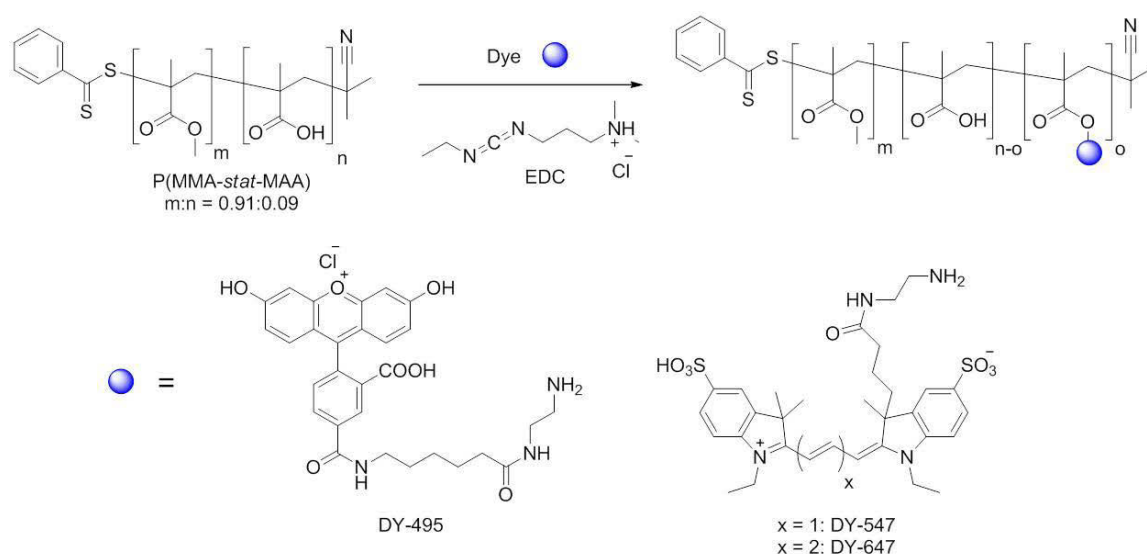


Figure 5.1. Confocal fluorescence images of L929 cells after 24 h incubation with polymeric p(MMA-*stat*-MA^y) nanoparticles (green). Cells incubated with polymer free culture medium served as control (not shown). All images were obtained with identical instrument settings (scale bars 10 µm).

Continuative studies aimed to explore the size dependent internalization of particles into cells in more detail. To this end, $p(\text{MMA-}i\text{stat-MAA})_{0.91:0.09}$ was post-functionalized with various fluorescent dyes (DY-495, DY-547 and DY-647) to obtain differently labeled copolymers for the preparation of nanoparticles (Scheme 5.1). For the labeling reaction (1-ethyl-3-(3-dimethylamino-propyl)carbodiimide (EDC) was used as coupling reagent. A low degree of labeling was sufficient due to the superior fluorescent properties of the selected dyes, and ensures similar properties for all copolymers as well as minimizes the influence of the dyes on the nanoprecipitation procedure. The fluorescence emission spectra of the purified copolymers $p(\text{MMA-}i\text{stat-MA}^{\text{green}})$, $p(\text{MMA-}i\text{stat-MA}^{\text{orange}})$, and $p(\text{MMA-}i\text{stat-MA}^{\text{red}})$ revealed distinct peaks at 525 nm, 568 nm, and 668 nm, respectively. In comparison to the initial emission of the pure dyes, no significant change in the fluorescence behavior was obtained. SEC measurements exhibited a minor change of the elution volume of the labeled copolymers in comparison to unmodified $p(\text{MMA-}i\text{stat-MAA})_{0.91:0.09}$, which indicated a slight increase of the molar mass as a result of the dye conjugation and supported the assumption that the polymer was not degraded or cross-linked during the labeling procedure. The overlay of the diode array detector and refractive index traces of the labeled samples further confirmed the successful covalent attachment of the dyes.



Scheme 5.1. Schematic representation of the reaction of $p(\text{MMA-}i\text{stat-MAA})_{0.91:0.09}$ with the DY-495 (green excitation), DY-547 (orange excitation), and DY-647 (red excitation) using EDC as coupling reagent.

After detailed characterization of the fluorescent copolymers, the nanoparticles were prepared only *via* nanoprecipitation in order to avoid any possible influence of other parameters (such as the presence of sugars on the surface). To achieve differently sized nanoparticles, the initial polymer concentration in the organic phase and the dropping method (polymer acetone solution into water or water into polymer acetone solution) were altered. The conditions used for the preparation of small, medium and large nanoparticles as well as their resulting sizes investigated by DLS are displayed in Table 5.1.

Table 5.1. Summary of the nanoprecipitation conditions as well as resulting Z average value (d_{DLS}) and polydispersity index (PDI_p) of representative nanoparticles prepared using p(MMA-*stat*-MA^{dye}). The solvent/non-solvent ratio was 0.25.

Polymer	Nanoprecipitation method	Polymer concentration [mg · mL ⁻¹]	d_{DLS} [nm]	PDI_p
p(MMA- <i>stat</i> -MA ^{green})	Dropping AW	1	80	0.26
p(MMA- <i>stat</i> -MA ^{orange})	Dropping AW	10	170	0.06
p(MMA- <i>stat</i> -MA ^{red})	Dropping WA	4	360	0.07

AW = Polymer acetone solution was dropped into water, WA = water was dropped into polymer acetone solution.

In detail, small nanoparticles in the range of 80 nm, medium particles with diameters of 170 nm and large nanospheres with an average size of 360 nm were obtained. Low PDI_p values indicated narrow size distribution, in particular for the medium and large particles, which were further verified by SEM investigations (Figure 5.2). Repetitive zeta potential measurements ascertained similar charge values in the range of 30 ± 10 mV for all nanoparticles indicating a good stability of the suspensions. Similar zeta potential values are furthermore essential since the focus was set on the influence of the size and not on the surface charge. To confirm the nanoparticles stability, the suspensions were centrifuged at 24.650 *g* for 20 min, autoclaved, incubated in PBS or cell culture media as well as titrated in a pH range of 4 to 10. Subsequent analysis by DLS, zeta potential measurements and SEM revealed that neither the size distributions nor the zeta potential values changed proving the high stability of the p(MMA-*stat*-MA^{dye}) nanoparticles as well as their eligibility to be used for further biological studies.

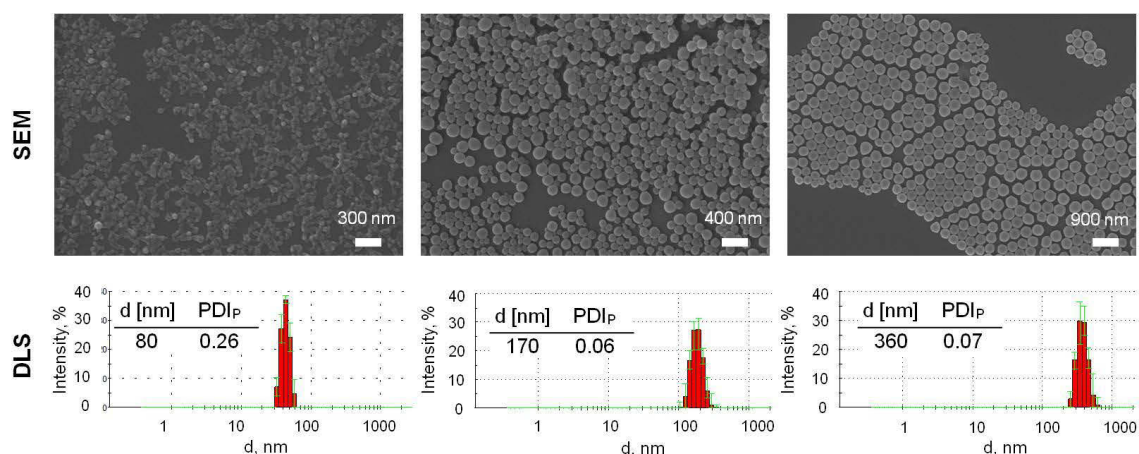


Figure 5.2. Representative SEM images and DLS intensity size distribution with corresponding Z average value and PDI_p of the small, medium and large particles of the p(MMA-*stat*-MA^{dye}) copolymer.

In first internalization studies with HeLa cells, a rapid uptake of medium sized particles was detected by flow cytometry investigations, whereas the large and small nanoparticles exhibited a slower internalization. In subsequent localization studies, mixtures of the various sized nanoparticles bearing different labels were applied simultaneously. Confocal

laser scanning microscopy measurements revealed the same cellular distribution of small and medium sized nanoparticles as both were detected in the late endosomes/lysosomes, whereas the large nanoparticles showed marginal co-localization with them. In additional experiments, different inhibitors for clathrin-dependent (chlorpromazine) and caveolin-dependent (filipin III) endocytosis as well as macropinocytosis (EIPA) were applied to confirm that small and medium nanoparticles with $d < 200$ nm were internalized *via* clathrin-dependent endocytosis, whereas larger nanoparticles with $d > 300$ nm were internalized *via* macropinocytosis.

In summary, highly fluorescent nanoparticles with different sizes were obtained *via* nanoprecipitation and PUC from various p(MMA-*stat*-MA^{dye}) copolymers that were labeled with a range of different fluorophores. It was evaluated that the nanoprecipitation technique is more suitable for the preparation of nanoparticles with defined surfaces, since the PUC samples might carry sugar moieties at the surface. Furthermore, it was proven that p(MMA-*stat*-MA^{dye}) copolymers represent excellent well-defined materials for the preparation of biocompatible nanoparticles: The size of the particles was easily tunable, the suspensions showed excellent stability without the usage of any surfactants and all particles were internalized into cellular compartments without any cytotoxic effects. Moreover, a size as well as a concentration dependent internalization of the particles was proven.

5.2 Active targeting

Although the adjustment of passive targeting parameters, e.g., the size and charge, is of vital importance, an active targeting of the nanoparticles *via* surface functionalization with ligands that bind selectively to specific cells represents the most promising concept for defined diagnostic and drug delivery applications.^[17] As mentioned in Chapter 2, sugar moieties are popular targeting units, which are broadly available and known to enhance the specific cellular uptake of nanoparticles.^[12,39] To explore the relationship between the sugar type attached to the particle and the resulting biorecognition and internalization, nanoparticles were prepared of fluorescence labeled poly(styrene-*block*-pentafluorostyrene)_{54:33} (PS-*b*-PTFS) copolymers that either contain β -D-thioglucose (PS-*b*-PTFSGlcOH) or β -D-thiogalactose (PS-*b*-PTFSGalOH) as different sugar moieties. The nanoparticles prepared were subsequently incubated with a human hepatocellular carcinoma cell line (HepG2 HCC) that expresses selective receptors for galactose. For the nanoparticle preparation, the glycopolymers PS-*b*-PTFSGlcOH and PS-*b*-PTFSGalOH were dissolved in a mixture of tetrahydrofuran (THF) and distilled water (1:1) with a concentration of $4 \text{ mg} \cdot \text{mL}^{-1}$ and water was added dropwise to cause nanoprecipitation of the polystyrene block.

After evaporation of the THF, both particle suspensions revealed final hydrodynamic diameters of 20 nm (Figure 5.3a), which was further confirmed by investigations *via* electron microscopy techniques, such as scanning electron microscopy (SEM) and cryo transmission electron microscopy (cryo-TEM) (Figure 5.3b). The similarity of the average

diameter and size distribution for both glycopolymers was essential in order to exclude an influence of the size on the cell internalization.^[64] DLS measurements furthermore confirmed a high stability of the glycosylated nanoparticles in suspension since storage at 5 °C in the dark for 12 months did not influence the size distribution. Moreover, no aggregation or sedimentation occurred. In subsequent biological studies, a carbohydrate specific biorecognition and cellular uptake of the galactose carrying nanoparticles into the HepG2 HCC cell line was detected. The nanoparticles internalized thereby in a concentration dependent manner with accumulation in the cytoplasm, most probably within lysosomal compartment, without any noticeable cytotoxic effect.

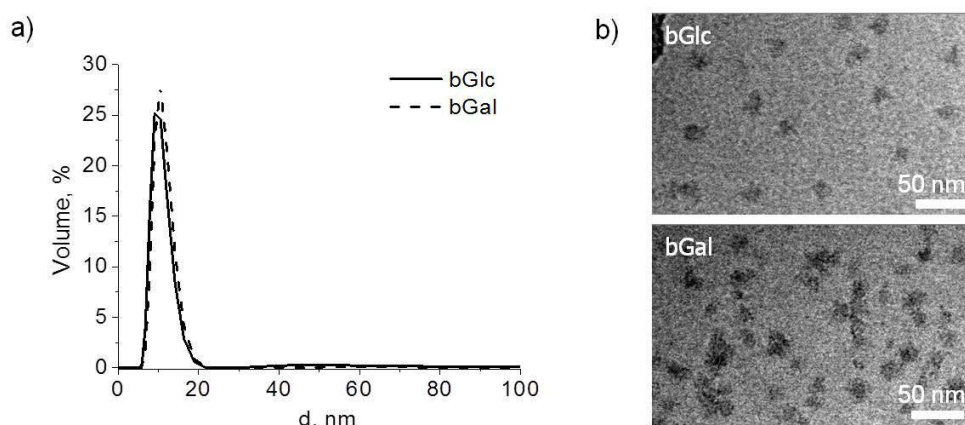


Figure 5.3. (a) Volume size distributions of the fluorescent glycosylated nanoparticles obtained by DLS and (b) cryo-TEM microscopy images of the glycosylated nanoparticles (bGlc = PS-*b*-PTFSGlcOH and bGal = PS-*b*-PTFSGalOH).

In conclusion, polymeric nanoparticles with specific targeted sugar moieties were prepared by nanoprecipitation from PS-*b*-PTFS that contain β -D-thioglucose or β -D-thiogalactose. The bioactivity of the carbohydrates remained after attachment to the polymer and led to a preferential internalization of galactosylated targeted nanoparticles by hepatocarcinoma cell line.

6. Nanoparticles for gene delivery

Parts of this chapter will be published: **P8)** S. Ochrimenko, A. Vollrath, K. Kempe, L. Tauhardt, S. Schubert, U. S. Schubert, D. Fischer, *Bioconjug. Chem.* **2013**, submitted. **P9)** A. Rinkenauer, A. Vollrath, A. Schallon, L. Tauhardt, K. Kempe, S. Schubert, D. Fischer, U. S. Schubert, *ACS Comb. Sci.* **2013**, submitted.

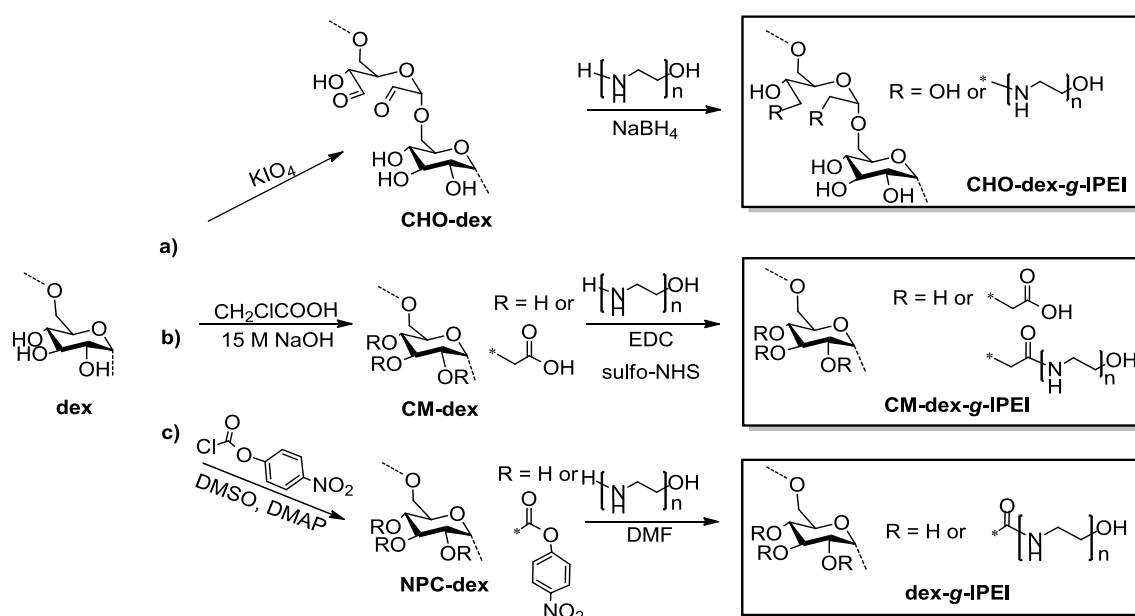
A new era in the field of pharmacotherapy began with the application of non-viral carrier vectors for gene delivery. Among cationic lipids or peptides which can be utilized as non-viral vectors, particularly cationic polymers like poly(ethylene imine) (PEI) and poly-(2-dimethylaminoethyl methacrylate) emerged as promising vector systems.^[69] Cationic polymers are able to compact the negatively charged nucleotides by counter charge complexation into nanoparticles. With implementation of such polymer based gene carriers, severe side effects accompanied with the usage of viruses, such as toxicity, immunogenic response or manufacturing limitations, can be avoided.^[70] However, for the evaluation and design of cationic polymers useful as transfection vectors two main aspects must be addressed: Optimal gene delivery with efficient protein expression as well as low cytotoxicity for safe administration. Unfortunately, it was investigated that many polycations (e.g., PEI) achieve high transfection rates only with rising positive charge which, in turn, effectuates high cytotoxicity. On the other hand, alternative polymer systems with lower charge density (e.g., chitosan) revealed indeed lower acute toxicity, but adversely also decreased transfection efficiency.^[69,71,72] Hence, continuative effort to understand the chemical nature and biological function of polymeric vectors is of vital importance, since researchers are still on the prospect of safe gene delivery agents with useful transfection levels.

6.1 Dextran-graft-linear poly(ethylene imine) synthesis

In the last decades, dextrans functionalized with cationic moieties were evaluated as promising gene delivery systems in various studies. Dextran is a natural, hydrophilic, biodegradable polysaccharide based of mainly α -1-6-linked D-glucose units and represents a well suitable material for the development of non-viral vectors. It offers the possibility of various chemical modifications with cationic moieties and captivates with a well-defined structure, excellent water-solubility, and perfect biocompatibility. Several attempts have been made to selectively modify dextran with cationic molecules such as PEI, diethylaminoethyl, spermine, protamine, or poly(L-lysine).^[73-77] Although different strategies for conjugation were followed and several linking strategies have been reported to covalently bind PEI to dextrans, the influence of the different linker strategies on biocompatibility, transgene expression, and DNA binding characteristics have received only little attention.^[73,78-82]

Thus, in order to directly study the influence of the different linker strategies, dextran with a molar mass of $60,000 \text{ g} \cdot \text{mol}^{-1}$ was functionalized with low molar mass linear PEI (lPEI) *via* altered synthesis routes. In detail, three synthesis strategies were applied to

synthesize a range of dextran-*graft*-linear poly(ethylene imine)s (dex-*g*-IPEI): (1) Reductive amination of aldehyde functionalized dextran (CHO-dex), (2) 1-ethyl-3-(3-dimethylamino-propyl) carbodiimide (EDC) coupling of carboxymethylated dextran (CM-dex) and (3) carbamate formation *via* reaction of 4-nitrophenyl carbonate-substituted dextran (NPC-dex) (Scheme 6.1).^[31,80,83]



Scheme 6.1. Schematic representation of the functionalization of dextran by (a) oxidation, (b) carboxymethylation and (c) 4-nitrophenyl carbonate-activation with subsequent reaction with IPEIs *via* (a) reductive amination, (b) EDC coupling and (c) carbamate formation.

To study further the impact of the degree of substitution (DS) of the dextran with IPEI as well as the IPEI chain length, two IPEIs consisting of $n = 20$ and 40 monomer units (IPEI₂₀ and IPEI₄₀) were allowed to react in various ratios with the different dextran precursors. For the grafting of IPEI to the dextran *via* reductive amination, aldehyde enriched dextrans were prepared by oxidation of dextran from *Leuconostoc mesenteroides* with different amounts of potassium periodate (KIO_4). Subsequently, the aldehyde containing precursors were each converted with the IPEI₂₀ and IPEI₄₀, whereas the DS of conjugated IPEIs per AGU was aimed to be at maximum 0.5. After subsequent reduction with sodium borohydride (NaBH_4) and purification by dialysis, the successful binding of the IPEI to the CHO-dex was confirmed by ^1H NMR spectroscopy measurements. The resulting DS of IPEI was calculated from the nitrogen content observed in the elemental analysis and determined to be between 0.13 to 0.38 per AGU (**A series, A1-A4**, Table 6.1).

For the EDC coupling strategy, dextran was first derivatized to CM-dex to introduce carboxylic moieties into the polymer. The carboxymethylation was performed under basic conditions using altered ratios of monochloroacetic acid (CH_2ClCOOH) and altered reaction times.^[84] The final degree of functionalization was determined according to the HPLC procedure described by Heinze *et al.* (Table 6.1).^[85] The subsequent grafting of IPEI₂₀ and IPEI₄₀ to the carboxymethylated carbohydrates was performed with usage of *N*-hydroxysulfosuccinimide (sulfo-NHS) and EDC owing to their well-known coupling

efficiency.^[73] The successful binding of the IPEIs to the CM-dextrans was confirmed by ¹H NMR spectroscopy measurements of the purified products (**B series, B1-B6**, Table 6.1). The coupling efficiency of IPEI per AGU was again calculated from the nitrogen content measured in the elemental analysis and found to be in the range of 0.06 to 0.18 (Table 6.1). In contrast to the previously described synthesis routes, the carbamate formation *via* reaction of 4-nitrophenyl carbonate-substituted dextran with the IPEIs was not qualified for the preparation of dex-*g*-IPEIs, due to the fact that adverse crosslinking occurred and led to insoluble products.

Table 6.1. Overview about the DS and nitrogen content of the synthesized dex-*g*-IPEI samples.

Samples	dex- <i>g</i> -IPEIs	CHO/COOH:NH ₂ -IPEI [mol]	N ^a [%]	DS ^b [IPEI/AGU]
A	Reductive amination			
A1	CHO _{0.5} -dex- <i>g</i> -IPEI ₂₀	1:0.5	15.78	0.18
A2	CHO _{0.5} -dex- <i>g</i> -IPEI ₄₀	1:0.5	19.12	0.13
A3	CHO _{1.0} -dex- <i>g</i> -IPEI ₂₀	1:0.5	21.45	0.38
A4	CHO _{1.0} -dex- <i>g</i> -IPEI ₄₀	1:0.5	21.73	0.19
B	EDC coupling			
B1	CM _{0.3} -dex- <i>g</i> -IPEI ₂₀	1:1.2	6.73	0.06
B2	CM _{0.3} -dex- <i>g</i> -IPEI ₄₀	1:1.2	12.80	0.07
B3	CM _{0.5} -dex- <i>g</i> -IPEI ₂₀	1:1.2	7.96	0.07
B4	CM _{0.5} -dex- <i>g</i> -IPEI ₄₀	1:1.2	14.83	0.1
B5	CM _{1.6} -dex- <i>g</i> -IPEI ₂₀	3:1	8.16	0.11
B6	CM _{1.6} -dex- <i>g</i> -IPEI ₄₀	3:1	18.38	0.18

^a Determined by elemental analysis measurements; ^b calculated from nitrogen content.

To evaluate the potential of the prepared dex-*g*-IPEI polymers to be useful as vectors for gene delivery applications, crucial characteristics such as the interaction with DNA, the complex formation, and the cell- and hemocompatibility as well as transgene expression were examined. Briefly, it could be shown that all cationic dextrans spontaneously formed interpolyelectrolyte complexes with the DNA as a result of cooperative electrostatic interactions depending on the N/P ratio. The efficiency to complex and stabilize the DNA was thereby increasing for both linker strategies with increasing N/P ratio, higher molar masses and DS of IPEI. In comparison to the CHO-dex-*g*-IPEIs synthesized by reductive amination, a weaker DNA complexation and stabilization ability was detected for the CM-dex-*g*-IPEIs. This may be attributed to the lower content of IPEI within the samples prepared by EDC coupling and to the presence of anionic charges, which presumably interfere with the positively charged amines of the IPEI polymer and lead to decreased DNA interactions. dynamic light scattering (DLS) measurements of the dex-*g*-IPEI/DNA nanoparticles revealed sizes in water in the range of 70 to 113 nm with monomodal size distributions (polydispersity indices (PDI) 0.13 to 0.31), which were comparable to the sizes obtained for the DNA complexes with IPEI₂₀ and IPEI₄₀. Moreover, all complexes were positively charged

with zeta potentials between +15 and +35 mV due to the excess of the cationic component with comparable results for N/P ratios 25 and 50. In comparison to the IPEI/DNA nanoparticles, the zeta potential values decreased indicating a shielding effect of the neutral dextran polymer. The shielding effect of the dextran was further supported by the observation that the zeta potential was rising with increasing DS and molar mass of IPEI grafted onto dextran.

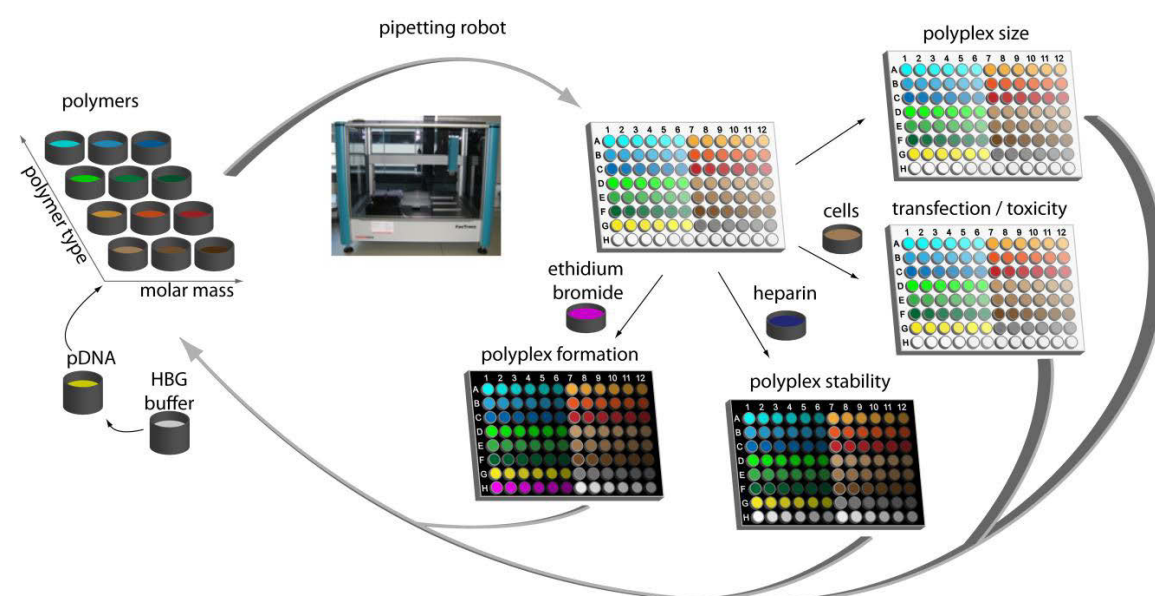
While the physicochemical properties were affected only marginally by the linker strategy, a remarkable difference between the **A** and **B series** was detected in the transfection efficiency as well as the cell- and hemocompatibility studies. The transfection efficiency obtained for the samples prepared by reductive amination (**A1-A4**) was higher than for the corresponding free IPEIs, but lower than for the cationized dextrans prepared by EDC coupling (**B1-B4**), which demonstrated the highest activity. The lower efficiency of the dextrans of the **A series** may be attributed to the higher DNA complexation efficiency of the polymer and, therefore, lower ability to release DNA from the complexes compared to the polymers of the **B series**. However, for the CHO-dex-*g*-IPEI polymers the transgene expression increased with higher molar mass of the IPEIs and N/P ratio, which was in agreement with literature.^[81] Contrary, the CM-dex-*g*-IPEI₄₀ conjugates revealed an approximately 1/3 lower transfection for **B4** at the N/P ratio 25 and **B2** at the N/P ratio 50 compared to their IPEI₂₀ counterparts. This could be due to higher interactions between the longer IPEI chain and COOH groups of the CM-dex than with the DNA. In conclusion, the best gene delivery properties at both N/P ratios in this study were provided by **B3**.

Moreover, all dex-*g*-IPEIs/DNA complexes were examined concerning their cytotoxicity and were found to be highly compatible under the transfection conditions applied.^[86] The compatibility was thereby independent of the linker technique, the DS, and the selected N/P ratios. In addition, no hemolytic potential of the dex-*g*-IPEIs was observed under the chosen conditions.^[87] Both polymer series induced higher red blood cell aggregation compared to free IPEIs, whereby the interactions with negatively charged cell membranes of the red blood cells were found to increase with the molar mass of IPEI. In general, the conjugates synthesized by reductive amination demonstrated a higher red blood cell aggregation potential compared to the modified dextrans prepared by EDC. The better compatibility of the **B series** polymers compared to the **A series** may be ascribed to the polyelectrolyte nature of the CM-dex-*g*-IPEIs, since polymers that contain both positive and negative charges revealed prolonged half life time in blood circulation experiments.^[88]

In conclusion, a library of several dex-*g*-IPEIs with varied linker units, different DS of IPEI as well as a range of cationic polymer chain length was synthesized. It was investigated that the variation of the linking strategy of cationic polymers to dextran affects particularly the biological properties. Although the reductive amination method achieved higher DS values of IPEI compared to the EDC coupling reaction, the latter synthesis route was more suitable as linking strategy since the conjugates showed improved hemocompatibility and enhanced transfection efficiencies.

6.2 High-throughput preparation and screening of nanoparticles for DNA delivery

Highly efficient cationic polymers suitable for gene delivery should provide (1) excellent binding and protection of genetic material during delivery, (2) enhanced cellular uptake, (3) superior biocompatibility and (4) high transfection efficiency. However, general synthesis rules for the construction of such efficient polymers are missing as a result of too diverse methods and polymer classes applied in the published studies. With the aim to realize a straightforward but comprehensive characterization of gene vectors that supports to understand how the polymers should be designed specifically to their task, an automatical combinatorial high-throughput (HT) workflow was developed that starts with the automated polyplex preparation *via* pipetting robots and continues with a parallel and HT-analysis of the size, binding affinity, stability, transfection efficiency, and toxicity (Scheme 6.2). Therefore, lPEI and branched PEI (bPEI) with a degree of polymerization (DP) of 20, 200 and 600 ($M_w = 860, 8,600$ and $25,800 \text{ g} \cdot \text{mol}^{-1}$, respectively) were chosen as model transfection agents to be complexed with plasmid DNA. For an automated preparation of complexes, liquid handling robots were used in a similar manner to the previously described HT-nanoprecipitation approach of synthetic polymers in Chapter 2. The benefit of such pipetting systems is the ability to systematically alter different parameters individually, such as polymer concentration, pH value, or buffer system. The HT-complex preparation was realized by automatic deposition of a buffered DNA solution to wells that contain various buffered cationic polymer solutions with the desired concentrations. Although this approach differs from conventional polymer/DNA complex preparation methods, where the polymer is pipetted to DNA solution with subsequent vortexing,^[89] previous experiments reveal similar results.



Scheme 6.2: HT-workflow for structure-property evaluation of cationic polymers/DNA nanocomplexes concerning molar ratio, size, binding, stability, release, transfection efficiency as well as cytotoxicity.

In order to investigate the dependency of the nanoparticle properties on different polymers and preparation conditions, several N/P ratios (2.5, 5, 10 and 20) were applied next to various PEIs. To this end, a dilution series ranging of previously produced polymer stock solutions was provided by using the pipetting robot. Afterwards, a DNA solution was added to each polymer solution, and the resulting suspensions were directly mixed by repetitive suction and release. After the nanoparticle formation, the nanosuspensions were distributed automatically into different well plates for subsequent parallel characterization studies (Scheme 6.2).

Since the complex size allows a first conclusion regarding the polymer capability to be used as transfection agent, DLS was applied as first analysis technique to determine the dependency of aggregation of the PEI/DNA assemblies on the conditions used for the complex formation.^[62] In order to realize the analysis of the complex size in an automatic HT-manner, a DLS plater reader was used. As displayed in Figure 6.1, all PEI/DNA nanoassemblies revealed diameters less than 600 nm. The smallest diameter of 140 nm was obtained for the bPEI₂₀₀. In comparison to previously performed manual size measurements, where complex sizes in a range of 80 to 200 nm were obtained, larger diameters with increased standard deviations were detected by the HT-DLS device. This could be explained by the different devices and settings for the DLS measurements. Although the HT-DLS results should be always considered with care, by application of the HT-DLS device information about the tendency of the polyplexes to aggregate can be obtained and conclusions about the polyplex stability in comparison to standard polymer controls are possible. According to these data, three tendencies were found: (i) With increasing N/P ratio, smaller complexes were formed; (ii) the bPEI revealed a stronger size dependency with higher molar masses in comparison to the IPEI, and (iii) the bPEI condensed the DNA into smaller particles compared to the IPEI (as also reported in literature).^[90] An influence of the degree of polymerization or the molar mass could not be observed under the chosen conditions.

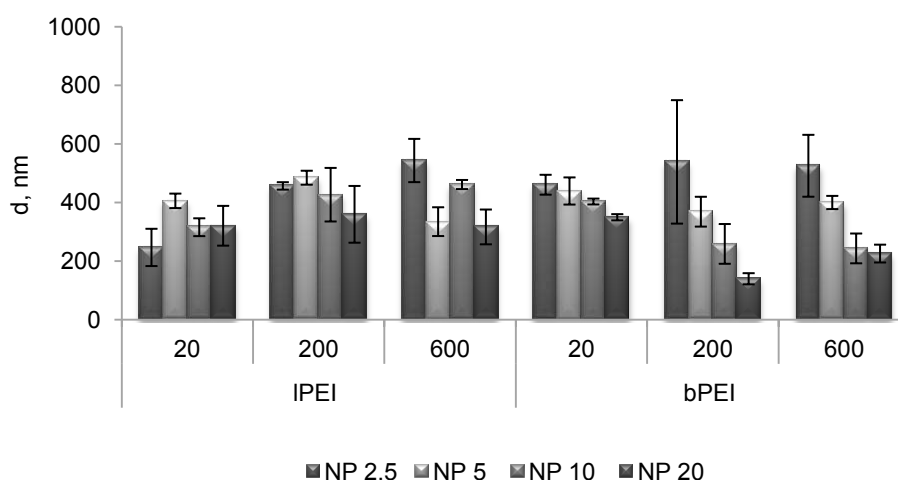


Figure 6.1 Hydrodynamic diameters of PEI/DNA complexes prepared by the pipetting robot. Values represent the mean, $n \geq 3$.

Afterwards, the DNA binding affinity of the polymers as well as the DNA release were evaluated *via* ethidium bromide and heparin assays, respectively. A proportional increase of the binding affinity was observed with increasing molar mass of the polymer. Furthermore, a higher binding affinity of branched structures (bPEI) was detected in comparison to linear architectures.^[90,91] In the case of lPEI₂₀, it can further be seen that the DNA binding affinity correlates with the N/P ratio until a plateau is reached (here at N/P 10). Simultaneous with the increased binding affinity, a decreased DNA release dependent on the N/P ratio, the architecture, and the molar masses of the various polymers was observed. These trends were also reported in literature and confirm that a rapid relationship analysis of polymer structure and conditions with respect to the DNA binding and release can be performed in an automated way within two hours by this HT-assay.^[92,93]

To allow conclusions about the transfection efficiency of the polymeric vectors, the expression of reporter genes was visualized by fluorescence using an EGFP reporter encoded plasmid (pEGFP-N1). Usually, this expression system is analyzed by flow cytometry analysis. But as this technique is not suitable for the HT-screening approach presented here, the transfection efficiency was studied using a microscope and a fluorescence plate reader. The following order of high to low transfection efficiency was obtained: lPEI₆₀₀ > bPEI₂₀₀ > lPEI₂₀₀ > bPEI₆₀₀ > bPEI₂₀ > lPEI₂₀. Since the results observed from the screening of the EGFP expression were comparable with non HT-transfection procedures, which use vortexed polymer/DNA complexes and flow cytometry, this observation confirms the potential of such a HT-screening of the transfection efficiencies of polymers.

Furthermore, the cytotoxicity of the nanosuspensions was studied in human embryonic kidney (HEK) cells in 96-well plates after 24 h incubation with the nanoparticles. The viability of the cells was explored after staining with Hoechst 33324 and detection of the fluorescence utilizing again the fluorescence plate reader device. After the HT-screening of the nanoparticles prepared from various PEIs with different molar masses and architectures, it was confirmed that lPEI₂₀ and bPEI₂₀ are non-cytotoxic at the investigated concentrations. However, with rising molar mass, the cytotoxic effect was increasing. The polymeric architecture itself showed no influence on the cell viability, but certainly on the DNA binding capability, since bPEI₂₀ revealed stronger DNA binding than lPEI₂₀. Although having relatively high binding affinities, the best transfection results were obtained for lPEI₆₀₀ and the bPEI₂₀₀.

In conclusion, the obtained results indicated in agreement with literature that PEIs with branched architectures and small molar masses have the highest potential to be used as gene vectors, as they offer the advantage of low cytotoxicity combined with high DNA binding affinity. It could be proven that the developed HT-workflow is applicable for different polymer systems as well as conditions enabling a fast and efficient analysis of polymer vectors in an automated way with respect to important polymer characteristics, such as molar mass, architecture, and N/P ratio used for the DNA binding and release. Then it is possible to identify and evaluate reams of polymers with regard to their capability to realize an efficient complexation, protection, and transfection of DNA.

7. Summary

In recent years, polymeric nanoparticles had their breakthrough within the area of nanotechnology and represent nowadays a new class of therapeutics with impressive potential. The straightforward encapsulation of multiple drug and dye molecules with high loading capacities as well as the possible introduction of additional functionalities for targeted delivery and controlled cargo release, are only a selection of the exquisite properties provided by polymeric nanoparticles. In particular, by combining the drug delivery with diagnostic application, multifunctional “theragnostic” agents for an improved medical treatment can be obtained. Although a couple of challenges associated with the development of polymeric nanoparticles for drug delivery and diagnostic are still unsolved, e.g., the reliable evaluation of their interaction with the environment and attended long-time consequences as well as their controlled and reproducible production, it is incontrovertible that nanomedicine is on the right path. Continuous effort on polymeric nanoparticles will thus represent an important scientific field in the future.

The presented thesis addresses the systematic formulation of polymeric nanoparticles, their physicochemical characterization, and the study of their resultant interaction with cells (Figure 7.1). Biocompatible polymers, such as poly(methyl methacrylate) (PMMA), poly(saccharides) and poly(lactic acid) derivatives were investigated with regard to their nanoparticle formation using the nanoprecipitation approach. This method is cost and time-efficient and provides the key benefit that no surfactants are required leading to more defined nanoparticles. The nanoprecipitation of the polymers was manually performed, but also in a high-throughput (HT) manner by the application of pipetting robots. In combination with the subsequent dynamic light scattering (DLS) plate reader analysis, the HT approach enabled an efficient screening of various polymer systems with regard to their precipitation behavior and crucial influencing parameters, such as concentration of the initial polymer solution or the solvent/non-solvent ratio in a 96-well plate format. It was investigated that almost all applied polymer systems were able to be formulated into nanoscale particles under distinct nanoprecipitation conditions. A vital contribution to the final size and size distribution revealed thereby the polymer characteristic itself (molar mass, hydrophobicity) as well as the route of adding the non-solvent (addition of the polymer solution to the non-solvent or *vice versa*).

After evaluation of important formulation parameters, well-defined nanoparticles were prepared from selected copolymers for cellular internalization studies. First, the fluorescent copolymer (p(MMA-*stat*-MA^y)_{0.97:0.03}), which already contained a thiazole chromophore in the backbone, was selected. Furthermore, a p(MMA-*stat*-MAA)_{0.91:0.09} copolymer was chosen to be post-functionalized with various fluorescent dyes yielding three polymers (p(MMA-*stat*-MA^{green}), p(MMA-*stat*-MA^{orange}), and p(MMA-*stat*-MA^{red})) with comparable properties, but different fluorescence. Nanoparticles with various sizes and altered fluorescent properties were also achieved by using diverse nanoprecipitation conditions for the differently labeled PMMA copolymers. After comprehensive characterization of the obtained

nanoparticles *via* orthogonal analysis techniques, e.g., DLS, scanning electron microscopy (SEM) and analytical ultracentrifugation (AUC), and ensurance of the nanosuspensions stability under various conditions (cell culture media, autoclavation, freeze drying, etc.), cellular uptake studies revealed an internalization of all particles examined into intracellular compartments without causing any adverse effects (cytotoxicity). This finding represents a crucial requirement for the utilization of the particles *in vitro* and *in vivo*. In subsequent studies by application of confocal microscopy, a concentration- as well as size dependent internalization of particles was proven. Furthermore, nanoparticles with specific targeted sugar moieties were prepared by nanoprecipitation from PS-*b*-PTFS copolymers that contain β -D-thioglucose or β -D-thiogalactose. The sugar-targeted nanoparticles were subsequently studied with regard to their cellular uptake by a hepatocarcinoma cell line. A preferential internalization of galactosylated targeted nanoparticles was detected proving the capability to actively targeted nanocarriers to reach a specific uptake.

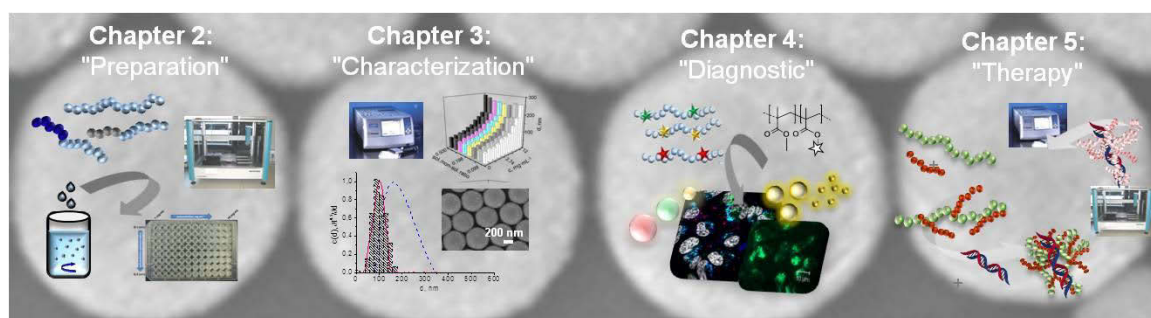


Figure 7.1 Overview of the thesis strategies: From preparation and characterization of polymeric nanoparticles to their application in diagnostic and therapy.

In addition to the formulation and characterization of polymeric nanoparticles for diagnostic purposes, the focus was also set on the investigation of the nanocarriers suitable for efficient gene delivery. In order to gain deeper insights into the structure-property relationships of polycations and their resulting nanoparticle formation, dextran, which is a water soluble, α -(1 \rightarrow 6) glycosidically linked polysaccharide that is characterized by superior biocompatibility and good availability, was functionalized with different linear poly(ethylene imine)s (IPEI) introducing the cationic charge into the dextran structure. The different cationic polymers were studied in terms of their nanoscale complexation with nucleic acids and their biophysicochemical properties. To evaluate the impact of the coupling strategies between dextran and the cationic polymers next to the influence of the molar mass and the degree of substitution of IPEI, different derivatives were synthesized *via* altered synthesis routes. The amidation reaction of carboxymethylated dextran and the reductive amination of previously oxidized dextrans are hereby noteworthy, since they enabled an efficient synthesis of several cationic dextrans with variable degree of substitution of IPEI. In subsequent studies, the capability of the synthesized polymer vectors to bind DNA into stable complexes in the nanoscale was proven. Moreover, the transfection efficiencies as well as the resulting toxicities were determined. Although the reductive amination method resulted in a higher degree of grafting of IPEI, the amidation reaction was

more suitable as linking strategy owing to the improved hemocompatibilities and enhanced transfection efficiencies of the obtained dextran-*graft*-IPEI conjugates.

In addition, a facile combinatorial HT-workflow that enables a straightforward but comprehensive characterization of cationic polymers as gene vectors was developed. As model polymers, well-known PEI derivatives were used. The complex formation between the cationic polymer and the plasmid DNA was realized *via* pipetting robots in an automated way. By subsequent parallel HT-analysis using a DLS platereader as well as biological assays, the size, the binding affinity, the complex stability as well as transfection and toxicity of the prepared nanoparticles were rapidly and efficiently explored.

In summary, within this thesis, well-defined nanoparticles based on a range of biocompatible polymers were synthesized and studied with regard to their resulting characteristics as well as interactions with biological systems. The presented results will contribute to the development and understanding of polymeric nanoparticle formulations and will support their future applications in the medical field.

8. Zusammenfassung

In den vergangenen Jahren erlebten polymerbasierte Nanopartikel im Bereich der Nanotechnology ihren wissenschaftlichen Aufschwung und stellen heutzutage eine neue Klasse von Therapeutika mit eindruckvollem Potenzial dar. Die unkomplizierte Einkapselung von Wirkstoff- und Farbstoffmolekülen mit hohen Ladungskapazitäten, sowie die Möglichkeit der Einführung von zusätzlichen Funktionalitäten für eine zielgerichtete Wirkstoffabgabe, sind nur eine Auswahl der herausragenden Eigenschaften, die diese Systeme aufweisen. Besonders die Kombination von kontrollierter Wirkstoffabgabe und Diagnostik führte zur Entwicklung von ersten multifunktionalen „Theragnostik“-Partikeln und ermöglichte eine verbesserte medizinische Behandlung. Obwohl einige Herausforderungen, die mit der Entwicklung von geeigneten polymeren Nanopartikeln zur Anwendung in Therapie und Diagnostik einhergehen, noch ungelöst sind (wie zum Beispiel die sichere Einschätzung der Interaktionen der Nanopartikel mit ihrer Umgebung und der damit verbundene Langzeitfolgen sowie ihre kontrollierte und reproduzierbare Herstellung), ist es unbestreitbar, dass die Nanomedizin sich auf dem richtigen Weg befindet. Weiterführende Bemühungen in Bezug auf polymerbasierte Nanopartikel stellen daher für die Zukunft ein entscheidendes Forschungsfeld dar.

Die vorliegende Schrift befasst sich mit der gezielten Formulierung polymerer Nanopartikel durch Nanofällung, deren biophysikochemischen Charakterisierung und der Untersuchung ihrer Wechselwirkung mit Zellen (Abbildung 8.1). Biokompatible Polymere, wie zum Beispiel Polysaccharidderivate, Polymilchsäurederivate oder Poly(methyl methacrylat) (PMMA)-Copolymere wurden hinsichtlich ihrer Nanopartikelbildung mittels Nanofällung untersucht. Diese Fällungsmethode ist kostengünstig, zeiteffizient und bietet den entscheidenden Vorteil, dass keine oberflächenaktiven Substanzen notwendig sind. Dies führt zu definierten Nanopartikeloberflächen und ist von zentraler Bedeutung für biologische Studien. Die Nanofällung wurde sowohl manuell als auch im Hochdurchsatzverfahren mit Hilfe von Pipettierrobotern realisiert. In Kombination mit der automatisierten dynamischen Lichtstreuunganalyse konnten verschiedene Polymersysteme sehr effizient hinsichtlich ihrer Fällungseigenschaften und entscheidende beeinflussenden Parameter, wie zum Beispiel die Konzentration der anfänglichen Polymerlösung oder die Fällbedingungen im 96-Plattenformat, untersucht werden. Dabei wurde festgestellt, dass nahezu alle verwendeten Polymere unter bestimmten Fällbedingungen zu nanoskaligen Partikeln formuliert werden können. Entscheidend zur resultierenden Größe und Größenverteilung der Partikel tragen dabei die Eigenschaften der Polymere (molare Masse, Hydrophobizität) sowie die Art der Zugabe des Nichtlösungsmittels bei (Zugabe der Polymerlösung zu dem Nichtlösungsmittel oder *vice versa*).

Nach Evaluierung der wichtigsten Formulierungsparameter wurden wohldefinierte Nanopartikel zur Untersuchung von Zellaufnahmemechanismen von ausgewählten Copolymeren hergestellt. Zunächst wurde das fluoreszierende Copolymer P(MMA-*stat*-MA)_{0.97:0.03}, welches bereits ein Thiazolchromophor im Polymerrückgrat

auswies, verwendet. Weiterhin wurde ein $P(\text{MMA-}stat\text{-MAA})_{0.91:0.09}$ Copolymer mit unterschiedlichen Fluoreszenzfarbstoffen funktionalisiert und so drei verschiedene Polymere ($P(\text{MMA-}stat\text{-MA}^{green})$, $P(\text{MMA-}stat\text{-MA}^{orange})$, and $P(\text{MMA-}stat\text{-MA}^{red})$) mit ähnlichen Eigenschaften, aber unterschiedlicher Fluoreszenz erhalten. Im Folgenden konnten Nanopartikel verschiedener Größe mit divergenter Fluoreszenz durch den Einsatz von unterschiedlichen Fluoreszenzfarbstoff-markierten PMMA Copolymeren und Anwendung verschiedenartiger Fällbedingungen erhalten werden. Nach umfassender Charakterisierung der erhaltenen Nanopartikel mit Hilfe orthogonaler Techniken, wie zum Beispiel der dynamischer Lichtstreuung, Rasterelektronenmikroskopie und der analytischen Ultrazentrifugation, sowie der Gewährleistung der Stabilität der Nanosuspensionen unter verschiedenen Bedingungen (Zellkulturmedium, Autoklavierung, Lyophilization, etc.), konnte in Zellexperimenten eine Aufnahme aller Partikel in intrazelluläre Kompartimente ohne toxische Nebenwirkungen (Zytotoxizität) nachgewiesen werden. Dies stellt eine notwendige Voraussetzung für den Einsatz der Partikel *in vitro* und *in vivo* dar. Mit Hilfe der konfokalen Fluoreszenzmikroskopie wurde in weiteren Studien neben einer konzentrationsabhängigen Aufnahme auch eine größenabhängige Partikelinternalisierung nachgewiesen. Desweiteren wurden Nanopartikel mit spezifischen Zuckermolekülen durch Nanofällung eines β -D-Thioglucose- oder β -D-Thiogalaktose-funktionalisierten Polystyrol-Copolymers hergestellt. Die mit Zucker funktionalisierten Nanopartikel wurden anschließend in Bezug auf ihre Aufnahme in Leberkrebszelllinien untersucht. Eine bevorzugte Aufnahme der Galaktose-funktionalisierten Nanopartikel bestätigte die Möglichkeit, Nanopartikel aktiv zu steuern und eine spezifische Zellaufnahme zu erhalten.

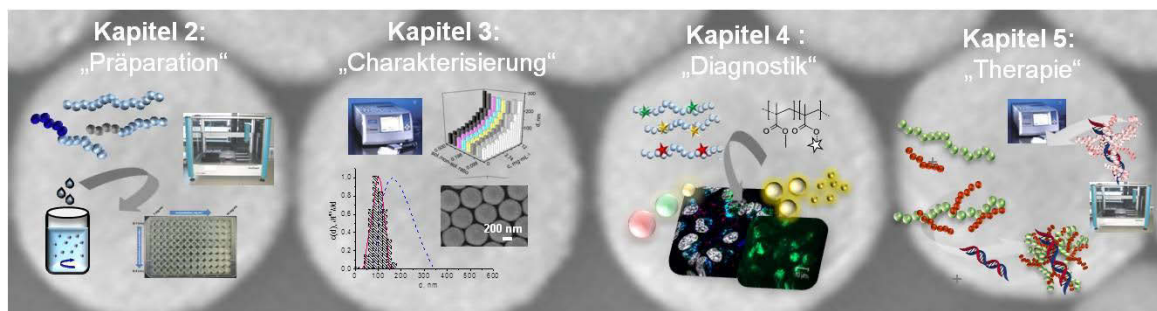


Figure 8.1 Übersicht über zentralen Themen der Dissertation: Von der Herstellung und Charakterisierung polymerer Nanopartikel zu deren Anwendung in Diagnostik und Therapie.

Im Fokus der Arbeit stand neben der Herstellung und Charakterisierung von polymeren Nanoobjekten für die Diagnostik auch die Untersuchung von Nanopartikeln zum therapeutischen Einsatz. Zu diesem Zweck wurden verschiedene kationische Polymere hergestellt und ihre nanoskalige Komplexbildung mit Nukleinsäuren erforscht. Zur genauen Analyse von Struktur-Eigenschaftsbeziehungen von Polykationen und ihrer Nanopartikelbildung wurde Dextran, ein wasserlösliches, α -(1→6) glycosidisch verknüpftes Polysaccharid, welches sich durch eine hohe Biokompatibilität und gute Verfügbarkeit

auszeichnet, gezielt mit verschiedenen linearen Polyethylenimininen (IPEI) funktionalisiert, um kationische Ladungen in die Dextran-Struktur einzuführen.

Um den Einfluss der molaren Masse und des Substitutionsgrades der IPEIs, aber auch die Bedeutung der verschiedenen Kopplungsstrategien zwischen Dextran und PEI zu studieren, wurde eine Reihe von Derivaten auf unterschiedlichen Syntheserouten hergestellt. Die Amidierung mit carboxymethyliertem Dextran sowie die reduktive Aminierung von zusätzlich oxidierten Dextranen sind hierbei hervorzuheben, da sie am effizientesten zur Herstellung verschiedener kationischer Dextranderivate mit variablen Substitutionsgraden führten. In anschließenden physikochemischen und biologischen Studien konnte gezeigt werden, dass die synthetisierten Polykationen mit Plasmid-DNS stabile Komplexe im Nanometerbereich bilden. Darüber hinaus wurden die Transfektionseffizienzen und Toxizitäten der jeweiligen Nanokomplexe bestimmt und die erfolgreichsten kationischen Polymere ermittelt. Obwohl mit der reduktiven Aminierung höhere Substitutionsgrade von IPEI an Dextran erhalten wurden, ist die Amidierungsreaktion die favorisierte Kopplungsstrategie, da die resultierenden Dextran-*graft*-IPEI Konjugate eine verbesserte Blutverträglichkeit als auch gesteigerte Transfektionseffizienzen aufwiesen.

Zur schnellen und umfassenden Analyse von kationischen Polymeren als Genvektoren wurde weiterhin ein automatisierter Arbeitsablauf entwickelt. Als Model polymere wurden dazu bekannte PEI-Derivate verwendet. Die automatisierte Formulierung der Nanopartikel zwischen dem kationischen Polymer und der Plasmid-DNS wurde mit Hilfe eines Pipettierroboters realisiert. Anschließende parallele Hochdurchsatzanalysen unter Zuhilfenahme von DLS Plattenlesern und biologischen Testverfahren ermöglichten eine zügige und effiziente Untersuchung der Komplexgröße, der Bindungsaffinität, der Komplexstabilität, sowie der Transfektionseffizienzen und der Toxizitäten.

Zusammenfassend konnten im Rahmen dieser Arbeit eine Vielzahl an maßgeschneiderten Nanopartikeln auf Basis verschiedener biokompatibler Polymere hergestellt und ihre Eigenschaften und Interaktion mit biologischen Systemen evaluiert werden. Die beschriebenen Ergebnisse werden zum tieferen Verständnis und zur Weiterentwicklung von polymeren Nanopartikeln beitragen und so deren zukünftigen Einsatz in medizinischen Anwendungsbereichen unterstützen.

9. References

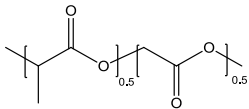
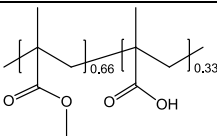
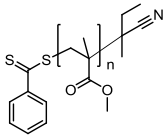
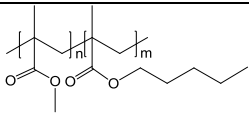
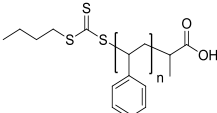
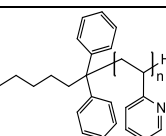
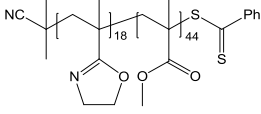
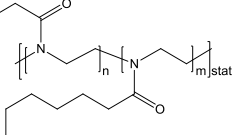
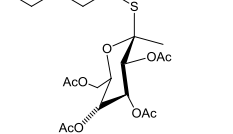
- [1] R. Duncan, R. Gaspar, *Mol. Pharm.* **2011**, *8*, 2101-2141.
- [2] M. Chakraborty, S. Jain, V. Rani, *Appl. Biochem. Biotechnol.* **2011**, *165*, 1178-1187.
- [3] N. Kamaly, Z. Xiao, P. M. Valencia, A. F. Radovic-Moreno, O. C. Farokhzad, *Chem. Soc. Rev.* **2012**, *41*, 2971-3010.
- [4] N. Sanvicens, M. P. Marco, *Trends Biotechnol.* **2008**, *26*, 425-433.
- [5] M. Nahar, T. Dutta, S. Murugesan, A. Asthana, D. Mishra, V. Rajkumar, M. Tare, S. Saraf, N. K. Jain, *Crit. Rev. Ther. Drug Carrier Syst.* **2006**, *23*, 259-318.
- [6] F. Danhier, E. Ansorena, J. M. Silva, R. Coco, A. Le Breton, V. Preat, *J. Control. Release* **2012**, *161*, 505-522.
- [7] T. K. Dash, V. B. Konkimalla, *J. Control. Release* **2012**, *158*, 15-33.
- [8] Z. Liu, Y. Jiao, Y. Wang, C. Zhou, Z. Zhang, *Adv. Drug Deliv. Rev.* **2008**, *60*, 1650-1662.
- [9] J. H. Park, G. Saravanakumar, K. Kim, I. C. Kwon, *Adv. Drug Deliv. Rev.* **2010**, *62*, 28-41.
- [10] C. Vauthier, K. Bouchemal, *Pharm. Res.* **2009**, *26*, 1025-1058.
- [11] J. P. Rao, K. E. Geckeler, *Prog. Polym. Sci.* **2011**, *36*, 887-913.
- [12] M. K. Yu, J. Park, S. Jon, *Theranostics* **2012**, *2*, 3-44.
- [13] J. Wang, J. D. Byrne, M. E. Napier, J. M. DeSimone, *Small* **2011**, *7*, 1919-1931.
- [14] T.-G. Iversen, T. Skotland, K. Sandvig, *Nano Today* **2011**, *6*, 176-185.
- [15] N. Desai, *AAPS Journal* **2012**, *14*, 282-295.
- [16] A. Musyanovych, J. Dausend, M. Dass, P. Walther, V. Mailaender, K. Landfester, *Acta Biomater.* **2011**, *7*, 4160-4168.
- [17] A. Albanese, P. S. Tang, W. C. W. Chan, *Annu. Rev. Biomed. Eng.* **2012**, *14*, 1-16.
- [18] M. Gaumet, A. Vargas, R. Gurny, F. Delie, *Eur. J. Pharm. Biopharm.* **2008**, *69*, 1-9.
- [19] J. Napp, J. E. Mathejczyk, F. Alves, *Pediatr. Radiol.* **2011**, *41*, 161-175.
- [20] J. Merian, J. Gravier, F. Navarro, I. Texier, *Molecules* **2012**, *17*, 5564-5591.
- [21] S. Foersch, A. Heimann, A. Ayyad, G. A. Spoden, L. Florin, K. Mpoukouvalas, R. Kiesslich, O. Kempfski, M. Goetz, P. Charalampaki, *Plos One* **2012**, *7*, e41760.
- [22] L. Thiberville, M. Salauen, S. Lachkar, S. Dominique, S. Moreno-Swirc, C. Vever-Bizet, G. Bourg-Heckly, *Eur. Respir. J.* **2009**, *33*, 974-985.
- [23] K. Polom, D. Murawa, Y.-s. Rho, P. Nowaczyk, M. Huenerbein, P. Murawa, *Cancer* **2011**, *117*, 4812-4822.
- [24] M. Hutteman, "Image-guided surgery using invisible near-infrared fluorescent light: from pre-clinical studies to clinical validation", Doctoral thesis, Leiden University, **2011**.
- [25] A. Wagh, S. Y. Qian, B. Law, *Bioconjug. Chem.* **2012**, *23*, 981-992.
- [26] A. Kumari, S. K. Yadav, S. C. Yadav, *Colloids Surf., B.* **2010**, *75*, 1-18.
- [27] J. Panyam, V. Labhasetwar, *Adv. Drug Deliv. Rev.* **2003**, *55*, 329-347.
- [28] M. A. Woodruff, D. W. Hutmacher, *Prog. Polym. Sci.* **2010**, *35*, 1217-1256.
- [29] R. Q. Frazer, R. T. Byron, P. B. Osborne, K. P. West, *J. Long. Term Eff. Med. Implants* **2005**, *15*, 629-639.
- [30] A. Bettencourt, A. J. Almeida, *J. Microencapsul.* **2012**, *29*, 353-367.
- [31] T. Heinze, T. Liebert, B. Heublein, S. Hornig, *Adv. Polym. Sci.* **2006**, *205*, 199-291.
- [32] J. H. Rao, A. Dragulescu-Andrasi, H. Q. Yao, *Curr. Opin. Biotechnol.* **2007**, *18*, 17-25.
- [33] R. K. Jain, T. Stylianopoulos, *Nat. Rev. Clin. Oncol.* **2010**, *7*, 653-664.
- [34] J. P. Best, Y. Yan, F. Caruso, *Adv. Healthc. Mater.* **2012**, *1*, 35-47.
- [35] F. Alexis, E. Pridgen, L. K. Molnar, O. C. Farokhzad, *Mol. Pharm.* **2008**, *5*, 505-515.
- [36] K. Knop, R. Hoogenboom, D. Fischer, U. S. Schubert, *Angew. Chem. Int. Ed.* **2010**, *49*, 6288-6308.
- [37] R. Gref, Y. Minamitake, M. T. Peracchia, V. Trubetskoy, V. Torchilin, R. Langer, *Science* **1994**, *263*, 1600-1603.
- [38] Y. H. Bae, K. Park, *J. Control. Release* **2011**, *153*, 198-205.

- [39] M. Wang, M. Thanou, *Pharmacol. Res.* **2010**, *62*, 90-99.
- [40] D. Peer, J. M. Karp, S. Hong, O. C. Farokhzad, R. Margalit, R. Langer, *Nature Nanotechnol.* **2007**, *2*, 751-760.
- [41] S. S. Moffatt, *J. Nanosci. Nanotechnol.* **2012**, *3*, 1-20.
- [42] U. Bilati, E. Allemann, E. Doelker, *Eur. J. Pharm. Sci.* **2005**, *24*, 67-75.
- [43] H. Fessi, F. Puisieux, J. P. Devissaguet, N. Ammoury, S. Benita, *Int. J. Pharm.* **1989**, *55*, R1-R4.
- [44] S. Schubert, J. T. Delaney, U. S. Schubert, *Soft Matter* **2011**, *7*, 1581-1588.
- [45] M. Lundqvist, J. Stigler, G. Elia, I. Lynch, T. Cedervall, K. A. Dawson, *Proc. Natl. Acad. Sci. U. S. A.* **2008**, *105*, 14265-14270.
- [46] R. L. Xu, *Particuology* **2008**, *6*, 112-115.
- [47] D. E. Koppel, *J. Chem. Phys.* **1972**, *57*, 4814-4820.
- [48] B. J. Frisken, *Appl. Opt.* **2001**, *40*, 4087-4091.
- [49] B. J. Berne, R. Pecora, "Dynamic Light Scattering – With applications to chemistry, biology and physics", John Wiley New York, **1975**.
- [50] K. Takahashi, H. Kato, T. Saito, S. Matsuyama, S. Kinugasa, *Part. Part. Syst. Char.* **2008**, *25*, 31-38.
- [51] A. Bootz, V. Vogel, D. Schubert, J. Kreuter, *Eur. J. Pharm. Biopharm.* **2004**, *57*, 369-375.
- [52] V. Klanga, N. B. Matskob, C. Valentaa, F. Hoferb, *Micron* **2012**, *43*, 85-103.
- [53] V. Klanga, C. Valentaa, N. B. Matsko, *Micron* **2013**, *44*, 45-74.
- [54] P. H. Brown, P. Schuck, *Biophys. J.* **2006**, *90*, 4651-4661.
- [55] P. Schuck, *Biophys. J.* **2000**, *78*, 1606-1619.
- [56] F. Bonaccorso, T. Hasan, P. H. Tan, C. Sciascia, G. Privitera, G. Di Marco, P. G. Gucciardi, A. C. Ferrari, *J. Physical Chem. C* **2010**, *114*, 17267-17285.
- [57] V. Vogel, K. Langer, S. Balthasar, P. Schuck, W. Maechtle, W. Haase, J. van den Broek, C. Tziatzios, D. Schubert, *Prog. Coll. Pol. Sci.* **2002**, *119*, 31-36.
- [58] H. Pertoft, *J. Biochem. Biophys. Methods* **2000**, *44*, 1-30.
- [59] M. Gaumet, R. Gurny, F. Delie, *Int. J. Pharm.* **2007**, *342*, 222-230.
- [60] M. K. Brakke, *J. Am. Chem. Soc.* **1951**, *73*, 1847-1848.
- [61] G. Sahay, D. Y. Alakhova, A. V. Kabanov, *J. Control. Release* **2010**, *145*, 182-195.
- [62] J. Rejman, V. Oberle, I. S. Zuhorn, D. Hoekstra, *Biochem. J.* **2004**, *377*, 159-169.
- [63] H. J. Gao, W. D. Shi, L. B. Freund, *Proc. Natl. Acad. Sci. U.S.A.* **2005**, *102*, 9469-9474.
- [64] S. Zhang, J. Li, G. Lykotrafitis, G. Bao, S. Suresh, *Adv. Mater.* **2009**, *21*, 419-424.
- [65] S. K. Sahoo, J. Panyam, S. Prabha, V. Labhasetwar, *J. Control. Release* **2002**, *82*, 105-114.
- [66] S. R. S. Ting, G. Chen, M. H. Stenzel, *Polym. Chem.* **2010**, *1*, 1392-1412.
- [67] J. J. Lundquist, E. J. Toone, *Chem. Rev.* **2002**, *102*, 555-578.
- [68] C. R. Becer, M. I. Gibson, J. Geng, R. Ilyas, R. Wallis, D. A. Mitchell, D. M. Haddleton, *J. Am. Chem. Soc.* **2010**, *132*, 15130-15132.
- [69] M. A. Mintzer, E. E. Simanek, *Chem. Rev.* **2009**, *109*, 259-302.
- [70] S. Y. Wong, J. M. Pelet, D. Putnam, *Prog. Polym. Sci.* **2007**, *32*, 799-837.
- [71] D. Pezzoli, F. Olimpieri, C. Malloggi, S. Bertini, A. Volonterio, G. Candiani, *PLoS One* **2012**, *7*, e34711.
- [72] S. Grund, M. Bauer, D. Fischer, *Adv. Eng. Mater.* **2011**, *13*, B61-B87.
- [73] Y.-X. Sun, X.-Z. Zhang, H. Cheng, S.-X. Cheng, R.-X. Zhuo, *J. Biomed. Mater. Res., Part A* **2008**, *84A*, 1102-1110.
- [74] Y. Eshita, J. Higashihara, M. Onishi, M. Mizuno, J. Yoshida, T. Takasaki, N. Kubota, Y. Onishi, *Molecules* **2009**, *14*, 2669-2683.
- [75] J. J. Thomas, M. R. Rekha, C. P. Sharma, *Colloids Surf. B. Biointerfaces* **2010**, *81*, 195-205.
- [76] A. Maruyama, H. Watanabe, A. Ferdous, M. Katoh, T. Ishihara, T. Akaike, *Bioconjug. Chem.* **1998**, *9*, 292-299.
- [77] T. Azzam, H. Eliyahu, A. Makovitzki, A. J. Domb, *Macromol. Symp.* **2003**, *195*, 247-262.

-
- [78] W.-C. Tseng, C.-M. Jong, *Biomacromolecules* **2003**, *4*, 1277-1284.
- [79] W.-C. Tseng, C.-H. Tang, T.-Y. Fang, *J. Gene Med.* **2004**, *6*, 895-905.
- [80] Y.-X. Sun, W. Xiao, S.-X. Cheng, X.-Z. Zhang, R.-X. Zhuo, *J. Control. Release* **2008**, *128*, 171-178.
- [81] D. Jiang, A. K. Salem, *Int. J. Pharm.* **2012**, *427*, 71-79.
- [82] S. K. Tripathi, R. Goyal, K. C. Gupta, *Soft Matter* **2011**, *7*.
- [83] T. Azzam, H. Eliyahu, L. Shapira, M. Linial, Y. Barenholz, A. J. Domb, *J. Med. Chem.* **2002**, *45*, 1817-1824.
- [84] J. Wotschadlo, T. Liebert, T. Heinze, K. Wagner, M. Schnabelrauch, S. Dutz, R. Mueller, F. Steiniger, M. Schwalbe, T. C. Kroll, K. Hoeffken, N. Buske, J. H. Clement, *J. Magn. Magn. Mater.* **2009**, *321*, 1469-1473.
- [85] T. Heinze, U. Erler, I. Nehls, D. Klemm, *Angew. Makromol. Chem.* **1994**, *215*, 93-106.
- [86] "ISO 10993-5: Biological evaluation of medical devices Part 5: Tests for in vitro cytotoxicity", **2009**.
- [87] "ASTM F 756-2000, Standard Practice for Assessment of Hemolytic Properties of Materials", in *Annual Book of ASTM Standards*, Philadelphia, **2008**.
- [88] S. Jiang, Z. Cao, *Adv. Mater.* **2010**, *22*, 920-932.
- [89] F. Schlenk, S. Grund, D. Fischer, *Ther. Delivery* **2013**, *4*, 95-113. doi: 110.4155/tde.4112.4128.
- [90] L. Parhamifar, A. K. Larsen, A. C. Hunter, T. L. Andresen, S. M. Moghimi, *Soft Matter* **2010**, *6*, 4001-4009.
- [91] M. Neu, D. Fischer, T. Kissel, *J. Gene Med.* **2005**, *7*, 992-1009.
- [92] A. C. Grayson, A. M. Doody, D. Putnam, *Pharm. Res.* **2006**, *23*, 1868-1876.
- [93] A. Kwok, S. L. Hart, *Nanomedicine-Uk* **2011**, *7*, 210-219.

Supplementary information

Table S.1. Summary nanoprecipitation conditions and size distributions of representative nanoparticles prepared from various synthetic polymers. Solvent/non-solvent ratio was kept constant at 0.25.

Polymer	Schematic representation of the chemical structure	Nanoprec. method	C_{polymer} [mg · mL ⁻¹]	d_{DLS} [nm]	PDI _p	ζ [mV]
PLGA ($M_w \approx 7,000 - 17,000$ g · mol ⁻¹)		A in W	0.25	30	0.28	-9
		W in A	4	242	0.11	-22
EUDRAGIT S100 ($M_w \approx 25,000$ g · mol ⁻¹)		A in W	0.25	64	0.20	-22
		W in A	4	89	0.43	-19
PMMA n = 50		W in A	4	453	0.30	-27
PMMA n = 120		W in A	4	731	0.24	-22
P(BuMA- <i>stat</i> -MMA) ($M_w \approx 150,000$ g · mol ⁻¹)		W in A	4	191	0.05	-26
PS n = 33		W in T	4	453	0.30	-26
PS n = 66		W in T	4	731	0.24	-22
P2VP n = 28		W in A	4	616	0.39	/
P(<i>i</i> POx- <i>stat</i> -MMA) _{18:44}		W in A	4	578	0.23	-8
P(EtOx- <i>stat</i> -Dec-GlcAc) _{16:4}		W in A	4	610	0.45	+17
P(EtOx- <i>stat</i> -Dec-GalAc) _{10:10}		W in A	4	590	0.19	-6

A in W = Polymer acetone solution was dropped into water, W in A = water was dropped into polymer acetone solution. W in T = Polymer THF solution was dropped into water.

Abbreviations: PLGA = poly(lactic-*co*-glycolic acid); EUDRAGIT S100 = poly(methyl methacrylate-*stat*-methyl methacrylate); PMMA = poly(methyl methacrylate); P2VP = p(2-vinylpyridine); P(BuMA-*stat*-MMA) = poly(butyl methacrylate-*stat*-methyl methacrylate); PS = poly(styrene); P(*i*POx-*stat*-MMA)_{18:44} = poly(*iso*-propyloxazoline-*stat*-methyl methacrylate)_{18:44}; P(EtOx-*stat*-Dec-GlcAc) = glucosylated poly((2-ethyl-2-oxazoline)-*stat*-poly(dec-9-enyl)-2-oxazoline); P(EtOx-*stat*-Dec-GalAc)_{10:10} = galactosylated poly((2-ethyl-2-oxazoline)-*stat*-poly(dec-9-enyl)-2-oxazoline).

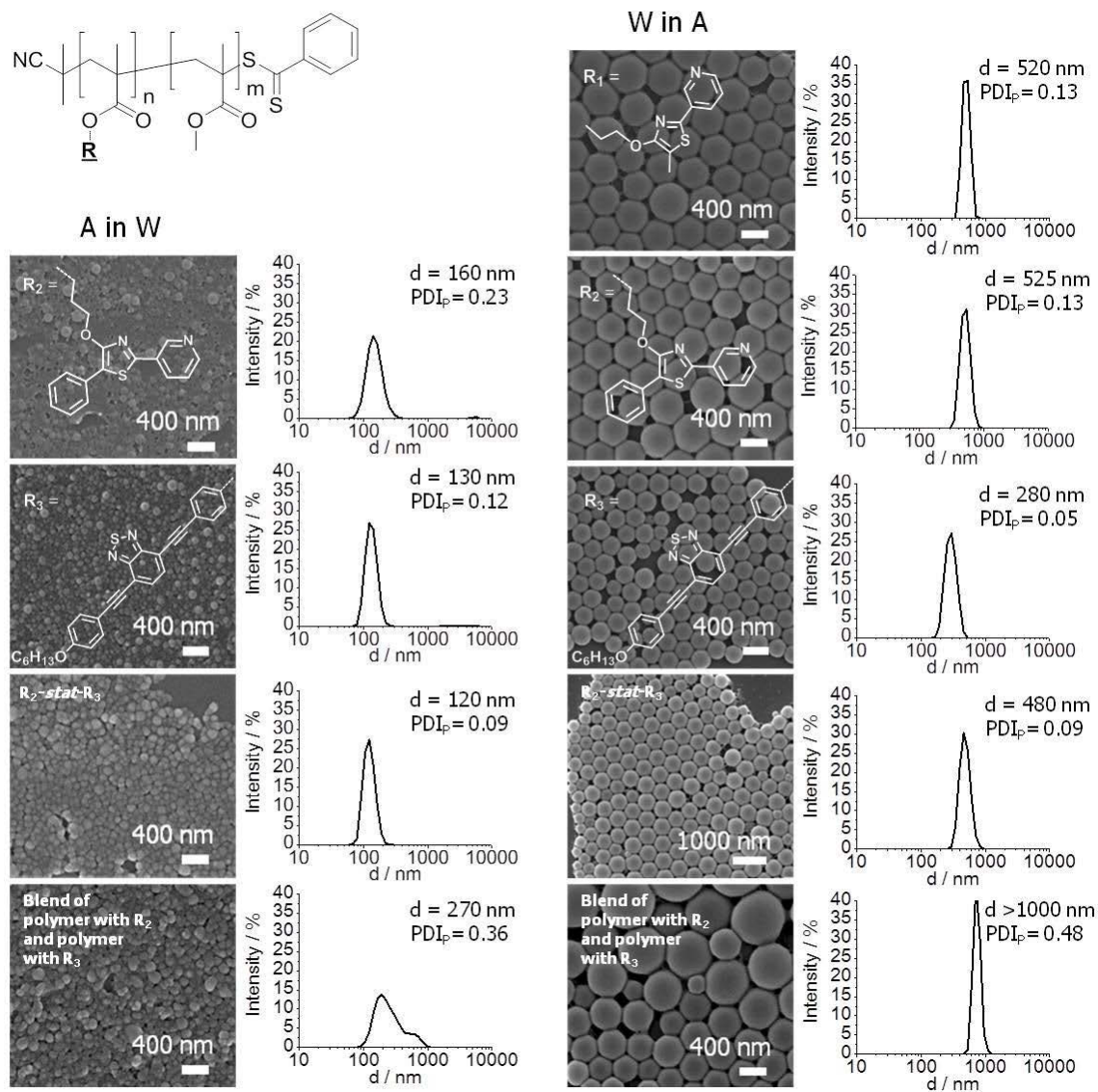


Figure S.1. Overview about nanoparticles prepared by nanoprecipitation using thiazole-functionalized PMMA copolymers: Intensity weighted size distribution, diameter and PDI_p values obtained by DLS measurements as well as representative SEM images. The particles were prepared by the dropping technique, applying a polymer acetone solution with $c = 3 \text{ mg} \cdot \text{mL}^{-1}$ and a solvent-non-solvent ratio of 0.25. A in W = polymer acetone solution was dropped into water, W in A = water was dropped into polymer acetone solution.

List of abbreviations

AGU	anhydroglucose unit
AUC	analytical ultracentrifugation
CLSM	confocal laser scanning microscopy
TEM	transmission electron microscopy
d	diameter
D	diffusion coefficient
d_h	hydrodynamic diameter
DLS	dynamic light scattering
DMEM	Dulbecco's modified Eagle's Medium
DS	degree of substitution
EDC	1-ethyl-3-(3-dimethylamino-propyl) carbodiimide
g	gravity
HBG	HEPES-buffered glucose
HEK	human embryonic kidney
HepG2 HCC	hepatocellular carcinoma cell line
HT	high-throughput
I	intensity
k_B	Boltzmann constant
mg	milligram
mL	milliliter
M_n	number average molar mass
M_w	weight average molar mass
N/P ratio	nitrogen (cationic polymer) to phosphate ratio (DNA)
NaBH_4	sodium borohydride
NMR	nuclear magnetic resonance
PBS	phosphate buffered saline
PDI	polydispersity index
PDI_p	polydispersity index particle (DLS)
PUC	preparative ultracentrifugation
RAFT	reversible addition-fragmentation chain transfer
SEC	size exclusion chromatography
SEM	scanning electron microscopy
THF	tetrahydrofuran
v/v	volume to volume
ζ	zeta potential
η_0	viscosity

Curriculum vitae



- 07/12/1984 Born in Weimar
- 1991 – 1995 School education in Buttstädt
- 1995 – 2003 School education in Kölleda
- 07/01/2003 University entrance qualification at Prof. Fritz Hofman Gymnasium
Kölleda
- 08/2003 – 03/2004 Temporary job as sales assistant
- 04/2004 Study of pharmacy at the Philipps-Universität Marburg
- 10/2004 – 11/2009 Study of chemistry at the Friedrich-Schiller-Universität Jena
- 09/2007 “Vordiplom” (equivalence to B. Sc. honors)
- 11/2008 – 11/2009 Diploma thesis at the Laboratory of Organic and Macromolecular
Chemistry (IOMC) at the Friedrich-Schiller-Universität Jena in the
group of Prof. Ulrich S. Schubert
- 11/03/2009 Academic degree diploma (equivalence to M. Sc.)
- Since 11/2009 PhD student at the Laboratory of Organic and Macromolecular
Chemistry (IOMC) at the Friedrich-Schiller-Universität Jena in the
group of Prof. Ulrich S. Schubert

Jena, 25.02.2013

Publications list

- P1) Antje Vollrath, Stephanie Schubert, Ulrich S. Schubert, "Fluorescence imaging of cancer tissue based on metal-free polymeric nanoparticles – Review", *J. Mater. Chem. B* **2013**, accepted.
- P2) Antje Vollrath, Anja Schallon, Christian Pietsch, Stephanie Schubert, Takahiro. Nomoto, Yu Matsumoto, Kazunori Kataoka, Ulrich S. Schubert, "A toolbox of differently sized and labeled PMMA nanoparticles for cellular uptake investigations", *Soft Matter* **2013**, 9, 99–108.
- P3) Antje Vollrath, David Pretzel, Christian Pietsch, Igor Y. Perevyazko, Roberto Menzel, Stephanie Schubert, George M. Pavlov, Dieter Weiß, Rainer Beckert, Ulrich S. Schubert, "Preparation, cellular internalization, and biocompatibility of highly fluorescent PMMA nanoparticles", *Macromol. Rapid Commun.* **2012**, 33, 1791–1797.
- P4) Igor Y. Perevyazko, Antje Vollrath, Christian Pietsch, Stephanie Schubert, George M. Pavlov, Ulrich S. Schubert, "Nanoprecipitation of poly(methyl methacrylate)-based nanoparticles: Effect of the molar mass and polymer behavior", *J. Polym. Sci., Part A: Polym. Chem.* **2012**, 50, 2906–2913.
- P5) Krzysztof Babiuch, David Pretzel, Tatjana Tolstik, Antje Vollrath, Sarmiza E. Stanca, Franziska Foertsch, C. Remzi Becer, Michael Gottschaldt, Christoph Biskup, Ulrich S. Schubert, "Uptake of well-defined, highly-glycosylated, pentafluorostyrene-based polymers and nanoparticles by human-heptocellular carcinoma cells", *Macromol. Biosci.* **2012**, 12, 1190–1199.
- P6) Christine Weber, Sarah Rogers, Antje Vollrath, Stephanie Höppener, Tobias Rudolph, Nicole Fritz, Richard Hoogenboom, Ulrich S. Schubert, "Aqueous solution behavior of comb shaped poly(2-ethyl-2-oxazoline)", *J. Polym. Sci., Part A: Polym. Chem.* **2012**, 51, 139–148.
- P7) Igor Y. Perevyazko, Joseph T. Delaney Jr., Antje Vollrath, George M. Pavlov, Stephanie Schubert, Ulrich S. Schubert, "Examination and optimization of the self-assembly of biocompatible, polymeric nanoparticles by high-throughput nanoprecipitation", *Soft Matter* **2011**, 7, 5030–5035.
- P8) Meta M. Bloksma, Christine Weber, Igor Y. Perevyazko, Anette Kuse, Anja Baumgärtel, Antje Vollrath, Richard Hoogenboom, Ulrich S. Schubert, "2-Cyclopropyl-2-oxazoline): From rate acceleration by cyclopropyl to thermoresponsive properties", *Macromolecules* **2011**, 44, 4057–4064.

- P9) Antje Vollrath, Stephanie Schubert, Norbert Windhab, Christoph Biskup, Ulrich S. Schubert, "Labeled nanoparticles based on pharmaceutical EUDRAGIT (R) S 100 polymers", *Macromol. Rapid Commun.* **2010**, *31*, 2053–2058.
- P10) Igor Y. Perevyazko, Antje Vollrath, Stephanie Hornig, George M. Pavlov, Ulrich S. Schubert, "Characterization of poly(methyl methacrylate) nanoparticles prepared by nanoprecipitation using analytical ultracentrifugation, dynamic light scattering, and scanning electron microscopy", *J. Polym. Sci., Part A: Polym. Chem.* **2010**, *48*, 3924–3931.
- P11) Kristian Kempe, Antje Vollrath, Hendrik W. Schaefer, Tobias G. Poehlmann, Christoph Biskup, Richard Hoogenboom, Stephanie Hornig, Ulrich S. Schubert, "Multifunctional poly(2-oxazoline) nanoparticles for biological applications", *Macromol. Rapid Commun.* **2010**, *31*, 1869–1873.
- P12) Christian Pietsch, Antje Vollrath, Richard Hoogenboom, Ulrich S. Schubert, "Fluorescent thermometer based on a pyrene-labeled thermoresponsive polymer" *Sensors* **2010**, *10*, 7979–7990.

Submitted publications:

- P13) Sofia Ochrimenko,# Antje Vollrath,# Kristian Kempe, Lutz Tauhardt, Stephanie Schubert, Ulrich S. Schubert, D. Fischer, "Dextran-*graft*-linear poly(ethylene imine) for gene delivery – influence of linker strategies on physicochemical and biological properties", *Bioconjug. Chem.* **2013**, submitted.
- P14) Alexandra C. Rinkenauer,# Antje Vollrath,# Anja Schallon, Lutz Tauhardt, Kristian Kempe, Stephanie Schubert, Dagmar Fischer, Ulrich S. Schubert, "Parallel high-throughput screening of polymer vectors for non-viral gene delivery: Evaluation of structure-property-relationships of transfection", *ACS Comb. Sci.* **2013**, submitted.

Equal contribution

Oral presentations:

- P1) "Formulation of polymeric nanoparticles *via* nanoprecipitation for drug delivery and diagnostic", DPI HTE Clustermeeting, Jena, Germany, **03.12.2012**.

- P2) "High-throughput nanoprecipitation of functional polymers", *International Symposium Controlled Release Society and NanoConSens*, Jena, Germany, **15.-16.3.2011**.
- P3) "Asymmetric field flow fractionation", *NanoConsSens Meeting*, Jena, Germany, **26.01.2011**.
- P4) "Nanoparticle formation and investigations of EUDRAGIT®", DPI HTE Clustermeeting, Jena, Germany, **16.12.2009**.

Poster presentations:

- P1) Antje Vollrath, Sofia Ochrimenko, Kristian Kempe, Lutz Tauhardt, Stephanie Schubert, Ulrich S. Schubert, Dagmar Fischer, "Dextran-graft-poly(ethylene imine) for gene delivery – structure-activity relationships", *Smart Polymers – Biennial Meeting of the GDCh-Division of Macromolecular Chemistry*, Mainz, Germany, **07.-09.10.2012**.
- P2) Antje Vollrath, Sofia Ochrimenko, Kristian Kempe, Lutz Tauhardt, Stephanie Schubert, Ulrich S. Schubert, Dagmar Fischer, "Dextran-graft-poly(ethylene imine) for gene delivery – structure-activity relationships", *International Conference on Polymer Synthesis & Polymer Colloids*; Warwick, United Kingdom, **08.-12.07.2012**.
- P3) Andreas Wild, Antje Vollrath, Andreas Winter, Martin D. Hager, Ulrich S. Schubert, "Polymer functionalized π -conjugated bisterpyridine metallopolymers", *Abstr. Pap. Am. Chem. Soc.* **2011**, 242, **28.08.-01.09.2011**.
- P4) Stephanie Schubert, Antje Vollrath, Igor Y. Perevyazko, Dagmar Fischer, Ulrich S. Schubert, "Polymeric nanoparticles for sensor and drug delivery applications" *Abstr. Pap. Am. Chem. Soc.* **2011**, 242, **28.08.-01.09.2011**.
- P5) Antje Vollrath, Igor Y. Perevyazko, Christian Pietsch, Joseph T. Delaney Jr., Stephanie Schubert, George M. Pavlov, Ulrich S. Schubert, "High-throughput nanoprecipitation of functional polymers", *Innovationskongress*, Potsdam, Germany, **19.05.2011**.
- P6) Antje Vollrath, Igor Y. Perevyazko, Christian Pietsch, Joseph T. Delaney Jr., Stephanie Schubert, George M. Pavlov, Ulrich S. Schubert, "High-throughput nanoprecipitation of functional polymers", *Materialtag*, Jena, Germany, **30.03.2011**.

- P7) Stephanie Schubert, Antje Vollrath, Igor Y. Perevyazko, Christian Pietsch, Joseph T. Delaney Jr., George M. Pavlov, Ulrich S. Schubert, "High-throughput nanoprecipitation of functional polymers", *Abstr. Pap. Am. Chem. Soc.* **2011**, 242, **28.08.-01.09.2011**.
- P8) Antje Vollrath, Igor Y. Perevyazko, Christian Pietsch, Joseph T. Delaney Jr., Stephanie Schubert, George M. Pavlov, Ulrich S. Schubert, "High-throughput nanoprecipitation of functional polymers", *International Symposium Controlled Release Society and NanoConSens*, Jena, Germany, **15.-16.03.2011**.
- P9) Antje Vollrath, Kristian Kempe, Hendrik Schäfer, Katrin Knop, Stephanie Hornig, Ulrich S. Schubert, "Formation of labeled nanoparticles of polymeric systems for drug delivery applications", *Thüringer Biomaterial Kolloquium*, Friedrichroda, Germany, **17.09.2009**.

Acknowledgements / Danksagung

Zuallererst möchte ich meinem wissenschaftlichem Betreuer Prof. Ulrich S. Schubert für die Möglichkeit bedanken, meine Doktorarbeit in seiner Arbeitsgruppe anzufertigen. Vielen Dank für die fortwährende Unterstützung, die vielen Hinweise und schnellen Korrekturen, aber auch für die hervorragenden Arbeitsplatzbedingungen, die verschiedenen Konferenzbesuche und die heiteren Gruppenausflüge. Desweiteren gebührt ein großer Dank meiner Betreuerin Dr. Stephanie Schubert für unzählige Diskussionen, Anregungen und Korrekturen. Ohne Deine große Unterstützung wäre diese Arbeit nicht möglich gewesen.

Ich danke Frau Prof. Dagmar Fischer für die gute Kooperation, Ihre stetige Unterstützung sowie für viele hilfreiche Diskussionen. Prof. Thomas Heinze, Prof. Rainer Beckert, Prof. Christoph Biskup, Prof. Felix Schacher, Prof. Alfred Fahr und Prof. Kazunori Kataoka danke ich ebenso für die vielen interessanten Kooperationen, aber auch für die Bereitstellung Ihrer technischen Geräte und Labore. In diesem Sinne danke ich auch Melanie Nikolayski, Thomas Elschner, Dr. Holger Wondrazeck, Jana Wodtschadlo, Dr. Alexander Mohn, Franziska Foertsch, Dr. Marius Bauer, Roberto Menzel, Takahiro Nomoto und Dr. Yu Matsumoto für Ihren wissenschaftlichen Rat und Beitrag. Was wäre eine Doktorarbeit in der Chemie ohne Analysen und Technische Unterstützung? Vielen lieben Dank Grit, Nicole, Sandra, Steffi, Frank wie auch Frau Lentvogt, Frau Sentis und Herr Dr. Günther für unzählige Messungen, die Licht in das Dunkel vieler Substanzen gebracht haben. Ein großer Dank geht ebenso an Anja, Tanja, Doreen, Sylvia und Frau Pfeifer für sämtliche Organisation. Dankeschön an Frau Kuse, Herrn Weigand, Herrn Schmäcke und Herrn Pohnert für den tollen Lieferservice sämtlicher Glasgeräte, Wasserkanister und all den anderen Kleinigkeiten, die man für den Laboralltag benötigt. Aber auch allen anderen Kollegen und Freunden der AG Schubert möchte ich von ganzem Herzen für die gute Zusammenarbeit und die tolle Zeit danken. Uwe unser Sicherheitsmann, Martin und Micha unsere Sorgentelefone – vielen Dank, dass Ihr immer auf uns Studenten aufpasst und mir bei wissenschaftlichen Fragen immer wieder weitergeholfen habt. Weiterhin danke ich Renzo und Jürgen für sämtliche technische Unterstützung, denn ohne Computer und Gefriertrocknung wäre meine Doktorarbeit wohl etwas anderes verlaufen. Thank you very much Igor, Georgy, Krzysztof und Joe for the very fruitful cooperation's, for all your helpful comments and advices. It was a pleasure to work with you. Vielen Dank für unzählige wertvolle Diskussionen und Hinweise Christine, Stephanie (H.) und Micha W. - Ihr hattet immer ein offenes Ohr für mich und irgendwie habe ich das Gefühl, dass ich auch in Zukunft mit einigen Fragen auf Euch zu kommen werde. Mit Franzi, Bernie und Andy durfte ich meine erste Messe erleben und mit so lieben und hilfsbereiten Kollegen wie Anke, Sebastian, Sarah, David, Banja, Justyna, Lutz, Stefan, Caro, Alex B., Annett und Torsten war die Arbeit nur halb so schwer. Vielen Dank für Eure Hilfe und alles Gute für Eure Zukunft! Ein riesiges Dankeschön verdienen an dieser Stelle außerdem meine lieben Laborpartner Matthias (Hans), Markus, Tobi und Uli, die sowohl meine unzähligen Dialysen als auch mein Rührfischklappern ertragen haben. Ich wünsche Euch perfekte PDIs und viel Erfolg bei Eurer Promotion!

Christian, Kristian und Andreas – Ihr seid schon alle drei was Besonderes! Vielen lieben Dank für Eure Freundschaft, Eure Unterstützung, die lustigen Streiche und Witze, aber natürlich auch für die wissenschaftliche Zusammenarbeit und all Eure hilfreichen Ratschläge. Ich wünsche Euch von ganzem Herzen viel Glück und Erfolg für Eure Zukunft! Chris und Tobi – meine Partyhelden! Euch danke ich für die heiteren Stunden in den letzten Monaten; Ihr habt Jena für mich nochmal richtig aufleben lassen. Ich wünsche Euch viel Schaffenskraft und alles Gute für die Promotion – Spaß habt Ihr sicherlich, da mache ich mir keine Sorgen...(und hin und wieder werde ich es hoffentlich schaffen dabei zu sein).

Katrin, Sofia, Anja, Alex – was wäre meine Doktorandenzeit ohne Euch gewesen? Nicht vorstellbar! Ich danke Euch unendlich für die bereichernden Diskussionen über Arbeit und die tollen gemeinsamen Projekte. Aber noch viel mehr bin ich für Eure Freundschaft und die unzähligen Gespräche über die privaten Dinge im Leben dankbar. Ihr ward und seid eine große Stütze und ich vermisse die Kaffeeklatschrunden mit den essentiellen Lebenserkenntnissen und Ratschlägen bereits jetzt. Alles Liebe für Eure zukünftigen Wege – ich hoffe wir bleiben in regem Kontakt!

Hannes, Thomas, Tanja, Daniel, Melanie, Julia, Simon und Amaya - Euch möchte ich dafür danken, dass Ihr ein Teil dieser schönen Zeit in Jena gewesen seid. Auch wenn wir nicht mehr im selben Haus wohnen, so hoffe ich doch hin und wieder von Euch zu hören. Weiterhin bedanke ich mich bei meinen guten Freunden zu Hause für die nun schon Jahr(zehnt)e andauernde Freundschaft. Im Besonderen bei Tina, Caro, Maria und Lina – Euch gilt ein außerordentlicher Dank, denn Euch kenne ich schon seit der Schulzeit und Ihr habt mich auf allen Höhen und Tiefen meines bisherigen Lebens begleitet. Wo auch immer unsere Wege hinführen werden, ich weiß ich kann auf Euch zählen...

Zum Schluss möchte ich meiner wunderbaren Familie für Ihre Unterstützung in allen Bereichen meines Lebens danken. Ohne meine lieben Eltern, die mir fortwährend ihr ganzes Vertrauen schenken, immer für mich da sind und mich in allem, was ich mir vornehme bestärken, wäre ich heute nicht da wo ich bin. Ihr seid wirklich großartig – fühlt euch umarmt...



Declaration of authorship / Selbstständigkeitserklärung

Hiermit erkläre ich, dass ich die vorliegende Arbeit selbständig angefertigt, nicht anderweitig zu Prüfungszwecken vorgelegt und keine anderen als die angegebenen Hilfsmittel verwendet habe. Sämtliche wissentlich verwendete Textausschnitte, Zitate oder Inhalte anderer Verfasser wurden ausdrücklich als solche gekennzeichnet.

I hereby certify that the work disclosed here is, to the best of my knowledge, original and the result of my own investigations, except as acknowledged, and has not been submitted, either in part or whole, for a degree at this or any other university.

Jena, den 25.02.2013

Antje Vollrath



Publications P1 – P9

P2: Reprinted with permission. Copyright 2010 WILEY-VCH.

P3: Reproduced with permission of The Royal Society of Chemistry. Copyright 2011.

P4: Reprinted with permission. Copyright 2011 WILEY-VCH.

P5: Reprinted with permission. Copyright 2012 WILEY-VCH.

P6: Reproduced with permission of The Royal Society of Chemistry. Copyright 2012.

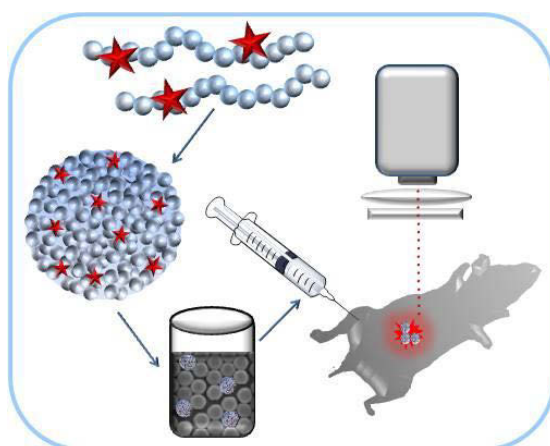
P7: Reprinted with permission. Copyright 2012 WILEY-VCH.

Publication 1

"Fluorescence imaging of cancer tissue based on metal-free polymeric nanoparticles – Review"

Antje Vollrath, Stephanie Schubert, Ulrich. S. Schubert

J. Mater. Chem. B **2013**, accepted.



Cite this: DOI: 10.1039/c0xx00000x

www.rsc.org/xxxxxx

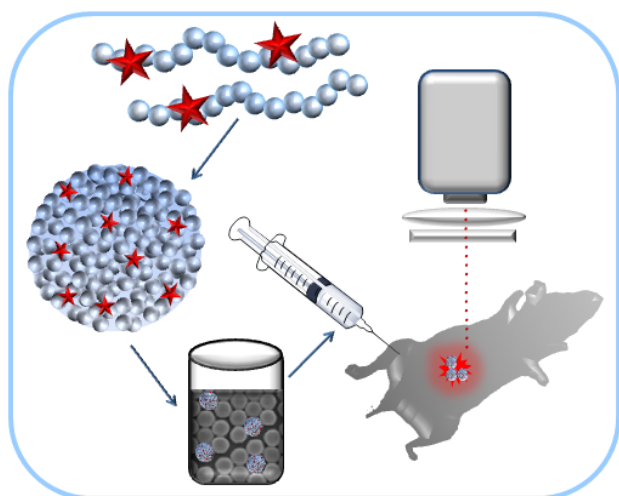
ARTICLE TYPE

Fluorescence imaging of cancer tissue based on metal-free polymeric nanoparticles - Review

Antje Vollrath,^a Stephanie Schubert,^{b,c} Ulrich S. Schubert^{a,b*}

5 Abstract

The utilization of fluorescent nanoparticles (FNPs), which consist of organic fluorophores embedded into a polymer matrix, seems to be a promising concept for *in vivo* cancer imaging showing good biocompatibility, biodegradability, and low toxicity of the agents. Polymeric nanoparticles as fluorescent nanocarriers can be systematically designed with regard to the requested task, *i.e.*, specific accumulation in the tumor tissue. Versatile organic fluorophores can be entrapped into polymers with fine-tuned properties, which were synthesized *via* polymerization techniques. Moreover, the formulation of the nanoparticles can be adjusted, and passive as well as active targeting strategies can be employed. Despite their evident benefits, fluorescent polymeric nanoparticles are still not in clinical application for cancer detection due to a still existing lack in the understanding of their *in vivo* interactions as well as their reproducible production. This review focuses on cancer imaging based on organic dyes and metal-free polymeric fluorescent nanoparticles highlighting recent interesting reports about their design and application as well as their limitations.



30 Keywords

Nanoparticle, polymers, fluorescence imaging, diagnostic, targeting



Antje Vollrath was born in 1984 in Weimar (Germany) and studied chemistry at the Friedrich-Schiller-University Jena (Germany; 2004–2009) She accomplished the master thesis in 2009 under the supervision of Prof. Ulrich S. Schubert and continued as a PhD student in Jena in the Organic and Macromolecular Chemistry Department. In her PhD studies she focussed on the synthesis of tailor-made

nanoparticles based on synthetic polymers for diagnostic and drug delivery.

Notes and references

^a Laboratory of Organic and Macromolecular Chemistry (IOMC), Friedrich Schiller University Jena, Humboldtstrasse 10, 07743 Jena, Germany;

^b Jena Center for Soft Matter (JCSM), Friedrich Schiller University Jena, Philosophenweg 7, 07743 Jena, Germany

^c Institute of Pharmacy, Department of Pharmaceutical Technology, Friedrich Schiller University Jena, Otto-Schott-Str. 41, 07745 Jena, Germany

E-mail: ulrich.schubert@uni-jena.de

Stephanie Schubert (née Hornig) was born in 1981 in Zwickau (Germany). She obtained her MS in chemistry at the Friedrich-Schiller-University of Jena (Germany) in 2005. After research activities at Virginia Tech (Blacksburg, USA), she finished her PhD studies in 2008 in the field of polysaccharide chemistry. During a postdoctoral training with J.M.J. Freché at Berkeley UC (USA), she gained further experiences in polymers as gene delivery

devices. She is currently working on projects related to nanoparticles for drug delivery and sensor applications in the Pharmaceutical Department at the University in Jena.

1 Introduction

Nanomedicine is an ever-growing scientific field within the multidisciplinary area of nanotechnology that addresses the design of novel nanosized therapeutics, which facilitates a target delivery of active species for an improved treatment of diseases.^[1-3] Likewise aspired in the nanomedicine area, is the development of diagnostic agents that enable the detection of manifold processes inside the body and form the major basis for the understanding of disfunctionalities and their subsequent occurrence of diseases.^[4] In particular for cancer treatment, an early detection of growing tumor cells is of vital importance and decides about the success of the therapy. A diagnostic technique that utilizes nanoimaging agents is fluorescence imaging. It is easy applicable and provide high spatial and temporal resolution, superb sensitivity as well as good selectivity.^[5-11] Thus, fluorescence imaging allows insights into living organisms with high sensitivity without the need of dissection, e.g. by usage of endoscopes or miniaturized fiber-based catheters.^[12-17] The examinations of vascular networks and sentinel lymph node mapping are only two examples of the successful application of fluorescence imaging.^[18] Besides an early detection, the surgical removal of the tumor is mostly efficient for cancer therapy, but it is a demanding task for the surgeon to remove the tumor tissue completely without damaging healthy tissue.^[19-21] In order to visualize tumors while surgery and to improve its radical resection, new systems were developed that enable the intraoperative identification of tumors. It was preclinically validated that by using specific fluorescent agents and image guided surgery, tumors can be detected and removed very efficiently with reduced complications.^[22]



Ulrich S. Schubert was born in Tübingen (Germany) in 1969. He studied chemistry in Frankfurt and Bayreuth (both Germany) and the Virginia Commonwealth University, Richmond (USA). His PhD studies were performed at the Universities of Bayreuth and South Florida/Tampa. After postdoctoral training with J.-M. Lehn at the University in Strasbourg (France), he moved to the TU München (Germany) and obtained his Habilitation in 1999.

1999–2000 he was professor at the Center for NanoScience, University of Munich (Germany), and 2000–2007 Full-Professor at TU Eindhoven. Since April 2007, he is Full-Professor at the Friedrich-Schiller-University Jena (Chair of Organic and Macromolecular Chemistry), Germany. His awards include the Bayerischen Habilitations-Förderpreis, the Habilitandenpreis of the GDCh (Makromolekulare Chemie), the Heisenberg-Stipendium of the DFG, the Dozenten-Stipendium of the Fonds der Chemischen Industrie, the VICI award of the NWO, the Piet-Lemstra innovation award of the DPI and the BPG biannual international award.

At the moment fluorescence image guided surgery is in transit to clinical practice. However, in order to enable a fast clinical realization, new fluorescence probes need to be established and approved for *in vivo* application. As the detection of light of fluorescence dyes emitted from the body is limited by tissue induced light absorption and reflection that decreases tremendously the fluorescence signals as well as signal-to-background ratios, researchers focused on the synthesis of stable near-infrared (NIR) fluorescent dyes that emit light between 650 to 900 nm, a range where the autofluorescence of tissue (hemoglobin) is reduced.^[21,23-25] In recent years, efficient fluorescent probes providing high quantum yields and absorption/emission spectra in regions beyond the physiological autofluorescence were developed.^[21] Suitable and preferred agents applied in fluorescence imaging are semiconductor nanocrystals (quantum dots, QD) and organic fluorophores due to their straightforward application compared to genetically engineered molecules (fluorescent proteins, bioluminescence).^[26-28] QD possess excellent fluorescent properties including broad excitation spectra, sharp fluorescence, and a bright emission with a high signal to noise ratio.^[29] Additionally, QD are stable against photobleaching due to the inorganic composition, and they possess long fluorescence lifetimes. Nevertheless, they are discussed controversially in terms of their health risks including cytotoxicity, induced apoptosis, and peroxidative stress.^[30] Significant effort was performed with the aim to enhance the biocompatibility of QD by coating with polymers like poly(ethylene glycol) (PEG) or polysaccharides.^[31] However, there are still open questions about their toxicity, and their future application in clinical settings is ambiguous. Contrary, new organic fluorophores exhibit similar fluorescent properties, but are established to be biocompatible and less toxic.^[15,19,32] Still, some problems come along with the application of free dyes, such as low photostability and low stability in the physiological environment.

With the objective to improve the fluorophore-based diagnostic and to develop new promising fluorescent agents suitable for clinical applications, dyes were entrapped into polymeric nanoparticles (NPs).^[28,33-36] The benefits of using polymeric particles as templates for dye encapsulation are thereby apparent: (1) Potential multiple loading of fluorophores into the NP leads to enhanced fluorescence intensities; (2) protection of the dye inside the NP core against the biological environment avoids undesired side effects such as reduced fluorescence because of interaction with proteins; (3) increased surface area for attachment of functional groups and targeting moieties.^[28] Furthermore, several polymeric NPs are already in clinical trials for drug delivery applications (without the use of any fluorescent label). Thus, the concept to encapsulate fluorophores into a polymeric NP that can be used as diagnostic agent seems promising in term of future clinical realization.^[37-41] This contribution reviews the design and application of organic dyes and fluorescent metal-free nanoparticles for cancer imaging. Thereby, advantages, challenges and available methods to

overcome some limitations are discussed in order to evaluate if metal-free imaging based on polymers is realistic for clinical application.

5 2 Organic fluorophores for *in vivo* imaging applications

As efficient imaging relies on the good detection of fluorophores, its final application depends on the properties of the chromophores. Desirable characteristics are high fluorescence quantum yields, high molar extinction coefficients, broad absorption ranges in visible field and a good tolerance to photobleaching.^[6,42] **Scheme 1** represents a selection of fluorophores commonly used for *in vivo* imaging.

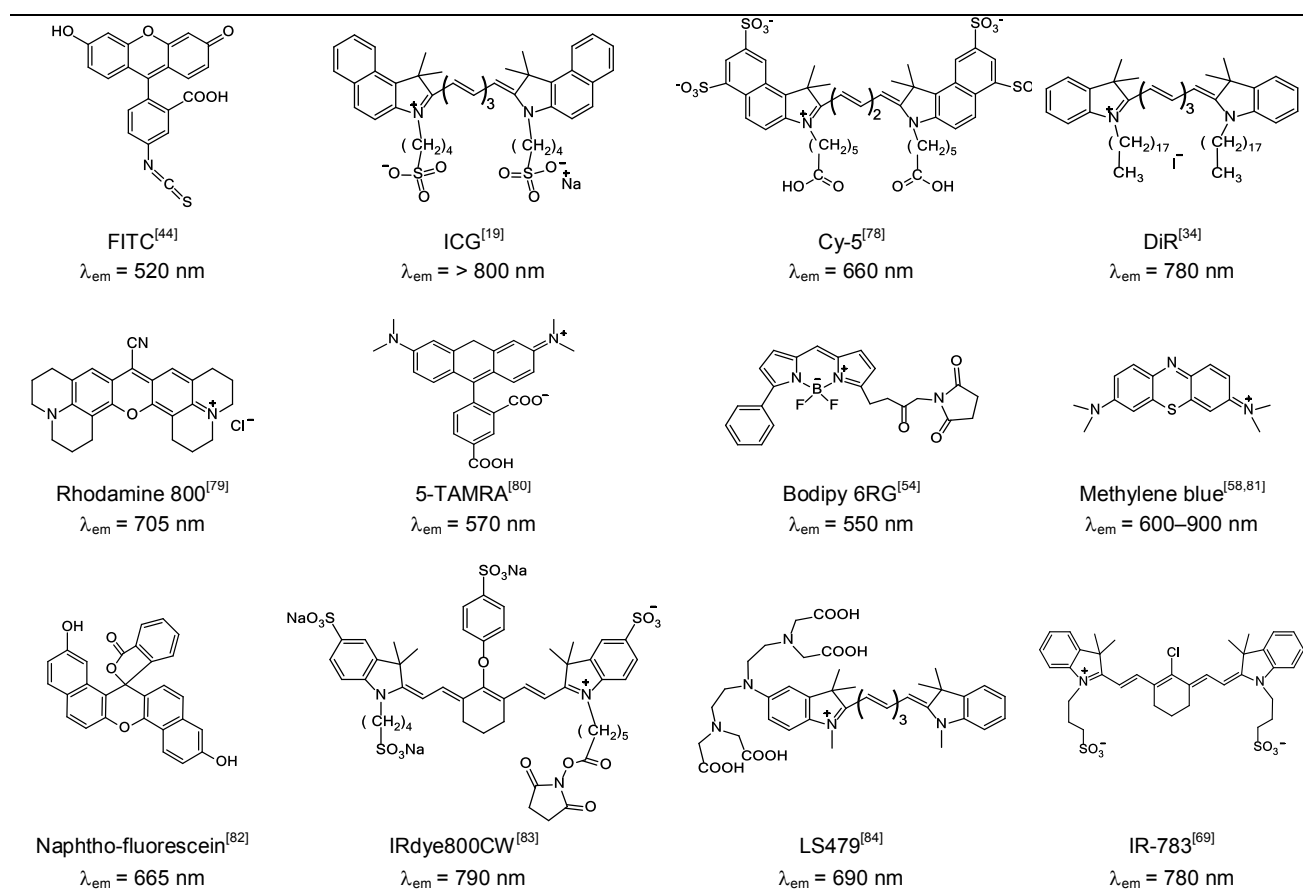
Fluorescein-5-isothiocyanate (FITC) and rhodamine B are members of the xanthene group and probably the most well-known and used dyes for cell, molecule or particle labelling. Besides its application *in vitro*, a fluorescein water based injection (10%) is approved by the Food and Drug Administration (FDA) to be used in diagnostic fluorescein angiography for blood flow examinations in surgical resections or in the ophthalmology for angiography of the retina and iris vasculature.^[17,43,44] However, the common xanthene members still suffer from low photostability and rapid photobleaching, which limits their utilization for diagnostic application. Though, it was found that the optical properties of common fluorophores can be enhanced and fine-tuned by introducing versatile substituents to the initial dye scaffold.^[45-47] For instance, Alexa fluorophores and DyLight Fluors are established derivatives of rhodamine, coumarin, cyanine and xanthene and were obtained, e.g., by the introduction of sulfonate groups at the chromophore.^[48-51] As a result of the sulfonation, the negatively charged dyes show an increased hydrophilic character and possess improved fluorescent properties in terms of emission intensity, photobleaching, pH stability and aggregation behavior of the dye molecules. Furthermore, these dyes cover a wide range of the fluorescence spectra including a good emission within the NIR range that was identified as ideal region for *in vivo* imaging owing to the ability of deeper penetration into tissue and decreased tissue autofluorescence. Most currently applied in diagnostic applications is the polymethine (cyanine) dye family. The spectra of available polymethine dyes ranges from 400 to 800 nm (and above) as a result of the ability to fine-tune the absorption *via* introduction of further vinylen units to the polymethine bridge that link the two aromatic nitrogen-containing heterocycles. A well-known representative of the polymethine class is the indocyanine green (ICG). ICG is approved by the FDA for intravenous administration and applied since several years in ophthalmic angiography and cardiac output determination. Recently, it is also used in the field of surgical oncology for sentinel lymph node mapping, for the imaging of vascular networks, demarcations of liver segments as well as intra operative staining.^[18,19,52] Other cyanine derivatives, such as 1,1'-dioctadecyltetramethyl indotricarbocyanine iodide (DiR), cyanine 5.5 (Cy5.5) and

cyanine 7 (Cy-7) are further utilized for fluorescence labelling of peptides or particles for *in vivo* imaging applications.^[6,15,34,42]

Besides the cyanines, new NIR fluorophores based on difluoroboron dipyrromethene (Bodipy, 4-bora-3a,4a-diaza-s-indacene) have gained significant attention for diagnostic application due to their robustness against light and chemicals, the good solubility, and their outstanding optical properties.^[45,53-55] Furthermore, the very inexpensive methylene blue (MB) fluorophore is utilized, e.g. in fluorescence-guided surgery for tissue staining, such as identification of bile ducts and ureters.^[56] MB is characterized by excellent water-solubility, low toxicity and emission wavelengths in the NIR range (600 to 900 nm).^[57,58]

Besides the synthesis of fluorophores with superb molar absorptions and quantum yields for high fluorescence intensity in the NIR spectral range was realized, the preferential accumulation in specific cells was requested for defined diagnostic and challenged researchers within the last years. The primary concentration of the fluorophores in specific cells can be achieved by attachment of targeting moieties. For instance, cancer specific NIR derivatives were synthesized by conjugation with cancer specific ligands, such as folate (FL), cyclic arginine-glycine-aspartic acid (cRGD) peptides, and various antibodies (AB).^[24,42,59-67] Surprisingly, two classes of heptamethine based dyes already prefer the accumulation in tumors. The so-called IR-808 and IR-783 dyes exhibit a favored tumor accumulation without the need of chemical conjugation with tumor specific ligands.^[68,69]

An alternative strategy for a defined imaging relies on imaging agents that only emit light *via* interaction and chemical reaction with the targeted tissue.^[23,70] For the synthesis of such "optically silent" NIR dyes, the quenching effect is often exploited. This effect of decreased fluorescence (due to the loss of absorption or decreasing quantum yield) occurs either if two or more of the same or different chromophores are linked close to each other or if they are coupled to a non-fluorescent quencher.^[71-73] By enzymatic cleavage of the linker, e.g. by a specific proteolytic enzyme that is mainly present in tumor tissue, the dyes are released and activated. As the fluorescence occurs only in the target site, interference and low signal-to-background ratios are avoided.^[74,75] One example is a protease activatable Cy5.5-based fluorochrome, so-called ProSense-680.^[27] The fluorophore/non-fluorescent quencher approach offers the advantage to utilize a target moiety as quencher and combine two superior properties: fluorescence activation as well as the targeting effect. To this end, responsive NIR optical probes were synthesized based on conjugation of various monoclonal antibodies (mABs) to ICG, AlexaFluor680 and others.^[60,61,76,77]



Scheme 1. Schematic representation of the structures and approximated emission wavelengths of organic fluorophores used for *in vivo* imaging.

Although the synthesis of versatile “smart” NIR dyes already improved the platform of *in vivo* fluorescent imaging applications, some limitations remain. For one, by shifting the fluorescence of the chromophore agents to the NIR region to enable deeper tissue imaging a decrease in the fluorescence intensities is observed due to the resultant higher degree of vibrations that increases the numbers of non-radioactive decay pathways. Moreover, these approaches still suffer from relatively low long-term photostability and low stability in the physiological environment, which can provoke aggregation of the dyes with a subsequent decrease in fluorescence. For some fluorophores, solubility issues in water are still not resolved. Though the water solubility of the fluorophores can be enhanced by attachment of biological molecules and/or polar groups, it should be mentioned that with conjugation of biomolecules or other ligands the chemical structure of the dyes might change leading to different fluorescence properties. Furthermore, it is challenging to adjust the dye-biomolecule conjugation. It should be sensitive enough to achieve a cleavage and subsequently a fluorescence signal in the targeted region, but not too sensitive against the biological environment to avoid a premature release of the dye from the conjugate.

3 Polymeric fluorescent nanoparticles (FNPs)

A promising way to amplify the fluorescence of dyes and to overcome the above mentioned limitations is to enclose dye molecules into NPs.^[28,33-36] Within this article, the term fluorescent nanoparticles (FNPs) refers to polymer-based particle systems that contain common organic dyes for optical imaging applications. Inorganic based particle systems will not be in the scope since there are excellent reviews discussing versatile systems based on inorganic (nano)materials, such as silica particles.^[85-88]

3.1 Opportunities and challenges

Manifold benefits are associated with the usage of FNPs.^[6] The particle formation on the nanoscale increases the *in vivo* distribution as well as the retention time of the dyes. Moreover, hundreds of dye molecules can be entrapped into the NP core that significantly enhances the fluorescence brightness in a single spot. The amount of fluorophores entrapped into the NP core is thereby only limited by the quenching effect which can occur if too many fluorophores are too close to each other. Thus, by application of NPs that contain fluorophores, a lower

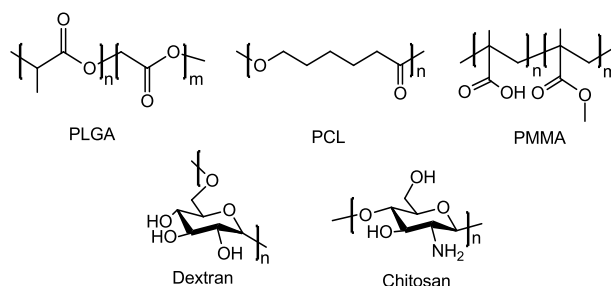
amount of dye molecules encapsulated into the NP might be more beneficial since it can lead to an enhanced detection ability. It was also observed that some fluorophores exhibit an increased quantum yield within the hydrophobic environment inside the particle core. Aside from that, the particle surface can be used for further reaction with functional groups, such as target moieties or stealth polymers. If two or more different chromophores are embedded in the polymer, it is also possible to obtain FRET systems, e.g. switchable emission and/or stimuli-responsive FNPs.^[34,89-91] Another important benefit of encapsulation of the dyes into a matrix material is the protection of the dye against the biological environment.

However, for the realistic application of FNPs for *in vivo* surgery practice, the agents have to fulfill a number of prerequisites. (1) FNPs have to exhibit high purity and must be non-toxic to ensure a safe administration. (2) Superior colloidal stability must be given in biological systems in order to avoid degradation or agglomeration and to enhance the blood circulation time. (3) Carriers should be targetable for a controlled imaging. (4) Complete clearance from biological systems must be warranted after the imaging process is completed. (5) Dye containing NPs should possess a high and stable fluorescence to ensure the long-term imaging and a good signal-to-noise ratio.

3.2 Polymer systems

In order to realize the development of nanocarriers that fulfill all prerequisites mentioned above, the polymers used as matrix material should offer excellent biocompatibility, low or non-toxicity and the ability to form stable particles that persist over a long time also in biological environments. To this end, a variety of formulations were tested, and a lot of effort was dedicated to the synthesis and characterization of biocompatible polymers as matrix material. Living and controlled polymerization techniques are applied for the preparation of polymers with a defined architecture, composition and constitution as well as molar mass.^[92-97] Thus, the chemical and physical properties of polymers can be easily adjusted. For the preparation of NPs, hydrophobic polymers such as poly(lactic-*co*-glycolic acid) (PLGA), poly(ϵ -caprolactone) (PCL) and poly(methyl methacrylate) (PMMA) derivatives are often used (Scheme 2).^[98-103] PLGA is the most extensively investigated matrix material for NP based diagnostic and drug delivery applications owing to its outstanding characteristics, such as excellent biocompatibility, biodegradability into metabolizable moieties, and good manufacturing abilities.^[104] PCL represents a good alternative that shows comparable properties and is also widely applied for NP-based drug delivery and imaging.^[99] Although NPs consisting of PMMA and its derivatives are not biodegradable, their proven biocompatibility and stability *in vitro* and *in vivo* declare them useful for *in vivo* applications.^[105-108] PMMA is a FDA approved polymer for some *in vivo* applications (contact and intraocular lenses, filler for bone cavities) and can be combined with versatile polymers to

obtained functional copolymers with fine-tuned properties.^[89,90] Besides synthetic compounds, biopolymers are also well-suited for the preparation of NPs as they offer excellent biocompatibility, good biodegradability as well as multiple functional groups for further conjugation with dyes or drugs. Important representatives amongst others are polysaccharides, such as dextran and chitosan.^[91-94]



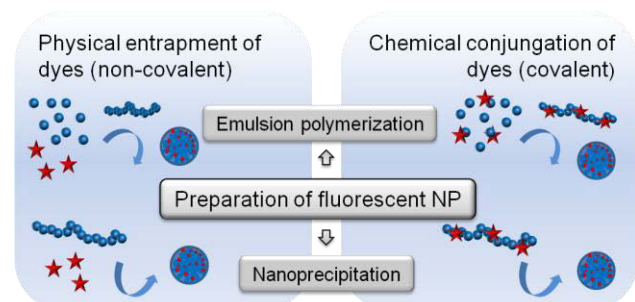
Scheme 2. Synthetic and natural polymers applied for the synthesis of NPs.

3.3 FNPs preparation

For the preparation of FNPs, two different techniques can be applied to embed the fluorophore in a polymer matrix (Figure 1). The non-covalent procedure is characterized by physical entrapment of the dye molecules in the matrix material, either by encapsulation during the particle formation or by diffusion of the dye molecules into the NP core. The physical inclusion method has the advantage that changes in the optical properties evoked by the attachment of the dye to the polymer backbone do not occur. Additionally, the manner of possible dyes is not limited as no functionality on the chromophore is necessary for chemical attachment. However, the dye may leak out of the nanoparticle shell. Such a leakage can be prevented by covalent attachment of the dye to the polymer scaffold.

The fabrication of FNPs is accomplished either by *in situ* polymerization of monomers in an emulsion polymerization or by forcing the polymer material to build nanostructures. For the latter method, single or double emulsification, solvent-displacement/nanoprecipitation, electro spraying, salting out, supercritical- and microfluidic processes as well as the inkjet printing of NPs were developed;^[95-99] thereby emulsion and nanoprecipitation technique are most frequently used. Emulsion polymerization relies on the formation of oil droplets containing the monomer units that are stabilized in water by surfactants.^[100] After the (nano-)emulsion is formed and homogenized, a polymerization reaction occurs within the existing nanodroplets leading to the formation of nanoparticles. Using this preparation technique, different particle sizes with narrow size-distributions can be achieved by controlling various parameters such as the type of surfactants, the solvent/non-solvent ratio, and the reaction time. Dye molecules can be mixed with monomer molecules leading to the entrapment of the dye into the

emerging matrix. The covalent attachment can be realized by copolymerization of original and dye-functionalized monomers.



5 **Figure 1.** Common preparation techniques of polymeric FNPs.

To obtain FNPs *via* the single emulsion technique, the labeled polymer units (covalent method) or a mixture of the polymer and the hydrophobic dye molecules (non-covalent method) are dissolved in a water-immiscible organic solvent (e.g. ethyl acetate, dichloromethane). Subsequently, the organic phase is emulsified in water with usage of appropriate surfactants (poly(vinylalcohol), polysorbate 20) to stabilize the particles, following the evaporation of the organic solvent. Hydrophilic dyes can be encapsulated by the double emulsion process.^[101,102] In this approach, the dye is dissolved in a small volume of an aqueous phase and emulsified in an organic phase that contains the polymer. The mixture is emulsified again in a larger amount of aqueous media. Comparable to emulsion polymerization, the particle size and degree of dye loading can be influenced by the type of polymer and solvents, concentrations, surfactants, emulsification time, and other formulation conditions.

Polymeric NPs are further produced by the nanoprecipitation method (also called solvent displacement) (**Figure 1**).^[97,103-105]

This method presents an alternative, easy, low cost as well as time efficient way to produce polymeric NPs and can be realized in a high-throughput manner.^[106,107] Thereby, particles are readily constructed by exposure of a polymer solution (organic phase) to a non-solvent (water). The major advantages of the nanoprecipitation process over the emulsification procedures are the non-requirement of surfactants and that no additional energy for sonification is required. Moreover, by variation of the initial conditions, such as the solvent/non-solvent ratio and the concentration of the polymer solution, the NP sizes can be tuned from a few nanometers up to 1 μm .^[106] For the dye labeling, the dye molecules are mixed with the polymer in the organic phase prior precipitation, and the dyes are encapsulated during the collapse or arrangement of the polymer molecules; not included dyes can be removed by washing procedures.

To achieve FNPs *via* a covalent procedure, active groups, such as carboxylic groups, amine functionalities or entities that may perform click reactions, are introduced into the polymer backbone for reaction with the dye molecules. Likewise, the dyes also have to provide at least one functionality that can react with the polymer without changing the fluorescence properties. By usage of coupling agents, high conversions can be reached,

though very often a low degree of dye substitution (e.g. few dye molecules per polymer chain) is sufficient as the particles contain multitudes of polymer molecules.

3.4 Design of smart NPs

Manifold biophysicochemical parameters are the key for NPs fate *in vivo*, which emphasizes that NP characteristics, such as size, shape, surface properties, and target unit, should be adjusted very carefully with regard to the final application of the nanocarriers.^[108-111] By implementation of targeting concepts, NPs can be directed to desired active sites (tumors) without adverse effects such as fast clearance by the macrophagocytotic system (MPS) or accumulation in healthy tissue. For improved diagnostic it is essential that the FNPs accumulate, but to a great extend, only in the target site to avoid interferences and to achieve high signal-to-background ratios for refined tumor detection.

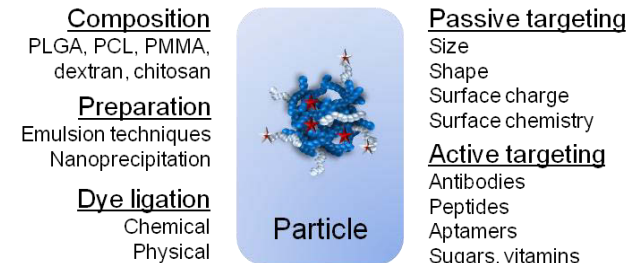


Figure 2. Important parameters for the design of polymeric NPs.

3.4.1 Passive targeting

Size

One of the most important parameters in the NP design is the size. It is evident that particles aimed for intravenous injection should be in a size range not larger than 1 μm in order to ensure long-term *in vivo* circulation without causing any thrombolytic reactions.^[1] In contrast, particles administered to the lung by aspiration of an aerosol can be in the range of several micrometers, and for GI tract imaging the particle size is supposed to be even less important.^[112] In literature, controversial size specifications are found for NPs to be used for *in vitro* and *in vivo* applications.^[107,110-114] The data range thereby from small particles below 10 nm up to 500 nm sized NPs. While NP with a diameter approximately below 30 nm show an efficient cell uptake, they are also rapidly cleared by glomerular filtration in the kidney. Contrary, larger NPs (> 200 nm) show a decreased internalization into cells and increased accumulation in spleen and liver.^[110] The optimal NP diameter is expected to be in the range of 30 to 200 nm, since NPs in that size range benefit from the enhanced permeation and retention (EPR) effect.^[115] The EPR effect exploits that the tumor tissue exhibits different structural features compared to normal cells, such as leaky vessels with enlarged gap functions

due to rapid angiogenesis.^[116] These features enable an enhanced extravasation of particulate material from the surrounding vessel into the tumor. Due to the lack of a lymphatic system, the retention time of NPs in tumors is prolonged, which further increases the preferential NPs accumulation. However, there is no general admitted optimum dimension for all NPs systems as the size dependent uptake also relies on other physicochemical properties and the tumor characteristics itself. Tumor tissue can be very heterogen, and the vascular permeability can be limited in a range of 100 nm up to 2 μm sized particles. Some tumor types show no EPR effect at all, and, accordingly, an active targeting is essential.^[117]

Shape

De Simone and co-workers studied the internalization of differently shaped NPs produced by the PRINT technology.^[118] Thereby, it was investigated that rod-like NPs with high aspect-ratios were internalized faster in comparison to spherical once with similar volume.^[108] Caruso et al. used the “surface-area to volume ratio” (SAV) as parameter to describe all geometric features (size, shape, surface area) in one value. It was found that the SAV affects the biodistribution and cellular uptake of the NPs significantly.^[119] In detail, with increasing SAV the phagocytotic uptake tends to decrease (due to flow alignment effects) whereas the cellular uptake increases (due to improved surface interaction).^[119] It was predicted that prolate ellipsoids and discoidal shapes possess prolonged circulation times in comparison to spherical NPs and are internalized most effectively. For the final conclusion, which SAV ratio is most beneficial for enhanced NP uptake, further studies are indispensable.

Surface charge and chemistry

In addition to the size and shape, the characteristics of the NPs surface greatly influences the retention time and cell recognition of the NP.^[120] Qualities, such as the surface charge, the surface hydrophobicity and further functionalization with ligands and polymers can significantly affect the interactions of the particles in suspension with cells and proteins. It was explored that positively charged particles reveal a high cellular uptake through endocytosis as a result of the intensified attraction with the negatively charged cell membrane (due to the presence of phospholipid groups). But, simultaneously, they also show increased non-specific interactions and non-desired internalization.^[110,111] Contrary, strong negatively charged NPs reveal decreased plasma protein absorption as well as non-specific interactions, but also lower cellular uptake efficiencies.^[111] Thus, for prolonged blood circulation times and an efficient cellular uptake, a neutral NP charge is recommended.^[109-111,114] For the influence of the hydrophilicity and hydrophobicity it was remarked that hydrophobic NPs revealed enhanced cellular uptake, but also an increased absorption of proteins that leads to a fast blood clearance.^[121] In order to achieve prolonged blood circulation times and to minimize the nonspecific protein binding, very often NPs are

surface-functionalized with additional ligands or polymers. Reactive groups, such as carboxylic acids and amino moieties, which are present at the surface, can be used for the ligand conjugation. Thereby, carbodiimide-mediated amide and maleimide coupling reactions as well as click chemistry represent exquisite techniques. Most frequently applied in the field of NPs surface functionalization is the attachment of poly(ethylene glycol) (PEG). The effect of PEGylation is nowadays well-known, intensively reviewed, and will be therefore not further discussed.^[122,123]

3.4.2 Active targeting

In cell culture experiments reproducible internalization rates at specific sites due to defined physical parameters of the NPs is possible, but for *in vivo* applications an active targeting of the NPs is essential to ensure a controlled accumulation in the desired tissue.^[41,124,125] The idea is to conjugate ligands to the NPs surface, which bind specifically to antigens or receptors that are only expressed on the target cells.^[126] By utilization of such ligand-receptor interactions, a specific tumor accumulation can be achieved.^[127,128] Although this concept seems simple, it has to be considered that the NPs are aimed for clinical usage. Hence, they should be manufactured in a reproducible manner with a controlled and defined ligand conjugation. Furthermore, the stability in biological environment, including also consistency against pH changes and hydrolysis must be guaranteed. At the same time, the bioactivity of the target unit after the conjugation to the particle should remain unchanged. The active targeting approach is realized most frequently *via* simple and efficient covalent bioconjugation techniques, or by electrostatic interactions of the ligands to the particle surface.^[124] Still, obstacles of weak reproducibility and poor control about the ligand density remain. To overcome these hurdles, a pre-targeting of the polymer with subsequent particle formation is feasible, and the number of target moieties can be tuned very efficiently.^[129]

Antibodies

As targeting ligands, often antibodies (AB), peptides, nucleic acids and other small molecules are used.^[128] Antibodies are large molecules, which are able to bind highly selectively to antigens, which are unique parts of each cell line. Common FDA approved representatives are the chimeric AB (rituximab) that binds to a CD20 antigen and is applied in the treatment of non-Hodgkins lymphoma as well as the humanized AB (trastuzumab) that is used in breast cancer therapy due to its selectivity to the HER2/neu antigen.^[130-132] Unfortunately, apart from their high selectivity, ABs are large (~150 kDa), expensive and potentially immunogenic. To lower the side effects of the AB, recently antibody fragments (Fab, nanobodies) including antigen-binding fragments or small antibody mimetics, such as affibodies, are applied as target units.^[133,134]

Peptides

The conjugation of peptides is convincing as they are of smaller size, increased stability with subsequent decreased immunogenicity, and easy to manufacture.^[131,135] Well-known members are the cyclo(arginine-glycine-aspartate) (cRGD) peptides that displays a selectivity to $\alpha_v\beta_3$ integrin receptors in tumor cells.^[136] The commercial derivative Cilengitide is tested in clinical phase III for lung cancer as well as pancreas treatment and in phase II for several other tumors.^[131,137] The drawback of peptides is their relatively low affinity for the aimed site and the subsequent occurrence of non-specific adhesion to normal tissue. Multiple peptide conjugation on the particle surface might reduce this problem, but still more effort is necessary to develop new derivatives with improved selectivity.

15 *Aptamers*

A high target specificity, owing to their unique conformations, is warranted by the usage of nucleic acids segments (aptamers).^[138,139] Aptamers are short single-stranded DNA or RNA oligonucleotides consisting of 15 to 40 base pairs and are low immunogenic as well as easy to manufacture and scale up.^[140] The 2'-fluoro-pyridine-RNA aptamer is known to targeted the prostate specific membrane antigen (PSMA) and is currently in clinical phase II.^[124]

25 *Sugars and vitamins*

Small molecules, such as sugars and vitamins, are also utilized as target moieties. For instance, folic acid (FA), a member of vitamin B family, participates in the biosynthesis of nucleic and amino acids and shows a high selectivity to folate receptors that are overexpressed in tumor cells.^[141] Important folate derivatives in clinical trails are the indium-111-labeled diethylenetriamine pentaacetic acid (DTPA)-folate and the vintafolide (EC145). EC145 is a FA-drug conjugate, which consists of FA attached to the vinca alkaloid desacetylvinblastine monohydrazone and showed a high anti-tumor effect against subcutaneous FR-positive tumor xenografts.^[124,142] Moreover, it was investigated that tumors show a high affinity to sugar units (glucose, mannose or galactose).^[143] The preferential accumulation of sugars is further supported by the presence of special carbohydrate-binding proteins (membrane lectins) on the cell surface. As a result, sugars are profitable targets, which are convincing with easy synthesis, good biocompatibility and high affinity. Despite the wide field of possible target moieties and the manifold reaction paths for their attachment, until now only three targeted polymeric NPs have progressed to clinical trials for drug delivery application.^[37-41] For one, a PEGylated cyclodextrin-based NP that contains human transferrin as a targeting ligand for binding to transferrin receptors, which are typically upregulated on cancer cells, is utilized to deliver siRNA.^[37] In addition, a PLGA-PEG based nanoparticle containing the anti-cancer drug docetaxel and a ligand that targets the prostate-specific membrane antigen (PSMA) is now in clinical trials in people (BIND-014).^[38] Moreover, a polymer based NP functionalized with nicotine and PEG containing a synthetic

TLR agonist, a novel universal T cell helper peptide, is applied against nicotine for smoking cessation (SEL-068).^[40] The low number of clinically applied targeted polymeric NPs clearly demonstrates the challenges that come along with the development of such designed nanocarriers.

A limiting factor of capital importance accompanied with the targeting concept is the controlled and reproducible production of NPs that fulfill the good manufacture practice (GMP) guidelines. Aside from that, there is still an insufficient understanding of the NP interactions and distributions *in vivo*. In order to realize the usage of targeted NPs in clinical applications, it is required to gain more knowledge about their *in vivo* stability, circulation behavior, their interactions with blood, proteins and cells as well as their definite faith. The development of new screening methods, which enable the study of various NPs systems, might help to gain more insights into the NP and their interplay with the biological environment.^[41] Nevertheless, in the past few years a great progress in the development of targeted nanosystems was observed, and many promising studies demonstrate the huge potential of targeted polymeric NPs for selective imaging as well as controlled drug delivery. A selection of recently performed *in vivo* studies of fluorescent NPs for cancer imaging applications are presented in **Table 1** and reviewed in the following.

80 **4. Recent *in vivo* studies of fluorescent NP systems**

4.1 PLGA/PLA and PCL based NPs

Due to the well-known biocompatibility and biodegradability, many studies utilize PLGA as matrix material for the NP preparation and encapsulation of cyanine dyes, such as ICG and Cy-5 to investigate the NP detection ability, biodistribution and circulation behavior *in vivo* in comparison to free fluorescent dye molecules (**Table 1**).^[144,145] Thereby, two major benefits of the FNPs were found: The particles could be nicely detected *in vivo* and the resulting dye concentrations in all organs (liver, spleen, lung, heart and kidney) were significantly increased compared to free dye molecules.^[145] The results clearly demonstrate the potential of polymeric NP for diagnostic application, though the accumulation of NPs was not specific. Since this is a fundamental requirement for excellent disease diagnostic, it becomes obvious that a targeting strategy is essential. As mentioned before a passive targeting can be realized *via* size dependent accumulation. To study the size effect in tumors, PEGylated fluorescent PLGA NPs with three different sizes were prepared by co-nanoprecipitation of the polymer with DiR fluorophores.^[146] The *in vivo* fate of the resulting NPs was studied in two different xenograft tumor types, the HT29 (colorectal carcinoma) and the A2780 (ovarian carcinoma) cell lines. It was observed that small NP batches (d = 111 and 141 nm) accumulated efficiently in the human xenograft tumor tissue, while slightly larger NPs (d = 166 nm) were rapidly eliminated by the liver. Nevertheless, passive

targeting does not solve the drawback of undesired accumulation of the NP in other organs.

To obtain a more tumor specific uptake, FA was attached to PLGA and FNPs were obtained *via* co-nanoprecipitation of the PLGA and ICG. The tagged nanocarriers (FA-ICG-PLGA) were evaluated *in vitro* with regard to their targeting characteristics using a human mammary gland adenocarcinoma cell line (MCF-7), which overexpresses the folate (FA) receptor.^[147] The fluorescence imaging properties and biodistribution of the FA-ICG-PLGA NPs were studied in nude mice bearing MCF-7 cell tumors. As expected, a prolonged circulation time in comparison to free ICG was obtained and uptake experiments proved the higher targeting efficiency of the FA-ICG-PLGA NPs in folate receptor overexpressing MCF-7 cells compared to folate receptor negative A549 cells. Furthermore, it was proven (Figure 3) that 24 h after injection no detectable signal of free ICG and ICG-PLGA NPs was recorded in the tumor. In contrast, the FA-ICG-PLGA NPs provided a significant fluorescence signal in the tumor. Similar PEGylated NPs consisting also of FA-targeted PLGA particles containing ICG were further studied in mice xenografted with MDA-MB-231 human breast cancer cells.^[148] The study demonstrated that the dual surface modification with PEG and FA significantly helped targeting and accumulating the nanoparticles in the tumor tissue.

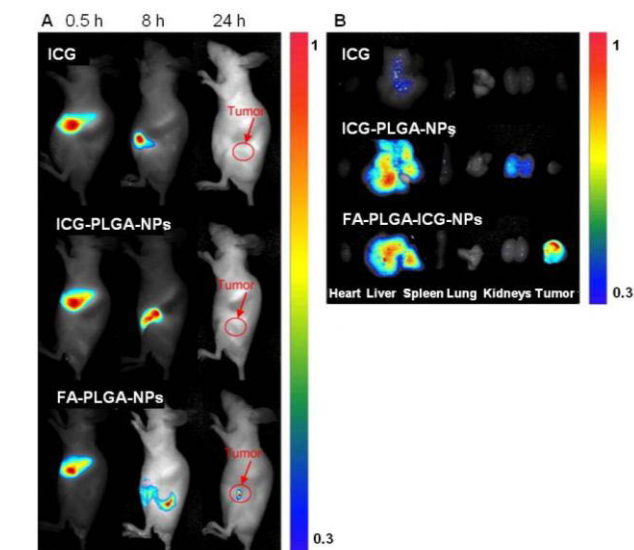


Figure 3. *In vivo* imaging of FA-ICG-PLGA NPs compared with ICG-PLGA NPs and free ICG as controls after injections in nude mice implanted with human breast tumors (MCF-7). (A) *In vivo* images taken at 0.5, 8, 24 h time point. (B) Fluorescence images of organs and tumors 24 h after injection. Reprinted with permission from ref 152. Copyright 2012 Elsevier.

In another example, NPs were obtained by nanoprecipitation of a PLA-PEG copolymer with covalently attached Cy-5 and aptamer.^[149] The resulting Cy-5-PLA-PEG-aptamer NPs revealed a size of 157 nm and high tumor specificity by *in vitro* measurements in PSMA-positive LNCaP cells. The *in vivo*

detection was proven with the non-targeted and non-PEG functionalized Cy5-PLA NPs. Other studies with PEG-PLGA based NP systems that utilized cRGD as target moiety examined the specific accumulation in breast cancer cells as well as pancreatic cancer in mouse models.^[150,151] In detail, 180 nm sized mPEG-PLGA-PLL-cRGD NPs with encapsulated rhodamine and the anti-tumor drug mitoxanthrone were prepared by nanoprecipitation and showed a preferentially tumor accumulation with decreased accretion in the heart.^[150] Furthermore, PLGA-4-arm-PEG NPs were loaded with the IR-140 dye, revealing sizes in the range of 150 to 180 nm.^[151] Similar to the previously mentioned study, an increased NP accumulation in the tumor in comparison to the controls was observed even after 1 h. The biodistribution of the NPs was studied *ex vivo* after 48 h and revealed primary accumulation in the tumor. Accumulation in liver and spleen was significantly reduced after one week of treatment, which proves the great potential of polymeric NP as imaging agents for cancer detection.

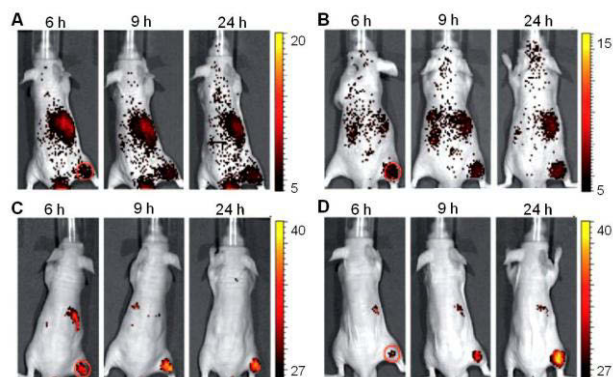


Figure 4. *In vivo* images of tumor-bearing mice after injection of ICG-PMMA-PEG NPs. Targeting concept: (A) Non-targeted, (B) folate (C), RGD, (D) GA. Color code: low intensity black, high intensity yellow, and tumor site red circle. Reprinted with permission from ref 160. Copyright 2012 John Wiley and Sons.

4.2 PS, PMMA and chitosan based NPs

Poly(acrylate-*co*-styrene) based imaging agents with entrapped coumarin 6 as fluorophore were prepared *via* nanoprecipitation.^[152-154] The PS nanospheres were targeted with peanut agglutinin (PNA) that binds to the glycoprotein Gal- β (1-3) GalNAc, which is over-expressed on tumor cells. As proven in a human colorectal cancer orthotropic mouse model, the PNA-PS-NPs recognize millimeter-sized tumors on the mucosal surface with high affinity and specificity.

Table 1. Selected studies of fluorescent NP systems prepared by nanoprecipitation for cancer detection *in vivo*.

	Polymer	Dye	Active target	Dye ligation	Size [nm]	Detection/ application	Ref
1	PLGA	ICG	-	Physical	300	Increased organ accumulation	[145]
2	PLGA	Cy-5	-	Chemical		Study of lymphatic biodistribution for detection of metastatic cancer	[144]
3	PLGA-PEG	DiR	-	Physical	110 – 160	Size-dependent passive tumor accumulation studies	[146]
4	PLGA	ICG	Folate	Physical	105	Breast cancer	[147]
5	PEG-PLGA	ICG	Folate	Physical	200 – 300	Breast cancer	[148]
6	PLA-mPEG	Cy-5	Aptamer	Chemical	157	Prostate carcinoma	[149]
7	mPEG-PLGA-PLL	Rhodamine B	cRGD	Chemical	180	Breast cancer	[150]
8	PLGA-4-arm-PEG	IR-140/nile red	cRGD	Physical	170	Pancreas carcinoma	[151]
9	PS-PNVA-PMMA	Coumarin 6	PNA	Chemical	180 – 300	Colorectal carcinoma	[152,153]
10	PCMS	Naphthalimide	Folate	Chemical	86	Breast cancer	[155]
11	PMMA-PEG	ICG	cRGD, GA	Chemical	200	Epithelial carcinoma	[156]
12	Chitosan	Cy-5.5	5 β -Cholanic acid	Chemical	260	Brain tumors, liver tumors, metastasis tumor models	[157,158]

Detailed biological studies also revealed good stability and no cytotoxicity. Also a high targeting efficiency to malignant cancer tissue compared to other organs was found for poly(chloromethyl-styrene) (PCMS) NPs ($d = 86$ nm) that were functionalized with a naphthalimide derivative (NA) as ligand and FA as target units.^[155] To study the specific tumor uptake, various targeting units, such as folic acid, glucose amine (GA) and RGD, were conjugated to an PMMA-PEG copolymer with covalently attached ICG.^[156] After assembly in water, the different NPs possess a size of 200 nm and were intravenously injected to mice with subcutaneous tumor xenograft. Non-targeted and FA tagged NPs showed accumulation in the tumor, liver, spleen, heart and lung (**Figure 4**). In contrast, the copolymers that were targeted with GA and RGD showed rapid and more efficient accumulation in tumor tissues with only low side accumulation in the liver. This effect was explained by the 10 times higher hydrophilicity of RGD and GA in comparison to folate molecules that might prefer to hide inside the more hydrophobic environment.^[156] Although the difference of the folate targeted copolymer is not yet fully understood, the study proved that stable NP systems combined with efficient targeting strategies enable selective tumor detection.

Furthermore, cancer-specific chitosan particles (CNPs) with an average diameter of about 260 nm were prepared from glycol chitosan that was chemically modified with hydrophobic 5 β -cholanic acid and labelled with Cy5.5. The NPs were also loaded with a drug for combined cancer detection and treatment (**Figure 5**).^[157] The Cy5.5-labeled CNPs exhibited significantly increased tumor accumulation in brain tumors, liver tumors, and metastasis tumor models with low nonspecific uptake by other tissues in tumor-bearing mice proving their great potential in both cancer imaging and therapy.^[158]

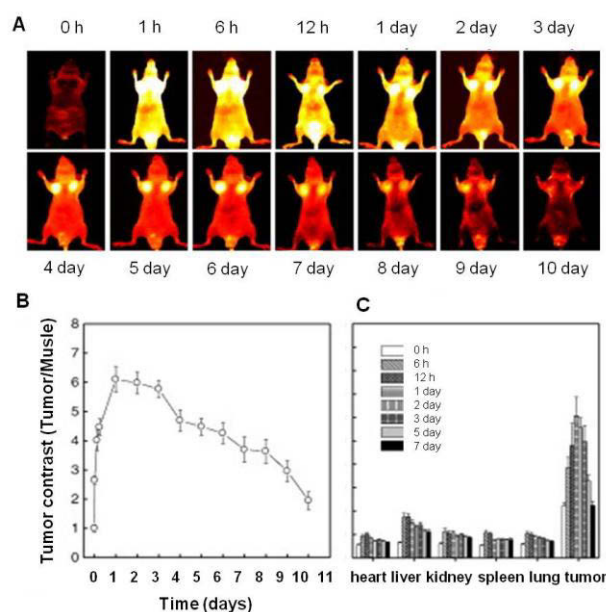


Figure 5. (A) *In vivo* biodistribution of Cy5.5-CNPs in SCC7 tumor-bearing mice after intravenously injection. (B) Time-dependent tumor contrast after administration of Cy5.5-labeled CNPs into tumor-bearing mice. (C) *Ex vivo* imaging of SCC7 xenograft tumor showed higher NIRF signal than other organs at all time points. Reprinted with permission from ref 162. Copyright 2012 Elsevier.

5 Conclusion and prospective

Within the last few years, a variety of novel fluorophores with emission in the NIR range were synthesized that enable a superior detection *in vivo*, and relieved the fluorescence imaging from the limitation to be only applied for thin sections. Besides the development of cancer targeted dyes, the concept of the encapsulation of dye molecules into a polymeric matrix seems advantageous, in particular in terms of fluorophores that are already approved by the FDA, e.g., ICG and MB. These dyes were not developed to be used as contrast agents for image-guided surgery and reveal only a low photostability. By using NPs as templates, multiple fluorophores can be loaded into the NPs and the dye molecules are protected against the biological environment leading to smart and tailor-made particles with enhanced fluorescence intensity and improved *in vivo* imaging. Another advantage of FNPs is the ability to precisely engineer them to their specific applications by variation of the polymer, the preparation method, and the kind of surface functionalization. Complementary to the passive targeting effect, which is mainly based on the size, shape, surface charge and chemistry of the NPs, also active targeting with ligands can be exploited to reach a high circulation time and tumor specificity. In all reviewed studies, an enhanced tumor accumulation of NPs compared to free dye molecules was reported. Furthermore, the ability to overcome various mentioned drawbacks of single dye molecules (instability, interaction with proteins, low signal-to-background ratios) by usage of targeted polymeric NPs as matrix for fluorescent dyes was proven. Although the results are difficult to interpret as various parameters affect the efficiency of the NPs, it was demonstrated that the targeting unit is one of the most important factors to affect the particle faith *in vivo* and is a prerequisite for improved diagnostic. The most promising systems seem to be PLGA-PEG copolymer based NPs that contain ICG dye molecules. Owing to the existing FDA approval for the polymers and the dye, these might be the first systems used in clinical studies. As targeting moieties, cRGD or aptamers seem convincing in terms of their high tumor specificity. Although folate is also often utilized as target moiety, it appears that folate receptors are also keenly expressed in other organs leading to increased accumulation in the non-target site. However, to become a clinical reality, the controlled and reproducible production of FNPs must be guaranteed. Fortunately, significant progress was made within the last years in the preparation of well-defined NPs. Nowadays, manifold advanced polymerization methods can be used to obtain (co-)polymers with distinct properties.^[159,160] For the fabrication of safe FNPs, it becomes obvious that the labelling of the polymers should be realized *via* chemical attachment to the polymer backbone in order to prevent adverse leakage of the fluorophores and to ensure a reproducible dye loading. Today, the labelling of multifunctional polymers with desired dyes can be performed using non-toxic coupling agents as well as click chemistry, and the resulting fluorescent polymers can be

comprehensively characterized by sophisticated techniques, such as multidimensional chromatography and modern mass spectrometry.^[107,161-163] Furthermore, with the application of high-throughput approaches, such as nanoprecipitation performed *via* pipetting robots, the reproducible and controlled preparation of NPs with adjustable properties could be realized.^[106]

Since there is still an insufficient understanding how NPs interact and distribute *in vivo*, the major goal within the next years will be the systematical study of promising systems with regard to their distribution and interaction within the body, in order to explore the optimal parameters in terms of dye loading, core/shell ratio, and specific target unit. While the theory appears very straightforward, reams of *in vitro* and *in vivo* studies remember consistently that the major problem remains: How can the knowledge be transferred from the cuvette to the cell to the mice and, finally, to the human body?

Acknowledgement

The Thuringian Ministry for Education, Science and Culture (grant #B514-09051, NanoConSens) is gratefully acknowledged.

6 References

- [1] M. Elsabahy, K. L. Wooley, *Chem. Soc. Rev.* **2012**, *41*, 2545-2561.
- [2] R. Duncan, R. Gaspar, *Mol. Pharm.* **2011**, *8*, 2101-2141.
- [3] M. Chakraborty, S. Jain, V. Rani, *Appl. Biochem. Biotechnol.* **2011**, *165*, 1178-1187.
- [4] P. Tallury, A. Malhotra, L. M. Byrne, S. Santra, *Adv. Drug Deliv. Rev.* **2010**, *62*, 424-437.
- [5] J. Napp, J. E. Mathejczyk, F. Alves, *Pediatr. Radiol.* **2011**, *41*, 161-175.
- [6] J. Merian, J. Gravier, F. Navarro, I. Texier, *Molecules* **2012**, *17*, 5564-5591.
- [7] L. Soon, F. Braet, J. Condeelis, *Microsc. Res. Tech.* **2007**, *70*, 252-257.
- [8] J. Wyckoff, B. Gligorijevic, D. Entenberg, J. Segall, J. Condeelis, *Cold Spring Harb Protoc.* **2011**, 1167-1184.
- [9] V. E. Centonze, J. G. White, *Biophys. J.* **1998**, *75*, 2015-2024.
- [10] M. Manfredini, F. Arginelli, C. Dunsby, P. French, C. Talbot, K. Koenig, G. Pellacani, G. Ponti, S. Seidenari, *Skin Res. Technol.* **2013**, *19*, E433-E443.
- [11] F. Leblond, S. C. Davis, P. A. Valdes, B. W. Pogue, *J. Photochem. Photobiol. B: Biol.* **2010**, *98*, 77-94.
- [12] N. Ramanujam, J. X. Chen, K. Gossage, R. Richards-Kortum, B. Chance, *IEEE Trans. Biomed. Eng.* **2001**, *48*, 1034-1041.
- [13] S. J. Miller, B. P. Joshi, Y. Feng, A. Gaustad, E. R. Fearon, T. D. Wang, *Plos One* **2011**, *6*, e17384.
- [14] S. Keereweer, J. D. F. Kerrebijn, P. B. A. A. v. Driel, B. Xie, E. L. Kaijzel, T. J. A. Snoeks, I. Que, M. Hutteman, J. R. v. d. Vorst, J. S. D. Mieog, A. L. Vahrmeijer, C. J. H. v. d. Velde, R. J. B. d. Jong, C. W. G. M. Löwik, *Mol. Imag. Biol.* **2011**, *13*, 199.
- [15] E. A. te Velde, T. Veerman, V. Subramaniam, T. Ruers, *Eur. J. Surg. Oncol.* **2010**, *36*, 6-15.
- [16] L. Thiberville, M. Salauen, S. Lachkar, S. Dominique, S. Moreno-Swirc, C. Vever-Bizet, G. Bourg-Heckly, *Eur. Respir. J.* **2009**, *33*, 974-985.

- [17] S. Foersch, A. Heimann, A. Ayyad, G. A. Spoden, L. Florin, K. Mpoukouvalas, R. Kiesslich, O. Kempfski, M. Goetz, P. Charalampaki, *Plos One* **2012**, *7*, e41760.
- [18] K. Polom, D. Murawa, Y.-s. Rho, P. Nowaczyk, M. Huenerbein, P. Murawa, *Cancer* **2011**, *117*, 4812-4822.
- [19] J. T. Alander, I. Kaartinen, A. Laakso, T. Patila, T. Spillmann, V. V. Tuchin, M. Venermo, P. Valisuo, *Int. J. Biomed. Imag.* **2012**, 940585.
- [20] J. S. D. Mieog, A. L. Vahrmeijer, M. Hutteman, J. R. van der Vorst, M. D. van Hooff, J. Dijkstra, P. J. K. Kuppen, R. Keijzer, E. L. Kaijzel, I. Que, C. J. H. van de Velde, C. W. G. M. Lowik, *Mol. Imag.* **2010**, *9*, 223-231.
- [21] S. Gioux, H. S. Choi, J. V. Frangioni, *Mol. Imag.* **2010**, *9*, 237-255.
- [22] M. Hutteman, "Image-guided surgery using invisible near-infrared fluorescent light: from pre-clinical studies to clinical validation", Doctoral thesis, Leiden University, **2011**.
- [23] H. Kobayashi, M. Ogawa, R. Alford, P. L. Choyke, Y. Urano, *Chem. Rev.* **2010**, *110*, 2620-2640.
- [24] S. L. Luo, E. L. Zhang, Y. P. Su, T. M. Cheng, C. M. Shi, *Biomaterials* **2011**, *32*, 7127-7138.
- [25] S. A. Hilderbrand, R. Weissleder, *Curr. Opin. Chem. Biol.* **2010**, *14*, 71-79.
- [26] C. E. Badr, B. A. Tannous, *Trends Biotechnol.* **2011**, *29*, 624-633.
- [27] B.-W. Xie, I. M. Mol, S. Keereweer, E. R. van Beek, I. Que, T. J. A. Snoeks, A. Chan, E. L. Kaijzel, C. W. G. M. Lowik, *Plos One* **2012**, *7*, e31875.
- [28] X. He, K. Wang, Z. Cheng, *Wiley Interdisciplinary Reviews-Nanomedicine and Nanobiotechnology* **2010**, *2*, 349-366.
- [29] A. Valizadeh, H. Mikaeili, M. Samiei, S. M. Farkhani, N. Zarghami, M. Kouhi, A. Akbarzadeh, S. Davaran, *Nanoscale Res. Lett.* **2012**, *7*, 480-480.
- [30] Kim M. Tsoi, Q. Dai, B. A. Alman, W. C. W. Chan, "Are Quantum Dots Toxic? Exploring the Discrepancy Between Cell Culture and Animal Studies.", in *Acc. Chem. Res.*, 201210.1021/ar300040z.
- [31] W. Liu, M. Howarth, A. B. Greytak, Y. Zheng, D. G. Nocera, A. Y. Ting, M. G. Bawendi, *J. Am. Chem. Soc.* **2008**, *130*, 1274-1284.
- [32] B. E. Schaafsma, J. S. D. Mieog, M. Hutteman, J. R. Van der Vorst, P. J. K. Kuppen, C. W. G. M. Lowik, J. V. Frangioni, C. J. H. Van de Velde, A. L. Vahrmeijer, *J. Surg. Oncol.* **2011**, *104*, 323-332.
- [33] A. Mukerjee, A. P. Ranjan, J. K. Vishwanatha, *Curr. Med. Chem.* **2012**, *19*, 3714-3721.
- [34] A. Wagh, S. Y. Qian, B. Law, *Bioconjug. Chem.* **2012**, *23*, 981-992.
- [35] J. Napp, T. Behnke, L. Fischer, C. Wuerth, M. Wottawa, D. M. Katschinski, F. Alves, U. Resch-Genger, M. Schaeferling, *Anal. Chem.* **2011**, *83*, 9039-9046.
- [36] S. Jiang, M. K. Gnanasammandhan, Y. Zhang, *J. R. Soc. Interface* **2010**, *7*, 3-18.
- [37] M. E. Davis, *Mol. Pharm.* **2009**, *6*, 659-668.
- [38] <http://clinicaltrials.gov/ct2/show/NCT01300533>, "A Study of BIND-014 Given to Patients With Advanced or Metastatic Cancer", Last updated: August 1, **2012**.
- [39] <http://clinicaltrials.gov/ct2/show/NCT01478893>, "Safety and Pharmacodynamics of SEL-068 Vaccine in Smokers and Non-Smokers", Last updated: November 21, **2011**.
- [40] L. Pittet, D. Altmutter, P. Ilyinskii, C. Fraser, Y. Gao, S. Baldwin, M. Keegan, L. Johnston, T. Kishimoto, *J. Immunol.* **2012**, *188*, 75.11.
- [41] N. Kamaly, Z. Xiao, P. M. Valencia, A. F. Radovic-Moreno, O. C. Farokhzad, *Chem. Soc. Rev.* **2012**, *41*, 2971-3010.
- [42] M. Fernandez-Suarez, A. Y. Ting, *Nat. Rev. Mol. Cell Bio.* **2008**, *9*, 929-943.
- [43] K. Koc, I. Anik, B. Cabuk, S. Ceylan, *Br. J. Neurosurg.* **2008**, *22*, 99-103.
- [44] P. J. Fenton, *Br. J. Ophthalmol.* **1965**, *49*, 205-&.
- [45] X.-D. Jiang, R. Gao, Y. Yue, G.-T. Sun, W. Zhao, *Org. Biomol. Chem.* **2012**, *10*, 6861-6865.
- [46] J. W. Park, Y. Kim, K.-J. Lee, D. J. Kim, *Bioconjug. Chem.* **2012**, *23*, 350-362.
- [47] Y. Duan, M. Liu, W. Sun, M. Wang, S. Liu, Q. X. Li, *Mini-Rev. Organic Chem.* **2009**, *6*, 35-43.
- [48] J. E. Berlier, A. Rothe, G. Buller, J. Bradford, D. R. Gray, B. J. Filanowski, W. G. Telford, S. Yue, J. X. Liu, C. Y. Cheung, W. Chang, J. D. Hirsch, J. M. Beechem, R. P. Haugland, *J. Histochem. Cytochem.* **2003**, *51*, 1699-1712.
- [49] N. Panchuk-Voloshina, R. P. Haugland, J. Bishop-Stewart, M. K. Bhalgat, P. J. Millard, F. Mao, W. Y. Leung, *J. Histochem. Cytochem.* **1999**, *47*, 1179-1188.
- [50] P. Sarkar, S. Sridharan, R. Luchowski, S. Desai, B. Dworecki, M. Nlend, Z. Gryczynski, I. Gryczynski, *J. Photochem. Photobiol. B.* **2010**, *98*, 35-39.
- [51] J. Pauli, R. Brehm, M. Spieles, W. A. Kaiser, I. Hilger, U. Resch-Genger, *J. Fluoresc.* **2010**, *20*, 681-693.
- [52] E. M. Sevick-Muraca, *Annu. Rev. Med.* **2012**, *63*, 217-231.
- [53] M. P. Shandura, V. P. Yakubovskiy, A. O. Gerasov, O. D. Kachkovskiy, Y. M. Poronik, Y. P. Kovtun, *Eur. J. Org. Chem.* **2012**, *9*, 1825-1834.
- [54] Y. Hama, Y. Urano, Y. Koyama, P. L. Choyke, H. Kobayashi, *Biochem. Biophys. Res. Commun.* **2006**, *348*, 807-813.
- [55] S. Shukla, A. P. Skoumbourdis, M. J. Walsh, A. M. S. Hartz, K. L. Fung, C.-P. Wu, M. M. Gottesman, B. Bauer, C. J. Thomas, S. V. Ambudkar, *Mol. Pharm.* **2011**, *8*, 1292-1302.
- [56] A. Matsui, E. Tanaka, H. S. Choi, V. Kianzad, S. Gioux, S. J. Lomnes, J. V. Frangioni, *Surgery* **2010**, *148*, 78-86.
- [57] X. He, X. Wu, K. Wang, B. Shi, L. Hai, *Biomaterials* **2009**, *30*, 5601-5609.
- [58] M. Chu, X. Xiao, J. Ma, A. Ji, R. Yuan, H. Yang, W. Xu, Y. Shao, J. Huang, J. Chen, *Curr. Nanosci.* **2010**, *6*, 388-396.
- [59] A. J. L. Villaraza, D. E. Milenic, M. W. Brechbiel, *Bioconjug. Chem.* **2010**, *21*, 2305-2312.
- [60] K. Sano, M. Mitsunaga, T. Nakajima, P. L. Choyke, H. Kobayashi, *Breast Cancer Res.* **2012**, *14*, R61.
- [61] M. Ogawa, N. Kosaka, P. L. Choyke, H. Kobayashi, *Cancer Res.* **2009**, *69*, 1268-1272.
- [62] J. Pauli, M. Grabolle, R. Brehm, M. Spieles, F. M. Hamann, M. Wenzel, I. Hilger, U. Resch-Genger, *Bioconjug. Chem.* **2011**, *22*, 1298-1308.
- [63] S. B. Qi, Z. Miao, H. G. Liu, Y. D. Xu, Y. Q. Feng, Z. Cheng, *Bioconjugate Chem.* **2012**, *23*, 1149-1156.
- [64] S. Qi, Z. Miao, H. Liu, Y. Xu, Y. Feng, Z. Cheng, *Bioconjug. Chem.* **2012**, *23*, 1149-1156.
- [65] S. Biswas, X. Wang, A. R. Morales, H.-Y. Ahn, K. D. Belfield, *Biomacromolecules* **2011**, *12*, 441-449.
- [66] D. J. Bharali, D. W. Lucey, H. Jayakumar, H. E. Pudavar, P. N. Prasad, *J. Am. Chem. Soc.* **2005**, *127*, 11364-11371.
- [67] X. Wang, A. R. Morales, T. Urakami, L. Zhang, M. V. Bondar, M. Komatsu, K. D. Belfield, *Bioconjug. Chem.* **2011**, *22*, 1438-1450.
- [68] X. Tan, S. Luo, D. Wang, Y. Su, T. Cheng, C. Shi, *Biomaterials* **2012**, *33*, 2230-2239.
- [69] C. Zhang, T. Liu, Y. Su, S. Luo, Y. Zhu, X. Tan, S. Fan, L. Zhang, Y. Zhou, T. Cheng, C. Shi, *Biomaterials* **2010**, *31*, 6612-6617.
- [70] H. Lee, W. Akers, K. Bhushan, S. Bloch, G. Sudlow, R. Tang, S. Achilefu, *Bioconjug. Chem.* **2011**, *22*, 777-784.
- [71] R. Weissleder, C. H. Tung, U. Mahmood, A. Bogdanov, *Nat. Biotechnol.* **1999**, *17*, 375-378.
- [72] M. Ogawa, N. Kosaka, M. R. Longmire, Y. Urano, P. L. Choyke, H. Kobayashi, *Mol. Pharm.* **2009**, *6*, 386-395.
- [73] K. E. Linder, E. Metcalfe, P. Nanjappan, T. Arunachalam, K. Ramos, T. M. Skedzielewski, E. R. Marinelli, M. F. Tweedle, A. D. Num, R. E. Swenson, *Bioconjug. Chem.* **2011**, *22*, 1287-1297.
- [74] J. Li, K. Chen, H. Liu, K. Cheng, M. Yang, J. Zhang, J. D. Cheng, Y. Zhang, Z. Cheng, *Bioconjug. Chem.* **2012**, *23*, 1704-1711.
- [75] V. M. Alexander, K. Sano, Z. Yu, T. Nakajima, P. L. Choyke, M. Ptaszek, H. Kobayashi, *Bioconjug. Chem.* **2012**, *23*, 1671-1679.

- [76] M. Ogawa, N. Kosaka, C. A. S. Regino, M. Mitsunaga, P. L. Choyke, H. Kobayashi, *Molecular Biosystems* **2010**, *6*, 888-893.
- [77] T. Nakajima, M. Mitsunaga, N. H. Bander, W. D. Heston, P. L. Choyke, H. Kobayashi, *Bioconjug. Chem.* **2011**, *22*, 1700-1705.
- [78] B. Ballou, G. W. Fisher, T. R. Hakala, D. L. Farkas, *Biotechnol. Prog.* **1997**, *13*, 649-658.
- [79] O. O. Abugo, R. Nair, J. R. Lakowicz, *Anal. Biochem.* **2000**, *279*, 142-150.
- [80] M. V. Kvach, I. A. Stepanova, I. A. Prokhorenko, A. P. Stupak, D. A. Bolibrukh, V. A. Korshun, V. V. Shmanai, *Bioconjug. Chem.* **2009**, *20*, 1673-1682.
- [81] R. Simmons, S. Thevarajah, M. B. Brennan, P. Christos, M. Osborne, *Ann. Surg. Oncol.* **2003**, *10*, 242-247.
- [82] E. Azuma, N. Nakamura, K. Kuramochi, T. Sasamori, N. Tokitoh, I. Sagami, K. Tsubaki, *J. Org. Chem.* **2012**, *77*, 3492-3500.
- [83] D. A. Heuveling, G. W. M. Visser, M. de Groot, J. F. de Boer, M. Baclayon, W. H. Roos, G. J. L. Wuite, C. R. Leemans, R. de Bree, G. A. M. S. van Dongen, *Eur. J. Nucl. Med. Mol. Imag.* **2012**, *39*, 1161-1168.
- [84] J. Han, K. Burgess, *Chem. Rev.* **2010**, *110*, 2709-2728.
- [85] F. Yang, C. Jin, S. Subedi, C. L. Lee, Q. Wang, Y. Jiang, J. Li, Y. Di, D. Fu, *Cancer Treat. Rev.* **2012**, *38*, 566-579.
- [86] S. Santra, *Methods Mol. Biol.* **2010**, *624*, 151-162.
- [87] H.-C. Huang, S. Barua, G. Sharma, S. K. Dey, K. Rege, *J. Control. Release* **2011**, *155*, 344-357.
- [88] J. E. Lee, N. Lee, T. Kim, J. Kim, T. Hyeon, *Acc. Chem. Res.* **2011**, *44*, 893-902.
- [89] R. Q. Frazer, R. T. Byron, P. B. Osborne, K. P. West, *J. Long. Term Eff. Med. Implants* **2005**, *15*, 629-639.
- [90] A. Bettencourt, A. J. Almeida, *J. Microencapsulation* **2012**, *29*, 353-367.
- [91] T. Heinze, T. Liebert, B. Heublein, S. Hornig, *Adv. Polym. Sci.* **2006**, *205*, 199-291.
- [92] S. Mao, W. Sun, T. Kissel, *Adv. Drug Deliv. Rev.* **2010**, *62*, 12-27.
- [93] Z. Liu, Y. Jiao, Y. Wang, C. Zhou, Z. Zhang, *Adv. Drug Deliv. Rev.* **2008**, *60*, 1650-1662.
- [94] S. Hornig, C. Biskup, A. Graefe, J. Wotschadlo, T. Liebert, G. J. Mohr, T. Heinze, *Soft Matter* **2008**, *4*, 1169-1172.
- [95] C. Wischke, S. P. Schwendeman, *Int. J. Pharm.* **2008**, *364*, 298-327.
- [96] T. K. Dash, V. B. Konkimalla, *J. Control. Release* **2012**, *158*, 15-33.
- [97] P. A. Grabnar, J. Kristl, *J. Microencapsulation* **2011**, *28*, 323-335.
- [98] R. Vehring, *Pharm. Res.* **2008**, *25*, 999-1022.
- [99] J. H. Rao, A. Dragulescu-Andrasi, H. Q. Yao, *Curr. Opin. Biotechnol.* **2007**, *18*, 17-25.
- [100] R. Sauer, A. Turshatov, S. Balushev, K. Landfester, *Macromolecules* **2012**, *45*, 3787-3796.
- [101] E. Pinon-Segundo, M. G. Nava-Arzaluz, D. Lechuga-Ballesteros, *Recent Pat. Drug Deliv. Formul.* **2012**, *6*, 224-235.
- [102] J. Liu, Z. Qiu, S. Wang, L. Zhou, S. Zhang, *Biomed. Mat.* **2010**, *5*.
- [103] H. Fessi, F. Puisieux, J. P. Devissaguet, N. Ammoury, S. Benita, *Int. J. Pharm.* **1989**, *55*, R1-R4.
- [104] S. Schubert, J. T. Delaney, U. S. Schubert, *Soft Matter* **2011**, *7*, 1581-1588.
- [105] J. P. Rao, K. E. Geckeler, *Prog. Polym. Sci.* **2011**, *36*, 887-913.
- [106] I. Y. Perevyazko, J. T. Delaney, Jr., A. Vollrath, G. M. Pavlov, S. Schubert, U. S. Schubert, *Soft Matter* **2011**, *7*, 5030-5035.
- [107] A. Vollrath, A. Schallon, C. Pietsch, S. Schubert, T. Nomoto, Y. Matsumoto, K. Kataoka, U. S. Schubert, *Soft matter* **2012**, *10.1039/C2SM26928G*.
- [108] J. Wang, J. D. Byrne, M. E. Napier, J. M. DeSimone, *Small* **2011**, *7*, 1919-1931.
- [109] S. E. A. Gratton, P. A. Ropp, P. D. Pohlhaus, J. C. Luft, V. J. Madden, M. E. Napier, J. M. DeSimone, *Proceedings of the National Academy of Sciences of the United States of America* **2008**, *105*, 11613-11618.
- [110] A. Albanese, P. S. Tang, W. C. W. Chan, *Annu. Rev. Biomed. Eng.* **2012**, *14*, 1-16.
- [111] F. Alexis, E. Pridgen, L. K. Molnar, O. C. Farokhzad, *Mol. Pharm.* **2008**, *5*, 505-515.
- [112] V. J. Pansare, S. Hejazi, W. J. Faenza, R. K. Prud'homme, *Chem. Mater.* **2012**, *24*, 812-827.
- [113] W. Jiang, B. Y. S. Kim, J. T. Rutka, W. C. W. Chan, *Nature Nanotechnology* **2008**, *3*, 145-150.
- [114] M. A. Woodruff, D. W. Huttmacher, *Prog. Polym. Sci.* **2010**, *35*, 1217-1256.
- [115] R. K. Jain, T. Stylianopoulos, *Nat. Rev. Clin. Oncol.* **2010**, *7*, 653-664.
- [116] H. Maeda, G. Y. Bharate, J. Daruwalla, *Eur. J. Pharm. Biopharm.* **2009**, *71*, 409-419.
- [117] A. Schaedlich, H. Caysa, T. Mueller, F. Tenambergen, C. Rose, A. Goepferich, J. Kuntsche, K. Maeder, *ACS Nano* **2011**, *5*, 8710-8720.
- [118] J. L. Perry, K. P. Herlihy, M. E. Napier, J. M. Desimone, *Acc. Chem. Res.* **2011**, *44*, 990-998.
- [119] J. P. Best, Y. Yan, F. Caruso, *Advanced Healthcare Materials* **2012**, *1*, 35-47.
- [120] S. Lorenz, C. P. Hauser, B. Autenrieth, C. K. Weiss, K. Landfester, V. Mailaender, *Macromol. Biosci.* **2010**, *10*, 1034-1042.
- [121] M. C. Garnett, P. Kallinteri, *Occup. Med.* **2006**, *56*, 307-311.
- [122] K. Knop, R. Hoogenboom, D. Fischer, U. S. Schubert, *Angew. Chem. Int. Ed.* **2010**, *49*, 6288-6308.
- [123] R. Gref, Y. Minamitake, M. T. Peracchia, V. Trubetskoy, V. Torchilin, R. Langer, *Science* **1994**, *263*, 1600-1603.
- [124] M. K. Yu, J. Park, S. Jon, *Theranostics* **2012**, *2*, 3-44.
- [125] Y. H. Bae, K. Park, *J. Control. Release* **2011**, *153*, 198-205.
- [126] M. Wang, M. Thanou, *Pharmacol. Res.* **2010**, *62*, 90-99.
- [127] D. Peer, J. M. Karp, S. Hong, O. C. Farokhzad, R. Margalit, R. Langer, *Nature Nanotechnol.* **2007**, *2*, 751-760.
- [128] S. S. Moffatt, *J. Nanosci. Nanotechnol.* **2012**, *3*, 1-20.
- [129] F. Gu, L. Zhang, B. A. Teply, N. Mann, A. Wang, A. F. Radovic-Moreno, R. Langer, O. C. Farokhzad, *Proc. Natl. Acad. Sci. U. S. A.* **2008**, *105*, 2586-2591.
- [130] G. L. Plosker, D. P. Figgitt, *Drugs* **2003**, *63*, 40.
- [131] A. Z. Wang, F. Gu, L. Zhang, J. M. Chan, A. Radovic-Moreno, M. R. Shaikh, O. C. Farokhzad, *Expert Opin. Biol. Ther.* **2008**, *8*, 1063-1070.
- [132] P. Yousefpour, F. Atyabi, E. Vasheghani-Farahani, A. A. Movahedi, R. Dinarvand, *Int. J. Nanomedicine* **2011**, *6*, 1977-1990.
- [133] F. V. Bockstaele, J. B. Holz, H. Revets, *Curr. Opin. Investig. Drugs* **2009**, *11*, 1212.
- [134] J. Majidi, J. Barar, B. Baradaran, J. Abdolalizadeh, Y. Omidi, *Hum. Antibodies* **2009**, *18*.
- [135] X.-X. Zhang, H. S. Eden, X. Chen, *J. Control. Release* **2012**, *159*, 11.
- [136] F. Danhier, A. L. Breton, V. Préat, *Mol. Pharmaceutics* **2012**, *9*, 12.
- [137] C. Mas-Moruno, F. Rechenmacher, H. Kessler, *Anticancer Agents Med. Chem.* **2010**, *10*, 5.
- [138] Z. Xiao, O. C. Farokhzad, *ACS Nano* **2012**, *6*, 3670-3676.
- [139] L. Yang, X. Zhang, M. Ye, J. Jiang, R. Yang, T. Fu, Y. Chen, K. Wang, W. Tan, *Adv. Drug Deliv. Rev.* **2011**, 1361.
- [140] G. Zhu, M. Ye, M. J. Donovan, E. Song, Z. Zhao, W. Tan, *Chem. Commun.* **2012**, *48*, 10472.
- [141] Y. J. Lu, P. S. Low, *Adv. Drug Deliv. Rev.* **2002**, *54*, 675-693.
- [142] P. S. Low, S. A. Kularatne, *Curr. Opin. Chem. Biol.* **2009**, *13*, 256-262.
- [143] T. Freire, E. Osinaga, *Immunotherapy* **2012**, *4*, 719-734.
- [144] E. J. Chaney, L. Tang, R. Tong, J. Cheng, S. A. Boppart, *Mol. Imag.* **2010**, *9*, 153-162.
- [145] V. Saxena, M. Sadoqi, J. Shao, *Int. J. Pharm.* **2006**, *308*, 200-204.

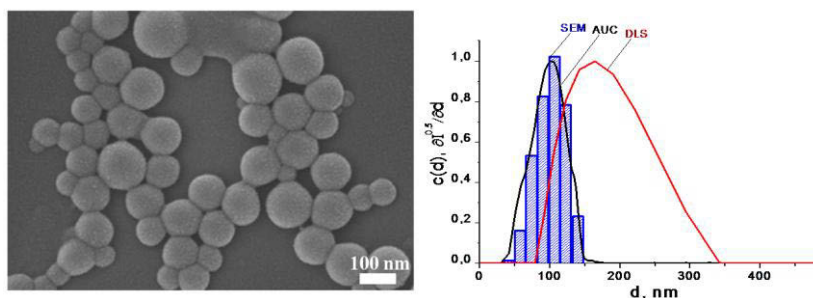
- [146] A. Schaedlich, C. Rose, J. Kuntsche, H. Caysa, T. Mueller, A. Göpferich, K. Mäder, *Pharm. Res.* **2011**, *8*, 1995.
- [147] C. Zheng, M. Zheng, P. Gong, D. Jia, P. Zhang, B. Shi, Z. Sheng, Y. Ma, L. Cai, *Biomaterials* **2012**, *33*, 5603-5609.
- 5 [148] Y. Ma, M. Sadoqi, J. Shao, *Int. J. Pharm.* **2012**, *436*, 25-31.
- [149] R. Tong, V. J. Coyle, L. Tang, A. M. Barger, T. M. Fan, J. Cheng, *Microsc. Res. Tech.* **2010**, *73*, 901-909.
- [150] P. Liu, L. Qin, Q. Wang, Y. Sun, M. Zhu, M. Shen, Y. Duan, *Biomaterials* **2012**, *33*, 6739-6747.
- 10 [151] H. Ding, K. T. Yong, I. Roy, R. Hu, F. Wu, L. L. Zhao, W. C. Law, W. W. Zhao, W. Ji, L. W. Liu, E. J. Bergey, P. N. Prasad, *Nanotechnology* **2011**, *22*.
- [152] S. Sakuma, M. Kataoka, H. Higashino, T. Yano, Y. Masaoka, S. Yamashita, K. Hiwatari, H. Tachikawa, R. Kimura, K. Nakamura, H.
- 15 Kumagai, J. C. Gore, W. Pham, *Eur. J. Pharm. Sci.* **2011**, *42*, 340-347.
- [153] S. Sakuma, T. Yano, Y. Masaoka, M. Kataoka, K. Hiwatari, H. Tachikawa, Y. Shoji, R. Kimura, H. Ma, Z. Yang, L. Tang, R. M. Hoffman, S. Yamashita, *J. Control. Release* **2009**, *134*, 2-10.
- [154] S. Sakuma, T. Yano, Y. Masaoka, M. Kataoka, K. Hiwatari,
- 20 H. Tachikawa, Y. Shoji, R. Kimura, H. Ma, Z. Yang, L. Tang, R. M. Hoffman, S. Yamashita, *Eur. J. Pharm. Biopharm.* **2010**, *74*, 451-460.
- [155] J. Hou, Q. Zhang, X. Li, Y. Tang, M. R. Cao, F. Bai, Q. Shi, C. H. Yang, D. L. Kong, G. Bai, *J. Biomed. Mater. Res. A* **2011**, *99A*, 684-689.
- 25 [156] K. Miki, A. Kimura, K. Oride, Y. Kuramochi, H. Matsuoka, H. Harada, M. Hiraoka, K. Ohe, *Angew. Chem. Int. Ed.* **2011**, *50*, 6567.
- [157] K. Kim, J. H. Kim, H. Park, Y.-S. Kim, K. Park, H. Nam, S. Lee, J. H. Park, R.-W. Park, I.-S. Kim, K. Choi, S. Y. Kim, K. Park, I. C. Kwon, *J. Control. Release* **2010**, *146*, 219-227.
- 30 [158] J. H. Na, H. Koo, S. Lee, K. H. Min, K. Park, H. Yoo, S. H. Lee, J. H. Park, I. C. Kwon, S. Y. Jeong, K. Kim, *Biomaterials* **2011**, *32*, 5252-5261.
- [159] K. Kempe, C. R. Becer, U. S. Schubert, *Macromolecules* **2011**, *44*, 5825-5842.
- 35 [160] U. Mansfeld, C. Pietsch, R. Hoogenboom, C. R. Becer, U. S. Schubert, *Polymer Chemistry* **2010**, *1*, 1560-1598.
- [161] A. Vollrath, S. Schubert, N. Windhab, C. Biskup, U. S. Schubert, *Macromol. Rapid Commun.* **2010**, *31*, 2053-2058.
- [162] A. Baumgaertel, E. Altuntas, U. S. Schubert, *J. Chromatogr. A* **2012**, *1240*, 1-20.
- 40 [163] A. C. Crecelius, A. Baumgaertel, U. S. Schubert, *J. Mass Spectrom.* **2009**, *44*, 1277-1286.

Publication 2

"Characterization of poly(methyl methacrylate) nanoparticles prepared by nanoprecipitation using analytical ultracentrifugation, dynamic light scattering, and scanning electron microscopy"

Igor Y. Perevyazko, Antje Vollrath, Stephanie Schubert,
George M. Pavlov, Ulrich S. Schubert

J. Polym. Sci., Part A: Polym. Chem. **2010**, *48*, 3924–3931.



Characterization of Poly(methyl methacrylate) Nanoparticles Prepared by Nanoprecipitation Using Analytical Ultracentrifugation, Dynamic Light Scattering, and Scanning Electron Microscopy

IGOR PEREVYAZKO,¹ ANTJE VOLLRATH,¹ STEPHANIE HORNIG,¹ GEORGES M. PAVLOV,^{1,2,3} ULRICH S. SCHUBERT^{1,2}

¹Laboratory of Organic and Macromolecular Chemistry, Friedrich-Schiller-University Jena, Humboldtstrasse 10, 07743 Jena, Germany

²Laboratory of Macromolecular Chemistry and Nanoscience, Eindhoven University of Technology, PO Box 513, 5600 MB Eindhoven, The Netherlands

³Department of Physics, St. Petersburg University, Ulianovskaya Strasse 1, 198504 St. Petersburg, Russia

Received 8 March 2010; accepted 25 May 2010

DOI: 10.1002/pola.24157

Published online in Wiley Online Library (wileyonlinelibrary.com).

ABSTRACT: Nanoprecipitation represents an effective method for the production of polymeric nanoparticles. This technique was used to prepare nanoparticles from solutions of poly(methyl methacrylate) and its copolymers. Since the regulation of main parameters like particle size, particle size distribution, and molar particle mass is very important for future applications, the stable nanoparticle dispersions were examined by scanning electron microscopy, velocity sedimentation, and dynamic light scattering, whereby advantages and disadvantages of each characterization techniques are discussed. Polydispersities of particle size distributions are determined by the ratio of d_w/d_n , where d_w and d_n are weight- and number-aver-

age diameters, respectively. The particle characteristics strongly depend on the chemical structure of the polymers and the way of preparation and, therefore, vary in the studied cases in the range of $6 < d_w < 680$ nm, whereas the polydispersity index d_w/d_n changes in the range of 1.02 to 1.40. It is shown that nanoparticles in a desirable size range can be prepared by solvent–nonsolvent methods (dialysis technique or dropping technique). © 2010 Wiley Periodicals, Inc. *J Polym Sci Part A: Polym Chem* 48: 3924–3931, 2010

KEYWORDS: dynamic light scattering; nanoparticles; SEM; ultracentrifugation; velocity sedimentation

INTRODUCTION The development of functional nanoparticles is of major interest because it was found that the unique properties of such nanoscale materials allow breakthroughs in technology, bioengineering, life sciences, and many others. To tune the properties of the nanoparticles for specific applications, not only the molecular structure but also the size of the systems needs to be well investigated. Therefore, imaging techniques such as atomic force microscopy and scanning and transmission electron microscopy (SEM and TEM) were used to investigate the nanoscale dimensions and morphologies up to the molecular level. In addition, dynamic light scattering (DLS) was applied because it provides more statistical information about the average size and size distribution of the particles in suspension. A further and less commonly used method is analytical ultracentrifugation (AUC), which allows a closer look on the flow characteristics of the nanoparticles. In the early 20th century, Svedberg already used AUC for the determination of the size and the size distribution of colloids.¹ None of the techniques mentioned provides ultimate information about the size, shape, morphology, and flow behavior of nanoparticulate systems. However, a combi-

nation of these techniques can lead to a satisfying characterization that is necessary for further improvements and prevention of undesired side effects, like aggregation (e.g., of drug-containing particles in the blood stream).

Synthetic polymers are widely used materials for the design of functional nanoparticles because they provide unique structural diversity and functionality. In this study, poly(methacrylate) nanoparticles were prepared and analyzed by SEM, DLS, and AUC. Poly(methacrylic acid)-*co*-(methyl methacrylate)s [poly(MAA-*co*-MMA)] show a pH-dependent solubility behavior, which makes it possible to use them as drug delivery systems both able to protect the drug and to release it at the targeted side.² In addition, the functionalization of the polymers with dyes allows the localization of the particles for cell studies or tissue examinations.^{3,4}

To prepare well-defined poly(methacrylate) nanoparticle suspensions, nanoprecipitation was applied as alternative technique besides emulsion techniques and spray drying processes usually used for polymers.⁵ The nanoprecipitation technique is based on precipitation of polymer molecules

Correspondence to: U. S. Schubert (E-mail: ulrich.schubert@uni-jena.de)

Journal of Polymer Science: Part A: Polymer Chemistry, Vol. 48, 3924–3931 (2010) © 2010 Wiley Periodicals, Inc.

into nanoscale particles during displacement of a solvent with a nonsolvent.^{6,7} Till now, nanoprecipitation is mainly used for poly(lactides) and its copolymers; however, it is, applicable in principle for all polymers under certain conditions.^{8–10} The latter could be shown not only for example for diverse polysaccharide derivatives, namely cellulose¹¹ and dextran esters,¹² several industrially prepared polymers¹³ but also highly functional pentafluorostyrenes.¹⁴ In this work, copolymers of MMA with MAA and ethylacrylate (EA), in particular poly(MMA-*stat*-MAA)_{1:2} and poly(MMA-*stat*-EA)_{1:4}, a homopolymer of poly(methyl methacrylate) (PMMA) and a fluorescence-labeled poly(MMA-*stat*-PyMMA) were formed into nanoscale particles, applying a dialysis and a dropping technique. The particle formation and, consequently, the resulting size and shape of the particles strongly depend on the concentration of the polymer solutions, the solvent, the solvent to nonsolvent ratio, and the course of the reaction. All these factors influence the self-assembly of the polymer molecules from the dissolved state into defined nanoparticulate systems. The nanoparticle suspensions formed were characterized extensively by SEM, TEM, and AUC including storage stability, to evaluate their ability as possible carriers for drug delivery and diagnostics.

EXPERIMENTAL

Materials

Poly(MMA-*stat*-MAA)_{1:2} and poly(MMA-*stat*-EA)_{1:4} were kindly provided by Evonik Röhm GmbH (Darmstadt, Germany). Pyren-1-ylmethylmethacrylate (PyMMA), P(MMA-*stat*-PyMMA), and PMMA were prepared by a reversible addition-fragmentation chain-transfer polymerization.^{15–17} Purified *N,N*-dimethylacetamide (DMA) was purchased from VWR (West Chester, PA).

METHODS

Size Exclusion Chromatography (SEC)

SEC was performed on a Shimadzu system, equipped with a SCL-10A VP system controller, a LC-10AD VP pump, a RID-10A refractive index detector, and a PSS SDV linear S column, with a mixture of chloroform:triethyl-amine:2-propanol (94:4:2) as eluent at 1 mL/min flow rate at 40 °C. Additional SEC measurements were performed on an Agilent 1200 series LC system (isocratic pump G1310A, refractive index detector G1362A) with a PSS Gram30 and a PSS Gram1000 column in series. DMA containing 0.21% LiCl (m/v) was used as eluent at a flow rate of 1 mL/min at 40 °C. As calibration standard, PMMA was used.

SEM

The nanoparticle suspensions were diluted with demineralized filtered water to a final concentration of 1 mg/mL. The suspensions were characterized by SEM using the system LEO-1450 VP (Leo, Oberkochen, Germany) operating at 10 kV. For this, one droplet (15–20 μL) of the suspension was placed on a mica surface, lyophilized for 3 h and finally covered with gold using a sputter coating device BAL-TEC SCD005 (Balzers, Lichtenstein; 60 mA, 80 s). The diameter of the nanoparticle was measured using the ImageJ software.¹⁸

Sedimentation Velocity Experiments

Sedimentation velocity experiments were performed with a Beckman XLI analytical ultracentrifuge (ProteomeLab XLI Protein Characterization System). They were carried out in conventional double-sector Epon centerpieces of 12-mm optical path length in a four holes rotor. Cells were filled with 420 μL of suspension and 440 μL of solvent (H₂O or D₂O). A rotor speed of 3,000 to 40,000 rpm was used depending on the sample. The nanoparticle suspensions were used without further purification. The rotor was equilibrated for ~2 h at 20 °C in the centrifuge. Sedimentation profiles were obtained every 15 s by interference optics, and the sedimentation data were evaluated by the program Sedfit.¹⁹

Particle Characterization by DLS

DLS was performed on a Zetasizer Nano ZS (Malvern instruments, Malvern, United Kingdom) equipped with a 10 mW He-Ne laser (633 nm) and operating at an angle of 173°. The nanoparticle suspensions were diluted with demineralized, filtered water to a final concentration of 0.02 mg/mL, and measured three times at 25 °C for 150 s. From the experimental data (autocorrelation function), the size information can be obtained by using the method of cumulants.^{20–22} In the cumulants method, the logarithm of the correlation function is given as:

$$\ln[g^2(\tau)] = -K_1\tau + K_2\tau^2/2 + \dots$$

where K_1 and K_2 are the cumulants and τ is a delay time. This method provides z -average size; the width of the distribution is related to the polydispersity index (PDI^{DLS}), which is defined as relation

$$\text{PDI}^{\text{DLS}} = \sqrt{\frac{K_2}{K_1^2}}$$

where K_1 and K_2 are the first- and the second-order cumulant of the light scattered intensity, respectively. It should be noted that the PDI^{DLS} cannot be related with the particle size ratio in a simple way.

Preparation of the Nanoparticles

Nanoparticles of different PMMA homopolymers and copolymers were obtained via nanoprecipitation.^{7,23} Two techniques were applied for the nanoparticle formation: dialysis and a dropping technique.^{13,24} For the dialysis process, 10 mg of the polymer was dissolved in 2.5 mL purified DMA as organic solvent, transferred into a regenerated cellulose membrane (Spectra/Por[®], Rancho Dominguez, CA, molar mass cutoff 6,000–8,000 g/mol), and dialyzed against 500 mL distilled water. The surrounding water was exchanged five times in a period of 12 h until all DMA was replaced. As a typical example for the dropping technique, 10 mg of the polymer was dissolved in 2.5 mL acetone, and the solution was added dropwise under stirring to 10 mL distilled water or deuterated water, respectively, or vice versa water was dropped into the polymer solution. The acetone was removed by evaporation at 40 °C overnight. The nanoparticle suspensions prepared were stored at 4 °C.

TABLE 1 Characterization of PMMA and PMMA Copolymers

Sample	Ratio	M_n (g/mol)	M_w (g/mol)	PDI
Poly(MMA)	–	10,100 ^a	11,200 ^a	1.11 ^a
Poly(MAA- <i>stat</i> -MMA) _{1:2}	1:2	10,000 ^b	19,600 ^b	1.96 ^b
Poly(MMA- <i>stat</i> -EA) _{1:4}	1:4	10,000 ^b	23,800 ^b	2.38 ^b
Poly(MMA- <i>stat</i> -PyMMA)	95:5	9,100 ^a	10,600 ^a	1.16 ^a

^a Calculated from SEC (CHCl₃) with PMMA standards.^b Calculated from SEC (DMA/LiCl) with PMMA standards.

RESULTS AND DISCUSSION

A homopolymer of PMMA and the copolymers poly(MMA-*stat*-MAA)_{1:2}, poly(MMA-*stat*-EA)_{1:4}, as well as poly(MMA-*stat*-PyMMA) were transformed into nanoscale materials by applying different nanoprecipitation techniques. The molar mass of the MMA-based polymers and their PDIs were estimated by size-exclusion chromatography (SEC) (Table 1). In the following, the particle suspensions of the synthetic polymers will be characterized and compared applying SEM, AUC, and DLS.

Distributions and Size Average Values

Because of the use of different methods for characterizing the nanoparticle suspensions, also different size distributions were obtained. SEM investigations yield number distributions. From velocity sedimentation, a weight-average distribution can be obtained. In addition, the translational diffusion coefficients D_z resulting from DLS represent z-averages. Usually, the weight-average distribution is shifted to higher values when compared with the number average distribution. However, at the same time, corresponding average values calculated from different kinds of distributions must coincide:

$$d_n = \frac{1}{\sum \frac{w_i}{d_i}} = \sum v_i d_i \text{ and } d_w = \sum w_i d_i = \frac{\sum v_i d_i^2}{d_n},$$

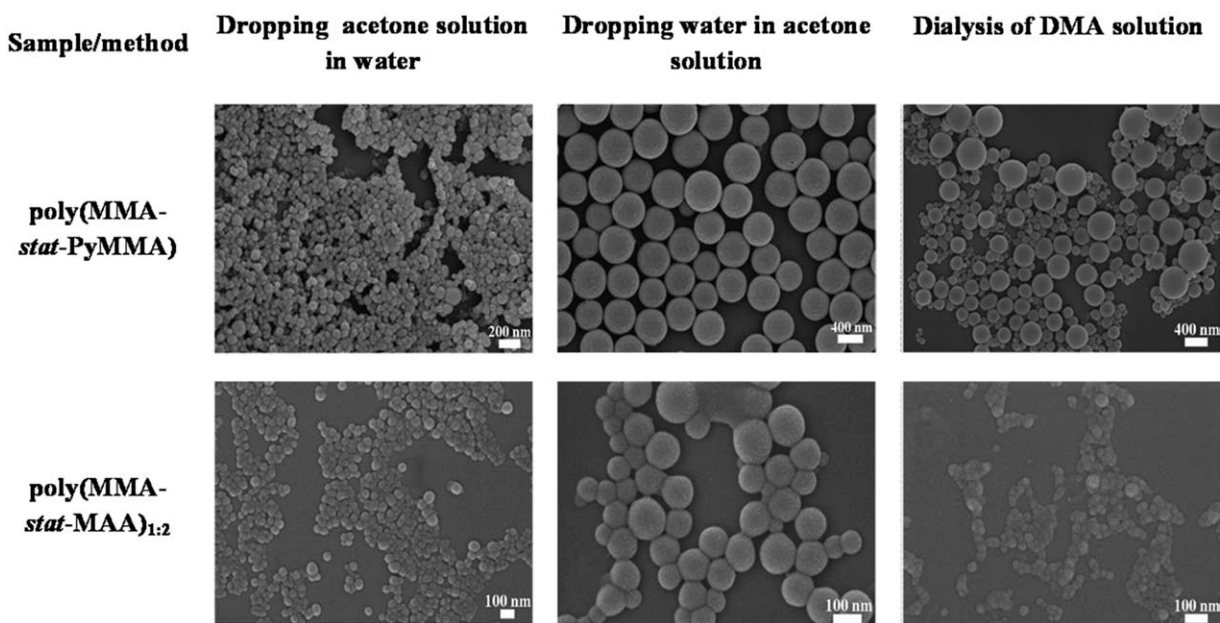
with $v_i = \frac{n_i}{N}$ being the number fraction and $w_i = \frac{nd_i}{\sum nd_i}$ being the weight fraction. For polydisperse samples, the relation $d_w > d_n$ can be applied. The heterogeneity of an ensemble of nanoparticles can further be characterized by the ratio of different size average values $PDI_d = \frac{d_w}{d_n}$. For particles with spherical shape, PDI_d is related by a simple way to the molar mass distribution $PDI_M = \frac{M_w}{M_n} = \left(\frac{d_w}{d_n}\right)^3$.

Particle Characterization by SEM

The morphology and size distribution of the PMMA nanoparticles was first investigated by SEM. Typical images of nanoparticles from poly(MMA-*stat*-MAA)_{1:2} and poly(MMA-*stat*-PyMMA) prepared by different precipitation techniques are shown in Figure 1. In all images, spherical-shaped particles in the nanoscale range can be observed. In some cases, adhesion of the particles is detected (dropping acetone solution of poly(MMA-*stat*-MAA)_{1:2} into water). The corresponding histograms are presented in Figure 2. Based on these number of histograms, the average values d_n and d_w were calculated. Weight-average diameters are listed in Table 2, and d_w/d_n values are presented in Table 3. The number of individual particles N considered in the calculations varies between 100 and 300.

Particle Characterization by AUC

In an ultracentrifuge, nanoparticles will be fractionated according to their size, density, and shape. Therefore, sedimentation analysis in combination with Sedfit software gives a reliable and adequate analysis of the nanoparticles including size and size distribution. A typical image obtained from the Sedfit program is shown in Figure 3. The data were

**FIGURE 1** SEM images of PMMA nanoparticles prepared by various techniques.

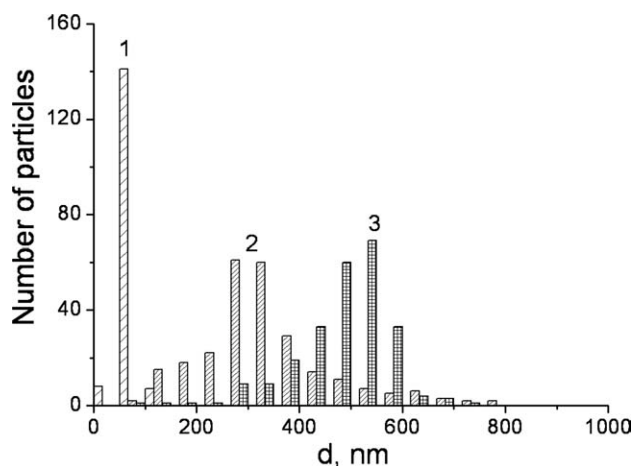


FIGURE 2 Size distribution, determined by SEM, of poly(MMA-*stat*-PyMMA) nanoparticles prepared by different nanoprecipitation techniques: (1) dropping a solution of the polymer in acetone into water, (2) dialysis of a solution in DMA against water, and (3) dropping water into the acetone/polymer solution.

modeled using two different analysis methods implemented in Sedfit: (1) $c(s)$ analysis, which is based on a numerical solution of the Lamm equation; it allows to estimate the weight-average frictional ratio of all particles, and (2) the least-squares boundary modeling $ls-g^*(s)$, which describes sedimentation of a non-diffusing species.²⁵ A parameter necessary for the quantitative interpretation of sedimentation data is the partial specific volume v , which was determined by the “density variation method”: by sedimentation velocity experiments on the nanoparticle suspensions using H_2O and D_2O ,^{26,27} assuming that the nanoparticles have the same size and molar mass in each solvent (which is equivalent to the assumption of a constancy of the intrinsic sedimentation coefficients $[s] \equiv \frac{s_0 \eta_0}{(1 - v\rho_0)}$). Applying this method, the partial specific volume value v of the particles can be obtained from the following equation:

$$v = \frac{s_2 \eta_2 - s_1 \eta_1}{s_2 \eta_2 \rho_1 - s_1 \eta_1 \rho_2}$$

where s_1 , η_1 , ρ_1 , and s_2 , η_2 , ρ_2 are sedimentation coefficients, dynamic viscosity, and solvent density measured in H_2O and D_2O , respectively. The partial specific volume of the particles was found as $v = 0.78 \text{ cm}^3/\text{g}$ with maximum deviation 0.01.

The nanoparticle suspensions were also investigated at different concentrations, to check for a possible concentration dependence of the sedimentation and frictional coefficient. However, no concentration dependence of s and f/f_{sph} could be observed in the concentration range of 0.025 to $0.10 \times 10^{-2} \text{ g/cm}^3$. The fitted frictional ratio $(f/f_{\text{sph}})_0$ obtained by $c(s)$ analysis is virtually equal to 1, which confirms the spherical shape of the nanoparticles and supports the investigations by SEM. By combining Svedberg’s equation,

$$s = \frac{M(1 - v\rho_0)}{N_A f},$$

where $f = 3\pi\eta d$ is the translational friction coefficient, and the hard sphere approximation $M = \frac{N_A \pi d^3}{6v}$, where N_A is Avogadro number. The diameter d of the particles can be easily calculated from the following expression²⁸:

$$d = 3\sqrt{2} \sqrt{[s]v} \quad (*)$$

Based on equation (*), the $c(s)$ and/or $ls-g^*(s)$ distributions can be converted to the distributions by sizes. The corresponding distributions are shown in Figure 4. Molar masses of the particles were estimated by applying the modified Svedberg’s equation

$$M_s = 9\pi\sqrt{2} N_A \sqrt{[s]^3 v}$$

Based on these mass distributions, the average values d_w were calculated and listed in Table 2 with the M_s estimations.

Particle Characterization by DLS

DLS is a commonly used technique to determine the size distribution profile of particles in suspension or of polymers in solution.^{29–31} The raw experimental data obtained in a DLS

TABLE 2 Weight-Average Sizes of Nanoparticles Determined by SEM, AUC, and DLS and Their Molar Masses Determined by AUC

<i>N</i>	Sample	Preparation	SEM, d_w (nm)	AUC, d_w (nm)	$M_{\text{sf}} \times 10^{-6}$ (g/mol)	DLS, d_w (nm)
1	poly(MMA)	D ^a	310	300	12,000	480
2	poly(MMA- <i>stat</i> -PyMMA)	D	280	570	73,000	480
3		A→W ^b	75	65	120	100
4		W→A ^c	490	380	22,500	680
5	poly(MMA- <i>stat</i> -MAA) _{1;2}	D	36	28	9.5	46
6		A→W	43	35	18	41
7		W→A	110	104	420	190
8	poly(MMA- <i>stat</i> -EA) _{1;4}	D	135	106	425	150
9		A→W	–	6.6	0.04	5.8
10		W→A	–	105	420	270

^a Dialysis preparation technique.

^b Dropping acetone solution of a polymer into water.

^c Dropping water into acetone solution of a polymer.

TABLE 3 Calculated PDI Values Obtained from DLS, AUC, and SEM

<i>N</i>	PDI _{DLS}	DLS, d_w/d_n	AUC, d_w/d_n	SEM, d_w/d_n
1	0.291	1.30	1.20	1.29
2	0.346	1.26	1.24	1.40
3	0.228	1.05	1.07	1.04
4	0.321	1.09	1.12	1.04
5	0.312	1.05	1.12	1.09
6	0.300	1.05	1.13	1.10
7	0.132	1.12	1.06	1.10
8	0.194	1.03	1.06	1.12
9	0.543	1.02	1.20	–
10	0.237	1.08	1.06	–

experiment is the intensity autocorrelation curve. For small particles, when $d \ll \lambda$, the Rayleigh scattering approximation is valid. The intensity I of light scattered by a single small particle from a beam of unpolarized light of wavelength λ and intensity I_0 is given by:

$$I = I_0 \frac{1 + \cos^2 \theta}{2R^2} \left(\frac{2\pi}{\lambda} \right)^4 \left(\frac{n^2 - 1}{n^2 + 2} \right)^2 \left(\frac{d}{2} \right)^6$$

with R being the distance to the particle, θ being the scattering angle, n being the refractive index of the particle, and d being its diameter. The scattering intensity of spherical particles is proportional to the sixth power of the diameter or the square of the molar mass: $I \sim d^6 \sim M^2$. Thus, a small amount of aggregates or larger particles can dominate the distribution, with the consequence that the intensity distribution can be somewhat misleading. The software of the Zetasizer Nano ZS transforms the intensity distribution into

volume and number distributions of the particles, with corresponding differential distribution $\partial V/\partial d$ and $\partial N/\partial d$, respectively, based on the Mie theory.³² In contrast to Rayleigh scattering, the Mie solution of the scattering problem is valid for all possible ratios of diameter to wavelength, although it results in a numerical summation of infinite sums.

For particles with $d \ll \lambda$, the Rayleigh approximation allows the following scaling of the intensity: $I^{0.5} \sim d^3 \sim M$. Therefore, the integral distribution $I = f(d)$ can be transformed into the corresponding $I^{0.5} = f_1(d)$ distribution, from which the differential distribution $\partial(I^{0.5})/\partial d$ was obtained. The distribution $\partial(I^{0.5})/\partial d$ may be close to $\partial V/\partial d$. A comparison of the three types of distributions is presented in Figure 5 for the examined poly(MMA-*stat*-MAA)_{1:2}. In an ideal case, the numerical size distribution shifts to smaller values in comparison with the weight distribution. In the majority of systems studied, this trend was observed; unexpectedly however, in some cases, the opposite of this trend was observed, where the weight distribution values were smaller than those of the corresponding numerical size distributions. The values of the weight-average diameter d_w obtained by DLS are presented in Table 2. In general, they are in acceptable (but in some cases only in rough) agreement with those obtained by the other methods applied. Values obtained from DLS using different distributions are listed in Table 4.

Comparison of Sizes and Distributions

It is obvious from Figures 1 and 4 as well as Table 2 that different preparation techniques lead to different particle sizes and size distributions (by comparing data of the same characterization technique; otherwise it is somewhat obscured due to the differences in the measuring principles applied). Apparently, what matters is the way of exchanging the solvent: The exchange of the solvent to the nonsolvent is either fast, in case of the dropwise addition of the polymer

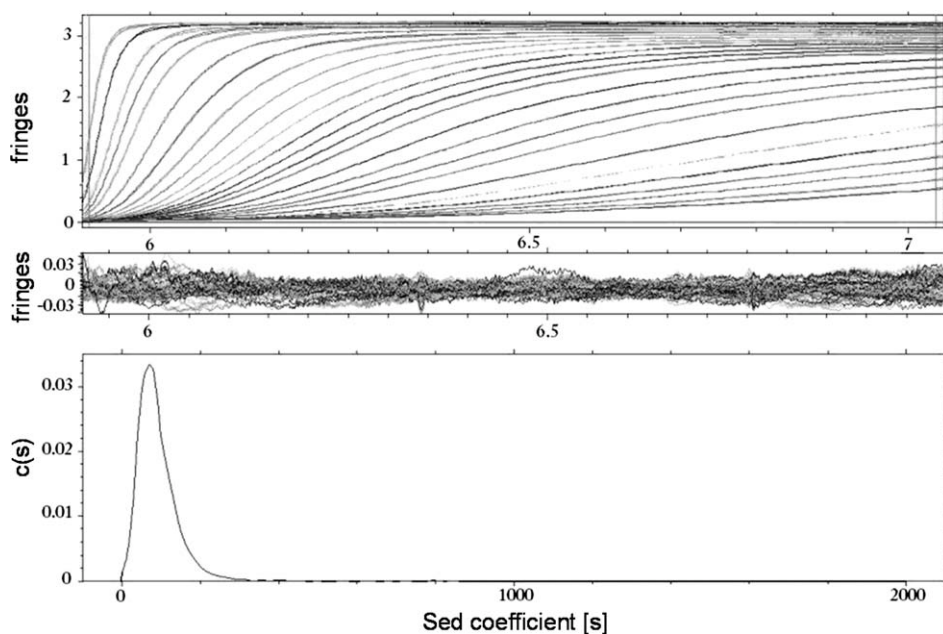


FIGURE 3 Sedimentation velocity experiments on poly(MMA-*stat*-MAA)_{1:2}. The experiment was carried out at 12,000 rpm, scans were collected every 15 s. Top panel: superposition of sedimentation profiles obtained with interference optics at 20 °C. Middle: corresponding residual plots. Bottom: differential distribution $c(s)$ of the sedimentation coefficients. The distributions were obtained with a regularization procedure with a confidence level of 0.9.

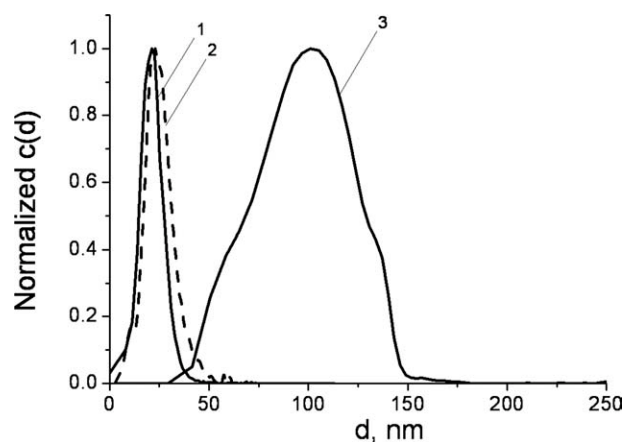


FIGURE 4 Size distributions, determined by DLS, of poly(MMA-*stat*-MAA)_{1:2} nanoparticles prepared by different nanoprecipitation techniques: (1: solid line) by dropping an acetone solution of the polymer into water, (2: dashed line) by dialysis of a DMA solution against water, (3: solid line) by dropping water to the acetone/polymer solution.

solution to water, or very slow, for the dialysis method as well as for dropping the water into acetone.

Considering all data obtained for the PMMA particle suspensions, some qualitative conclusions can be drawn. By dropping the acetone/polymer solution into water, the polymer precipitates rapidly in the surplus of water. As a result, the formation of comparatively small nanoparticles (less than 100 nm in diameter) could be observed. On the other hand, the successive dropping of water into the polymer/acetone solution leads to a more defined precipitation of the polymer molecules into nanoparticles. However, significantly larger particles are formed. The slow exchange of DMA as polymer

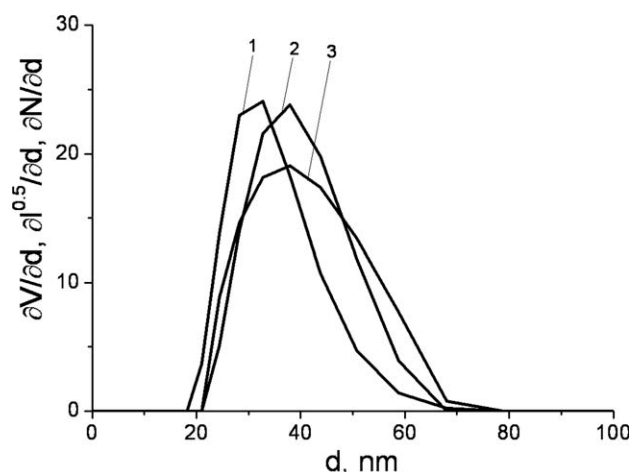


FIGURE 5 Comparison of different size distributions of a poly(MMA-*stat*-MAA)_{1:2} sample (prepared by dropping an acetone solution into water), all determined from DLS data: (1) number distribution, (2) volume distribution, and (3) square root of scattered intensity. Number and volume distributions were automatically calculated from the intensity distribution by using the Mie theory.

TABLE 4 Weight-Average Diameters Calculated from DLS Data Using Different Distributions

N	d_w (nm)			d_w^{av} (nm)
	Square Root of Intensity	Volume	Number	
1	484	406	344	410 ± 50
2	476	455	451	460 ± 10
3	100	105	85	97 ± 8
4	684	661	637	650 ± 10
5	46	41	45	44 ± 2
6	41	40	40	40 ± 1
7	187	177	179	181 ± 4
8	150	149	150	150 ± 1
9	5.83	5.81	5.89	5.8 ± 0.1
10	269	267	261	266 ± 3

solvent against water applying dialysis yields particles with sizes in between the two dropping techniques, though with a broad size distribution.

As a typical example, the size distributions for poly(MMA-*stat*-MAA)_{1:2} particles obtained by DLS, SEM, and AUC are shown in Figure 6. The shapes of the distributions obtained from the different techniques have a similar appearance (i.e., similar modalities of distribution). In Figure 7, the average measured weight diameter values of nanoparticles from corresponding distributions are compared from the different techniques, where the dotted straight line represents parity between the two measurements. In the size range below 150 nm, a satisfactory correlation between the measurements from the different methods is observed. However, at larger sizes (> 300 nm) the measurement values collected by DLS exceed those of d_w^{SEM} . To understand this disparity in the measurements for this size domain, more data must be obtained. The parameter d_w/d_n , which characterizes the

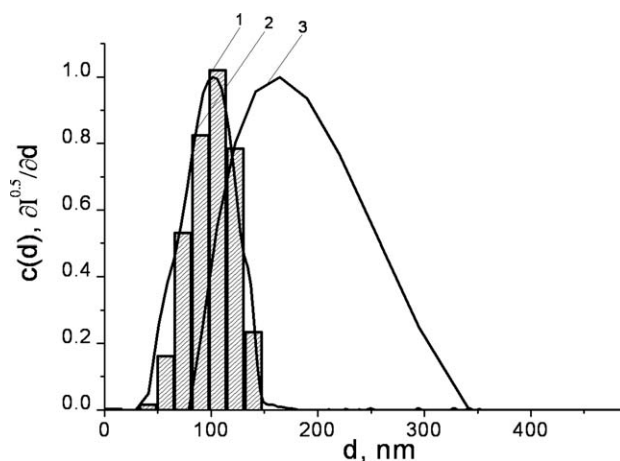


FIGURE 6 Size distribution of nanoparticles (prepared from an acetone solution of poly(MMA-*stat*-MAA)_{1:2} by dropping water into it) as analyzed by (1) SEM (in bars), (2) AUC, and (3) DLS.

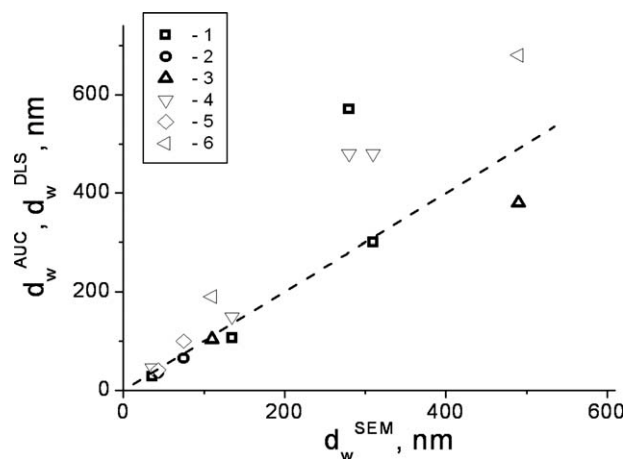


FIGURE 7 A comparison of particle weight-average sizes obtained by different methods. Values obtained by AUC (1–3) and DLS (4–6) plotted against measurements taken using SEM. Particles obtained by the dialysis technique (1,4), by dropping polymer solution into water (2,5), and by dropping water into the polymer solution (3,6), were compared. The dashed line slope is equal to measurement parity.

dimensional polydispersity of the ensemble of nanoparticles, changes in the limits $1.02 \leq d_w/d_n \leq 1.40$, which means that the corresponding molar mass polydispersity M_w/M_n will change in the limits $1.06 \leq M_w/M_n \leq 2.75$. Figure 8 demonstrates the slight increase of the d_w/d_n values with increasing diameter of the particles. The corresponding PDI values are listed in a Table 3.

Analysis of Storage Stability

The effect of storage of the dispersions (in the refrigerator at +4 °C) on particle diameters and size distributions was investigated by velocity sedimentation runs. Figure 9A shows the distributions of the sedimentation coefficient of poly(MMA-*stat*-PyMMA) nanoparticles after different periods of time (1, 2, 4, 7, and 26 weeks, respectively). The shapes

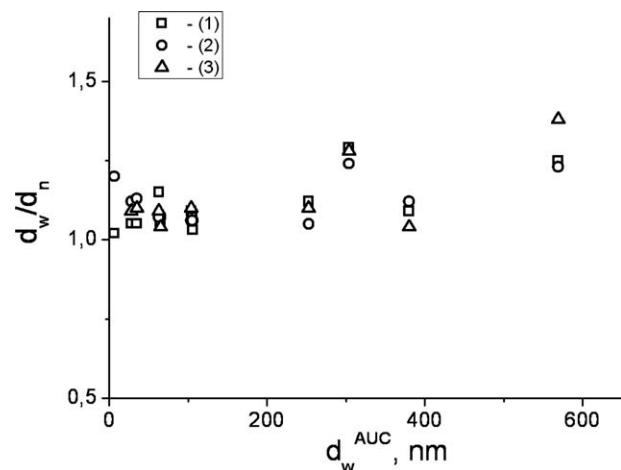


FIGURE 8 Correlation between the PDI values calculated from (1) AUC, (2) DLS, and (3) SEM data and the weight-average sizes estimated from AUC.

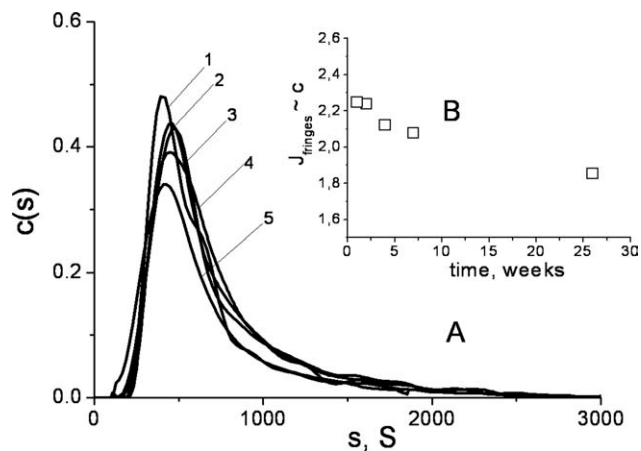


FIGURE 9 Effect of storage on the distribution of the sedimentation coefficients (A) and on the number of interference fringes (B) of a poly(MMA-*stat*-PyMMA) suspension after (1) 1, (2) 2, (3) 4, (4) 7, and (5) 26 weeks of storage.

of the distribution remain virtually the same, whereas the peak position fluctuates around 500 S. The area under the distribution curve is related to the total number of fringes which, in turn, is directly related to the concentration of the dispersed species by the following equation:

$$J = c \left[\frac{kl \Delta n / \Delta c}{\lambda} \right],$$

where λ is the light wavelength, k the magnifying coefficient, and l the optical path.³³ After 6 months, the particle concentration in suspension decreased only by 20% (see Fig. 9B), which could also be confirmed by monitoring the small amounts of sediment in the bottom of the flasks.

CONCLUSIONS

Nanoparticles of homopolymers and copolymers of PMMA were obtained by nanoprecipitation using three different methods. The characteristics of the particle suspensions were investigated by applying SEM, AUC, and DLS measurements. Each of these analysis tools provides information about the characteristics of the particles, however, also coming along with some benefits and disadvantages. SEM imaging shows the approximate shape of the particles but only for a comparatively small section. AUC and DLS measurements provide more statistical information about nanoparticles in suspensions and do not require any drying processes. However, only a few larger aggregates are necessary to influence the DLS results yielding misleading data. Although requiring longer preparation and measurement times, AUC provides information about multimodal size distributions over a wide range of sizes. In this study, the diameters of the nanoparticles obtained by the nanoprecipitation method were in the range of $6 \leq d \leq 600$ nm as revealed and discussed by various measuring principles. The PMMA-based polymers form dispersions of spherical-shaped

particles in the nanoscale range, which are stable for at least 6 months.

The authors thank the Dutch Polymer Institute (DPI), Evonik Röhm GmbH and the Thuringian Ministry for Education, Science and Culture (grant #B514-09,051, NanoConSens) for financial support. The authors thank Evonik Röhm GmbH for providing the PMMA-PAA and PMMA-PEA copolymers; the other polymers were prepared by C. Pietsch (FSU Jena). The authors thank Dr. Richard Hoogenboom and in particular Prof. Dr. Dieter Schubert for helpful comments.

REFERENCES AND NOTES

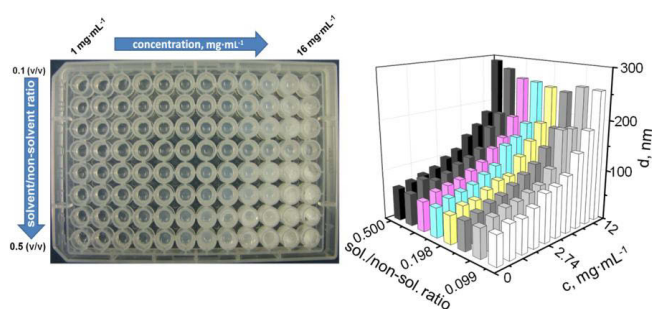
- Svedberg, T.; Rinde, H. *J Am Chem Soc* 1924, 46, 2677.
- Ashford, M.; Fell, J. T.; Attwood, D.; Woodhead, P. J. *Int J Pharm* 1993, 91, 241–245.
- Josephson, L.; Kircher, M. F.; Mahmood, U.; Tang, Y.; Weisleder, R. *Bioconjug Chem* 2002, 13, 554–560.
- Santra, S.; Dutta, D.; Walter, G. A.; Moudgil, B. M. *Technol Cancer Res Treat* 2005, 4, 593–602.
- Mundargi, R. C.; Babu, V. R.; Rangaswamy, V.; Patel, P.; Aminabhavi, T. M. *J Control Release* 2008, 125, 193–209.
- Fessi, H.; Devissaguet, J.; Puisieux, F.; Thies, C. U.S. Patent 5,118,528, 1990.
- Fessi, H.; Puisieux, F.; Devissaguet, J.; Ammoury, N.; Benita, S. *Int J Pharm* 1989, 55, R1–R4.
- Govender, T.; Stolnik, S.; Garnett, M.; Illum, L.; Davis, S. *J Control Release* 1999, 57, 171–185.
- Guterres, S.; Fessi, H.; Barrat, G.; Puisieux, F.; Devissaguet, J. *Int J Pharm* 1995, 113, 57–63.
- Lassalle, V.; Ferreira, M. *Macromol Biosci* 2007, 7, 767–783.
- Hornig, S.; Heinze, T. *Biomacromolecule* 2008, 9, 1487–1492.
- Hornig, S.; Heinze, T.; Biskup, C.; Gräfe, A.; Wotschadlo, J.; Liebert, T.; Mohr, G. *Soft Matter* 2008, 4, 1169–1172.
- Hornig, S.; Heinze, T.; Becer, C.; Schubert, U. S. *J Mater Chem* 2009, 19, 3838–3840.
- Becer, C.; Babiuch, K.; Pilz, D.; Hornig, S.; Heinze, T.; Gottschaldt, M.; Schubert, U. S. *Macromolecules* 2009, 42, 2387–2394.
- Jiang, J.; Tong, X.; Zhao, Y. *J Am Chem Soc* 2005, 127, 8290–8291.
- Pietsch, C.; Fijten, M.; Lambermont-Thijs, H.; Hoogenboom, R.; Schubert, U. S. *J Polym Sci Part A: Polym Chem* 2009, 47, 2811–2820.
- Pietsch, C.; Hoogenboom, R.; Schubert, U. S. *Polym Chem* 2010, DOI: 10.1039/c0py00162g.
- Collins, T. *BioTechniques* 2007, 43, 25–30.
- Schuck, P. *Biophys J* 2000, 78, 1606–1619.
- Friskens, B. *Appl Opt* 2001, 40, 4087–4091.
- Koppel, D. *J Chem Phys* 1972, 57, 4814–4820.
- Pecora, R. *J Nanopart Res* 2000, 2, 123–131.
- Lassalle, V.; Ferreira, M. *Macromol Biosci* 2007, 7, 767–783.
- Jeong, Y.; Cheon, J.; Kim, S.; Nah, J.; Lee, Y.; Sung, Y.; Akaite, T.; Cho, C. *J Control Release* 1998, 51, 169–178.
- Schuck, P.; Rossmannith, P. *Biopolymers* 2000, 54, 328–341.
- Mächtle, W. *Makromol Chem* 1984, 185, 1025–1039.
- Müller, H. G.; Herrmann, F. *Prog Colloid Polym Sci* 1995, 99, 114–119.
- This type of relation was first used by Svedberg and Estrup for an estimation of the sizes of particles of various dispersions sedimenting in the Earth gravitation field. Later, the relation was used by Dumanski, Zobotinski, and Ewsejew for colloidal gold particles sedimenting in a low speed ultracentrifuge. (a) Svedberg, T.; Estrup, K. *Kolloid-Zeitschr* 1911, 9, 259–261; (b) Dumanski, A.; Zobotinski, E.; Ewsejew, M. *Kolloid-Zeitschr* 1913, 12, 6–11.
- McCracken, M.; Sammons, M. *J Pharm Sci* 1987, 76, 56–59.
- Hallet, F.; Watton, J.; Krygsman, P. *Biophys J* 1991, 59, 357–362.
- Bootz, A.; Vogel, V.; Schubert, D.; Kreuter, J. *Eur J Pharm Biopharm* 2003, 72, 369–375.
- Mie, G. *Annalen der Physik Vierte Folge* 1908, 25, 377–445.
- Pavlov, G.; Finet, S.; Tatarenko, K.; Korneeva, E.; Ebel, C. *Eur Biophys J* 2003, 32, 437–449.

Publication 3

"Examination and optimization of the self-assembly of biocompatible, polymeric nanoparticles by high-throughput nanoprecipitation"

Igor Y. Perevyazko, Joseph T. Jr. Delaney, Antje Vollrath,
George M. Pavlov, Stephanie Schubert, Ulrich S. Schubert

Soft Matter **2011**, 7, 5030–5035.



Cite this: *Soft Matter*, 2011, **7**, 5030

www.rsc.org/softmatter

PAPER

Examination and optimization of the self-assembly of biocompatible, polymeric nanoparticles by high-throughput nanoprecipitation†

Igor Y. Perevyazko,^{ab} Joseph T. Delaney, Jr.,^{abc} Antje Vollrath,^{ab} Georges M. Pavlov,^{abc} Stephanie Schubert^{abd} and Ulrich S. Schubert^{*abc}

Received 17th January 2011, Accepted 21st March 2011

DOI: 10.1039/c1sm05079f

In recent years, the development of polymer nanoparticle suspensions by nanoprecipitation has gained increased attention both by industry and academia. However, the process by which such formulations are prepared is a highly empirically driven enterprise, whereby developing optimized formulations remains an iterative process. In this contribution, a new approach towards exploration of the materials space for these systems is reported, based on systematically varying processing and formulation to understand their influence on the characteristics of the resulting materials. Taking advantage of the tools and techniques that have already been standardized by informatics-driven life sciences disciplines, we have prepared libraries of nanoparticle formulations of poly(methyl methacrylate-*stat*-acrylate), poly(lactic-*co*-glycolic acid), and acetal-derivatized dextran by using a pipetting robot. They were subsequently characterized using a dynamic light scattering plate reader, analytical ultracentrifugation, and scanning electron microscopy. With this high-throughput nanoprecipitation approach, large numbers of materials can be prepared, screened, and the formulation rationally optimized.

Introduction

Polymer-based nanoparticle dispersions offer tremendous opportunities for tailoring biologically active materials, such as drugs,^{1,2} transfection agents,³ and agrochemicals, with respect to improved bioavailability and specificity of delivering.^{4,5} Several techniques like emulsification–solvent diffusion, salting out, and nanoprecipitation (solvent shifting) are established for the production of the polymeric particles.⁶ Nanoprecipitation is a very mild and common method and represents the process of nanoparticle formation by self-assembly of polymer molecules during an exchange of a solvent against a non-solvent that is miscible with the solvent.⁷ For this approach, various synthetic polymers as well as biopolymers can be used.^{8–10}

Besides its application for completely hydrophobic polymers, nanoprecipitation is also used for the preparation of nanovesicles and micelles on the basis of amphiphilic block copolymers.^{11,12} The process and mechanism of the nanoparticle formation were

intensively investigated in the last decades.^{13–15} Recent publications on this topic come up with the theory of the “Ouzo effect”.^{16–19} The “Ouzo effect” or the spontaneous emulsification effect is a phenomenon observed when water is added to Ouzo (Greek liquor) forming a milky and highly stable oil-in-water microemulsion. This effect also occurs if a solution of the hydrophobic polymer is rapidly brought into a metastable region by the addition of a non-solvent.¹⁶

However, in order to identify suitable nanoparticle formulations with predictable performance as well as the process parameters leading to them, knowledge and understanding of the relationships between formulation, process parameters, and properties of the end product are beneficial. While many publications are available in this area, there is still no “unified theory” for predicting particle size, size distribution, and dispersion stability *ab initio* for complex systems.^{20–24} Thus, even if significant efforts are spent in order to create a manageable workflow, large numbers of samples are required to explore a particular materials space. To elucidate the material relationships more rigorously, the nanoprecipitation technique was applied as a tool of high-throughput experimentation. In this study, we applied nanoprecipitation on poly(methyl methacrylate-*stat*-acrylate) (p(MMA-*stat*-MAA)_{2:1}), poly(lactic-*co*-glycolic acid) (PLGA) and a hydrophobic dextran derivative. These biocompatible and biodegradable polymers have been widely used in the biomedical industry (p(MMA-*stat*-MAA)_{2:1}, PLGA), but also in basic research (dextran), *e.g.* as nanoparticles for sustained-release formulations.^{25–30} When preparing nanoparticles from these

^aLaboratory of Organic and Macromolecular Chemistry (IOMC), Friedrich-Schiller-University, Humboldtstrasse 10, D-07743 Jena, Germany. E-mail: ulrich.schubert@uni-jena.de

^bJena Center for Soft Matter (JCSM), Friedrich-Schiller-University, Humboldtstrasse 10, D-07743 Jena, Germany

^cDutch Polymer Institute (DPI), Post Office Box 902, Eindhoven, 5600 AX, The Netherlands

^dLaboratory of Pharmaceutical Technology, Friedrich-Schiller-University, Otto-Schoott-Strasse 41, D-07743 Jena, Germany

† Electronic supplementary information (ESI) available. See DOI: 10.1039/c1sm05079f

compounds, a number of questions immediately emerge related to the processing conditions, *e.g.*, concerning the influence of the initial polymer concentration and the solvent-to-non-solvent ratio.^{13,20} In order to investigate such an influence directly, we have systematically prepared nanoparticle populations of various polymers under varied conditions using liquid handling robots, and we have characterized plates of different formulations in an automated manner using high-throughput dynamic light scattering (HT-DLS). Such systems are usually applied for the characterization of proteins and other nanostructured biological samples, but surprisingly only few reports can be found that deal with non-biological nanoparticles.^{31–33} Selected samples were further characterized using different analytical techniques, including analytical ultracentrifugation (AUC) and scanning electron microscopy (SEM). This side-by-side comparison allows for the general evaluation of the reliability of the HT measurement and supplies additional opportunities for the analysis of the process–property relationships.^{34–37} This high-throughput approach may lead to improved particle formulations, *e.g.* for drug delivery; it may also be useful for systematic biotechnological screenings.

Experimental section

Materials

The statistical copolymer p(MMA-*stat*-MAA)_{2:1} (Eudragit® S100), with $M_w = 25\,000\text{ g mol}^{-1}$ and PDI = 1.96, was kindly provided by Evonik Röhm GmbH (Darmstadt, Germany). PLGA (50 : 50, acid terminated, $M_w = 13\,900\text{ g mol}^{-1}$ and PDI = 2.03) was purchased from Sigma Aldrich and used without further treatment. Dextran acetal (ac-dex) was prepared as previously described³⁸ from pharma grade dextran (*Leuconostoc mesenteroides* strain no. NRRL B-512(F) with $M_w = 61\,600\text{ g mol}^{-1}$), as purchased from Pharmacosmos. The reaction time was 20 minutes, leading to degrees of substitution (DS) with cyclic acetals of 1.37 and with acyclic acetals of 0.80, as confirmed by ¹H NMR spectroscopy in DCI/D₂O. The molar mass was determined to be $M_w = 45\,000\text{ g mol}^{-1}$ (PDI = 1.98). Molar masses and PDI indexes were estimated by size exclusion chromatography (SEC) (performed on a Shimadzu system equipped with a SCL-10A VP system controller, a LC-10AD VP pump, and a RID-10A refractive index detector). DMA containing 0.21% LiCl (m/v) was used as eluent, at a flow rate of 1 mL min^{-1} at 40 °C. The calibration standard used during SEC was polystyrene. The chemical structures of the polymers are presented in the ESI†.

Preparation of the nanoparticle suspensions

Nanoparticles were prepared by the nanoprecipitation method from a stock polymer solution in acetone, with solute concentrations of 10 mg mL^{-1} and 16 mg mL^{-1} . The initial polymer solutions were filtered *via* a $0.45\text{ }\mu\text{m}$ filter. In order to formulate the particles in a 96 well microtiter plate, a pipetting robot (FasTrans, Analytik Jena GmbH, Jena, Germany) was used.

Nanoparticles can be prepared by nanoprecipitation in two general ways: (1) by addition of the non-solvent into the polymer solution, or (2) by adding the polymer solution to the non-solvent. In general, due to fast evaporation of the acetone, it was

much more convenient to add the polymer solution to water, rather than *vice versa*. Nevertheless, particle preparation was done in both ways. Nanoprecipitation was performed in an automated way by the fast injection of the polymer solution (or the non-solvent water) to a well containing water (or the polymer solution). The effective final volume of the well was $300\text{ }\mu\text{L}$. The formed nanosuspension was then mixed three times by suction, using $200\text{ }\mu\text{L}$ tips. Subsequently, the plate was placed in a fume hood where the acetone was completely removed from the suspension by evaporation. For the ac-dex nanoparticles, water adjusted to pH > 7 with triethylamine was used, to prevent deacetalization.³⁸

Scanning electron microscopy (SEM)

The nanoparticle suspensions were diluted with filtered deionized water to a final concentration of 1 mg mL^{-1} . They were characterized using a LEO-1450 VP SEM (Leo, Oberkochen, Germany), operating at 10 kV. One droplet (15 to $20\text{ }\mu\text{L}$) of the suspension was placed on a mica surface and lyophilized for 3 h. Finally, the sample was coated with gold, using a BAL-TEC SCD005 sputtering device (Balzers, Lichtenstein) and applying a current of 60 mA for 80 s.

Sedimentation velocity experiments

Sedimentation velocity experiments were performed with a ProteomeLab XLI Protein Characterization System analytical ultracentrifuge (Beckman Coulter, Brea, CA), using conventional double-sector Epon centerpieces of 12 mm optical path length and a four hole rotor. Rotor speed was 3000 to 40 000 rpm, depending on the sample. Cells were filled with $420\text{ }\mu\text{L}$ of nanoparticle suspension at initial concentration and $440\text{ }\mu\text{L}$ of solvent (H₂O). The nanoparticle suspensions were used without further purification. Before the run, the rotor was equilibrated for approximately 2 h at 20 °C in the centrifuge. Sedimentation profiles were obtained every 15 s at the same temperature by interference optics.

Particle characterization by DLS

DLS was performed on the DynaPro Plate Reader Plus (Wyatt Technology Corporation, Santa Barbara, CA) equipped with a 60 mV linearly polarized gallium arsenide (GaAs) laser of $\lambda = 832.5\text{ nm}$ and operating at an angle of 156°. The data were analyzed with the Dynamics software ver. 6.10 by the method of cumulants.³⁹ The percent of polydispersity is given by,

$$\%Pd = 100 \frac{\mu_2}{\mu_1^2}, \quad (1)$$

where μ_1 and μ_2 are the first and the second order cumulant, respectively. The level of homogeneity is considered high when the percent polydispersity is less than 15%. If the level of homogeneity is low (percent polydispersity larger than 30%), the particle population can be considered as being polydisperse.

For selected samples, the determination of the particles size and ζ potential measurements were performed using a Zetasizer Nano ZS (Malvern instruments, Malvern, UK). In these measurements, a laser beam at 633 nm was used and a scattering angle of 173°. Each sample was measured in triplicate at 25 °C

for 30 s in a low volume polycarbonate cell. For this purpose, 20 μL nanoparticle suspensions were diluted with 1 mL demineralized, filtered water. The mean particle size was approximated as the effective (Z average) diameter obtained by the cumulant method.

Results and discussions

In a first set of experiments, the pipetting robot was used to create a dilution series of $\text{p(MMA-}i\text{stat-MAA)}_{2:1}$ ranging from 1 to 16 mg mL^{-1} (12 different solutions in acetone with logarithmically scattered concentrations). These samples were then each combined with eight different proportions of water, in a way that the acetone solution/water ratios varied from 0.099 to 0.500 (again scattered logarithmically). To ensure the reproducibility of the preparation procedure, particles were formulated three times under the same conditions. The net result were three arrays of each 96 different formulations, which exhibited a visually observable trend in appearance, following the changes made in the nanoprecipitation process (Fig. 1). At the lowest concentrations, a faintly opalescent suspension was obtained; as the concentration increased, the opalescence became more apparent. At the highest concentrations, macroscopic precipitates were evident. In terms of solvent/non-solvent ratios, a similar trend could be observed, though only at higher polymer concentrations. By taking a closer look at the instrumental analysis data, one can identify trends and try to account for the visual observations in the array.

Initially, a DLS plate reader was used to measure the mean particle size. In Fig. 2, the average particle size of the $\text{p(MMA-}i\text{stat-MAA)}_{2:1}$ samples is presented as a function of the polymer concentration and the solvent/non-solvent ratio (A—particles prepared by adding the polymer solution into water; B—particles prepared by adding water into the polymer solution). The $\text{p(MMA-}i\text{stat-MAA)}_{2:1}$ particles of A have sizes between 60 nm and 290 nm, whereas those of B vary from 30 nm to 180 nm. At dilute polymer concentrations, the nanoprecipitation process yields a single particle population with narrowly distributed

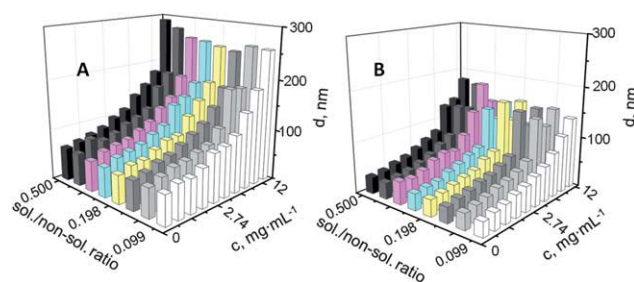


Fig. 2 3D-Representation of a size distribution as a function of initial concentration of the polymer and solvent to non-solvent ratio obtained by DLS. Particle suspensions of $\text{p(MMA-}i\text{stat-MAA)}_{2:1}$ prepared by (A) dropping the polymer solution into water and (B) by dropping water into the polymer solution.

diameters. For both preparation techniques, the mean particle diameter increases as a function of the initial polymer concentration. Fig. 3A shows the double logarithmic plot of the average size on the initial polymer concentration at different solvent/non-solvent ratios. It is worth noting that two distinct areas can be distinguished: low and intermediate concentration of the polymer (1–6 mg mL^{-1}) can correspond to the Ouzo region.¹⁶ This region is located between the binodal (miscibility limit curve) and spinodal (stability limit curve) on a three component phase diagram based on hydrophobic solute, solvent, and non-solvent.¹⁶ It was previously claimed that the volume of the particle is proportional to the initial concentration of the polymer, based on the fact that the slopes of the resulting lines are close to 1/3 (for PMMA; use of surfactants).¹⁸ The slope of the linear fit in our case is 0.44 ± 0.01 , whereas for higher concentrations, the slope of the linear fit is increasing to 1.01 ± 0.08 . In combination with higher particle polydispersity indexes observed in this range, such a behavior may testify a shift beyond the Ouzo region. After exceeding the concentration of 10 mg mL^{-1} , nanoprecipitation additionally produces particles with diameters larger than ~ 300 nm as well as macroscopic aggregates with diameters >1000 nm; the latter are immediately apparent upon

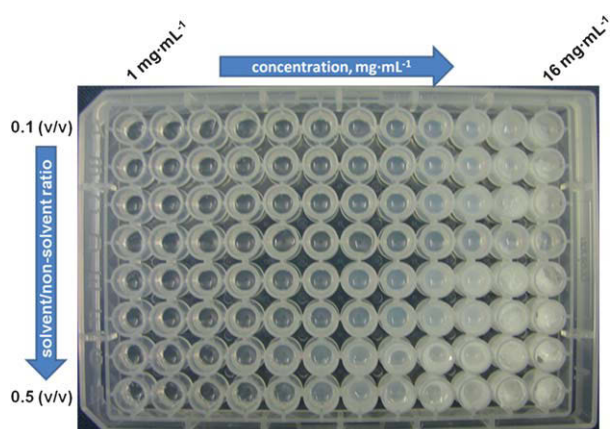


Fig. 1 Layout of a nanoprecipitation experiment: the concentration of copolymer $\text{p(MMA-}i\text{stat-MAA)}_{2:1}$ is varied along the x -axis and the ratio of solvent/non-solvent solution along the y -axis. The polymer concentration in each well is a product of the initial concentration of the polymer and the solvent/non-solvent ratio.

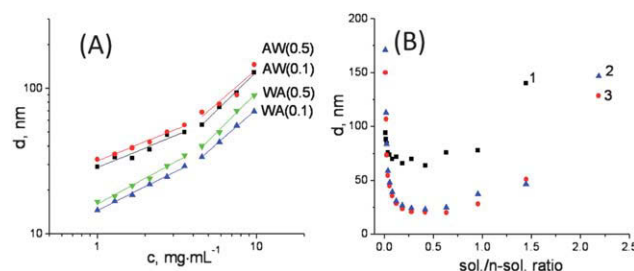


Fig. 3 (A) Double logarithmic plot of the average diameters of $\text{p(MMA-}i\text{stat-MAA)}_{2:1}$ nanoparticles as a function of the initial polymer concentration at solvent/non-solvent ratios of 0.1 and 0.5. The particles were prepared by addition of the polymer acetone solution to water (AW) or by addition of water to the polymer acetone solution (WA). Straight lines are the linear fits. (B) Dependence of the mean sizes of the formed particles on the solvent/non-solvent ratio where (1) the initial polymer concentration was kept constant at 3.57 mg mL^{-1} , (2) polymer concentration in the final mixture was kept constant at 0.1 mg mL^{-1} , and (3) amount of the polymer in the final mixture was kept constant at 0.1 mg. The particles were prepared by adding polymer solution to water.

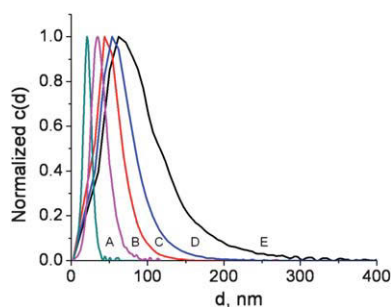


Fig. 4 Normalized size distributions obtained by analytical ultracentrifugation of the p(MMA-*stat*-MAA)_{2:1} nanoparticle suspensions prepared by dropping polymer solution into water at various concentrations: A—1.00 mg mL⁻¹, B—3.53 mg mL⁻¹, C—5.84 mg mL⁻¹, D—7.51 mg mL⁻¹, E—9.67 mg mL⁻¹. The corresponding weight average sizes are: 25, 45, 52, 73 and 130 nm. The value of the solvent/non-solvent ratio was kept constant at 0.157.

visual inspection. In the set of three experiments performed in parallel, the reproducibility was found to be good: average diameters differ from the mean by less than 10%.

Interestingly, the solvent/non-solvent ratio had a comparatively small effect on the sizes of the formed particles in the studied region. Therefore, another set of nanoparticle suspensions representing a broader range of the solvent ratio was prepared and analyzed by DLS. Since the amount of the polymer in the final solution will increase with the solvent/non-solvent ratio, the size of the particles may also be affected. Thus, the experiment was prepared at different conditions: at constant initial concentration (1), at constant final polymer concentration (2), and at constant amount of the polymer in the final mixture (3). The dependence of the mean particles diameter on the ratio is shown in Fig. 3B, where various regions can be distinguished. At low solvent/non-solvent ratios (0.01 to 0.1), the particle diameter is decreasing with increasing solvent/non-solvent ratio. Since the particle formation occurs through nucleation, such a behavior

can apparently be interpreted as an increase in nucleation sites, which leads to the formation of smaller particles.¹⁸ The minimum size was reached in all cases at ratio values from 0.3 to 0.4, which corresponds to the maximum number of nucleation sites. At a higher solvent content with ratios from 1.44 to 3.3, the nucleation process is more difficult, thus, less nuclei will be formed.¹⁸ As a consequence, a sharp increase in the mean size of the particles is observed. The formation of microparticles and large aggregates was detected at ratios starting from 2.5. The polydispersity of the nanoparticle suspensions was also found to be affected by the solute concentration: From $c = 1 \text{ mg mL}^{-1}$ to $c = 10 \text{ mg mL}^{-1}$, the polydispersity increased from $(15 \pm 1)\%$ to $(35 \pm 4)\%$, as found by HT-DLS measurements (Table S1†).

The mean size of the particles and the polydispersity do not provide full information on the size-distribution. In an effort to evaluate the applicability and reliability of HT-DLS measurements for the latter problem, a selected subset of samples was also characterized using SEM and AUC. For the AUC experiments, series of nanoparticle samples were prepared from the stock p(MMA-*stat*-MAA)_{2:1} solution with concentrations of 1, 3.57, 5.84, 7.51, and 9.67 mg mL⁻¹ and solvent/non-solvent ratios of 0.099, 0.157, and 0.280, respectively. The resulting size distributions obtained as a function of polymer concentration for a solvent/non-solvent ratio of 0.157 are presented in Fig. 4. The mean diameter increases with the polymer concentration of the polymer while the distribution becomes broader, which corresponds to an increase in the polydispersity of the particles.⁴⁰ The polydispersity index in this case can be calculated as a ratio of the weight average size of the particles, d_w , to the number average size of the particles, d_n , and can be considered as the PDI index in its classical sense;³⁷ d_w and d_n were calculated from the initial size distribution obtained by AUC. The calculated values of the polydispersity indexes are ranging from 1.05 up to 1.20.

The morphology and size distribution of the same nanoparticle suspensions were further investigated by SEM and compared to the DLS and AUC results. In Fig. 5, SEM images and size distributions obtained by SEM and AUC are presented.

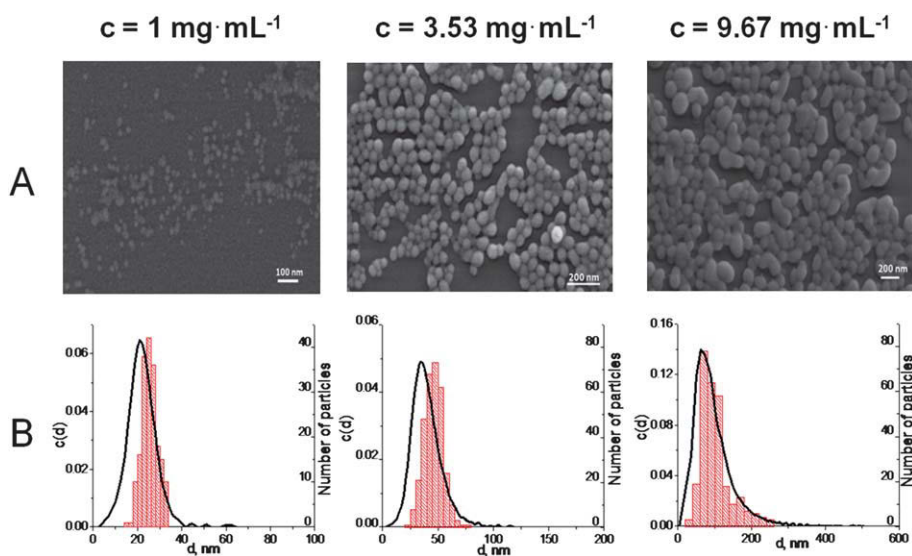


Fig. 5 (A) SEM images of p(MMA-*stat*-MAA)_{2:1} nanoparticles at different concentrations and (B) the corresponding size-distributions obtained by SEM (bars) and by AUC (—). The particles were prepared by dropping the polymer solution into water.

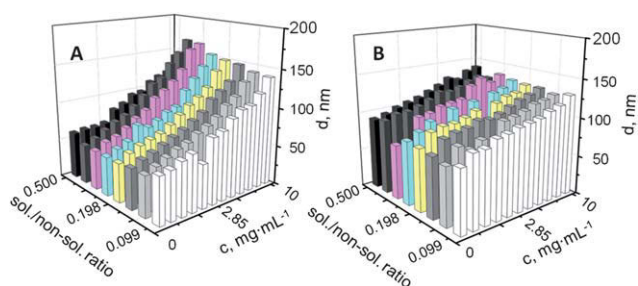


Fig. 6 3D-Representation of a size distribution as a function of initial concentration of PLGA (A) and ac-dex (B) and solvent to non-solvent ratio obtained by DLS. The particle suspensions were prepared by dropping the polymer solution into water.

In the case of low and intermediate polymer concentrations, the SEM results only show nanoparticles with smooth surfaces, regular shapes, and narrow size distribution. The number of individual particles considered for calculating the size distributions was 260 ± 40 . The calculated weight average sizes are 27, 49 and 141 nm, respectively. Polydispersity values were estimated to be 1.02, 1.09, and 1.18 by the same manner as for AUC. It is apparent that a satisfactory correlation exists between the sizes and polydispersity indexes obtained from either AUC or SEM, whereas the size values collected by DLS exceed those from both AUC and SEM. A detailed comparison of the various characterization techniques for polymeric nanoparticles, performed on the same $p(\text{MMA-}i\text{stat-MAA})_{2:1}$ samples, was published recently.³⁷

Surface charge is another important characteristic of polymeric nanoparticles. It provides information about the stability and is also a significant factor affecting cellular uptake.^{41,42} The charge distribution is typically quantified by the ζ (zeta) potential. In this study, a correlation between the ζ potential and the mean size of the particles was identified. ζ Potential measurements were performed for the same series of samples as for the AUC experiments. It was found that the surface charge increased with increasing polymer concentration. On the other hand, the measured ζ potential remained unchanged when the solvent/non-solvent ratio was varied, indicating a correlation between ζ potential and particle size. The value of the ζ potential changed from -17 ± 7 mV for the particles prepared from dilute polymer solution ($c = 1 \text{ mg mL}^{-1}$, solvent/non-solvent ratio: 0.099) to -63 ± 1 mV for the highest concentration used ($c = 9.67 \text{ mg mL}^{-1}$, solvent/non-solvent ratio: 0.099).

In order to present additional examples on the feasibility of high-throughput nanoprecipitation, nanoparticles were also prepared from two other biocompatible polymers, namely poly (lactic-*co*-glycolic acid) (PLGA) spheres and an acetylated dextran (ac-dex). These polymers are suitable as medical delivery devices in the form of nano- or microparticles.^{27,38} PLGA and ac-dex were nanoprecipitated by adding the polymer dissolved in acetone in the non-solvent water. The concentration of the polymer/acetone solutions ranged logarithmically from 1 to 10 mg mL^{-1} . Fig. 6(A and B) show the dependence of the particle size on the solute concentration and on the solvent/non-solvent ratio for particles based on PLGA (A) and ac-dex (B). Again, a concentration dependency is clearly shown. The sizes of PLGA particles vary from 40 nm for $c = 1 \text{ mg mL}^{-1}$ to 170 nm

for $c = 10 \text{ mg mL}^{-1}$, whereas ac-dex particles show the formation of particles from 80 nm to 140 nm for the same range of concentrations. On the other hand, the particle size is only weakly dependent on the solvent/non-solvent ratio.

By comparing the dependencies of nanoparticle size on the polymer concentration (Fig. 7), different trends can be revealed. As mentioned before, the size dependence of $p(\text{MMA-}i\text{stat-MAA})_{2:1}$ changes at different concentration ranges. In contrast, the sizes of the ac-dex and PLGA particles increase linearly in the whole interval of concentration examined. The slopes of the resulting lines for the ac-dex and PLGA are 0.21 and 0.44, respectively (an overview of slopes is presented in Table S3† in the ESI). These differences could be due to the differences in hydrophobicity of the two polymers: ac-dex contains a certain amount of OH groups (0.83 mol hydroxyls per mol anhydroglucose unit), which are assumed to be preferentially located at the particle surface and might stabilize the particle in addition to the surface charge, thus, preventing their further growth and aggregation. PLGA nanoparticles follow a trend between the two other polymers. This may imply a hydrophobicity of PLGA in between $p(\text{MMA-}i\text{stat-MAA})_{2:1}$ and ac-dex. Recently, the effect of hydrophobic-hydrophilic interactions on the formation and properties of nanoparticles was discussed in the literature.^{43,44} However, additional studies seem to be necessary to settle this problem, whereas using the present HT approach might be the appropriate tool.

Selected samples of PLGA and ac-dex were also investigated by a second DLS equipment (Zetasizer Malvern instruments) and compared to the data obtained by HT-DLS. The resulting values are in satisfactory agreement (Table S2†). For an accurate size and molar mass estimation by AUC, complementary experiments were carried out in order to determine the dynamic viscosities and densities of the nanoparticle suspensions. Viscosity and density of the suspensions are very close to water values at ambient conditions and only at high concentrations a slight increase is detected. More detailed information about the size, polydispersity, and ζ potential of the different polymers are presented in the ESI†.

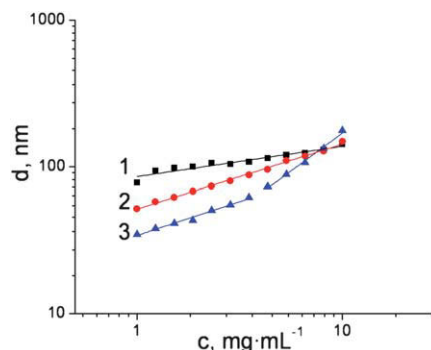


Fig. 7 (1) Ac-dex, (2) PLGA, and (3) $p(\text{MMA-}i\text{stat-MAA})_{2:1}$ nanoparticle sizes as a function of the initial polymer concentration on a double logarithmic dependence. The plotted sizes of $p(\text{MMA-}i\text{stat-MAA})_{2:1}$ particles are average diameters of three formulations under the same conditions. Straight lines represent a linear fit of the experimental data. The solvent/non-solvent ratio was kept constant at 0.157.

Conclusions

We have presented a new approach for the production of nanoparticles using nanoprecipitation technology. This approach allows the automated, reproducible preparation of nanoparticle suspensions in large numbers and thus identifying the optimal conditions for the preparation of particles with desired size and polydispersity. The work presents the formulation of p(MMA-*stat*-MAA)_{2:1}, PLGA and a dextran acetal including fast characterization of the suspensions by high-throughput dynamic light scattering. More detailed information were obtained by using additional analysis techniques, like analytical ultracentrifugation and scanning electron microscopy, in order to evaluate and prove the results. For selected polymer/solvent/non-solvent systems, the influence of the polymer concentration and the solvent/non-solvent ratio as well as the polymer structure on the particle formation was studied. The appropriate conditions were found to “dial in” particle sizes from 20 to 300 nm, depending on the way of preparation and initial conditions. The stability of the particles was confirmed in terms of ζ potential measurements. In summary, the formulation of different nanosuspensions can be performed in an automatic, reproducible manner, which opens an easy and efficient way for exploring various compositions. In the future, structure–property relationship will be elucidated using this high-throughput approach in order to prepare tailor-made particle formulations with desired sizes and loadings.

Acknowledgements

The authors are grateful to the Thuringian Ministry for Education, Science, and Culture (grant #B514-09051, NanoConSens) and to the Dutch Polymer Institute (DPI, Technology Area HTE) for financial support. They would also like to thank Evonik Röhm GmbH for providing polymers, Frank Steininger from the Elektronenmikroskopie Zentrum (EMZ), Jena, for the SEM measurements, and Prof. Dr. Dieter Schubert for helpful comments. Dedicated to Kazunori Kataoka on the occasion of his 60th birthday.

Notes and references

- 1 E. Allemann, R. Gurny and E. Doelker, *Eur. J. Pharm. Biopharm.*, 1993, **39**, 173–191.
- 2 C. E. Mora-Huertas, H. Fessi and A. Elaissari, *Int. J. Pharm.*, 2010, **385**, 113–142.
- 3 K. Tahara, H. Yamamoto, H. Takeuchi and Y. Kawashima, *J. Pharm. Soc. Jpn.*, 2007, **127**, 1541–1548.
- 4 A. L. Boehm, I. Martinon, R. Zerrouk, E. Rump and H. Fessi, *J. Microencapsulation*, 2003, **20**, 433–441.
- 5 A. L. L. Boehm, R. Zerrouk and H. Fessi, *J. Microencapsulation*, 2000, **17**, 195–205.
- 6 C. Vauthier and K. Bouchemal, *Pharm. Res.*, 2009, **26**, 1025–1058.
- 7 H. Fessi, F. Puisieux, J. P. Devissaguet, N. Ammoury and S. Benita, *Int. J. Pharm.*, 1989, **55**, R1–R4.
- 8 R. Labruère, R. Sicard, R. Cormier, E. Turos and L. West, *J. Controlled Release*, 2010, **148**, 234–240.
- 9 S. Hornig, H. Bunjes and T. Heinze, *J. Colloid Interface Sci.*, 2009, **338**, 56–62.
- 10 V. Lassalle and M. L. Ferreira, *Macromol. Biosci.*, 2007, **7**, 767–783.
- 11 D. Li, C. Li, G. Wan and W. Hou, *Colloids Surf., A*, 2010, **372**, 1–8.
- 12 N. Karanikolopoulos, M. Zamurovic, M. Pitsikalis and N. Hadjichristidis, *Biomacromolecules*, 2009, **11**, 430–438.
- 13 S. Stainmesse, A. M. Orecchioni, E. Nakache, F. Puisieux and H. Fessi, *Colloid Polym. Sci.*, 1995, **273**, 505–511.
- 14 D. Horn and J. Rieger, *Angew. Chem., Int. Ed.*, 2001, **40**, 4330–4361.
- 15 M. C. Brick, H. J. Palmer and T. H. Whitesides, *Langmuir*, 2003, **19**, 6367–6380.
- 16 S. A. Vitale and J. L. Katz, *Langmuir*, 2003, **19**, 4105–4110.
- 17 F. O. Ganachaud and J. L. Katz, *ChemPhysChem*, 2005, **6**, 209–216.
- 18 J. Aubry, F. Ganachaud, J. P. Cohen Addad and B. Cabane, *Langmuir*, 2009, **25**, 1970–1979.
- 19 M. Beck-Broichsitter, E. Rytting, T. Lebbardt, X. Wang and T. Kissel, *Eur. J. Pharm. Sci.*, 2010, **41**, 244–253.
- 20 E. Plasari, P. H. Grisoni and J. Villermaux, *Chem. Eng. Res. Des.*, 1997, **75**, 237–244.
- 21 O. Thioune, H. Fessi, J. P. Devissaguet and F. Puisieux, *Int. J. Pharm.*, 1997, **146**, 233–238.
- 22 M. Chorny, I. Fishbein, H. D. Danenberg and G. Golomb, *J. Controlled Release*, 2002, **83**, 389–400.
- 23 P. Legrand, S. Lesieur, A. Bochot, R. Gref, W. Raatjes, G. Barratt and C. Vauthier, *Int. J. Pharm.*, 2007, **344**, 33–43.
- 24 S. Galindo-Rodriguez, E. Allémann, H. Fessi and E. Doelker, *Pharm. Res.*, 2004, **21**, 1428–1439.
- 25 A. Vollrath, S. Schubert, N. Windhab, C. Biskup and U. S. Schubert, *Macromol. Rapid Commun.*, 2010, **31**, 2053–2058.
- 26 T. Govender, S. Stolnik, M. C. Garnett, L. Illum and S. S. Davis, *J. Controlled Release*, 1999, **57**, 171–185.
- 27 R. Manchanda, A. Fernandez-Fernandez, A. Nagesetti and A. J. McGoron, *Colloids Surf., B*, 2010, **75**, 260–267.
- 28 C. E. Astete and C. M. Sabilov, *J. Biomater. Sci., Polym. Ed.*, 2006, **17**, 247–289.
- 29 T. T. Beaudette, J. A. Cohen, E. M. Bachelder, K. E. Broaders, J. L. Cohen, E. G. Engleman and J. M. J. Fréchet, *J. Am. Chem. Soc.*, 2009, **131**, 10360–10361.
- 30 S. Hornig, C. Biskup, A. Grafe, J. Wotschadlo, T. Liebert, G. J. Mohr and T. Heinze, *Soft Matter*, 2008, **4**, 1169–1172.
- 31 F. He, G. W. Becker, J. R. Litowski, L. O. Narhi, D. N. Brems and V. I. Razinkov, *Anal. Biochem.*, 2010, **399**, 141–143.
- 32 T. Q. Chastek, K. L. Beers and E. J. Amis, *Rev. Sci. Instrum.*, 2007, **78**, 072201–072208.
- 33 A. D. Hanlon, M. I. Larkin and R. M. Reddick, *Biophys. J.*, 2010, **98**, 297–304.
- 34 A. Bootz, V. Vogel, D. Schubert and J. Kreuter, *Eur. J. Pharm. Biopharm.*, 2004, **57**, 369–375.
- 35 M. S. McCracken and M. C. Sammons, *J. Pharm. Sci.*, 1987, **76**, 56–59.
- 36 U. Duclairoir and E. Nakache, *Int. J. Polym. Anal. Charact.*, 2002, **7**, 284–313.
- 37 I. Perevyazko, A. Vollrath, S. Hornig, G. M. Pavlov and U. S. Schubert, *J. Polym. Sci., Part A: Polym. Chem.*, 2010, **48**, 3924–3931.
- 38 E. M. Bachelder, T. T. Beaudette, K. E. Broaders, J. Dashe and J. M. J. Fréchet, *J. Am. Chem. Soc.*, 2008, **130**, 10494–10495.
- 39 D. E. Koppel, *J. Chem. Phys.*, 1972, **57**, 4814–4820.
- 40 W. Mächtle and L. Börger, *Analytical Ultracentrifugation of Polymers and Nanoparticles*, Springer, Berlin, Heidelberg, 2006.
- 41 C. He, Y. Hu, L. Yin, C. Tang and C. Yin, *Biomaterials*, 2010, **31**, 3657–3666.
- 42 M. Gaumet, A. Vargas, R. Gurny and F. Delie, *Eur. J. Pharm. Biopharm.*, 2008, **69**, 1–9.
- 43 S. K. Filippov, L. Starovoytova, C. Koňák, M. Hrubý, H. Macková, G. Karlsson and P. Štěpánek, *Langmuir*, 2010, **26**, 14450–14457.
- 44 D. A. Rao, M. L. Forrest, A. W. G. Alani, G. S. Kwon and J. R. Robinson, *J. Pharm. Sci.*, 2010, **99**, 2018–2031.

Electronic supplementary information

Instrumentation

Sedimentation velocity experiments.

The raw sedimentation data were evaluated by the program Sedfit using continuous $c(s)$, which is based on the numerical resolution of the Lamm equation. It allows the least-squares boundary modeling $ls - g^*(s)$, which describes sedimentation of a non-diffusing species, and to determine the average frictional ratio (f/f_{sph}) of the particles.^{1,2} The partial specific volume v was determined by the density variation method, *i.e.*, by sedimentation velocity experiments on the nanoparticle suspensions, using in parallel H₂O and D₂O. The partial specific volume was found to be $v = (0.78 \pm 0.01) \text{ cm}^3 \cdot \text{g}^{-1}$. Molar masses of the particles were estimated applying the modified Svedberg equation:

$$10 \quad M_s = 9\pi\sqrt{2}N_A\sqrt{[s]^2v}$$

where N_A is the Avogadro's number, v the partial specific volume and $[s]$ is the intrinsic sedimentation coefficient which is defined as:

$$[s] = \frac{s_0\eta_0}{(1-v\rho_0)}$$

where s_0 is the sedimentation coefficient at zero concentration, η_0 the dynamic viscosity of the solvent, and ρ_0 the density of the solvent. The diameters were calculated from the Stokes approximation for a sphere:

$$d = 3\sqrt{2}\sqrt{[s]v}$$

Notes and references

1. P. Schuck, *Biophys. J.*, 2000, **78**, 1606-1619.
2. P. Schuck, P. Rossmannith, *Biopol.*, 2000, **54**, 328-341.
- 20 3. W. G. Martin, W. H. Cook, C. A. Winkler, *Can. J. Chem.*, 1956, **34**, 809-814.
4. W. Maechtler, *Makromolekulare Chemie-Macromolecular Chemistry and Physics*, 1984, **185**, 1025-1039.

25

30

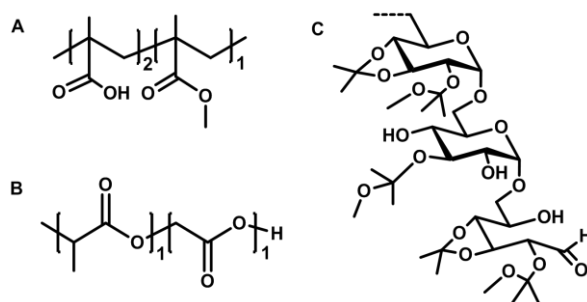


Fig. 1 Chemical structure of the polymers. A - p(MMA-*stat*-MAA)_{2:1}, B - poly(lactic-*co*-glycolic acid) (50:50), C - dextran acetal (DS = 2.17).

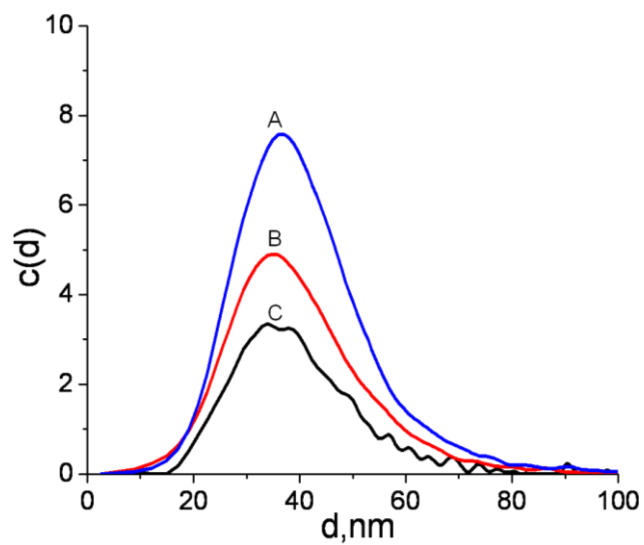


Fig. 2 Size distributions of the nanoparticles at different solvent/non-solvent ratios. The distributions were obtained by sedimentation velocity analysis. The values of the solvent/non-solvent ratio were 0.280 (A), 0.157 (B), and 0.099 (C). The polymer concentration was 3.57 mg·mL⁻¹. The particles were prepared by dropping the polymer solution into water.

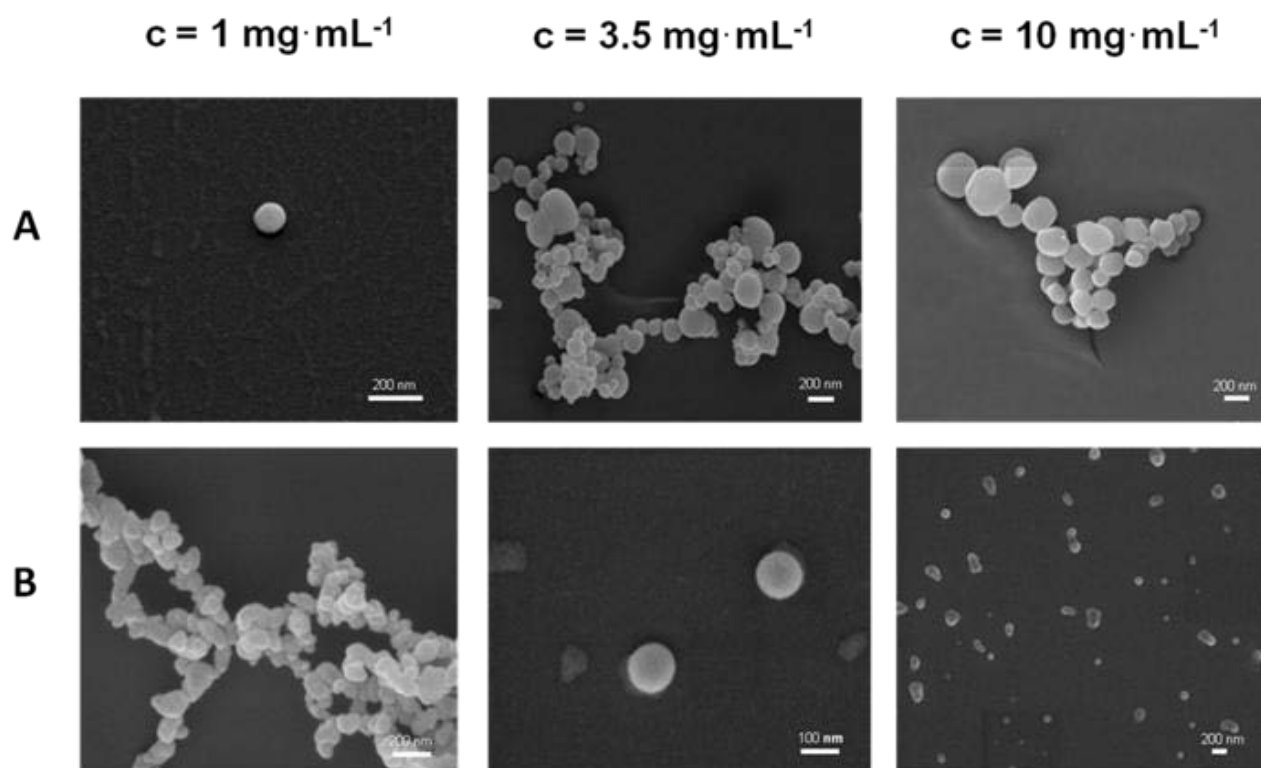


Fig. 3 SEM images of nanoparticles prepared from A) ac-dex and B) PLGA at different polymer concentrations. The particles were prepared by dropping the polymer solution into water.

5

10

15

20

25

30

Table 1 Summary of analytical data for p(MMA-*stat*-MAA)_{2:1} particles

C, mg·mL ⁻¹	sol/n-sol ratio	d _{DLS} ^a nm	d _{AUC} ^a nm	PDI _{AUC}	%Pd _{DLS}	M _n ×10 ⁻⁶ , g·mol ⁻¹	ξ, mV	ρ, g·cm ⁻³	η, cP
1	0.099	46	25	1.05	14.1	6.2	-(17±7)	0.9979	1.0218
	0.157	44	25	1.06	16.0		-(22±4)	0.9978	1.0236
	0.280	42	25	1.04	15.1		-(31±7)	0.9978	1.0220
3.53	0.099	71	43	1.12	25.6	37	-(44±5)	0.9979	1.0234
	0.157	74	45	1.11	26.0		-(59±6)	0.9979	1.0238
	0.280	70	45	1.11	25.2		-(49±3)	0.9980	1.0230
9.67	0.099	240	130	1.19	31.0	1300	-(63±1)	0.9981	1.0292
	0.157	240	130	1.18	35.4		-(62±1)	0.9980	1.0312
	0.280	260	150	1.20	38.9		-(65±1)	0.9983	1.0468

^a ρ denotes the density and η the viscosity of the nanoparticle suspensions

Table 2 Summary of analytical data for ac-dex and PLGA particles

Polymer	C, mg·mL ⁻¹	d _{DLS} ^a Platereader nm	%Pd _{DLS} Platereader	d _{DLS} ^a Zetasizer nm	%Pd _{DLS} Zetasizer	ξ, mV
ac-dex	1	78	14.3	112	22.5	-(16±11)
	3.5	108	17.8	138	20.2	-(16±14)
	10	142	25.2	172	22.2	-(22±10)
PLGA	1	52	14.9	78	18.2	-(14±14)
	3.5	88	16.9	89	16.4	-(22±12)
	10	148	22.2	132	23.5	-(22±12)

Table 3 Slope and best fit coefficient obtained from the linear fit of the mean particle size vs initial concentration plots

Sample	slope [*]	slope ^{**}	slope ^{***}	r ²
p(MMA- <i>stat</i> -MAA) _{2:1}	0.44 ^a	1.01 ^a	0.66 ^b	0.98 ^a 0.94 ^b
PLGA	–	–	0.44	0.99
ac-dex	–	–	0.21	0.93

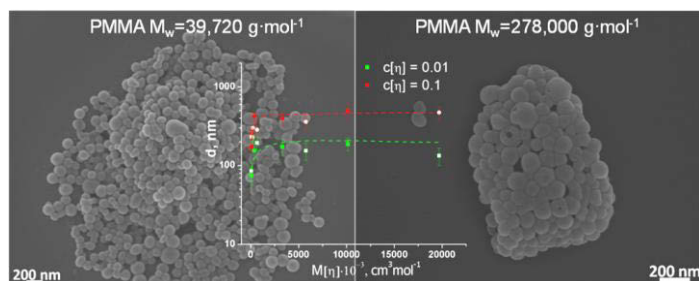
^{*}Linear fit for the data in the 1 – 6 mg·mL⁻¹ range of concentration. ^{**}Linear fit for the data in the 6 – 10 mg·mL⁻¹ range of concentration. Linear fit through all data points.

Publication 4

"Nanoprecipitation of poly(methyl methacrylate)-based nanoparticles: Effect of the molar mass and polymer behavior"

Igor Y. Perevyazko, Antje Vollrath, Christian Pietsch,
Stephanie Schubert, George M. Pavlov, Ulrich S. Schubert

J. Polym. Sci., Part A: Polym. Chem. **2012**, *50*, 2906–2913.



Nanoprecipitation of Poly(methyl methacrylate)-Based Nanoparticles: Effect of the Molar Mass and Polymer Behavior

Igor Y. Perevyazko,^{1,2} Antje Vollrath,^{1,2} Christian Pietsch,^{1,2,3} Stephanie Schubert,^{1,2,4} Georgy M. Pavlov,^{1,2} Ulrich S. Schubert^{1,2,3}

¹Laboratory of Organic and Macromolecular Chemistry (IOMC) Friedrich-Schiller-University, D-07743 Jena, Germany

²Jena Center for Soft Matter (JCSM), Friedrich-Schiller-University, D-07743 Jena, Germany

³Dutch Polymer Institute (DPI), Eindhoven 5600 AX, The Netherlands

⁴Institute of Pharmacy, Department of Pharmaceutical Technology, Friedrich-Schiller-University, D-07743 Jena, Germany

Correspondence to: U. S. Schubert (E-mail: ulrich.schubert@uni-jena.de)

Received 8 March 2012; accepted 14 March 2012; published online 28 April 2012

DOI: 10.1002/pola.26071

ABSTRACT: The current investigation describes in detail the influence of the polymer molar mass as well as polymer-solvent interactions on the formation of nanoparticles using the nanoprecipitation methodology. For this purpose, a homologous series of poly(methyl methacrylates) with molar masses ranging from 7,700 to 274,000 g mol⁻¹ was prepared. Subsequently nanoprecipitation was performed in an automated and systematic manner using liquid handling robots and a variation of different initial concentrations of the polymers and solvent/nonsolvent ratios. To elucidate information about the polymer behavior in the solvents used for the nanoprecipitation proce-

dures (acetone, tetrahydrofuran), intrinsic viscosity measurements were performed. The nanoparticle formulations were examined in terms of particle size and size distribution, particle shape as well as zeta-potential. The conditions for the preparation of stable and uniform nanoparticles, regardless of molar mass and hydrodynamic volume of the initial polymer, were determined. © 2012 Wiley Periodicals, Inc. *J Polym Sci Part A: Polym Chem* 50: 2906–2913, 2012

KEYWORDS: nanoparticles; nanoprecipitation; molar mass; PMMA; synthetic polymers; ultracentrifugation; viscosity

INTRODUCTION Polymeric nanoparticles have been extensively studied in the last decades as potential drug delivery devices. Nanoparticle formation using the nanoprecipitation method¹ is nowadays a commonly used technique. Among the numerous other manufacturing methods, it is known to be a very simple and convenient way for the production of polymeric nanoparticles with desired sizes.^{2,3} A variety of different polymers can be used, such as poly(lactide-co-glycolide),⁴ poly(ϵ -caprolactone),⁵ poly(acrylics), poly(styrene), poly(methyl methacrylate) (PMMA), and its different copolymers as well as various amphiphilic block copolymers.^{6–9} Nanoprecipitation represents a process based on the diffusion of the organic solution (i.e., polymer solvent) into an aqueous phase leading to the precipitation of the polymer into small colloidal particles. The formation of nanoparticles by the process complies with the nucleation theory and consists of several steps like particle nucleation, molecular growing, and aggregation.^{10,11} Stable nanoparticle suspensions are only formed applying specific conditions, which promote a supersaturation of polymer molecules in a ternary polymer/solvent/nonsolvent system and shifts it into a metastable region (Ouzo region).^{9,11–13} This region is located

between the binodal (miscibility limit curve) and spinodal (stability limit curve) on a three component phase diagram based on the hydrophobic solute, the solvent, and the nonsolvent. The resulting properties of the particles primarily depend on the polymer behavior in the organic phase but also on the nature and ratio of the external phase as well as on concentration and nature of the used surfactants.^{14–18} It could be shown repeatedly that the particle size is strongly affected by the initial polymer concentration: higher concentrations lead to an increasing number of molecules per volume of the solvent, which, in turn, leads to the formation of larger particles. At the same time, the ratio between solvent and nonsolvent was found to have a more complex, nonlinear influence on the size of the particles.^{9,18,19} Thorough investigation of the molar mass influence on the production of biodegradable nanoparticles based on poly(lactic acid) was first presented by Legrand et al.¹⁶ This study was designed to determine in detail and to extend the understanding of the effect of the polymer characteristics, in particular the molar mass, on the nanoprecipitation results of synthetic polymers. For this purpose, PMMA samples were investigated in a wide range of molar masses (between M_w

= 7,700 and 274,000 g mol⁻¹) to obtain information about the polymer-solvent interactions and the size of the particles formed. The investigations were carried out in two solvents, namely acetone and tetrahydrofuran (THF). Nanoparticles were prepared in a reproducible and systematic manner by using a liquid handling robot.¹⁹ All formulations were subsequently characterized using dynamic light scattering (DLS) for a fast size determination. In addition, selected samples were studied by analytical ultracentrifugation (AUC) and scanning electron microscopy (SEM).

EXPERIMENTAL

Synthesis of the PMMA Polymers

Methyl methacrylate (MMA) and 2-cyano-2-propyl dithiobenzoate (CPDB) were purchased from Sigma-Aldrich. MMA was purified by treating the monomer with inhibitor-remover (Aldrich). The initiator 2,2'-azobisisobutyronitrile (AIBN) was recrystallized from methanol prior to use. All analytical grade solvents were purchased from commercial sources (Fluka, Aldrich, Alfa Caesar and Acros Organics).

The following procedure illustrates the standard conditions for the reversible addition-fragmentation chain transfer (RAFT) polymerization of MMA.^{20,21} The desired amount of MMA (3.0 mL, 28.12 mmol) was transferred into a reaction vial and dissolved in ethanol (1 mL). Thereafter, the calculated volumes of stock solutions of CPDB (5.19 mg, 0.023 mmol) as well as AIBN (1.92 mg, 0.012 mmol) in ethanol were added. Before closing the vial, the reaction solution was purged with a flow of argon for at least 30 min. Subsequently, the reaction was performed in an oil bath at 70 °C (see Table 1 for exact reaction times, MMA concentration and [M]/[chain transfer agent, CTA] ratios). After the polymerization, acetone was added to the final mixtures, and the polymers were then manually precipitated in cold methanol. The polymers were dried under reduced pressure at 40 °C.

Size-Exclusion Chromatography

Size-exclusion chromatography (SEC) was performed using an Agilent1200 series system, a G1310A pump, a G1362A refractive index detector and both a PSS Gram30 and a PSS Gram1000 column in series, whereby *N,N*-dimethylacetamide with 5 mmol lithium chloride was used as an eluent at 1 mL min⁻¹ flow rate. The column oven was set to 40 °C. The system was calibrated with PMMA standards of narrow dispersity.

Sedimentation Velocity Experiments

Sedimentation velocity experiments were performed with a ProteomeLab XLI Protein Characterization System analytical ultracentrifuge (Beckman Coulter, Brea, CA), using conventional double-sector Epon centerpieces of 12-mm optical path length and a four hole rotor. Rotor speed was 3,000 to 20,000 rpm, depending on the sample. Cells were filled with 420 μL of nanoparticle suspension at the initial concentration and 440 μL of solvent (H₂O). The nanoparticle suspensions were used without further purification. Before the run, the rotor was equilibrated for ~2 h at 20 °C in the centrifuge. Sedimentation profiles were obtained every 15 s by in-

TABLE 1 Selected Characterization Data of the Obtained PMMA Polymers

Sample	[M]:[CTA]: [AIBN]	Conc. mol L ⁻¹	Time, h	<i>M</i> _{w, SEC} g mol ⁻¹	PDI _{SEC}	DP _{SEC}
1	40:1:0.25	2.0	13	7,700	1.13	66
2	200:1:0.25	2.0	13	20,200	1.17	170
3	400:1:0.25	2.0	20.5	39,700	1.26	312
4	1,200:1:0.5	7.03	16	106,000	1.25	846
5	4,000:1:0.5	7.03	16	274,000	1.34	2,035

terference optics. For the analysis of the particle size distribution, the sedimentation velocity data were treated by ls-g*(s) analysis with a Tikhonov-Phillips regularization procedure (confidence level of 0.9 was used) implemented into the Sedfit program. This method is based on a boundary modeling of a superposition of sedimentation profiles of ideal nondiffusing particles.²² For the appropriate size determination by sedimentation velocity, the knowledge of the partial specific volume is essential. A value of $v = 0.78 \pm 0.01$ cm³ g⁻¹ was used, which was determined previously for PMMA and its copolymers.⁸

DLS and Zeta Potential

DLS was performed on the DynaPro Plate Reader Plus (Wyatt Technology Corporation, Santa Barbara, CA) equipped with a 60 mV linearly polarized gallium arsenide (GaAs) laser at 832.5 nm and operating at an angle of 156°. The data were analyzed with the Dynamics software ver. 6.10 by the method of cumulants. The percent of polydispersity is given by,

$$\% Pd = 100 \frac{\mu_2}{\mu_1^2} \quad (1)$$

where μ_1 and μ_2 are the first and the second order cumulant, respectively.

For selected samples, the determination of the particles size and zeta potential measurements was performed using a Zetasizer Nano ZS (Malvern instruments, Malvern, UK). In these measurements, a laser beam at 633 nm was used and a scattering angle of 173°. Each sample was measured in triplicate at 25 °C for 30 s in a low volume polycarbonate cell. For this purpose, 20 μL nanoparticle suspensions were diluted with 1 mL demineralized, filtered water. The mean particle size was approximated as the effective (Z average) diameter obtained by the cumulant method.

SEM

The nanoparticle suspensions were diluted with filtered, deionized water to a final concentration of 1 mg mL⁻¹. They were characterized using a LEO-1450 VP SEM (Leo, Oberkochen, Germany), operating at 10 kV. One droplet (15–20 μL) of the suspension was placed on a mica surface and lyophilized for 3 h. Finally, the sample was coated with platinum,

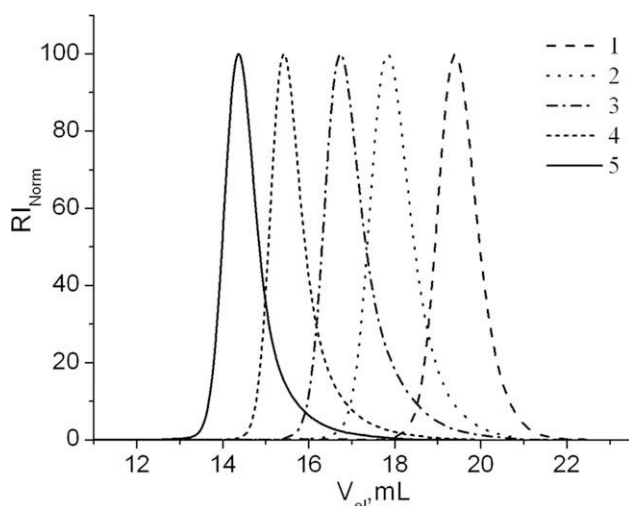


FIGURE 1 SEC chromatograms of the obtained PMMA polymers used. 1 – ($M_w = 7,700 \text{ g mol}^{-1}$), 2 – ($M_w = 20,200 \text{ g mol}^{-1}$), 3 – ($M_w = 39,700 \text{ g mol}^{-1}$), 4 – ($M_w = 106,000 \text{ g mol}^{-1}$), and 5 – ($M_w = 274,000 \text{ g mol}^{-1}$).

using a BAL-TEC SCD005 sputtering device (Balzers, Lichtenstein) and applying a current of 60 mA for 80 s.

Viscosity Measurements

Viscosity measurements were conducted using a AMVn (Anton Paar, Graz, Austria) rolling ball viscometer with a manually filled capillary with an internal diameter of 0.9 mm. The viscosities of the solution, η , and of the solvent, η_0 , were obtained from the rolling times of the steel ball, measured at three inclination angles (30° , 50° , and 70°) of the capillary. The viscosity of each solution was calculated from the average of six measurements; the measurements were conducted at 20°C .

Preparation of the Nanoparticle Suspensions

Nanoparticles were prepared by the nanoprecipitation method from a stock polymer solution in acetone or THF at different concentrations of the polymers. The initial polymer solutions were filtered via a $0.45 \mu\text{m}$ filter. To formulate the particles in a 96-well microtiter plate, a pipetting robot (Fas-Trans, Analytik Jena GmbH, Jena, Germany) was used. Nanoprecipitation was performed in an automated way by the fast injection of the polymer solution into a well containing different amounts of water depending on the solvent/nonsolvent ratio. The effective final volume of the well was $300 \mu\text{L}$. The nanosuspension formed was then mixed three times by aspiration and release of a volume of $200 \mu\text{L}$. Subsequently, the plate was placed in a fume hood, where the organic solvent was completely removed from the suspension by evaporation.

RESULTS AND DISCUSSION

Synthesis and Characterization of the Polymers

A range of PMMA samples were synthesized using the RAFT polymerization technique. The RAFT polymerization was carried out using AIBN as radical initiator, ethanol as solvent,

and CPDB as CTA. Different molar masses of PMMA were obtained by changing the polymerization time, the MMA concentration and the $[M]:[\text{CTA}]$ ratio (see Table 1 for detailed reaction conditions). High molar masses up to $M_w = 274,000 \text{ g mol}^{-1}$ could be realized via the RAFT process. All PMMA samples are well-defined with polydispersity indices ranging from 1.13 to 1.34. The SEC chromatographs of the different PMMAs are depicted in Figure 1.

Intrinsic Viscosity Measurements

Prior to compare the influence of various PMMA samples on the nanoparticle formation, intrinsic viscosity measurements of polymer solutions were performed. The knowledge of the intrinsic viscosity is essential to evaluate the interaction between the polymer and solvent molecules at various polymer molar masses. The intrinsic viscosities were obtained by applying Huggins extrapolation to zero concentration procedure:

$$\frac{\eta_{\text{sp}}}{c} = [\eta] + k'[\eta]^2 c + \dots \quad (2)$$

where $[\eta]$ and η_{sp} are the intrinsic and specific viscosity respectively, k' is the Huggins dimensionless parameter (interaction parameter), and c is the polymer concentration. The resulting plot of the reduced viscosity and the concentration for the samples investigated in acetone and THF is presented in Figure 2. As expected, solutions of PMMA in acetone have a lower viscosity in comparison to THF. According to Flory's equation,²³ this can indicate that the volume of the polymer coil in acetone is lower than in THF solutions. The corresponding values of the intrinsic viscosity are listed in Table 2. It is also well known that for a homologous series of macromolecules the intrinsic viscosity can be related to the molar mass through scaling relations of the Kuhn-Mark-Houwink-Sakurada type (KMHS relations):²³

$$[\eta] = K_\eta \cdot M^a \quad (3)$$

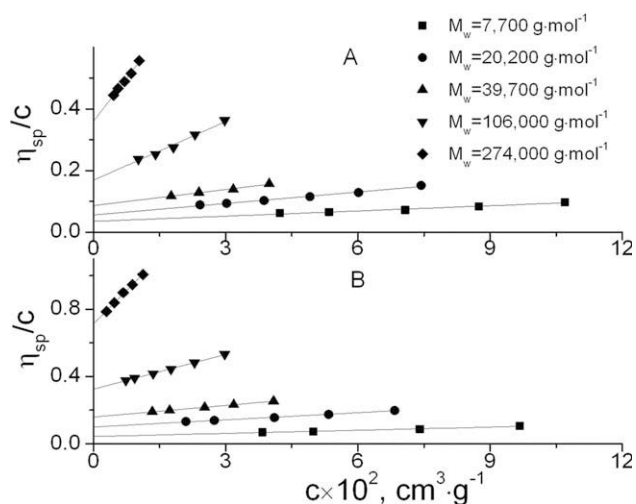


FIGURE 2 Dependence of the reduced viscosity on the polymer concentration for PMMA samples in acetone (A) and THF (B), respectively. Lines represent linear fitting procedures.

TABLE 2 Intrinsic Viscosity Data for the PMMA Polymers

Sample	$[\eta]_{\text{acetone}}, \text{cm}^3 \text{g}^{-1}$	$[\eta]_{\text{THF}}, \text{cm}^3 \text{g}^{-1}$
1	4.1 ± 0.5	6 ± 1
2	6.2 ± 0.6	10.6 ± 0.5
3	9.2 ± 0.6	16.3 ± 0.6
4	19 ± 1	33.2 ± 0.5
5	37 ± 1	71.8 ± 0.5

The parameters of this equation are characteristic for the polymer-solvent system. They can be evaluated from the log-log dependence of the $[\eta]$ versus M_w . The exponent in the KMHS equation varies in the range of $0.5 < a < 0.85$ for random coils. A value of 0.5 is indicating theta solvent conditions, which means that the polymer coil behaves as an undisturbed Gaussian coil. In this study, the following values: $K_\eta = 1.33 \cdot 10^{-2}$, $a = 0.63$ and $K_\eta = 0.70 \cdot 10^{-2}$, $a = 0.74$ were found for the polymer solution in acetone and THF, respectively. This, in turn, testifies a good affinity of the polymer to the solvents. However, according to the collected data THF seems to be a thermodynamically better solvent for the PMMA than acetone.

Nanoparticle Formation

To study the influence of the polymer molar mass on the nanoparticle formation via nanoprecipitation, it is crucial to maintain the same initial conditions for each nanoprecipitation process. The characteristic “degree of dilution” assesses the contribution of the different intrinsic viscosities of polymer solutions, which were introduced and represented by the Debye parameter: $c \cdot [\eta]$, where c is the polymer concentration and $[\eta]$ is the intrinsic viscosity of the polymer. The degree of dilution evaluates the volume fraction of the macromolecular coils in the solution. If the value of $c \cdot [\eta] \ll 1$, the solution can be considered as diluted, and no overlapping of the macromolecular coils occurs.

In detail, the nanoparticles were precipitated from 12 different initial polymer solutions with concentrations (logarithmically scattered) corresponding to the following range of $c \cdot [\eta]$ values: 0.004–0.120. Each solution was then combined with eight different proportions of water in a way that the solvent/nonsolvent ratio was ranged from 0.1 to 0.5 (again scattered logarithmically) representing in total 96 different populations of nanoparticles. The same procedure was applied for each PMMA sample. After preparation, one can notice a visually observable trend in appearance following the changes made in the nanoprecipitation process. At the lowest concentrations, a faintly opalescent suspension was obtained; with increasing concentration, the opalescence became more apparent. The particles suspensions were analyzed after complete evaporation of acetone or THF, respectively. Initially, the DLS plate reader was used for the particle characterization. Figure 3 shows a size distribution as a function of initial polymer concentration and solvent/nonsolvent ratio of nanoparticles based on **PMMA 1**. The size of the particles is increasing from around 70 to 180 nm

depending on the concentration (degree of dilution) and solvent/nonsolvent ratio. The polydispersity of the nanoparticles based on **PMMA 1** to **PMMA 3** increases from $5 \pm 2\%$ to $20 \pm 5\%$ for the lowest and highest concentration, respectively. In the case of particles based on **PMMA 4** and **PMMA 5**, the nanoparticle suspensions were found to be more polydisperse; the polydispersity constitutes $12 \pm 3\%$ and $30 \pm 16\%$ for the lowest and highest concentration, respectively.

Morphology Study

In Figure 4, the SEM micrographs and the corresponding size-distributions, determined by ImageJ analysis, are shown for nanoparticles based on **PMMA 1**, **3**, and **5** prepared in acetone and THF, respectively, at a degree of dilution $c[\eta] = 0.01$ and a solvent/nonsolvent ratio of 0.1. The sizes of the particles of **PMMA 1**, **3**, and **5** were virtually the same. The calculated weight average particle size constitutes 74 ± 4 nm for the preparation procedure in acetone and 100 ± 20 nm for the THF preparations. However, particles prepared from acetone solution are only uniform and spherically shaped for the low molar mass **PMMA 1** ($M_w = 7,700 \text{ g mol}^{-1}$), whereas with increasing molar mass less spherical particles with rough surfaces appeared. In contrast, particles prepared from THF solution are spherical and uniform within the whole molar mass range.

Sedimentation Velocity Experiments

Sedimentation velocity analyses were performed for various nanoparticle suspensions in water to gain detailed information about the size distribution of the particles. In Figure 5(A) typical size-distributions obtained by AUC are shown for **PMMA 1** and **PMMA 5** particles. The differential distribution of sedimentation coefficients were subsequently

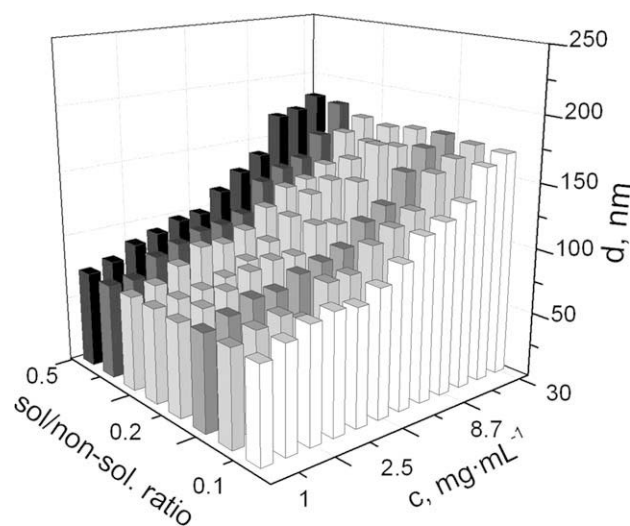


FIGURE 3 3D representation of the nanoprecipitation experiment using a PMMA with $M_w = 7,700 \text{ g mol}^{-1}$: an average particle size (Z-axis) as function of initial polymer concentration (X-axis) and solvent/nonsolvent ratio (Y-axis). Sizes were obtained by DLS measurements. The nanoparticles were prepared by dropping a polymer acetone solution into water.

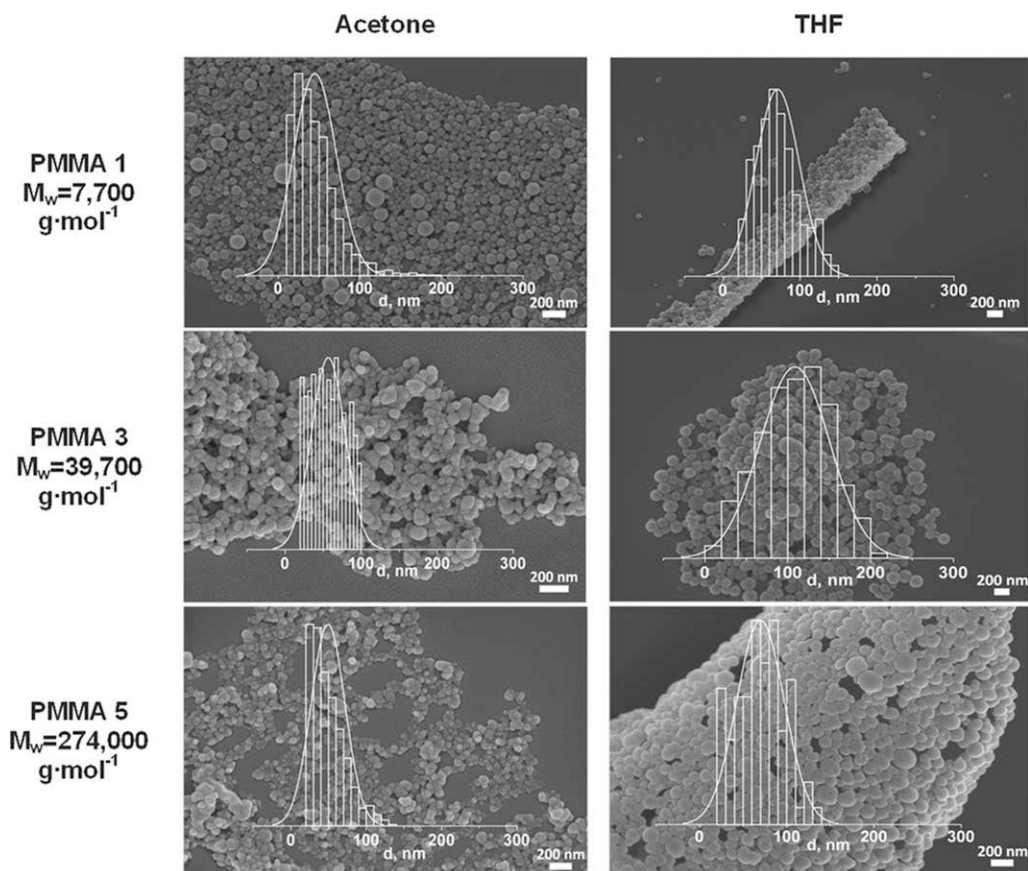


FIGURE 4 SEM images and corresponding size-distributions of nanoparticles prepared from polymer solutions of PMMA with different molar masses in acetone and THF. The particles were prepared by dropping a polymer solution into water. The initial polymer concentration was adjusted to obtain the same degree of dilution ($c[\eta] = 0.01$) of all polymer solutions. Solvent/nonsolvent ratio was kept constant at 0.1.

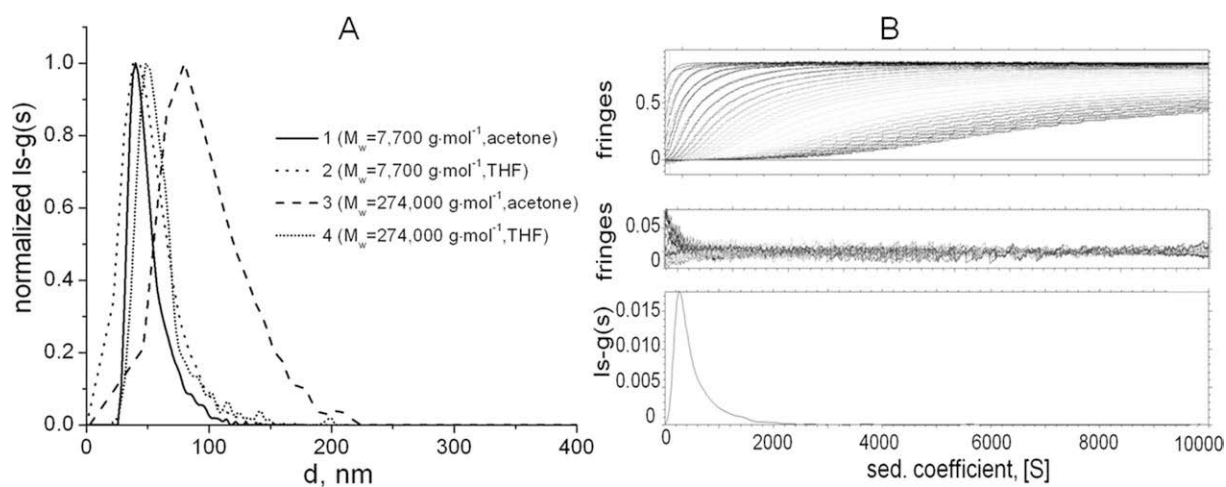


FIGURE 5 A: Comparison of normalized size-distributions obtained by sedimentation velocity experiment for the nanoparticles based on **PMMA 1** ($M_w = 7,700 \text{ g mol}^{-1}$) and **PMMA 5** ($M_w = 274,000 \text{ g mol}^{-1}$) in acetone and THF. The initial polymer concentration corresponds to the degree of dilution $c[\eta] = 0.01$ at a solvent/nonsolvent ratio of 0.1. B: Example of sedimentation velocity experiments for nanoparticles based on **PMMA 1** in acetone. The experiment was carried out at 3,000 rpm, scans were collected every 15 s. Top panel: superposition of sedimentation profiles obtained with interference optics at 20 °C. Middle: corresponding residual plots. Bottom: differential distribution $I_s-g(s)$ of the sedimentation coefficients. The distributions were obtained with a regularization procedure at a confidence level of 0.9.

transformed into the size distribution, and an average diameter was calculated according to the Stokes-Einstein equation assuming a spherical shape of the particles. Particles prepared from acetone solution are slightly smaller comparing to the THF preparation. The majority of the particles prepared from the different molar mass samples at similar degree of dilution $c[\eta] = 0.01$ have virtually the same sizes: 74 ± 5 nm and 100 ± 20 nm for the particles prepared from acetone and THF polymer solution, respectively. However, it should be noted that the distributions of high molar mass samples are slightly shifted to larger diameters.

Zeta-Potential Measurements

The surface charge of particles represents an additional important parameter for the characteristics of nanoparticles besides size and shape. In particular, the stability of nanoparticle suspensions as well as the cellular uptake are strongly affected by the zeta-potential. The correlation between zeta-potential and initial polymer molar mass is presented in Figure 6. The magnitude of the zeta-potential decreases with increasing molar mass of the initial polymer. The maximum value was observed for the nanoparticles based on **PMMA 1** and constitutes -33 and -37 mV for the acetone and THF preparations, respectively. The minimum values were observed for the particles based on **PMMA 3**, which do not change significantly at larger molar mass: $-(13 \pm 1)$ mV and $-(20 \pm 3)$ mV for the acetone and THF preparations, respectively.

DISCUSSION

Many factors have to be taken into account to obtain stable nanoparticle suspension with desired size and properties during the nanoprecipitation process. It was shown before that one of the key-factors, which define the particle size, is the initial polymer concentration: the higher the concentration of the polymer in the organic phase, the lower the velocity of diffusion owing to the increasing viscosity of the polymer solution; consequently, more polymer molecules per unit volume of solvent are present, and the resulting particles will have a larger size.^{13,15,16} However, equality of the initial polymer concentration will not reflect the same conditions for the nanoprecipitation process in case of polymers with various molar mass or different chemical structure, since macromolecular coils will occupy different volumes owing to the different length of a polymer chain. Furthermore, the volume of the macromolecular coil of a polymer depends on the equilibrium rigidity of the chain and on the nature of the polymer-solvent interaction. A physical quantity, which reflects the volume occupied by the polymer molecule, is the intrinsic viscosity.

$$[\eta] = \Phi \frac{\langle h^2 \rangle^{3/2}}{M} \quad (4)$$

where $\langle h^2 \rangle$ is the mean square end-to-end distance of the coil, Φ is the Flory hydrodynamic parameter, and M is the molar mass of the polymer. The product of the intrinsic viscosity $[\eta]$ and the concentration of the solution (Debye pa-

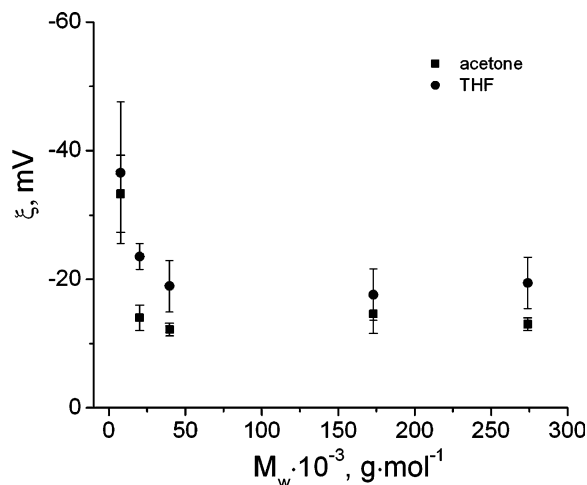


FIGURE 6 Zeta-potential of the nanoparticles as a function of initial polymer molar mass. The nanoparticles were obtained by nanoprecipitation of polymers dissolved in acetone and THF. The initial polymer concentration corresponds to the degree of dilution $c[\eta] = 0.01$ at a solvent/nonsolvent ratio of 0.1.

rameter) represents a good approximation of the volume fraction of the macromolecular coils in the solution ϕ and can be specified as follows:

$$\phi \equiv \frac{nv}{V} = \frac{mvN_A}{VM} = \frac{c \times 0.36 \langle h^2 \rangle^{3/2} N_A}{M} = \left(\frac{0.36N_A}{\phi} \right) c[\eta] \approx c[\eta] \quad (5)$$

$$v = 0.36 \langle h^2 \rangle^{3/2} \quad (6)$$

Therein, v is the volume occupied by the macromolecular coil in solution, m is the mass of the polymer in volume V , N_A is the Avogadro number. If $c[\eta] \ll 1$, the polymer solution can be considered as diluted-then, no overlapping of macromolecular coils occurs.

Based on these data, nanoparticle suspensions were prepared with a degree of dilution from $0.004 < c[\eta] < 0.12$. In Figure 7, the size of the nanoparticles as a function of the Debye parameter is presented in a double logarithmic scale. A comparison is made for particles prepared from the polymer solutions of **PMMA 1** and **PMMA 5** in acetone and THF, respectively. As expected, the particles size increases as the solution becomes more concentrated-corresponding to the higher values of the Debye parameter. However, the slopes of the regression lines (0.20 and 0.32 for **PMMA 1** and **PMMA 5**, respectively) show that the size increases more rapidly for the nanoparticles on the basis of high molar mass polymer. It is further obvious that higher molar mass polymers lead to the formation of the particles with larger diameters, which actually contradicts data obtained from SEM and AUC. Such a difference in sizes can be related to the fact that, in accordance with the measured values of zeta-potential, nanoparticles on the basis of high molar mass polymers (**PMMA**

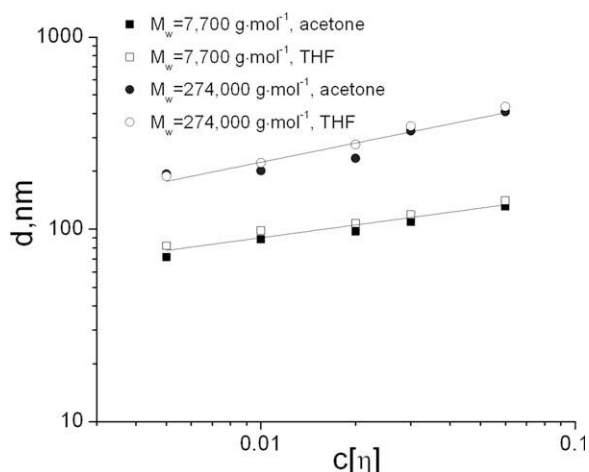


FIGURE 7 Double logarithmic dependence of the particle diameters on the degree of dilution (Debye parameter) obtained by DLS measurements. Nanoparticles based on **PMMA 1** ($M_w = 7,700 \text{ g mol}^{-1}$) and **PMMA 5** ($M_w = 274,000 \text{ g mol}^{-1}$) in acetone and THF.

4, PMMA 5) were found to have low values of surface charge. This, in turn, can provoke formation of agglomerates, which will influence the final particle distribution. The resulting comparison of the particles sizes (an average from the AUC, DLS, and SEM data) as a function of the polymer molar mass is presented in Figure 8(A). Indeed, a slight increase of the particle sizes with the molar mass is noticeable. This effect is more evident when the particles were nanoprecipitated from the polymer solution in acetone. It can also be concluded that, regardless to the solvent used, the increase in particle size is followed by a plateau. A maximum size could be observed for the particles based on **PMMA 2** with $M_w = 20,200 \text{ g mol}^{-1}$. Figure 8(B) represents the semi logarithmic dependence of the particle size on the product of polymer molar mass and intrinsic viscosity.

product of molar mass M on the intrinsic viscosity $[\eta]$ for two values of $c[\eta]$: 1, 2 – 0.01 and 3, 4 – 0.1. Since this work was generally performed using dilute polymer solutions, the parameter $M[\eta]$ will reflect the volume of the macromolecular coils in the initial solution. It is clear that in both cases an increase of the volume of the macromolecular coil leads to the formation of nanoparticles with larger sizes. The magnitude of the particle size increases ~ 2.5 –3 times compared to the first data point. With further increase of the macromolecular volume, the size of the nanoparticles remains constant within the experimental error. It is also clear that in case of more concentrated solutions ($c[\eta] = 0.1$) the final nanoparticle size is larger. It was generally observed that stable nanoparticle suspensions were only produced when $c[\eta] \leq 0.1$. Applying concentrations corresponding to the values of $c[\eta] > 0.1$, nanoparticle suspensions were found to be highly polydisperse, with diameters larger than 500 nm. Such a behavior may testify to the shift beyond the Ouzo region. Regardless to concentration and molar mass, the particles obtained from the polymer solution in acetone are relatively smaller than those prepared from THF solution. This size difference can simply be related to the lower viscosity of the acetone polymer solution in comparison to THF. SEM micrographs showed the formation of more uniform nanoparticles if THF was used as solvent. This is in agreement with the viscosity data, which show higher values of the exponent in the KMHS equation for the polymer in THF solution resulting in the higher affinity of the polymer to the solvent. When acetone was used as solvent, uniform nanoparticles with smooth surfaces were only observed in case of **PMMA 1** based nanoparticles.

CONCLUSION

To obtain well-defined particles on the basis of a certain polymer, it is crucial to work with highly diluted polymer solutions. Regardless to the polymer molar mass,

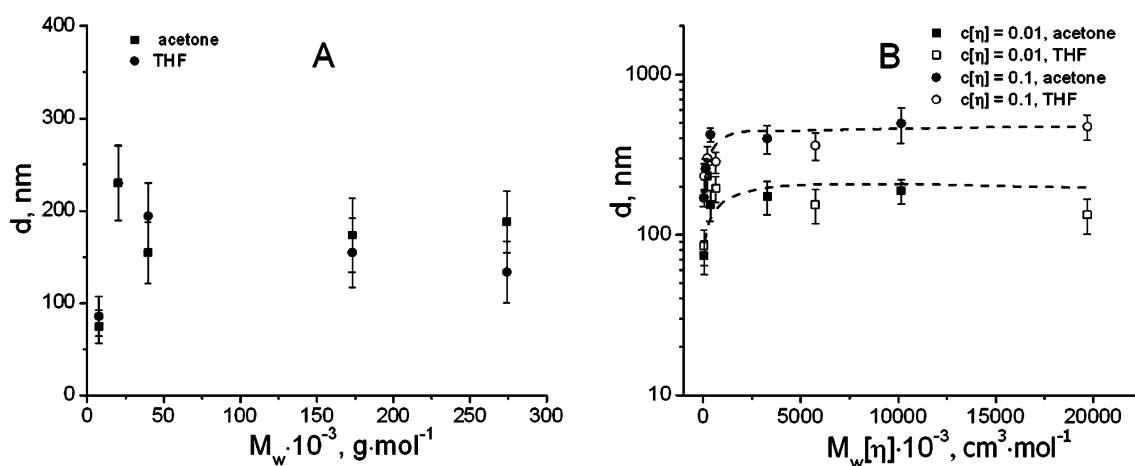


FIGURE 8 A: Dependence of the resulting weight average sizes on the initial polymer molar mass for the nanoparticles obtained by nanoprecipitation of polymers dissolved in acetone and THF. Initial polymer concentrations correspond to the degree of dilution $c[\eta] = 0.01$. B: Semi logarithmic dependence of the particle size on the product of polymer molar mass and intrinsic viscosity. Initial polymer concentrations correspond to the degree of dilution $c[\eta] = 0.01$ and $c[\eta] = 0.1$ in acetone and THF. Deviations are related to the difference in the nanoparticle sizes obtained from various characterization techniques (AUC, DLS, and SEM).

hydrodynamic volume and solvent quality, the formation of stable nanoparticle suspensions could only be observed at a Debye parameter $c[\eta] \ll 0.1$. According to this, it could be shown that the key factor during the particle preparation is the volume fraction occupied by the polymer macromolecular coil in the initial solution instead of the polymer concentration. The morphology of the nanoparticles depends on the affinity of the polymer molecules to the solvent. It appeared that “good” solvents are preferable to formulate uniform nanoparticles with smooth surfaces. Taking together these findings, it can be concluded that knowledge of the hydrodynamic properties of the initial polymer solution is essential for tuning and optimizing conditions for the nanoprecipitation process.

ACKNOWLEDGMENTS

The authors are grateful to the Thuringian Ministry for Education, Science, and Culture (grant #B514-09051, NanoConSens), to the Carl-Zeiss Stiftung (Strukturantrag JCSM) and to the Dutch Polymer Institute (DPI, Technology Area HTE) for financial support.

REFERENCES AND NOTES

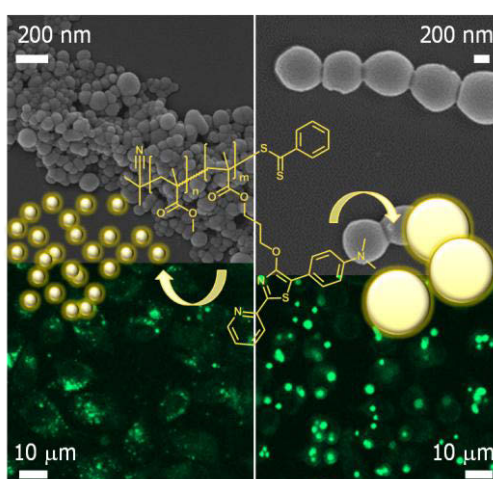
- 1 Fessi, H.; Puisieux, F.; Devissaguet, J. P.; Ammoury, N.; Benita, S. *Int. J. Pharm.* **1989**, *55*, R1–R4.
- 2 Mora-Huertas, C. E.; Fessi, H.; Elaissari, A. *Int. J. Pharm.* **2010**, *385*, 113–142.
- 3 Vauthier, C.; Bouchemal, K. *Pharm. Res.* **2009**, *26*, 1025–1058.
- 4 Govender, T.; Stolnik, S.; Garnett, M. C.; Illum, L.; Davis, S. S. *J. Controlled Release* **1999**, *57*, 171–185.
- 5 Zhang, H.; Cui, W.; Bei, J.; Wang, S. *Polym. Degrad. Stab.* **2006**, *91*, 1929–1936.
- 6 Dutta, P.; Shrivastava, S.; Dey, J. *Macromol. Biosci.* **2009**, *9*, 1116–1126.
- 7 Hornig, S.; Heinze, T.; Becer, C. R.; Schubert, U. S. *J. Mater. Chem.* **2009**, *19*, 3838–3840.
- 8 Perevyazko, I.; Vollrath, A.; Hornig, S.; Pavlov, G. M.; Schubert, U. S. *J. Polym. Sci., Part A: Polym. Chem.* **2010**, *48*, 3924–3931.
- 9 Aubry, J.; Ganachaud, F.; Cohen Addad, J. P.; Cabane, B. *Langmuir* **2009**, *25*, 1970–1979.
- 10 Horn, D.; Rieger, J. *Angew. Chem. Int. Ed.* **2001**, *40*, 4330–4361.
- 11 Brick, M. C.; Palmer, H. J.; Whitesides, T. H. *Langmuir* **2003**, *19*, 6367–6380.
- 12 Vitale, S. A.; Katz, J. L. *Langmuir* **2003**, *19*, 4105–4110.
- 13 Beck-Broichsitter, M.; Rytting, E.; Lehardt, T.; Wang, X.; Kissel, T. *Eur. J. Pharm. Sci.* **2010**, *41*, 244–253.
- 14 Chorny, M.; Fishbein, I.; Danenberg, H. D.; Golomb, G. *J. Controlled Release* **2002**, *83*, 389–400.
- 15 Plasari, E.; Grisoni, P. H.; Villiermaux, J. *Chem. Eng. Res. Des.* **1997**, *75*, 237–244.
- 16 Legrand, P.; Lesieur, S.; Bochot, A.; Gref, R.; Raatjes, W.; Barratt, G.; Vauthier, C. *Int. J. Pharm.* **2007**, *344*, 33–43.
- 17 Galindo-Rodriguez, S.; Allémann, E.; Fessi, H.; Doelker, E. *Pharm. Res.* **2004**, *21*, 1428–1439.
- 18 Stainmesse, S.; Orecchioni, A. M.; Nakache, E.; Puisieux, F.; Fessi, H. *Colloid. Polym. Sci.* **1995**, *273*, 505–511.
- 19 Perevyazko, I. Y.; Delaney, J. T.; Vollrath, A.; Pavlov, G. M.; Schubert, S.; Schubert, U. S. *Soft Matter* **2011**, *7*, 5030–5035.
- 20 Moad, G.; Rizzardo, E.; Thang, S. H. *Aust. J. Chem.* **2009**, *62*, 1402–1472.
- 21 Chiefari, J.; Chong, Y. K.; Ercole, F.; Krstina, J.; Jeffery, J.; Le, T. P. T.; Mayadunne, R. T. A.; Meijs, G. F.; Moad, C. L.; Moad, G.; Rizzardo, E.; Thang, S. H. *Macromolecules* **1998**, *31*, 5559–5562.
- 22 Schuck, P.; Rossmannith, P. *Biopolymers* **2000**, *54*, 328–341.
- 23 Fujita, H. *Polymer Solutions*; Elsevier: Amsterdam, **1990**.

Publication 5

"Preparation, cellular internalization, and biocompatibility of highly fluorescent PMMA nanoparticles"

Antje Vollrath, David Pretzel, Christian Pietsch, Igor Y. Perevyazko,
Roberto Menzel, Stephanie Schubert, George M. Pavlov,
Dieter Weiß, Rainer Beckert, Ulrich S. Schubert

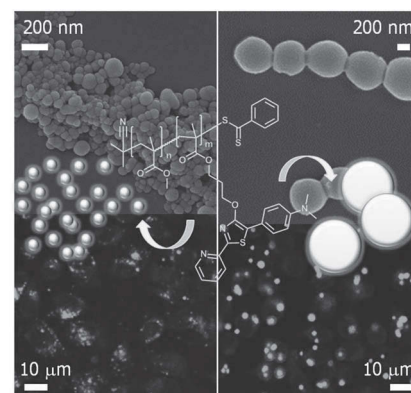
Macromol. Rapid Commun. **2012**, *33*, 1791–1797.



Preparation, Cellular Internalization, and Biocompatibility of Highly Fluorescent PMMA Nanoparticles

Antje Vollrath, David Pretzel, Christian Pietsch, Igor Perevyazko, Stephanie Schubert, George M. Pavlov, Ulrich S. Schubert*

Methacrylate monomers were functionalized with a 4-hydroxythiazole chromophore and copolymerized with methyl methacrylate via RAFT. Nanoparticles of 120 and 500 nm in size were prepared without using stabilizers/surfactants. For comparative studies, preparative ultracentrifugation was applied for the separation into small and large particle fractions. All suspensions were characterized by DLS, AUC, and SEM and tested regarding their stability during centrifugation and re-suspension, autoclavation, and incubation in cell culture media. In vitro studies with mouse fibroblast cell line and differently sized NP showed a particle uptake into cells. Biocompatibility, non-toxicity, and hemocompatibility were demonstrated using a XTT assay, a live/dead staining, and an erythrocyte aggregation and hemolysis assay.



1. Introduction

Recent progress in the area of nanosciences enabled the development of various nanoparticle (NP) devices as powerful tools in the pharmaceutical area for drug delivery

systems, but also in other scientific fields, for example, chemistry, biology, and electronics.^[1–3] In particular for diagnostic applications, like live cell imaging, the investigation of labeled nanosystems (1 to 1000 nm) is rapidly expanding.^[4–8] Such nanodevices can consist of various materials, such as silica, carbon, metal oxides, pure metals, and polymers.^[6,9,10] In particular, quantum dots have revolutionized the biological research with their fascinating light-emitting properties, though still having safety issues due to the liberation of heavy metals.^[2,11] The use of fluorescent polymeric NP represents a suitable alternative to avoid the obstacle of the potential toxicity of metal-based NP. A diversity of biocompatible polymers, such as poly(lactide-*co*-glycolide) and poly(ϵ -caprolactone), are used for formulation.^[12–14] The incorporation of dyes into the polymer shell during NP preparation or the use of labeled polymer systems provides a protection against external influences while keeping their spectral properties, which are essential for the subsequent analysis of particle–cell interactions via confocal laser scanning microscopy.^[7,13,15] A further benefit of polymeric NP is the variety of formulation techniques such as emulsification–solvent diffusion,

A. Vollrath, D. Pretzel, C. Pietsch, I. Perevyazko, G. M. Pavlov, U. S. Schubert

Laboratory of Organic and Macromolecular Chemistry,
Friedrich-Schiller-University Jena,
Humboldtstr. 10, 07743 Jena, Germany
E-mail: ulrich.schubert@uni-jena.de

C. Pietsch, U. S. Schubert

Dutch Polymer Institute (DPI), Post Office Box 902,
Eindhoven 5600 AX, the Netherlands
S. Schubert, U. S. Schubert

Jena Center for Soft Matter (JCMS),
Friedrich-Schiller-University Jena,
Humboldtstr. 10, 07743 Jena, Germany
S. Schubert

Institute of Pharmacy, Department of Pharmaceutical
Technology Friedrich-Schiller-University Jena,
Otto-Schott-Str. 41, 07745 Jena, Germany

nanoprecipitation, spray drying, salting out, and milling processes.^[16–18] By using the appropriate conditions for formulation, specific drugs can be encapsulated resulting in labeled drug carriers of desired sizes and with suitable charges.^[16,18,19]

In the herein presented study, polymethylmethacrylate (PMMA) copolymers were chosen as a model system to demonstrate that functional PMMA-based nanoparticles are well suitable for diagnostic applications such as the imaging of cells. The biocompatibility of PMMA microspheres enables their use in many biomedical applications, for example, as injectable dermal fillers, as PMMA-based NPs for in vitro gene delivery approaches, and also for orthopedic bone reconstruction.^[20–28] For the design of labeled nanosystems, a luciferin-based 4-hydroxythiazole derivative was incorporated into the PMMA polymer backbone, showing benefits as high fluorescence at room temperature with high quantum yields, easy adjustment of the fluorescent properties, and excellent stability.^[29,30] For this purpose, methacrylates were functionalized with the thiazole chromophore (MA^y) and then copolymerized with methyl methacrylate (MMA) using the reversible addition–fragmentation chain transfer (RAFT) polymerization technique.^[29,31–33] For the NP preparation, nanoprecipitation (solvent-evaporation) was chosen as a simple, fast, reliable, and cost-effective method.^[34–36] Different particle sizes were obtained by varying the initial conditions of the formulation. Additionally, preparative ultracentrifugation (pUC) was utilized for the fractionation of particles into discretely sized NP suspensions. It provides another dimension of physical control of the size distribution of particles on the nanoscale.^[14,37–39]

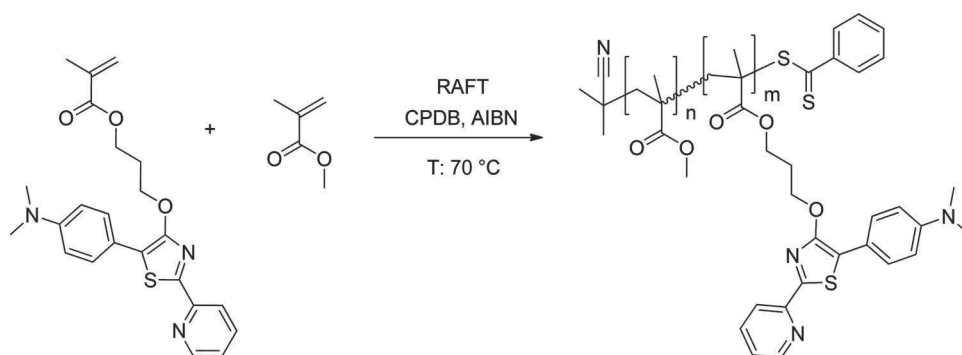
Since the size strongly influences the biodistribution of NPs and the way of internalization into target cells, it is imperative to have well-defined particles with narrow size distributions. Unfortunately, it is a matter of fact that in literature the accuracy of particle size determination is disputable.^[40–42] Consequently, in this distribution,

all suspensions were characterized comprehensively by dynamic light scattering (DLS), scanning electron microscopy (SEM), and analytical ultracentrifugation (AUC) to allow a detailed characterization of the NPs.^[43] The stability of the resulting nanosuspensions after long-time storage, autoclavation, and incubation in cell culture media was studied by measurements of size and zeta potential. The internalization of the differently sized nanoparticles into adherent cells was monitored by confocal laser scanning microscopy (CLSM). The biocompatibility of the particle suspensions in terms of their non-toxicity was proven by XTT cytotoxicity assay and microscopic evaluation of viability after a live/dead staining. Compatibility with blood was analyzed by checking the induction of hemolysis and aggregation of erythrocytes.

2. Results and Discussion

2.1. Synthesis of P(MMA-*stat*-MA^y)

The yellow light-emitting thiazole-dye 3-((5-(4-(dimethylamino)phenyl)-2-(pyridin-3-yl)thiazol-4-yl)oxy)propan-1-ol was attached to the methacrylate monomer by an esterification reaction. The non-classical 4-hydroxy-1,3-thiazole chromophore structure is similar to the luciferin dye of fireflies and shows excellent fluorescent properties.^[44] The resulting dye-functionalized methacrylate MA^y was copolymerized statistically with MMAs using the RAFT polymerization methodology (Scheme 1).^[31–33] The reaction was carried out using AIBN as a radical initiator, toluene as a solvent, and 2-cyano-2-propyl dithiobenzoate (CPDB) as a chain transfer agent. The ratio of MMA to the dye-functionalized monomers was 69:1, leading to a final conversion rate of 70% of the copolymers with a DP of 100. The dye-functionalized methacrylates were statistically distributed in the polymer backbone due to the same reactivity of both monomers.^[29] The low degree of labeling (1 to 3%) ensured the preservation of the properties of the PMMA



■ Scheme 1. Schematic representation of the synthesis of p(MMA-*stat*-MA^y).

Table 1. Summary of the size distributions of the nanoparticles based on p(MMA-*stat*-MA^y).

Sample	d_{DLS} [nm]	$\text{PDI}_{\text{particle}}$	d_{SEM} [nm]	d_{AUC} [nm]	ζ [mV]
S1	118	0.10	111	120	-36
L1	488	0.03	696	503	-35
S2	120	0.26	131	97	-32
L2	597	0.19	502	381	-33

homopolymer. As determined by SEC, the final p(MMA-*stat*-MA^y) revealed a molar mass (\bar{M}_n) of 8500 g mol⁻¹ with a polydispersity index value of 1.19 (Table S1, Supporting Information). Similar molar mass distributions recorded by both RI and UV detector clearly demonstrate that the thiazole dye was incorporated into the copolymer. The ratio of the MMA units and the thiazole dye in the copolymer was determined to be 2.9 mol% by ¹H NMR spectroscopy. The final copolymer showed the same absorbance and emission behavior like the monomeric thiazole chromophore (solvent acetonitrile; $\lambda_{\text{Abs}} = 413$ nm, $\lambda_{\text{Em}} = 557$ nm, Stokes-shift 6259 cm⁻¹, Figure S1, Supporting Information) with a quantum yield of $\Phi_{\text{PL}} = 0.29$.

2.2. Nanoparticle Preparation and Characterization

The so-called nanoprecipitation or solvent evaporation process was found to be a suitable method for the preparation of differently sized NPs. Therefore, this simple, fast, and cost effective technique was applied for the preparation of p(MMA-*stat*-MA^y) NPs.^[34,45] The final particle size was tuned by variation of the initial polymer concentration in the organic phase and/or by changing the dropping method (polymer solution into water or water into polymer solution).^[46] In order to obtain small particles (**S1**), a polymer solution with a concentration of 4 mg mL⁻¹ was dropped into water. For larger particles (**L1**), water was dropped into the polymer solution with a concentration of 3 mg mL⁻¹. In general, a solvent/non-solvent ratio of 0.25 was used and continuous stirring was applied. After evaporation of the acetone, the particle sizes were examined by DLS. The Z-average diameter for the nanoparticles suspensions **S1** and **L1** was determined to be $d_{\text{S1}} = 118$ nm ($\text{PDI}_{\text{P}} = 0.10$) and $d_{\text{L1}} = 488$ nm ($\text{PDI}_{\text{P}} = 0.03$), respectively (Table 1). The resulting size distributions were monomodal (Figure 1). In addition to nanoprecipitation, preparative ultracentrifugation (pUC)^[47] in a density gradient was used for the separation of defined NP. For pUC, a thin layer of a particle suspension to be fractionated is layered on the top of a solution containing the density gradient. When a centrifugal field is applied, the various components move through the gradient at different rates depending on their sizes, densities, and shapes.^[37–39,48] In this respect, a particle

suspension with a broad size distribution was separated by pUC into fractions **S2** and **L2**. DLS and AUC measurements indicated particle sizes of $d_{\text{S2}} = 120$ nm ($\text{PDI}_{\text{P}} = 0.29$) and $d_{\text{L2}} = 600$ nm ($\text{PDI}_{\text{P}} = 0.19$, Table 1). The small increase of the PDI_{P} values of **S2** and **L2** compared with **S1** and **L1** might be caused by a slight agglomeration of the NP during the pUC treatment. The zeta potential of all suspensions were in the same range ($\zeta = -32$ to -36 mV) and thereby testified a good stability of the NP in suspension. SEM investigations were performed to obtain further information about the size and shape of the particles (Figure 1). The small particles **S1** and **S2** revealed more irregular shapes than the larger ones (**L1** and **L2**), which might be caused by the preparation technique, that is, dropping acetone in water, which is characterized by the fast exchange of the solvent against the non-solvent environment.^[34,35] For the small particles, the calculated diameters were in good agreement with the DLS results ($d_{\text{S1}} = 111$ nm, $d_{\text{S2}} = 131$ nm), whereas the large particle samples were characterized by slightly increased sizes in the particle fractions ($d_{\text{L1}} = 696$ nm, $d_{\text{L2}} = 502$ nm, Table 1). Complementary, the analysis of the samples by AUC revealed diameters of $d_{\text{S1}} = 120$ nm and $d_{\text{L1}} = 503$ nm as well as $d_{\text{S2}} = 97$ nm and $d_{\text{L2}} = 381$ nm, respectively. In order to exclude the occurrence of bulk precipitation and Ostwald ripening even over a long period of time, the nanosuspensions were stored at 5 °C for 6 months and examined again regarding their zeta potential and size distribution. No signs of instability of the initial nanosuspensions were found in terms of agglomeration or creaming up. It should be mentioned that no surfactants were added to inhibit particle aggregation. In addition, samples of the initial NP suspension were analyzed by DLS and SEM after centrifugation at 24.650 g for 20 min, autoclavation, lyophilization, and subsequent resuspension. Neither the size distributions nor the zeta potential values changed, which ensured the high stability of the p(MMA-*stat*-MA^y) nanoparticles. The absorption and emission spectra of the nanosuspensions in comparison to the monomer were equal within the range of the measurement errors (± 5 nm). This implies that the fluorescence properties of the monomers were unaffected by polymerization and NP formation.

2.3. Biological Experiments

In order to prove the efficient internalization of the particles into cells, mouse fibroblasts L929 were incubated with 120 and 500 nm sized nanosuspensions prepared by nanoprecipitation and pUC separation, respectively. The internalization of the NP into the cells was monitored by CLSM (representative micrographs are shown in Figure 2). On the basis of the relative size distribution of their corresponding fluorescence signal, a clear discrimination of small and large particles was possible. Furthermore, a concentration-dependent internalization of all

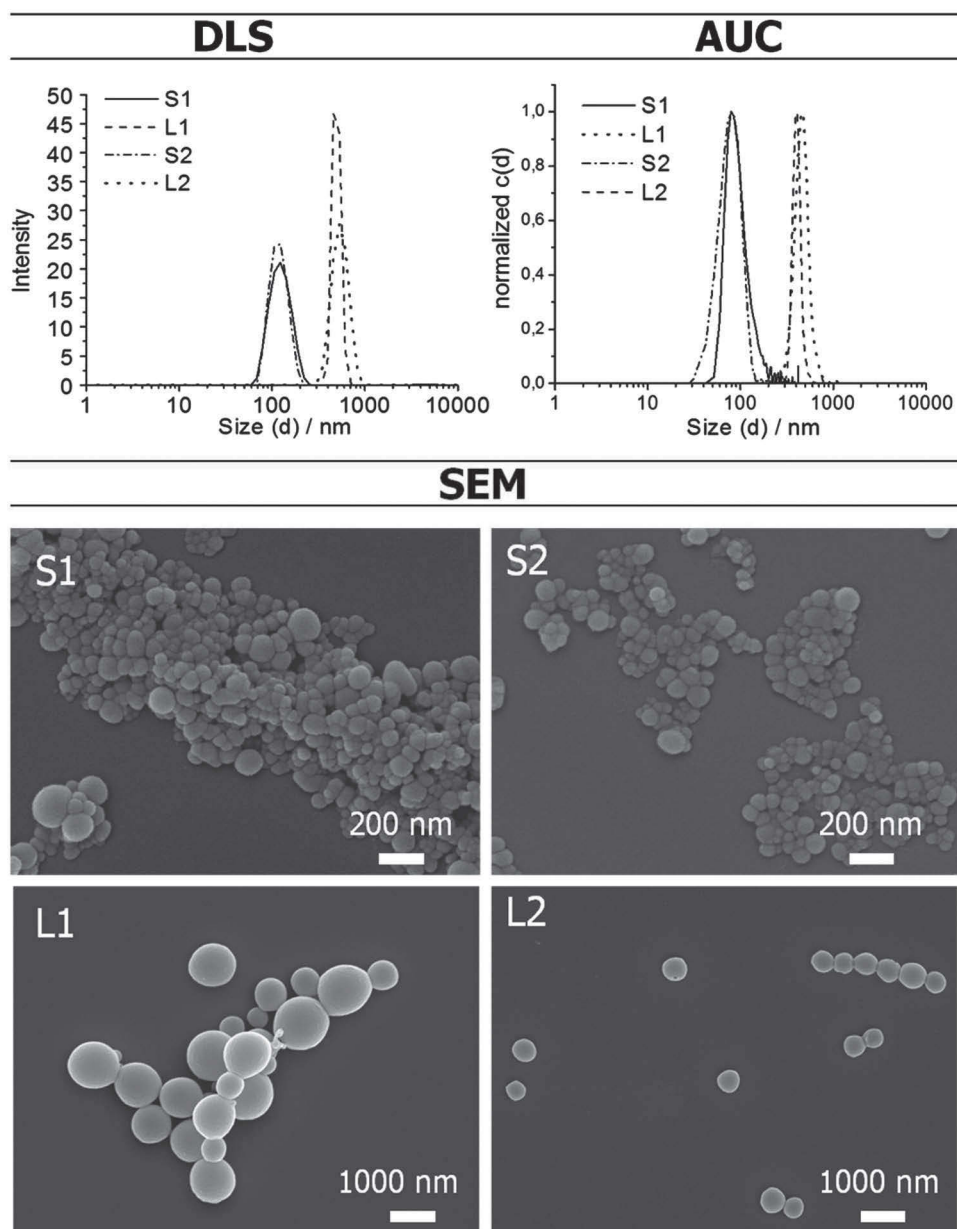


Figure 1. Size distributions of the particles in water ($c = 0.5 \text{ mg mL}^{-1}$) obtained by DLS and AUC as well as SEM images of the particle suspensions.

fluorescent NP into the cytoplasm in the range of $c = 0.1$ to $10 \text{ } \mu\text{g mL}^{-1}$ was observed. The more particles added for incubation with adherent cells, the more particles were consequently found in the cytoplasm. It was further obvious that the pUC prepared samples **S2** and **L2** were internalized to a higher degree than the particles **S1** and **L1**. This might be due to traces of sucrose attached to the particle surface. As described in literature, carbohydrate moieties can act as ligands for diverse receptors. Hence, their appearance on the particle surface could lead to an enhanced cellular recognition and internalization of the particle **S2** and **L2**.^[49–51]

It is known that PMMA particles are phagocytosable and it can be assumed that the cellular uptake of PMMA particles in the size range studied is presumable mediated in a similar fashion via an endocytotic pathway.^[27] The negative surface charge of the PMMA NP does not alter the cellular uptake and most probably yields to a reduction of the non specific binding of anionic proteins present in the cell culture medium and also in the body fluid, for example, in the blood, thus rendering opportunities for in vivo administration of NP.^[26]

For diagnostic applications, the biocompatibility and non-toxicity of the nanosuspensions are important

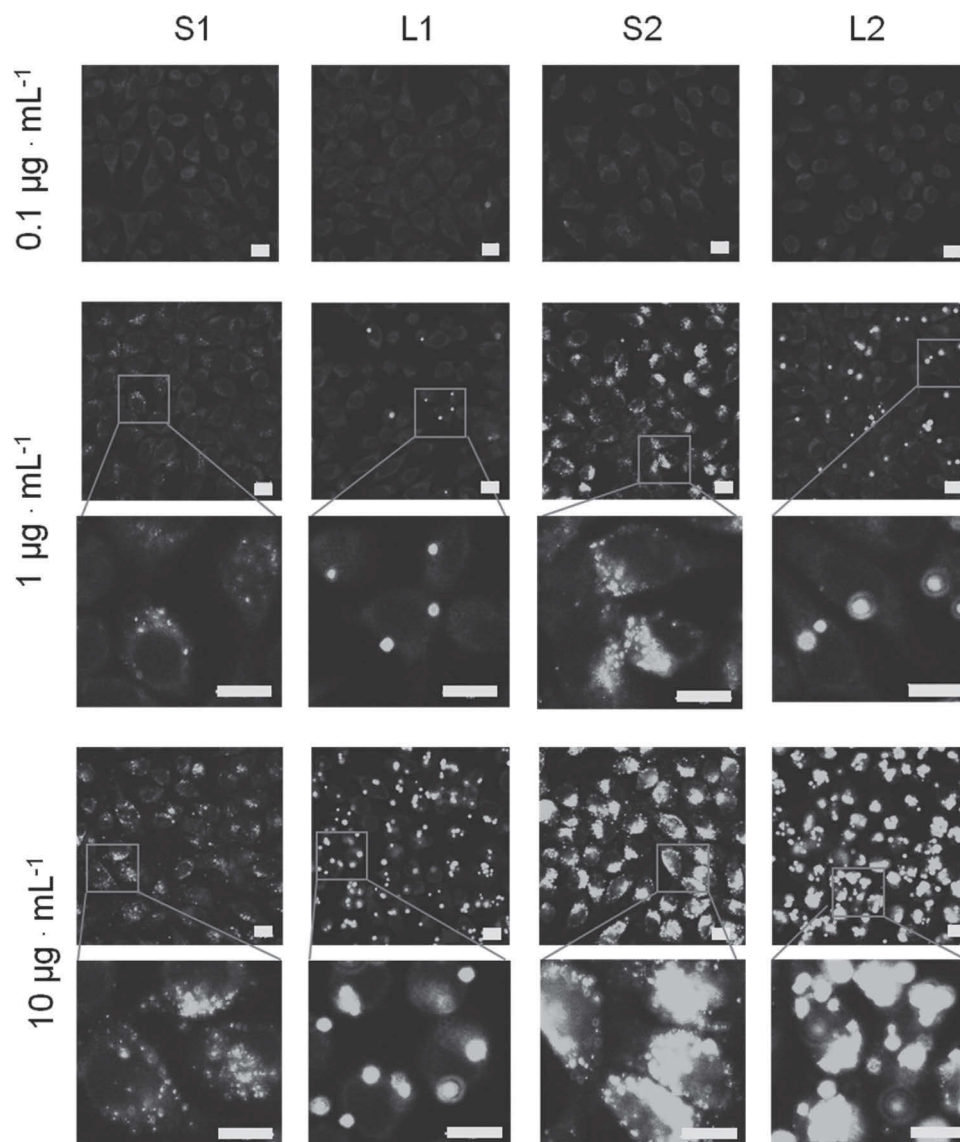


Figure 2. Confocal fluorescence images of L929 cells after 24 h incubation with polymeric p(MMA-*stat*-MA)^y nanoparticles. Cells incubated with polymer free culture medium served as control (not shown). All images were obtained with identical instrument settings (scale bars 10 μm).

prerequisites. The *in vitro* cytotoxicity experiment was performed on the basis of the XTT assay using L929 mouse fibroblasts, according to the German standard institution guideline DIN ISO 10993-5 as a reference for biomaterial testing. After 24 h of incubation with different NP concentrations ($c = 0.1\text{--}10\ \mu\text{g mL}^{-1}$), the metabolic activity of cells treated with test-samples was found to be on the level of untreated controls, which proves the absence of a toxic effect mediated by the NPs (Figure S2, Supporting Information). A detailed live/dead microscopy study of cells that were treated with NP confirmed the cell-membrane integrity (exclusion of red fluorescent PI from cell nuclei) and their excellent viability (strong green fluorescence

of FDA in cytoplasm) (Figure S3, Supporting Information). In addition, the interaction of NP suspensions with blood cells was investigated in terms of their potential to induce hemolysis (membrane damage and cell disruption) and/or aggregation of erythrocytes, one of the major cellular blood components. Whereas the treatment of erythrocytes with 1% Triton X-100 as positive control led to a complete disruption of the erythrocytes and subsequent release of the incorporated hemoglobin, none of the NP suspensions nor the PBS-treated negative control showed any hemolytic activity, indicating the absence of any harmful effect on the erythrocyte membrane integrity (Figure S4, Supporting Information). Furthermore,

the capability of NP suspensions to induce a formation of erythrocyte aggregates as an unwanted sign of blood incompatibility was studied microscopically and photometrically. None of the NP suspensions induced any red blood cell aggregation, even at the highest concentration of $10 \mu\text{g mL}^{-1}$ (Figure S5 and S6, Supporting Information). In contrast, the treatment with 25 kDa bPEI as positive control caused the clear formation of aggregates, whereas PBS-treated samples used as negative control did not yield in any aggregate formation. This observed absence of any nanoparticle-mediated blood incompatibility is in line with clinical evaluations of PMMA membranes dedicated for the use in blood dialysis.^[26] It is reported that due to their relatively hydrophobic and anionic surface PMMA particles show less nonspecific protein and peptide binding, and, thereby reduce the initial steps of opsonization leading to cell recognition/binding and possible immunological reactions.^[52] It is known that PMMA NP may be ingested and most probably can pass through the epithelial barrier and will likely end up in the bloodstream. Large particles are usually trapped by the liver,^[53] while smaller pass on and are captured by the kidneys.^[54] However, because of the very low toxicity documented for PMMA NPs, even in view of a chronic/continuous disease treatment in vivo, the possibility of obtaining sustainable effects by using PMMA NPs is presumably realistic. In addition, the good stability of the nanoparticles during autoclavation, centrifugation, and lyophilization/resuspension is basic requirements for the possible administration of lyophilized, resuspended/reconstituted, and autoclaved particles.

3. Conclusion

Consequently, the 4-hydroxythiazole-functionalized PMMA NPs are suitable for fluorescence-based long-term studies of biological processes at the molecular level. On the contrary to traditional fluorophores, the PMMA NPs combine small size and high photostability, and, in contrast to widely used quantum dots, they do not contain hazardous components, which need to be shielded by protective layers. The bio-analytical applications based on functionalized polymeric PMMA NPs are of emerging interest and provide opportunities like minimal-invasive intracellular monitoring of key components like pH value and oxygen content as well as ions like calcium, potassium or sodium. They can be combined with state-of-the-art imaging techniques like flow cytometry, fluorescence microscopy, and sophisticated imaging approaches, such as confocal imaging providing the opportunity for 3D analysis. In combination with dyes emitting in the near-infrared wavelength range, it offers an optical window for in vivo tissue imaging into several mm depth. By the immobilization of ligands to the

PMMA particles surface, also a specific binding to biomolecules can be mediated, thereby enabling approaches like specific cell targeting.^[55]

Supporting Information

Supporting Information is available from the Wiley Online Library or from the author.

Acknowledgements: The Thüringer Ministerium für Bildung, Wissenschaft und Kultur (TMBWK, ProExzellenz-Programm NanoConSens) is acknowledged for financial support. We gratefully thank Roberto Menzel and Prof. Dr. Rainer Beckert, Friedrich-Schiller-University of Jena, for providing the 4-hydroxyl thiazole dye and Steffi Stumpf and Dr. Frank Steininger, EMZ Jena, for assistance in the SEM investigations.

Received: May 13, 2012; Revised: June 28, 2012; Published online: August 7, 2012; DOI: 10.1002/marc.201200329

Keywords: fluorescent nanoparticles; 4-hydroxythiazoles; nanoprecipitation; particle size distribution; preparative ultracentrifugation; analytical ultracentrifugation; poly(methyl methacrylate); size-dependent cell uptake; solvent-evaporation technique

- [1] D. F. Emerich, C. G. Thanos, *J. Drug Targeting* **2007**, *15*, 163.
- [2] W. J. Stark, *Angew. Chem. Int. Ed.* **2011**, *50*, 1242.
- [3] N. Sanvicens, M. P. Marco, *Trends Biotechnol.* **2008**, *26*, 425.
- [4] A. Merkoci, *Biosens. Bioelectron.* **2010**, *26*, 1164.
- [5] C. J. Xu, L. Y. Mu, I. Roes, D. Miranda-Nieves, M. Nahrendorf, J. A. Ankrum, W. A. Zhao, J. M. Karp, *Nanotechnology* **2011**, *22*, 1.
- [6] K. H. Chung, M. Y. Cho, M. H. Sung, H. Poo, Y. T. Lim, *Chem. Commun.* **2011**, *47*, 8889.
- [7] G. Tosi, L. Bondioli, B. Ruozi, L. Badiali, G. M. Severini, S. Biffi, A. De Vita, B. Bortot, D. Dolcetta, F. Forni, M. A. Vandelli, *J. Neural Transm.* **2011**, *118*, 145.
- [8] M. Mahmoudi, V. Serpooshan, S. Laurent, *Nanoscale* **2011**, *3*, 3007.
- [9] A. H. Faraji, P. Wipf, *Biorg. Med. Chem.* **2009**, *17*, 2950.
- [10] H. S. Cho, Z. Dong, G. M. Pauletti, J. Zhang, H. Xu, H. Gu, L. Wang, R. C. Ewing, C. Huth, F. Wang, D. Shi, *ACS Nano* **2010**, *4*, 5398.
- [11] K. H. Lee, *J. Nucl. Med.* **2007**, *48*, 1408.
- [12] Z. Zili, S. Sfar, H. Fessi, *Int. J. Pharm.* **2005**, *294*, 261.
- [13] G. Tosi, F. Rivasi, F. Gandolfi, L. Costantino, M. A. Vandelli, F. Forni, *Biomaterials* **2005**, *26*, 4189.
- [14] M. Gaumet, R. Gurny, F. Delie, *Int. J. Pharm.* **2007**, *342*, 222.
- [15] A. E. Nel, L. Maedler, D. Velegol, T. Xia, E. M. V. Hoek, P. Somasundaran, F. Klaessig, V. Castranova, M. Thompson, *Nat. Mater.* **2009**, *8*, 543.
- [16] C. Vauthier, K. Bouchemal, *Pharm. Res.* **2009**, *26*, 1025.
- [17] R. A. Jain, *Biomaterials* **2000**, *21*, 2475.
- [18] J. P. Rao, K. E. Geckeler, *Prog. Polym. Sci.* **2011**, *36*, 887.
- [19] C. Pinto Reis, R. J. Neufeld, A. J. Ribeiro, F. Veiga, *Nanomed. Nanotechnol. Biol. Med.* **2006**, *1*, 8.

- [20] C. H. Lohmann, D. D. Dean, G. Koster, D. Casasola, G. H. Buchhorn, U. Fink, Z. Schwartz, B. D. Boyan, *Biomaterials* **2002**, *23*, 1855.
- [21] L. Araujo, M. Sheppard, R. Lobenberg, J. Kreuter, *Int. J. Pharm.* **1999**, *176*, 209.
- [22] I. Perevyazko, A. Vollrath, S. Hornig, G. M. Pavlov, U. S. Schubert, *J. Polym. Sci., Part A: Polym. Chem.* **2010**, *48*, 3924.
- [23] A. Vollrath, S. Schubert, N. Windhab, C. Biskup, U. S. Schubert, *Macromol. Rapid Commun.* **2010**, *31*, 2053.
- [24] J. W. Yoo, N. Giri, C. H. Lee, *Int. J. Pharm.* **2011**, *403*, 262.
- [25] R. Q. Frazer, R. T. Byron, P. B. Osborne, K. P. West, *J. Long. Term Eff. Med. Implants* **2005**, *15*, 629.
- [26] H. Horikawa, H. Naitoh, M. Agatsuma, S. Hashimoto, T. Miyazaki, H. Nagasaka, A. Fujimori, *Kidney Dial.* **1994**, *94*.
- [27] A. Bettencourt, A. J. Almeida, *J. Microencapsul.* **2012**, *29*, 353.
- [28] M. L. W. Knetsch, N. Olthof, L. H. Koole, *J. Biomed. Mater. Res., Part A* **2007**, *82A*, 947.
- [29] R. Menzel, A. Breul, C. Pietsch, J. Schaefer, C. Friebe, E. Tauscher, D. Weiss, B. Dietzek, J. Popp, R. Beckert, U. S. Schubert, *Macromol. Chem. Phys.* **2011**, *212*, 840.
- [30] D. Weiss, R. Menzel, E. Tauscher, R. Beckert, H. Goerls, *Z. Anorg. Allg. Chem.* **2010**, *636*, 1380.
- [31] G. Moad, S. H. Thang, *Aust. J. Chem.* **2009**, *62*, 1379.
- [32] R. Hoogenboom, C. Pietsch, U. S. Schubert, *Polym. Chem.* **2010**, *1*, 1005.
- [33] J. Chiefari, Y. K. Chong, F. Ercole, J. Krstina, J. Jeffery, T. P. T. Le, R. T. A. Mayadunne, G. F. Meijs, C. L. Moad, G. Moad, E. Rizzardo, S. H. Thang, *Macromolecules* **1998**, *31*, 5559.
- [34] H. Fessi, F. Puisieux, J. P. Devissaguet, N. Ammoury, S. Benita, *Int. J. Pharm.* **1989**, *55*, R1.
- [35] S. Schubert, J. T. Delaney, U. S. Schubert, *Soft Matter* **2011**, *7*, 1581.
- [36] U. Bilati, E. Allemann, E. Doelker, *Eur. J. Pharm. Sci.* **2005**, *24*, 67.
- [37] F. Bonaccorso, T. Hasan, P. H. Tan, C. Sciascia, G. Privitera, G. Di Marco, P. G. Gucciardi, A. C. Ferrari, *J. Phys. Chem. C* **2010**, *114*, 17267.
- [38] V. Vogel, K. Langer, S. Balthasar, P. Schuck, W. Maechtle, W. Haase, J. van den Broek, C. Tziatzios, D. Schubert, *Prog. Colloid Polym. Sci.* **2002**, *119*, 31.
- [39] H. Pertoft, *J. Biochem. Bioph. Methods* **2000**, *44*, 1.
- [40] M. Gaumet, A. Vargas, R. Gurny, F. Delie, *Eur. J. Pharm. Biopharm.* **2008**, *69*, 1.
- [41] M. Gaumet, R. Gurny, F. Delie, *Eur. J. Pharm. Sci.* **2009**, *36*, 465.
- [42] C. He, Y. Hu, L. Yin, C. Tang, C. Yin, *Biomaterials* **2010**, *31*, 3657.
- [43] J. C. Giddings, *Science* **1993**, *260*, 1456.
- [44] E. Tauscher, D. Weiss, R. Beckert, J. Fabian, A. Assumpcao, H. Goerls, *Tetrahedron Lett.* **2011**, *52*, 2292.
- [45] S. Hornig, T. Heinze, C. R. Becer, U. S. Schubert, *J. Mater. Chem.* **2009**, *19*, 3838.
- [46] I. Y. Perevyazko, J. T. Delaney, Jr., A. Vollrath, G. M. Pavlov, S. Schubert, U. S. Schubert, *Soft Matter* **2011**, *7*, 5030.
- [47] M. K. Brakke, *J. Am. Chem. Soc.* **1951**, *73*, 1847.
- [48] X. Sun, S. M. Tabakman, W. S. Seo, L. Zhang, G. Zhang, S. Sherlock, L. Bai, H. Dai, *Angew. Chem. Int. Ed.* **2009**, *48*, 939.
- [49] S. R. S. Ting, G. Chen, M. H. Stenzel, *Polym. Chem.* **2010**, *1*, 1392.
- [50] J. J. Lundquist, E. J. Toone, *Chem. Rev.* **2002**, *102*, 555.
- [51] C. R. Becer, M. I. Gibson, J. Geng, R. Ilyas, R. Wallis, D. A. Mitchell, D. M. Haddleton, *J. Am. Chem. Soc.* **2010**, *132*, 15130.
- [52] D. H. Sun, M. C. D. Trindade, Y. Nakashima, W. J. Maloney, S. B. Goodman, D. J. Schurman, R. L. Smith, *J. Biomed. Mater. Res., Part A* **2003**, *65A*, 290.
- [53] G. Borchard, J. Kreuter, *Pharm. Res.* **1996**, *13*, 1055.
- [54] A. M. Gatti, F. Rivasi, *Biomaterials* **2002**, *23*, 2381.
- [55] Y. K. Gong, F. M. Winnik, *Nanoscale* **2012**, *4*, 360.

Supporting Information

for *Macromol. Rapid Commun.*, DOI: 10.1002/marc.201200329

Preparation, Cellular Internalization, and Biocompatibility of Highly Fluorescent PMMA Nanoparticles

Antje Vollrath,¹ David Pretzel,¹ Christian Pietsch,^{1,2} Igor Perevyazko,¹ Stephanie Schubert,^{3,4}
George M. Pavlov,¹ Ulrich S. Schubert^{1,2,3*}

¹ Laboratory of Organic and Macromolecular Chemistry (IOMC), Friedrich-Schiller-University Jena, Humboldtstr. 10, 07743 Jena, Germany. Fax: +49(0) 3641 9482 02; E-mail: ulrich.schubert@uni-jena.de

² Dutch Polymer Institute (DPI), Post Office Box 902, Eindhoven 5600 AX, The Netherlands

³ Jena Center for Soft Matter (JCMS), Friedrich-Schiller-University Jena, Humboldtstr. 10, 07743 Jena, Germany

⁴ Institute of Pharmacy, Department of Pharmaceutical Technology Friedrich-Schiller-University Jena, Otto-Schott-Str. 41, 07745 Jena, Germany

Materials

All reagents were purchased from commercial sources (Fluka, Aldrich, Alfa Aesar and Acros Organics). MMA was purchased from Sigma-Aldrich and purified with an inhibitor-remover before use. 2,2'-Azobis(*iso*-butyronitrile) (AIBN) was recrystallized from methanol prior to use. The RAFT agent 2-cyano-2-propyl dithiobenzoate (CPDB) was purchased from Sigma-Aldrich. The thiazol functionalized methacrylate monomer was synthesized according to the

literature.^[1,2] Purified *N,N*-dimethylacetamide (DMA) was purchased from VWR. Unless otherwise stated, the chemicals were used without further purifications.

Synthesis of p(MMA-*stat*-MA^y) The RAFT polymerization technique was used according to already established methods.^[3-5] The desired amounts of MMA (592 mg, 0.63 mL) and dye-functionalized methacrylate (MA^y, 37.0 mg) were transferred into 5 mL reaction vials and dissolved in toluene. Thereafter, the calculated amounts of CPDB (9.5 mg) as well as AIBN (1.8 mg) dissolved in toluene (in total 2.07 mL) and anisole (0.3 mL), respectively, were added. The ratio of [CPDB] to [AIBN] was 4/1 using a monomer concentration of 2 mol · L⁻¹. Before closing the vial, the reaction solution was purged with a flow of argon for at least 30 min. Subsequently, the reaction solution was placed in a preheated oil bath at 70 °C for 14 h. The polymers obtained were purified by precipitation into cold methanol and dried under reduced pressure. Conversion was measured by ¹H NMR spectroscopy using anisole as internal standard.

p(MMA-*stat*-MA^y) ¹H NMR (CDCl₃, 300 MHz): δ = 8.57, 8.11 (Ar-H pyridine), 7.89, 7.78, 7.62, 7.51, 6.77 (Ar-H), 4.57 (OCH₂), 4.20 (OCH₂), 3.60 (OCH₃), 3.00 (NCH₃), 2.21 – 0.63 (backbone) ppm. SEC (CHCl₃, PMMA standard): M_n = 8,500 g · mol⁻¹, PDI = 1.19 ($M_{n,theo}$ = 9,900 g · mol⁻¹). UV/Vis (acetonitrile) λ_{max} = 413 nm, emission (acetonitrile) λ_{max} = 557 nm.

Preparation of the nanoparticle suspensions NP were prepared by the nanoprecipitation method from a stock polymer solution in acetone.^[6,7] The polymer solution was filtered through a 2 μ m filter before use. Since the route of nanoprecipitation has an influence on the size of the particles, the technique was performed in two ways: By dropping the acetone polymer solution into water (AW) or by dropping water in the polymer solution (WA). For route AW, the polymer was dissolved in acetone at a concentration of 4 mg · mL⁻¹. For route WA, the concentration was 3 mg · mL⁻¹. The solvent/non-solvent ratio was chosen to be 0.25. Subsequently, the acetone was completely removed from the suspensions by evaporation. The nanoparticle suspensions were diluted to a final concentration of 1.5 mg · mL⁻¹ and stored at 4 °C until further use.

Density gradient centrifugation The linear density gradients were prepared in 14 mm diameter, 13.2 mL capacity ultracentrifuge tubes (ultra clear tubes, Beckman) using a gradient maker consisting of two chambers connected *via* a channel with a stopcock; final gradient volume was 11.7 mL. In order to create a border for pelleting particles, 0.5 mL of 60% w/w sucrose solution was placed on the bottom of the tube before the main gradient solution was

loaded. The main gradient was obtained by mixing 5.6 mL of 20% w/w and 5.6 mL of 40% w/w sucrose solution in a mixing chamber by the way that the lower density solution was loaded first into the centrifugal tube. The gradient prepared was then stored for an hour at room temperature. The initial particle solution (0.5 mL) with a concentration of $1.5 \text{ mg} \cdot \text{mL}^{-1}$ was placed on top of the gradient. The centrifugal tube was then placed in a swinging bucket rotor and centrifuged at 10,000 rpm for 40 minutes. After centrifugation, the solution was collected by using a peristaltic pump and a narrow tube, inserted from above to the bottom of the centrifuge vial. Depending on the sample each 0.5 mL or 1 mL of the solution was collected. The fractions containing nanoparticles were then dialyzed against pure water and analyzed by AUC, DLS and SEM.

Instrumentation

Size Exclusion chromatograms (SEC) were recorded using a SEC Shimadzu SCL-10A system controller, a LC-10AD pump, a RID-10A refractive index detector and a PSS SDV column with chloroform:triethylamine:2-propanol (94:4:2) as eluent. The column oven was set to 40 °C with a flow rate of $1 \text{ mL} \cdot \text{min}^{-1}$. The system was calibrated with narrow polydispersity PMMA standards.

^1H NMR and ^{13}C NMR spectra were recorded in CDCl_3 on a Bruker Avance 250 MHz or 300 MHz spectrometer. Chemical shifts are given in ppm relative to signals from the NMR solvents. Conversions were calculated from ^1H NMR spectra using anisole as an internal standard.

Elemental analysis (EA) was carried out at an Elementaranalysator Vario EL III CHNS from Elementar Analysensysteme GmbH, Hanau.

UV/VIS spectroscopy measurements were set out on a Specord 250, Analytik Jena GmbH. The emission spectra were recorded using the FP 6500, Jasco. The polymers were dissolved in acetonitrile and measured in a quartz cuvette.

Dynamic light scattering (DLS) and zeta potential were recorded on a Zetasizer Nano ZS (Malvern Instruments, Malvern, U.K.) operating with a laser beam at 633 nm and a scattering angle of 173° . Each sample was measured in triplicate at 25 °C in a polycarbonate zeta cell. For size measurements, 3 runs for 30 s were chosen, and for the zeta potential, 3 runs for 10 s. For this purpose, 20 μL nanoparticle suspensions were diluted with 1 mL demineralized, filtered water. The mean particle size was approximated as the effective (Z average) diameter obtained by the cumulant method, and the particle polydispersity index (PDI_p) was calculated as a square root of the ratio of the second order cumulant to the first order cumulant

$PDI_p = (K2/K1)^{1/2}$.^[8] Furthermore, the intensity and the volume distribution of the particle size were calculated applying the NNLS mode.

Scanning electron microscopy (SEM) was performed on a LEO-1450 VP (Leo Elektronenmikroskopie GmbH, Oberkochen, Germany). One droplet (20 μ L) of the nanoparticle suspension (1 mg mL⁻¹) was placed on a mica surface, lyophilized for 3 h, and covered with platinum or gold using a sputter coating device BAL-TEC SCD005 (Balzers, Lichtenstein; 60 mA, 80 s). The system was operating from 8 to 10 kV. The average size of the particles was determined using the software Image J.

Analytic Ultracentrifugation (AUC): A ProteomeLab XLI Protein Characterization system analytical ultracentrifuge (Beckman Instruments, Palo Alto, USA) was used for sedimentation velocity runs. Experiments were carried out in conventional double-sector Epon centerpieces of 12 mm optical path length in a four holes rotor. Cells were filled with 400 μ L of suspension ($c = 1.2 \text{ mg} \cdot \text{mL}^{-1}$) and 420 μ L of solvent (H₂O). The rotor speed was set to 6,000 rpm. The rotor temperature was equilibrated for approximately 2 h at 20 °C in the chamber of the centrifuge. Sedimentation profiles were obtained every 15 s by interference optics, and the sedimentation runs were evaluated by the program Sedfit.^[9] As partial specific volume, $v = 0.832 \text{ cm}^3 \text{ g}^{-1}$ was used.

Density gradient centrifugation was set up in a Beckman Optima L-XP ultracentrifuge (Beckman Instruments, Palo Alto, USA) using the swinging bucket rotor SW 41 Ti rotor.

Laser scanning microscopy: For the analysis of the uptake of particles by L929 cells, fluorescence images were obtained with a confocal laser-scanning microscope (LSM 510 Meta, Carl Zeiss, Jena, Germany), using a Plan-Apochromat 63 \times oil immersion objective (NA 1.4, Zeiss). The thiazole dye was excited with a 458 nm laser. The emitted fluorescence was collected with a 505 nm longpass filter. To facilitate a comparison between the images, all images of a series were captured under identical conditions and instrument settings (e.g. laser power, pinhole diameter and detector gain).

Fluorescence microscopy: To visualize the viability of L929 cells after incubation with different particle suspensions, the blue/red/green fluorescence signal of cells cultured in 96 well plate and stained with Hoechst/PI/FDA was observed on a fluorescence microscope (Cell Observer Z1, Carl Zeiss, Jena, Germany) equipped with a mercury arc UV lamp and the appropriate filter combinations for excitation and detection of emission. Images of a series were captured with a 10 \times objective using identical instrument settings (e.g. UV lamp power, integration time, camera gain) and spots of the 96-well plate were addressed using an automated XY table.

Photometric absorbance measurement: A TECAN Infinite M200 PRO platereader (TECAN, Crailsheim, Germany) was used to measure the absorbance of samples from a) the XTT cytotoxicity assay (570 nm with a background correction of the OD at 690 nm) b) the hemolysis of erythrocytes (540 nm with a background correction of the OD at 690 nm) and c) the photometric evaluation of erythrocyte aggregation (645 nm). Each well containing the sample was measured in 4 different spots each with 10 flashes per scan.

Biological studies

Cell line: The mouse fibroblast cell line L929 used in the biological experiments was purchased from the German Collection of Microorganisms and Cell Cultures (DSMZ, Braunschweig, Germany). Cells were cultured in Dulbecco's modified eagle's medium (DMEM) supplemented with 10% FCS, 100 U · mL⁻¹ penicillin, and 100 µg · mL⁻¹ streptomycin (all components from Biochrom, Berlin, Germany) at 37 °C in a humidified atmosphere with 5% (v/v) CO₂.

Uptake study: To assess the particle uptake in adherent L929 cell monolayers by CLSM, 8 × 10⁴ cells were initially seeded onto sterile glass coverslips placed into 6 well plates. The cells were grown for 48 hours until 75% confluency was reached and then incubated separately with different concentrations (0.1, 1.0, and 10.0 µg · mL⁻¹, respectively) of particle suspensions for 24 h. Control cells were incubated with fresh culture medium. After incubation, the solutions were aspirated from the wells, and any unbound conjugates were removed by washing the cell layer three times with PBS. Subsequently, the cells were fixed directly on the glass coverslips for 10 minutes at room temperature using 4% paraformaldehyde dissolved in PBS followed by 2 times washing with PBS. The glass coverslips were mounted on glass slides using 25 µL Moviol 4-88 solution containing 625 µg 1.4-diazabicyclo-(2,2,2) octane. Samples were then characterized by CLSM.

Cytotoxicity test: In order to assess the short-term cytotoxicity of the polymeric nanoparticles, the XTT cytotoxicity test was used, according to ISO/EN 10993 part 5 guidelines: For the XTT test, L929 cells were seeded in 96-well plates at a density of 1 × 10⁴ cells/well and were grown as monolayer cultures for 24 h. The cells were then incubated separately with different concentrations (0.01, 0.1, 1.00 and 10.00 µg · mL⁻¹ (n = 6)) for 24 h. Control cells were incubated with fresh culture medium. After incubation, 50 µL of a XTT solution prepared according to the manufacturer's instructions were added to each well. After 4 h at 37 °C 100 µL of each solution were transferred to a new microtiter

plate and the optical density (OD) was measured photometrically. The negative control was standardized as 0% of metabolism inhibition and referred as 100% viability.

Cytotoxicity test: In order to assess the short-term cytotoxicity of the polymeric nanoparticles, the XTT cytotoxicity test was used, according to ISO/EN 10993 part 5 guidelines: For the XTT test, L929 cells were seeded in 96-well plates at a density of 1×10^4 cells/well and were grown as monolayer cultures for 24 h. The cells were then incubated separately with different concentrations (0.01, 0.1, 1.0 and 10.0 $\mu\text{g} \cdot \text{mL}^{-1}$ ($n = 6$)) for 24 h. Control cells were incubated with fresh culture medium. After incubation, 50 μL of a XTT solution prepared according to the manufacturer's instructions was added to each well. After 4 h at 37 °C, 100 μL of each solution were transferred into a new microtiter plate, and the optical density (OD) was measured photometrically. The negative control was standardized as 0% of metabolism inhibition and referred to 100% viability.

Viability staining with FDA/PI/Hoechst: In addition to the XTT assay as a method for determination of metabolic activity, the influence of the particle suspensions on viability of L929 mouse fibroblasts was examined microscopically by using the fluorescein diacetate (FDA)/propidium iodide (PI) viability assay. The cell line was treated with particle suspensions as described for the XTT assay. After incubation for 24 h a viability staining was performed. For that, cells were covered for 10 min with a solution of cell culture medium containing Hoechst 33342 dye ($1 \mu\text{g} \cdot \text{mL}^{-1}$), PI ($1 \mu\text{g} \cdot \text{mL}^{-1}$) and FDA ($1 \mu\text{g} \cdot \text{mL}^{-1}$). After removal of the staining solution, cells were washed twice and finally covered with PBS. The blue, red and green fluorescence was observed within 10 min after staining using a fluorescence microscope.

Hemolysis of erythrocytes and erythrocyte aggregation: For testing the hemolytic activity of the particle suspensions, blood from sheep, collected in heparinized-tubes, was centrifuged at $4.500 \times g$ for 5 min and the pellet was washed three times with cold PBS. The suspension of red blood cells was always freshly prepared and used within 24 h after collection. The stock solutions were diluted with PBS to a final erythrocyte-concentration of approx. $3 \times 10^6/\text{mL}$. Polymer solutions with concentrations of 0.01, 0.1, 1.00 and 10.00 $\mu\text{g} \cdot \text{mL}^{-1}$ were prepared in PBS buffer, added to the erythrocytes in a ratio of 1:1 and were then incubated for 60 min at 37 °C. The release of hemoglobin was determined after centrifugation ($2,400 g$ for 5 min) by measurement of absorption. Complete hemolysis was achieved using 1% Triton X-100 reflecting the 100% value. PBS served as negative control. Less than 5% hemolysis rate were taken as non-hemolytic. For the analysis of erythrocyte aggregation, 100 μL of polymers with concentrations of 0.01, 0.1, 1.00 and 10.00 $\mu\text{g} \cdot \text{mL}^{-1}$ were dissolved in PBS buffer,

incubated at 37 °C for 2 h with 100 µL of erythrocytes isolated as described above for the hemolysis assay. PBS served as negative control and 50 µg · mL⁻¹ 25 kDa branched poly(ethylene imine) displayed the positive control. Erythrocyte aggregation was measured photometrically at $\lambda = 645$ nm.^[10] Additionally, a microscopic evaluation was performed with samples that were diluted after photometric measurement 1:10 with PBS. Experiments for hemolysis and erythrocyte aggregation were run in triplicate from 3 different donor sheep and were repeated once.

- [1] R. Menzel, A. Breul, C. Pietsch, J. Schaefer, C. Friebe, E. Tauscher, D. Weiss, B. Dietzek, J. Popp, R. Beckert, U. S. Schubert, *Macromol. Chem. Phys.* **2011**, *212*, 840.
- [2] D. Weiss, R. Menzel, E. Tauscher, R. Beckert, H. Goerls, *Z. Anorg. Allg. Chem.* **2010**, *636*, 1380.
- [3] G. Moad, S. H. Thang, *Aust. J. Chem.* **2009**, *62*, 1379.
- [4] G. Moad, J. Chiefari, Y. K. Chong, F. Ercole, J. Krstina, J. Jeffery, T. P. T. Le, R. T. A. Mayadunne, G. F. Meijs, C. L. Moad, E. Rizzardo, S. H. Thang, *Macromolecules* **1998**, *31*, 5559.
- [5] R. Hoogenboom, C. Pietsch, U. S. Schubert, *Polym. Chem.* **2010**, *1*, 1005.
- [6] S. Schubert, J. T. Delaney, U. S. Schubert, *Soft Matter* **2011**, *7*, 1581.
- [7] H. Fessi, F. Puisieux, J. P. Devissaguet, N. Ammoury, S. Benita, *Int. J. Pharm.* **1989**, *55*, R1.
- [8] D. E. Koppel, *J. Chem. Phys.* **1972**, *57*, 4814.
- [9] P. Schuck, *Biophys. J.* **2000**, *78*, 1606.
- [10] A. V. Cardoso, M. H. Pereirab, G. d. A. Marcondesa, A. R. Ferreira, P. R. d. Araújo, *J. Mater. Res.* **2006**, *10*, 31.

Polymer characterization

Table S1. Characterization data of the copolymer p(MMA-*stat*-MA^y).

[MMA]: [dye]	[M]: [CTA]: [AIBN]	Conv. MMA ^a (%)	$M_{n, \text{theo}}$ (g/mol)	$M_{n, \text{SEC}}$ (RI) ^b (g/mol)	PDI _{SEC} (RI) ^b	DP _{SEC} (RI) ^b	Dye content (NMR) ^c (%)
138:2	140:1:0.25	68	9,900	8,500	1.19	81	2.9

a) Calculated from vinyl integrals of ¹H NMR spectra using anisole as internal standard.

b) Calculated from SEC (CHCl₃), PMMA calibration.

c) Calculated from integrated areas of aromatic dye signals and the methyl signals of MMA.

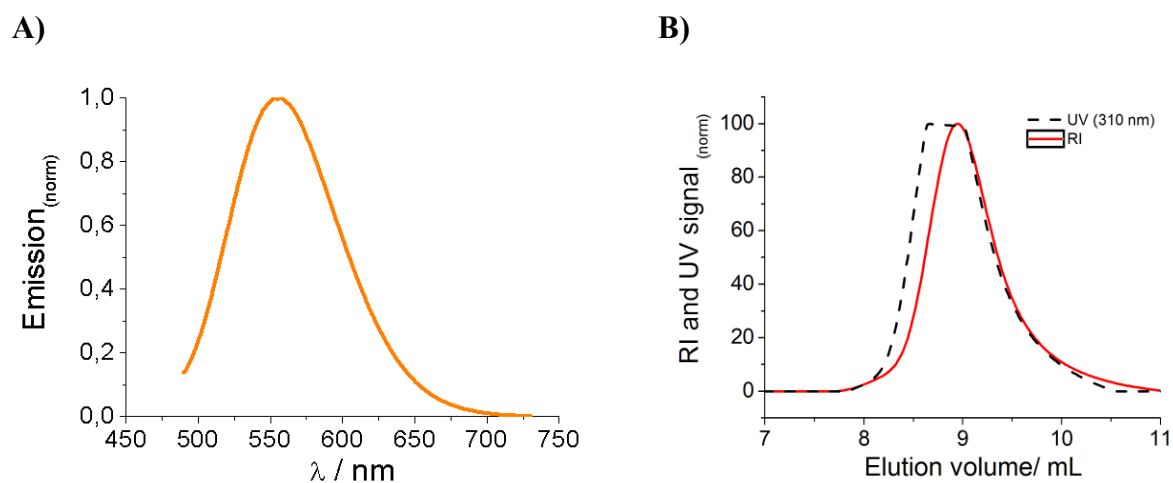


Figure S1. A) Fluorescence emission spectra of p(MMA-*stat*-MA^y) in acetonitrile (excited at $\lambda = 418$ nm). B) SEC measurements (CHCl₃) of p(MMA-*stat*-MA^y). The refractive index trace (--) and the UV trace at 310 nm (-) of the labeled polymer occur at the same retention time confirming the covalent attachment.

Biological experiments

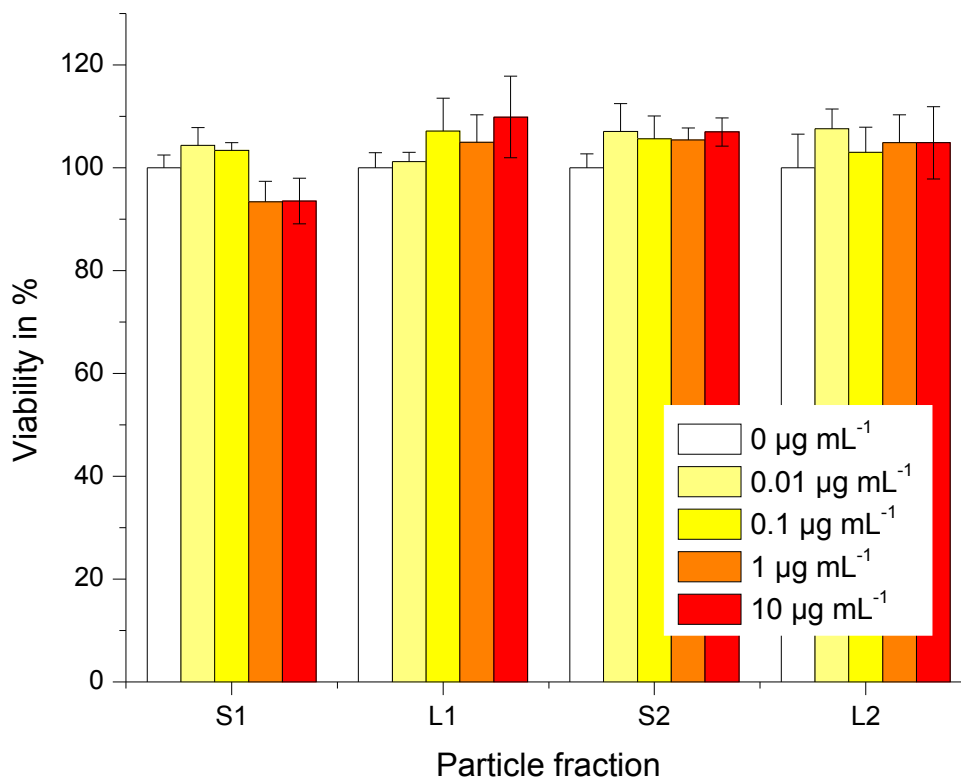


Figure S2. Cell viability of L929 mouse fibroblasts after incubation with small (**S1/S2**) and large (**L1/L2**) polymeric p(MMA-*stat*-MA^y) nanoparticles up to 10 µg · mL⁻¹ for 24 hours. Cells incubated with polymer free culture medium served as control. The cell viability was determined by XTT assay according to ISO 10993-5, where values below 70% viability were regarded as cytotoxic. Data are expressed as mean ±SD of six determinations.

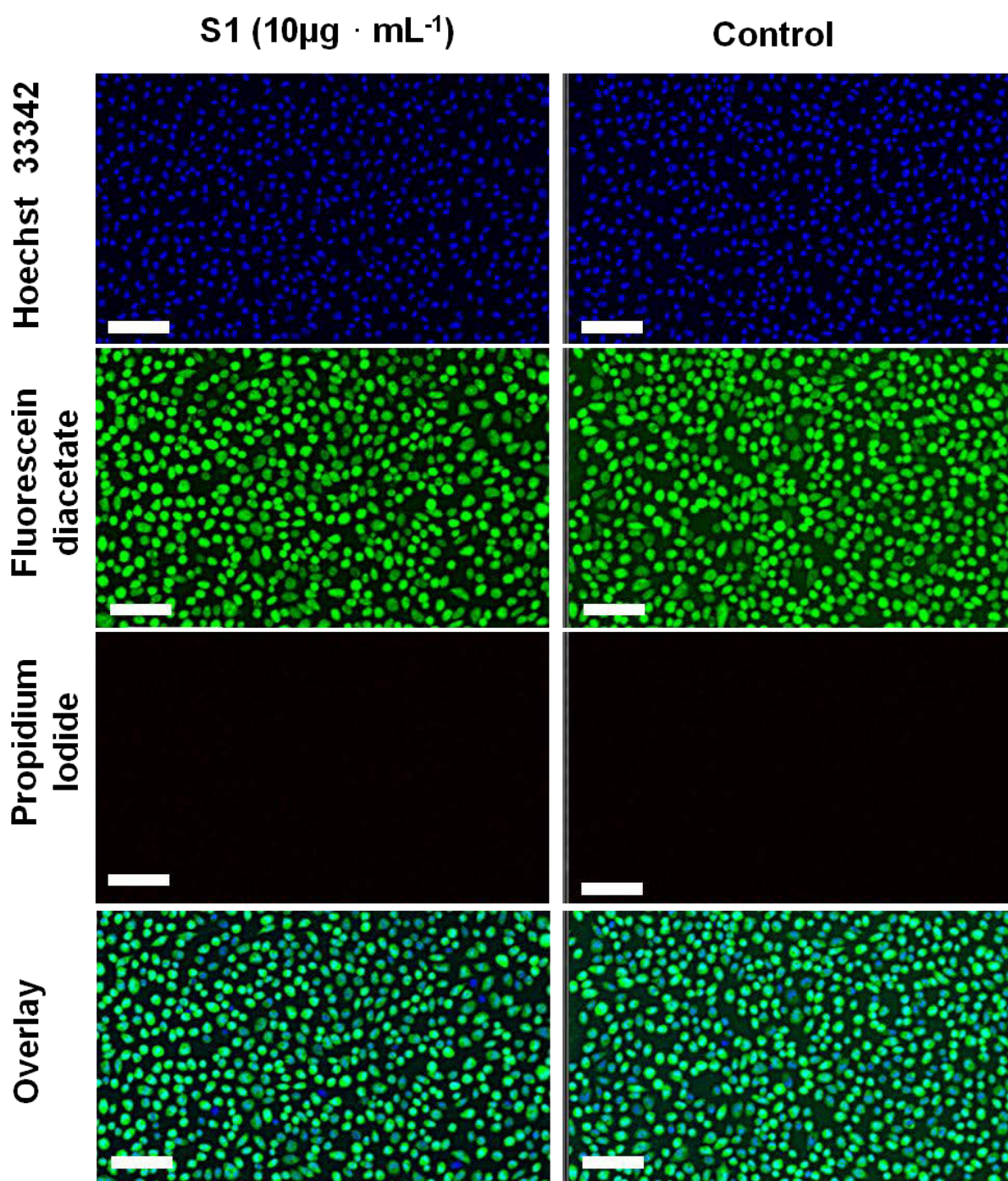


Figure S3. Representative fluorescence microscopy micrographs of Hoechst 33342/FDA/PI stained L929 mouse fibroblast cells cultured for 24 hours in the presence of the small (**S1/S2**) and large (**L1/L2**) polymeric p(MMA-*stat*-MA^y) nanoparticles up to 10 $\mu\text{g} \cdot \text{mL}^{-1}$ for 24 hours. Blue fluorescent Hoechst dye labels nuclei of all cells present, green fluorescent FDA dye indicates cytoplasm of vital cells, red fluorescent PI signals tag nuclei of dead cells. Left: 10 $\mu\text{g} \cdot \text{mL}^{-1}$ particle suspension added (small (**S1**); same results for small (**S2**) and large (**L1/L2**) particle suspensions), right: control culture without particles.

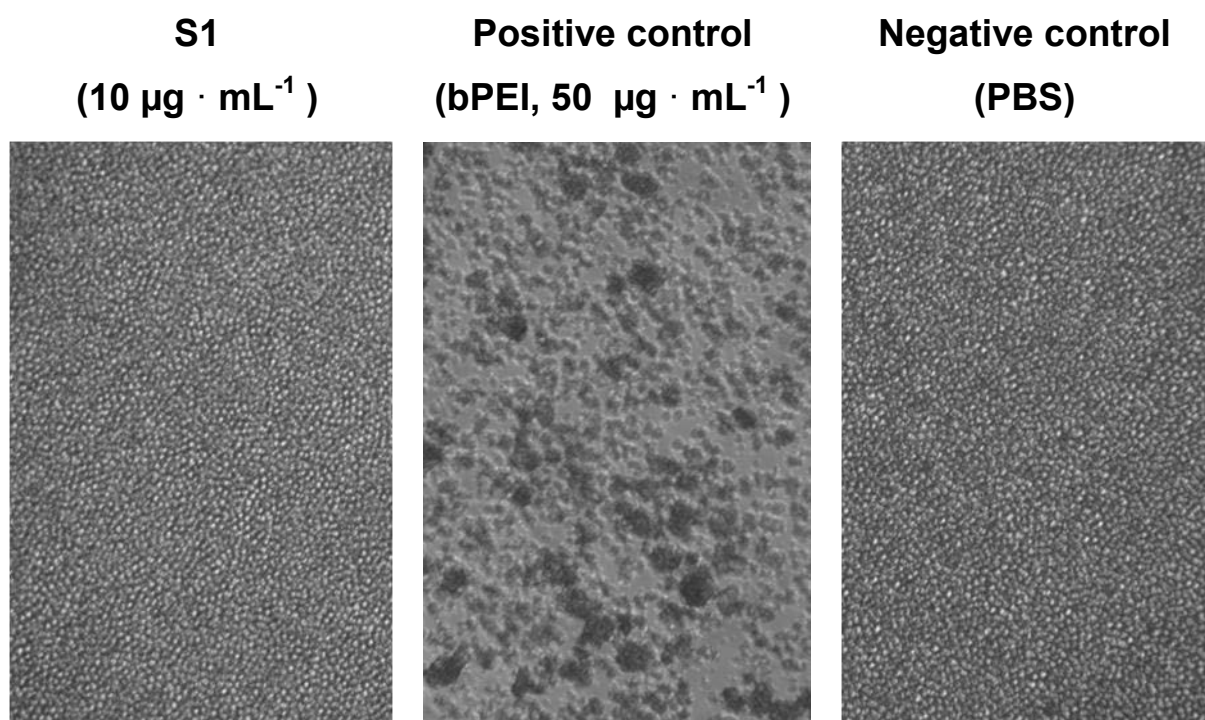


Figure S4. Representative micrographs of red blood cell aggregation after 2 h incubation at 37 °C with small polymeric p(MMA-*stat*-MA^y) nanoparticles (**S1**, 10 $\mu\text{g} \cdot \text{mL}^{-1}$). Same results as for **S1** were obtained for **S2/L1/L2**. 25 kDa bPEI (50 $\mu\text{g} \cdot \text{mL}^{-1}$) served as positive and PBS as negative control. Magnification 320 \times .

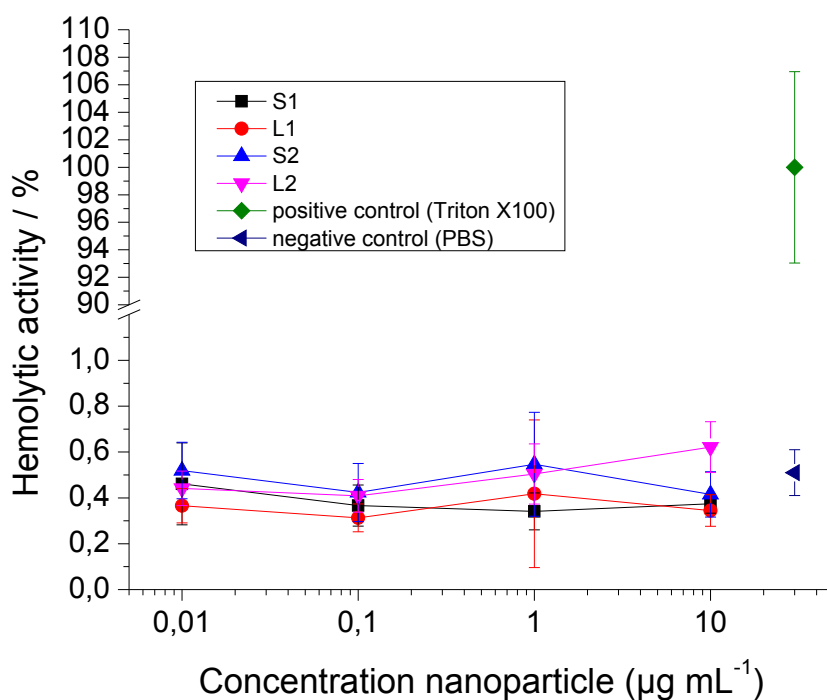


Figure S5: Photometric determination of hemolytic activity after 1 h incubation at 37 °C with small (S1/S2) and large (L1/L2) polymeric p(MMA-*stat*-MA^y) nanoparticles. Triton X-100 (1%) served as positive and PBS as negative control. Data are presented as the mean percentage \pm SD of hemolytic activity compared to the positive control set as 100%.

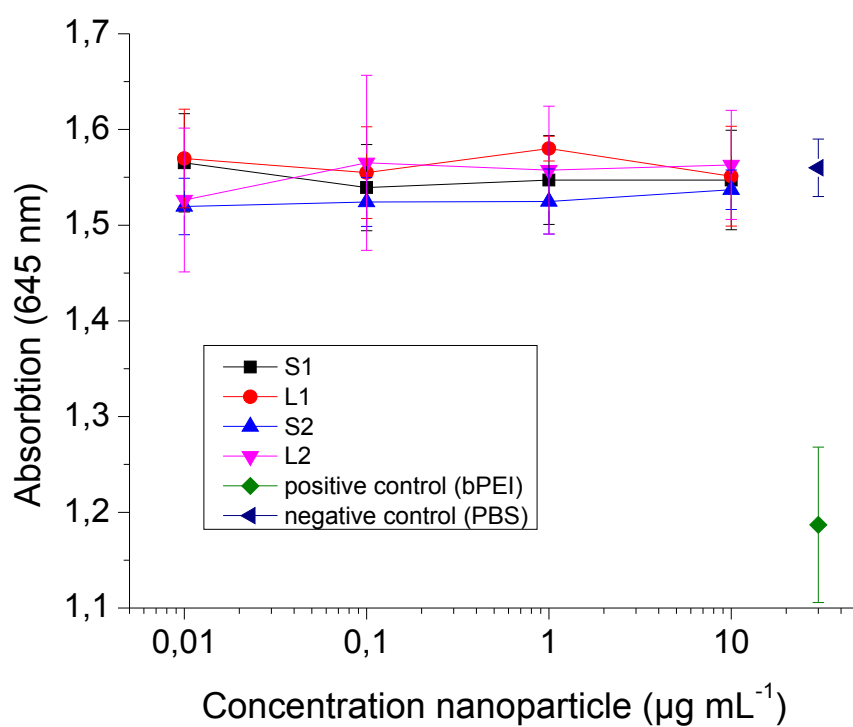


Figure S6: Photometric determination of erythrocyte aggregation after 2 h incubation at 37 °C with small (S1/S2) and large (L1/L2) polymeric p(MMA-*stat*-MA^y) nanoparticles. 25 kDa bPEI ($50 \mu\text{g} \cdot \text{mL}^{-1}$) served as positive and PBS as negative control. Data are presented as the mean measured absorbance \pm SD.

Preparation, Cellular Internalization, and Biocompatibility of Highly Fluorescent PMMA Nanoparticles

Antje Vollrath, David Pretzel, Christian Pietsch, Igor Perevyazko, Stephanie Schubert, George M. Pavlov, Ulrich S. Schubert*

DOI: 10.1002/marc.201200329

The authors regret that there were important omissions in the above article. The synthesis of the yellow light-emitting thiazole-dye 3-((5-(4-(dimethylamino)phenyl)-2-(pyridin-3-yl)thiazol-4-yl)oxy)propan-1-ol as well as the corresponding methacrylate monomer was not described in reference 29 of the manuscript or in reference 1 of the Supporting Information (in this publication only the related blue emitting monomer is described). The resulting yellow and blue polymers were both investigated – however, due to the non-visibility of the blue polymer only the yellow one was continued in the published study. In order to allow an exact reproduction of the monomer synthesis, a detailed description has been added as Supporting Information of this Correction.

In the original version of the above article, three co-authors' names (Roberto Menzel, Dieter Weiß, and Rainer Beckert) were missing from the byline and affiliation. The correct author byline is as follows:

Antje Vollrath, David Pretzel, Christian Pietsch, Igor Perevyazko, Roberto Menzel, Stephanie Schubert, George M. Pavlov, Dieter Weiß, Rainer Beckert, Ulrich S. Schubert*

Finally, the Acknowledgments section in the above article should be replaced with the following paragraph.

The Thüringer Ministerium für Bildung, Wissenschaft und Kultur (TMBWK, ProExzellenz-Programm NanoConSens) is acknowledged for financial support. We gratefully thank Steffi Stumpf and Dr. Frank Steininger, EMZ Jena, for assistance in the SEM investigations.

A. Vollrath, D. Pretzel, C. Pietsch, I. Perevyazko, R. Menzel,
G. M. Pavlov, D. Weiß, R. Beckert, U. S. Schubert
Laboratory of Organic and Macromolecular Chemistry (IOMC),
Friedrich-Schiller-University Jena, Humboldtstr. 10,
07743 Jena, Germany
E-mail: ulrich.schubert@uni-jena.de
C. Pietsch, I. Perevyazko, G. M. Pavlov, U. S. Schubert
Dutch Polymer Institute (DPI), Post Office Box 902,
Eindhoven 5600 AX, The Netherlands
S. Schubert, R. Beckert, U. S. Schubert
Jena Center for Soft Matter (JCMS), Friedrich-Schiller-
University Jena, Humboldtstr. 10, 07743 Jena, Germany
Stephanie Schubert
Institute of Pharmacy, Department of Pharmaceutical
Technology Friedrich-Schiller-University Jena,
Otto-Schott-Str. 41, 07745 Jena, Germany

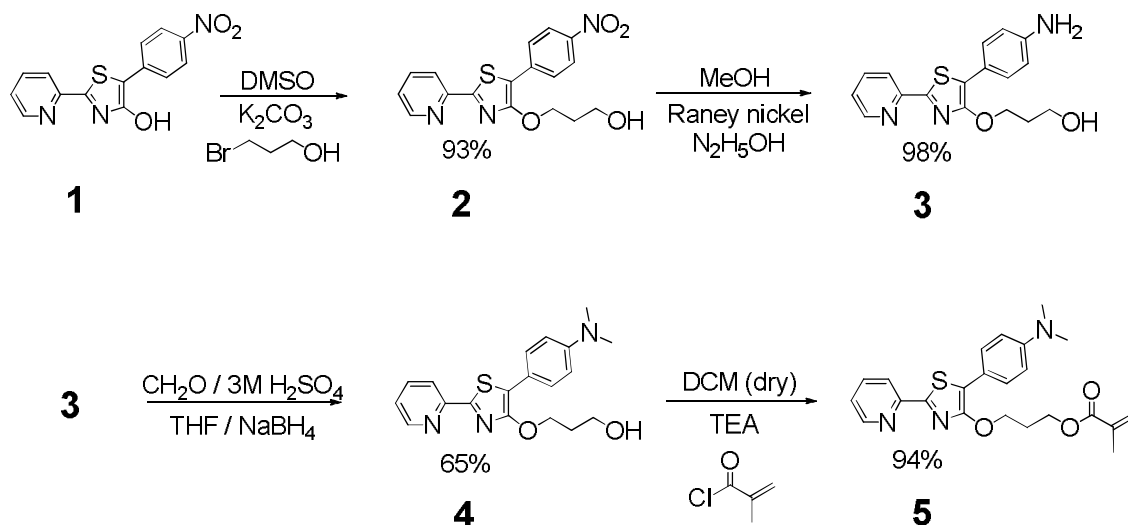
Preparation, Cellular Internalization, and Biocompatibility of Highly Fluorescent PMMA Nanoparticles

Antje Vollrath, David Pretzel, Christian Pietsch, Igor Perevyazko, Roberto Menzel, Stephanie Schubert, George M. Pavlov, Dieter Weiß, Rainer Beckert, Ulrich S. Schubert*

Materials

The hydrazinium hydroxide solution and the Raney nickel were purchased from Sigma-Aldrich. The educt 5-(4-nitrophenyl)-2-(pyridin-2-yl)thiazol-4-ol (**1**) for the synthesis of the thiazol-functionalized methacrylate monomer was prepared according to the literature.^[1]

[1] *Arylamine-Modified Thiazoles as Donor-Acceptor Dyes: Quantum Chemical Evaluation of the Charge-Transfer Process and Testing as Ligands in Ruthenium(II) Complexes*, R. Menzel, S. Kupfer, R. Mede, D. Weiss, H. Goerls, L. Gonzalez, R. Beckert, *Eur. J. Org. Chem.* **2012**, 5231.



Synthesis of the monomer used for the polymerization.

Synthesis of 3-((5-(4-nitrophenyl)-2-(pyridin-2-yl)thiazol-4-yl)oxy)propan-1-ol (2). Fine ground K_2CO_3 (1.44 g, 10.4 mmol, 1.2 equiv) was added to a suspension of 5-(4-nitrophenyl)-2-(pyridin-2-yl)thiazol-4-ol (2.60 g, 8.69 mmol) and 3-bromopropane-1-ol (1.33 g, 9.56 mmol, 1.1 equiv) in DMSO (100 mL). The deep blue mixture was stirred for four days at room temperature followed by the addition of H_2O (400 mL). The product was extracted with CHCl_3 (3 · 100 mL). The combined organic phases were washed additionally with H_2O (3 · 100 mL) to remove the DMSO, dried over MgSO_4 and concentrated *in vacuo*. The brown solid was purified with a short gel filtration (silica, $\text{CHCl}_3/\text{EtOAc}$ 3:1) to yield the pure ether.

The product can also be recrystallized from *n*-heptane/CHCl₃ by slow evaporation of the CHCl₃ and addition of a seed crystal; yield: 2.85 g (7.97 mmol, 92%). ¹H NMR (250 MHz, CDCl₃): δ = 8.62 (ddd, *J* = 4.8, 1.6, 0.9 Hz, 1H), 8.28 - 8.18 (m, 2H), 8.08 (dt, *J* = 8.0, 0.9 Hz, 1H), 7.95 - 7.86 (m, 2H), 7.81 (td, *J* = 7.7, 1.7 Hz, 1H), 7.35 (ddd, *J* = 7.5, 4.8, 1.1 Hz, 1H), 4.76 (t, *J* = 6.0 Hz, 2H), 3.88 (t, *J* = 5.9 Hz, 2H), 2.40 (s, 1H), 2.14 ppm (p, *J* = 6.0 Hz, 2H). ¹³C NMR (63 MHz, CDCl₃): δ = 163.89, 161.18, 150.52, 149.81, 145.71, 138.64, 137.31, 126.86, 125.13, 124.31, 119.40, 112.21, 68.08, 59.29, 32.81 ppm. MS (Micro-ESI): 380.2 [M + Na]⁺. Anal. Calcd for C₁₇H₁₅N₃O₄S: C, 57.13; H, 4.23; N, 11.76; S, 8.97. Found: C, 57.01; H, 4.35; N, 11.90; S, 8.91.

Synthesis of 3-((5-(4-aminophenyl)-2-(pyridin-2-yl)thiazol-4-yl)oxy)propan-1-ol (3). A suspension of 3-((5-(4-nitrophenyl)-2-(pyridin-2-yl)thiazol-4-yl)oxy)propan-1-ol (1.90 g, 5.32 mmol) in MeOH (100 mL) was heated to 50 °C. An 80% solution N₂H₅OH in H₂O and freshly prepared Raney nickel (catalytic amounts) were added till no educt was left as indicated by TLC. The reaction mixture was filtered through a frit, on which a two centimeter thick silica bed was applied to remove the Raney nickel after the reaction was finished. The silica bed was washed with a mixture of EtOH/CHCl₃ 1:1 and the two fractions were combined and concentrated. The product was purified using gradient gel filtration (silica, CHCl₃ to CHCl₃/EtOAc 1:1) yielding the amine almost quantitatively as a yellow solid; yield: 1.72 g (5.52 mmol, 98%). ¹H NMR (250 MHz, CDCl₃): δ = 8.56 (d, *J* = 4.2 Hz, 1H), 8.01 (d, *J* = 8.0 Hz, 1H), 7.74 (td, *J* = 7.8, 1.7 Hz, 1H), 7.60 - 7.52 (m, 2H), 7.25 (ddd, *J* = 8.7, 4.7, 1.0 Hz, 1H), 6.74 - 6.66 (m, 2H), 4.63 (t, *J* = 5.9 Hz, 2H), 3.85 (t, *J* = 5.9 Hz, 2H), 3.77 (s, 2H), 3.03 (s, 1H), 2.14 - 1.99 ppm (m, 2H). ¹³C NMR (63 MHz, CDCl₃): δ = 159.02, 158.21, 151.24, 149.58, 145.83, 137.12, 128.47, 124.05, 121.79, 118.82, 116.34, 115.34, 67.86, 59.37, 33.02 ppm. MS (Micro-ESI): 350.2 [M + Na]⁺. Anal. Calcd for C₁₇H₁₇N₃O₂S: C, 62.36; H, 5.23; N, 12.83; S, 9.79. Found: C, 62.21; H, 5.35; N, 12.90; S, 9.86.

Synthesis of 3-((5-(4-(dimethylamino)phenyl)-2-(pyridin-2-yl)thiazol-4-yl)oxy)propan-1-ol (4). To a solution of 37% CH₂O in H₂O (1.80 g, approx. 22.1 mmol, 7 equiv.) and 3 M H₂SO₄ (15 mL), a mixture of 3-((5-(4-aminophenyl)-2-(pyridin-2-yl)thiazol-4-yl)oxy)propan-1-ol (1.03 g, 3.15 mmol) and NaBH₄ (600 mg, approx. 15.8 mmol, 5 equiv.) suspended in THF (30 mL) was added successively in small portions over a period of one hour. The resulting deep orange mixture was diluted with CHCl₃ (50 mL) and washed with water (3 · 50 mL) after neutralization with a saturated K₂CO₃ solution. The organic phase was dried over MgSO₄, filtered and concentrated *in vacuo*. Gel filtration (silica, CHCl₃/EtOAc 4:1) yielded the product as brownish yellow oil, which solidifies after a few minutes to form a yellow solid; yield: 730 mg (2.06 mmol, 65%).

Synthesis of 3-((5-(4-(dimethylamino)phenyl)-2-(pyridin-2-yl)thiazol-4-yl)oxy)propyl methacrylate (5). To a solution of 3-((5-(4-(dimethylamino)phenyl)-2-(pyridin-2-yl)thiazol-4-yl)oxy)propan-1-ol (480 mg, 1.35 mmol) and TEA (180 mg, 1.6 mmol, 1.2 equiv.) in dry CH₂Cl₂ (20 mL), methacryloyl chloride (170 mg, 1.6 mmol, 1.2 equiv.) were added. The reaction was stirred under a nitrogen atmosphere at room temperature and was monitored by TLC. After the reaction was finished (typically after 24 h), the organic phase was washed thoroughly with a saturated NaHCO₃ solution and H₂O (3 · 20 mL), dried over MgSO₄ and evaporated to dryness at T < 40 °C to give a yellow oil. The crude product was purified using column chromatography (silica, CHCl₃) affording the pure methacrylate as a yellow oil, which solidifies at T < 0 °C; yield: 540 mg (1.28 mmol, 94%). ¹H NMR (250 MHz, CDCl₃): δ = 8.57 (d, *J* = 4.7 Hz, 1H), 8.00 (d, *J* = 7.8 Hz, 1H), 7.91 (t, *J* = 7.6 Hz, 1H), 7.57 (d, *J* =

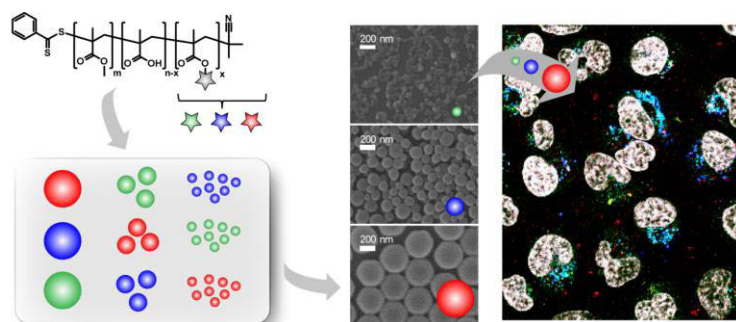
8.7 Hz, 2H), 7.48 - 7.37 (m, 1H), 6.75 (d, $J = 8.8$ Hz, 2H), 6.03 (s, 1H), 5.65 (s, 1H), 4.53 (t, $J = 6.2$ Hz, 2H), 4.29 (t, $J = 6.3$ Hz, 2H), 2.92 (s, 6H), 2.16 (p, $J = 6.2$ Hz, 2H), 1.86 ppm (s, 3H). ^{13}C NMR (63 MHz, CDCl_3): $\delta = 167.53, 158.16, 157.75, 151.68, 149.61, 149.49, 136.88, 136.50, 128.17, 125.59, 123.74, 119.76, 118.83, 116.54, 112.62, 67.04, 61.93, 40.54, 29.20, 18.45$ ppm. MS (EI): 423 (60) [M^+], 296 (10), 164 (100). Anal. Calcd for $\text{C}_{23}\text{H}_{25}\text{N}_3\text{O}_3\text{S}$: C, 65.23; H, 5.95; N, 9.92; S, 7.57. Found: C, 65.20; H, 5.99; N, 10.13; S, 7.73. UV/Vis (acetonitrile) λ_{max} (log ϵ): 226 (4.192), 283 (4.058), 413 (4.302).

Publication 6

"A toolbox of differently sized and labeled PMMA nanoparticles for cellular uptake investigations"

Antje Vollrath, Anja Schallon, Christian Pietsch, Stephanie Schubert,
Takahiro Nomoto, Yu Matsumoto, Kazunori Kataoka, Ulrich S. Schubert

Soft Matter **2013**, 9, 99–108.



A toolbox of differently sized and labeled PMMA nanoparticles for cellular uptake investigation†

Cite this: *Soft Matter*, 2013, 9, 99

Antje Vollrath,^{ab} Anja Schallon,^{ab} Christian Pietsch,^{ab} Stephanie Schubert,^{bc} Takahiro Nomoto,^d Yu Matsumoto,^e Kazunori Kataoka^{*defg} and Ulrich S. Schubert^{*ab}

The cellular internalization of defined PMMA nanoparticles was investigated. For this purpose, the biocompatible copolymer p(MMA-*stat*-MAA)_{0.91:0.09} was synthesized by RAFT polymerization and labeled with three different fluorescent dyes ($\lambda_{\text{Ex}} = 493, 557, \text{ and } 653 \text{ nm}$). Nanoparticles were formulated from the differently labeled copolymers into samples with relatively narrow size distribution (diameter $d < 100 \text{ nm}$, $100 \text{ to } 200 \text{ nm}$, $>300 \text{ nm}$) under appropriate conditions of nanoprecipitation and were subsequently characterized by DLS and SEM. Mixtures of the differently sized nanoparticle samples were applied for internalization studies using monolayer cultured HeLa cells. The localization of the nanoparticles was detected after certain time points up to 24 h by CLSM, using LysoTracker as a marker for late endosomes and lysosomes. In investigations by flow cytometry, a fast uptake of medium sized nanoparticles was found, whereas the large and small nanoparticles exhibited a slower internalization. However, small and medium sized nanoparticles were detected in the late endosomes/lysosomes, whereas the large nanoparticles exhibit little co-localization with LysoTracker. Moreover, it could be shown by using different inhibitors for clathrin-dependent (chlorpromazine), caveolin-dependent (filipin III) endocytosis and macropinocytosis (EIPA) that nanoparticles with $d < 200 \text{ nm}$ were internalized *via* clathrin-dependent endocytosis, whereas those with $d > 300 \text{ nm}$ were internalized *via* macropinocytosis.

Received 20th August 2012

Accepted 25th September 2012

DOI: 10.1039/c2sm26928g

www.rsc.org/softmatter

Introduction

Polymeric nanoparticles (NPs) can provide manifold opportunities for drug and gene delivery,^{1,2} because molecules and particles at the nanometer scale offer important benefits like an enhanced permeability and retention effect (EPR), resulting in an improved bioavailability and fewer side effects. In addition, NPs offer the possibility of delivering nucleic acids (siRNA, DNA), proteins or other active substances into targeted organs or cells.^{1–6} However, many points in the field of nanotechnology

still need to be considered very carefully with regard to unknown long-time consequences such as the accumulation of the particles in the vessels/liver, the uptake through skin and lungs, and the removal by the reticuloendothelial system.⁷ Hence, a detailed understanding of the interaction of NPs with their environment is essential for the development of defined drug delivery systems as well as for specific diagnostic applications.

Since the last decade, a number of studies have been published investigating the cellular uptake mechanisms of NPs with respect to various physical, chemical, and biological parameters.^{8–13} The size of the NPs was found to play the key role in the final particle–cell interaction.^{14–16} In detail, depending on their size, particles can enter cells either by phagocytosis or pinocytosis; the latter mechanism can be further subdivided into clathrin- and caveolin-dependent endocytosis as well as clathrin/caveolin-independent endocytosis such as macropinocytosis.^{17–20} Phagocytosis and macropinocytosis are processes to engulf large particles up to the range of $10 \mu\text{m}$, whereas the clathrin- and caveolin-dependent endocytosis are the main processes for the internalization of smaller particles below 500 nm .¹⁸ In addition, the shape of the NPs significantly influences uptake of NPs by phagocytosis. Rod-like and oblate ellipsoidal NPs with a high aspect ratio were taken up more efficiently in comparison to their spherical counterparts, due to their higher surface area and, therefore, a better attachment to

^aLaboratory of Organic and Macromolecular Chemistry (IOMC), Friedrich Schiller University Jena, Humboldtstrasse 10, 07743 Jena, Germany. E-mail: ulrich.schubert@uni-jena.de

^bJena Center for Soft Matter (JCSM), Friedrich Schiller University Jena, Philosophenweg 7, 07743 Jena, Germany

^cInstitute of Pharmacy, Department of Pharmaceutical Technology, Friedrich Schiller University Jena, Otto-Schott-Str. 41, 07745 Jena, Germany

^dDepartment of Bioengineering, Graduate School of Engineering, The University of Tokyo, 7-3-1 Hongo, Bunkyo-ku, Tokyo 113-8656, Japan

^eCenter for Disease Biology and Integrative Medicine, Graduate School of Medicine, The University of Tokyo, 7-3-1 Hongo, Bunkyo-ku, Tokyo 113-0033, Japan

^fDepartment of Materials Engineering, Graduate School of Engineering, The University of Tokyo, 7-3-1 Hongo, Bunkyo-ku, Tokyo 113-8656, Japan

^gCenter for NanoBio Integration (CNBI), The University of Tokyo, 7-3-1 Hongo, Bunkyo-ku, Tokyo 113-8656, Japan. E-mail: kataoka@bmw.t.u-tokyo.ac.jp

† Electronic supplementary information (ESI) available: See DOI: 10.1039/c2sm26928g

the cell membrane.^{13,16,21,22} In addition, the internalization of particles into the cells is influenced by their surface charge: an increased positive charge leads to a higher cellular uptake due to electrostatic interactions with the negatively charged cell membrane.²³ As the surface of NPs can be further functionalized with different reactive groups (COOH and NH₂), amino acids, sugar units, antibodies, or peptides, cellular uptake of NPs can be inhibited or advanced.^{24–26} Nevertheless, no final conclusion can be drawn about the size, shape and charge dependency of cellular uptake of NPs, as the studies published so far are all based on different materials. Inorganic (gold,^{27,28} silica particles,^{29,30} and quantum dots³¹) and organic (poly(lactic-co-glycolic acid) (PLGA),¹⁵ polystyrene (PS),^{32,33} and chitosan^{34,35}) materials were studied and many contradictory results were reported by different investigators.³⁶ Furthermore, cell internalization studies frequently used NP beads with non-defined surfaces because conventional preparation techniques (e.g. the emulsion technique) require the use of surfactants, which also influence cellular uptake.³⁷ Hence, further studies on NP–cell-interactions with well-defined NPs, in the absence of any surfactants, would be helpful to gain a better insight into the involved parameters and structure–property relationships.

The present study aims at investigating the cell interaction of polymeric NPs with well-defined characteristics based on poly(methyl methacrylate) (PMMA) derivatives, poly(methyl methacrylate)-*stat*-poly(methacrylic acid) (p(MMA-*stat*-MAA)) copolymer. The p(MMA-*stat*-MAA) copolymer is based on the same monomers as the pharmaceutically important coating material EUDRAGIT® S100, which is applied for pH-dependent drug release.³¹ Recently, it has been demonstrated that PMMA systems are suitable for diagnostic applications in cell imaging and as a gene carrier due to their non-toxicity and good biocompatibility.^{38–41} Here, the poly(methacrylic acid) segment of p(MMA-*stat*-MAA) was labeled with various dyes (DY-495 (green), DY-547 (orange), and DY-647 (red)) for tracking of the NPs.⁴² NPs of the labeled p(MMA-*stat*-MAA) copolymers (p(MMA-*stat*-MA^{dye} (green, orange, or red))) were prepared by the solvent-evaporation (nanoprecipitation) method⁴³ and characterized comprehensively by dynamic light scattering (DLS) and scanning electron microscopy (SEM).⁴⁴ The stability of the NPs was demonstrated by DLS measurements after autoclave treatment, after incubation in cell culture media, and during pH titration studies, respectively. Cytotoxicity assays were performed to prove the biocompatibility and non-toxicity of the NPs. The cellular uptake studies used HeLa cells and three differently sized and individually labeled NPs. Flow cytometry was applied for studies on time- and concentration-dependent cellular uptake and confocal laser scanning microscopy (CLSM) for cellular distribution and co-localization studies. In addition, cellular internalization was investigated by inhibitors of clathrin- and caveolin-dependent endocytosis as well as of macropinocytosis.

Experimental

Materials

All reagents were purchased from commercial sources (Fluka and Sigma Aldrich). MMA and MAA were purchased from Sigma Aldrich and purified with an inhibitor-remover before use. 2,2'-

Azobis(iso-butyronitrile) (AIBN) was recrystallized from methanol prior to use. 2-Cyano-2-propyl dithiobenzoate (CPDB) was purchased from Sigma Aldrich. Purified *N,N*-dimethylacetamide (DMA) and dimethylformamide (DMF) were obtained from VWR. The fluorescent dyes $\lambda = 495$ nm (DY-495), $\lambda = 557$ nm (DY-547), and $\lambda = 653$ nm (DY-647) were purchased from DYOMICS GmbH. AlamarBlue, LysoTracker Green, and Opti-MEM were obtained from Life Technologies. Hoechst 33342, 5-(*N*-ethyl-*N*-isopropyl)amiloride (EIPA), filipin III, and chlorpromazine were purchased from Sigma Aldrich. Cell culture materials were received from Greiner Bio One, cell culture media and solutions from Biochrome, Greiner, and PAA. Unless otherwise stated, the chemicals were used without further purification.

Synthesis of p(MMA-*stat*-MAA)

P(MMA-*stat*-MAA) was prepared by copolymerization of MMA with MAA using the reversible addition–fragmentation chain transfer (RAFT) polymerization method.^{37,38} In a typical RAFT copolymerization experiment, 4.325 g of MMA monomer (43.2×10^{-3} mol), 0.413 g of MAA monomer (4.8×10^{-3} mol), 19.7 mg of AIBN initiator (0.12×10^{-3} mol), 106.3 mg of CPDB RAFT agent (0.48×10^{-3} mol) and 5.8 mL of ethanol were mixed together with anisole as the internal standard (1.2 mL) in a 25 mL reaction vial. The monomer concentration was kept at 4 mol L⁻¹. Subsequently, the reaction solution was placed in a preheated oil bath at 70 °C for 10 hours. The copolymer was purified by precipitation into a large volume of cold diethyl ether and dried under reduced pressure. Conversion was measured by ¹H NMR spectroscopy using anisole as the internal standard. ¹H NMR (DMSO-d₆, 300 MHz): $\delta = 12.5$ (–OH), 7.83, 7.64, and 6.46 (Ar–H, CPDB), 3.55 (OCH₃), 2.25–0.3 (backbone) ppm. SEC (DMA, LiCl, and PMMA standard): $M_n = 16\,000$ g mol⁻¹ and PDI = 1.19. Elemental analysis: p(MMA-*stat*-MAA) C: 58.18 and H: 7.91%.

Labeling of p(MMA-*stat*-MAA)

500 mg of the p(MMA-*stat*-MAA) polymer (3.1×10^{-4} mol) were dissolved in 2 mL of dried DMF, and 50 μ L (3.0×10^{-4} mol) of 1-ethyl-3-(3-dimethylaminopropyl)carbodiimide (EDC) was added as well as 500 μ L of a stock solution ($c = 0.1$ mg mL⁻¹ in DMF) of the desired dye DY-495 (green, 8.5×10^{-8} mol), DY-547 (orange, 7.5×10^{-8} mol), or DY-647 (red, 7.1×10^{-8} mol). The labeled polymers were purified by repeated precipitation in water and extensive dialysis afterwards. The products were obtained by freeze drying in 70% overall yield. SEC (DMA, LiCl, and PMMA standard): p(MMA-*stat*-MA^{green}): $M_n = 23\,500$ g mol⁻¹ and PDI = 1.21; p(MMA-*stat*-MA^{orange}): $M_n = 21\,800$ g mol⁻¹ and PDI = 1.22; p(MMA-*stat*-MA^{red}): $M_n = 23\,800$ g mol⁻¹ and PDI = 1.22; elemental analysis: p(MMA-*stat*-MA^{green}) C: 56.85, H: 8.18, and N: 2.43; p(MMA-*stat*-MA^{orange}) C: 58.51, H: 8.12, and N: 2.40; p(MMA-*stat*-MA^{red}) C: 58.17, H: 8.08, and N: 2.46.

Preparation of the NP suspension

NPs were prepared by nanoprecipitation with subsequent solvent evaporation. For this purpose, the polymers were dissolved in acetone and filtered through a 2 μ m filter prior to use.

NP suspensions with different sizes were prepared by variation of the initial conditions of the formulation. For the small (diameter $d < 100$ nm) and medium (100 to 200 nm) sized NPs, the acetone solution was dropped into deionized water (AW) with a concentration of 1 mg mL^{-1} and 10 mg mL^{-1} , respectively. By dropping water to the polymer solution (WA) with a concentration of 4 mg mL^{-1} , large NPs ($d > 300$ nm) were prepared. For all suspensions, the acetone–water ratio was chosen to be 0.25. Furthermore, the dropping speed was approximately $50 \mu\text{L}$ per second, and the stirring speed was set to 1000 rpm (Magnetic Stirrer MR Hei-Standard). Afterwards, the acetone was evaporated from the solution by stirring overnight at room temperature, the suspensions were filtered using a filter paper and diluted to a final concentration of 0.5 mg mL^{-1} . The suspensions were stored in a fridge at 4°C and before further usage they were vortexed to ensure a homogenous particle suspension.

Dynamic light scattering (DLS) and zeta potential measurements

For DLS investigations, a Zetasizer Nano ZS (Malvern Instruments, Malvern, UK) operating with a laser beam at 633 nm and a scattering angle of 173° was used. Each sample was analyzed in triplicate at 25°C in a polycarbonate zeta cell. For size measurements, three runs were applied for 30 s; for the zeta potential measurements, three runs were applied for 10 s. The intensity, volume and number distribution of the NPs were calculated applying the NNLS mode.

Scanning electron microscopy (SEM)

SEM images were obtained using a LEO-1450 VP, Leo Elektronenmikroskopie GmbH, Oberkochen, Germany. The sputter coating device BAL-TEC SCD005 (Balzers, Liechtenstein; 60 mA, 80 s) was used. The system was operated from 8 to 10 kV.

Cell lines and culture conditions

The HeLa (CCL-2, ATCC) and L929 (CCL-1, ATCC) cell lines used in the uptake and cytotoxicity experiments were maintained in suitable cell culture media supplemented with 10% fetal calf serum (FCS), $100 \mu\text{g mL}^{-1}$ streptomycin, 100 IU mL^{-1} penicillin, and 2 mM L-glutamine (4 mM for L929). The cells were cultured at 37°C in a humidified 5% CO_2 atmosphere.

Flow cytometry analysis

For the determination of cellular uptake of NPs *via* flow cytometry, 10^5 cells per well were seeded in 12-well plates and incubated for 24 h. Thirty minutes prior to the incubation with the NPs, the cells were rinsed with PBS and supplemented with OptiMEM. The NPs were added to the cells and the plates were incubated for the indicated time. Afterwards, the cells were harvested by trypsinization and resuspended in PBS supplemented with 10% FCS. To determine the relative uptake of NPs, 10 000 cells were quantified by flow cytometry using a Cytomics FC 500 (Beckman Coulter).

Microscopy studies

HeLa cells were cultured on 35 mm glass dishes (Iwaki, Japan) at 2×10^5 cells per dish. After 24 h, the medium was exchanged with OptiMEM, and the cells were incubated for 30 min before the addition of the NP suspensions. The nuclei and the late endosomes/lysosomes were stained with Hoechst 33342 and LysoTracker Green, respectively, before CLSM imaging. CLSM images were acquired 24 h after the administration of NPs, using a Zeiss LSM 780 (Carl Zeiss). Excitation wavelengths were 405 nm, 488 nm, 561 nm and 633 nm for Hoechst 33342, LysoTracker Green or DY-495 stained NPs, DY-547 stained NPs, and DY-647 stained NPs, respectively. Co-localization was quantified, using Imaris software (Bitplane AG, Zurich, Switzerland).

Inhibition of endosomal pathways

The cells were seeded as described before. The growth media were changed to OptiMEM and incubated for 30 min before $10 \mu\text{g mL}^{-1}$ chlorpromazine, $1 \mu\text{g mL}^{-1}$ filipin III, or $100 \mu\text{M}$ EIPA were added and incubated for a further 30 min. Afterwards, the NPs were added, and the cells were incubated for the indicated time.

Cell viability

For L929 cells, the cytotoxicity assay was performed according to ISO10993-5. In detail, the cells were seeded at 10 000 cells per well in a 96-well plate and incubated for 24 h. No cells were seeded in the outer wells. The growth media were replaced by OptiMEM. Afterwards, NP dilutions in the concentration range from 78 to $254 \mu\text{g mL}^{-1}$ were added, and the cells were incubated at 37°C for further 24 h. Subsequently, the medium was replaced by DPBS and AlamarBlue, as recommended by the supplier. After incubation for 4 h, the fluorescence was measured at Ex 570/Em 610 nm in a microplate reader (Genios Pro, Tecan GmbH), with untreated cells serving as controls.

Results and discussions

Polymer preparation and characterization

To provide the possibility of functionalization after the polymerization, carboxylic acid groups were introduced into the PMMA chain. Therefore, MMA was copolymerized with MAA using the RAFT polymerization method.^{37,38} This technique allows the synthesis of tailored polymers with control over molar mass and the composition of the copolymer, *i.e.*, the ratio between MAA and MMA.

In the copolymerization reaction, a final conversion of 87% (both monomers) was reached. MMA and MAA are statistically distributed in the polymer backbone due to the same reactivity ratio of the MMA and MAA units.⁴⁵ The ratio between both MMA and MAA in $p(\text{MMA-}stat\text{-MAA})$ was determined by ^1H NMR spectroscopy. The observed ratio of 91 to 9% agrees well with the theoretical value of 90 to 10%. The low content of MAA ensures the stability at $\text{pH} > 7$ of the NPs and seems to be beneficial for a well-defined NP formation in aqueous systems. A molar mass of $M_n = 16\,000 \text{ g mol}^{-1}$ with a polydispersity

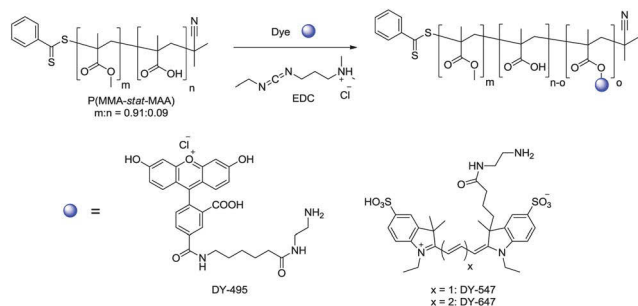
Table 1 Selected characterization data of the p(MMA-*stat*-MAA)_{0.91:0.09} polymer and the fluorescent labeled p(MMA-*stat*-MA^{dye}) copolymers

Sample	M_n^a [g mol ⁻¹]	PDI _{SEC} (RI) ^a	C [%]	H [%]	N [%]
P(MMA- <i>stat</i> -MAA) _{0.91:0.09}	16 000	1.15	58.18	7.91	—
P(MMA- <i>stat</i> -MA ^{green})	23 500	1.21	56.85	8.18	2.43
P(MMA- <i>stat</i> -MA ^{orange})	21 800	1.22	58.51	8.12	2.40
P(MMA- <i>stat</i> -MA ^{red})	23 800	1.22	58.17	8.08	2.46

^a Calculated from SEC (DMA and LiCl) and PMMA calibration.

index of 1.15 (DMA, LiCl) was determined by size exclusion chromatography (SEC) for the final copolymer p(MMA-*stat*-MAA)_{0.91:0.09} (Table 1).

In order to obtain differently labeled polymers, three different dyes (DY-495, DY-547 and DY-647) were chosen, because the dyes provide high quantum yields, good photostability, and are available with different functional groups (Scheme 1).⁴² The labeling procedure was performed by the reaction of the COOH groups with the NH₂-functionalized dyes using EDC as the coupling reagent. The absence of free dye was proven by fluorescence measurements of the washing water after purification. The fluorescence emission spectra of the labeled copolymers p(MMA-*stat*-MA^{green}), p(MMA-*stat*-MA^{orange}), and p(MMA-*stat*-MA^{red}) are displayed in the ESI, Fig. S1.† All the copolymers show distinct peaks at 525 nm, 568 nm, and 668 nm, respectively. In comparison to the initial emission of the pure dyes, no significant change in the fluorescence behavior was obtained even after conjugation into the copolymer segments. A comparison of the SEC graphs of the unmodified p(MMA-*stat*-MAA) and the labeled copolymers revealed a slight change in the elution volume, indicating that the molar mass slightly increased due to dye conjugation and that the polymer was not degraded or cross-linked during the labeling procedure. The overlay of the diode array detector (DAD) and refractive index (RI) traces of the labeled samples confirm the covalent attachment of the dyes (ESI, Fig. S2†). Furthermore, the elemental analysis revealed an increase in the nitrogen content, which also indicates the attachment of the dyes in the polymer backbone.

**Scheme 1** Schematic representation of the reaction of p(MMA-*stat*-MAA)_{0.91:0.09} with the DY-495, DY-547, and DY-647 using EDC as a coupling reagent.

Preparation and characterization of NPs

Differently sized NPs were prepared by nanoprecipitation with subsequent solvent evaporation, a technique, which is not only simple and cost-effective but also fast and easy.⁴³ By variation of the initial conditions of the formulation, such as the solvent/non-solvent ratio and the concentration of the polymer solution, well-defined NPs with different sizes can be prepared. In comparison to other procedures commonly used, *e.g.*, the emulsification technique, no surfactants are necessary for the NP preparation. This represents an important benefit of the nanoprecipitation technique. It was proven that surfactants significantly affect the interaction of NPs with cells as well as their cellular uptake.³⁷ Using nanoprecipitation, it is known that the final NP sizes can be tuned from 50 nm up to 1 μm by varying the initial polymer concentration in the organic phase and/or by changing the dropping method (polymer solution into water or water into polymer solution). In order to yield small (S; $d < 100$ nm), medium (M; d between 100 and 200 nm), and large (L, $d > 300$ nm) NPs, different nanoprecipitation conditions were applied. By dropping the acetone-polymer solution into water, smaller NPs were obtained in comparison to the reverse technique. For the preparation of the small NPs, polymer acetone solutions with a concentration of 1 mg mL⁻¹ were dropped into water. For the medium sized NPs the same procedure with an increased concentration of 10 mg mL⁻¹ was used. The large NPs were generated by dropping water into polymer solutions with a concentration of 4 mg mL⁻¹. For all suspensions, a solvent/non-solvent ratio of 0.25 and no surfactants were used. After subsequent removal of the acetone by overnight evaporation, the NPs were filtered, diluted to a concentration of 0.5 mg mL⁻¹, and characterized by DLS and SEM. These complementary techniques give sufficient information about the size, shape, and surface characteristics of the particle systems.⁴⁴ For the small NPs, a size of 80 (±10) nm was measured by DLS in water. The medium NPs revealed a size of 150 (±10) nm, whereas for the large NPs a size of 400 (±50) nm was obtained. Low PDI^P values confirm a narrow size distribution of the NPs, which was further verified by the SEM investigations. A detailed analysis of a representative small, medium and large NP batch is displayed in Fig. 1. As the major focus of this research was set on the influence of the size on the cell internalization, a charge effect needs to be excluded. Thus, only a low degree of labeling was performed in order to keep the charge density similar. The zeta potential of the NP was measured in water (pH = 6), resulting in comparable values with 30 ± 10 mV for all nanoparticle suspensions. The zeta potential values larger than 20 mV further indicate high repulsion forces and colloidal stability of the NPs in suspension. However, the stability of the NPs should also be confirmed under different conditions, and, therefore, a NP suspension with medium sized NPs was investigated in more detail. For this purpose, all NPs were centrifuged at 15 000 rpm for 20 min, autoclaved, or incubated in PBS or cell culture media as well as titrated in the pH range of 4 to 10. The resulting suspensions were analyzed again by DLS and SEM. Neither the size distribution nor the zeta potential value changed, which proves the

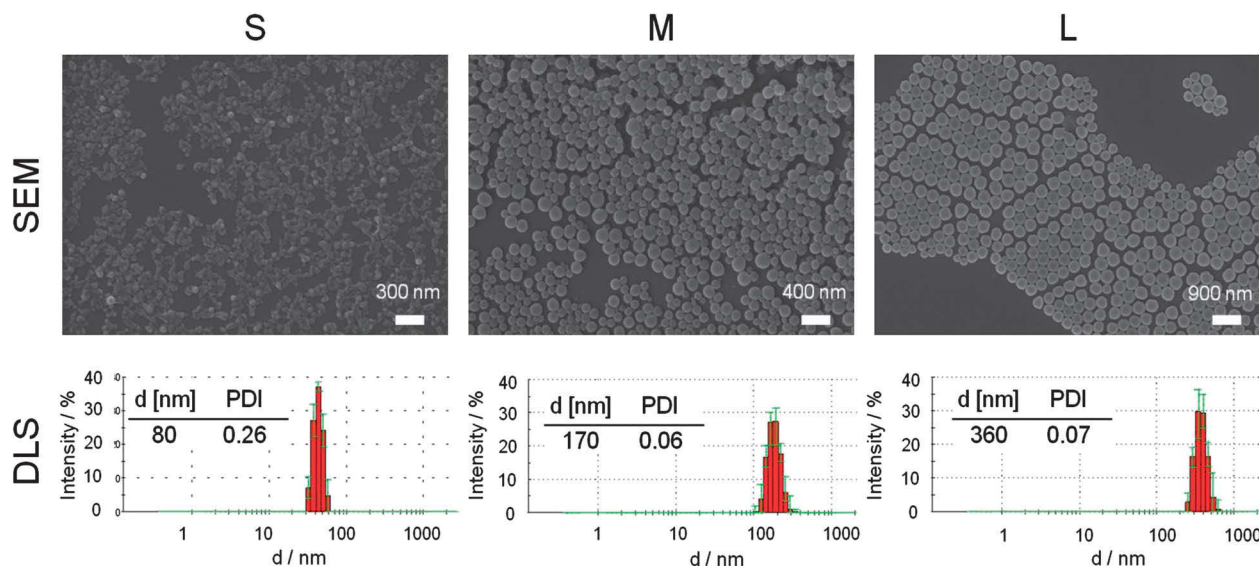


Fig. 1 Representative SEM images and DLS intensity size distribution with corresponding Z average value and polydispersity PDI^P of the small, medium and large particles of the p(MMA-*stat*-MA^{dye}) copolymer.

high stability of the p(MMA-*stat*-MA^{dye}) NPs (ESI, Fig. S3[†]). In combination with the easily tunable NP size, the absence of surfactants, and the variety on possible modifications/labels of the original polymers, the NPs represent excellent and well-defined materials for further cell internalization experiments.

Cytotoxicity of the polymers in L929 cells

To evaluate the cytotoxicity of the NPs, we used L929 cells, because they were commonly used for the investigation of cytotoxicity, as they are sensitive and recommended by ISO10993-5. For the cell experiments, the NPs (which originally were in distilled water) were buffered with DPBS before being added to the cells. In preliminary experiments, cytotoxicity tests with AlamarBlue were performed for 24 h, to evaluate the metabolic activity of L929 cells exposed to the NPs. Small (<100 nm) and large (>300 nm) labeled NPs were investigated. As shown in Fig. S4 (ESI[†]), all types of NPs did not cause a significant cytotoxicity after 24 h of incubation at the investigated concentrations up to 260 $\mu\text{g NPs per mL}$ ($p > 0.01$; ANOVA). Moreover, neither size nor labeling of the NPs showed an influence on the cytotoxicity. This is in agreement with studies of other groups using EUDRAGIT S100.^{38–40} Thus, the NPs used here are not toxic even at the maximum concentration of 150 $\mu\text{g mL}^{-1}$.

Validation of cellular uptake measurement by flow cytometry *via* fluorescence and side scatter

To investigate cellular uptake of the NPs into HeLa cells by flow cytometry, we first confirmed the validation of cellular uptake measurement by flow cytometry. The fluorescence channel as well as the side scatter (SSC) and forward scatter (FSC) channels were used. The SSC is directly related to the cell granularity and was used as an indicator of cellular uptake.⁴⁶ On the other hand, the FSC is correlated with the cell size and was used as an additional factor. After overnight incubation with the NPs, the cells showed a high cellular uptake that was detected by the

fluorescence intensity measurements. This result was also confirmed by an increase in the SSC channel (ESI, Fig. S5[†]): the SSC signal increased with the increase of the incubation time, whereas the FSC signal did not change. Moreover, a strong correlation between fluorescence and SSC was detected when HeLa cells were incubated with increasing sizes of DY-547 labeled NPs. To exclude a high influence of NPs on the cell surface, the outer fluorescence was quenched with trypan. No differences in the non-quenched ones could be observed. Therefore, the uptake of NPs can be detected by fluorescence and SSC measurements.

Dependency of cellular uptake on the NP concentration

A concentration-dependent cellular uptake was investigated after 24 h using four different NP concentrations (25, 50, 100, and 150 $\mu\text{g mL}^{-1}$, respectively). The cellular uptake was quantified using flow cytometry. It should be noted that larger NPs contain a higher content of labeled polymers leading to an increased fluorescence signal compared to smaller NPs. To suppress the influence of the cell size on granularity, the SSC was measured relative to the FSC as the cofactor. For analysis, the fluorescence (mean fluorescence intensity = MFI) and SSC/FSC of the treated cells were plotted relative to untreated cells (Fig. 2). It was observed that higher NP concentrations lead to an increase in MFI and SSC/FSC (Fig. 2A). In particular, for the medium and large sized NPs, a clear concentration-dependent cellular uptake was observed. In detail, for incubation with 150 $\mu\text{g mL}^{-1}$, a three times higher relative SSC/FSC value was obtained for the medium and large sized NPs (3.4 ± 0.2 and 3 ± 0.4 , respectively) in comparison to the control cells. For the small NPs only a relative SSC/FSC value of 2.6 ± 0.4 was detected. The fluorescence measurement also confirmed these results, but is influenced by the amount of fluorescent polymer per particle. The number of “positive cells” (cells that

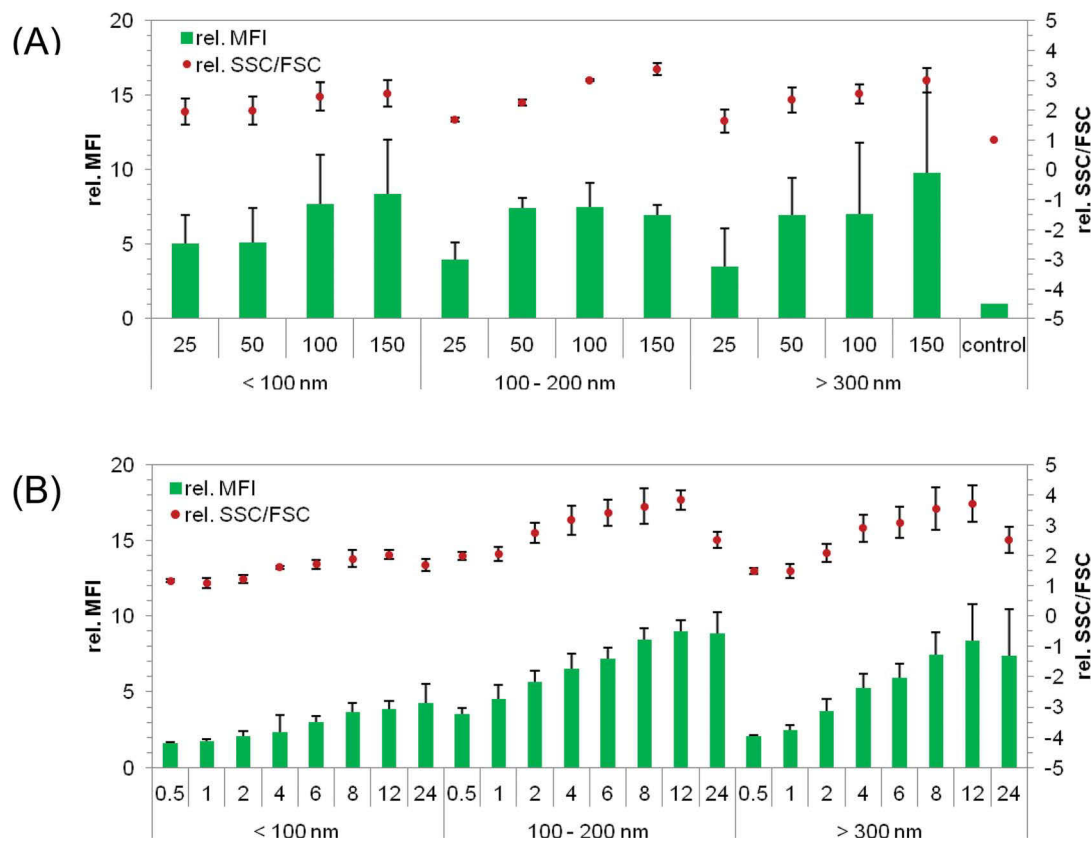


Fig. 2 Cellular uptake of NPs into HeLa cells measured by flow cytometry: the cells were seeded at a concentration of 10^5 cells per mL 24 h before particle incubation with NPs. The uptake of NPs was investigated in serum-reduced media and measured by two methods: the relative change of fluorescence (MFI) and granularity (SSC/FSC) compared to non-treated cells. (A) Different concentrations of differently sized particles were analyzed after 24 h of incubation. (B) Time-dependent uptake of 50 μg NPs per mL. Data represent mean \pm SD, $n \geq 3$.

internalize NPs) was increased with higher NP concentration: 95% positive cells were found for $c = 150 \mu\text{g mL}^{-1}$ and 75% for $50 \mu\text{g mL}^{-1}$, respectively (data not shown). Furthermore, the relative SSC/FSC as well as the relative MFI showed no significant differences between small, medium and large NPs at $50 \mu\text{g mL}^{-1}$ ($p > 0.05$). It could be shown that all NPs were taken up by HeLa cells at the used concentrations.

Cultivation conditions – influence on the NP uptake by HeLa cells

The majority of experiments were performed with serum-reduced media (OptiMEM), but additionally the cellular uptake of NPs was further investigated in growth media to exclude an influence of serum proteins on the uptake. No significant differences could be obtained between serum-reduced and serum-containing (growth media) conditions for $50 \mu\text{g mL}^{-1}$ small and large NPs. In all cases, 60% to 70% of positive cells and an increased SSC/FSC signal could be detected after 24 h. The results indicate that the used media have no influence on the cellular uptake.

Dependency of cellular uptake on the incubation time

The size of the NPs showed no influence on the cytotoxicity and cellular uptake after 24 h incubation at a NP concentration of $50 \mu\text{g mL}^{-1}$ as described above. To gain a deeper understanding

of the cellular uptake, a time-dependent cellular uptake was evaluated. In these experiments, HeLa cells were incubated with p(MMA-*stat*-MA^{orange}) NPs for 30 min up to 24 h, and MFI as well as SSC/FSC were analyzed by flow cytometry. In Fig. 2B, the cellular uptake is presented as relative MFI and SSC/FSC of treated cells to non-treated cells. It could be observed that all the NPs were taken up by the cells in a time-dependent manner. In detail, small NPs < 100 nm reached a relative MFI of around 4 and an increase of SSC/FSC of around 2 after 24 h at $50 \mu\text{g mL}^{-1}$. This is in agreement with the results observed by the concentration-dependent uptake in Fig. 2A. A significant increase ($p < 0.01$) in granularity (relative SSC/FSC) was detectable after 4 h incubation. The highest relative SSC/FSC was found after 12 h incubation. This was also the case for medium and large sized NPs (medium NP: MFI 8.5, SSC/FSC 3.5; large NP: MFI 7.5–8, SSC/FSC 3.5). Furthermore, no significant differences were detected between medium and large NPs after 4 to 24 h incubation ($p > 0.05$). The internalization of all NPs reached a plateau after 8 h, as indicated by the lack of further significant increase in fluorescence and granularity ($p > 0.05$). A difference in the cellular uptake of the differently sized NPs was, however, observed at early time points. In detail, small NPs < 100 nm and large NPs > 300 nm showed no increase in granularity for 2 h and 1 h, respectively ($p > 0.05$). In contrast to this, an increase in granularity was detectable with medium sized NPs ($p < 0.01$),

which can be due to different reasons. First of all, the effect may be caused by different endosomal pathways. The delayed cellular uptake of small NPs can also be explained by a slower sedimentation of the NPs compared to the larger ones. This could lead to a later contact between the membrane of cells and NPs, and an eventual delayed cellular uptake. Besides, a decrease in relative SSC/FSC was observed at 24 h compared to that at 12 h in particular with medium and large sized NPs. This could not be observed by fluorescence. The reason for this decrease in granularity is not understood by now and requires further investigations.

In conclusion, medium NPs of 100 to 200 nm were found to have the fastest cellular uptake in HeLa cells compared to smaller and larger ones. A fast cellular uptake of medium sized NPs could be due to fast sedimentation and fast internalization into cells, indicating an endosomal pathway. Large NPs were taken up very slowly despite fast sedimentation, indicating a macropinocytotic uptake, because endosomal pathways like clathrin- or caveolin-dependent endocytosis are faster compared to macropinocytosis.⁴⁷

Intracellular localization study of differently sized NPs

The cellular uptake mechanisms of HeLa cells were investigated by CLSM. For this purpose, the intracellular distribution of NPs after 24 h incubation was studied in living cells. Small NP^{green}, medium NP^{orange} and large NP^{red} suspensions were used at 50 $\mu\text{g mL}^{-1}$ each. The nuclei of the cells were stained with Hoechst 33342. A representative NP distribution in HeLa cells is presented in Fig. 3. Cells containing NPs of different sizes are plotted separately (Fig. 3A–C) as well as the corresponding cell nuclei (Fig. 3D). In addition, two overlays are presented. The overlay of all channels is presented in Fig. 3F. No NPs could be observed in the cell nuclei. The intracellular distribution of small and medium sized NPs is comparable. In detail, a peri-nuclear localization was observed (compare Fig. 3A and B) in the cytoplasm. Hence, a strong co-localization was found with NPs below 200 nm. In contrast, the intracellular localization of small and large NPs is different, as presented in Fig. 3A and C, and merged in Fig. 3E. Co-localizations between small and large sized NPs would be indicated by yellow signals. Here, only a few yellow signals were detectable indicating only some co-localization. This could also be observed in Fig. 3F, where the observed cyan staining indicates a co-localization of small and medium sized NPs, whereas only a few purple (co-localization of medium and large NPs) and yellow signals could be found. Furthermore the co-localization was quantified by Pearson's correlation coefficient (PCC) (Fig. 3G). The PCC between the small and medium sized NPs showed the highest value, suggesting that the small and medium sized NPs might have a similar cellular uptake pathway. To exclude the possibility that this cellular distribution is caused by the dye, other NPs with comparable sizes but different dyes were investigated (*e.g.* small NP^{orange} and large NP^{green}). This combination of NPs was also incubated with HeLa cells and treated as described before. Thereby, the intracellular distribution shows no dependency on the dye and, thus, indicates no influence of the chemical nature

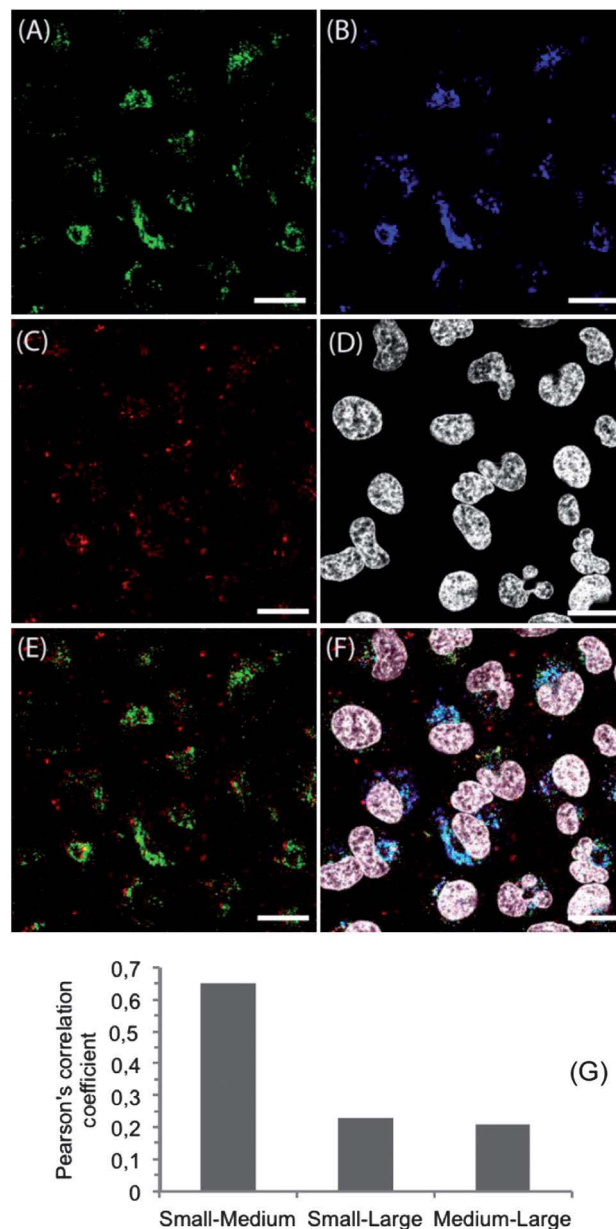


Fig. 3 Confocal microscope images of HeLa cells incubated with NPs. Cells were seeded at a density of 10^5 cells per mL for 24 h in medium before particle incubation. NPs with different sizes and labels (A: small NP^{green}; B: medium NP^{orange}; C: large NP^{red}) were added at 50 $\mu\text{g mL}^{-1}$ simultaneously and incubated for 24 h. (D) Cell nuclei were stained with Hoechst 33342. (E) Overlay of small NP^{green} and large NP^{red}. (F) Overlay image of labeled NPs and cell nuclei. (G) Pearson's correlation coefficient of labeled NPs. The scale bars indicate 20 μm .

of dyes used on the uptake behavior of HeLa cells. Additionally, HeLa cells incubated with small, medium, and large NPs at 4 °C revealed no fluorescence inside the cells (ESI, Fig. S6†). This indicates an active cellular uptake mechanism of all sized NPs *via* endocytosis. Hence, a different intracellular distribution of large NPs (>300 nm) compared to small (<100 nm) and medium (100 to 200 nm) sized NPs was clearly proven. This indicates a different internalization of NPs below 200 nm compared to larger ones. Furthermore, the microscopy data support the results observed by flow cytometry, where differences in time-dependent uptake

could be found with regard to the NP size. Although, medium and large sized NPs sediment faster onto the cells, the large NPs were not internalized within the first hour, whereas medium sized NPs were detected in cells after 30 min.

Investigation of cellular pathways

The intracellular localization and the cellular uptake kinetics of NPs showed strong dependency on size (Fig. 2B and 3). To further elucidate this observation, the intracellular localization was investigated by using LysoTracker, a well known substance for staining acidic late endosomes and lysosomes. As NPs <200 nm showed the same cellular localization in all experiments, only medium (100 to 200 nm) NPs are presented here. They show a stronger fluorescence signal and could be detected more easily compared to small NPs, due to more labeled polymers inside the NPs. In Fig. 4, the stained lysosomes (A), medium NPs (B), large NPs (C), and cell nuclei (D) are presented. Moreover, the overlay of lysosomes and large NPs (E) and the overlay of all dyes used (F) are shown. Again, no NPs were found in the nuclei. It should be noted that almost all medium sized NPs were detected in the late endosomes or lysosomes indicated by a high PCC of 0.61 and a cyan staining in Fig. 4F due to the merging of medium sized NP^{orange} (plotted in blue) with LysoTracker (A). An adverse intracellular localization was found by using large NPs

showing little co-localization with medium sized NPs and a PCC of 0.19, as described before. Furthermore, little co-localization was observed with late endosomes or lysosomes, indicated by slight yellow signals in Fig. 4E and a PCC of only 0.15.

The large NPs were taken up by the cells, but the internalization or the cellular pathway seems to be different to the medium ones. Whereas smaller NPs revealed a fate in late endosomes or lysosomes, the cellular uptake mechanism of larger NPs is not fully understood. It can be postulated that NPs smaller than 200 nm were internalized *via* endocytosis and ended up in the late endosomes or lysosomes. The missing co-localization of larger NPs > 300 nm with late endosomes or lysosomes indicates an uptake mechanism that does not end in the lysosomes at the investigated time points, as a release of NPs into the cytoplasm is not supported.

Inhibition of endocytic pathways

To investigate the cellular uptake mechanism of differently sized NPs, internalization routes were inhibited. Chlorpromazine was used for inhibition of clathrin-dependent and filipin III for inhibition of caveolin-dependent endocytosis. It was described in the literature that NPs < 200 nm are predominantly taken up by these pathways.^{18,48} In contrast to smaller NPs, larger NPs can be taken up by macropinocytosis or phagocytosis and were inhibited by

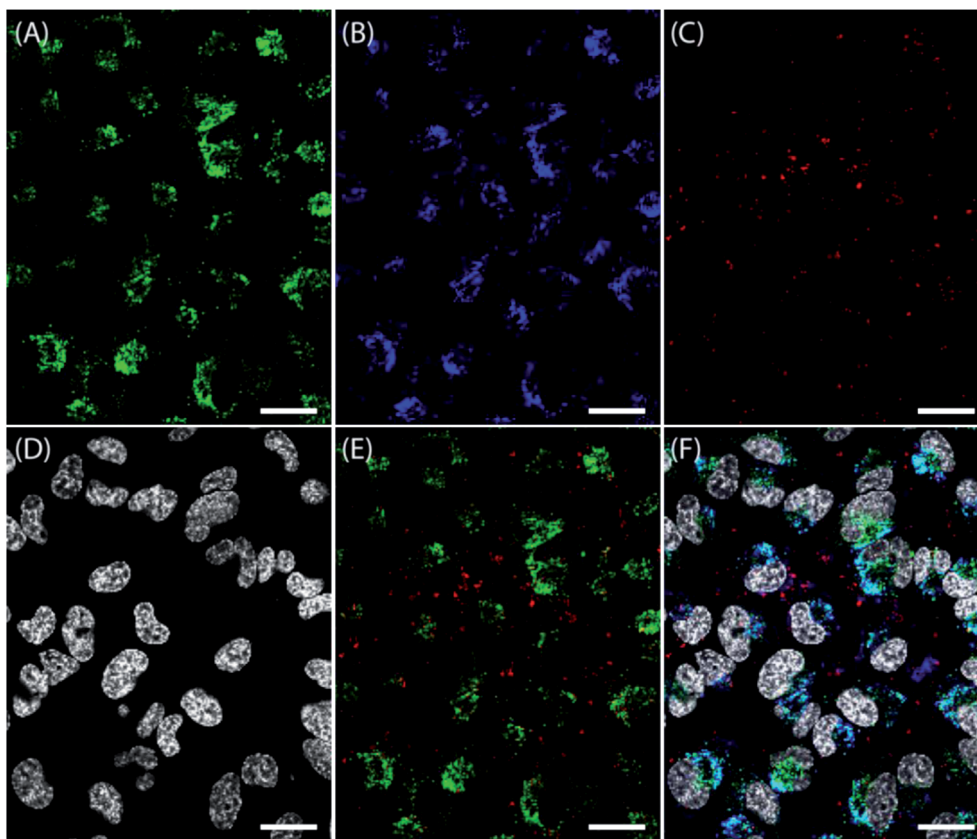


Fig. 4 Confocal microscope images of HeLa cells incubated with particles. Cells were seeded at a density of 10^5 cells per mL for 24 h. The medium was changed and incubated for 30 min. NPs at different sizes and labels (B: medium NP^{orange}; C: large NP^{red}) were added at $50 \mu\text{g mL}^{-1}$ simultaneously and incubated for 24 h. (A) LysoTracker Green was added 10 min before microscopic analysis and incubated at 37°C to stain acidic late endosomes and lysosomes. (D) Cell nuclei were stained with Hoechst 33342. (E) Overlay of stained lysosomes and large NP^{red}. (F) Overlay image of labeled NPs, lysosomes and cell nuclei. The scale bars indicate 20 μm .

EIPA.^{18,48} The NP internalization was analyzed by flow cytometry (ESI, Fig. S7†). Inhibition of cellular uptake was investigated with small and large sized NPs, as it was shown that the intracellular localization of small and medium sized NPs is comparable. As mentioned above, the MFI and the SSC/FSC showed no strong increase after 2 h (Fig. 2), because the NP concentration in cells has an influence on the signal intensity of SSC/FSC and MFI. As the cells internalize only a few NPs after 2 hours, the SSC/FSC and MFI could not be used in this case. Therefore, the percentage of cells taking up NPs was used (ESI, Fig. S7†). In the case of using small NPs and the three different inhibitors, it was found that NPs < 200 nm were excluded not by filipin III and EIPA but by chlorpromazine, indicating an uptake *via* clathrin-dependent endocytosis. To prove this result, CLSM studies were also performed. In Fig. S8 (ESI†), medium sized NPs (green) were not detectable in cells incubated with chlorpromazine (A) but detectable in cells incubated with filipin III. As controls, polystyrene (PS) beads of 150 nm were used (blue emission). These PS beads could be excluded by filipin III, indicating an uptake *via* caveolin-dependent endocytosis, as also confirmed in the literature.¹⁸ This suggests that surfactants, which are usually necessary to prepare commercial NPs, have an influence on the uptake in cells. By using inhibitors, it can be assumed that NPs < 200 nm internalize *via* clathrin-dependent endocytosis, in particular the 100 nm NPs used in this study. In the case of internalization of large NPs, an exclusion could be observed by using EIPA, but not when chlorpromazine and filipin III are used (ESI, Fig. S7†), indicating an uptake of larger NPs *via* macropinocytosis. As already reported in the literature,⁴⁹ EIPA caused also a weak inhibition of small sized NPs. These blocking study of differently sized NPs showed that defined small p(MMA-*stat*-MAA) NPs were predominantly taken up by clathrin-dependent endocytosis, whereas larger ones were predominantly taken up by macropinocytosis.

Conclusion

The preparation of a differently labeled p(MMA-*stat*-MAA) copolymer and its nanoprecipitation into defined NPs with various sizes (<100 nm, 100 to 200 nm, and >300 nm) without the usage of surfactants were demonstrated. These tailor-made NPs are promising for studying the influence of the surface, charge or size of the NPs on their internalization into cells, as no stabilizers were used, which have an influence on cellular uptake. We showed that the size itself of the NPs has a strong influence on the uptake in HeLa cells. This is further influenced by the concentration used and incubation time. The medium sized NPs were taken up faster compared to small and large ones. All NPs were found inside the cells, whereas small and medium sized NPs showed the same cellular distribution and were detectable in lysosomes. In contrast, large NPs showed less co-localization with smaller NPs and were not detectable in the lysosomes. By using inhibitors, we have shown that clathrin-dependent endocytosis is the predominant pathway for smaller NPs < 200 nm, whereas macropinocytosis is responsible for larger NPs. In further studies, the influence of the zeta potential and of the additional functional groups on the particle surface will be studied, again in the absence of surfactants.

Acknowledgements

The financial support from the Thuringian Ministry for Education, Science and Culture (grant #B514-09051, Nano-ConSens), the Deutsche Forschungsgemeinschaft (Japan-Germany exchange program, DFG and JSPS), the Carl-Zeiss Foundation (JCSM Strukturantrag), the Funding Program for World-Leading Innovative R&D on Science and Technology (FIRST Program, JSPS), and the Core Research Program for Evolutional Science and Technology (CREST) from the Japan Science and Technology Corporation (JST) is gratefully acknowledged. We express our gratitude to Steffi Stumpf, EMZ Jena, for assistance in the SEM investigations, Melanie Nikolajski, University of Jena, for help with the pH dependent zeta measurements, Tomoya Suma, the University of Tokyo, for help with FC studies, and Dr Xueying Liu, the University of Tokyo, for the CLSM measurements.

References

- 1 K. Riehemann, S. W. Schneider, T. A. Luger, B. Godin, M. Ferrari and H. Fuchs, *Angew. Chem., Int. Ed.*, 2009, **48**, 872.
- 2 N. Sanvicens and M. P. Marco, *Trends Biotechnol.*, 2008, **26**, 425.
- 3 J. Fang, H. Nakamura and H. Maeda, *Adv. Drug Delivery Rev.*, 2011, **63**, 136.
- 4 K. Miyata, T. Nomoto, H. Takemoto, H. J. Kim, Y. Matsumoto, M. Oba, N. Nishiyama and K. Kataoka, *Abstr. Pap. Am. Chem. Soc.*, 2010, **110**, 178.
- 5 Y. Liu, H. Miyoshi and M. Nakamura, *Int. J. Cancer*, 2007, **120**, 2527.
- 6 X. A. Wu and H. M. Mansour, *Int. J. Nanotechnol.*, 2011, **8**, 115.
- 7 G. Oberdorster, V. Stone and K. Donaldson, *Nanotoxicology*, 2007, **1**, 2.
- 8 J. A. Kim, C. Aberg, A. Salvati and K. A. Dawson, *Nat. Nanotechnol.*, 2012, **7**, 62.
- 9 V. Mailander and K. Landfester, *Biomacromolecules*, 2009, **10**, 2379.
- 10 L. E. Euliss, J. A. DuPont, S. Gratton and J. M. DeSimone, *Chem. Soc. Rev.*, 2006, **35**, 1095.
- 11 F. Alexis, E. Pridgen, L. K. Molnar and O. C. Farokhzad, *Mol. Pharmacol.*, 2008, **5**, 505.
- 12 M. Mahmoudi, I. Lynch, M. R. Ejtehadi, M. P. Monopoli, F. B. Bombelli and S. Laurent, *Chem. Rev.*, 2011, **111**, 5610.
- 13 J. Wang, J. D. Byrne, M. E. Napier and J. M. DeSimone, *Small*, 2011, **7**, 1919.
- 14 G. M. Whitesides, *Nat. Biotechnol.*, 2003, **21**, 1161.
- 15 M. Gaumet, R. Gurny and F. Delie, *Eur. J. Pharm. Sci.*, 2009, **36**, 465.
- 16 J. P. Best, Y. Yan and F. Caruso, *Adv. Healthcare Mater.*, 2012, **1**, 35.
- 17 G. Sahay, D. Y. Alakhova and A. V. Kabanov, *J. Controlled Release*, 2010, **145**, 182.
- 18 J. Rejman, V. Oberle, I. S. Zuhorn and D. Hoekstra, *Biochem. J.*, 2004, **377**, 159.

- 19 H. J. Gao, W. D. Shi and L. B. Freund, *Proc. Natl. Acad. Sci. U. S. A.*, 2005, **102**, 9469.
- 20 S. Zhang, J. Li, G. Lykotrafitis, G. Bao and S. Suresh, *Adv. Mater.*, 2009, **21**, 419.
- 21 S. E. A. Gratton, P. A. Ropp, P. D. Pohlhaus, J. C. Luft, V. J. Madden, M. E. Napier and J. M. DeSimone, *Proc. Natl. Acad. Sci. U. S. A.*, 2008, **105**, 11613.
- 22 N. Doshi and S. Mitragotri, *PLoS One*, 2010, **5**, 1.
- 23 J. Dausend, A. Musyanovych, M. Dass, P. Walther, H. Schrezenmeier, K. Landfester and V. Mailander, *Macromol. Biosci.*, 2008, **8**, 1135.
- 24 A. Musyanovych, J. Dausend, M. Dass, P. Walther, V. Mailaender and K. Landfester, *Acta Biomater.*, 2011, **7**, 4160.
- 25 S. Lorenz, C. P. Hauser, B. Autenrieth, C. K. Weiss, K. Landfester and V. Mailander, *Macromol. Biosci.*, 2010, **10**, 1034.
- 26 M. Gaumet, R. Gurny and F. Delie, *Int. J. Pharm.*, 2010, **390**, 45.
- 27 W. Jiang, B. Y. S. Kim, J. T. Rutka and W. C. W. Chan, *Nat. Nanotechnol.*, 2008, **3**, 145.
- 28 Arnida, M. M. Janat-Amsbury, A. Ray, C. M. Peterson and H. Ghandehari, *Eur. J. Pharm. Biopharm.*, 2011, **77**, 417.
- 29 W.-K. Oh, S. Kim, M. Choi, C. Kim, Y. S. Jeong, B.-R. Cho, J.-S. Hahn and J. Jang, *ACS Nano*, 2010, **4**, 5301.
- 30 P. Decuzzi, B. Godin, T. Tanaka, S. Y. Lee, C. Chiappini, X. Liu and M. Ferrari, *J. Controlled Release*, 2010, **141**, 320.
- 31 Z. Popovic, W. Liu, V. P. Chauhan, J. Lee, C. Wong, A. B. Greytak, N. Insin, D. G. Nocera, D. Fukumura, R. K. Jain and M. G. Bawendi, *Angew. Chem., Int. Ed.*, 2010, **49**, 8649.
- 32 W. Zauner, N. A. Farrow and A. M. R. Haines, *J. Controlled Release*, 2001, **71**, 39.
- 33 O. Lunov, T. Syrovets, C. Loos, J. Beil, M. Delecher, K. Tron, G. U. Nienhaus, A. Musyanovych, V. Mailander, K. Landfester and T. Simmet, *ACS Nano*, 2011, **5**, 1657.
- 34 C. He, Y. Hu, L. Yin, C. Tang and C. Yin, *Biomaterials*, 2010, **31**, 3657.
- 35 Y.-L. Chiu, Y.-C. Ho, Y.-M. Chen, S.-F. Peng, C.-J. Ke, K.-J. Chen, F.-L. Mi and H.-W. Sung, *J. Controlled Release*, 2010, **146**, 152.
- 36 T.-G. Iversen, T. Skotland and K. Sandvig, *Nano Today*, 2011, **6**, 176.
- 37 S. K. Sahoo, J. Panyam, S. Prabha and V. Labhasetwar, *J. Controlled Release*, 2002, **82**, 105.
- 38 M. Feng and P. Li, *Acta Pharm. Sinica*, 2005, **40**, 893.
- 39 K. M. Ho, W. Y. Li, C. H. Wong and P. Li, *Colloid Polym. Sci.*, 2010, **288**, 1503.
- 40 P.-J. Lou, W.-F. Cheng, Y.-C. Chung, C.-Y. Cheng, L.-H. Chiu and T.-H. Young, *J. Biomed. Mater. Res., Part A*, 2009, **88**, 849.
- 41 A. Vollrath, D. Pretzel, C. Pietsch, I. Perevyazko, S. Schubert, G. M. Pavlov and U. S. Schubert, *Macromol. Rapid Commun.*, 2012, DOI: 10.1002/marc.201200329.
- 42 J. Pauli, T. Vag, R. Haag, M. Spieles, M. Wenzel, W. A. Kaiser, U. Resch-Genger and I. Hilger, *Eur. J. Med. Chem.*, 2009, **44**, 3496.
- 43 S. Schubert, J. T. Delaney and U. S. Schubert, *Soft Matter*, 2011, **7**, 1581.
- 44 I. Y. Perevyazko, A. Vollrath, S. Hornig, G. M. Pavlov and U. S. Schubert, *J. Polym. Sci., Part A: Polym. Chem.*, 2010, **48**, 3924.
- 45 J. Brandrup, E. H. Immergut and E. A. Grulke, in *Polymer Handbook*, Wiley-Interscience, 4th edn, 1999.
- 46 A. Palecanda and L. Kobzik, *Methods*, 2000, **21**, 241.
- 47 C. S. S. R. Kumar, "Nanocomposites, Nanomaterials for Life Sciences", in *Nanocomposites*, Wiley-VCH, 1st edn, 2010, p. 466.
- 48 S. Grosse, Y. Aron, G. Thevenot, M. Monsigny and I. Fajac, *J. Controlled Release*, 2007, **122**, 111.
- 49 M. Fretz, J. Jin, R. Conibere, N. A. Penning, S. Al-Taei, G. Storm, S. Futaki, T. Takeuchi, I. Nakase and A. T. Jones, *J. Controlled Release*, 2006, **116**, 247.

Supporting information

A toolbox of differently sized and labeled PMMA nanoparticles for cellular uptake investigations

5 Antje Vollrath,^{a,b} Anja Schallon,^{a,b} Christian Pietsch,^{a,b} Stephanie Schubert,^{b,c} Takahiro Nomoto,^d Yu
Matsumoto,^e Kazunori Kataoka,^{d,e,f,g,*} Ulrich S. Schubert^{a,b,*}

Received 20th August 2012, Accepted 25th September 2012

DOI: 10.1039/c2sm26928g

10 Notes and references

^a Laboratory of Organic and Macromolecular Chemistry (IOMC), Friedrich Schiller University Jena, Humboldtstrasse
10, 07743 Jena, Germany; e-mail: ulrich.schubert@uni-jena.de

^b Jena Center for Soft Matter (JCSM), Friedrich Schiller University Jena, Philosophenweg 7, 07743 Jena, Germany

^c Institute of Pharmacy, Department of Pharmaceutical Technology, Friedrich Schiller University Jena, Otto-Schott-Str.
15 41, 07745 Jena, Germany

^d Department of Bioengineering, Graduate School of Engineering, The University of Tokyo, 7-3-1 Hongo, Bunkyo-ku,
Tokyo 113-8656, Japan

^e Center for Disease Biology and Integrative Medicine, Graduate School of Medicine, The University of Tokyo, 7-3-1
Hongo, Bunkyo-ku, Tokyo 113-0033, Japan

^f Department of Materials Engineering, Graduate School of Engineering, The University of Tokyo, 7-3-1 Hongo, Bunkyo-
ku, Tokyo 113-8656, Japan

^g Center for NanoBio Integration (CNBI), The University of Tokyo, 7-3-1 Hongo, Bunkyo-ku, Tokyo 113-8656, Japan; e-
mail: kataoka@bmw.t.u-tokyo.ac.jp

25

Experimental part

Size exclusion chromatography (SEC)

SEC were recorded using a Shimadzu SCL-10A system controller, a LC-10AD pump, a RID-10A refractive
30 index detector and a PSS SDV column with chloroform:triethylamine:2-propanol (94:4:2) as eluent. The
column oven was set to 40 °C with a flow rate of 1 mL · min⁻¹. Furthermore, an Agilent 1200 Series system
equipped with an isocratic pump G1310A, a G1329A auto sampler, a G1362A refractive index detector and
both a PSS Gram30 and a PSS Gram1000 column in series was used for SEC with DMA containing
0.21 mmol LiCl as eluent with a flow rate of 1 mL · min⁻¹ at 40 °C. The systems were calibrated with narrow
35 dispersity PMMA standards.

¹H NMR and ¹³C NMR spectroscopy

Spectra were recorded in CDCl₃ on a Bruker Avance 250 MHz or 300 MHz spectrometer. Chemical shifts are
given in ppm relative to signals from the NMR solvents.

Elemental analysis (EA)

EA was carried out at an Elementaranalysator Vario EL III CHNS from Elementar Analysensysteme GmbH, Hanau, Germany.

UV/VIS spectroscopy

5 Measurements were performed on a Specord 250 (Analytik Jena GmbH). The emission spectra of the dyes and polymers were recorded in acetone using the FP 6500 from Jasco. The particle suspensions were measured in water.

Statistical analysis

Data sets are reported as mean \pm SD. To determine the significance of more than two groups of data, ANOVA
10 was used.

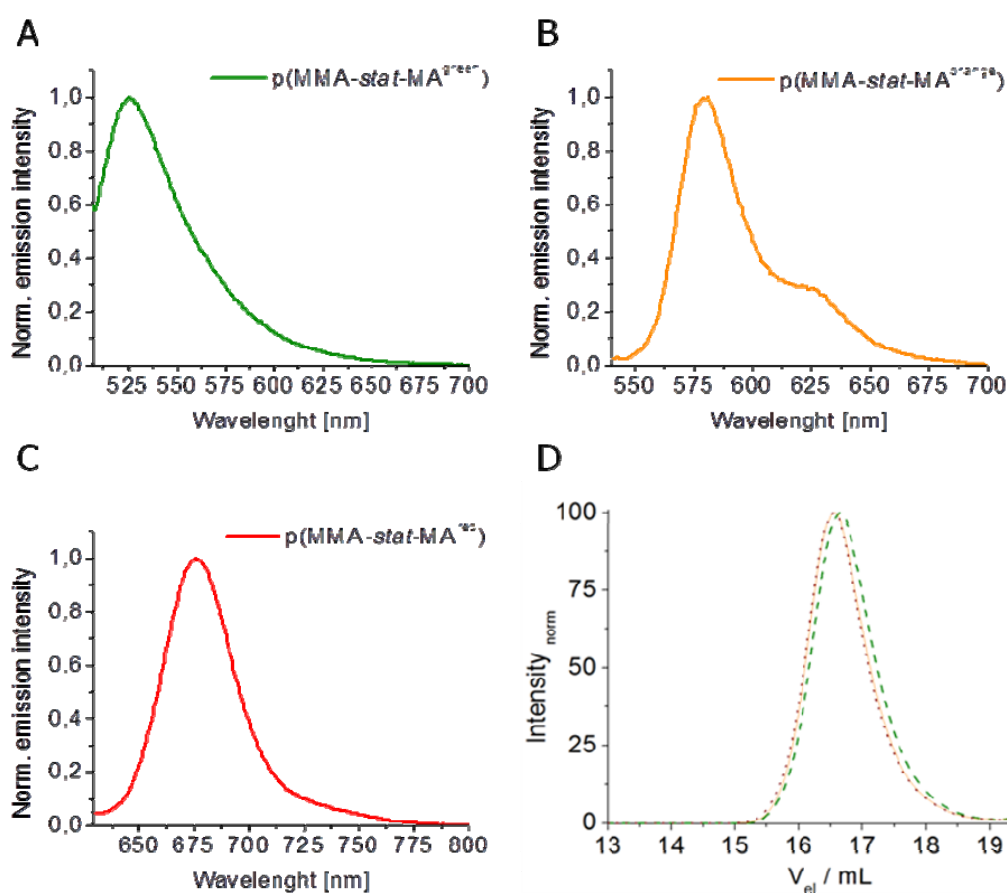


Figure S1. Fluorescence spectra of labeled p(MMA-*stat*-MA^{dye}) copolymers for the labeled copolymers p(MMA-*stat*-MA^{green, orange, red}) (A,B,C). (D) SEC traces of the final copolymers measured in DMAc/LiCl using PMMA standards (dashed line - p(MMA-*stat*-MA^{green}); solid line - p(MMA-*stat*-MA^{orange}); dotted line - p(MMA-*stat*-MA^{red})).

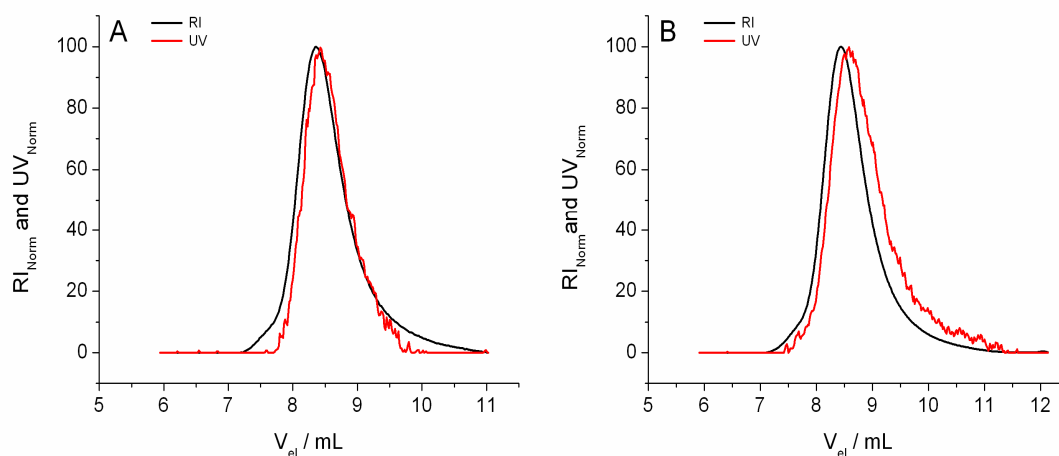


Figure S2. SEC traces of the final copolymers measured in CHCl₃/triethylamine/2-propanol (94:4:2) using RI and UV detector (at 590 nm); A: P(MMA-*stat*-MA^{green}) and B: P(MMA-*stat*-MA^{red}).

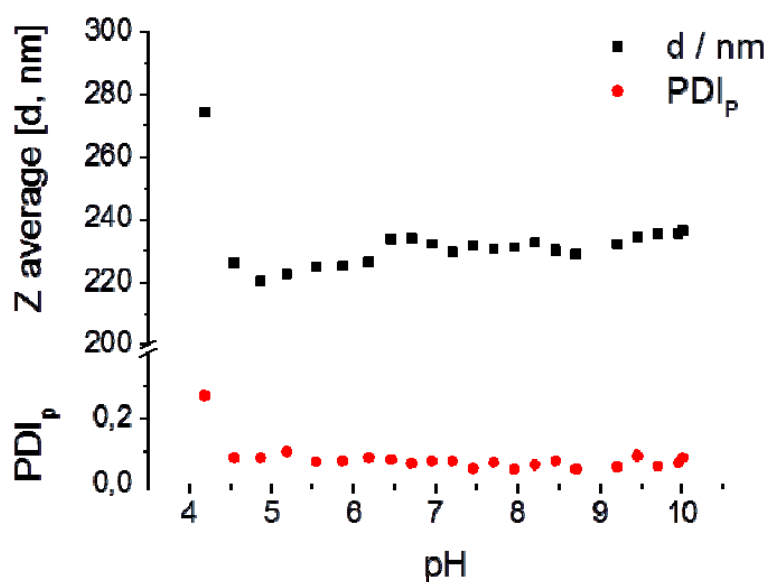


Figure S3. Z average values and corresponding PDI^P of the p(MMA-*stat*-MA^{dye}) particles in water titrated against HCl and NaOH in a pH range of 4 to 10.

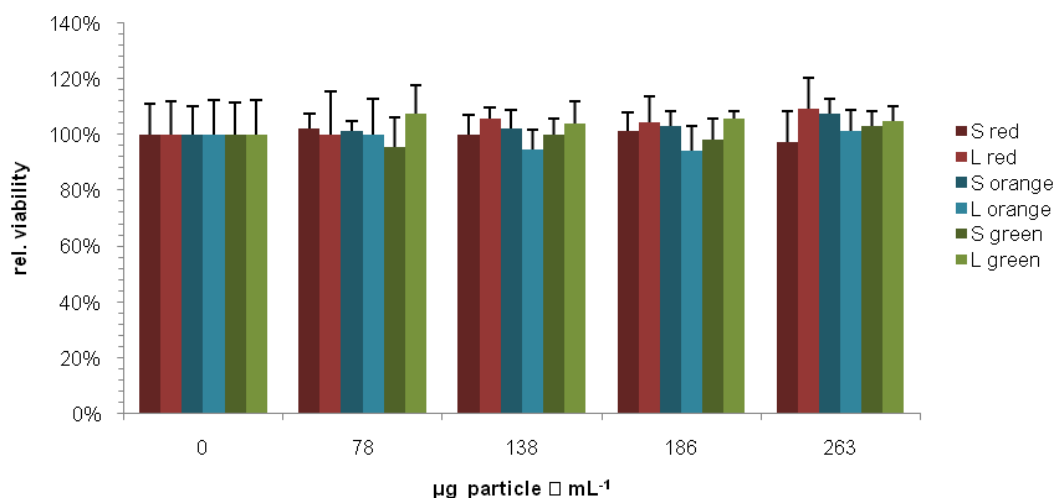


Figure S4. Cytotoxicity test of particles at different sizes and labels in L929 cells. The relative viability is expressed as percentage to control cells not treated with particles. Data represent mean \pm SD, $n \geq 12$.

5

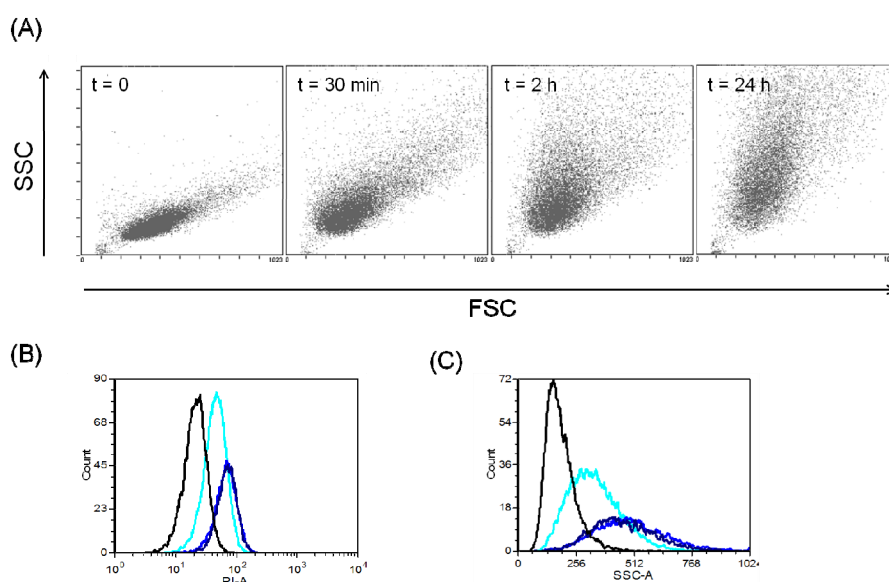


Figure S5. (A) Flow cytometry data show a time-dependent uptake of particles by an increase in SSC. (B) and (C) Histograms of non treated cells (black) and cells incubated with small (light blue), medium (blue), and large (dark blue) NP^{orange}. (B) Increase in fluorescence measured in PI (orange fluorescence) detector. (C) Increase in SSC signal.

15

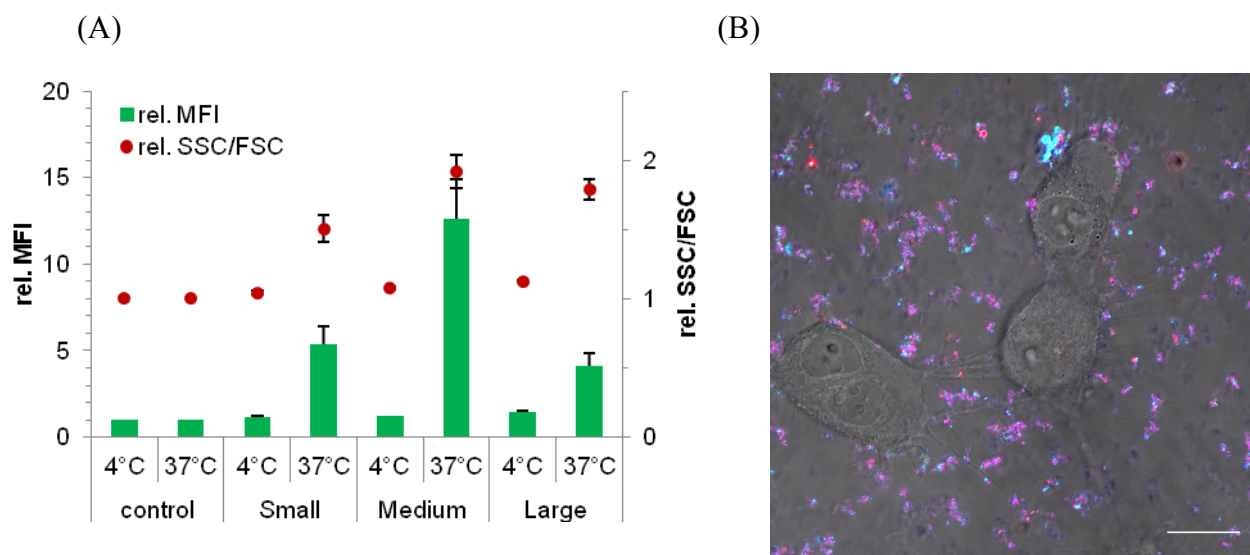


Figure S6. (A) Flow cytometry data show analysis of HeLa cells incubated with particles. Cells were seeded at a density of 10^5 cells · mL⁻¹, after 24 h medium was replaced with OptiMEM. NP^{orange} at different sizes were added at $50 \mu\text{g} \cdot \text{mL}^{-1}$ each and incubated for 24 h at 4 °C and 37 °C. No uptake at 4 °C was detectable in SSC/FSC or MFI compared to non treated cells ($p > 0.05$). Data represent mean \pm SD, $n \geq 3$. (B) Confocal microscope images of HeLa cells incubated with $50 \mu\text{g} \cdot \text{mL}^{-1}$ of each NP (small NP^{green}; medium NP^{orange}; large NP^{red}; 150 nm latex^{blue}) for 18 h in OptiMEM. The scale bars indicate 20 μm.

10

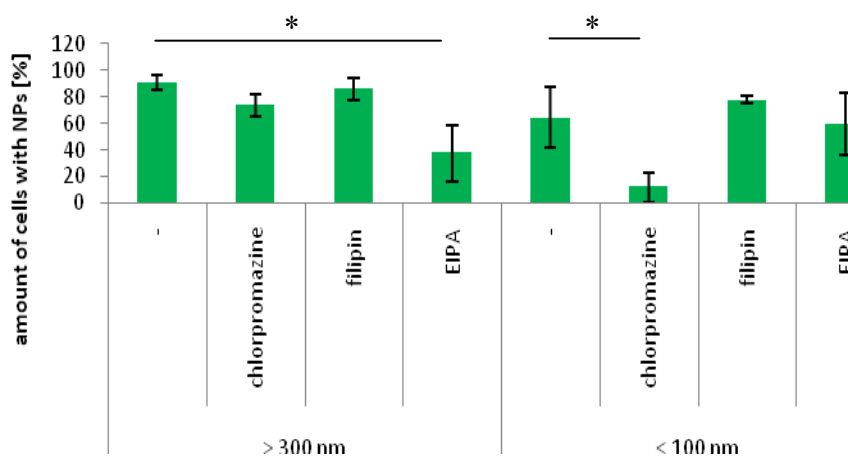


Figure S7: Flow cytometry analysis of HeLa cells incubated with particles. Cells were seeded at a density of 10^5 cells · mL⁻¹, after 24 h medium was replaced with OptiMEM supplemented with indicated inhibitors. NP^{orange} at different sizes were added at $50 \mu\text{g} \cdot \text{mL}^{-1}$ each and incubated for 2 h. * indicates statistical significance (t-test, $p < 0.05$).

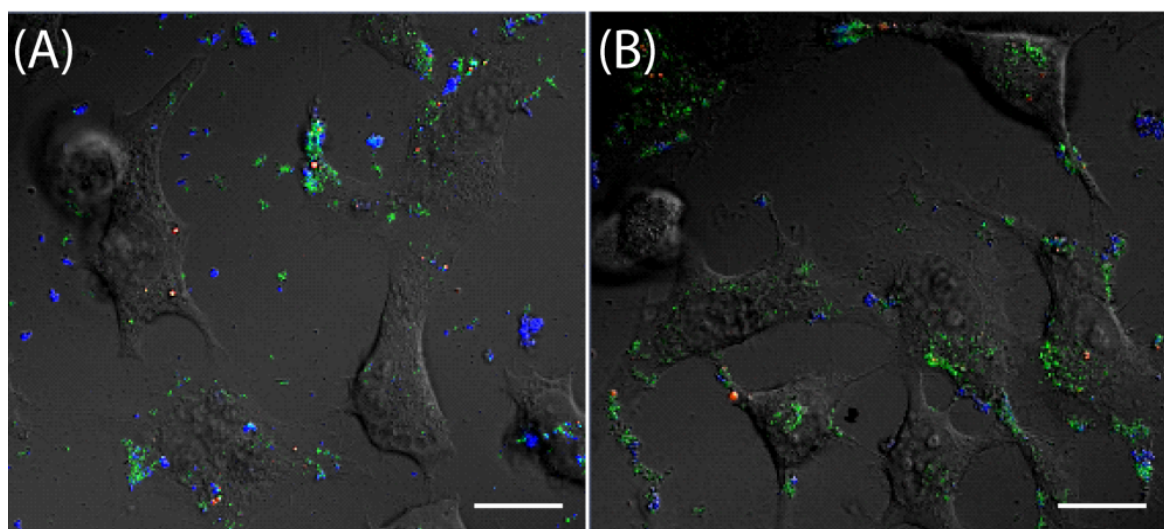


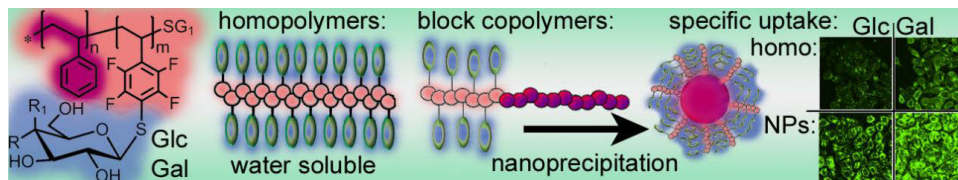
Figure S8: Confocal microscope images of HeLa cells incubated with NPs and inhibitors. Cells were seeded at a density of $10^5 \text{ cells} \cdot \text{mL}^{-1}$ for 24 h, medium was replaced with OptiMEM supplemented with chlorpromazine (A) and filipin (B). NPs with different sizes and labels (medium NP^{green}; large NP^{red}) were added at $50 \mu\text{g} \cdot \text{mL}^{-1}$ each simultaneously and incubated for 5 h. The scale bars indicate 20 μm .

Publication 7

"Uptake of well-defined, highly-glycosylated, pentafluorostyrene-based polymers and nanoparticles by human-heptocellular carcinoma cells"

Krzysztof Babiuch, David Pretzel, Tatjana Tolstik, Antje Vollrath,
Sarmiza E. Stanca, Franziska Foertsch, C. Remzi Becer,
Michael Gottschaldt, Christoph Biskup, Ulrich S. Schubert

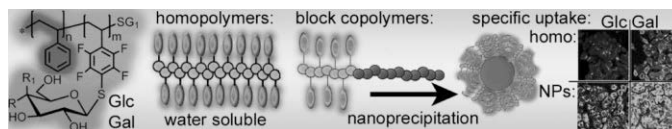
Macromol. Biosci. **2012**, *12*, 1190–1199.



Uptake of Well-Defined, Highly Glycosylated, Pentafluorostyrene-Based Polymers and Nanoparticles by Human Hepatocellular Carcinoma Cells^a

Krzysztof Babiuch, David Pretzel, Tatiana Tolstik, Antje Vollrath, Sarmiza Stanca, Franziska Foertsch, C. Remzi Becer, Michael Gottschaldt, Christoph Biskup, Ulrich S. Schubert*

Chain length, size, composition, surface charge, and other properties of polymeric materials affect their recognition and uptake by cells and must be optimized to deliver polymers selectively to their target. However, it is often not possible to precisely modify selected properties without changing other parameters. To overcome these difficulties, well-defined poly(pentafluorostyrene)-based polymers are prepared that can be grafted via thiol/*para*-fluorine “click” reaction with 1-thio- β -D-glucose and 1-thio- β -D-galactose. Fluorescence microscopy and flow cytometry show that nanoparticles are taken up by HepG2 cells to a higher degree than the respective water-soluble polymers, and that internalization of both galactosylated homo- and nanoprecipitated block copolymers is enhanced.



1. Introduction

Synthetic polymers offer the possibility to introduce biologically active moieties and to design tailor-made

macromolecules with well-defined architectures and properties.^[1,2] Glycopolymers, consisting of a synthetic polymeric backbone and pendant sugar moieties, are currently applied for affinity separations, bioassays, and

K. Babiuch, Dr. D. Pretzel, T. Tolstik, A. Vollrath, Dr. C. Remzi Becer, Dr. M. Gottschaldt, Prof. U. S. Schubert

Laboratory of Organic and Macromolecular Chemistry (IOMC), Friedrich-Schiller-University Jena, Humboldtstr. 10, 07743 Jena, Germany

E-mail: ulrich.schubert@uni-jena.de

K. Babiuch, Dr. D. Pretzel, A. Vollrath, Dr. M. Gottschaldt, Prof. C. Biskup, Prof. U. S. Schubert

Jena Center for Soft Matter (JCSM), Friedrich-Schiller-University Jena, Humboldtstr. 10, 07743 Jena, Germany

T. Tolstik

Current address: Division of Gastroenterology, Hepatology and Infectious Diseases, University Hospital Jena, Erlanger Allee 101, 07747 Jena, Germany

S. Stanca, F. Foertsch, Prof. C. Biskup

Biomolecular Photonics Group, University Hospital Jena, Nonnenplan 2-4, 07740 Jena, Germany

S. Stanca

Current address: Institute of Photonic Technology, Albert-Einstein-Str. 9, 07745 Jena, Germany

Dr. C. Remzi Becer

Current address: Department of Chemistry, University of Warwick, Library Road, CV4 7AL Coventry, UK

Prof. U. S. Schubert

Dutch Polymer Institute (DPI), John F. Kennedylaan 2, 5612 AB Eindhoven, The Netherlands

^a **Supporting Information** is available from the Wiley Online Library or from the author.

biocapture analysis, in clinical diagnostics, as well as in targeted drug delivery systems.^[3] They represent a highly versatile tool allowing the precise modification of their material and biological traits for the synthesis of various, cell (organ)-targeting systems. Modern polymerization techniques enable the adjustment of the polymeric backbone composition and to control in this way the solubility behavior of the material as well as offer the possibility to introduce responsiveness to stimuli such as a change of temperature or pH values.^[4] Since the carbohydrate units act as ligands for a broad spectrum of receptors, glycopolymers that actively target specific cells or organs can be obtained by selecting appropriate types of sugar moieties.^[5] Recognition by cell type specific receptors is significantly enhanced by multivalent representation of the carbohydrate ligand along the polymeric backbone, exploiting the cluster glycoside effect.^[6,7]

By introducing a hydrophobic block into an otherwise water soluble glycopolymer, materials that aggregate in water to nanoparticles (NPs) can be created. Their significance in biomedical fields for the delivery of drugs, genes as well as imaging agents has been thoroughly reviewed.^[8,9] Adjustment of the formulation conditions during the preparation of NPs allows a tuning of the physicochemical properties (size, charge, and surface properties) over a wide range and in a high-throughput manner.^[10] By fine-tuning of macromolecular composition and processing parameters, biodistribution and pharmacokinetics of particulate carriers can be modified to reach an enhanced accumulation within specific tissues.^[11] NPs have also been used in the treatment of liver diseases.^[12] In order to successfully target liver the particles should efficiently pass through the liver sinusoidal endothelium.^[12] To be biocompatible they should not interact with serum proteins, avoid mechanical entrapment by the capillaries in the lung and the body, and evade uptake by macrophages or provoke immune responses. Glycopolymers have revealed some protein repellent properties, therefore, their interaction with serum can be minimized and formation of agglomerates that are captured in capillaries can be avoided.^[13,14]

In order to study the interaction between polymers and cells well-defined and characterized materials are essential.^[15] Chain length, composition, and topology are the factors that influence the spatial distribution of sugars on the backbone of the macromolecule, thus, affecting their recognition by cells.^[16] The synthesis of glycopolymers can be performed via the polymerization of glycosylated monomers or the grafting of sugar moieties onto a preformed polymeric backbone.^[17] In this study, the second approach was applied. Utilizing controlled polymerization techniques in combination with a highly efficient introduction of carbohydrate moieties, for example, by “click

chemistry,” ensures a precise control over the structure of the glycosylated product.^[18]

Poly(pentafluorostyrene)-based glycopolymers reveal high thermal stability (up to 220 °C) and do not decompose under acidic conditions.^[19,20] In addition, the carbohydrate attachment via *S*-glycosidic bonds offers resistance toward enzymatic degradation.^[21] Previously, the glucosylated, fluorescently labeled, water soluble, pentafluorostyrene (PFS)-based homopolymers were applied as coating for superparamagnetic iron oxide NPs.^[20] It was shown that they act as an appropriate stabilizing agent without any cytotoxicity towards 3T3 fibroblasts. Furthermore, films prepared from the water insoluble polystyrene block copolymers were proven as synthetic biocompatible coatings on poly(propylene) (PP) substrates for culturing 3T3 fibroblasts and MC3T3-E1 preosteoblasts.^[22] Both cell types showed stable adhesion and proliferation on the glycopolymer-coated surfaces.

In order to confirm that the cellular recognition of carbohydrates, attached via thiol/*para*-fluorine “click” reaction to poly(pentafluorostyrene) (PPFS), is maintained, we report in this contribution the interactions of a HepG2 human hepatocellular carcinoma cell (HCC) line with water soluble homopolymers as well as nanoprecipitated polystyrene block copolymers, carrying β -D-thiogluco- or β -D-thiogalactose moieties. Internalization of fluorescently labeled water soluble compounds and NPs by a hepatocarcinoma cell line is studied by confocal laser scanning microscopy (CLSM) as well as flow cytometry (FC).

2. Experimental Section

2.1. Materials

Styrene ($\geq 99\%$, Aldrich), PFS (99%, Aldrich) and BlocBuilder[®] (Arkema) were used as received. 2,3,4,6-Tetra-*O*-acetyl-1-thio- β -D-glucopyranose ($>99\%$) was purchased from Glycon Biochem. GmbH, triethylamine (TEA) from Merck (for synthesis, $\geq 99\%$), *N,N*-dimethylformamide ($\geq 99.5\%$) and *N,N*-dimethylacetamide (DMA) from Fluka and methanol (anhydrous 99.8%) from Aldrich. 2,3,4,6-Tetra-*O*-acetyl-1-thio- β -D-galactopyranose was synthesized as previously reported.^[23] Fluorescein 5(6)-isothiocyanate (FITC, Sigma) and dry *N,N*-dimethylformamide (DMF) from Fluka were used for labeling. For nanoprecipitation of the polymers, distilled water and THF from Aldrich was utilized. Wheat germ agglutinin (WGA) coupled to Alexa Fluor 633 nm, which was applied to stain the cell membrane, was purchased from Molecular Probes/Invitrogen. For embedding fixed cells Moviol 4–88 solution containing 625 μ g 1,4-diazabicyclo-(2,2,2)octane from Roth, was used.

2.2. General Methods and Instrumentation

¹H and ¹³C NMR spectra were recorded on a Bruker Avance 300 MHz spectrometer, and ¹⁹F NMR spectra on a Bruker Avance 200 MHz

spectrometer in deuterated DMF. The chemical shifts were calibrated with respect to residual DMF peaks. Size-exclusion chromatography (SEC) was measured on an Agilent Technologies 1200 Series SEC system equipped with a G131A isocratic pump, a G1329A autosampler, a G1362A refractive index detector, and both a PSS Gram 30 and a PSS Gram 1000 columns in series. 2.1% LiCl solution in DMA was used as eluent at $1 \text{ mL} \cdot \text{min}^{-1}$ flow rate at a column oven temperature of 40°C . The reported number-average molar masses were determined by using polystyrene standards. Thermogravimetric analyses were performed on a Netzsch TG 209 F1 Iris with $10^\circ\text{C} \cdot \text{min}^{-1}$ heating rates from room temperature up to 900°C under nitrogen flow. Dynamic light scattering measurements (DLS) were performed on a Zetasizer Nano ZS device from Malvern Instruments (Worcestershire, UK). In these measurements, a 633 nm He/Ne laser beam was used and scattered light was detected at an angle of 173° . Scanning electron microscopy (SEM) images were recorded on a LEO-1450 VP SEM (Leo, Oberkochen, Germany), operating at 10 kV. For platinum coating of the sample a BAL-TEC SCD005 sputtering device (Balzers, Lichtenstein) was used, applying a current of 60 mA for 80 s. Cryo-TEM images were recorded using a Technai G2 Sphera (FEI) transmission electron microscope (TEM) with an acceleration voltage of 200 kV. Fluorescence excitation and emission spectra of the polymers and NPs were obtained with a Cary Eclipse fluorescence spectrofluorometer (Varian, Darmstadt, Germany) using Hellma quartz cuvettes. The slit width of the emission and excitation monochromator was adjusted such that the resulting resolution was 5 nm. Excitation spectra were recorded at an emission wavelength of 515 nm. The emission spectra were measured by exciting the polymers at 488 nm. Fluorescence images were obtained with confocal laser-scanning microscopes (LSM 510 Meta and LSM 710, Zeiss, Jena, Germany), using a Plan-Apochromat $63\times$ oil immersion objective (NA 1.4, Zeiss) and a C-Apochromat $40\times$ water immersion objective (NA 1.2, Zeiss). FITC was excited with the 488 nm line of the argon laser. The emitted fluorescence was collected with a 505 nm longpass filter (LSM510) or with the built-in grating in the 505–550 nm wavelength range (LSM710). To excite the WGA Alexa Fluor 633 membrane stain, the He/Ne 633 nm laser was used. Fluorescence was recorded in the 640–700 nm range using the built-in grating (LSM710). To allow a comparison, all images of a series were captured under identical conditions and instrument settings (laser power, pinhole diameter and detector gain). Quantitative image analysis was performed on grayscale converted images using the ImageJ software. FC was measured on a Beckmann Coulter Cytomics FC-500 equipped with Uniphase Argon ion laser, 488 nm, 20 mW output and analyzed with the Cytomics CXP software.

2.3. Glycopolymer Synthesis

The glycopolymers were synthesized as previously reported.^[22] Briefly, acetylated carbohydrate thiols were grafted onto a PPFs or a polystyrene-*block*-PPFs backbones, which were prepared by nitroxide-mediated, living, radical polymerization.^[19] The reaction was carried out in DMF in presence of TEA yielding polymers with high degrees of functionalization ($\geq 90\%$ of substitution). The glycopolymers were obtained by subsequent deprotection of the acetyl groups, using sodium methoxide as base.

2.4. Glycopolymer Labeling

Labeling was achieved by an analogous method to the previously reported for glucosylated homopolymers.^[20] In an oven-dried, round bottom flask, glycopolymer and FITC (0.5 mol equiv. per polymer chain) were weighed in and dried for 1 h under vacuum. DMF (10 mL) was added, and the sealed mixture was stirred for 24 h in the dark. The reaction was quenched by dropping the mixture into ethanol. The precipitated polymers were centrifuged and washed at least six times with ethanol until the fluorescence in the supernatant disappeared completely as shown by thin-layer chromatography (TLC) monitoring.

2.5. Nanoprecipitation Procedure

8 mg of the labeled polystyrene block glycopolymers were dissolved in a mixture of 1 mL THF and 1 mL of distilled water. After 10 min stirring, 7 mL water were added dropwise to cause nanoprecipitation of the materials. THF was evaporated at 60°C under reduced pressure and the solution was sterile filtered using a $2 \mu\text{m}$ filter.

2.6. Characterization of Nanoparticles

2.6.1. DLS Characterization

Dynamic light scattering was used to determine the size and zeta potentials of the particles. For this purpose, $20 \mu\text{L}$ of the suspension were added to 1 mL of demineralized, filtered water ($\text{pH} = 6.0$) and this solution was transferred into a polycarbonate zeta cell. For size measurements, three runs were applied for 150 s, and for the zeta potential three runs for 10 s.

2.6.2. SEM Characterization

For the SEM measurements one droplet ($15\text{--}20 \mu\text{L}$) of the suspension was placed on a mica surface and lyophilized for 3 h. Finally, the sample was sputtered with platinum applying a current of 60 mA for 80 s.

2.6.3. Cryo-TEM Characterization

Samples for cryo-TEM were prepared using a FEI Vitrobot system. $3 \mu\text{L}$ of the sample solution were transferred onto a Quantifoil (R2/2) grid, and blotting was performed at 3 mm and 3.5 s of blotting time. Samples were rapidly transferred into liquid ethane and stored in liquid nitrogen until the measurements were performed using a Gatan cryo holder.

2.7. Measurements of Fluorescence Spectra

To measure the fluorescence by the spectrofluorometer (Varian, Darmstadt, Germany), the water soluble homopolymers were dissolved in phosphate-buffered saline (PBS), $\text{pH} = 7.4$, at the indicated concentrations. The aqueous suspensions of the NPs, obtained from the block copolymers, were diluted to the indicated concentrations with PBS.

2.8. Uptake Studies

2.8.1. Cell Culture

The human hepatocarcinoma cell line HepG2 was purchased from the German Collection of Microorganisms and Cell Cultures (DSMZ, Braunschweig, Germany). For uptake studies, 8×10^4 cells were initially seeded into 6 well plates in 4 mL of RPMI medium supplemented with 10% fetal calf serum (FCS), $100 \text{ U} \cdot \text{mL}^{-1}$ penicillin, and $100 \mu\text{g} \cdot \text{mL}^{-1}$ streptomycin (all components from Biochrom, Berlin, Germany). To assess the polymer uptake in adherent HepG2 cell monolayers by CLSM, cells were seeded on sterile glass coverslips. The cells were grown at 37°C in a humidified atmosphere containing 5 vol% CO_2 for 48 h until 75% confluency was reached and then subjected to incubation with the polymers.

2.8.2. Incubation of Cells With Polymers

The cells were incubated separately with different concentrations (0.10, 1.00, and 10.00 $\mu\text{g} \cdot \text{mL}^{-1}$, respectively) of the sugar containing polymers for 24 h at 37°C under 5% CO_2 atmosphere. Control cells were incubated with fresh culture medium. After incubation, the solutions were aspirated from the wells and any unbound conjugates were removed by washing the cell layer three times with PBS. Subsequently, the cells were subjected to further treatment for CLSM and FC analysis.

2.8.3. Analysis of Glycopolymer and Nanoparticle Uptake by CLSM

After incubation with the sugar containing polymers, the cells were fixed directly onto the glass coverslips for 10 min at room temperature using 4% paraformaldehyde (PFA) dissolved in PBS and subsequently washed twice with PBS. The glass coverslips were mounted on glass slides using 25 μL Moviol 4-88 solution containing 625 μg 1,4-diazabicyclo-(2,2,2)octane. After 24 h CLSM images were recorded using a Carl Zeiss 510. Quantification of the cell-associated fluorescence signal was performed using 8 bit, grayscale-converted images and ImageJ software. The cell boundaries were identified by the user and the average fluorescence intensity per pixel was obtained. Values from at least 100 cells were averaged.

2.8.4. Proof of Glycopolymer and Nanoparticle Internalization by CLSM

To show that the fluorescence resulted from internalized polymers and not from materials bound to the cell membrane, an aliquot of enzymatically detached and fixed cells was stained for 10 min with a solution of 5 μg WGA coupled to Alexa Fluor 633 nm in 1 mL phosphate-buffered saline (PBS). The cells were then centrifuged for 5 min at 1500 rpm and resuspended in 400 μL PBS. The suspension was transferred into a custom built microscope chamber and allowed to sediment. CLSM images were recorded on a Carl Zeiss 710. The emitted fluorescence was collected in the 505–550 nm wavelength range.

2.8.5. FC Analysis

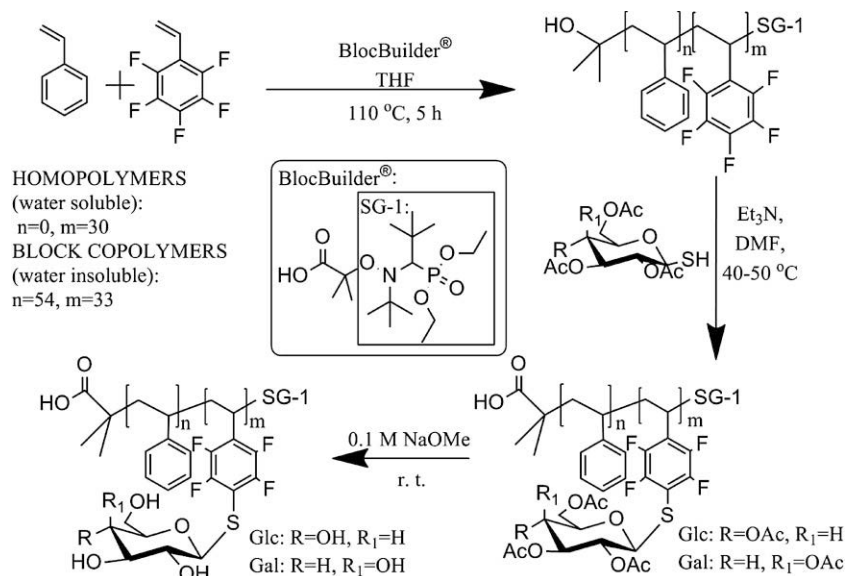
After detaching the adherent cells by trypsin treatment, the cell suspension was washed twice with PBS supplemented with 10%

FCS. For the investigation of cytotoxic effects, dead cells were labeled with a propidium iodide (PI) staining for 15 min at room temperature using $100 \mu\text{g} \text{ PI} \cdot \text{mL}^{-1}$ PBS. The cells were then incubated with 4% PFA dissolved in PBS for 10 min at room temperature and subsequently washed twice with PBS. A total of 2×10^4 cells were resuspended and subjected to FC using gates of forward and side scatters to exclude debris and cell aggregates.

3. Results and Discussion

3.1. Glycopolymer Synthesis and Labeling

The glycopolymers were synthesized as previously reported (Scheme 1).^[22] In brief, glucosylated (hGlc) and galactosylated (hGal) homopolymers as well as the respective polystyrene block copolymers, bGlc and bGal, were obtained by post-polymerization modification using the thiol/*para*-fluorine “click” reaction to graft acetylated 1-thio- β -D-glucopyranose and 1-thio- β -D-galactopyranose onto a homopolymer of PFS as well as onto a block copolymer of styrene and PFS (PS-*b*-PFS). Subsequent deprotection of the carbohydrate moieties yielded well-defined, glucose- or galactose-modified polymers. The obtained glycopolymers were stable up to 220°C , as confirmed by thermogravimetric analysis (see the Supporting Information). The post-polymerization modification approach, unlike the polymerization of glycosylated monomers, ensures that the materials investigated in this study are of the same degree of polymerization, since the grafting step was performed on the same batches of PFS and PS-*b*-PFS. In addition, the monomers used in the backbone synthesis are commercially available and thoroughly studied. Consequently, the synthetic problems connected with polymerization of unknown, sterically hindered carbohydrate containing units can be avoided.^[24] The lengths of the obtained starting polymers were determined from ^1H NMR spectra, by integration of the signals derived from the initiator and the backbone (see Supporting Information) and SEC measurements. Furthermore, this method reduces the practical complications connected with the characterization of glycopolymers caused by the bulky carbohydrate moieties, which result in hydrodynamic diameter values that significantly deviate from the commonly applied SEC standard polymers (Table 1). In order to precisely determine the amount of attached carbohydrate moieties, after thiol/*para*-fluorine “click” reaction, ^{19}F NMR spectroscopy was used (Supporting Information).^[19] The deprotected glycopolymers exhibited narrow molar mass distributions and carried equal amounts of carbohydrate units. Synthesis and characterization details for the obtained glycopolymers can be found in ref. ^[22] as well as in the Supporting Information (^1H , ^{13}C , and ^{19}F NMR spectroscopy).



■ Scheme 1. Schematic representation of the synthesis of the glucosylated and galactosylated homo and block copolymers.

Subsequently, the glycopolymers were labeled with FITC, as reported previously.^[20] In order to ensure that the bioactivity of the carbohydrate moieties is maintained and the label is equally distributed, 0.5 equivalents of FITC per one polymeric chain were used for the labeling. SEC analyses of the fluorescent polymers (Figure 1) did not show any significant differences in the molar masses of the respective Glc and Gal derivatives. The low polydispersity index values were maintained for the labeled glycopolymers, indicating no coupling reactions of the polymeric backbone or its decomposition. Furthermore, the SEC traces show that the labeled homopolymers and block copolymers have the same molar masses and distributions as the respective non-labeled substrates. Successful introduction of the fluorescent label was further confirmed by the fluorescence spectra (Figure 2). For the same concentrations, the fluorescence of glucosylated polymer was 1.4 times

higher than for the galactosylated one. This can be attributed to different amounts of FITC attached to the glycopolymers and has to be taken into account when interpreting the FC and CLSM measurements.

3.2. Preparation and Characterization of Nanoparticles

For the preparation of NPs the nanoprecipitation technique was chosen. The process of NP formation by solvent displacement method, i.e., mixing of the polymer solution with an anti-solvent that is miscible with the solvent, has already been applied for various synthetic polymers and biopolymers.^[25–28] Important advantages are the fast and easy preparation and no necessity of surfactants. In particular, the absence of surface active agents like poly(vinyl alcohol) is essential for this study, as their

■ Table 1. Selected characterization data for the obtained glycopolymers.

Name	Structure	Carbohydrate amount ^{a)} [mol%]	\bar{M}_n theo [g mol ⁻¹]	\bar{M}_n , SEC ^{b)} [g mol ⁻¹]	\bar{M}_w/\bar{M}_n ^{b)}
PFS	PPFS ₃₅	0	7200	5700	1.06
hGlc	PTFSGlcOH	100	13 300	20 600	1.10
hGal	PTFSGalOH	99	13 200	19 300	1.06
PS- <i>b</i> -PFS	PS ₅₄ - <i>b</i> -PPFS ₃₃	0	12 400	14 300	1.16
bGlc	PS- <i>b</i> -PTFSGlcOH	90	17 600	40 000	1.13
bGal	PS- <i>b</i> -PTFSGalOH	94	17 900	39 900	1.10

^{a)}Calculated from ¹⁹F NMR spectroscopy; ^{b)}Calculated according to polystyrene standards (PSS) using 2.1% LiCl solution in DMA as eluent.

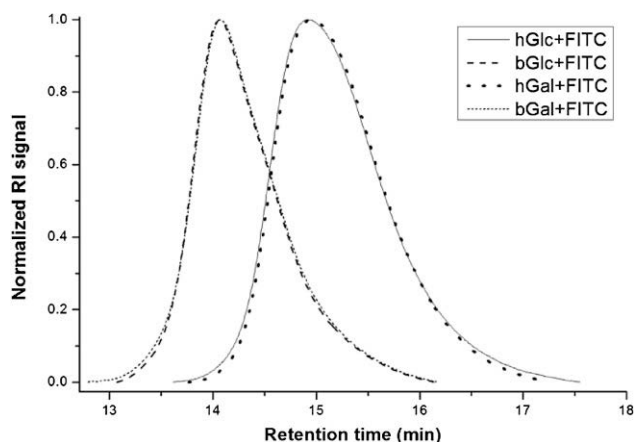


Figure 1. Normalized SEC traces of the FITC-labeled glycopolymers using 2.1% LiCl solution in DMA as eluent.

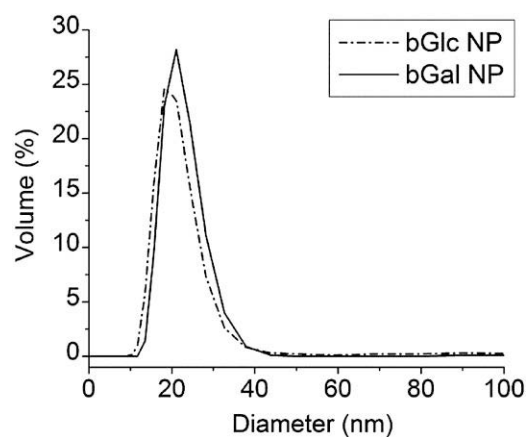


Figure 3. Volume size distributions of the fluorescent glycosylated nanoparticles, obtained by DLS.

presence may affect the cell uptake of the particles.^[29] The particles for the cell study were obtained by dissolving the amphiphilic block glycopolymers in a water/THF mixture (1:1) and subsequent precipitation by successive dropwise addition of water to this solution (the homopolymers were water soluble and could, therefore, not be nanoprecipitated). THF provides good solubility for the PS block of the macromolecule and water is a good solvent for the glycosylated part, as shown for the homo-glycopolymers. Therefore, this solvent mixture gave visibly clear solutions of the amphiphilic block copolymers. The further addition of water caused the collapse of the polystyrene block, because of the water insolubility, and self-assembly of these hydrophobic parts into NPs. The resulting NP suspensions were characterized by DLS and the measurement of the zeta potential. The volume size distributions obtained by DLS are displayed in Figure 3. Both, glucosy-

lated and galactosylated particles revealed the same hydrodynamic diameters of 20 nm. The zeta potentials of the particle suspensions (pH = 6) were determined to be -15 mV for bGlcNPs and -30 mV for bGalNPs. The negative zeta potential values can be attributed to the presence of electron rich hydroxyl groups of the sugar units as well as fluorine atoms, since the NPs prepared from unmodified, hydrophobic PS-*b*-PFS also revealed strongly negative (below -30 mV) values.^[19] Apart from DLS investigations, the particles were characterized by electron microscopy techniques such as SEM and cryo-TEM (Figure 4). In the displayed images very small and spherical particles with diameters of 15–40 nm are visible, confirming the DLS results. The apparent larger sizes for glucosylated NPs result from the sample preparation technique and particle agglomeration during the drying process. Additional SEM images can be found in Supporting Information (Figure S7). In order to prove the long-term stability of the particles the suspensions were stored at 5 °C in the dark for twelve months. DLS measurements of these particles did not show any significant change in the size distribution. Furthermore, no aggregation or sedimentation of the particles was observed, confirming a very good stability of these glycosylated NPs in suspension. It is very important that the average diameters and size distributions are similar for both glycopolymers, in order to exclude any influence of the particle size on the cellular uptake.^[30] Moreover, the shape of the particle as well as the morphology also affects its uptake.^[31] The investigated NPs were all spherical with smooth surfaces; hence, the differences in their uptake can only result from the type of attached carbohydrate. The fluorescence of the particles at different concentrations in PBS was examined (Figure 5). The fluorescence intensities of the glucosylated NPs were, similarly to the water soluble glycopolymers, approximately 1.4-fold higher than of the galactose-functionalized NPs (also in this case the

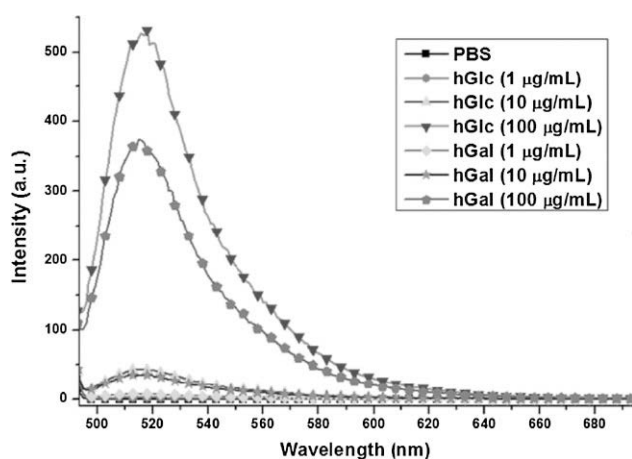


Figure 2. Fluorescence emission spectra of the FITC-labeled, water soluble glycopolymers.

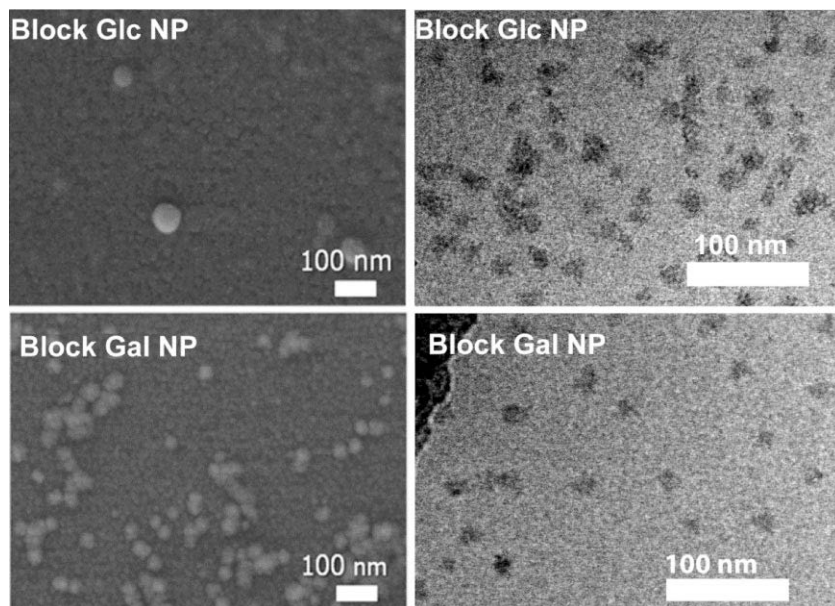


Figure 4. SEM (left) and cryo-TEM (right) images of the glycosylated nanoparticles, which reveal small and spherical particles with sizes between 15 and 40 nm.

difference has to be taken into account when evaluating the results of uptake studies performed by CLSM and FC).

3.3. Investigation of PFS-Based Glycopolymers Uptake by HepG2 Cells

3.3.1. CLSM Investigation of Uptake Dependence on Polymer Concentration and Type of Carbohydrate

Hepatocellular carcinoma HepG2 cells were seeded on sterile glass coverslips and incubated with the sugar containing polymers in order to investigate their interaction as described in the experimental section. Subsequently,

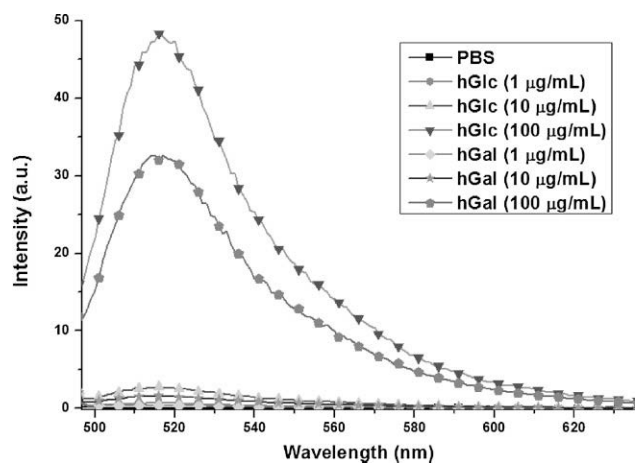


Figure 5. Fluorescence emission spectra of the FITC-labeled, glucosylated, and galactosylated nanoparticles.

the cells were fixed, using PFA, and the coverslips were mounted onto glass slides for microscopy observations. Representative CLSM micrographs of the cells are shown in Figure 6, left. The results reveal an increase of intracellular fluorescence after incubation with both, water soluble polymers and polymeric NPs in a concentration-dependent manner, confirming the uptake of the polymers by the HepG2 cells. To quantify the uptake, images were subjected to quantitative analysis using ImageJ software determining the mean fluorescence intensity per cell. At a concentration of $1 \mu\text{g} \cdot \text{mL}^{-1}$ a clear increase of the fluorescence was observed for the internalized galactosylated, but not for the glucosylated materials (Figure 6, right). At higher concentrations the fluorescence resulting from the internalized NPs was much higher than from the water soluble homo-glycopolymers, but

still galactosylated compounds were taken up to a higher degree than glucosylated ones.

3.3.2. Proof of Internalization by CLSM Investigations

To confirm that the particles as well as the soluble polymers did not adsorb to the outer leaflet of the plasma membrane but were truly internalized by the HepG2 cells, an aliquot of the cells was investigated by CLSM (Figure 7). To delineate the cell membrane, cells were stained with WGA conjugated to Alexa Fluor 633. WGA is a lectin (carbohydrate-binding protein), which selectively binds to the glycocalyx of cellular membranes. The overlay of the fluorescence originating from the labeled polymers (green) and the red stained membrane clearly shows that all particles are located inside the cells. This is further confirmed by z-stacks and a 3D reconstruction of the cells (see movie in Supporting Information). Both water-soluble polymers and NPs were accumulated in HepG2 cells.

3.3.3. Flow Cytometric Investigations of the Uptake

The uptake of the fluorescent labeled glycopolymers was further quantified by FC measurements. For this purpose, cells were incubated with different concentrations (0.10 , 1.00 , and $10.00 \mu\text{g} \cdot \text{mL}^{-1}$) of the materials for 24 h. Unbound polymers were removed by washing with PBS, and the cells were trypsinized, fixed with PFA and subjected to FC analysis. The mean fluorescence intensities per cells increased with increasing concentrations of the compounds. Since the intrinsic fluorescence intensities of the glucosylated compounds were 1.4 times higher than of the galactosylated materials (Figure 2 and 5), the results

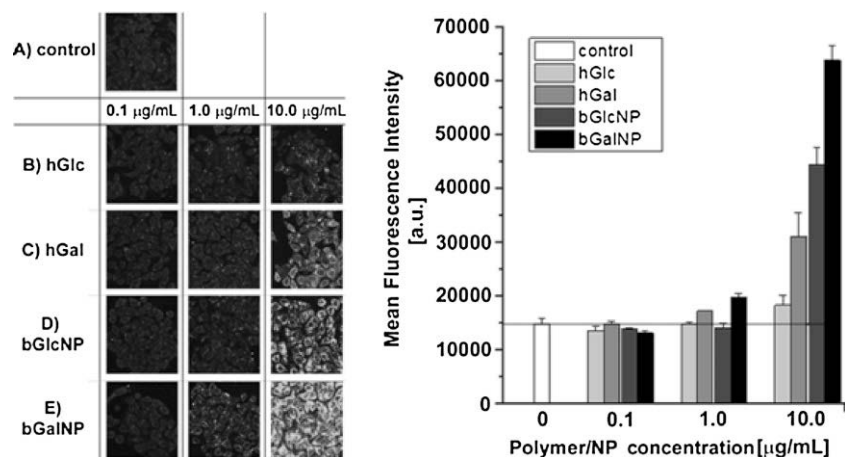


Figure 6. Confocal fluorescence microscopy images (left) of HepG2 cells after incubation with the water soluble polymers (hGlc and hGal) and polymeric nanoparticles (bGlcNP and bGalNP) for 24 h at 37 °C (left). Cells incubated with polymer free culture medium served as control. All images were obtained with identical instrument settings. Results from quantitative image analysis (right) of confocal fluorescence micrographs (left). Values for the mean fluorescence intensity per a HepG2 cell were assessed from grayscale-converted images using ImageJ software. A color version of this figure is available in the Supporting Information.

distinctly reveal the preferential uptake of the galactosylated compounds and confirm the results obtained from the image analysis of the CLSM micrographs (Figure 6). Furthermore, the fluorescence of the internalized glucose- and galactose-modified particles at concentration of 10 µg · mL⁻¹ was much higher than of the respective homopolymers pointing to some additional uptake mechanism.

Additionally, FC investigation of cellular membrane integrity with PI exclusion assays showed that the analyzed materials did not affect the cell membrane integrity confirming the findings from CLSM experiments (see Supporting Information).^[22]

The obtained results confirm the enhanced internalization of galactosylated PFS-based polymers and NPs. They are in good correlation with the previous studies, where both galactosylated and glucosylated materials show differences in their uptake via the asialoglycoprotein

were normalized by this factor in order to enable an accurate comparison of the carbohydrate-specific uptake. The histogram plots (Figure 8) clearly show a concentration-dependent increase of the fluorescence intensity distributions (observable as a shift to the right) for all types of the polymers from a concentration of 1.0–10.0 µg · mL⁻¹. The results, depicted in the bar chart, for the mean fluorescence intensities of the analyzed cell populations

receptors (ASGPR).^[32] Poly(*N-p*-vinylbenzyl-*O*-β-D-galactopyranosyl-[1 → 4]-D-gluconamide) (PVLA) was previously employed as a model ligand for ASGPR in order to examine the effect of the density of the carbohydrates attached to the polymeric backbone on binding and internalization of fluorescent polystyrene NPs by hepatocytes.^[33] The uptake of particles (500 nm), coated with various concentrations of water soluble PVLA and non-galactosylated poly(vinylbenzyl-D-gluconamide), by rat hepatocytes, was found to be proportional to the galactose content.

These findings can be exploited to target liver cells selectively. So far, amphiphilic, galactose-functionalized polycarbonate block copolymers, prepared by ring opening polymerization, have been already employed to prepare doxorubicin-loaded micelles with diameters below 100 nm and narrow size distributions.^[34] The micelles were taken up selectively by an ASGPR-expressing HepG2 HCC cell line and had a significantly higher cytotoxicity of the drug as compared to the ASGPR-negative HEK293 cell line. Herein, the fluorescence intensities of hGal and bGalNP, internalized by the HepG2 cells, are distinctly higher, at the concentration of 1.0 µg · mL⁻¹, than the cellular autofluorescence (control) as well as the fluorescence of cells cultured with the glucosylated materials (Figure 6). Therefore, the galactosyl moieties attached to PFS backbones via thiol-*p*-fluorine “click” reaction retain their hepatocyte-uptake enhancing properties.

On the other hand, the uptake of glucosylated polymers and NPs was higher than expected, when comparing with similar glucose-modified glycopolymers having a hydro-

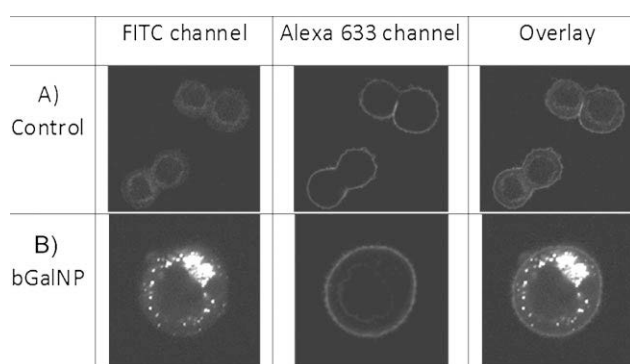


Figure 7. Representative CLSM micrographs of cells incubated with 10 µg · mL⁻¹ of polymeric nanoparticles from bGal for 24 h at 37 °C. The cells were detached and stained with WGA conjugated to Alexa Fluor 633 to mark the plasma membrane. Fluorescence originating from the labeled polymers was collected in the FITC channel (1st column) whereas fluorescence originating from the plasma membrane was collected in the Alexa 633 channel (2nd column). The overlay of both channels (3rd column) clearly shows that the particles are located inside the cells. A color version of this figure is available in the Supporting Information.

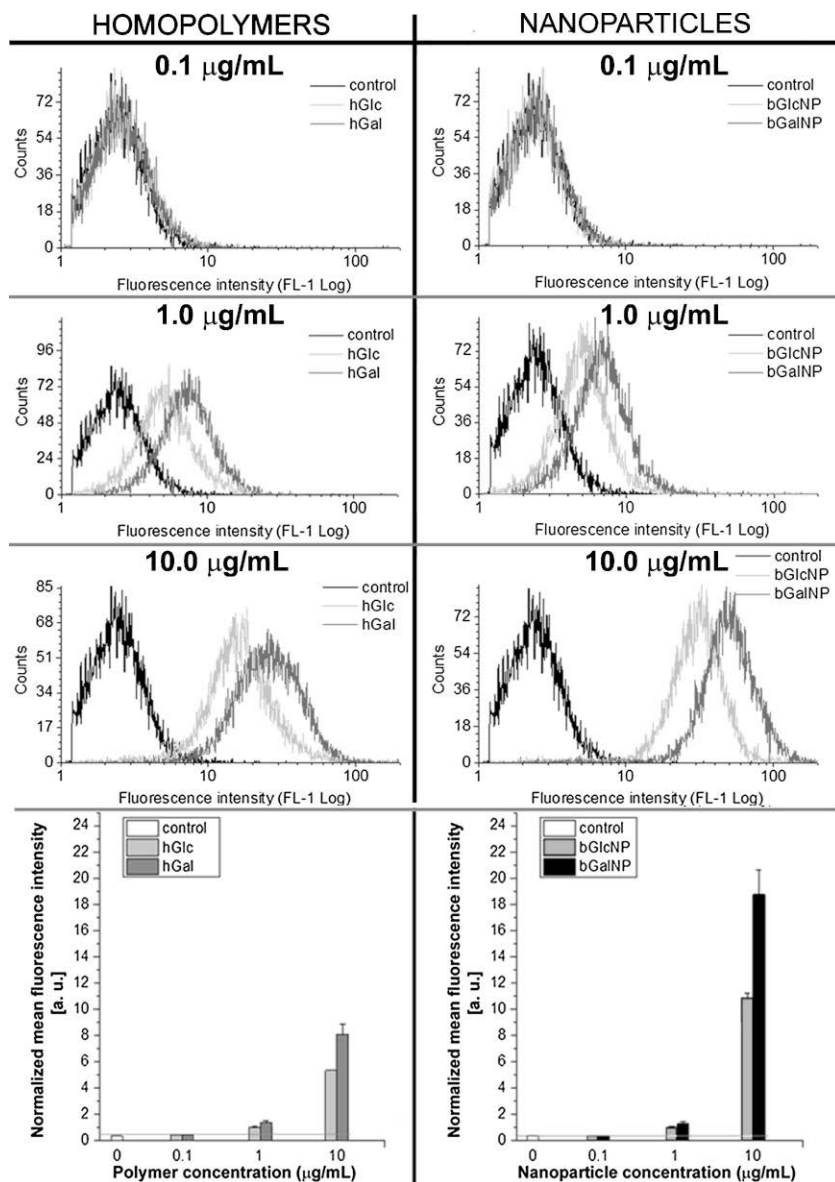


Figure 8. Histogram plots from flow cytometry on the uptake of water soluble polymers (hGlc and hGal) and polymeric nanoparticles (bGlcNP and bGalNP) by HepG2 cells after 24 h incubation at 37 °C. Cells incubated with polymer free culture medium served as control. The fluorescence intensity on the x-axis is plotted against the number of events on the y-axis. A shift of the histogram toward the right side demonstrates an increasing amount of FITC-labeled polymers/nanoparticles attached to or taken up by the cells. The bar charts depict the results for the mean fluorescence intensities, obtained from flow cytometry of the analyzed cell populations. Various polymer concentrations, physical forms (water soluble: hGlc and hGal; nanoparticles: bGlcNP and bGalNP), as well as carbohydrate moieties, are taken up to a different degree.

phobic polystyryl backbone, namely poly[*N-p*-vinylbenzyl-*O*- α -D-glucopyranosyl-[1 \rightarrow 4]-D-gluconamide] (PVMA) and poly[3-*N-p*-vinyl-benzyl-D-glucose] (PVG).^[35] These polymers carry glucose substituted at C-1 and C-3, respectively, and did not show any clear interaction with hepatocytes.

However, hepatocytes took up the polymer with the carbohydrate attached via C6 (poly[*N-p*-vinylbenzyl-D-glucuronamide], PV6Gna) but to a lower degree than galactosylated PVLA.^[36] It has to be taken into account that not only the type of sugar but also the rotational restriction, stiffness and hydrophobicity can influence the glycopolymer/hepatocyte interactions, as was shown for chitosan beads functionalized with lactonamide units.^[37] Our observation concerning the higher uptake (at the concentration of 10 $\mu\text{g} \cdot \text{mL}^{-1}$) of nanoparticulate materials, as compared to the soluble homopolymers, is in line with studies on the interaction of poly(ethylene glycol)-*block*-poly(ϵ -caprolactone) block copolymeric micelles with HepG2. They have shown that even non-targeted particulated materials were taken up by hepatocellular carcinoma cells following 24 h of incubation.^[38] This uptake was attributed to unspecific interactions and non-receptor-mediated endocytosis. The ratio between internalized non-glycosylated and galactosylated micelles, in ref.,^[38] corresponds well to the ratio between bGlcNPs and bGalNPs taken up by the cells in this work.

4. Conclusion

Through nanoprecipitation of water-insoluble galactosylated or glucose-modified compounds NPs of the same sizes and similar morphologies were obtained. As a consequence, an influence of the polymeric architecture as well as of the particle diameter and shape on the interaction with cells could be excluded. Fluorescent labeling of the water soluble polymers and particles facilitated the use of CLSM and FC to confirm the carbohydrate specific uptake of the water soluble galactosylated polymer as well as of the NPs prepared from galactose-modified polystyrene block copolymer and show that internalization of galactosylated homo- and nanoprecipitated block copolymers is enhanced as compared to the respective glucose substituted compounds. NPs are taken up to a higher degree than respective water soluble polymers. All materials did not show any acute cytotoxicity.

Since these results revealed that the preferential internalization of β -D-galactose by HepG2 cells is maintained upon grafting onto PPFs-based polymers, these glycopolymers can find a multitude of potential applications in, for example, liver tumor-targeted chemotherapy, imaging, and as extracellular matrices for hepatocytes. Additionally, the PPFs-based glycopolymers can be modified with other thiolated glycosides for lectin-mediated drug targeting as reported for other classes of carbohydrate-containing polymers.

Acknowledgements: We thank the Thuringian Ministry for Education, Science, and Culture (grant #B514-09051, NanoConsens) and the Dutch Polymer Institute (DPI, Technologic Area HTE) for funding and Dr. Stephanie Hoepfner for the cryo-TEM measurements.

Received: January 24, 2012; Revised: April 19, 2012; Published online: June 25, 2012; DOI: 10.1002/mabi.201200024

Keywords: cellular uptake; glycopolymers; graft copolymers; hepatocellular carcinoma cells; nanoparticles

- [1] B. Le Droumaguet, J. Nicolas, *Polym. Chem.* **2010**, *1*, 563.
- [2] B. D. Ulery, L. S. Nair, C. T. Laurencin, *J. Polym. Sci., Part B: Polym. Phys.* **2011**, *49*, 832.
- [3] S. G. Spain, N. R. Cameron, *Polym. Chem.* **2011**, *2*, 60.
- [4] K. Kempe, C. Weber, K. Babiuch, M. Gottschaldt, R. Hoogenboom, U. S. Schubert, *Biomacromolecules* **2011**, *12*, 2591.
- [5] S. R. S. Ting, G. Chen, M. H. Stenzel, *Polym. Chem.* **2010**, *1*, 1392.
- [6] J. J. Lundquist, E. J. Toone, *Chem. Rev.* **2002**, *102*, 555.
- [7] C. R. Becer, M. I. Gibson, J. Geng, R. Ilyas, R. Wallis, D. A. Mitchell, D. M. Haddleton, *J. Am. Chem. Soc.* **2010**, *132*, 15130.
- [8] S. Chen, S.-X. Cheng, R.-X. Zhuo, *Macromol. Biosci.* **2011**, *11*, 576.
- [9] W. J. Stark, *Angew. Chem. Int. Ed.* **2011**, *50*, 1242.
- [10] I. Y. Perevyazko, J. T. Delaney, A. Vollrath, G. M. Pavlov, S. Schubert, U. S. Schubert, *Soft Matter* **2011**, *7*, 5030.
- [11] M. E. Davis, Z. Chen, D. M. Shin, *Nat. Rev. Drug Discovery* **2008**, *7*, 771.
- [12] L. J. Li, H. Y. Wang, Z. Y. Ong, K. J. Xu, P. L. R. Ee, S. S. Zheng, J. L. Hedrick, Y. Y. Yang, *Nano Today* **2010**, *5*, 296.
- [13] Q. Yang, Z.-K. Xu, Z.-W. Dai, J.-L. Wang, M. Ulbricht, *Chem. Mater.* **2005**, *17*, 3050.
- [14] S. Azarmi, W. H. Roa, R. Löbenberg, *Adv. Drug Delivery Rev.* **2008**, *60*, 863.
- [15] B. Voit, D. Appelhans, *Macromol. Chem. Phys.* **2010**, *211*, 727.
- [16] L. L. Kiessling, L. E. Strong, J. E. Gestwicki, in *Annual Reports in Medicinal Chemistry*, Vol. 35 (Eds: W. Hagmann, A. Doherty), Academic Press, San Diego **2000**, pp. 321–330.
- [17] S. G. Spain, M. I. Gibson, N. R. Cameron, *J. Polym. Sci., Part A: Polym. Chem.* **2007**, *45*, 2059.
- [18] S. Slavin, J. Burns, D. M. Haddleton, C. R. Becer, *Eur. Polym. J.* **2011**, *47*, 435.
- [19] C. R. Becer, K. Babiuch, D. Pilz, S. Hornig, T. Heinze, M. Gottschaldt, U. S. Schubert, *Macromolecules* **2009**, *42*, 2387.
- [20] K. Babiuch, R. Wyrwa, K. Wagner, T. Seemann, S. Hoepfner, C. R. Becer, R. Linke, M. Gottschaldt, J. Weisser, M. Schnabelrauch, U. S. Schubert, *Biomacromolecules* **2011**, *12*, 681.
- [21] J. C. Wilson, M. J. Kiefel, D. I. Angus, M. von Itzstein, *Org. Lett.* **1999**, *1*, 443.
- [22] K. Babiuch, C. R. Becer, M. Gottschaldt, J. T. Delaney, J. Weisser, B. Beer, R. Wyrwa, M. Schnabelrauch, U. S. Schubert, *Macromol. Biosci.* **2011**, *11*, 535.
- [23] M. Gottschaldt, D. Koth, D. Muller, I. Klette, S. Rau, H. Gorls, B. Schafer, R. P. Baum, S. Yano, *Chem. Eur. J.* **2007**, *13*, 10273.
- [24] C. Ott, R. Hoogenboom, U. S. Schubert, *Chem. Commun.* **2008**, 3516.
- [25] H. Fessi, F. Puisieux, J. P. Devissaguet, N. Ammoury, S. Benita, *Int. J. Pharm.* **1989**, *55*, R1.
- [26] R. Labrière, R. Sicard, R. Cormier, E. Turos, L. West, *J. Controlled Release* **2010**, *148*, 234.
- [27] S. Hornig, H. Bunjes, T. Heinze, *J. Colloid Interface Sci.* **2009**, *338*, 56.
- [28] V. Lassalle, M. L. Ferreira, *Macromol. Biosci.* **2007**, *7*, 767.
- [29] S. K. Sahoo, J. Panyam, S. Prabha, V. Labhasetwar, *J. Controlled Release* **2002**, *82*, 105.
- [30] S. Zhang, J. Li, G. Lykotraftitis, G. Bao, S. Suresh, *Adv. Mater.* **2009**, *21*, 419.
- [31] H. Gao, W. Shi, L. B. Freund, *Proc. Natl. Acad. Sci. USA* **2005**, *102*, 9469.
- [32] Y. Watanabe, X. Liu, I. Shibuya, T. Akaike, *J. Biomater. Sci., Polym. Ed.* **2000**, *11*, 833.
- [33] N. Adachi, A. Maruyama, T. Ishihara, T. Akaike, *J. Biomater. Sci., Polym. Ed.* **1994**, *6*, 463.
- [34] F. Suriano, R. Pratt, J. P. K. Tan, N. Wiradharma, A. Nelson, Y.-Y. Yang, P. Dubois, J. L. Hedrick, *Biomaterials* **2010**, *31*, 2637.
- [35] S.-H. Kim, M. Goto, C.-S. Choi, T. Akaike, *Biotechnol. Lett.* **2000**, *22*, 1049.
- [36] S.-H. Kim, M. Goto, T. Akaike, *J. Biol. Chem.* **2001**, *276*, 35315.
- [37] M. G. H. Yura, H. Okazaki, K. Kobayashi, T. Akaike, *J. Biomed. Mater. Res.* **1995**, *29*, 1557.
- [38] R. Yang, F. Meng, S. Ma, F. Huang, H. Liu, Z. Zhong, *Biomacromolecules* **2011**, *12*, 3047.

Supporting Information

for *Macromol. Biosci.*, DOI: 10.1002/mabi.201200024

Uptake of Well-Defined, Highly Glycosylated, Pentafluorostyrene-Based Polymers and Nanoparticles by Human Hepatocellular Carcinoma Cells

Krzysztof Babiuch, David Pretzel, Tatiana Tolstik, Antje Vollrath, Sarmiza Stanca, Franziska Foertsch, C. Remzi Becer, Michael Gottschaldt, Christoph Biskup, Ulrich S. Schubert*

Contents:

1. Selected data of the polymer characterization
 - 1.1. ^1H NMR spectra of the homopolymers and block copolymers
 - 1.2. ^{13}C NMR spectra of the galactosylated homopolymers and block copolymers
 - 1.3. ^{19}F NMR spectra of the homopolymers and block copolymers
 - 1.4. Thermogravimetric analysis of the glucosylated materials
2. Additional SEM images of the glucosylated and galactosylated particles
3. Confirmation of the viability of HepG2 cells after incubation with water soluble polymers or polymeric particles
4. Movie composed of a stack of CLSM micrographs showing the internalization of galactosylated particles
5. Color versions of Figure 6 and 7

1. Selected data of the polymer characterization

1.1.

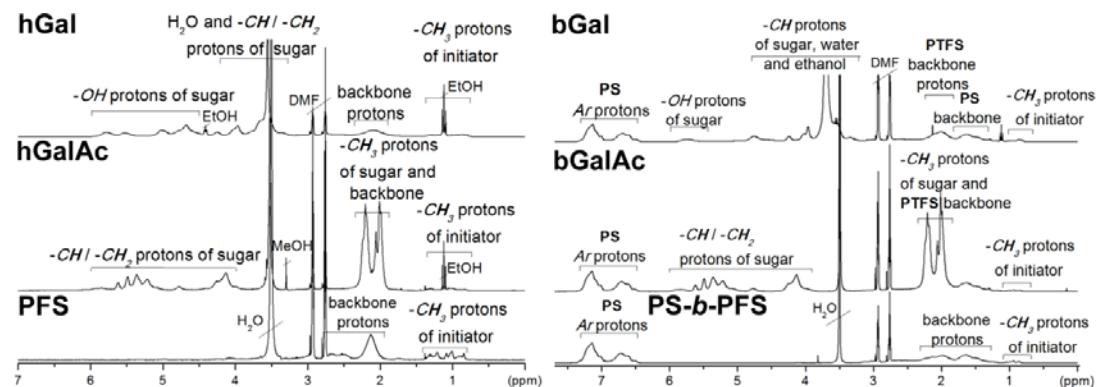


Figure S1. Details from the ^1H NMR spectra (300 MHz, DMF-d_7) of the galactosylated homopolymers (left) and the galactosylated block copolymers (right).

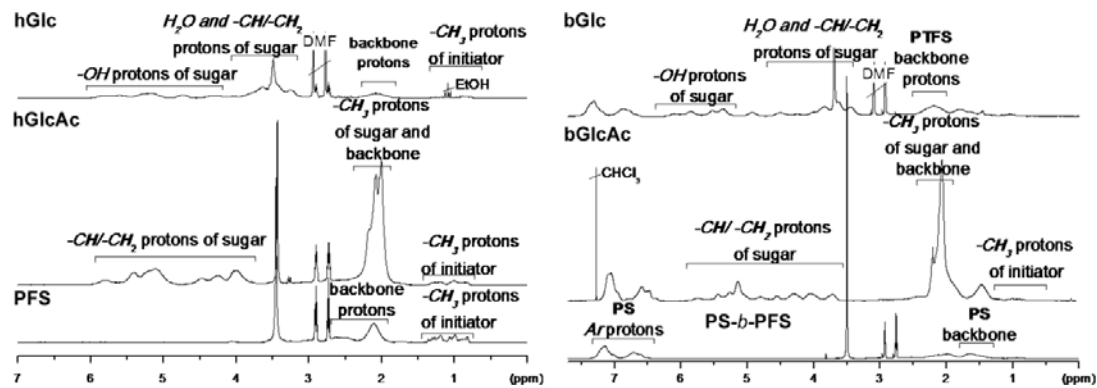


Figure S2. ^1H NMR spectra (300 MHz, DMF-d_7) of the gluco-sylated and deacetylated homopolymers (left) and block copolymers (right).

1.2.

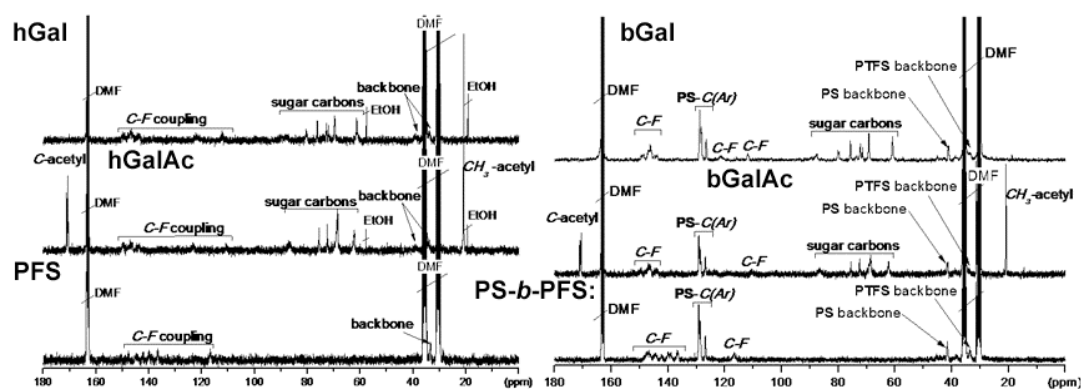


Figure S3. Details from the ^{13}C NMR spectra (300 MHz, DMF- d_7) of the galactosylated homopolymers (left) and block copolymers (right).

1.3.

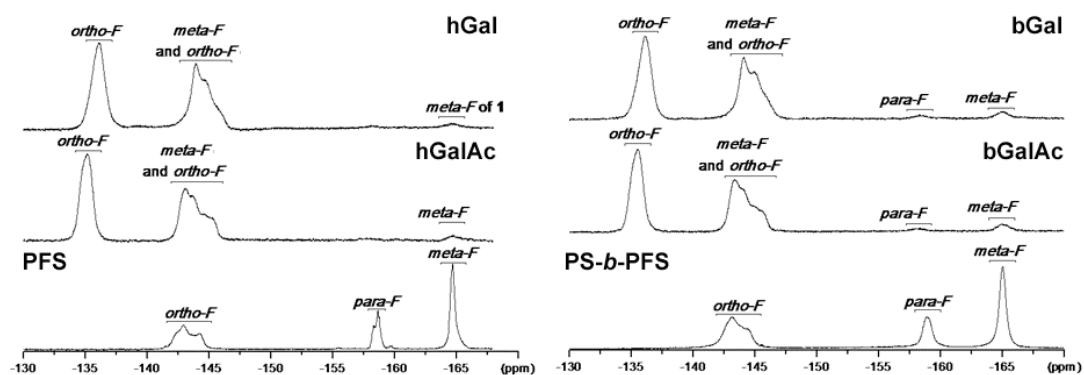


Figure S4. ^{19}F NMR spectra (200 MHz, DMF- d_7) of the galactosylated and deacetylated homopolymers (left) and block copolymers (right).

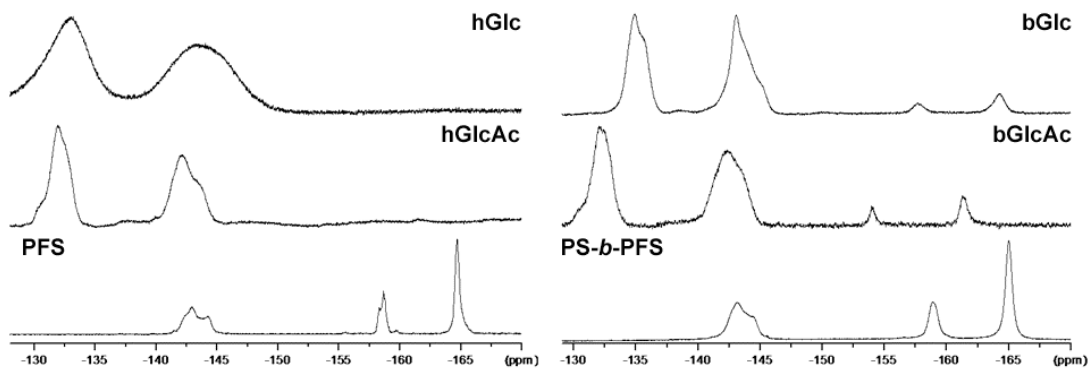


Figure S5. ^{19}F NMR spectra (200 MHz, DMF-d_7) of the glucosylated and deacetylated homopolymers (left) and block copolymers (right).

1.4.

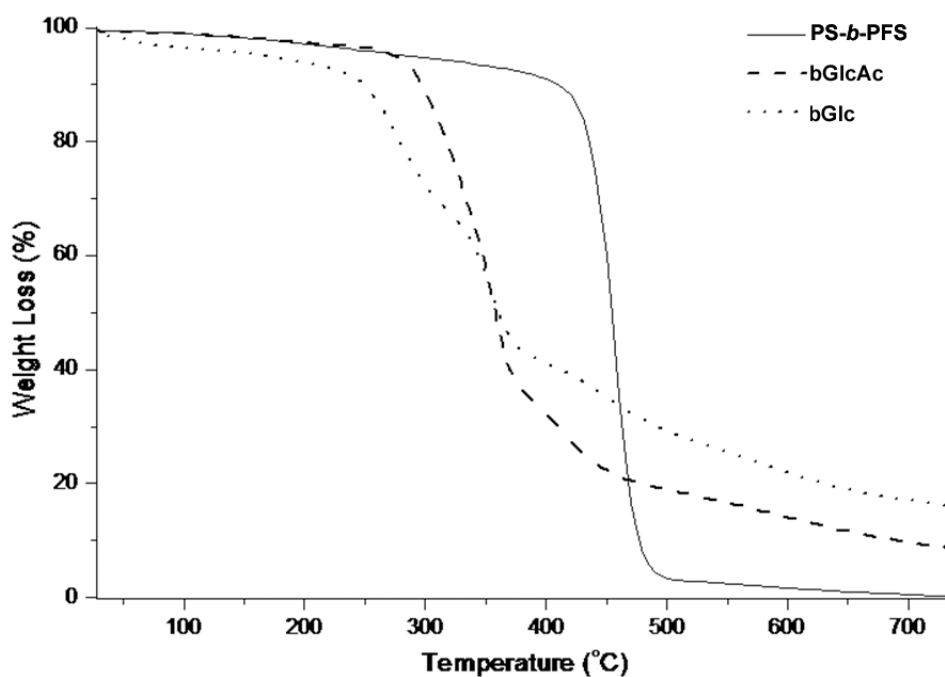


Figure S6. Thermogravimetric analysis of glucose-carrying block copolymers.

2. Additional SEM images of the obtained particles

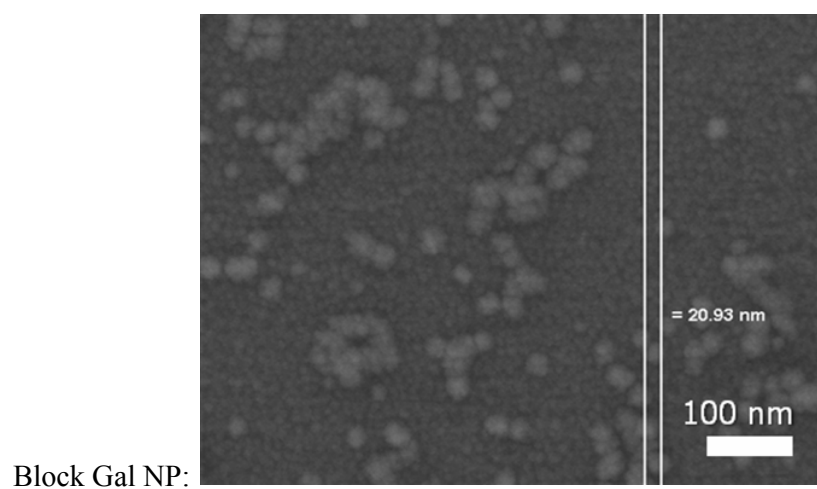
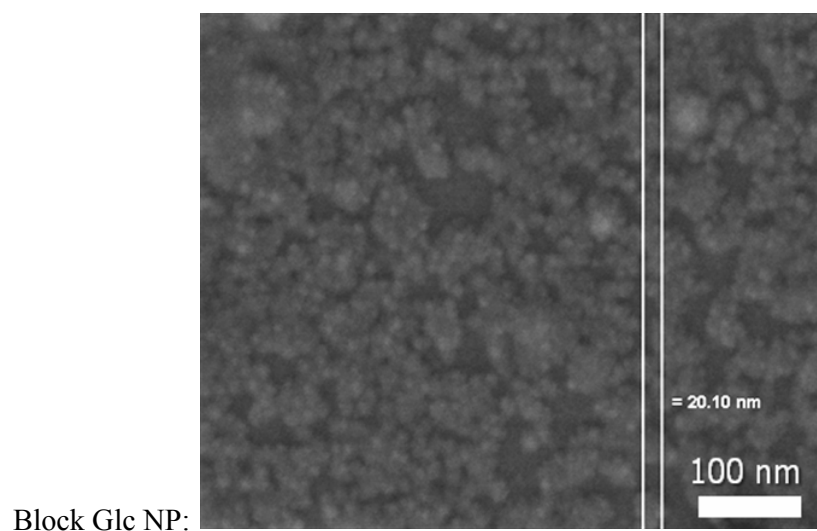


Figure S7. SEM images of the obtained nanoparticles.

3. Flow cytometric analysis of the HepG2 viability (PI exclusion)

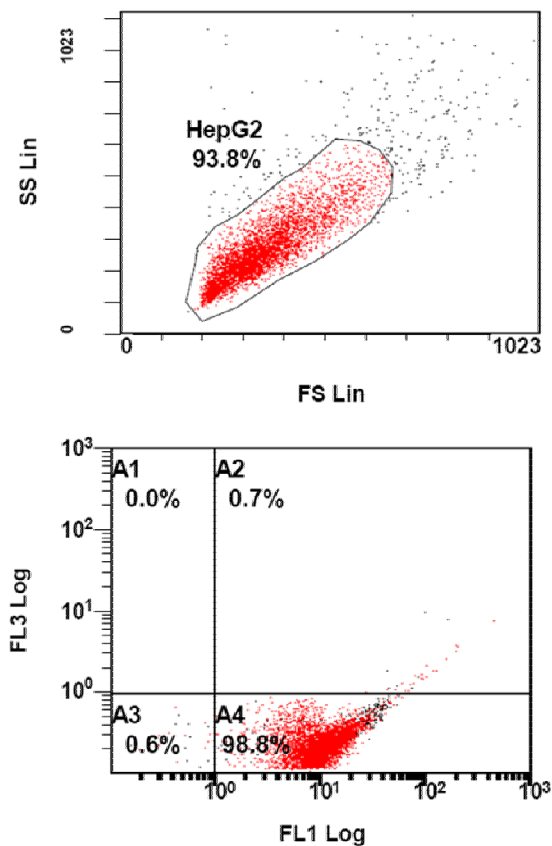


Figure S8: Flow cytometry analysis demonstrated an exclusion of propidium iodide as exemplarily shown for cells incubated with FITC labeled bGalNPs (10 $\mu\text{g}/\text{mL}$). Fluorescence channel FL1 detects the FITC labeled cells (98.8%), whereas FL3 determines dead cells after inclusion of PI staining (0.7%).

4.

Movie S1: Stack of CLSM micrographs of a cell incubated with 10 $\mu\text{g/mL}$ of polymeric nanoparticles from bGal for 24 h at 37 $^{\circ}\text{C}$. The cells were stained with wheat germ agglutinin (WGA) conjugated to Alexa Fluor 633 to mark the plasma membrane. Fluorescence originating from the labeled polymers was collected in the FITC channel and is displayed in green color, whereas fluorescence originating from the plasma membrane was collected in the Alexa 633 channel and is displayed in red color. The pinhole was adjusted such that each cross section has a thickness of 1 μm . The movie shows an overlay of both channels and starts with a confocal cross section close to the bottom of the cell. The focus is then shifted by steps of 0.5 μm to the top of the cell, and the respective cross sections are shown. The z-stack shows that almost all particles (except for those sticking to the surface of the coverslip) are located inside the cells. Only few particles are sticking to the outer surface of the membrane.

((Typesetter: Please insert movie mabi.201200024_Movie_S1.avi here))

5. Color versions of Figures 6 and 7

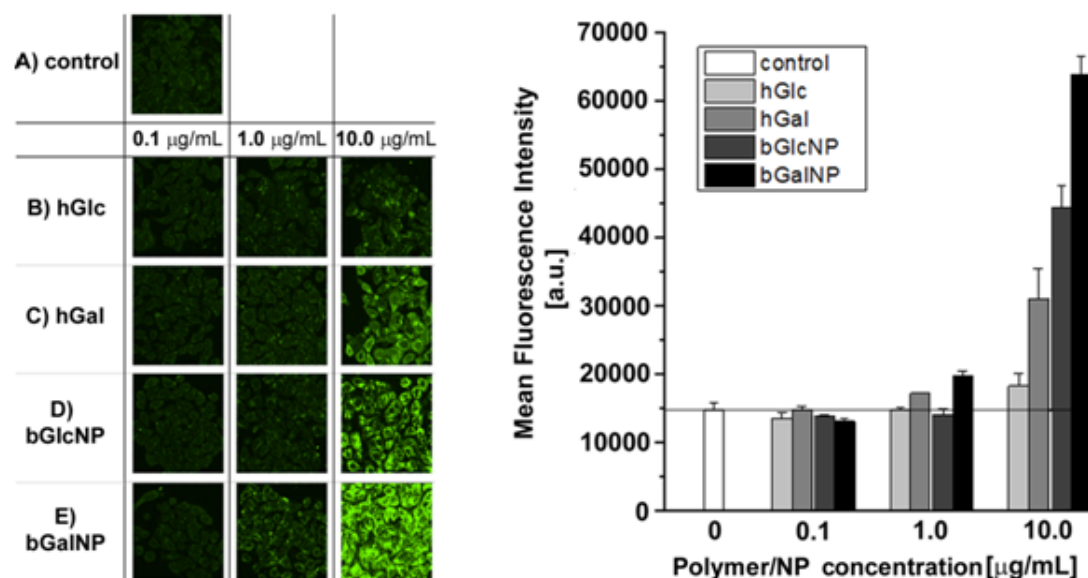


Figure S9: Color version of Figure 6.

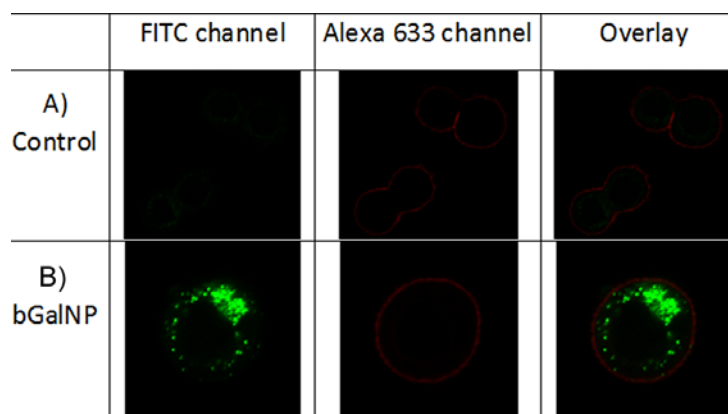


Figure S10: Color version of Figure 7.

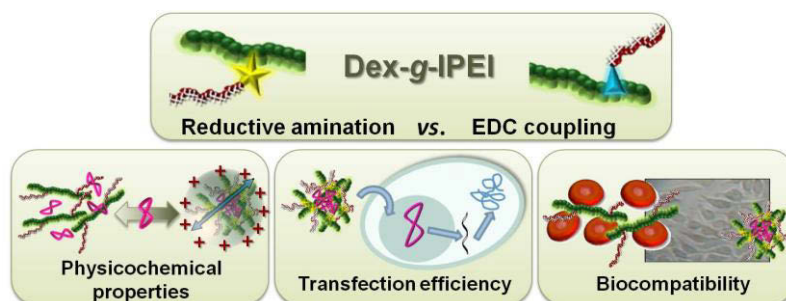
Publication 8

"Dextran-*graft*-linear poly(ethylene imine) for gene delivery – influence of linker strategies on the physicochemical and biological properties"

Sofia Ochrimenko,[#] Antje Vollrath,[#] Kristian Kempe, Lutz Tauhardt,
Stephanie Schubert, Ulrich S. Schubert, Dagmar Fischer

[#]equal contribution

Bioconjug. Chem. **2013**, submitted.



Dextran-*graft*-linear poly(ethylene imine)s for gene delivery: Influence of linking strategies on physicochemical and biological properties

Sofia Ochrimenko,^{†‡#} Antje Vollrath,^{‡#} Lutz Tauhardt,[‡] Kristian Kempe,[‡] Stephanie Schubert,^{†§} Ulrich S. Schubert,^{‡§*} Dagmar Fischer^{†§*}

Abstract

Two low molar mass linear poly(ethylene imine)s (IPEI) with 20 and 40 repeating units were synthesized by acidic hydrolysis of poly(2-ethyl-2-oxazoline) and grafted onto dextran *via* different synthesis routes aiming at the evaluation of structure-property relationships of dextran-*graft*-linear poly(ethylene imine) (dex-g-IPEI) conjugates for gene delivery applications. Using reductive amination of oxidized dextran and 1-ethyl-3-(3-dimethylamino-propyl) carbodiimide (EDC) promoted coupling of IPEI to carboxymethylated dextran resulted in various derivatives with altered linkers. Beside the molar mass of IPEIs and the linker unit, also the degree of functional groups (CHO, COOH) per anhydroglucose unit within the dextran precursors and the content of IPEI in the final polymeric vectors were varied. The synthesized dextran modifications were characterized by an enhanced complexation and stabilization of DNA against enzymatic degradation with increasing DS and molar mass of IPEI as well as with rising polymer nitrogen to DNA phosphate (N/P) ratio. All derivatives formed complexes with DNA of about 100 nm in highly purified water and revealed positive zeta potentials. The transfection efficiency of dex-g-IPEIs was increased compared to free IPEI and revealed a dependency of the used linking strategy as determined by luciferase assay using chinese hamster ovary (CHO-) K1 cells. Whereas in a cell viability assay all complexes of DNA and dex-g-IPEIs were found to be nontoxic, for free polymers the synthesis route revealed a strong impact on the aggregation of red blood cells. In conclusion, the linking strategy of IPEI to dextran has a high influence on physicochemical characteristics of DNA/polymer complexes, the biocompatibility as well as on the resulting transfection properties.

Author information

Corresponding Author

*E-mail: dagmar.fischer@uni-jena.de, ulrich.schubert@uni-jena.de

Author contributions

#These authors contributed equally.

Notes

The authors declare no competing financial interest.

Affiliation:

[†]Department of Pharmaceutical Technology, Institute of Pharmacy, Otto-Schott-Str. 41, 07745 Jena, Germany

[‡]Laboratory of Organic and Macromolecular Chemistry (IOMC), Friedrich-Schiller-University Jena, Humboldtstr. 10, 07743 Jena, Germany

[§]Jena Center for Soft Matter (JCMS), Friedrich-Schiller-University Jena, Philosophenweg 7, 07743 Jena, Germany

Submitted to:

Bioconjugate Chemistry

Address for correspondence:

*Prof. Dr. Dagmar Fischer, Department of Pharmaceutical Technology, Institute of Pharmacy, Otto-Schott-Str. 41, 07745 Jena, Germany

*Prof. Ulrich S. Schubert, Laboratory of Organic and Macromolecular Chemistry (IOMC), Friedrich-Schiller-University Jena, Humboldtstr. 10, 07743 Jena, Germany

Keywords: cationized dextran; gene delivery; polyethylenimine; non-viral vector; linking strategy

Introduction

Dextran, natural hydrophilic, biodegradable polysaccharides based of mainly α -1-6-linked D-glucose units, have widely been used in medical, pharmaceutical and drug delivery applications.¹ More than 50 years of clinical use provided an impressive proof of their safety in parenteral and oral administration, e.g. as lubricant in ophthalmic solutions, creams, and ointments or as coating material for diagnostic nanoparticles.^{2, 3} Additionally, many modern drug delivery systems containing dextran are under preclinical development, for instance bioadhesive microspheres, nanoparticles or hydrogels.⁴ In the field of gene therapy, dextran itself has not been found to be suitable as non-viral vector system due to the missing positive charge that is required for the electrostatic interaction with negatively charged nucleic acids. Consequently, several attempts have been made to selectively modify dextran to introduce cationic moieties such as diethylaminoethyl,⁵ spermine,^{6, 7} protamine,⁸ poly(L-lysine),⁹ poly(ethylene imine) (PEI)¹⁰⁻¹⁴ or 2,3-epoxypropyl-trimethylammonium chloride¹⁵ in order to improve the formation of polyelectrolyte complexes. PEI was thereby one of the most favored cationic polymers applied for conjugation to dextran owing to its excellent transfection efficiency. Several studies have evaluated dextran-*graft*-poly(ethylene imine) (dex-g-PEI) conjugates as promising gene delivery systems in recent years. Three different strategies for conjugation were followed: (i) Low molar mass dextrans (1,500 to 10,000 g · mol⁻¹) were covalently grafted onto high

molar mass PEIs (e.g. 25,000 g · mol⁻¹ branched or linear PEI) in order to mask the cationic charge of PEI, decrease its cytotoxicity and enhance the complex stability.^{10, 16} The biocompatible, uncharged dextran decreased the charge effects of salts and proteins present in the extracellular environment as also observed for stealth polymers like poly(ethylene glycol) (PEG).¹⁷ Depending on the molar mass of dextran and the degree of grafting used, transfection efficiencies of dex-g-PEI were reported to be comparable or lower than that of the unmodified high molar mass PEI. This finding was ascribed to a steric hindrance of protonation of PEI after conjugation and decreased buffering capacity dependent on the molar mass of the dextran.¹⁸ (ii) The grafting of branched PEIs (bPEI) of low molar masses (800 to 2,000 g · mol⁻¹) onto large dextran backbones (15,000 to 200,000 g · mol⁻¹) was investigated. Due to the conjugation the cytotoxicity was lower compared to high molar mass bPEI, whereas the transfection could be enhanced compared to 25,000 g · mol⁻¹ bPEI by increasing the degree of substitution (DS) of low molar mass bPEIs conjugated to dextran or the N/P ratio of DNA/dextran-g-bPEI complexes or using serum containing media.^{11, 12, 14} (iii) Dextran nanoparticles were formed by crosslinking of 40,000 g · mol⁻¹ dextran and grafted in different extents with 25,000 g · mol⁻¹ bPEI by reductive amination. In this way, the steric hindrance of the dextran molecules to form stable complexes of PEI and plasmid could be decreased and the transgene expression as well as cell viability were enhanced compared to unconjugated 25,000 g · mol⁻¹ bPEI and lipofectamine.¹⁹

Several linking strategies have been reported to covalently bind PEI to dextrans. A commonly used approach is the conjugation by primary amines, for which the following strategies were described: Tseng *et al.* synthesized cationized dextrans by conjugation of 25,000 g · mol⁻¹ PEI to oxidized 1,500 g · mol⁻¹ dextran (reductive amination) demonstrating improved complex stability, lower cytotoxicity and higher or comparable transfection efficiency than 25,000 g · mol⁻¹ PEI dependent on the DS of grafted dextran.¹⁶ This oxidation process followed by conjugation represent a convenient method to form irreversible linkages in aqueous solution, but it yields adverse products with undefined chemical structures due to the occurrence of various chain scission reactions during the oxidation reaction of dextran. To keep the dextran structure intact and avoid undesired changes of the biocompatibility, Sun *et al.* functionalized dextrans with hexamethylene diisocyanate (HMDI).¹¹ The HMDI linkage was found to be advantageous since the functionalization reaction could be conducted fast and effectively without addition of any catalyst owing to the high reactivity of the isocyanate. Furthermore, the urea and urethane bonds in the final product are hydrolytically stable. A disadvantage of this linker might be the occurrence of crosslinking as a result of the multivalence of both, dextran and bPEI. Dextran structure can also be maintained by grafting of PEI to carboxymethylated dextran (CM-dex). However, by application of this method negatively charged carboxyl groups are introduced into the molecule what might result in different properties of the polymer.¹²

Since so far the influence of the different linker strategies on biocompatibility, transgene expression and DNA binding characteristics have received only little attention, in the present study a direct comparison was performed. To this end, dextran with a molar mass of 60,000 g · mol⁻¹ typically used in medical and pharmaceutical applications, was functionalized with low molar mass PEI. In contrast to previously published studies, linear PEI (IPEI) was chosen because it could be synthesized in a controlled manner with low molar mass distributions and well-defined structures as well as with tailored end groups.^{20, 21} Two well-defined IPEIs with molar masses of 860 g · mol⁻¹ and 1,720 g · mol⁻¹, consistent with 20 (IPEI₂₀) and 40 repeating units (IPEI₄₀), respectively, were synthesized and subsequently grafted onto different dextran-precursors, namely dextran aldehyde (CHO-dex), carboxymethylated dextran (CM-dex), and 4-nitrophenyl carbonate-substituted dextran (NPCF-dex). The degree of the functional groups (CHO, COOH) per anhydroglucose unit (AGU) of dextran as well as the DS and molar mass of conjugated IPEI were varied. Subsequently, the influence of the type of linkage, the DS and the molar mass of IPEI of the various dex-g-PEI conjugates was examined regarding the interaction with DNA, the complex formation and the cell- and hemocompatibility as well as transgene expression.

Materials and Methods: see supporting information

Results and discussion

Synthesis of dextran-graft-poly(ethylene imine) polymers

To create a library of various dextran-graft-linear poly(ethylene imine)s (dex-g-IPEI), which enables the analysis of structure-property relationships, diverse dex-g-IPEIs copolymers were synthesized containing different dextran-precursors with varying linkers as well as type and degree of functional groups. In detail, three synthesis strategies were utilized to graft IPEIs to dextran: (i) Reductive amination of aldehyde functionalized dextran (CHO-dex), (ii) EDC promoted coupling of IPEI to carboxymethylated dextran (CM-dex), and (iii) carbamate formation *via* reaction of 4-nitrophenyl carbonate-substituted dextran (NPC-dex) with IPEI (**Scheme 1**).^{7, 12, 22} The reductive amination method was selected since it is known as very efficient conjugation technique and provides the benefit that no coupling agents are required. By application of the coupling reaction with EDC, dextran remains non-oxidized and adverse side-reactions which appear by the oxidation of dextran do not occur. Due to the beneficial fact that 4-nitrophenyl carbonate-substituted dextran reacts with amines without any coupling agent or catalysts and introduces no additional functional groups or structural changes to the dextran backbone during the reaction, this conjugation method was selected as third synthesis route. In preliminary studies (data not shown) these synthesis routes were examined with regard to their capability to enable a straightforward reaction of the primary amino functionality of

IPEI with the respective active groups introduced to dextran. It was found that the reductive amination and the EDC coupling are well-suited techniques for the synthesis of various dex-g-IPEIs. Contrary, the carbamate formation method was not qualified as adverse crosslinking occurred during reaction of 4-nitrophenyl carbonate-activated dextran with IPEIs resulting in insoluble products for higher DS (data not shown).

To evaluate the influence of the linker unit, but also of the DS and molar mass of IPEI, various IPEIs were reacted in various ratios with dextran-precursors. To this end, well-defined, proton initiated poly(2-ethyl-2-oxazoline)s (PEtOx) were synthesized and subsequently hydrolyzed to IPEI under acidic conditions (**Scheme S1**). LPEIs with a molar mass of $M_n = 860 \text{ g} \cdot \text{mol}^{-1}$ (IPEI₂₀) and $1,720 \text{ g} \cdot \text{mol}^{-1}$ (IPEI₄₀) were obtained, which both carried an active primary amino group at one polymer chain end that was utilized for subsequent conjugation to the dextran (**Table S1, Scheme S1**). A detailed characterization of the LPEIs is published elsewhere.^{20, 21}

Reductive amination

For the attachment of IPEI to dextran *via* reductive amination, CHO-dextran precursors were prepared by oxidation of $60,000 \text{ g} \cdot \text{mol}^{-1}$ pharmaceutical grade dextran from *Leuconostoc mesenteroides* ($M_w = 65,900 \text{ g} \cdot \text{mol}^{-1}$) with potassium periodate (KIO₄). The molar mass of $60,000 \text{ g} \cdot \text{mol}^{-1}$ was selected, since it was most frequently applied in previous studies as well as in preclinical and clinical applications.^{2, 12} For the oxidation, two different ratios of KIO₄ per anhydroglucose unit (AGU) (1:3 and 1:10, respectively) were chosen to react with dextran. The final degree of oxidation (degree of aldehyde groups per AGU) of the products (after purification by dialysis against water at 25 °C) was determined to be 0.51 (**CHO-dex_{0.5}**) and 1.09 (**CHO-dex_{1.0}**), as examined by hydroxylamine chloride titration according to Zhao *et al.*, 1991.²³ Further investigations by SEC exhibited a slight decrease in the molar mass due to chain degradation. In comparison to unmodified dextran, the oxidized CHO-dex samples revealed molar masses with $M_w = 55,100 \text{ g} \cdot \text{mol}^{-1}$ for **CHO-dex_{0.5}** and $M_w = 52,500 \text{ g} \cdot \text{mol}^{-1}$ for **CHO-dex_{1.1}**, respectively (**Table S2**). As expected, the final molar mass was thereby influenced by the amount of KIO₄ used for the oxidation. With increasing amount of KIO₄ applied per AGU, the degree of oxidation also increased, whereas the molar mass of the dextran decreased due to few unavoidable chain scissions. The final products were further characterized by ¹H NMR spectroscopy and elemental analysis (**Table S2, Figure S3**). In the ¹H NMR spectra, the signals at 3.4 ppm to 4.1 ppm can be assigned to the protons of the AGU, and the peak at 5.2 ppm to 5.3 ppm is attributed to the anomeric proton (**Figure S3**). Additionally, the ¹H NMR spectra showed several distinctive signals in the region of 4.0 ppm to 6.0 ppm that were not present in the original dextran ¹H NMR spectrum indicating the structural changes due to the oxidation reaction (hints for different C-C bond breaking reactions as well as the formation of various hemiacetals).²⁴⁻²⁶

Subsequently, the two aldehyde containing precursors were converted each with **IPEI₂₀** and **IPEI₄₀** by reductive amination reaction in water at a temperature of 60 °C (**Scheme 1A**). To reduce aminolysis side reactions caused by a fast conjugation rate, the pH value of the IPEI solution was adjusted to pH 6, which additionally improved the solubility of the IPEI. The DS of conjugated IPEIs per AGU was aimed to be highest 0.5 and, thus, the molar ratio of NH₂-IPEI to CHO was set to 1:2 for the higher oxidized sample **CHO-dex_{1.0}** and 1:1 for the lower oxidized dextran **CHO-dex_{0.5}**. After subsequent reduction with sodium borohydride (NaBH₄), all obtained dex-g-IPEIs (**A series, A1-A4**) were purified by extensive dialysis against water at 60 °C, lyophilized and investigated by ¹H NMR spectroscopy, elemental analysis as well as SEC measurements (**Table S3, Figure S4**). In the ¹H NMR spectra, the signals of the CHO-dex samples are still detectable (protons of AGU = 3.4 ppm – 4.1 ppm; anomeric proton = 5.2 ppm – 5.3 ppm). The additional peaks at 3.1 ppm to 3.3 ppm corresponds to the protons of the IPEI backbone and confirms the successful covalent conjugation of the IPEI to the CHO-dex. Furthermore various DS of IPEI per AGU were obtained with values between DS = 0.13 to 0.38 as calculated from the nitrogen content found in the elemental analysis (**Table 1**). SEC measurements showed an increasing molar mass of the synthesized CHO-dex-g-IPEIs with increasing DS of IPEI. The molar mass ranged from $M_w = 24,000 \text{ g} \cdot \text{mol}^{-1}$ for CHO_{0.5}-dex-g-IPEI₂₀ up to $M_w = 36,500 \text{ g} \cdot \text{mol}^{-1}$ for the CHO_{1.0}-dex-g-IPEI₄₀ (**SI, Table S3**). However, these results are not reliable as a result of the dramatic rise in charge density of the polymers, which leads to a considerable change in the elution behavior from the column.

EDC coupling

For the second synthetic strategy, carboxylic moieties, which are able to react with the primary amino groups of the IPEIs, were introduced in the $60,000 \text{ g} \cdot \text{mol}^{-1}$ dextran backbone by carboxymethylation. The derivatization of dextran to CM-dex was performed using monochloroacetic acid (MCA) under basic conditions according to literature.^{12, 27} In order to obtain different CM-dex precursors with varying DS of carboxylic groups, the ratios of the reagents (dextran-AGU:MCA:NaOH = 2.2:1:1 or 1:5:10) as well as the reaction times (90 or 300 min) were altered. After purification by dialysis against water at 25 °C, the lyophilized samples were characterized with regard to their content of the carboxymethyl groups according to a HPLC procedure described by Heinze *et al.*^{28, 29} Three degrees of carboxymethyl functionalization per AGU were found, namely 0.32 (**CM_{0.3}-dex**), 0.54 (**CM_{0.5}-dex**), and 1.60 (**CM_{1.6}-dex**) (**Table S4**). Furthermore, all CM-dex samples were characterized by SEC and ¹H NMR spectroscopy measurements (**Table S4, Figure S5**). The ¹H NMR spectra (600 MHz, D₂O) of the products showed the expected methylene peak of the carboxymethyl group in the CM-dex at 4.1 ppm to 4.3 ppm, and the proton signals of the AGU (3.4 ppm – 4.1 ppm) as well as the anomeric proton peak at

5.2 ppm to 5.3 ppm. SEC data revealed increasing molar masses with increasing attachment of the carboxymethyl groups, ranging from $M_w = 51,100 \text{ g} \cdot \text{mol}^{-1}$ for **CM_{0.3}-dex** up to $60,100 \text{ g} \cdot \text{mol}^{-1}$ for **CM_{1.6}-dex**.

The subsequent grafting of IPEI₂₀ and IPEI₄₀ to the various CM-dex samples was performed in water in the presence of *N*-hydroxysulfosuccinimide (sulfo-NHS, Sigma Aldrich) and EDC (Sigma Aldrich). Both reagents are frequently used in peptide chemistry and assure efficient coupling reactions.¹² Similar to the reductive amination, several CM-dex-*g*-IPEIs with altered DS were targeted. Both **CM-dex_{0.3}** and **CM-dex_{0.5}** were allowed to react with a slight excess of IPEI (COOH:NH₂ = 1:1.2), whereas the COOH:NH₂ ratio was reduced to 3:1 for **CM-dex_{1.6}**. After purification by extensive dialysis against water at 60 °C and lyophilization, the products (**B series, B1-B6**) were characterized by ¹H NMR spectroscopy, SEC and elemental analysis measurements. In agreement with the literature data, the chemical shifts of the protons of the IPEI backbone are detected at 3.1 to 3.3 ppm confirming the successful binding of the IPEIs to the CM-dextrans.^{12, 30} The resulting DS of IPEI per AGU was as well as the reductive amination samples calculated from the nitrogen content obtained by the elemental analysis and found to be in the range between 0.06 to 0.18 (**Table 1**). Furthermore, SEC analysis revealed a change in the elution volume with increasing chain length and DS of IPEI, indicating an increase of molar mass due to attachment of the IPEIs to the CM-dex. Like the results of the **A series**, the molar mass values presented are not absolute values due to the drastic difference in the charge density of the polymers that lead to an unpredictable elution behavior from the column.

By comparing the strategies applied for the grafting of IPEI to dextran, it is apparent that both ways enabled the synthesis of various dex-*g*-IPEIs with different DS of IPEI in a straightforward manner. Although the reductive amination method reached considerably higher DS values, this technique has the drawback that the required oxidization of dextran led to ring opening reactions of the glucose, chain degradation and other adverse side-reactions, which resulted in hardly predictable chemical structures and biophysicochemical characteristics. In contrast, during dextran activation *via* carboxymethylation the glucose units of the dextran kept their ring structure and no chain degradation occurred. However, dex-*g*-IPEIs prepared by EDC coupling additionally contained carboxylic acid functionalities (COOH) in the dextran backbone, which resulted in polyelectrolyte structures including both cationic and anionic charges that might influence the physicochemical and the biological properties as well.

Binding and protection of DNA

Based on electrostatic interactions between the cationic carrier material and the anionic DNA, nanoassemblies can be formed spontaneously by masking the anionic charge of the DNA. This is necessary to protect DNA against enzymatic digestion as

well as to enable cell uptake. To study the DNA binding properties, complexes of modified dextrans were formed with herring testes DNA as model DNA³¹ applying different N/P ratios (0.5 to 40) and analyzed by agarose gel electrophoresis (**Figure S7**, the N/P ratios of 0.5 to 10 are shown). The analysis of the free DNA as control (left lane of each gel), which was detected by ethidium bromide intercalation, revealed a broad fluorescent band corresponding to its broad molar mass distribution. Free polymers were used as controls (data not shown) to exclude unspecific interactions between polymer and dye and exhibited no signal. Free 60,000 $\text{g} \cdot \text{mol}^{-1}$ dextran was not able to interact with DNA due to the missing charge since the bands showed the same signal as the DNA control (data not shown).

All cationic dextrans spontaneously formed interpolyelectrolyte complexes with the DNA as a result of cooperative electrostatic interactions depending on the N/P ratio. As the cationic dextran concentration increased, the amount of DNA migrating into the gel with unchanged electrophoretic mobility decreased indicating that the complexes were larger in size and/or less negatively charged than free DNA. The influence of the N/P ratio on the stability and complex size has been described by several authors for many cationic polymers.^{31, 32} Anyway, it was explored that all dex-*g*-IPEIs prepared by reductive amination (**A1-A4**) fully complexed herring testes DNA already at a N/P ratio of 1 (**Figure S7**) indicating charge balance. The complexation was found to be slightly increased with higher molar mass of IPEI coupled to CHO-*g*-dex. Comparable observations were reported for low molar mass branched PEI conjugated to 15 and 100 to 200 kDa dextran where the increase of molar mass branched PEI resulted in a higher binding capacity independent of the degree of grafting.¹⁴ For comparison, both linear PEIs (20 and 40 monomers) also fully retarded the DNA at a N/P ratio 1 in accordance with the data of Lungwitz *et al.*³² Furthermore, dex-*g*-IPEIs prepared by EDC coupling (**B1-B4**) were found to completely retard DNA migration into the gel at a N/P ratio 2, which indicates a weaker complexation ability than free IPEIs and CHO-dex-*g*-IPEI samples. This may be attributed to the lower nitrogen content and to the presence of the anionic charges that could interfere with IPEI and, therefore, might decrease the interactions with DNA. This assumption is supported by polymer **B5**, which contained the highest number of anionic charges and demonstrated the lowest interaction with DNA with a total complexation earliest at a N/P ratio 5. The negative “charge effect” on DNA binding can be balanced by a higher DS and molar mass of IPEI grafted on the CM-dex backbone as demonstrated for sample **B6**. It was characterized by the highest nitrogen content in the B series and complexed DNA already at a N/P ratio 1. Again a slight trend to higher compaction with increasing the molar mass of IPEI could be observed. Sun *et al.* reported comparable effects with an improved binding capability of CMD-*g*-PEI to DNA with increasing DS for 800 $\text{g} \cdot \text{mol}^{-1}$ bPEI grafted to 60,000 to 90,000 $\text{g} \cdot \text{mol}^{-1}$ dextran.¹²

Compaction of plasmid DNA (pDNA) by cationized dextrans should substantially hinder the access of enzymes to the pDNA by physical or electrostatic barriers and, thus, increase the stability.¹⁹ To study the integrity of pDNA after enzymatic treatment by gel electrophoresis (**Figure 1**), pDNA/cationized dextran complexes of different N/P ratios were treated with DNase I for 45 min. After inactivation of the enzyme by heat and release of the plasmid by dissociation of the complex using dextran sulfate, free pDNA was detected on agarose gels. Intact plasmid revealed two major fluorescent bands corresponding to the supercoiled and open circular form (**Figure 1 a-c**, lane 1, “untreated”). Free plasmid was rapidly degraded after DNase I incubation at 37 °C already after 5 min (data not shown). Thus, the characteristic bands disappeared due to degradation to lower molar mass products (**Figure 1 a-c**, lane 3, “DNase I”). Plasmid treated by the same procedure but without enzyme remained stable and served as control to exclude nonspecific degradation (**Figure 1 a-c**, lane 2, “treated”).

Although a full pDNA complexation by cationic dextrans already occurred at low N/P ratios, higher N/P ratios were selected for physicochemical analysis based on later transfection results. The results of the stability assay indicated that the efficiency to stabilize DNA by electrostatic interactions was increased with increasing N/P ratio of complexes, higher molar masses and DS of IPEI. The trend to a higher protection of plasmid against enzymatic degradation by complexes of N/P ratio 50 compared to that with N/P ratio 25 could be shown for IPEI and all dex-g-IPEI derivatives independent of the type of linker. The stabilization of plasmids against enzymatic and mechanical destruction with increasing amount of the cationic component was described for many different polycations and correlated to a higher compaction of DNA.³¹ For free IPEI, a molar mass dependent interaction with pDNA could be observed (**Figure 1**, lanes 8 and 10). The higher the molar mass of free IPEI, the more effective was the stabilizing effect of the complex. This effect could also be observed for the dex-g-IPEIs, but was more pronounced for the copolymers than for the free IPEIs. In particular, at N/P ratio 25 the stability increased with rising molar mass which might be related to the increase in charge density within the macromolecules.

In the **A series** the stabilization effect was most obvious for **A1** and **A3** since they revealed at a N/P ratio 25 a different pattern of DNA bands than the other CHO-dex-g-PEI complexes. Changes in the topology of the plasmids were observed as reported in many other studies, e.g. after enzymatic treatment of DNA complexes with PEI derivatives or poly(diallyldimethylammonium chloride).^{31, 33} **A2** and **A4** (both conjugated with IPEI₄₀) protected the plasmid better than their IPEI₂₀ counterparts, since at N/P ratio 25 no degradation product was visible and just a weak fluorescent band between the expected supercoiled and the open circular band appeared (**Figure 1 a** lanes 8 and 10). At N/P ratio 50 for both conjugates even a low fluorescent supercoiled plasmid band is still visible (**Figure 1 a**, lanes 9 and 11). The CM-dex-g-IPEIs

protected the plasmid against enzymatic degradation in an IPEI molar mass dependent matter as well. The conjugates with IPEI₂₀ (**B1**, **B3** and **B5**) were not able to protect the pDNA as good as their IPEI₄₀ counterparts. **B1** with the lowest DS of IPEI and, thus, the lowest nitrogen content demonstrated at N/P ratio 25 a high plasmid damaging effect. In contrast for **B2** and **B4**, both substituted with IPEI₄₀, a certain amount of supercoiled plasmid could be conserved. In accordance to the finding of the low DNA binding efficiency described above, **B5** was not able to stabilize plasmid DNA even at N/P ratio 50, whereas for **B6** characterized by a higher percentage of nitrogen a protective effect could be observed.

Comparing the polymers with the aspect of two different linker strategies, for both series a stabilization of plasmid could be obtained depending on the molar mass of IPEI and the N/P ratio of the complexes. In contrast to the **B series**, all conjugates of the **A series** were able to achieve a certain protection at the chosen N/P ratios. This might be attributed to the higher DS of the IPEIs (0.13 to 0.38). Additionally, as also observed in the binding study above, the negative charges of the **B series** might hinder the interaction with pDNA and, consequently, its tight compaction. In the literature, crosslinked dextran nanoparticles were conjugated to bPEI and the DNA was shielded against DNase I for at least 2 h of treatment. This was observable for one of the conjugates with a medium percentage of grafting (7%) of the dextran onto bPEI.¹⁹ Likewise, dextran-spermine protected plasmid against enzymatic digestion just in a certain way that only a slight decreased fluorescence of the plasmid band was observable. Unfortunately, the plasmid was not released from the complex after stopping the DNase I incubation and, hence, the integrity of the plasmid was not shown.³⁴ Therefore, it can be concluded that neutral and negatively charged polymers conjugated to positively charged polymers are able to shield complexed nucleotides against nucleases. For the combination of negatively and positively charged copolymers a certain content of polycation is required for protection of the complexed pDNA.

Size and zeta potential of complexes

The efficiency of the dex-g-IPEI-mediated cellular DNA delivery will also be determined by the size and the surface charge of the complexes formed, because both might be one of the limits for an adequate cellular uptake. A positive surface charge represents a prerequisite to stabilize the included nucleic acid against enzymatic degradation in small sized complexes, which are able to interact with the negatively charged cell membrane for an effective endocytosis into cellular compartments.³⁵ Complexes were prepared with two different N/P ratios (25 and 50) in bidistilled water and studied by laser light scattering with regard to the effect of the functional groups (CH₂OH, COOH) on the final size and surface charge without any influence of the ionic strength of the solvent.

All dex-g-IPEI/pDNA assemblies revealed sizes in water in the range of 70 to 113 nm with monomodal size distributions (polydispersity indices (PDI) 0.13 to 0.31, data not shown) (**Figure 2 a**), which were comparable to the sizes obtained for the DNA complexes with IPEI₂₀ and IPEI₄₀. Since an excess of polymer was used, no major differences could be observed between N/P ratio 25 and 50. For polymer **B5**, a relatively high hydrodynamic diameter of 113 nm could be measured at N/P ratio 50. The insufficient DNA binding and stabilization of DNA by **B5** observed in the electrophoresis experiments correlated with a lower DNA compaction, and consequently, higher complex size. A similar trend could be observed for **B1** at N/P ratio 25 (hydrodynamic diameter = 110 nm).

Moreover, all complexes were positively charged with zeta potentials between +15 and +35 mV due to the excess of the cationic component with comparable results for N/P ratios 25 and 50 (**Figure 2 b**). This finding was in accordance with the results of Jiang *et al.* and Tseng *et al.*^{14, 16}

In the **A series**, an increase of zeta potential with higher molar mass of IPEI could be detected, which correlated well with the observations of the enzymatic stability testing. In the **B series** for **B1-B4** nearly comparable surface charges were measured for the polymers except for **B1** with lower zeta potentials of 20.7 and 19.8 mV at N/P ratio 25 and 50, respectively. Polymer **B5** reached also only a zeta potential of 20 mV at N/P ratio 50. The low zeta potentials of **B1** and **B5** correlated with the large particle sizes ascribed above and supported the hypothesis of an incomplete DNA compaction. Compared to the free IPEIs, the zeta potential of the dex-g-IPEIs decreased when IPEI was covalently attached to dextran, which can be explained by the shielding effect of the dextran backbone and was also observed for other dextran-PEI conjugations in earlier studies.^{16, 19}

Additionally, complexes were prepared in 50 mM NaCl solution at pH 7.4 (data not shown). All complexes of the **A series** prepared with N/P ratio 25 tended to aggregate in 50 mM NaCl solution as indicated by formation of complexes with hydrodynamic diameters larger than 800 nm with broad and multimodal size distributions. Such large assemblies were also reported earlier.^{12, 36} In contrast, at N/P 50 smaller sized complexes were obtained with diameters of about 170 to 320 nm due a more intense compaction of the plasmid by the modified dextrans. In comparison to free IPEI_{20/40}, pDNA complexes with CHO-dex conjugated IPEIs revealed a decrease in complex size, thus demonstrating a positive impact of dextran on the complex formation. Measurements of complexes of the **B series** with pDNA in 50 mM NaCl did not lead to evaluable results due to strong aggregation, forming complexes larger 1 µm with multimodal size distributions (data not shown).

Transfection mediated by pDNA/dex-g-IPEI complexes

CHO-K1 cells were transfected with complexes of the cationized dextrans and the plasmid pGL3 at different N/P ratios for 4 h. Based on preliminary experiments, N/P

ratios 25 and 50 were found to be suitable and were selected for the following experiments. Luciferase expression was presented by normalizing the measured relative light units (RLU) to the total protein mass of the cells per culture well. For all tested samples cytotoxicity-related effects as the reason for the declining transfection efficiencies were unlikely, since the protein concentrations in cell lysates (determined by a BCA assay), an indicator for cell growth, when treated with the different polymers were very similar (data not shown). Free plasmid itself revealed only a limited ability to transfect cells. Unmodified 60,000 g · mol⁻¹ dextran was tested in concentrations up to 25 µg · µg⁻¹ pGL3 plasmid in a preliminary study and failed to produce any detectable level of transgene expression (data not shown). Also IPEI₂₀ and IPEI₄₀, which were found before to be too small to form small and fully stabilized complexes, were characterized by a low transgene expression. The dependency of the transfection efficiency on the molar mass could slightly be observed at N/P ratio 25 and 50 as described before.³⁷

The transfection efficiency obtained for the samples prepared by reductive amination (**A1-A4**) was higher than for the corresponding free IPEIs, but lower than for the cationized dextrans prepared by EDC coupling (**B1-B4**), which demonstrated the highest activity (**Figure 3**). The covalent binding of the IPEIs to the dextran backbone may increase the cationic charge density and, conclusively, the electrostatic interaction with and protection of pDNA (as seen in the stability tests). As observed before in the physicochemical characterization, for the CHO-dex-g-IPEI polymer the transgene expression increased with higher molar mass of the IPEIs and N/P ratio. Similar results were reported by Jiang *et al.*¹⁴ For the CM-dex-g-IPEIs the transfection rate increased from **B1** to **B3** at a N/P ratio 25, whereas for **B4** a decrease could be observed (**Figure 3 a**). It has to be highlighted that **B1**, **B3** and **B4** at N/P ratio 50 (1.8 to 2.3 · 10⁶ RLU/µg protein, **Figure 3 b**) showed transfer efficiencies that were comparable to that of a commercially available linear 2,500 g · mol⁻¹ PEI at N/P ratio 25 (2.55 · 10⁶ RLU/µg protein, data not shown). A similar effect could be observed earlier for CM-dex-PEIs.¹² Unexpected was the observation of transfection by the CM-dex-g-IPEI₄₀ conjugates. It was estimated that **B2** and **B4** would induce higher transfection rates than **B1** and **B3**, as it is known from the higher molar mass dex-g-bPEI conjugates¹⁴ and what was also shown by the **A series**. But a contrary effect was revealed for **B4** at N/P ratio 25 and **B2** at N/P ratio 50, since an approximately 1/3 lower transfection could be observed compared to their IPEI₂₀ counterparts. This could be due to higher interactions between the longer IPEI chain and COOH groups of the CM-dex than with the pDNA. From the results shown in **Figure 3**, it can be concluded that **B3** provides the best gene delivery properties in this study at both N/P ratios, what might be related to the ratio of cationic charges to anionic charges per monomer (**Table 1**). Additionally, the lower efficiency of the dextrans of the **A series** may be attributed to the higher DNA complexation efficiency of the polymer and, therefore, lower ability to

release pDNA from the complexes compared to the polymers of the **B series** as shown by the electrophoresis assays. Dissociation of DNA from the complexes is one of the critical steps in the biological process, since only released and intact DNA can be transcribed. The observed trends are in line with the results of the physicochemical experiments: As uptake of complexes into cells imposes certain size and stability requirements on the endocytosed material, it is necessary for a successful gene transfer that the cation in polyplexes not only bind DNA, but also compact it. Since the condensation of DNA is also known to protect the genetic material from enzymatic degradation,³⁸ the decrease of transfection ability of the complexes formed by polymers **B5** and **B6** could result from the insufficient interactions with pDNA based on the highest number of anionic charges.

***In vitro* biocompatibility testing**

Biocompatibility testing has been performed with respect to cyto- and hemotoxicity. The *in vitro* cytotoxicity of the non-viral vectors was evaluated by the 3-(4,5-Dimethylthiazol-2-yl)-2,5-diphenyltetrazolium bromide (MTT) assay representing the metabolic activity of cells (**Figure 4**). L929 mouse fibroblasts were selected since they were recommended as target cells for *in vitro* toxicity testing by many standard institutions.³⁹ The same conditions as in the transfection experiments were used. Independent of the N/P ratio (N/P 25 and 50), complexes with the two linear PEIs did not cause any cytotoxic effect, which is supported by results from earlier studies demonstrating the low cytotoxicity of complexes formed with low molar mass IPEIs.^{37, 40, 41} Taking the DIN ISO 10993-5 guideline³⁹ into consideration which defines a reduction of cell viability lower than 30% as nontoxic, all tested dex-g-IPEI/DNA complexes were found to be highly compatible (84 to 110%) at N/P ratios 25 and 50 under the transfection conditions applied. The compatibility was thereby independent of the linker technique, the DS and the selected N/P ratios (**Figure 4**). For comparison, the positive control thiomersal solution (0.02%) reduced the mean cell viability to 0.6% (data not shown). Consequently, cytotoxic effects could be excluded for the variations in transfection efficiency which were described above. The results of the MTT assay correlated well with the observation of the BCA assay (data not shown) in the transfection experiments. Similar results were reported in earlier studies as well.^{12, 14}

Furthermore, the compatibility of non-viral vectors with blood indicates their suitability for administration directly into the systemic circulation. The hemolytic behavior of the free polymers was tested as worst case scenario and classified according to the ASTM F756-08 standard (data not shown).⁴² According to this standard, neither free IPEIs nor dex-g-IPEIs did show any detectable disturbance of the red blood cell membranes (hemolysis < 2%) up to 1 mg · mL⁻¹ under the chosen conditions. In agreement with the results of Moreau *et al.*, the observed behavior was attributed to the low DS and the low molar mass of the cationic polymers.⁴³ For comparison

dextran itself showed up to 16 mg · mL⁻¹ with 0.2% hemolytic activity no erythrocyte membrane disturbance.⁴⁴ Conclusively, under the chosen conditions no polymer structure related differences could be detected concerning the hemolytic potential of the cationic dextrans and were comparable to the negative control (RBC in PBS buffer, 0% hemolysis).

To avoid clinical complications like thrombosis and embolism by systemic use of the dextran-based vectors, their potential to aggregate red blood cells was investigated by qualitative light microscopy (**Figure 5 a-b**) and classified into three stages (**Figure 5 b**) as well as quantitatively by UV-Vis spectroscopy (**Figure 5 c**). Both methods gave comparable results and displayed a concentration-dependent red blood cell aggregation behavior of the polymers up to 50 µg · mL⁻¹. Applying the three stage classification system as described in the supporting information, in microscopic experiments the negative control did not show any signs of cluster formation (stage 1), whereas the positive control (25,000 g · mol⁻¹ bPEI, 15 µg · mL⁻¹) caused the formation of large aggregates (stage 3) as described before (**Figure 5a**).⁴⁵ Additionally, the $\Delta\text{Abs}_{\text{max}}$ value was introduced, meaning the difference of the highest reduction in absorbance to the negative control absorbance. Correspondingly to the microscopic data, the highest $\Delta\text{Abs}_{\text{max}}$ value (0.12) was calculated for 25,000 g · mol⁻¹ bPEI as positive control attributed to the formation of large clusters (**Figure 5 c**). In contrast to the high molar mass bPEI, IPEI₂₀ was well tolerated and classified as stage 1 ($\Delta\text{Abs}_{\text{max}} = 0.026$), whereas an increase in molar mass (IPEI₄₀) initiated rouleaux formation only at the highest tested concentration of 50 µg · mL⁻¹ (stage 2, $\Delta\text{Abs}_{\text{max}} = 0.04$). The molar mass and concentration dependent effects of PEIs on red blood cell aggregation were described by several authors.^{17, 46} Correlated to the increasing number of charges with size, the interactions with negatively charged cell membranes increase as well. In accordance to the results obtained for the free IPEIs, also for the dex-g-IPEIs an increase of red blood cell aggregation could be observed with higher molar mass of IPEI (**Figure 5**).

In the **A series** erythrocyte aggregation could be observed starting at concentrations of 6.25 and 25 mg · mL⁻¹ for **A3**, **A4** and **A2**, respectively. In contrast, **A1** did not show any signs of interaction up to the highest tested concentration of 50 µg · mL⁻¹ (**Figure 1 b**). Therefore, interactions with negatively charged cell membranes of the red blood cells were found to increase with the molar mass of IPEI; this observation correlated well with the percentage nitrogen content of the **A series** polymers. While **A1** (N = 15.8%) did not induce aggregation of erythrocytes (stage 1, $\Delta\text{Abs}_{\text{max}} = 0.03$), **A2** (N = 19.1%) reached stage 2 at 25 µg · mL⁻¹ and $\Delta\text{Abs}_{\text{max}}$ of 0.04. **A3** and **A4** demonstrated nearly comparable aggregation results (stage 3 at 12.5 and 25 µg · mL⁻¹, $\Delta\text{Abs}_{\text{max}} = 0.08$) due to the similar percentage of nitrogen contents of about 21%. In general, the conjugates synthesized by reductive amination demonstrated a higher red blood cell aggregation potential compared to the modified dextrans prepared by EDC. The CM-dex-g-IPEIs **B2**, **B3** and **B4** reached only stage 2 with maximum $\Delta\text{Abs}_{\text{max}}$ values of 0.06, even at the highest

concentration of $50 \mu\text{g} \cdot \text{mL}^{-1}$. Again, for the IPEI₄₀-containing polymers **B2** and **B4** the aggregation effects were more pronounced than for the IPEI₂₀-based polymers (**B1** and **B3**). The higher compatibility of the **B series** polymers compared to the **A series** may be ascribed to the polyelectrolyte nature of the CM-Dex-g-IPEIs since they contain both positive and negative charges. This was particularly demonstrated by the polymer **B6**, that possess a higher number of anionic charges and revealed the lowest effects on red blood cells (stage 1 at $50 \mu\text{g} \cdot \text{mL}^{-1}$, $\Delta\text{Abs}_{\text{max}} = 0.02$). Hence, the high number of anionic charges within the **CM-dex-g-IPEI** polymers seems to interfere with the electrostatic interactions between the anionic cell membranes and the cationic polymers resulting in a decreased cell aggregation. De facto, for polyelectrolytes (e.g. zwitterionic polymers) a higher resistance to non-specific protein adsorption and blood cell interactions, which lead to a prolonged half life time in blood circulation, have been shown.⁴⁷

Conclusion

With the objective to evaluate the influence of the linking strategy of IPEI to dextran, several dextran-g-IPEIs were prepared. For this purpose, different IPEIs ($M = 860$ and $1720 \text{ g} \cdot \text{mol}^{-1}$) were synthesized and conjugated to dextran *via* two altered routes, namely reductive amination or EDC coupling. For a detailed study of structure-activity relationships, the content of functional groups (CHO, COOH) within the dextran precursors and the DS of IPEI were varied as well. Subsequently, the final dex-g-IPEI samples were investigated with regard to their physicochemical properties (DNA binding and stabilization, complex size and surface charge), transfection efficiency as well as biocompatibility and, in the end, compared to each other as well as to free IPEIs. The investigations were performed in terms of dependency on the linking strategy, the molar mass of conjugated IPEIs and the N/P ratio of the formed DNA/dex-g-IPEI complexes. Independent from the linking strategy, DS and molar mass of IPEI, it was observed that almost all conjugates formed with DNA complexes stable against enzymatic degradation in the range of 100 nm (in water) at N/P ratio 25 and 50 and revealed a positive surface charge. Differences between the types of conjugation were visible when IPEI was conjugated with CM_{1,6}-dex (**B5**): The binding capacity was reduced, as well as the stability and the zeta potential which was attributed to the higher content of COOH groups along the dextran backbone. Moreover, cell viability studies revealed the good cytocompatibility of the resulting dex-g-IPEI/DNA complexes under the chosen conditions since cell viabilities of 84 to 110% were observed with no crucial influence of the synthesis route or the DS and molar mass of IPEI. Instead, a remarkable effect of these parameters was detected on the transfection efficiency, since the cationic dextrans prepared by EDC coupling showed a more than one order of magnitude increased transgene expression compared to the **A series** despite much lower IPEI content. Nevertheless, the dex-g-IPEI obtained by reductive

amination still showed higher transfection values than the free IPEIs. The efficiency was found to be dependent on the molar mass and DS of conjugated IPEI as well as on the N/P ratio: With increasing these parameters also the transfection efficiency was enhanced. The transfection efficiencies of the CM-dex-g-IPEIs might depend additionally on the ratio of positive to negative charges of the molecules. However, further investigations would be necessary for deeper insights and final conclusions. It was also explored that both polymer series induced higher red blood cell aggregation compared to unconjugated IPEIs, while CHO-dex-g-IPEIs showed a stronger erythrocyte aggregation activity than CM-dex-g-IPEIs. In conclusion, the variation of the linking strategy of cationic polymers to dextran affects the biological properties, while the physicochemical properties were affected only marginal which was ascribed due to the high excess of polymer used for the experiments. Furthermore, for the grafting of low molar mass IPEIs to dextran the EDC coupling was more suitable as linking strategy compared to the polymers obtained by reductive amination, since the conjugates showed improved hemocompatibility and enhanced transfection efficiencies.

Associated content

Supporting Information

Materials and Methods: Instrumentation, methods of synthesis of the conjugates, methods of biological studies. Scheme of cationic ring-opening polymerization of pEtOxs (**Scheme S1**), tables of analytical data of the synthesized polymers and the conjugates (**Table S1-S5**), kinetics of cationic ring-opening polymerization of pEtOx (**Figure S1**), SEC traces of pEtOx (**Figure S2**), ¹H NMR spectra of the synthesized conjugates (**Figure S3-S6**), DNA binding capacity of the dex-g-IPEIs and free IPEIs (**Figure S7**) and references affiliated to the methods. This material is available free of charge via the Internet at <http://pubs.acs.org>.

Acknowledgements

Financial support from the Thuringian Ministry for Education, Science and Culture (grant #B514-09051, NanoConSens) is gratefully acknowledged. The authors also thank Angela Herre, Ramona Brabetz and Maxi Prange for their excellent laboratory assistance.

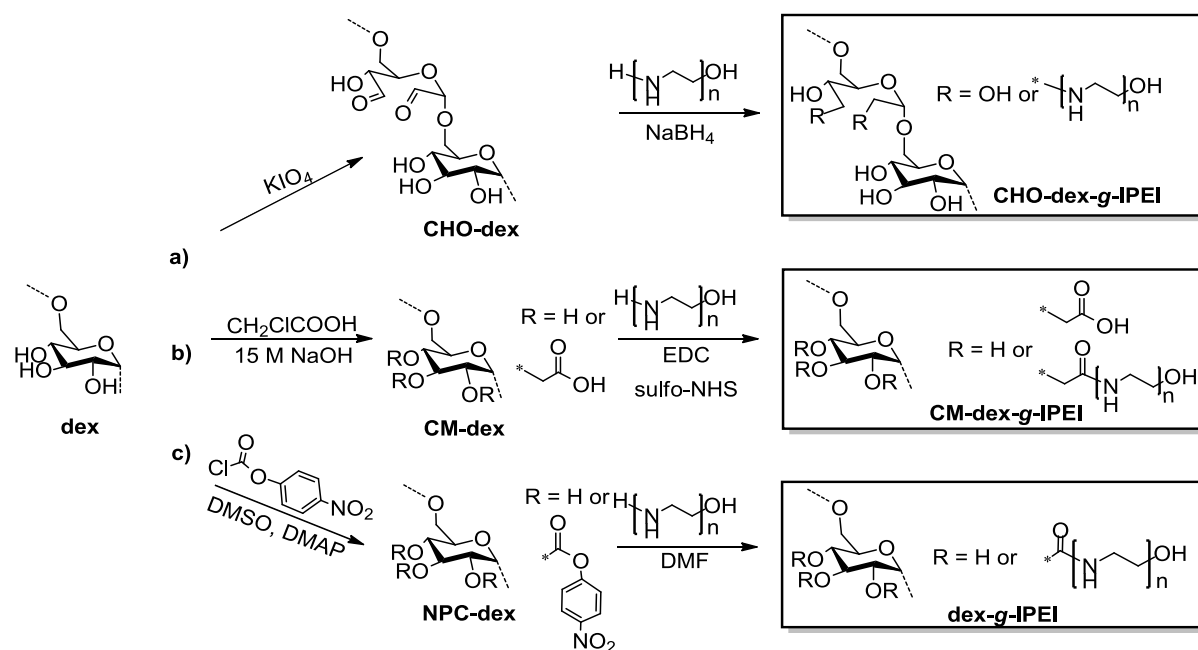
References

- (1) Varshosaz, J. (2012) Dextran conjugates in drug delivery. *Expert Opin. Drug Del.* 9, 509-523.
- (2) Mehvar, R. (2000) Dextran for targeted and sustained delivery of therapeutic and imaging agents. *J. Control. Release* 69, 1-25.
- (3) Heinze, T., Liebert, T., Heublein, B., and Hornig, S. (2006) Functional polymers based on dextran. *Adv. Polym. Sci.* 205, 199-291.
- (4) Liebert, T., Wotschadlo, J., Laudeley, P., and Heinze, T. (2011) Melttable dextran esters as biocompatible and

- functional coating materials. *Biomacromolecules* 12, 3107-3113.
- (5) Eshita, Y., Higashihara, J., Onishi, M., Mizuno, M., Yoshida, J., Takasaki, T., Kubota, N., and Onishi, Y. (2009) Mechanism of introduction of exogenous genes into cultured cells using DEAE-dextran-MMA graft copolymer as non-ciral gene carrier. *Molecules* 14, 2669-2683.
- (6) Cohen, J. L., Schubert, S., Wich, P. R., Cui, L., Cohen, J. A., Ynar, . . ., and Fr chet, J. M. J. (2011) Acid-degradable cationic dextran particles for the delivery of siRNA therapeutics. *Bioconjugate Chem.* 22, 1056-1065.
- (7) Azzam, T., Eliyahu, H., Shapira, L., Linial, M., Barenholz, Y., and Domb, A. J. (2002) Polysaccharide-oligoamine based conjugates for gene delivery. *J. Med. Chem.* 45, 1817-1824.
- (8) Thomas, J. J., Rekha, M. R., and Sharma, C. P. (2010) Dextran-protamine polycation: An efficient nonviral and haemocompatible gene delivery system. *Colloids Surf. B* 81, 195-205.
- (9) Maruyama, A., Watanabe, H., Ferdous, A., Katoh, M., Ishihara, T., and Akaike, T. (1998) Characterization of interpolyelectrolyte complexes between double-stranded DNA and polylysine comb-type copolymers having hydrophilic side chains. *Bioconjugate Chem.* 9, 292-299.
- (10) Tseng, W.-C., and Jong, C.-M. (2003) Improved stability of polycationic vector by dextran-grafted branched polyethylenimine. *Biomacromolecules* 4, 1277-1284.
- (11) Sun, Y.-X., Xiao, W., Cheng, S.-X., Zhang, X.-Z., and Zhuo, R.-X. (2008) Synthesis of (dex-HMDI)-g-PEIs as effective and low cytotoxic nonviral gene vectors. *J. Control. Release* 128, 171-178.
- (12) Sun, Y.-X., Zhang, X.-Z., Cheng, H., Cheng, S.-X., and Zhuo, R.-X. (2008) A low-toxic and efficient gene vector: Carboxymethyl dextran-graft-polyethylenimine. *J. Biomed. Mater. Res. A* 84A, 1102-1110.
- (13) Sun, K., Wang, J., Zhang, J., Hua, M., Liu, C., and Chen, T. (2011) Dextran-g-PEI nanoparticles as a carrier for co-delivery of adriamycin and plasmid into osteosarcoma cells. *Int. J. Biol. Macromol.* 49, 173-180.
- (14) Jiang, D., and Salem, A. K. (2012) Optimized dextran-polyethylenimine conjugates are efficient non-viral vectors with reduced cytotoxicity when used in serum containing environments. *Int J Pharm* 427, 71-79.
- (15) Thomas, J. J., Rekha, M. R., and Sharma, C. P. (2010) Dextran-glycidyltrimethylammonium chloride conjugate/DNA nanoplex: A potential non-viral and haemocompatible gene delivery system. *Int J Pharm* 389, 195-206.
- (16) Tseng, W.-C., Tang, C.-H., and Fang, T.-Y. (2004) The role of dextran conjugation in transfection mediated by dextran-grafted polyethylenimine. *J. Gene Med.* 6, 895-905.
- (17) Petersen, H., Fechner, P. M., Martin, A. L., Kunath, K., Stolnik, S., Roberts, C. J., Fischer, D., Davies, M. C., and Kissel, T. (2002) Polyethylenimine-graft-poly(ethylene glycol) copolymers: Influence of copolymer block structure on DNA complexation and biological activities as gene delivery system. *Bioconjugate Chem.* 13, 845-854.
- (18) Tseng, W.-C., Fang, T.-Y., Su, L.-Y., and Tang, C.-H. (2005) Dependence of transgene expression and the relative buffering capacity of dextran-grafted polyethylenimine. *Mol. Pharm.* 2, 224-232.
- (19) Tripathi, S. K., Goyal, R., and Gupta, K. C. (2011) Surface modification of crosslinked dextran nanoparticles influences transfection efficiency of dextran-polyethylenimine nanocomposites. *Soft Matter* 7, 11360-11371.
- (20) Tauhardt, ., Kempe, K., Knop, K., Altuntaş, E., Jäger, M., Schubert, S., Fischer, D., and Schubert, U. S. (2011) Linear polyethylenimine: Optimized synthesis and characterization – on the way to “Pharmagrade” batches. *Macromol. Chem. Phys.* 212, 1918-1924.
- (21) Altuntaş, E., Knop, K., Tauhardt, ., Kempe, K., Crecelius, A. C., Jäger, M., Hager, M. D., and Schubert, U. S. (2012) Tandem mass spectrometry of poly(ethylene imine)s by electrospray ionization (ESI) and matrix-assisted laser desorption/ionization (MALDI). *J. Mass Spectrom.* 47, 105-114.
- (22) Vandoorne, F., Bruneel, D., Vercauteren, R., and Schacht, E. (1991) New approach to dextran derivatives containing primary amino functions. *Makromol. Chem.* 192, 673-677.
- (23) Zhao, H., and Heindel, N. D. (1991) Determination of degree of substitution of formyl groups in polyaldehyde dextran by the hydroxylamine hydrochloride method. *Pharm. Res.* 8, 400-402.
- (24) Kent, P. W. (1949) Periodate oxidation in the study of the structure of dextrans. *Science* 110, 689-690.
- (25) Jeanes, A., and Wilham, C. A. (1950) Periodate oxidation of dextran. *J. Am. Chem. Soc.* 72, 2655-2657.
- (26) Rankin, J. C., and Jeanes, A. (1954) Evaluation of the periodate oxidation method for structural analysis of dextrans. *J. Am. Chem. Soc.* 76, 4435-4441.
- (27) Wotschadlo, J., Liebert, T., Heinze, T., Wagner, K., Schnabelrauch, M., Dutz, S., Mueller, R., Steiniger, F., Schwalbe, M., Kroll, T. C., Hoeffken, K., Buske, N., and Clement, J. H. (2009) Magnetic nanoparticles coated with carboxymethylated polysaccharide shells – Interaction with human cells. *J. Magn. Magn. Mater.* 321, 1469-1473.
- (28) Liebert, T., and Heinze, T. (1998) Cellulose derivatives: Synthesis, characterization and nanostructures. *ACS Symp. Ser.*, 61.
- (29) Heinze, T., Eler, U., Nehls, I., and Klemm, D. (1994) Determination of the substituent pattern of heterogeneously and homogeneously synthesized carboxymethyl cellulose by using high-performance liquid chromatography. *Angew. Makromol. Chem.* 215, 93-106.
- (30) Park, M. R., Han, K. O., Han, I. K., Cho, M. H., Nah, J. W., Choi, Y. J., and Cho, C. S. (2005) Degradable polyethylenimine-alt-poly(ethylene glycol) copolymers as novel gene carriers. *J. Control. Release* 105, 367-380.
- (31) Fischer, D., Dautzenberg, H., Kunath, K., and Kissel, T. (2004) Poly(diallyldimethylammonium chlorides) and their N-methyl-N-vinylacetamide copolymer-based DNA-polyplexes: Role of molecular weight and charge density in

- complex formation, stability, and in vitro activity. *Int J Pharm* 280, 253-269.
- (32) Lungwitz, U., Breunig, M., Liebl, R., Blunk, T., and Goepferich, A. (2008) Methoxy poly(ethylene glycol) – low molecular weight linear polyethylenimine-derived copolymers enable polyplex shielding. *Eur. J. Pharm. Biopharm.* 69, 134-148.
- (33) Gebhart, C. L., Sriadibhatla, S., Vinogradov, S., Lemieux, P., Alakhov, V., and Kabanov, A. V. (2002) Design and formulation of polyplexes based on pluronic-polyethylenimine conjugates for gene transfer. *Bioconjugate Chem.* 13, 937-944.
- (34) Abdullah, S., Wendy-Yeo, W. Y., Hosseinkhani, H., Hosseinkhani, M., Masrawa, E., Ramasamy, R., Rosli, R., Rahman, S. A., and Domb, A. J. (2010) Gene transfer into the lung by nanoparticle dextran-spermine/plasmid DNA complexes. *J. Biomed. Biotechnol.* 2010, DOI: 10.1155/2010/284840.
- (35) Grund, S., Bauer, M., and Fischer, D. (2011) Polymers in drug delivery – state of the art and future trends. *Adv. Eng. Mater.* 13, B61-B87.
- (36) Petersen, H., Fechner, P. M., Fischer, D., and Kissel, T. (2002) Synthesis, characterization, and biocompatibility of polyethylenimine-graft-poly(ethylene glycol) block copolymers. *Macromolecules* 35, 6867-6874.
- (37) Breunig, M., Lungwitz, U., Liebl, R., Fontanari, C., Klar, J., Kurtz, A., Blunk, T., and Goepferich, A. (2005) Gene delivery with low molecular weight linear polyethylenimines. *J. Gene Med.* 7, 1287-1298.
- (38) Godbey, W. T., Barry, M. A., Saggau, P., Wu, K. K., and Mikos, A. G. (2000) Poly(ethylenimine)-mediated transfection: A new paradigm for gene delivery. *J Biomed Mater Res* 51, 321-328.
- (39) "Biological evaluation of medical devices part 5: Tests for in vitro cytotoxicity", 2nd edition, International Organization for Standardization/ANSI; ISO ISO 10993-5, Geneva, Switzerland (2009).
- (40) Thomas, M., Ge, Q., Lu, J. J., Chen, J., and Klibanov, A. (2005) Cross-linked small polyethylenimines: While still nontoxic, deliver DNA efficiently to mammalian cells in vitro and in vivo. *Pharm. Res.* 22, 373-380.
- (41) Yu, J.-H., Quan, J.-S., Kwon, J.-T., Xu, C.-X., Sun, B., Jiang, H.-L., Nah, J.-W., Kim, E.-M., Jeong, H.-J., Cho, M.-H., and Cho, C.-S. (2009) Fabrication of a novel core-shell gene delivery system based on a brush-like polycation of α , β -poly (L-aspartate-graft-PEI). *Pharm. Res.* 26, 2152-2163.
- (42) ASTM F756, 2008, "Standard practice for assessment of hemolytic properties of materials" in *Annual Book of ASTM Standards, Vol. 13. 01, ASTM, Philadelphia* DOI: 10.1520/F0756-08, www.astm.org.
- (43) Moreau, E., Domurado, M., Chapon, P., Vert, M., and Domurado, D. (2002) Biocompatibility of polycations: In vitro agglutination and lysis of red blood cells and in vivo toxicity. *J. Drug Target.* 10, 161-173.
- (44) Yang, J., Liu, Y., Wang, H., Liu, L., Wang, W., Wang, C., Wang, Q., and Liu, W. (2012) The biocompatibility of fatty acid modified dextran-arginine bioconjugate gene delivery vector. *Biomaterials* 33, 604-613.
- (45) Bauer, M., Lautenschlaeger, C., Kempe, K., Tauhardt, L., Schubert, U. S., and Fischer, D. (2012) Poly(2-ethyl-2-oxazoline) as alternative for the stealth polymer poly(ethylene glycol): Comparison of in vitro cytotoxicity and hemocompatibility. *Macromolecular Bioscience*, 986–998.
- (46) Jeon, O., Yang, H. S., Lee, T.-J., and Kim, B.-S. (2008) Heparin-conjugated polyethylenimine for gene delivery. *J. Control. Release* 132, 236-242.
- (47) Jiang, S., and Cao, Z. (2010) Ultralow-fouling, functionalizable, and hydrolyzable zwitterionic materials and their derivatives for biological applications. *Adv. Mater.* 22, 920-932.

Figures and Tables



Scheme 1. Schematic representation of the functionalization of dextran by (a) oxidation, (b) carboxymethylation and (c) 4-nitrophenyl carbonate-activation with subsequent reaction with IPEIs *via* (a) reductive amination, (b) EDC coupling and (c) carbamate formation.

Table 1. Overview about the DS and nitrogen content of all synthesized dex-g-IPEI samples.

P	dex-g-IPEIs	CHO/ COOH: NH ₂ [mol]	DS [IPEI/ AGU]	N [%]	Cationic charge/M _{Monomer} ^a	Anionic charge/M _{Monomer} ^b
A	Reductive amination					
A1	CHO _{DS=0.5} -dex-g-IPEI ₂₀	1:0.5	0.18	15.78	0.0114	-
A2	CHO _{DS=0.5} -dex-g-IPEI ₄₀	1:0.5	0.13	19.12	0.0135	-
A3	CHO _{DS=1.0} -dex-g-IPEI ₂₀	1:0.5	0.38	21.45	0.0156	-
A4	CHO _{DS=1.0} -dex-g-IPEI ₄₀	1:0.5	0.19	21.73	0.0156	-
B	EDC coupling					
B1	CM _{DS=0.3} -dex-g-IPEI ₂₀	1:1.2	0.06	6.73	0.0052	0.0013
B2	CM _{DS=0.3} -dex-g-IPEI ₄₀	1:1.2	0.07	12.80	0.0093	0.0010
B3	CM _{DS=0.5} -dex-g-IPEI ₂₀	1:1.2	0.07	7.96	0.0056	0.0020
B4	CM _{DS=0.5} -dex-g-IPEI ₄₀	1:1.2	0.1	14.83	0.0110	0.0014
B5	CM _{DS=1.6} -dex-g-IPEI ₂₀	3:1	0.11	8.16	0.0063	0.0046
B6	CM _{DS=1.6} -dex-g-IPEI ₄₀	3:1	0.18	18.38	0.0127	0.0028

a) Calculated cationic charge/molar mass of monomer unit

b) Calculated anionic charge/molar mass of monomer unit

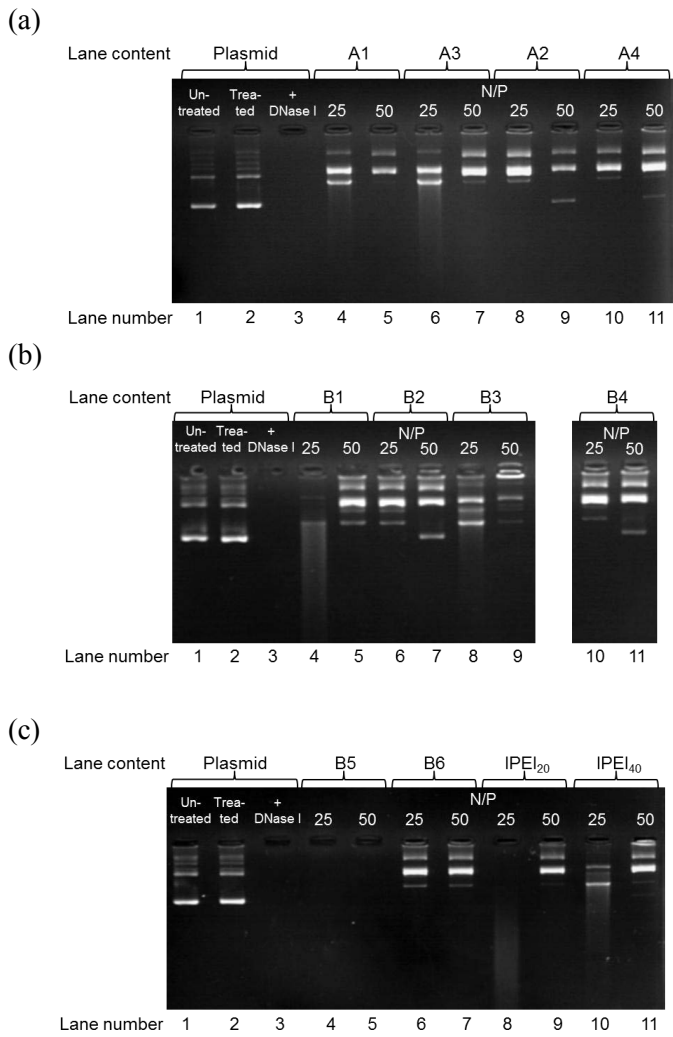


Figure 1: Stability of dex-g-IPEI/plasmid complexes against enzymatic degradation (DNase I, 37 °C, 45 minutes) at N/P ratio 25 and 50: (a) dex-g-IPEIs by reductive amination; (b + c) dex-g-IPEIs by EDC-coupling, (c) IPEIs. Controls: lane 1: untreated free plasmid; lane 2: free plasmid treated in the same way as complexes but without enzyme; lane 3: free plasmid treated with enzyme.

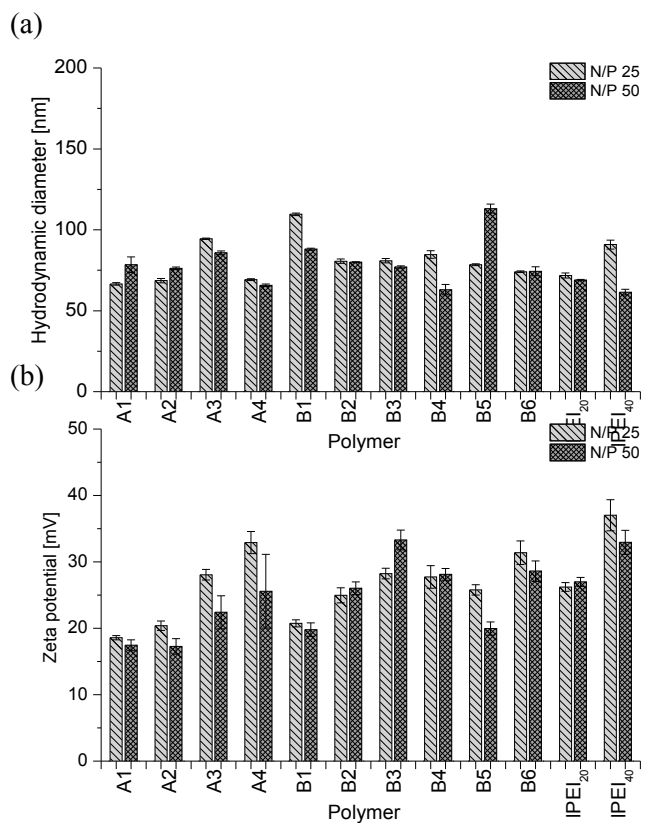


Figure 2: (a) Hydrodynamic diameter and (b) zeta potential of dex-g-IPEI and IPEI complexes with plasmid DNA at N/P ratio 25 and 50 measured in water. Results are shown as mean of six measurements \pm SD.

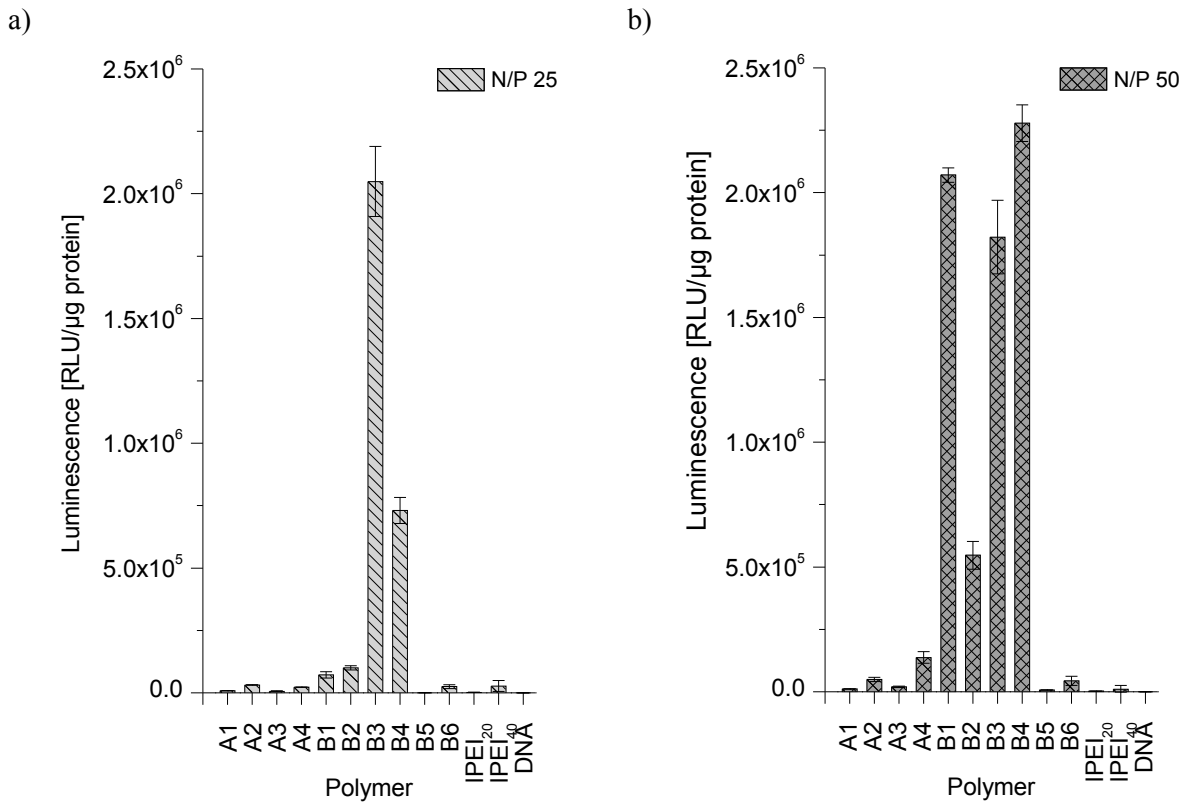


Figure 3: Transfection efficiency of dex-g-IPEIs and free IPEIs complexed with plasmid pGL3 at (a) N/P ratio 25 and (b) N/P ratio 50 in CHO-K1 cells determined by luciferase assay; in comparison to the control naked plasmid (DNA).

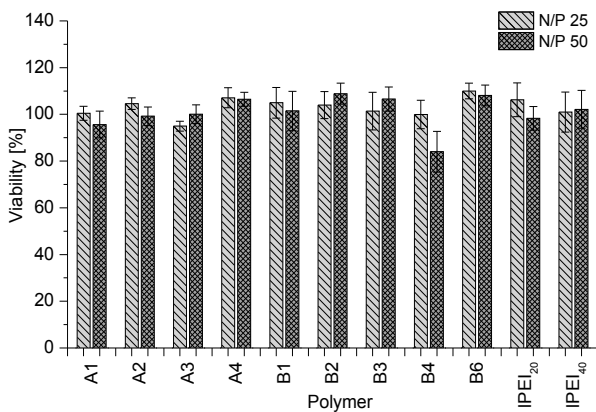


Figure 4: Viability of L929 mouse fibroblasts treated with dex-g-IPEI/DNA and IPEI/DNA complexes at N/P ratio 25 and 50 for 24 h, determined by MTT assay. Complexes were formed with herring testes DNA as model DNA. Results are shown as mean of seven values \pm SD.

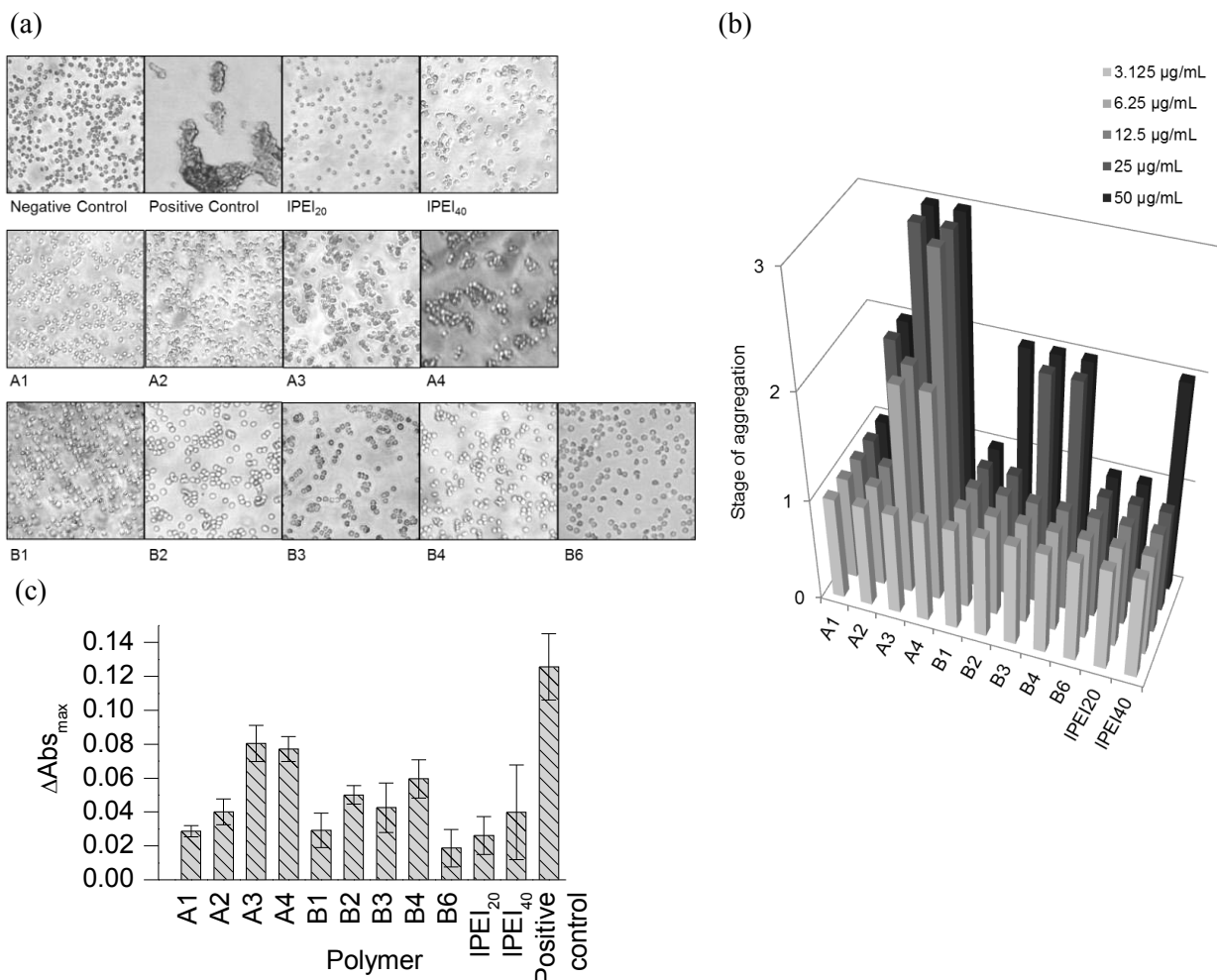


Figure 5: Aggregation of sheep red blood cells after treatment with free dex-g-IPEI and IPEI polymers incubated at 37 °C for 2 h. (a) Representative pictures of microscopic observation at 50 µg · mL⁻¹ (negative control = PBS; positive control = 15 µg · mL⁻¹ bPEI 25,000 g · mol⁻¹) with magnification 200×. (b) Stages of sheep blood erythrocyte aggregation of dex-g-IPEIs and IPEIs at concentrations up to 50 µg · mL⁻¹. Classification: 1 = no aggregation of erythrocytes, 2 = moderate aggregation with rouleau formation, 3 = strong aggregation with cluster formation. (c) ΔAbs_{max} of polymers. The RBC aggregation experiments were performed with n = 2 and repeated once (mean ± SD).

Supporting information for

Dextran-*graft*-linear poly(ethylene imine)s for gene delivery: Influence of linking strategies on physicochemical and biological properties

Sofia Ochrimenko,^{†‡#} Antje Vollrath,^{‡#} Lutz Tauhardt,[‡] Kristian Kempe,[‡] Stephanie Schubert,^{†§} Ulrich S. Schubert,^{‡§*} Dagmar Fischer^{†§*}

#Equal Contributors

*Corresponding Authors

[†]Department of Pharmaceutical Technology, Institute of Pharmacy, Otto-Schott-Str. 41, 07745 Jena, Germany

[‡]Laboratory of Organic and Macromolecular Chemistry (IOMC), Friedrich-Schiller-University Jena, Humboldtstr. 10, 07743 Jena, Germany

[§]Jena Center for Soft Matter (JCMS), Friedrich-Schiller-University Jena, Philosophenweg 7, 07743 Jena, Germany

This file includes:

Material and Methods	Page 2
Table S1	Page 3
Table S2	Page 5
Table S3	Page 6
Table S4	Page 8
Table S5	Page 9
Scheme S1	Page 3
Figure S1-S2	Page 4
Figure S3	Page 6
Figure S4	Page 7
Figure S5	Page 8
Figure S6	Page 9
Figure S7	Page 11
References	Page 15

Material and Methods

1. Instrumentation

Size exclusion chromatograms (SEC) of poly(2-ethyloxazoline) was measured on an Agilent Technologies 1200 Series gel permeation chromatography system equipped with a G1310A isocratic pump, a G1329A autosampler, a G1362A refractive index detector, and both a PSS Gram 30 and a PSS Gram 1000 column placed in series. A 0.21% lithium chloride (LiCl, ACROS Organic, New Jersey, USA) solution in *N,N*-dimethylacetamide (DMA, HiPerSolv CHROMANORM, VWR Prolabo, Darmstadt, Germany) was used as eluent at $1 \text{ mL} \cdot \text{min}^{-1}$ flow rate and a column oven temperature of $40 \text{ }^\circ\text{C}$. The molar masses were calculated against poly(ethylene glycol) (PEG, Polymer Standards Service, Mainz, Germany). The dextran aldehyde and carboxymethylated dextran were investigated on a Jasco SEC system composed of a DG-2080-53 degasser, a PU-980 pump and a RI-930 refractive index detector running in dimethyl sulfoxide (DMSO, ROTIPURAN 99.8%, Carl-Roth GmbH, Karlsruhe, Germany) containing 0.5% lithium bromide (LiBr, Riedel-de Haën, Seelze, Germany) at $0.5 \text{ mL} \cdot \text{min}^{-1}$ at $65 \text{ }^\circ\text{C}$. The samples were separated on PSS NOVEMA 3000 and 300 \AA columns and their molar masses calculated against narrow distributed dextran standards (Polymer Standards Service, Mainz, Germany).

Moreover, all dextran-*graft*-linear poly(ethylene imine)s were measured on a Jasco SEC system equipped with a PU-980 pump, a AS-1555 autosampler, a DG-980-50 degasser, a RI-930 refractive index detector, and a PSS SUPREMA-MAX column. As eluent, a solution of 0.1% trifluoroacetic acid (TFA, Uvasol, MERCK, Darmstadt, Germany) and 0.05 M NaCl (Sigma Aldrich, Deisenhofen, Germany) in water (pH 2), running at a flow rate of $1 \text{ mL} \cdot \text{min}^{-1}$ and a column oven temperature of $60 \text{ }^\circ\text{C}$, was used. The molar masses were calculated against pullulan (Polymer Standards Service, Mainz, Germany).

^1H NMR and ^{13}C NMR spectra were recorded in deuterated water (D_2O , Eurisotop, Gif sur Yvette Cedex, France) or deuterated dichloromethane (CD_2Cl_2 , Eurisotop, Gif sur Yvette Cedex, France) on a Bruker Avance 250 MHz or 300 MHz spectrometer. Chemical shifts are given in ppm relative to signals from the NMR solvents. Conversions were calculated from ^1H spectra using anisole as an internal standard.

Elemental analysis (EA) was carried using an the Elementaranalysator Vario EL III CHNS from Elementar Analysensysteme GmbH, Hanau.

2. Synthesis

Synthesis of poly(2-oxazolines) (pEtOx)

The pEtOxs used in this study as starting materials for the preparation of linear polyethylene imines (IPEIs) were synthesized according to literature procedures.^{1, 2} Briefly, poly(2-ethyl-2-oxazoline)s (pEtOx) with monomer-to-initiator ratios of 20 and 40 were synthesized under microwave irradiation. In order to obtain solely proton initiated chains *p*-toluene sulfonic acid

(Sigma Aldrich) was used as initiator for the cationic ring-opening polymerization (Scheme S1). Polymerization kinetics revealed a linear increase of $\ln([M]_0/[M]_t)$ with time demonstrating a constant concentration of propagating species indicative of a living polymerization mechanism. The resulting first-order kinetic plot is shown in Figure S1, left. The linear increase in the molar mass with conversion as well as low polydispersity index (PDI) values (< 1.3) further support the living character of the polymerization (Figure S1, right). Based on these results two large batches of pEtOx₂₀ and pEtOx₄₀ were synthesized. The molar mass determined by ¹H NMR spectroscopy was in accordance with the feed ratio (pEtOx₂₀: 2,000 g · mol⁻¹, pEtOx₄₀: 4,000 g · mol⁻¹) and SEC measurements revealed reasonable molar mass distributions with low PDI values (PEtOx₂₀: 3,530 g · mol⁻¹, PDI = 1.14; PEtOx₄₀: 5,900 g · mol⁻¹, PDI = 1.2) (Figure S2).

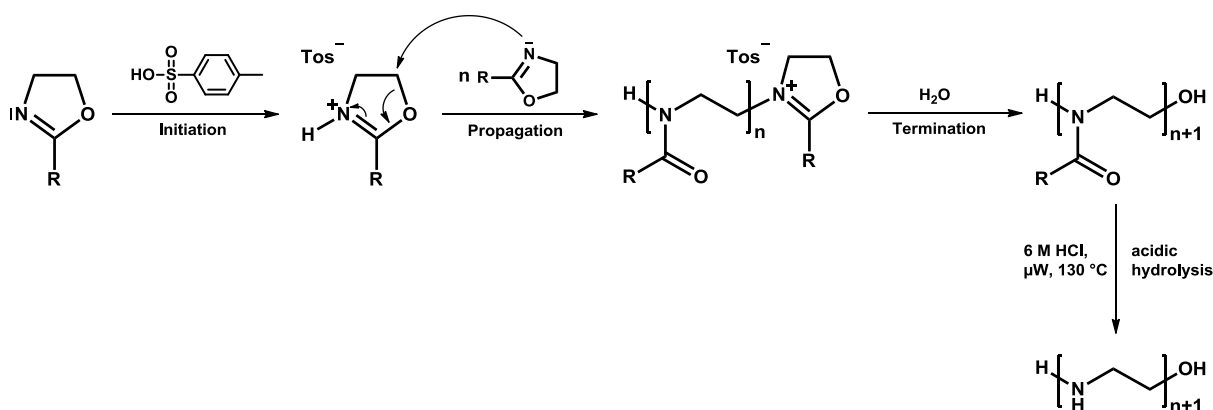
Synthesis of linear poly(ethylene imines) (IPEI)

The IPEI synthesis was performed according to a modified procedure described in literature.² Briefly, corresponding pEtOx (30 g) was dissolved in 6 M HCl (400 mL, Sigma Aldrich) and heated for 24 h at 150 °C. The solvent was removed under reduced pressure. The residue was dissolved in water (500 mL) and 3 M NaOH (Sigma Aldrich) was added until precipitation occurred. The precipitate was filtered off and recrystallized from water (600 mL). After filtration the IPEI was dissolved in methanol (200 mL, Mineralöl Albert, Jena, Germany) and precipitated into ice-cold diethyl ether (1,300 mL, Mineralöl Albert). The white precipitate was filtered off and dried under reduced pressure at 40 °C for 5 d. The purity and degree of hydrolysis of the resulting IPEI were determined by ¹H NMR spectroscopy.^{2,3}

Table S1. Analytical data of poly(2-ethyloxazoline) and the resulting linear poly(ethylene imine)s.

	M_n^a [g · mol ⁻¹]	PDI
PEtOx ₂₀	3,550 ^a	1.14 ^a
PEtOx ₄₀	5,900 ^a	1.20 ^a
IPEI ₂₀	860 ^b	-
IPEI ₄₀	1,720 ^b	-

^a SEC, DMA, ^b theoretical values calculated from the PEtOx precursor



Scheme S1. Scheme of the cationic ring-opening polymerization of pEtOxs followed by the subsequent acidic hydrolysis to IPEI.

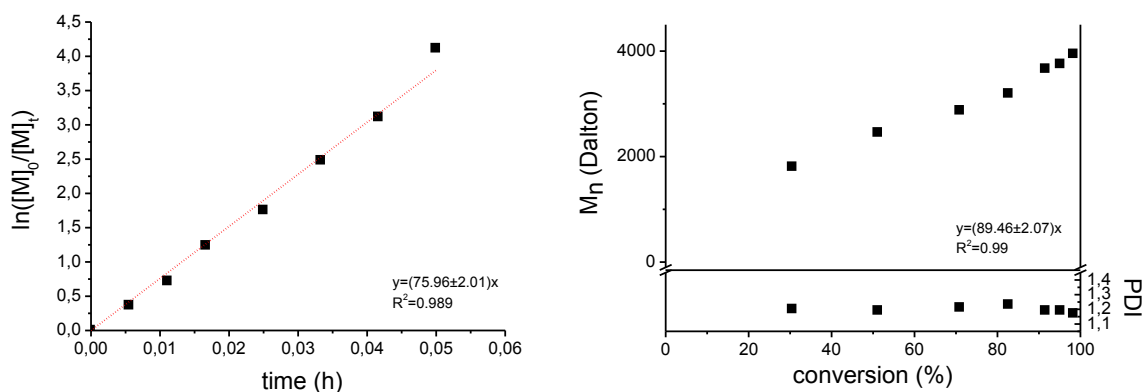


Figure S1. Kinetics of the cationic ring-opening polymerization of pEtOx: Resulting first-order kinetic plot of $\ln([M]_0/[M]_t)$ (left) linear increase in the molar mass with conversion as well as low polydispersity index (PDI) values (right).

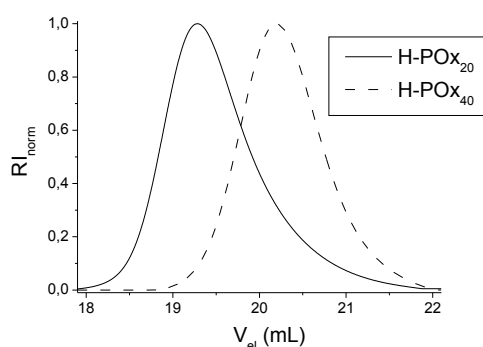


Figure S2. SEC traces of pEtOx₂₀ and pEtOx₄₀ using DMA as eluent.

Synthesis of dextran aldehyde (CHO-dex)

Pharmaceutical grade dextran with an average molar mass of $65,900 \text{ g} \cdot \text{mol}^{-1}$ (Pharmacosmos, Holbaek, Denmark) (5 g, 0.0136 mol per anhydroglucose unit (AGU)) was dissolved in 20 mL distilled water, and the adequate amount (0.0045 or 0.00136 mol) of potassium periodate (KIO_4 , Sigma Aldrich) was added. After stirring in the dark at room temperature for 24 h, the products were dialyzed for 5 days (10 times exchange of water) and were transferred into tare glass vials and lyophilized in an Alpha 1-2/LD Plus freeze dryer (Martin Christ, Osterode Germany) at a pressure of 0.006 mbar for 72 h (yield 90%). The final CHO-dextran were characterized by elemental analysis, SEC (Table S2) as well as ^1H NMR spectroscopy (Figure S3, a, b).

The degree of oxidation in the CHO-dex was determined according to the hydroxylamine chloride titration after Zhao *et al.* in distilled water.⁴ CHO-dex samples (100 mg) were dissolved in 25 mL of 0.25 M hydroxylamine hydrochloride solution (Sigma Aldrich). After 2 h incubation at room temperature, the solution was titrated against 1 N NaOH solution. Thereby, the degree of substitution (DS) of CHO was calculated based on the sample weights (formula) and subscripted as CHO_X-dex.

$$DS [CHO_x - dex] = \frac{V_{mL} \times 10^{-3}(L) \times M_{NaOH} (mol \times L^{-1})}{\frac{m_{dex} (g)}{M_{dex}(g \times mol^{-1})}}$$

Table S2. Overview of analytical data of the oxidation of dextran with KIO₄.

	KIO ₄ :AGU [mol]	[CHO/AGU] ^a	M _w [g · mol ⁻¹] ^b	PDI ^b	C [%]	H [%]	N [%]
Dextran	-	-	65,900	1.86	40.49	6.79	-
CHO _{0.5} -dex	1:10	0.51	55,100	2.51	42.34	6.39	-
CHO _{1.0} -dex	1:3	1.09	52,500	2.35	41.43	6.25	-

^a Determined by hydroxylamine chloride titration

^b SEC were performed in DMSO containing 0.5 % LiBr using pullulan as standard

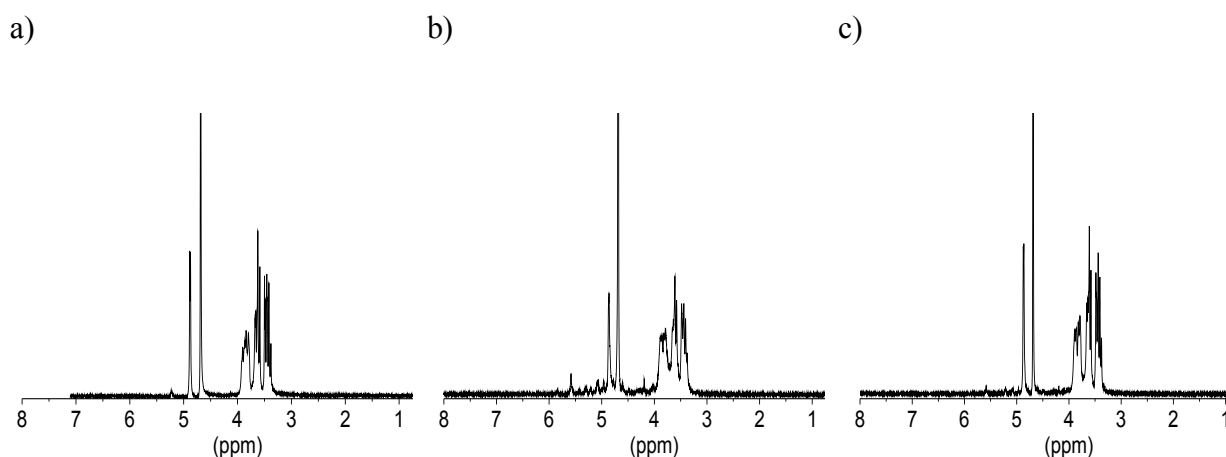


Figure S3. ¹H NMR spectra of (a) dextran, (b) CHO_{0.5}-dex and (c) CHO_{1.0}-dex prepared by oxidation with KIO₄. The ¹H NMR spectra were measured at 25 °C in D₂O.

Synthesis of CHO-dex-g-IPEI

For the synthesis of various dextran conjugated IPEIs, 200 mg (0.0012 mol AGU) CHO_{0.5}-dex and CHO_{1.0}-dex as well as the desired amount of IPEI (CHO:NH₂-PEI ratio = 1:1 or 1:0.5) were dissolved in water at 60 °C. After mixing both solutions, the color turned to yellow indicating an imine bond formation. The mixture was stirred for 24 h at 60 °C following the slow addition of a 5 times excess of sodium borohydride (NaBH₄, Sigma Aldrich). The solutions became colorless due to the reduction of the imine bond to an amine formation and were stirred for 2 days at room temperature. Subsequently, the product was purified from uncoupled IPEI and NaBH₄ residues by extensive dialysis against water at 60 °C. The water was exchanged at least 10 times within 5 days until the pH of the dialysis water was neutral (pH 6-7). The product was lyophilized in an Alpha 1-2/LD Plus freeze dryer (Martin Christ) at a pressure of 0.006 mbar for 72 h reaching 30 to 40% overall yield. The absence of

unbound IPEI was proven by ^1H NMR measurement (600 MHz, D_2O , 60 °C) of the collected dialysis water and the final DS of IPEI was calculated by the nitrogen content obtained from elemental analysis (Table S3). The polymers were further characterized by SEC measurements (in H_2O , 0.1% TFA) and ^1H NMR spectroscopy (600 MHz, D_2O , 60 °C) (Figure S4).

Table S3. Overview of analytical data of the dex-g-IPEI samples obtained by reductive amination.

Products	CHO: NH ₂ -IPEI [mol]	DS ^a [IPEI/ AGU]	C [%]	H [%]	N [%]	M _w [g · mol ⁻¹] ^b	PDI ^b
CHO _{0.5} -dex-g-IPEI ₂₀	1:1	0.18	41.95	9.75	15.78	24,000	1.21
CHO _{0.5} -dex-g-IPEI ₄₀	1:1	0.13	43.00	10.38	19.12	27,600	1.26
CHO _{1.0} -dex-g-IPEI ₂₀	2:1	0.38	43.74	10.58	21.45	31,300	1.20
CHO _{1.0} -dex-g-IPEI ₄₀	2:1	0.19	43.62	10.45	21.73	36,500	1.20

^a Calculated from the nitrogen content N [%] of the elemental analysis

^b SEC measurements were performed in H_2O containing 0.1% TFA and 0.05 M NaCl (pH 2) using pullulan as standard.

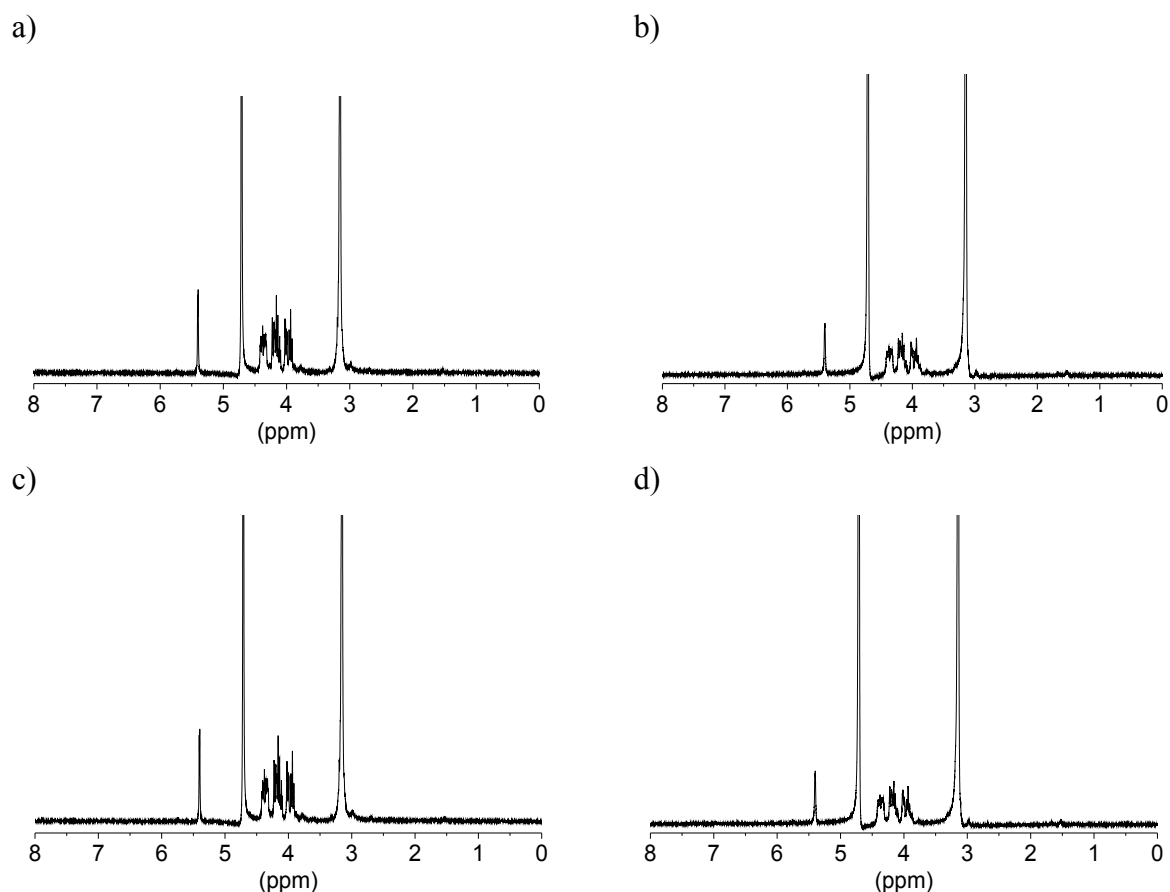


Figure S4. ^1H NMR spectra of dex-g-IPEI samples obtained by reductive amination. The ^1H NMR spectra were measured at 60 °C in D_2O . (a) CHO_{0.5}-dex-g-IPEI₂₀, (b) CHO_{0.5}-dex-g-IPEI₄₀ (c) CHO_{1.0}-dex-g-IPEI₂₀, (d) CHO_{1.0}-dex-g-IPEI₄₀.

Synthesis of carboxymethyl dextran (CM-dex)

Pharmaceutical grade dextran with an average molar mass of $65,900 \text{ g} \cdot \text{mol}^{-1}$ (Pharmacosmos) (5 g, 0.0136 mol per AGU) was dissolved in 50 mL water and stirred for 20 minutes at room temperature. The desired amount of 15 M NaOH was added dropwise, and the reaction mixture stirred for further 60 minutes. Subsequently, the desired amount of monochloroacetic acid (Sigma Aldrich) was added dropwise and the temperature was increased to $60 \text{ }^\circ\text{C}$. The reaction was stopped after 90 minutes or 300 minutes by neutralization with acetic acid (pH 6-7, Sigma Aldrich). After precipitation in 1.5 L of cold methanol (Mineralöl Albert), the solid product was filtered off over a G3 frit and washed (at least 3 times) with methanol. After dialysis (5 times exchange of water, 3 days) the products were obtained in 80% yield by lyophilization in an Alpha 1-2/LD Plus freeze dryer (Martin Christ) at a pressure of 0.006 mbar for 72 h. The DS of carboxymethyl groups was determined according to the HPLC procedure described by Wotschadlo *et al.*⁵ Furthermore, the products were characterized by ^1H NMR spectroscopy (600 MHz, D_2O), SEC (in DMSO) and EA measurements (Table S4).

Table S4. Overview of analytical data of the CM-dex samples obtained by reductive amination.

	AGU:ClCH ₂ COOH :NaOH [mol]	DS ^a [CH ₂ COOH /AGU]	M _w [g · mol ⁻¹] ^b	PDI ^b
CM _{0.3} -dex	2.2:1:1 (90 minutes)	0.32	51,100	2.36
CM _{0.5} -dex	2.2:1:1 (300 minutes)	0.54	54,400	2.37
CM _{1.6} -dex	1:5:10 (300 minutes)	1.6	60,100	2.04

^a Determined by HPLC measurement

^b SEC were performed in DMSO containing 0.5 % LiBr using pullulan as standard

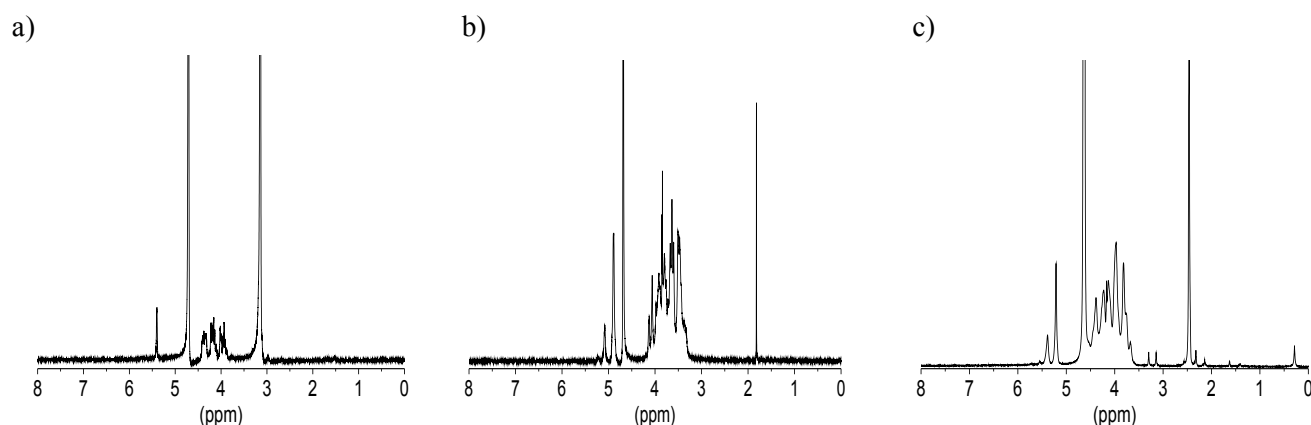


Figure S5. ^1H NMR spectra of (a) CM_{0.3}-dex, (b) CM_{0.5}-dex and (c) CM_{1.6}-dex obtained by carboxymethylation with monochloroacetic acid. The ^1H NMR spectra were measured at $25 \text{ }^\circ\text{C}$ in D_2O .

Synthesis of CM-dex-g-IPEI

The reactions of the CM-dex with the IPEIs were performed using 1-ethyl-3-(3-dimethylaminopropyl)carbodiimide (EDC, Sigma-Aldrich) as coupling reagent. Firstly, 300 mg of each CM-dex and the desired amount of IPEI (NH₂:COOH = 1.2:1) were dissolved in distilled water at 60 °C to ensure complete dissolution of the IPEIs. Subsequently, the pH value of the solution was adjusted to 6.0 by 1 M HCl solution. After 20 minutes stirring at 60 °C EDC (COOH:EDC = 1:1) and *N*-hydroxysulfosuccinimide (sulfo-NHS, Sigma Aldrich) (EDC:sulfo-NHS = 1:1) were added. The reaction mixture was stirred for 24 h at 60 °C, and the product was purified by extensive dialysis (at least 10 times exchange of water within 5 days) at 60 °C. The products were obtained by lyophilization (Alpha 1-2/LD Plus freeze dryer, Martin Christ) at a pressure of 0.006 mbar for 72 h in 30 to 40% overall yield. The absence of free unbound IPEI was proven by ¹H NMR (600 MHz, D₂O) measurement of the collected dialysis water. Furthermore, SEC analyses (in H₂O, 0.1% TFA) as well as ¹H NMR spectroscopy (600 MHz, D₂O, 60°C) and elemental analysis investigations of the products were performed. The final DS of IPEI was calculated by the nitrogen content obtained from elemental analysis (Table S5).

Table S5. Overview of analytical data of the dex-g-IPEI samples obtained by EDC coupling.

Products	COOH:EDC: NH ₂ -IPEI	DS ^a [IPEI /AGU] ^b	M _w [g · mol ⁻¹] ^b	PDI ^b	C [%]	H [%]	N [%]
CM _{0.3} -dex-g-IPEI ₂₀	1:1.2	0.06	22,900	1.06	40.91	7.35	6.73
CM _{0.3} -dex-g-IPEI ₄₀	1:1.2	0.07	36,500	1.09	38.91	8.07	12.80
CM _{0.5} -dex-g-IPEI ₂₀	1:1.2	0.07	25,000	1.07	40.55	7.11	7.96
CM _{0.5} -dex-g-IPEI ₄₀	1:1.2	0.1	36,000	1.09	37.89	8.51	14.83
CM _{1.6} -dex-g-IPEI ₂₀	3:1	0.11	15,600	1.14	43.29	7.09	8.16
CM _{1.6} -dex-g-IPEI ₄₀	3:1	0.18	17,200	1.18	33.91	8.57	18.38

^a Calculated from the nitrogen content N [%] of the elemental analysis

^b SEC measurements were performed in H₂O containing 0.1% TFA and 0.05 M NaCl (pH 2) using pullulan as standard

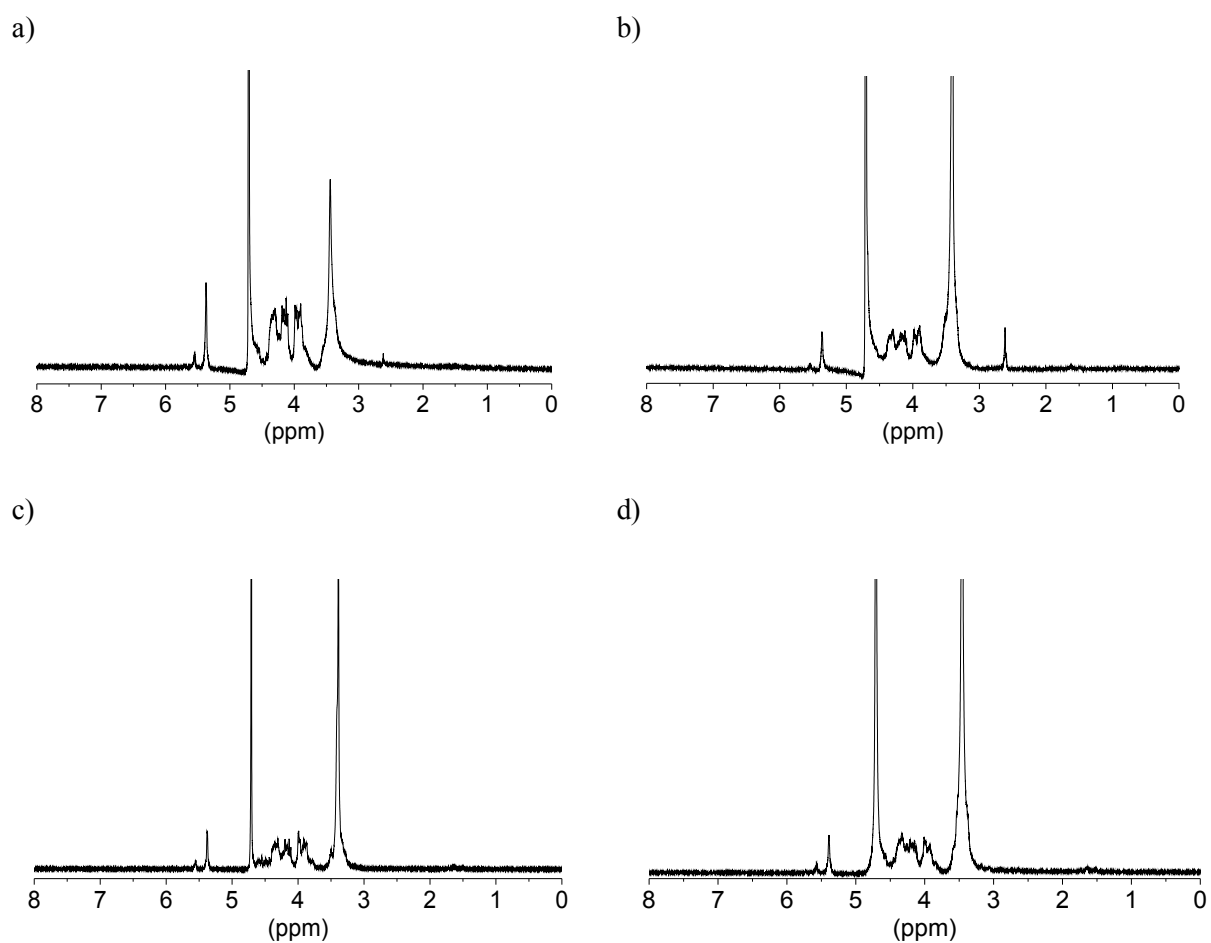


Figure S6. Representative ^1H NMR spectra of dex-g-PEI samples obtained by EDC coupling of CM-dex and IPEI: (a) $\text{CM}_{0.3}$ -dex-g-IPEI₂₀ (b) $\text{CM}_{0.3}$ -dex-g-IPEI₄₀ (c) $\text{CM}_{0.5}$ -dex-g-IPEI₂₀ (d) $\text{CM}_{0.5}$ -dex-g-IPEI₄₀. The ^1H NMR spectra were measured at 60 °C in D_2O .

3. Biological studies

DNA preparation

Luciferase reporter gene encoding plasmid pGL3 (Promega, Madison, WI, USA) was transferred to competent *E. coli* TG1 (kind gift of Hans-Knoell-Institute, Jena) and isolated with the plasmid Maxi kit according to manufacturer's protocol (E.Z.N.A[®], OMEGA bio-tek, Norcross, GA, USA). Herring testes DNA Type XIV (Sigma Aldrich) was used as model DNA.

Preparation of polymer/DNA complexes

Stock solutions of dextran derivatives and IPEIs were prepared in highly purified water at a concentration of $1 \text{ mg} \cdot \text{mL}^{-1}$, and pH was adjusted to 7.4. The solutions were sterile filtered ($0.2 \text{ } \mu\text{m}$, VWR international, Darmstadt, Germany). Polymer concentrations after filtration

were quantified as copper(II) (Cu^{2+}) complexes according to Perrine *et al.* (1967)⁶ by measurement of the absorbance at 645 nm in 96-well plates (Greiner Bio-One, Frickenhausen, Germany) with a microplate reader (Fluostar OPTIMA, BMG Labtech, Offenburg, Germany) using a calibration curve of the corresponding derivatives. The complexes were formed according to Fischer *et al.* (1999)⁷ and Tseng *et al.* (2003).⁸ The N/P ratio was calculated by the molar ratio of the nitrogen (N) (determined by elemental analyses) of each dex-g-IPEI sample to phosphorus (P) in the DNA. Five μg DNA and the appropriate amount of polymer solution were each diluted in 125 μL 150 mM NaCl (Roth, Karlsruhe, Germany) pH 7.4 and vortexed for 10 minutes. Afterwards, the polymer solution was added to the DNA solution, vortexed for 10 seconds and incubated at room temperature for 10 minutes.

Horizontal gel retardation assay

A 50 μL aliquot (containing 1 μg herring testes DNA type XIV) of the complex dilution was mixed with 5 μL loading buffer (40 mM Tris, 50% (v/v) glycerol 85%, 1 mM EDTA, pH 7.4, all from Roth). Subsequently, 5 μL dilution was applied on a 1% agarose gel (PeqGold Universal agarose, Peqlab Biotechnology GmbH, Erlangen, Germany). Electrophoretic separation was carried out in TAE running buffer (40 mM Tris, 1% acetic acid, 1 mM EDTA, all from Roth) in a horizontal electrophoresis chamber (Biometra, Goettingen, Germany) at 80 V for 1 h. For DNA detection, the fluorescence of intercalated ethidium bromide (Roth) was determined using a UV transilluminator (Intas GmbH, Goettingen, Germany) at 312 nm. Photographs were taken with a gel documentation system (Digit Store UNO, Intas GmbH).

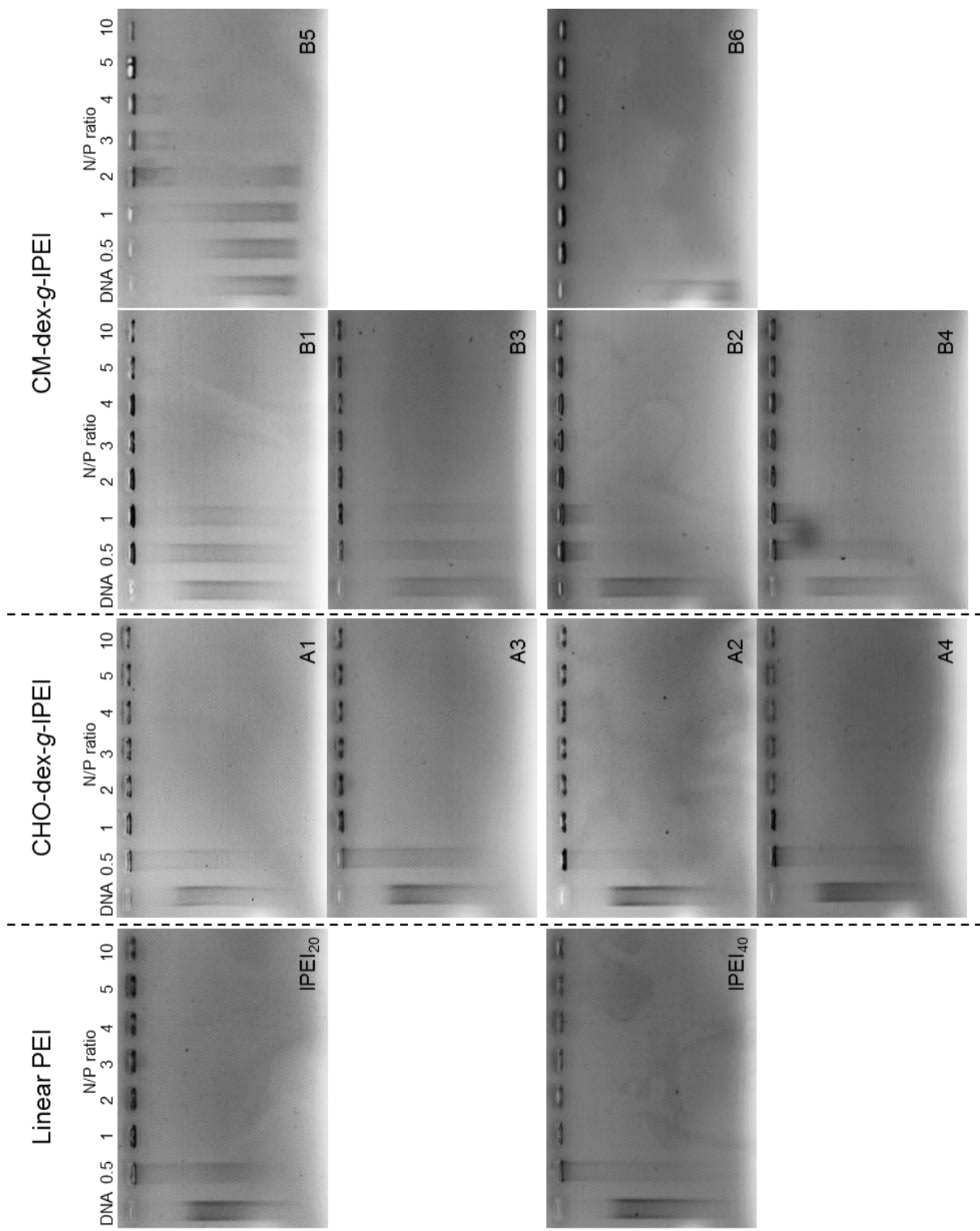


Figure S7. DNA binding capacity of IPEI_{20/40} and dex-g-IPEIs at different N/P ratios in comparison to free DNA, determined by agarose gel electrophoresis.

Complex stability against enzymatic degradation

Complexes were prepared as described above with 4 µg pGL3 plasmid in a total volume of 200 µL 150 mM NaCl solution. DNase I (2.5 Kunitz units/µL, Applichem, Darmstadt, Germany) diluted in 150 mM NaCl and 20 mM MgCl₂ pH 7.4 with an activity of 1.5 Kunitz units/µg plasmid was added to the complex solution, gently mixed and incubated for 45 minutes in a water bath at 37 °C. The enzyme was inactivated in a water bath at 70 °C for 30 minutes. Subsequently, plasmid was released from the complexes by incubation with 10 µL dextran sulfate solution (5,000 g · mol⁻¹, 10 mg · mL⁻¹, Sigma) per µg plasmid at 37 °C for 20 minutes. Naked plasmid treated with DNase I, untreated plasmid, as well as plasmid incubated in the same way like complexes but without enzyme were used as controls. An aliquot of 50 µL complex solution (containing 1 µg plasmid) of each sample were mixed with 5 µL TAE loading buffer and electrophoresed as described above.

Complex size measurement and zeta potential

Size and zeta potential of complexes with N/P ratios of 25 and 50 with 2 µg plasmid were measured with the Zetasizer Nano ZS (Malvern Instruments, Herrenberg, Germany) in 50 mM NaCl and highly purified water. Photon correlation spectroscopy was carried out in a minimal volume cuvette ZEN 0040 (BRAND GmbH, Wertheim, Germany) with a laser beam at 633 nm and a scattering angle of 173° at 25 °C. The viscosity (0.89 mPa · s) and refractive index (1.33) of purified water at 25 °C were used for data analysis. Results are shown as the mean of Z-average of 6 runs ± standard deviation (SD) and calculated with the “General purpose” (normal resolution) algorithm using the Malvern software 6.20. Zeta potential of the complexes was performed in a zetasizer cuvette (DTS1060, Malvern Instruments) by measuring the electrophoretic mobility at 25 °C. The results were calculated with the Malvern software 6.20 and shown as the mean of 6 runs ± SD. All measurements were repeated once.

Cell culture

L929 mouse fibroblasts (German Collection of Microorganisms and Cell Cultures, DSMZ, Braunschweig, Germany) were cultured in Roswell Park Memorial Institute 1640 (RPMI 1640) culture medium supplemented with 2 mM L-glutamine and 10% fetal bovine serum gold (FBS) (all PAA, Pasching, Austria). CHO-K1 (Chinese hamster ovary cells, DSMZ) cells were cultured in Ham's F12 (PAA) supplemented with 1 mM L-alanyl-L-glutamine and 10% FBS (PAA). Cells were subcultured once a week and incubated at 37 °C, 5% CO₂ and 95% relative humidity. To test the absence of squirrel monkey retrovirus, DNA of the cells was isolated (QIAamp[®] DNA Mini kit, Qiagen, Hilden, Germany) and regularly screened by PCR (polymerase chain reaction). Absence of mycoplasma in the cells was periodically tested with a standard test kit (Venor[®] GeM, Minerva Biolabs, Berlin, Germany).

Cytotoxicity of complexes

In vitro cytotoxicity of complexes was tested by the 3-(4,5-Dimethylthiazol-2-yl)-2,5-diphenyltetrazolium bromide (MTT) assay as described by Mosman⁹ and Fischer *et al.*¹⁰ Briefly, complexes were prepared as described above with 3.2 µg herring testes DNA (in 10 mM Tris buffer) and the appropriate amount of polymer to receive N/P ratios of 25 and 50. Afterwards, RPMI 1640 culture medium was added to each complex solution up to 1,210 µL.

L929 mouse fibroblasts (8500/well) were seeded in 96-well plates (Greiner Bio-One, Frickenhausen, Germany) and incubated for 24 h. Afterwards, culture medium was replaced by 110 μL complex dilution/well. Cells were incubated with the complexes for 4 h. Afterwards the test solution was removed and replaced by 200 μL RPMI 1640 medium followed by incubation for further 20 h. The following MTT assay procedure was performed as described before. Absorbance (A) of the samples was measured in a microplate reader (Fluostar OPTIMA) at 570 nm. As blank control culture medium without cells was used. Negative control (100% viability) was determined using cells treated only with culture medium. The positive control (0% viability) was obtained by treatment of the cells with 0.02% thiomersal solution (Synopharm, Barsbüttel, Germany). Relative cell viability was calculated as follows:

$$\text{Relative viability [\%]} = \frac{A_{\text{sample}} - A_{\text{blank}}}{A_{\text{negative control}} - A_{\text{blank}}} \times 100$$

Relative cell viability < 70% was regarded as cytotoxic according to DIN ISO 10993-5.¹¹ All experiments were run with n = 7 and repeated once.

Aggregation of erythrocytes

To investigate the erythrocyte aggregation of the polymers a modified method of Ogris *et al.*¹² was applied. Polymers were tested in phosphate buffered saline (PBS) [8 mM disodium hydrogen phosphate, 1.5 mM potassium dihydrogen phosphate, 137 mM sodium chloride and 2.7 mM potassium chloride (all from Roth)] pH 7.4 at concentrations of 0.024 to 50 $\mu\text{g} \cdot \text{mL}^{-1}$. Sheep blood was collected in heparinized tubes and the serum was removed by centrifugation at 2,880 g for 7 minutes (Eppendorf Centrifuge 5804R, Eppendorf, Hamburg, Germany). The pellet was washed three times with PBS by centrifugation at 2,880 g for 7 minutes and was resuspended in PBS to the initial volume. The red blood cell suspensions were used within 24 h after collection. Erythrocyte suspension (100 μL) containing 20×10^6 erythrocytes/mL was mixed with 100 μL test compound in a 96-well plate (Greiner Bio-One). The plates were incubated under vigorous shaking at 37 °C for 2 h. Afterwards, erythrocyte aggregation was evaluated by microscopic observations (Leica DM IL, Achromat 10/0.20 Phaco 1a objective, 200fold magnifications, Wetzlar, Germany) and the results were classified in three stages. In stage 1 the erythrocytes stay discrete in suspension, no aggregation is detectable. At stage 2 the majority of red blood cells stays separate and shows only a moderate aggregation with rouleau formation. In stage 3 almost all erythrocytes are aggregated in clusters. As negative control for the determination of stage 1, erythrocytes were treated with PBS. As stage 3 (positive control), erythrocytes were treated with a 15 $\mu\text{g} \cdot \text{mL}^{-1}$ solution of 25,000 $\text{g} \cdot \text{mol}^{-1}$ branched poly(ethylene imine) (bPEI, a kind gift of BASF corporation, Ludwigshafen, Germany). Additionally, the aggregation of erythrocytes was analyzed by quantitative measurement of total absorbance at 645 nm with a microplate reader (Fluostar OPTIMA) according to Bauer *et al.*¹³ To quantify the erythrocyte aggregation the calculation of $\Delta\text{Abs}_{\text{max}}$ was established by using the following equation according to Florian Schlenk (personal communication):

$$\Delta Abs_{max} = (A_{negative\ control} - A_{blank}) - (A_{sample\ min} - A_{blank})$$

The experiments were run in duplicate and repeated once. The results are shown as the mean of two experiments ($n = 4$) \pm SD.

Hemolysis of erythrocytes

According to Bauer *et al.*¹³ the hemolytic activity of the dex-g-IPEIs was determined. The erythrocytes were isolated as described in the previous section. Polymers were tested in PBS buffer with concentrations of 0.125 to 1 mg \cdot mL⁻¹. They were mixed with the erythrocyte dilution and incubated on a shaker (Heidolph Instruments Titrimax 100, Schwabach, Germany) at 450 rpm at 37 °C for 1 h. Hemoglobin release was determined by spectrophotometric analysis of 100 μ L supernatant at 544 nm with a microplate reader (Infinite[®] M200 PRO, Tecan, Maennedorf, Switzerland) after centrifugation at 2,250g for 5 minutes (Eppendorf Centrifuge 5804R). As positive control 0.05% Triton X-100 solution (Ferak, Berlin, Germany) was used. Erythrocytes treated with PBS provided the negative control. Percentage hemolysis was calculated according to the following equation:

$$Hemolysis [\%] = \frac{(A_{sample} - A_{blank}) - (A_{negative\ control} - A_{blank})}{A_{positive\ control} - A_{blank}} \times 100$$

Hemolytic activity of the polymers was evaluated with the limit values of the ASTM F756-08 standard.¹⁴ A hemoglobin release of 0%–2%, 2%–5%, or >5% of the total hemoglobin release was classified as non-hemolytic, slightly hemolytic, or hemolytic, respectively. Experiments were run in duplicate and repeated once. The results are shown as the mean of the two experiments \pm SD.

Transfection

CHO-K1 cells (50,000/well) were seeded in 12-well plates (Greiner bio one) and incubated for 24 h. Afterwards, culture medium and complex solution (200 μ L/well) prepared as described above containing 4 μ g pGL3 plasmid at N/P ratios 25 and 50 were added to the wells. Cells were incubated with complexes for 4 h. As controls were used cells treated with 200 μ L physiological saline, free plasmid as well as complexes formed with 2,500 g \cdot mol⁻¹ IPEI (Polysciences Europe GmbH, Eppelheim, Germany) N/P 25. Culture medium was changed, and the cells were incubated for further 44 h. Cells were washed twice with PBS buffer. Lysis of cells and luciferase assay were carried out according to manufacturer's protocol (Luciferase assay system, Promega). Protein mass was quantified with a standard BCA assay kit (Thermo Scientific, Rockford, USA) according to manufacturer's protocol with minor modifications: cell lysate (25 μ L) was incubated with 10 μ L 0.05 M iodacetamide solution (Applichem) to inactivate dithiothreitol (DTT) of the lysis reagent at 37 °C for 20 minutes. The transfection efficiency was calculated as RLU/ μ g protein and presented as the mean of a duplicate testing \pm SD. The experiment was repeated twice.

4. References

- (1) Hoogenboom, R., Paulus, R. M., Pilotti, A., and Schubert, U. S. (2006) Scale-up of microwave-assisted polymerizations in batch mode: The cationic ring-opening polymerization of 2-ethyl-2-oxazoline. *Macromol. Rapid Commun.* 27, 1556-1560.
- (2) Tauhardt, L., Kempe, K., Knop, K., Altuntaş, E., Jäger, M., Schubert, S., Fischer, D., and Schubert, U. S. (2011) Linear polyethyleneimine: Optimized synthesis and characterization – on the way to “Pharmagrade” batches. *Macromol. Chem. Phys.* 212, 1918-1924.
- (3) Altuntaş, E., Knop, K., Tauhardt, L., Kempe, K., Crecelius, A. C., Jäger, M., Hager, M. D., and Schubert, U. S. (2012) Tandem mass spectrometry of poly(ethylene imine)s by electrospray ionization (ESI) and matrix-assisted laser desorption/ionization (MALDI). *J. Mass Spectrom.* 47, 105-114.
- (4) Zhao, H., and Heindel, N. D. (1991) Determination of degree of substitution of formyl groups in polyaldehyde dextran by the hydroxylamine hydrochloride method. *Pharm. Res.* 8, 400-402.
- (5) Wotschadlo, J., Liebert, T., Heinze, T., Wagner, K., Schnabelrauch, M., Dutz, S., Mueller, R., Steiniger, F., Schwalbe, M., Kroll, T. C., Hoeffken, K., Buske, N., and Clement, J. H. (2009) Magnetic nanoparticles coated with carboxymethylated polysaccharide shells – Interaction with human cells. *J. Magn. Magn. Mater.* 321, 1469-1473.
- (6) Perrine, T. D., and Landis, W. R. (1967) Analysis of polyethylenimine by spectrophotometry of its copper chelate. *Journal of Polymer Science Part A-1: Polymer Chemistry* 5, 1993-2003.
- (7) Fischer, D., Bieber, T., Li, Y. X., Elsasser, H. P., and Kissel, T. (1999) A novel non-viral vector for DNA delivery based on low molecular weight, branched polyethylenimine: Effect of molecular weight on transfection efficiency and cytotoxicity. *Pharm. Res.* 16, 1273-1279.
- (8) Tseng, W.-C., and Jong, C.-M. (2003) Improved stability of polycationic vector by dextran-grafted branched polyethylenimine. *Biomacromolecules* 4, 1277-1284.
- (9) Mosmann, T. (1983) Rapid colorimetric assay for cellular growth and survival: Application to proliferation and cytotoxicity assays. *Journal of Immunological Methods* 65, 55-63.
- (10) Fischer, D., Li, Y. X., Ahlemeyer, B., Krieglstein, J., and Kissel, T. (2003) In vitro cytotoxicity testing of polycations: influence of polymer structure on cell viability and hemolysis. *Biomaterials* 24, 1121-1131.
- (11) "Biological evaluation of medical devices part 5: Tests for in vitro cytotoxicity", 2nd edition, International Organization for Standardization/ANSI; ISO ISO 10993-5, Geneva, Switzerland (2009).
- (12) Ogris, M., Brunner, S., Schuller, S., Kircheis, R., and Wagner, E. (1999) PEGylated DNA/transferrin-PEI complexes: Reduced interaction with blood components, extended circulation in blood and potential for systemic gene delivery. *Gene Therapy* 6, 595-605.

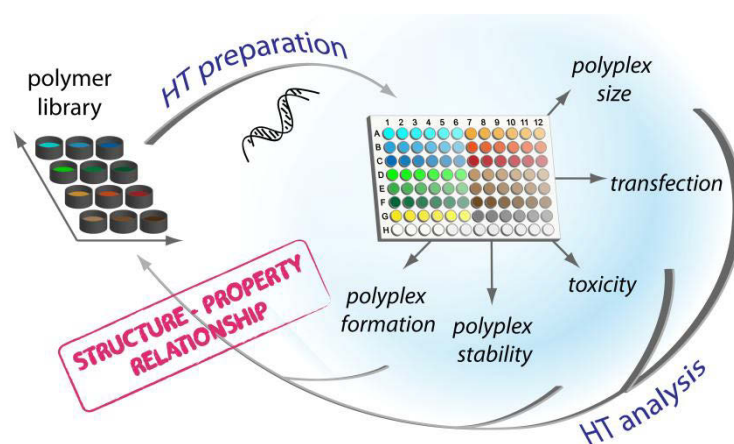
- (13) Bauer, M., Lautenschlaeger, C., Kempe, K., Tauhardt, L., Schubert, U. S., and Fischer, D. (2012) Poly(2-ethyl-2-oxazoline) as alternative for the stealth polymer poly(ethylene glycol): Comparison of in vitro cytotoxicity and hemocompatibility. *Macromolecular Bioscience*, 986–998.
- (14) ASTM F756, 2008, "Standard practice for assessment of hemolytic properties of materials" in *Annual Book of ASTM Standards, Vol. 13. 01*, ASTM, Philadelphia DOI: 10.1520/F0756-08, www.astm.org.

Publication 9

"Parallel high-throughput screening of polymer vectors for non-viral gene delivery: Evaluation of structure-property-relationships of transfection"

Alexandra C. Rinkenauer, #Antje Vollrath, # Anja Schallon, Lutz Tauhardt, Kristian Kempe, Stephanie Schubert, Dagmar Fischer, Ulrich S. Schubert
#equal contribution

ACS Comb. Sci. **2013**, submitted.



Parallel high-throughput screening of polymer vectors for non-viral gene delivery: Evaluation of structure-property-relationships of transfection

Alexandra C. Rinkenauer,^{+,§,#} Antje Vollrath,^{+,§,#} Anja Schallon,^{+,§} Lutz Tauhardt,^{+,§} Kristian Kempe,^{+,§} Stephanie Schubert,^{§,&} Dagmar Fischer,[&] Ulrich S. Schubert^{+,§,#*}

equal contribution

⁺Laboratory of Organic and Macromolecular Chemistry (IOMC), Friedrich Schiller University Jena, Humboldtstrasse 10, 07743 Jena, Germany

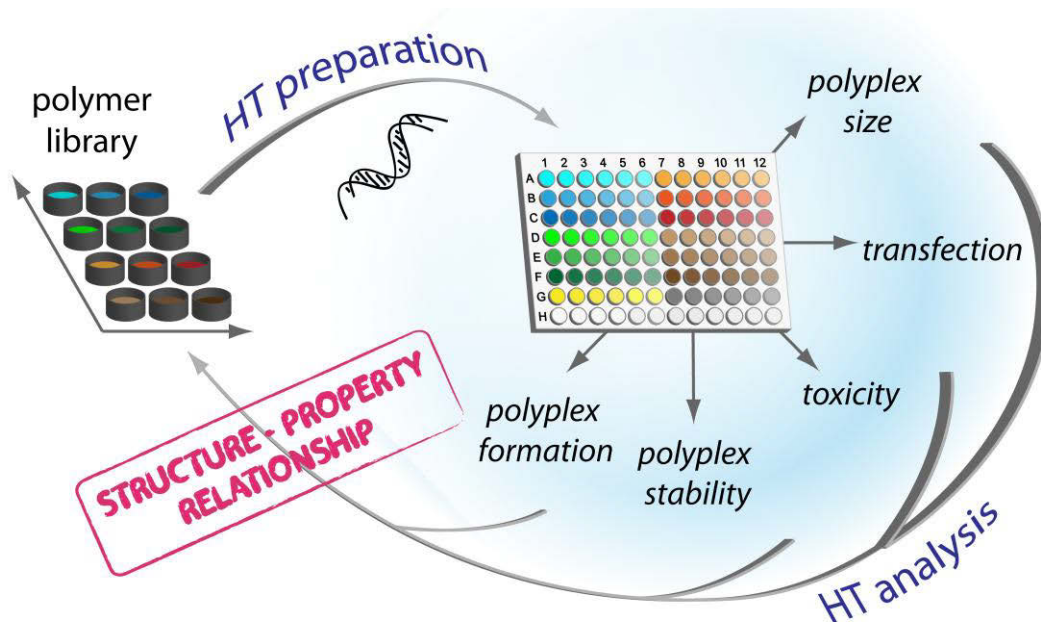
[§]Jena Center for Soft Matter (JCSM), Friedrich Schiller University Jena, Philosophenweg 7, 07743 Jena, Germany

[&]Institute of Pharmacy, Department of Pharmaceutical Technology, Friedrich-Schiller-University Jena, Otto-Schott-Str. 41, 07745 Jena, Germany

[#]Dutch Polymer Institute, P.O. Box 902, 5600 AX Eindhoven, The Netherlands

* Address correspondence to: ulrich.schubert@uni-jena.de

Keywords High-throughput screening, transfection, non-viral gene delivery, polyplex stability, polyethylene imine, heparin, combinatorial workflow



Abstract Within the last years, high-throughput (HT) turned into a keyword in polymer research. In this study we present a novel HT workflow for the investigation of cationic polymers for gene delivery applications. For this purpose, various poly(ethylene imine)s (PEI) were used as representative vectors and investigated *via* HT-assays in a 96-well plate format starting from the polyplex preparation up to the examination of the transfection process. In detail, polyplex preparation, complex size determination, DNA binding affinity, polyplex stability, cytotoxicity, and transfection efficiency were performed in the well plate format. Usually, biological studies are time consuming and, thus, only a few polymers can be investigated under altered conditions (such as pH value, buffer systems, concentration). But with the presented approach, manifold parameters can be tested, and different polymers can be screened in terms of their transfection properties. The HT-workflow represents a great facilitation to gain deeper insights into physiochemical properties as well as biological parameters of polyplexes, like transfection efficiency and cytotoxicity.

Introduction

Beside the evolutionary qualified and very efficient viral gene delivery, non-viral gene delivery (transfection) is of high interest. In particular, the strategy of using cationic polymers as non-viral vectors to form complexes (polyplexes) with the negatively charged plasmid DNA (pDNA) was discovered as promising concept with increased safety and control.^[1, 2] For the evaluation of polymers as transfection agents, two main aspects must be considered: The efficiency of the gene delivery with subsequent reporter gene expression as well as the resulting cytotoxicity.^[3] Biophysical properties, such as polyplex size and surface charge of the polyplexes play thereby a crucial role for the required cellular uptake.^[4, 5] In addition, the interaction between the polymer and the genetic material (binding affinity) has a critical impact since the binding within the interelectrolyte complex of polymer and pDNA has to be strong enough to protect the pDNA, but at the same time must be reversible to release the pDNA inside the cells.^[6, 7] Although strenuous effort was performed to understand the chemical nature as well as the biological function of polymers and the resulting polyplexes, there is still an insufficient knowledge how polymers should be constructed to be highly efficient gene vectors. Certainly, some demands on ideal polymers have already been proposed: (i) Efficient binding and protection of genetic material during delivery, (ii) efficient cellular uptake, (iii) high biocompatibility and (iv) high transfection efficiency.^[8, 9] However, general synthesis rules for the construction of efficient polymers are missing as a result of too diverse methods and polymer classes applied in the published studies. For instance, the transfection protocols differ notably in the used cells and media. Also for the preparation of the polyplexes often different polymer solutions and buffers were used leading to results that are hard to compare.^[10, 11] Up to now, no polymer based transfection agent reached the marketing approval, although they were used for *in vitro* application and in biotechnology since decades.^[12-14] The high-throughput (HT) synthesis and characterization of cationic polymers represents thereby no obstacle, since nowadays manifold polymers can be prepared quasi overnight by synthesis robots.^[15-20] Using this synthetic approach, polymer properties, *e.g.*, molar mass, functional groups, architecture, or the combination of different monomers in statistic

or block copolymers can be altered, yielding systematic polymer libraries, which enable the elucidation of structure-property relationships.^[15-23] But unfortunately, the subsequent biological evaluation is still time consuming and limited regarding a combinatorial HT workflow.^[24] Thus, the biological outcome must be increased to gain deeper insights into the transfection mechanism to allow tailor-made synthesis rules for polymers aimed to be used as transfection vectors. A combinatorial HT workflow, which combines analytic and biological methods, would help to understand how the polymers should be designed specifically to their task.^[25-27] Biological studies such as binding affinity and polyplex stability are commonly performed *via* agarose gel electrophoresis, but are not recommended for HT screenings. However, in recent years, HT experiments using assays in a 96-well plate format have been established to study the binding affinity by usage of an intercalating dye.^[28] Also transfection as well as cytotoxicity assays are performed in 96-well plates, but with repeating samples to reduce measurement mistakes. Moreover, HT screening of a wide range of polymers as transfection agents were described by Langer and coworkers with regard to synthesis and transfection efficiency.^[29] Massing and coworkers presented a HT screening for lipofection reagents also concerning transfection efficiency and toxicity.^[30]

With the aim to solve the bottle-neck in the biological screening of various polymers regarding their complexation behavior with pDNA, a combinatorial high-throughput workflow was developed and is presented herein. The HT workflow starts with the automated polyplex preparation *via* pipetting robots and continues with a parallel and HT analysis of analytical and biological properties like size, binding affinity, stability, transfection, and toxicity. Therefore, poly(ethylene imine) (PEI), the most prominent cationic polymer and most efficient transfection agent for pDNA *in vitro*, was used.^[31] It is a well known system and was studied in detail with regard to the polyplex properties and the transfection efficiency since the 90ies. Thus, it represents an excellent model polymer to be investigated in a HT manner in order to allow a comparison to results described in literature.^[14] In detail, linear PEI synthesized of poly(2-ethyl-2-oxazoline)s of different molar masses, was chosen.^[32, 33] By application of automated microwave synthesizers, poly(2-ethyl-2-oxazoline)s can be obtained within 10 minutes and converted into “pharma-grade” PEI within 1 hour by acidic hydrolysis. The cationic PEI polymers offer the advantage to be molecularly designed in a highly reproducible manner for specific applications in pharmacy or biotechnology. In addition, also commercial branched PEI completed this study. The demonstrated novel workflow is applicable for versatile polymer systems as well as conditions and allows a fast and efficient screening in terms of important vector parameters, such as polyplex formation, pDNA release, cytotoxicity and transfection.

Results and Discussions

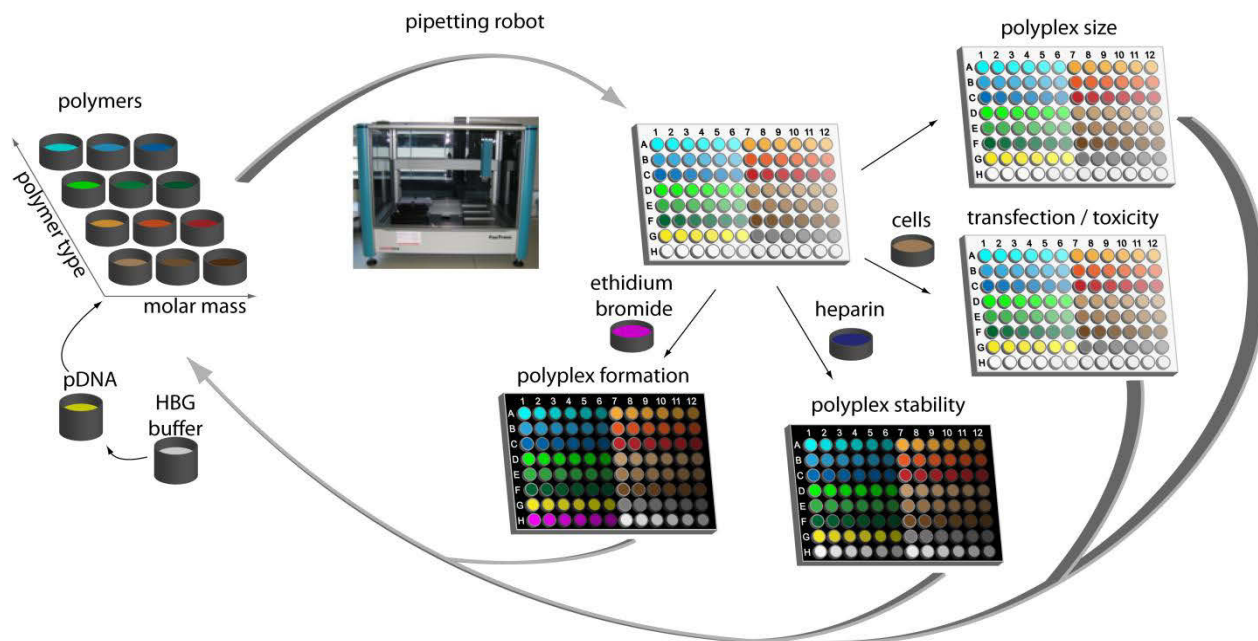
Evaluation of an appropriate buffer system

The polyplex formation of cationic polymers and anionic genetic material is driven by electrostatic interactions and a gain of entropy.^[34] Thus, the ionic strength, the pH value and the final polyplex concentration in the buffer system applied have a major impact on the complexation behavior and the resulting polyplex size.^[35, 36] For the *ex cellular* characterization, polyplexes are often prepared in high ionic strength buffers, such as 150 mM sodium chloride (NaCl) or buffer systems using phosphate (PBS) or TRIS (TBS). It was reported that the high ionic strength of the media has a negative impact on particle size as well as stability and leads to fast aggregation of the polyplexes.^[36] Thus, a low ionic strength 20 mM HEPES buffer with 5% glucose for physiological osmolarity (HBG buffer) was examined for the polyplex preparation. Preliminary studies with linear PEI₆₀₀ revealed that smaller polyplexes were formed in HBG.^[35] A lower tendency to aggregate over time compared to physiological salt solutions (150 mM NaCl) was observed if the polyplexes were prepared in HBG.^[37-39] To confirm the decreased aggregation tendency, the sizes of the polyplexes in HBG prepared by the conventional polyplex preparation methods were compared to the polyplexes prepared using the pipetting robots. No tendency to aggregate or differences in polyplex size were observed (data not shown). Furthermore, the polyplexes in HBG revealed no aggregation or particle growth before and after the addition to serum containing culture media.^[36, 37, 40] This prevents misinterpretation of physicochemical properties as size and biological investigations regarding the cellular uptake behavior. Also convincing is the fact that HBG buffer can be used for zeta potential measurements in this concentration range as well as for electron microscopic evaluations, where salts cause electrophoresis or artifacts, respectively. Consequently, HBG was selected as best appropriate buffer system for the HT approach and was used for all polyplex preparations and its analytical investigations, showing improved potential for structure properties studies.

Polyplex preparation using pipetting robots

For an automated preparation of polyplexes formed of cationic polymers and DNA liquid handling robots, which were usually utilized in peptide chemistry and recently discovered to be also beneficial for the production of polymeric nanoparticles, were used.^[41] The benefit of such pipetting systems is the ability to systematically alter different parameters individually, such as polymer concentration, pH value or buffer system.^[42] The HT polyplex preparation was realized by automatic deposition of a buffered pDNA solution into wells that contain various buffered cationic polymer solutions with the desired concentrations. Although the preparation *via* pipetting robots differs from the conventional preparation methods^[1] (pipetting polymer to DNA solution, vortexing after polymer addition), it was evaluated that similar results could be observed in previous experiments with lPEI₆₀₀ and bPEI₆₀₀ (see methods).

Scheme 1. Workflow of the high-throughput transfection studies for structure-property evaluations concerning molar ratio, size, polyplex formation, polyplex stability, release, transfection efficiency and cytotoxicity.



In order to evaluate the dependency of the polyplex properties on different polymers and preparation conditions, various linear and branched cationic poly(ethylene imine) (LPEI and BPEI, respectively) with varied degree of polymerization ($DP = 20, 200$ and 600) were used to form polyplexes with pDNA. Besides the molar mass and architecture, also several nitrogen (polymer) to phosphate (DNA) ratios ($N/P = 2.5, 5, 10$ and 20) were applied. To this end, a dilution series of previously prepared polymer solutions was provided by using the pipetting robot. Afterwards, pDNA solution was added to each polymer solution, and the resulting suspensions were directly mixed by repetitive suction and release. After the polyplex formation, the prepared polyplex suspensions were distributed each automatically into different well plates for subsequent parallel analysis studies. Although it was reported that a reverse order of pipetting (polymer to pDNA solution) results in higher transfection results,^[43] we observed no influence of the pipetting order. This could be explained by more reversible interelectrolyte formation in the low ionic strength buffer HBG compared to high ionic strength buffer (150 mM NaCl) commonly used.

Investigation of polyplex size and stability

The polyplex size allows a first hint regarding the polymer capability to be used as transfection agent, since it is known that polyplexes larger than 500 nm show a decreased uptake.^[44] For this purpose, dynamic light scattering (DLS) was applied as first analysis technique to determine the dependency of aggregation of the polyplexes on the conditions used for the complex formation.^[45] To evaluate the polyplex formation with regard to the preparation procedure, in first experiments the polyplex sizes were measured manually using the Zetasizer (Malvern).

Polyplexes for all N/P ratios and all PEIs revealed thereby radii between 40 to 100 nm with polydispersities in a range of 0.09 to 0.50 (data not shown). Additionally, selected polyplexes were studied over 2 h and revealed no change in their size (data not shown), which further confirmed the formation of stable polyplexes by utilization of the pipetting robot. However, in order to realize the analysis of the polyplex size in an automatic HT manner, a DLS plate reader was applied. As displayed in Figure 1, all polyplexes revealed here a radius of less than 270 nm, whereby in particular polyplexes with N/P ratios above 5 showed radii below 250 nm. The smallest radius of 70 nm was obtained for the BPEI₂₀₀. It is obvious that higher radii with increased standard deviations were detected by the HT-DLS device. This could be explained by the altered preparation procedure as well as by the different devices and settings. Although HT-DLS results should be always considered with care by application of the HT-DLS device information about the tendency of the polyplexes to aggregate can be obtained and conclusions about the polyplex stability in comparison to standard polymer controls are possible. According to these data, three tendencies were found, also reported in literature: (i) With increasing N/P ratio smaller polyplexes were observed (ii) BPEI with higher DPs showed a stronger size dependency compared to LPEI and (iii) BPEI condensed DNA into smaller particles compared to LPEI.^[31] An influence of the degree of polymerization or the molar mass could not be observed under the chosen conditions.

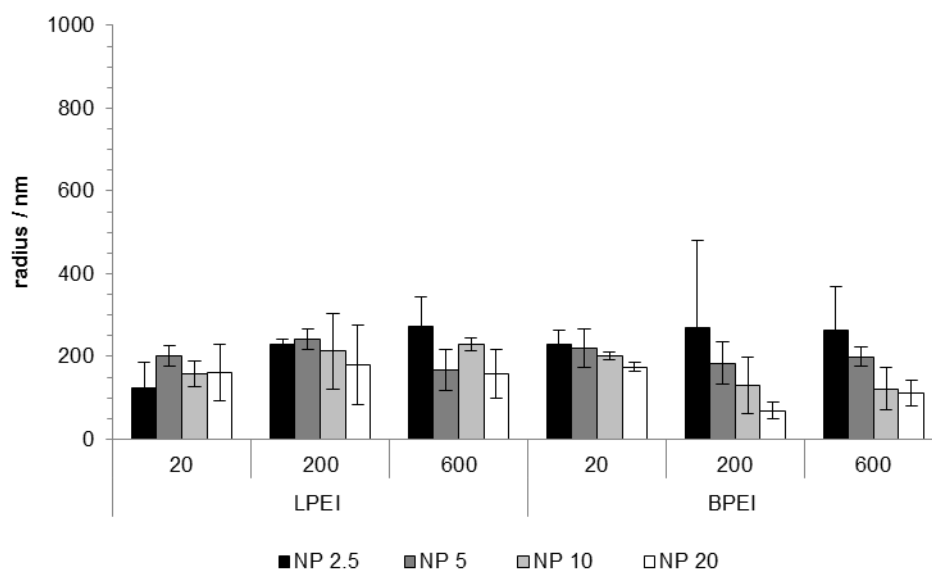


Figure 1. Hydrodynamic radii of polyplexes prepared using they pipetting robot. The values represent the mean ($n \geq 3$) of each polymer at different N/P ratios.

Fluorescence displacement assay

Besides the polyplex size, also the determination of the binding affinity of the polymers to the genetic material is of vital importance for the interpretation of the transfection results. As mentioned before, an optimal polyplex binding is a compromise of a strong, but also reversible interaction in order to protect and transport the genetic material as well as to release the DNA inside the cell. Moreover, by determination of the binding affinity the N/P ratio at which the

polyplexes are formed, could be estimated. This can either be investigated by usage of gel retardation assays or by application of intercalating dyes, such as ethidium bromide (EB) or Pico Green. As the gel retardation method is not suitable for a HT screening in a 96-well plate format, the fluorescence displacement assay with EB was chosen. It is generally known that the binding of EB with the pure pDNA leads to a high fluorescence signal. However, if the pDNA form interelectrolyte complexes with the polymers, the dyes are displaced leading to decreased fluorescence signals. For the investigation of the binding affinity *via* an EB assay, 100 μ L of the polyplex suspension were mixed with EB in each well and analyzed using a fluorescence plate reader. In Figure 2, the fluorescence signals (RFU) of all investigated PEI polymers with increasing N/P ratio are shown. It was found that BPEI₂₀₀ and BPEI₆₀₀ reached a comparable RFU of around $30.5 \pm 1.4\%$ ($p > 0.5$) indicating a strong DNA binding. Furthermore, BPEI₂₀ as well as the higher molar mass LPEIs (LPEI₂₀₀ and LPEI₆₀₀) revealed comparable RFUs in the range of $37.1 \pm 6.2\%$ ($p > 0.1$), whereas the weakest binding was obtained by LPEI₂₀ showing further a strong N/P dependency. In detail, polyplexes formed at N/P -20 revealed a mediate RFU of $48.7 \pm 8\%$ ($p > 0.5$) compared to $73.8 \pm 8.5\%$ at N/P 5. The obtained results demonstrate that the binding affinity depends on the molar mass and the architecture of the polymer as well as on the N/P ratio applied. A proportional increase of the binding affinity was observed with increasing molar mass of the polymer. Furthermore, a higher binding affinity of branched structures (BPEI) was detected in comparison to linear architectures.^[8, 31] Additionally, in the case of LPEI₂₀ it can be seen that the binding affinity correlates with the N/P ratio until a plateau is reached (here at N/P 10). These trends were also reported in literature and confirm the possibility of polyplex analysis by this HT assay.^[46, 47] It should be noted that already at this stage of the workflow, after performing size measurements and binding affinity assays, it is possible to exclude polymers non-suitable as transfection agents, which showed undesired interaction like aggregation or no polyplex formation, respectively.

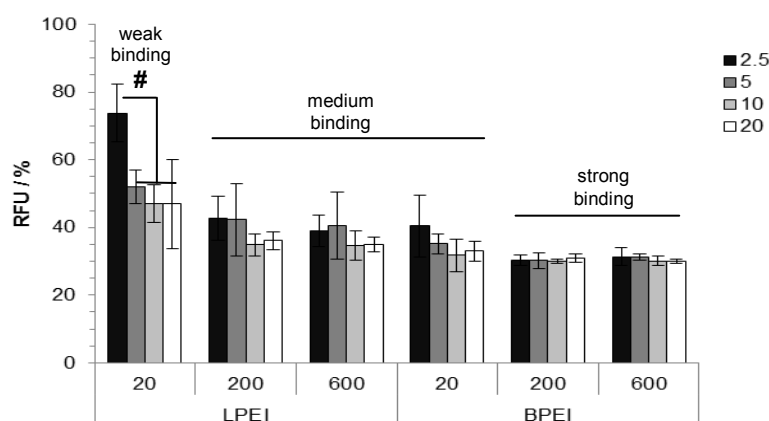


Figure 2. Fluorescence displacement assay using LPEI and BPEI with varying DP. The RLU of single pDNA represent 100% RLU. N/P ratios of 2.5 up to 20 were studied using EB as intercalating agent. The values represent the mean \pm S.D., $n \geq 3$, # indicate significant statistical difference (ANOVA, $p < 0.05$).

DNA release

After determination of the binding affinity, the release of the pDNA from the polyplexes was investigated using the heparin assay. Heparin is a polyanion and was explored to be a good competitor to the negatively charged pDNA.^[47] Thus, it is able to form interelectrolyte complexes with the cationic polymers and, as a result of this polymer-heparin interaction, the pDNA is released and able to interact with the EB as intercalating dye leading to increased fluorescence intensities. The heparin study is often performed *via* gel retardation assays or using one single N/P ratio, which might lead to misinterpretations due to the fact that the given N/P ratio does not represent the molar ratio at each step of the transfection procedure. In particular for *in vitro* cultivations of adherent cells, the concentration at the cell membrane differs between the beginning of the transfection and after incubation due to the polyplex sedimentation process.^[8, 48, 49] In order to determine the critical heparin concentration at different N/P ratios for a more reliable conclusion, all polyplex suspensions were titrated against two heparin stock solutions ($c = 10 \text{ U mL}^{-1}$ and 200 U mL^{-1}) in the fluorescence plate reader at $37 \text{ }^\circ\text{C}$. With this approach, a high range of heparin concentrations (20) can be tested for one sample. The results obtained from the performed assay are displayed in Figure 3. A detailed fluorescence plot for N/P ratios up to 20 for LPEI₆₀₀ is shown in Figure 3 A, whereas a summary of all is presented in Figure 3 C.

As expected, the release of pDNA detected by RFU was dependent on the heparin concentration. Moreover, it was explored that higher N/P ratios required an increased amount of heparin to reach a full pDNA release. This effect was detected for all investigated polymers (Figure 3 C) and is explained by the fact that at high N/P ratios the amount of free polymer is increased, whereas the amount of complexed polymer remains constant.^[50] Thus, by adding heparin to the polyplex suspensions with high N/P ratios, first all free polymers complex with the heparin and no pDNA is released. Only above a critical concentration the pDNA is released, and an increase of RFU can be detected. For an improved comparability, the inflection point of the titration curves in Figure 3 A was defined as the critical heparin concentration (HC_{50}) and implemented as representative value of the concentration at which usually 50% of the complexed pDNA were released.

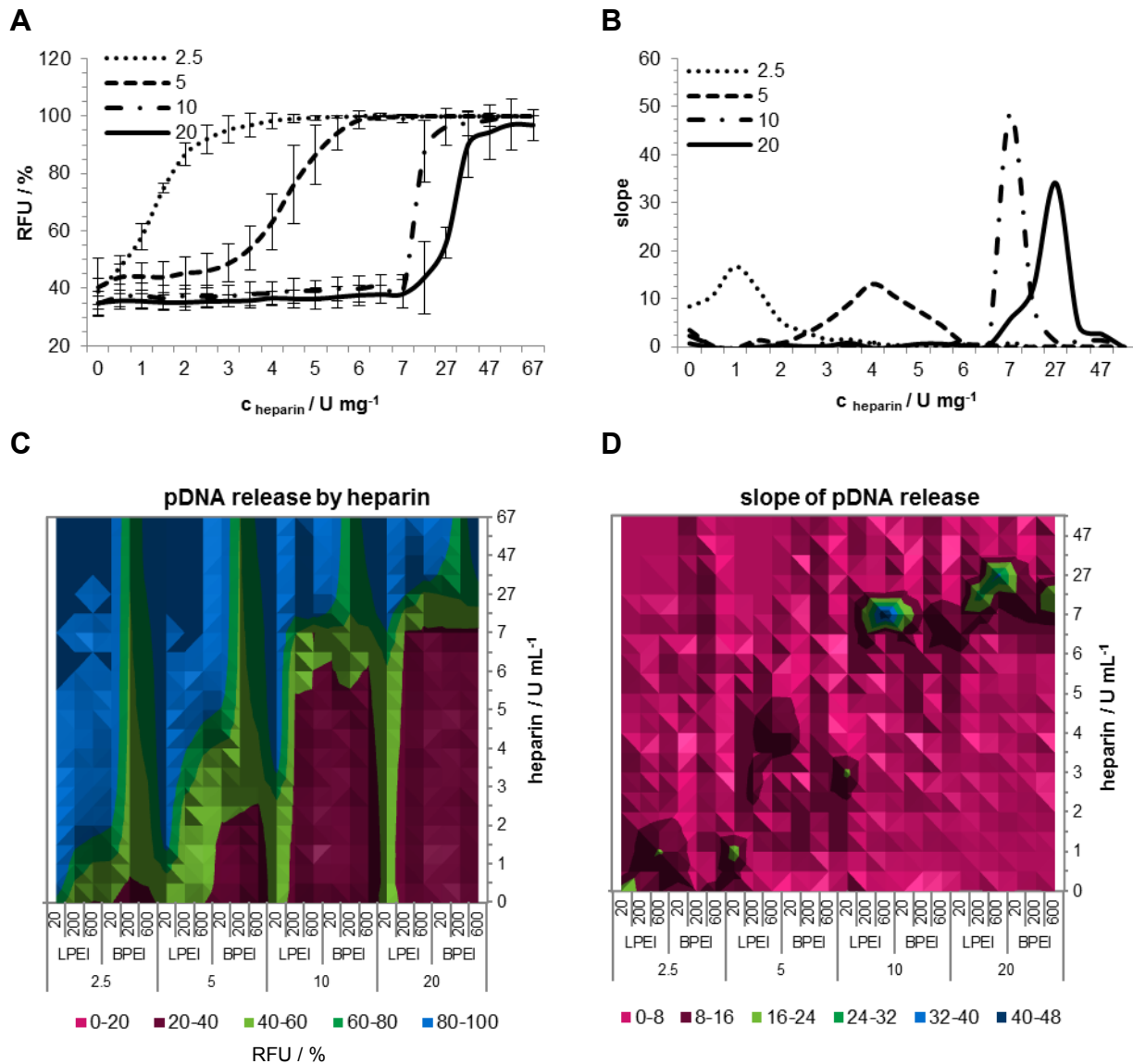


Figure 3. The pDNA release of polyplexes after titration with heparin. Release of pDNA was measured by incubation of polyplexes with increasing heparin concentrations. A) RFU of polyplexes prepared from LPEI₆₀₀ at different N/P ratios and increasing heparin concentrations. B) Slope of RFU of LPEI₆₀₀ polyplexes at different N/P ratios. C) RFU of all polyplexes at different N/P ratios and increasing heparin concentrations. Color represents the RFU. D) Slope of RFU of all polyplexes at different N/P ratios. Color represents the slope. The values represent the mean \pm S.D., $n \geq 3$.

A detailed example of RFU plots of the LPEI₆₀₀ polyplexes is shown in Figure 3 B, and an overview of the HC₅₀ values of all studied polyplex samples is displayed in Figure 3 D. The correlation between the N/P ratio and the heparin concentration was obvious and confirmed already published trends, which are also based on the complex formation of heparin with PEI polymers. However, beside the influence of the N/P ratio, it was observed that the architecture of PEI plays a role in the kinetic of the release. Polyplexes prepared from branched polymers

showed higher HC_{50} values (indicated by larger purple areas in particular at N/P 2.5 and 5, Figure 3 C and D) in comparison to the linear polycations. Furthermore, the polyplexes prepared with the $LPEI_{20}$ showed an early release of the pDNA at low heparin concentrations in comparison to its branched counter piece ($BPEI_{20}$), but also compared to the linear PEIs with higher molar masses ($LPEI_{200}$ and $LPEI_{600}$). These results correlate well to the weak binding affinity obtained with the fluorescence displacement assay (Figure 2).

Cytotoxicity

To study the cytotoxicity of the polyplexes, HEK cells were seeded in 96-well plates and incubated for 24 h with the prepared polyplex suspensions. In order to measure the viability of the cells, they were washed after the incubation and stained with Hoechst 33324, a dye that crosses the cell membrane and stains the chromosomal DNA of attached cells. Subsequently, the fluorescence was measured utilizing the fluorescence plate reader. The obtained RFU signals of Hoechst of all treated cells are presented in Figure 4 A. No indication for cytotoxic effects of the polyplexes was found since the detected values are comparable to non-treated cells (ANOVA, $p > 0.05$). The polyplexes exhibited a lower cytotoxicity than the single polymers due to neutralized cationic groups. Polyplex toxicity at N/P 20 would be a knock out criteria. However, for a comprehensive analysis, the polymers were also screened with regard to their toxicity using polymer concentrations up to $72 \mu\text{g mL}^{-1}$, which is equal to N/P 500 in this case (data not shown). With increasing DP of the cationic polymers a higher cytotoxicity was observed, though no significant difference between linear and branched PEI could be detected.^[31] Interestingly, the polymers with the lowest DP showed no cytotoxicity at all investigated concentrations.

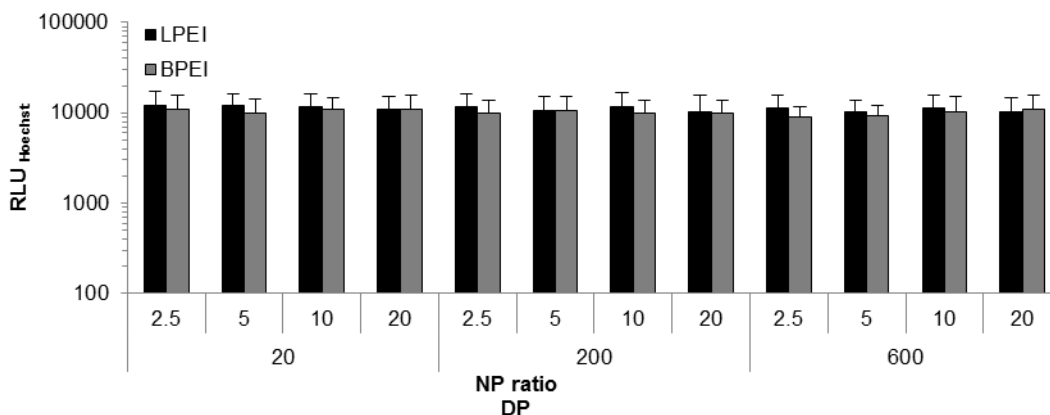


Figure 4. Investigation of cytotoxicity. The viability of cells after incubation of the polyplexes up to N/P 20. Non-treated cells served as controls and gave comparable results. The bottom of 96-well plates were measured at Em_{350}/Ex_{461} (Hoechst 33324).

Transfection efficiency

To allow conclusions about the transfection efficiency of the polymeric vectors, the expression of reporter genes was visualized by fluorescence using an EGFP reporter encoded plasmid. Usually, this expression system is analyzed by flow cytometry analysis. But as this technique is

not suitable for the HT screening approach presented here the transfection efficiency was studied using a microscope and a fluorescence plate reader. To this end, cells were seeded in 96-well plates, incubated with polyplexes for 24 h, stained with Hoechst 33324 and, subsequently, studied with regard to the amount of green fluorescent cells by automatically scanning the wells with the microscope. In Figure 5 A, a representative overview of the cells transfected with LPEI₆₀₀ is displayed. Since a simple microscopic analysis is not sufficiently efficient for a rapid HT screening with regard to the data processing and does not allow a direct comparison of the samples, the mean fluorescence in each picture was measured and calculated. The obtained values are presented in Figure 5 B. In order to study the capability for the quantification of EGFP using a fluorescence plate reader, which would be more efficient and faster, the well plates were additionally screened with this technical device regarding their fluorescence. As demonstrated in Figure 5 B, a good correlation between the microscopic analysis and the fluorescence plate reader results was found, proving the capability to screen the EGFP amount in a fast and easy manner. In general it can be stated that there are some decent advantageous of a fluorescence screening with a plate reader compared to luciferase or galactose based assays, namely: (1) An easy and cheap detection, (2) the possibility to perform single cell analysis by flow cytometry or microscope afterwards of the same cells, and (3) the fact that EGFP is a more stable reporter protein.

The expression of EGFP for all investigated PEI polymers is presented in Figure 5 C. The following order of high to low transfection efficiency was obtained: LPEI₆₀₀ > LPEI₂₀₀ > BPEI₂₀₀ > BPEI₆₀₀ > BPEI₂₀ > LPEI₂₀. Obviously, the standard deviation was increased compared to flow cytometry measurements. However, the HT investigation showed clearly trends confirming that the method is suitable to elucidated high potential candidates, which should be investigated subsequently in more detail. LPEI₂₀ revealed no transfection efficiency, while LPEI₆₀₀ shows the highest one. In between, also branched and linear PEI₂₀₀ reached high transfection efficiencies. The most efficient N/P ratio seemed to be dependent on the specific cationic polymer. While N/P 5 and N/P 10 were optimal for the linear PEIs, BPEI₂₀₀ showed the highest transfection efficiency at N/P 2.5. The results obtained from the screening of the EGFP expression were comparable with non HT transfection procedures, using vortexed polyplexes and flow cytometry (data not shown). This observation further confirms the potential of such a HT screening of the transfection efficiencies of polymers using a fluorescent plate reader.

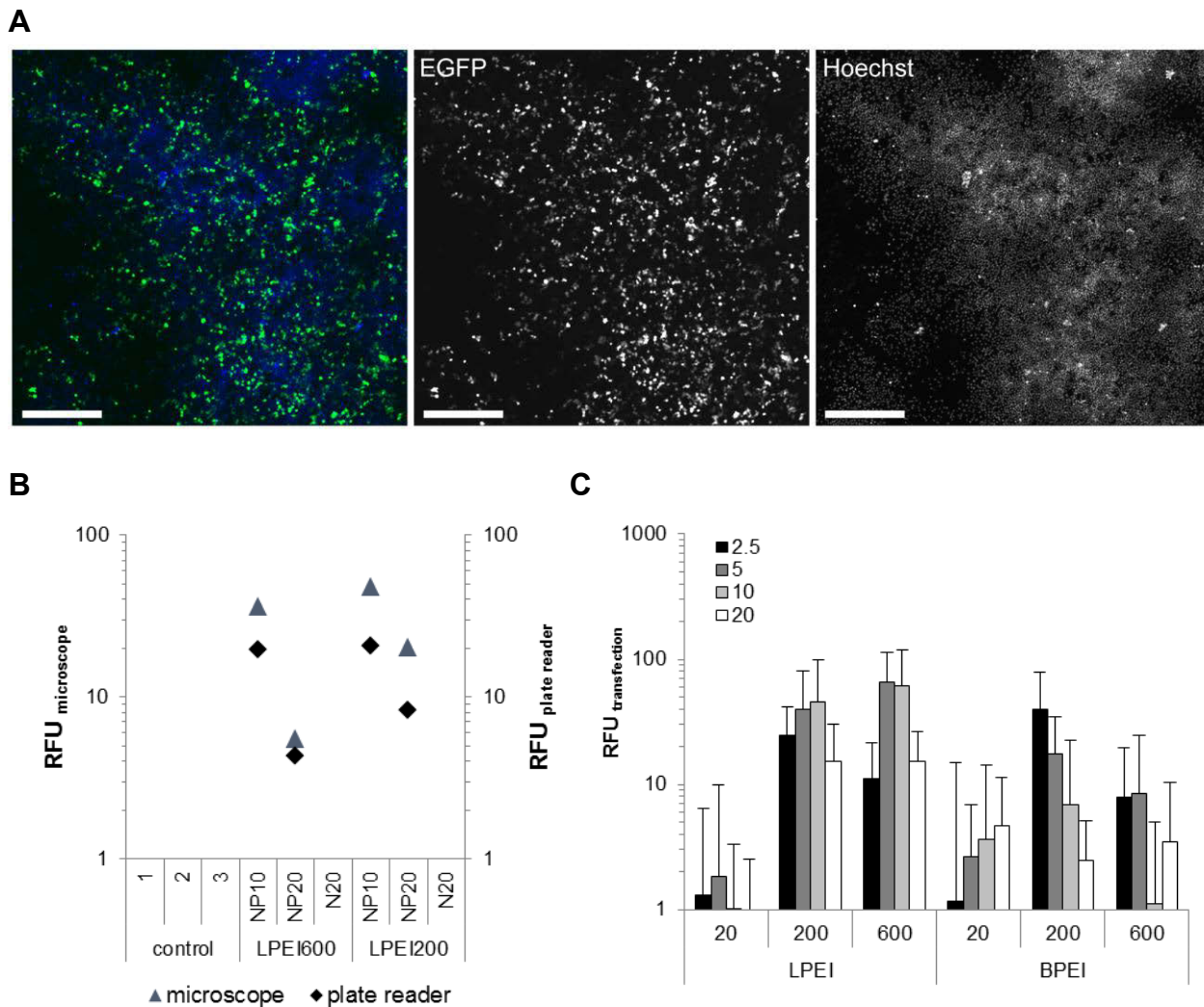


Figure 5. Transfection efficiency by microscopic evaluation and fluorescence intensity measurements. A) HEK cells transfected with EGFP coding pDNA and LPEI₆₀₀ at N/P 10. Cell nuclei were stained with Hoechst 33324 (blue). Scale bare indicates 500 μm . B) Correlation of the microscopic evaluation of EGFP content determined ($\text{RFU}_{\text{microscope}}$) and bottom measurements using a plate reader ($\text{RFU}_{\text{plate reader}}$). Three control wells, where cells were not transfected, as well as cells only incubated with the polymer at concentrations correspond N/P 20 (N20) showed no RFU. C) Transfection efficiency and number of cells transfected with a pipetting robot in a 96-well plate. Values represent the mean \pm S.D., $n \geq 3$.

Conclusion

Since HT synthesis and characterization of polymers could be managed by synthetic robots and microwave synthesizers combined with the subsequent characterization of the molecular properties using fast and automated characterization tools, polymer libraries for biological applications can be prepared with a high variety of parameters in a rapid manner.^[15-20] However, an efficient and fast HT screening of these polymers for gene delivery purposes regarding

structure-property relationship was up to now not possible. In this contribution, a solution for the biological screening bottleneck has been found for gene delivery applications. The discussed HT workflow enables a rapid analysis of polymer vectors in an automated way with respect to important polymer characteristics, such as molar mass, architecture, and N/P ratio used for the pDNA binding and release. By its application it is possible to identify and evaluate reams of polymers with regard to their capability to realize an efficient complexation, protection and transfection of pDNA. For instance, the described heparin assay can be used for 23 polymers at four different N/P ratios resulting in 92 samples plus controls ($n = 1$).^[15-20] By using only one N/P ratio, a further increase in polymer samples up to 30 (triplicate), 46 (duplicate), or 94 (single) is possible. This enables a possible screening of around 360 polymers (one N/P ration, triplicate or three N/P ratios, single) or 1100 polymers (one N/P ration, single) within 24 h. Furthermore, it was demonstrated that the screening of the cytotoxicity and the transfection efficiency of the polyplexes is also possible in a HT manner. As expected, the study of the different PEI model polymers revealed that linear and branched PEI are non-cytotoxic at the investigated concentrations, but that with rising molar mass and polymer concentration the cytotoxic effect was increasing. The polymeric architecture itself showed thereby no influence on the cell viability. At low molar masses the DNA binding affinity is influenced by the polymeric architecture, since BPEI₂₀ revealed a stronger pDNA binding than LPEI₂₀. The obtained results indicated that PEIs with branched architectures and small molar masses have the highest potential to be used as gene vectors, as they offer the advantage of low cytotoxicity combined with high pDNA binding affinity. Although having relatively high binding affinities, the best transfection results were obtained for LPEI₆₀₀ and the BPEI₂₀₀.

It could be proven that the developed workflow is applicable for polymer systems and conditions enabling a fast and efficient screening in terms of important vector parameters, such as polyplex formation, transfection and release. The possible screening of polymer libraries for the best transfection candidate will help to elucidate main polymer characteristics and to understand why some polymers are high performers and others not. Thus, an enhanced development of more efficient polymers and polyplexes can be realized.

Experimental section

Material

Ethidium bromide solution 1% was purchased from Carl Roth (Karlsruhe, Germany). AlamarBlue was obtained from Life Technologies (Darmstadt, Germany). If not otherwise stated, cell culture materials, cell culture media, and solutions were obtained from PAA (Pasching, Austria). Plasmid pEGFP-N1 (4.7 kb, Clontech, USA) was isolated using Qiagen Giga plasmid Kit (Hilden, Germany). All other chemicals were purchased from Sigma Aldrich (Steinhausen, Germany) and are of analytical grade or better and used without further purification. Linear PEI was synthesized according to procedure described in literature.^[32]

Synthesis of LPEI

LPEIs were synthesized from the corresponding poly(2-ethyl-2-oxazoline)s (PEtOx) by acidic hydrolysis as described in literature.^[32, 33] Briefly, PEtOx (2 g) was dissolved in 6 M aqueous hydrochloric acid (15 mL) and heated at 130 °C for 1 h in a Initiator Sixty single-mode microwave synthesizer from Biotage, equipped with a noninvasive IR sensor (accuracy: $\pm 2\%$). The acid was removed under reduced pressure. The residue was dissolved in water and 3 M aqueous NaOH was added until precipitation occurred. The precipitate was filtered off, recrystallized from water, filtered, dissolved in methanol, and precipitated into ice-cold diethyl ether. Subsequently, the LPEI was dried for 3 day at 40 °C. The degrees of hydrolysis were determined by ¹H NMR spectroscopy and found to be 99% for all LPEIs. A detailed characterization of the short LPEI₂₀ can be found elsewhere.^[32, 33, 51] ¹H NMR (300 MHz, CD₃OD): $\delta = 3.65$ (t, CH₂-OH), 2.73 (br., N-CH₂), 2.39 (s, CH₃-N). IR (FT-IR): $\nu = 3217$ (NH), 2 873 (CH₃), 2804 (CH), 1 446 (CH₂/CH₃), 1330 (C-N), 1134 (C-N), 1103 (C-N) cm⁻¹

Table 1. SEC-Data of the PEtOx precursors.

PEtOx precursor	Repeating units ^{a)}	M _n (g/mol) ^{b)}	PDI ^{b)}
PEtOx ₂₀	20	3,600	1.11
PEtOx ₂₀₀	200	58,200	1.14
PEtOx ₆₀₀	600	40,600	1.79

^{a)}Calculated from ¹H NMR; ^{b)}Determined by size exclusion chromatography (solvent: chloroform/triethylamine/ iso-propanol [94/4/2]; calibration standard: PS)

Polyplex preparation using pipetting robot

For an automated polyplex preparation, 100 μ L buffered DNA solution ($c = 15 \mu\text{g mL}^{-1}$) were injected into wells that contain 300 μ L of the desired polymer solution. As cationic polymers, linear PEI with a DP of 20, 200, and 600 as well as branched PEI with a DP of 20, 200, and 600 were applied. In order to achieve different polymer to DNA ratios (N/P ratios), a dilution series in HBG of four different polymer concentrations (N/P ratio 2.5, 5, 10, 20) was prepared using a pipetting robot from a polymer stock solution of $c = 72 \mu\text{g mL}^{-1}$. After addition of the DNA solution, the polyplex suspension was mixed five times by suction and release using 200 μ L tips and incubated at least 20 min. Subsequently, 100 μ L of each polyplex suspension were transferred into three different well plates for a detailed analysis studies. The following assays were performed up to 2 h after polyplex preparation.

Table 2. Hydrodynamic diameter of polyplexes prepared by conventional preparation (vortexed for 10sec, incubated for at least 15 min) and pipetting. Radii were measured with Zetasizer Nano ZS (Malvern Instruments, Herrenberg, Germany).

	METHOD	PEI (μL)	DNA (μL)	HB (μL)	Z Avg (nm)	PDI
lPEI ₆₀₀	pipetted 3x mix	100	50	50	160	0.40
	vortexed 10s	100	50	50	158	0.38
bPEI ₆₀₀	pipetted 3x mix	100	50	50	135	0.23
	vortexed 10s	100	50	50	150	0.43

Investigation of polyplex size and stability

For first studies, the polyplex sizes were studied by utilization of a Zetasizer Nano ZS (Malvern Instruments, Herrenberg, Germany). The measurements were carried out in a minimal volume cuvette ZEN 0040 (BRAND GmbH, Wertheim, Germany) with a laser beam at 633 nm and a scattering angle of 173° at 25 °C. The viscosity (0.89 mPa s) and refractive index (1.33) of purified water at 25 °C were used for data analysis. 40 μL of polyplex suspensions were measured five times for 20 sec. The mean particle size was approximated as the effective (Z average) diameter and calculated with the General purpose (normal resolution) algorithm using the Malvern software 6.20. For the polyplex size analysis by dynamic light scattering, a DynaPro Plate Reader Plus (Wyatt Technology Corporation, Santa Barbara, CA) equipped with a 60 mV linearly polarized gallium arsenide (GaAs) laser of $\lambda = 832.5$ nm and operating at an angle of 156° was utilized. Again, the viscosity (0.89 mPa s) and refractive index (1.33) of purified water at 25 °C were used for data analysis. The data were analyzed with the Dynamics software ver. 6.10 by the method of cumulants as previously described for nanoparticle analysis.^[42] The measurement time was set to 10 seconds per run and 10 acquisitions were collected five times per well and repeated 3 times in independent experiments.

Binding affinity

The polyplex formation and binding affinity responsible for complexation of pDNA and polymers were detected by quenching of the ethidium bromide (EB) fluorescence as described previously.^[52] After the polyplex preparation via pipetting robot, 100 μL of the polyplex solution were incubated with EB (0.4 $\mu\text{g mL}^{-1}$) for 10 min at room temperature in black 96-well plates (Nunc, Langensfeld, Germany). The fluorescence was measured using a Tecan Genios Pro fluorescence microplate reader (Tecan, Crailsheim, Germany) with excitation and emission wavelength at 525 and 605 nm, respectively. A sample containing only pDNA and EB was used to calibrate the device to 100% fluorescence. The percentage of dye displaced upon polyplex formation was calculated using equation (1):

$$\text{RFU} [\%] = \frac{F_{\text{sample}}}{F_{\text{pDNA}}} \quad (1)$$

Here, RFU is the relative fluorescence. F_{sample} and F_{siRNA} are the fluorescence intensities of a given sample and the EB intercalated into pDNA alone.

DNA release by heparin

To investigate the release of pDNA from polyplexes, the heparin dissociation assay was used. For this purpose, 100 μL of polyplex solution were incubated for 10 min with EB ($0.4 \mu\text{g mL}^{-1}$) in a black 96-well plate. After transferring into the Tecan Genios Pro fluorescence microplate reader, heparin solutions were automatically added at the indicated concentrations. Therefore, 20 cycles of the following procedure were used: 5 μL of heparin stock solutions (10 U mL^{-1} or 200 U mL^{-1}) were dropped to each well. Afterwards the plate was shaken (orbital, 10 sec, 2 mm) and incubated for 5 min at $37 \text{ }^\circ\text{C}$. After each cycle, the fluorescence of EB was measured, and the percentage of intercalated EB was calculated as described before (1).

Cell Culture

HEK-293 (CRL-1573, ATCC) cells were maintained in RPMI 1640 culture medium, L929 (CCL-1, ATCC) in DMEM culture medium. Both media were supplemented with 10% fetal calf serum (FCS), 100 $\mu\text{g/mL}$ streptomycin, 100 IU mL^{-1} penicillin, and 2 mM L-glutamine. Cells were cultivated at $37 \text{ }^\circ\text{C}$ in a humidified 5% CO_2 atmosphere.

The cytotoxicity of the single polymers was tested with L929 cells, as this cell line is recommended by ISO10993-5. In detail, cells were seeded at 10^4 cells per well in a 96-well plate and incubated for 24 h. No cells were seeded in the outer wells. Afterwards, polymers at the indicated concentrations were added, the plates were slued, and incubated at $37 \text{ }^\circ\text{C}$ for further 24 h. Subsequently, the medium was replaced by PBS and AlamarBlue as recommended by the supplier. After incubation for 4 h, the fluorescence was measured at Ex 570 / Em 610 nm, with untreated cells on the same well plate serving as controls (2).

$$\text{viability} [\%] = \frac{F_{\text{sample}} - F_0}{F_{\text{control}} - F_0} \quad (2)$$

Here, viability is the relative fluorescence and F_{sample} , F_0 , and F_{control} are the fluorescence intensities of a given sample, the blank wells without cells, and the control cells without polymer treatment.

For transfection experiments, HEK cells were seeded at a density of 10^4 cells per well in 96-well plates 24 h before transfection. In order to avoid any misleading measurement results and to prevent a systematic mistake, the polyplexes were always placed and measured at different positions in the 96-well plate to avoid alterations due to differences in the gas exchange between outer and inner wells and 25 measuring points per well were taken. One hour prior transfection, cells were washed with PBS and supplemented with 100 μL OptiMEM (Life Technologies). Polyplex solutions were added (10 μL) to the cells and the plates were slued and incubated for 4

h at 37 °C. Afterwards, the supernatant was replaced by 100 µL of fresh growth medium (RPMI1640 based), and the cells were further incubated for 20 h. Before analysis, the cells were incubated with 1 µg mL⁻¹ Hoechst 33324 for 10 min at 37 °C, washed twice with PBS, and the plates were transferred to the plate reader. The expression of EGFP fluorescence (Ex 475 nm / Em 509 nm) and viability (Hoechst, Em 350 nm / Ex 461 nm) was quantified by using the fluorescence measured from the bottom of the plates. The transfection efficiency was calculated relative to cell number and control cells using the following equation (3), where EGFP_{sample}, EGFP_{control}, Hoechst_{sample}, Hoechst_{control} are the fluorescence signal of EGFP and Hoechst of treated (sample) and non treated (control) cells, respectively. Experiments were repeated 3 times independently.

$$\text{transfection efficiency [\%]} = \frac{\text{EGFP}_{\text{sample}} - \text{EGFP}_{\text{control}}}{\text{Hoechst}_{\text{sample}} / \text{Hoechst}_{\text{control}}} \quad (3)$$

Acknowledgment

The financial support from the Thuringian Ministry for Education, Science and Culture (grant #B514-09051, NanoConSens), the Dutch Polymer Institute (DPI, technology area HTE, project #729) and the Carl-Zeiss Foundation (JCSM Struktur Antrag) are gratefully acknowledged. We express our gratitude to Caroline Fritzsche for assistance in the cell culture, Dr. David Pretzel for assistance at the microscope as well as Michael Wagner for helpful discussions.

References

- [1] F. Schlenk, S. Grund, D. Fischer, *Ther. Delivery* **2013**, *4*, 95-113. doi: 110.4155/tde.4112.4128.
- [2] D. Pezzoli, R. Chiesa, L. De Nardo, G. Candiani, *J. Appl. Biomater. Function. Mater.* **2012**, *10*, e82-91. doi: 10.5301/JABFM.2012.9707.
- [3] M. Breunig, U. Lungwitz, R. Liebl, A. Goepferich, *Proc. Natl. Acad. Sci. U. S. A.* **2007**, *104*, 14454-14459.
- [4] K. Kunath, A. von Harpe, D. Fischer, H. Petersen, U. Bickel, K. Voigt, T. Kissel, *J. Control. Release* **2003**, *89*, 113-125.
- [5] P. Pereira, A. F. Jorge, R. Martins, A. A. Pais, F. Sousa, A. Figueiras, *J. Colloid Interface Sci.* **2012**, *387*, 84-94.
- [6] Z. Dai, C. Wu, *Macromolecules* **2012**, *45*, 4346-4353.
- [7] K. Itaka, A. Harada, Y. Yamasaki, K. Nakamura, H. Kawaguchi, K. Kataoka, *J. Gene Med.* **2004**, *6*, 76-84.
- [8] M. Neu, D. Fischer, T. Kissel, *J. Gene Med.* **2005**, *7*, 992-1009.
- [9] S. D. Patil, D. G. Rhodes, D. J. Burgess, *AAPS J.* **2005**, *7*, E61-77.
- [10] X. Jiang, W. Qu, D. Pan, Y. Ren, J. M. Williford, H. Cui, E. Luijten, H. Q. Mao, *Adv. Mater.* **2013**, *25*, 227-232.
- [11] R. Iwai, R. Haruki, Y. Nemoto, Y. Nakayama, *Bioconjugate Chem.* **2013**, *29*, 29.

- [12] M. Derouazi, P. Girard, F. Van Tilborgh, K. Iglesias, N. Muller, M. Bertschinger, F. M. Wurm, *Biotechnol. Bioeng.* **2004**, *87*, 537-545.
- [13] M. W. Florian, *Nat. Biotechnol.* **2004**, 1393-1398.
- [14] O. Boussif, F. Lezoualch, M. A. Zanta, M. D. Mergny, D. Scherman, B. Demeneix, J. P. Behr, *Proc. Natl. Acad. Sci. U. S. A.* **1995**, *92*, 7297-7301.
- [15] R. Hoogenboom, M. W. M. Fijten, H. M. L. Thijs, B. M. Van Lankvelt, U. S. Schubert, *Designed Monomers and Polymers* **2005**, *8*, 659-671.
- [16] R. Hoogenboom, U. S. Schubert, *Macromol. Rapid Commun.* **2007**, *28*, 368-386.
- [17] R. Hoogenboom, F. Wiesbrock, H. Y. Huang, M. A. M. Leenen, H. M. L. Thijs, S. F. G. M. van Nispen, M. Van der Loop, C. A. Fustin, A. M. Jonas, J. F. Gohy, U. S. Schubert, *Macromolecules* **2006**, *39*, 4719-4725.
- [18] F. Wiesbrock, R. Hoogenboom, C. H. Abeln, U. S. Schubert, *Macromol. Rapid Commun.* **2004**, *25*, 1895-1899.
- [19] F. Wiesbrock, R. Hoogenboom, M. Leenen, S. F. G. M. van Nispen, M. van der Loop, C. H. Abeln, A. M. J. van den Berg, U. S. Schubert, *Macromolecules* **2005**, *38*, 7957-7966.
- [20] F. Wiesbrock, R. Hoogenboom, M. A. M. Leenen, M. A. R. Meier, U. S. Schubert, *Macromolecules* **2005**, *38*, 5025-5034.
- [21] M. A. R. Meier, R. Hoogenboom, U. S. Schubert, *Macromol. Rapid Commun.* **2004**, *25*, 21-33.
- [22] R. Hoogenboom, M. A. R. Meier, U. S. Schubert, *Macromol. Rapid Commun.* **2003**, *24*, 16-32.
- [23] R. Potyrailo, K. Rajan, K. Stoewe, I. Takeuchi, B. Chisholm, H. Lam, *ACS Comb. Sci.* **2011**, *13*, 579-633.
- [24] S. C. Abeylath, S. Ganta, A. K. Iyer, M. Amiji, *Acc. Chem. Res.* **2011**, *44*, 1009-1017.
- [25] A. Akinc, D. M. Lynn, D. G. Anderson, R. Langer, *J. Am. Chem. Soc.* **2003**, *125*, 5316-5323.
- [26] A. Peters, D. M. Brey, J. A. Burdick, *Tissue Eng., Part B* **2009**, *15*, 225-239.
- [27] A. L. Hook, C. Y. Chang, J. Yang, J. Luckett, A. Cockayne, S. Atkinson, Y. Mei, R. Bayston, D. J. Irvine, R. Langer, D. G. Anderson, P. Williams, M. C. Davies, M. R. Alexander, *Nat. Biotechnol.* **2012**, *30*, 868-U899.
- [28] R. Batchelor, D. Hagen, I. Johnson, J. Beechem, *Comb. Chem. High Throughput Screening* **2003**, *6*, 287-291.
- [29] D. G. Anderson, D. M. Lynn, R. Langer, *Angew. Chem., Int. Ed.* **2003**, *42*, 3153-3158.
- [30] A. E. Regelin, E. Fernholz, H. F. Krug, U. Massing, *J. Biomol. Screen* **2001**, *6*, 245-254.
- [31] L. Parhamifar, A. K. Larsen, A. C. Hunter, T. L. Andresen, S. M. Moghimi, *Soft Matter* **2010**, *6*, 4001-4009.
- [32] L. Tauhardt, K. Kempe, K. Knop, E. Altuntas, M. Jager, S. Schubert, D. Fischer, U. S. Schubert, *Macromol. Chem. Phys.* **2011**, *212*, 1918-1924.
- [33] N. Adams, U. S. Schubert, *Adv. Drug Del. Rev.* **2007**, *59*, 1504-1520.
- [34] A. Schallon, C. V. Synatschke, D. V. Pergushov, V. Jerome, A. H. E. Müller, R. Freitag, *Langmuir* **2011**, *27*, 12042-12051.

- [35] E. V. B. van Gaal, G. Spierenburg, W. E. Hennink, D. J. A. Crommelin, E. Mastrobattista, *J. Control. Release* **2010**, *141*, 328-338.
- [36] E. V. B. van Gaal, R. van Eijk, R. S. Oosting, R. J. Kok, W. E. Hennink, D. J. A. Crommelin, E. Mastrobattista, *J. Control. Release* **2011**, *154*, 218-232.
- [37] M. Breunig, U. Lungwitz, R. Liebl, J. Klar, B. Obermayer, T. Blunk, A. Goepferich, *Biochim. Biophys. Acta, Gen. Subj.* **2007**, *1770*, 196-205.
- [38] D. Goula, J. S. Remy, P. Erbacher, M. Wasowicz, G. Levi, B. Abdallah, B. A. Demeneix, *Gene Ther.* **1998**, *5*, 712-717.
- [39] L. Wightman, R. Kircheis, V. Rossler, S. Carotta, R. Ruzicka, M. Kursa, E. Wagner, *J. Gene Med.* **2001**, *3*, 362-372.
- [40] S. J. Sung, S. H. Min, K. Y. Cho, S. Lee, Y. J. Min, Y. I. Yeom, J. K. Park, *Biol. Pharm. Bull.* **2003**, *26*, 492-500.
- [41] I. Perevyazko, A. Vollrath, S. Hornig, G. M. Pavlov, U. S. Schubert, *J. Polym. Sci., Part A: Polym. Chem.* **2010**, *48*, 3924-3931.
- [42] I. Y. Perevyazko, J. T. Delaney, A. Vollrath, G. M. Pavlov, S. Schubert, U. S. Schubert, *Soft Matter* **2011**, *7*, 5030-5035.
- [43] C. L. Gebhart, A. V. Kabanov, *J. Control. Release* **2001**, *73*, 401-416.
- [44] J. Rejman, A. Bragonzi, M. Conese, *Mol. Ther.* **2005**, *12*, 468-474.
- [45] J. Rejman, V. Oberle, I. S. Zuhorn, D. Hoekstra, *Biochem. J.* **2004**, *377*, 159-169.
- [46] A. C. Grayson, A. M. Doody, D. Putnam, *Pharm. Res.* **2006**, *23*, 1868-1876.
- [47] A. Kwok, S. L. Hart, *Nanomedicine-Uk* **2011**, *7*, 210-219.
- [48] D. Luo, W. M. Saltzman, *Nat. Biotech.* **2000**, *18*, 893-895.
- [49] C. Tros de Ilarduya, Y. Sun, N. Duzgunes, *Eur. J. Pharm. Sci.* **2010**, *40*, 159-170.
- [50] I. Y. Perevyazko, M. Bauer, G. M. Pavlov, S. Hoepfener, S. Schubert, D. Fischer, U. S. Schubert, *Langmuir* **2012**, *28*, 16167-16176.
- [51] E. Altuntaş, K. Knop, L. Tauhardt, K. Kempe, A. C. Crecelius, M. Jäger, M. D. Hager, U. S. Schubert, *J. Mass Spectrom.* **2012**, *47*, 105-114.
- [52] M. X. Tang, F. C. Szoka, *Gene Ther.* **1997**, *4*, 823-832.

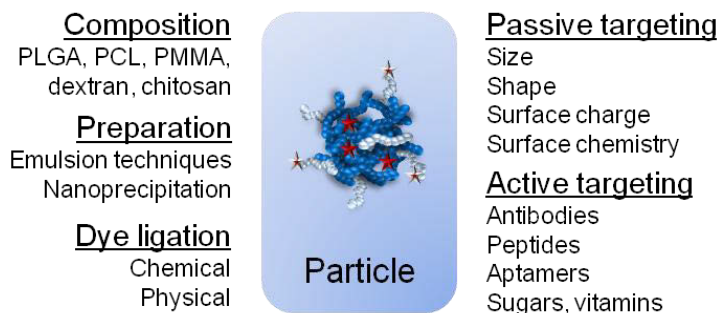


Figure 2.1. Important parameters for the design of polymeric nanoparticles.

Moreover, for *in vivo* applications an active targeting strategy of the nanoparticles is beneficial to ensure a controlled accumulation in the desired tissue.^[38] The idea is to conjugate ligands, such as antibodies, peptides, nucleic acids and other small molecules to the nanoparticle surface, which bind specifically to antigens or receptors that are only expressed on the target cells.^[39] Manifold studies demonstrated that the attachment of targeting units, in particular in combination with a PEG surface modification, significantly increased the accumulation of the nanoparticles in the tumor tissue.^[40,41] The undesired accumulation in healthy organs, such as liver, spleen, heart and lung was thereby decreased, which is beneficial in terms of enhanced cancer detection and unknown long-time consequences that might be accompanied with the application of fluorescent nanoparticles.

In the past few years a great progress in the development of polymer based nanoscale agents could be observed and many promising studies demonstrated the large potential of targeted fluorescent particles for selective imaging. However, in order to realize the usage of polymeric nanoparticles in clinical applications it is certainly required to gain deeper knowledge about their production and design, *in vivo* stability, circulation behavior and their interactions with blood, proteins and cells as well as their definite faith.

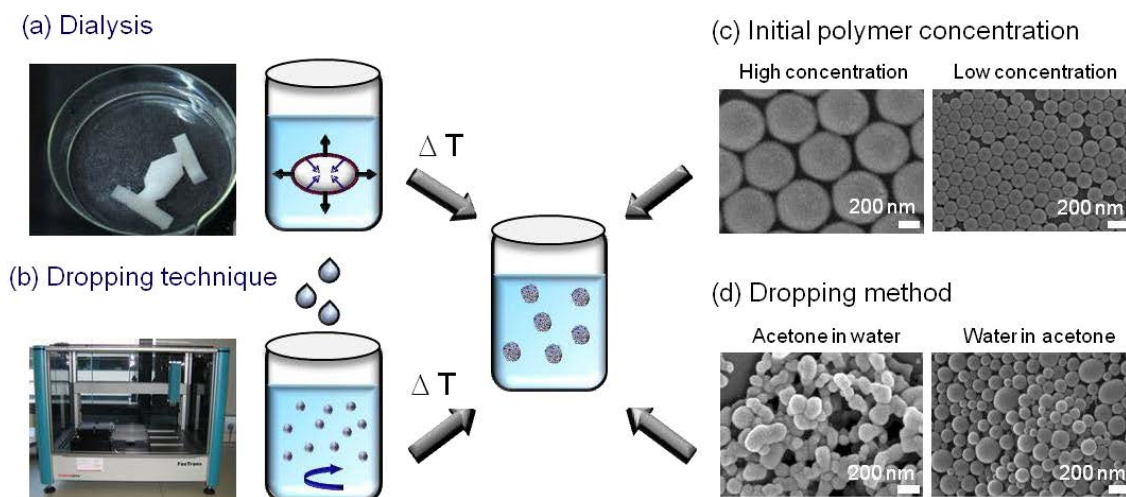


Figure 3.1. Left: Overview about the nanoprecipitation methods (a) of dialysis and (b) dropping technique. Right: Tuning possibilities of the size and shape of the nanoparticles by variation of (c) initial polymer concentration and (d) dropping method.

Stimulated by the successful application of nanoprecipitation for various synthetic polymers, the dropping technique was accomplished in a high-throughput (HT) manner *via* utilization of pipetting robots, in order to facilitate a faster, reproducible, and more in-depth exploration of process-property relationships of the materials. In particular, for the development of improved particle formulations for drug delivery or systematic biotechnological studies, the HT-nanoprecipitation represents a highly suitable tool. In a first set of experiments, the biocompatible polymers poly(methyl methacrylate-*stat*-methylacrylic acid) (p(MMA-*stat*-MAA)_{0.66:0.33}), poly(lactide-*co*-glycolide)_{0.5:0.5} (PLGA) and acetal-derivatized dextran (ac-dex) were chosen to be processed *via* HT-nanoprecipitation (Figure 3.2a). The interplay of the manufacture process and the resulting characteristics of the nanoparticles was thereby investigated by alteration of the initial polymer concentration and the solvent-to-non-solvent ratio (Figure 3.2b). For this purpose, a dilution series of the respective polymer solution with concentrations ranging from 1 mg · mL⁻¹ up to 12 mg · mL⁻¹ was created and combined with different proportions of water, in a way that the solvent (acetone) to non-solvent (water) ratios varied from 0.1 to 0.5 (v/v). After each polymer solution was added dropwise into water, the net result was an array of 96 different formulations, which exhibits a visually observable trend in appearance, following the changes made in the nanoprecipitation process (Figure 3.2b).

The fabricated plates of the different nanoparticle formulations were subsequently characterized with regard to their particle size distribution in an automated manner using a high-throughput dynamic light scattering (HT-DLS) device (Figure 3.2c). The HT-DLS measurements confirmed the dependency of the final average particle sizes on the polymer concentration (Figure 3.3a-c). At diluted polymer concentrations, the nanoprecipitation process yielded small nanoparticle sizes below 100 nm with monomodal and narrow size distributions for all polymers. But with rising concentration, the particle diameters

increased, which was indicated before by the increased turbidity of the suspensions. In detail, 60 nm to 290 nm sized nanoparticles were obtained by nanoprecipitation of the $p(\text{MMA-}i\text{stat-MAA})_{0.66:0.33}$ polymer within a concentration range from $1 \text{ mg} \cdot \text{mL}^{-1}$ to $12 \text{ mg} \cdot \text{mL}^{-1}$ (Figure 3.3a). The sizes of the PLGA nanoparticles varied from 40 nm for $1 \text{ mg} \cdot \text{mL}^{-1}$ to 170 nm for $10 \text{ mg} \cdot \text{mL}^{-1}$, while ac-dex particles revealed increasing sizes from 80 nm to 140 nm for the same range of concentrations (Figure 3.2b,c).

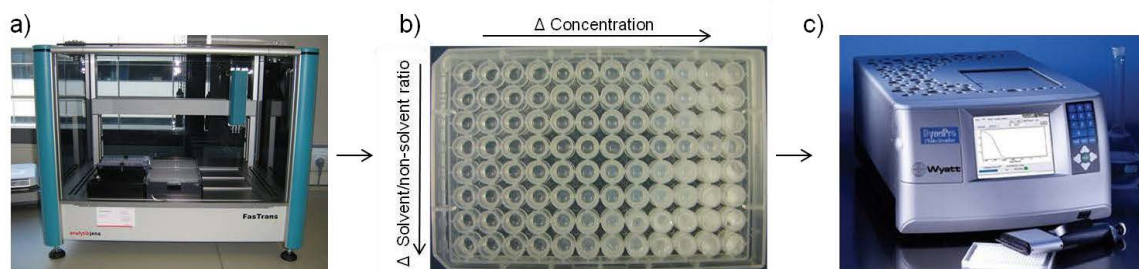


Figure 3.2. HT-experimental set-up: (a) HT-nanoprecipitation of polymers a pipetting robot. (b) Layout of a 96 well plate after nanoprecipitation. The concentration of the polymer is varied along the x-axis and the ratio of solvent/non-solvent solution along the y-axis. (c) The final well plates of different nanoparticle formulations were characterized using HT-DLS.

For all examined polymers the tendency of a growth of the mean particle diameter as a function of initial polymer concentration was detected. This effect was expected since with higher concentration of the polymer in the organic phase more polymer molecules per unit volume of solvent are present. A comparatively small effect on the nanoparticle sizes exhibited the solvent to non-solvent ratio in the studied region. Merely a slight decline in the mean nanoparticle diameter with increasing solvent/non-solvent ratio was observed. Furthermore, the polymer characteristics itself revealed a high impact on the nanoparticle size as well. Regarding to its hydrophobicity and molar mass, a difference in the particle formation for the different polymers is the consequence. By HT-DLS investigations, an exponential growing in the particle size was observed for the $p(\text{MMA-}i\text{stat-MAA})_{0.66:0.33}$ copolymer, while the sizes of the ac-dex particles increase less considerably, and the concentration dependence tends to play a minor role (Figure 3.3d). The tendency obtained for PLGA-nanoparticles is located between the $p(\text{MMA-}i\text{stat-MAA})_{0.66:0.33}$ and ac-dex, and it also tends to show a linear correlation between concentration and size, contrary to the exponential one of the $p(\text{MMA-}i\text{stat-MAA})_{0.66:0.33}$ copolymer. To evaluate the influence of the polymers and the manufacturing parameters on the resulting surface charge of the nanoparticles, zeta potential (ζ) measurements were performed of selected samples. As mentioned in Chapter 2, the zeta potential provides vital information about the nanoparticle stability and affects the cellular internalization as well as the biodistribution *in vivo*.^[17,45] $p(\text{MMA-}i\text{stat-MAA})_{0.66:0.33}$ particles revealed values between $\zeta = -17$ to -65 mV , while a lower surface charge of $\zeta = -14$ to -22 mV was obtained for ac-dex and PLGA particles. A correlation of the zeta potential and particle size was evident due to the fact that the surface charge was increasing with higher polymer concentrations, whereas with varying solvent/non-solvent ratio the measured zeta potential remained unchanged.

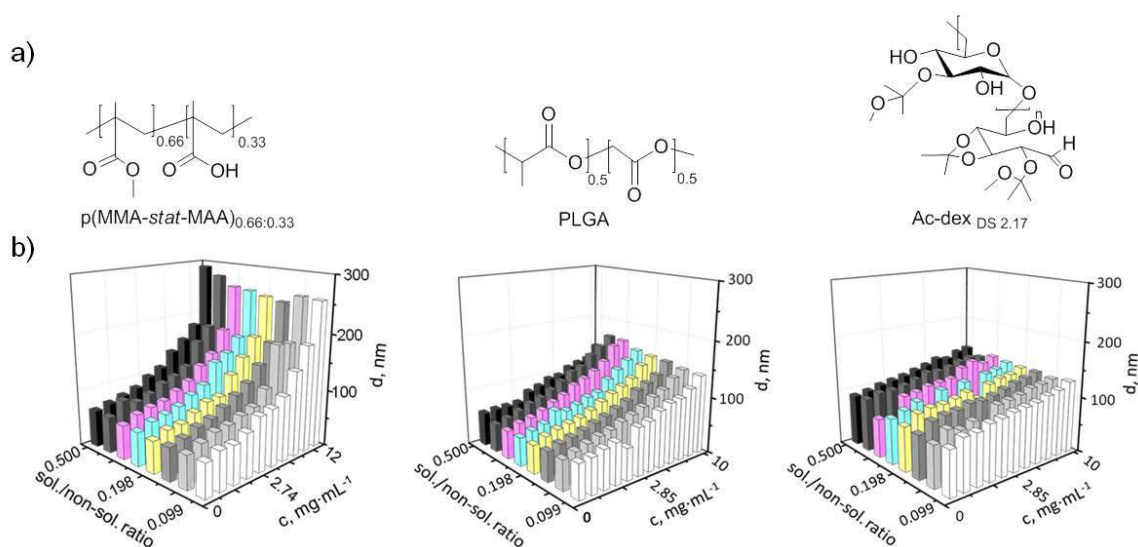


Figure 3.3. (a) $P(\text{MMA-}stat\text{-MAA})_{0.66:0.33}$, PLGA, and ac-dex applied for HT-nanoprecipitation and (b) corresponding 3-D representation of the size distribution obtained by HT-DLS as a function of initial polymer concentration and solvent to non-solvent ratio. The particle suspensions were prepared by dropping the polymer acetone solution into water.

Additional studies were addressed to extend the understanding of the effect of the molar mass of the polymer on the nanoparticle formation. For this purpose, a homologous series of a poly(methyl methacrylate) (PMMA) polymer with molar masses ranging from $3,000 \text{ g}\cdot\text{mol}^{-1}$ to $278,000 \text{ g}\cdot\text{mol}^{-1}$ was applied for the HT-nanoprecipitation process. In first studies identical to previous experiments, the polymer concentration and the solvent to non-solvent ratio were altered. HT-DLS measurements revealed that with increasing molar mass of the PMMA polymer the range of particle sizes was rising as well, while the critical polymer concentration for aggregation was decreased (Figure 3.4). For instance, PMMA with a molar mass of $38,000 \text{ g}\cdot\text{mol}^{-1}$ showed an aggregation of the particles already at an initial concentration above $10 \text{ mg}\cdot\text{mL}^{-1}$, whereas PMMA with a molar mass of $6,000 \text{ g}\cdot\text{mol}^{-1}$ formed stable nanoparticles up to a concentration of $c = 30 \text{ mg}\cdot\text{mL}^{-1}$.

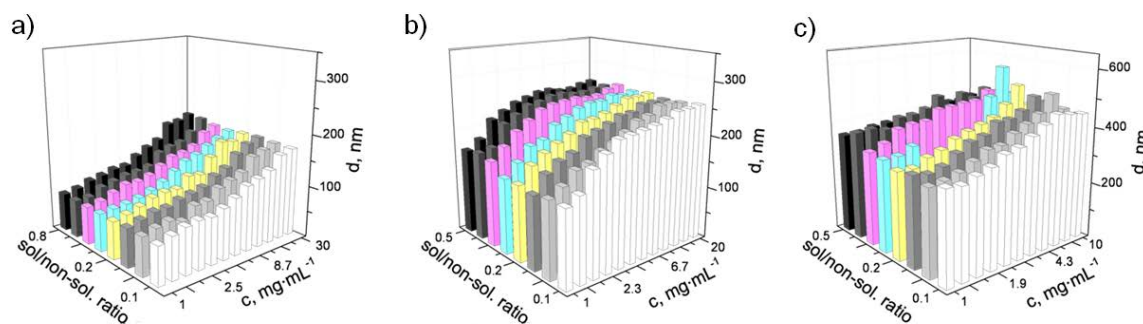


Figure 3.4. 3D-Representation of a size distribution obtained by DLS of PMMA polymers with different molar masses: (a) $M_w = 6,000 \text{ g}\cdot\text{mol}^{-1}$, (b) $M_w = 18,000 \text{ g}\cdot\text{mol}^{-1}$, and (c) $M_w = 38,000 \text{ g}\cdot\text{mol}^{-1}$. The particles were prepared by dropping polymer acetone solution in water.

Table 4.2. Summary of the size distributions of the nanoparticles based on $p(\text{MMA-}i\text{stat-MA}^y)_{0.97:0.03}$.

Sample	Preparation method	d_{DLS} [nm]	PDI _p	d_{SEM} [nm]	d_{AUC} [nm]
S1	Nanoprecipitation	118	0.10	111	120
L1	Nanoprecipitation	488	0.03	696	503
S2	PUC fractionation	120	0.26	131	97
L2	PUC fractionation	597	0.19	502	381

It was explored that the small $p(\text{MMA-}i\text{stat-MA}^y)_{0.97:0.03}$ particle batches (**S1** and **S2**) revealed similar average sizes and size distributions proving the superior qualification of the nanoprecipitation to prepare narrow, defined nanoparticles in a straightforward manner. Contrary, for the larger particles (**L1** and **L2**) diverging sizes were obtained ranging from 400 up to 600 nm, depending on the characterization method applied. Although no remarkable discrepancy in the size plots of the differently prepared particle suspensions could be observed by DLS (Figure 4.2a), the distributions obtained by AUC already illustrate broader size distribution for the samples prepared by nanoprecipitation (Figure 4.2b). This was further confirmed by a detailed analysis of the SEM images, in which the fractionated samples were obviously more uniform in their size than the initial, non-fractionated samples (Figure 4.2c). Yet, it is difficult to predict if a fractionation process by PUC is actually more efficient than using a defined nanoprecipitation process. The precipitation method convinces due to its fast and easy applicability. Furthermore, it already led to monomodal and narrow size distributions for the small nanoparticles. In contrast, for the large particles prepared by nanoprecipitation a broader size distribution was observed (as revealed by AUC and SEM measurements) indicating that the effort to use PUC for more distinct size distribution might be profitable.

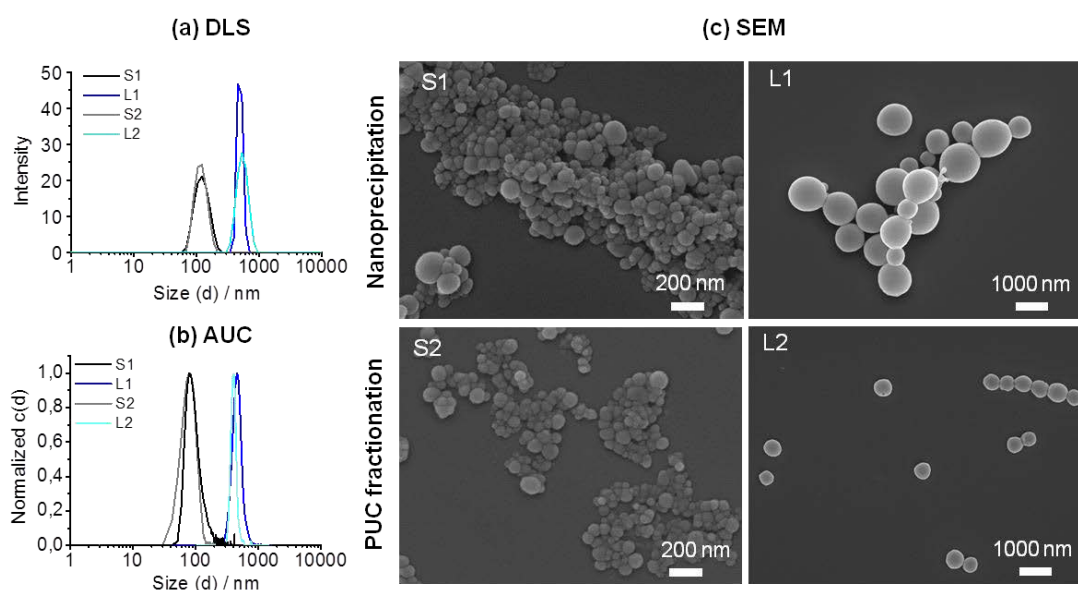
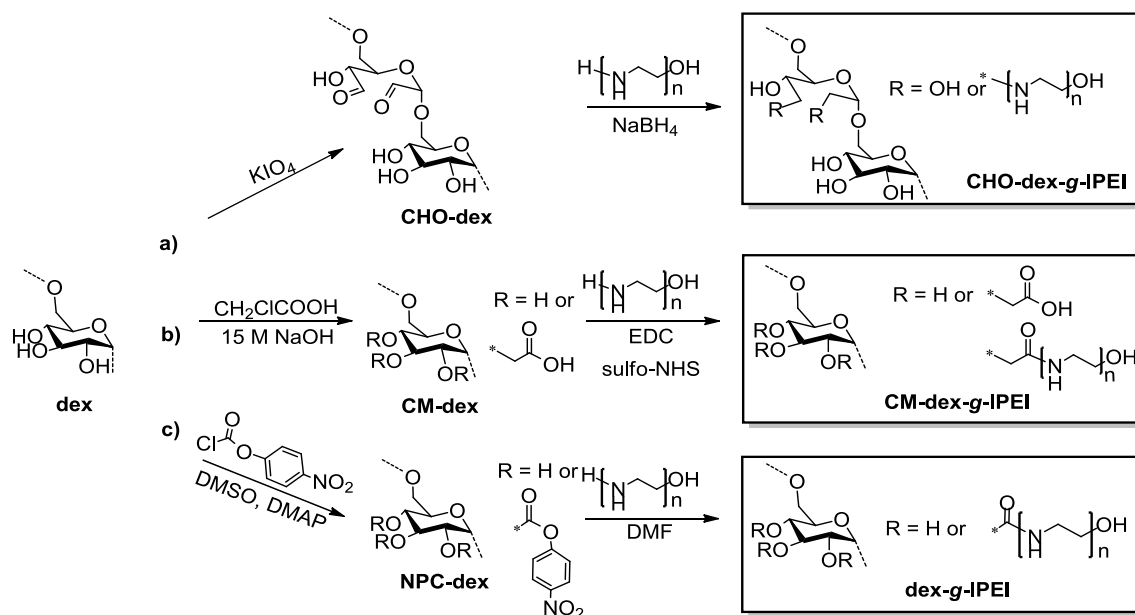


Figure 4.2. Characterization of small and large nanoparticles of $p(\text{MMA-}i\text{stat-MA}^y)_{0.97:0.03}$ prepared by nanoprecipitation and fractionation *via* PUC. Size distributions of the particles in water determined by DLS (a) and AUC (b) as well as SEM images of the particle suspensions (c).

synthesize a range of dextran-*graft*-linear poly(ethylene imine)s (dex-*g*-IPEI): (1) Reductive amination of aldehyde functionalized dextran (CHO-dex), (2) 1-ethyl-3-(3-dimethylamino-propyl) carbodiimide (EDC) coupling of carboxymethylated dextran (CM-dex) and (3) carbamate formation *via* reaction of 4-nitrophenyl carbonate-substituted dextran (NPC-dex) (Scheme 6.1).^[31,80,83]



Scheme 6.1. Schematic representation of the functionalization of dextran by (a) oxidation, (b) carboxymethylation and (c) 4-nitrophenyl carbonate-activation with subsequent reaction with IPEIs *via* (a) reductive amination, (b) EDC coupling and (c) carbamate formation.

To study further the impact of the degree of substitution (DS) of the dextran with IPEI as well as the IPEI chain length, two IPEIs consisting of $n = 20$ and 40 monomer units (IPEI₂₀ and IPEI₄₀) were allowed to react in various ratios with the different dextran precursors. For the grafting of IPEI to the dextran *via* reductive amination, aldehyde enriched dextrans were prepared by oxidation of dextran from *Leuconostoc mesenteroides* with different amounts of potassium periodate (KIO_4). Subsequently, the aldehyde containing precursors were each converted with the IPEI₂₀ and IPEI₄₀, whereas the DS of conjugated IPEIs per AGU was aimed to be at maximum 0.5. After subsequent reduction with sodium borohydride (NaBH_4) and purification by dialysis, the successful binding of the IPEI to the CHO-dex was confirmed by ^1H NMR spectroscopy measurements. The resulting DS of IPEI was calculated from the nitrogen content observed in the elemental analysis and determined to be between 0.13 to 0.38 per AGU (**A series, A1-A4**, Table 6.1).

For the EDC coupling strategy, dextran was first derivatized to CM-dex to introduce carboxylic moieties into the polymer. The carboxymethylation was performed under basic conditions using altered ratios of monochloroacetic acid (CH_2ClCOOH) and altered reaction times.^[84] The final degree of functionalization was determined according to the HPLC procedure described by Heinze *et al.* (Table 6.1).^[85] The subsequent grafting of IPEI₂₀ and IPEI₄₀ to the carboxymethylated carbohydrates was performed with usage of *N*-hydroxysulfosuccinimide (sulfo-NHS) and EDC owing to their well-known coupling

In order to investigate the dependency of the nanoparticle properties on different polymers and preparation conditions, several N/P ratios (2.5, 5, 10 and 20) were applied next to various PEIs. To this end, a dilution series ranging of previously produced polymer stock solutions was provided by using the pipetting robot. Afterwards, a DNA solution was added to each polymer solution, and the resulting suspensions were directly mixed by repetitive suction and release. After the nanoparticle formation, the nanosuspensions were distributed automatically into different well plates for subsequent parallel characterization studies (Scheme 6.2).

Since the complex size allows a first conclusion regarding the polymer capability to be used as transfection agent, DLS was applied as first analysis technique to determine the dependency of aggregation of the PEI/DNA assemblies on the conditions used for the complex formation.^[62] In order to realize the analysis of the complex size in an automatic HT-manner, a DLS platerreader was used. As displayed in Figure 6.1, all PEI/DNA nanoassemblies revealed diameters less than 600 nm. The smallest diameter of 140 nm was obtained for the bPEI₂₀₀. In comparison to previously performed manual size measurements, where complex sizes in a range of 80 to 200 nm were obtained, larger diameters with increased standard deviations were detected by the HT-DLS device. This could be explained by the different devices and settings for the DLS measurements. Although the HT-DLS results should be always considered with care, by application of the HT-DLS device information about the tendency of the polyplexes to aggregate can be obtained and conclusions about the polyplex stability in comparison to standard polymer controls are possible. According to these data, three tendencies were found: (i) With increasing N/P ratio, smaller complexes were formed; (ii) the bPEI revealed a stronger size dependency with higher molar masses in comparison to the IPEI, and (iii) the bPEI condensed the DNA into smaller particles compared to the IPEI (as also reported in literature).^[90] An influence of the degree of polymerization or the molar mass could not be observed under the chosen conditions.

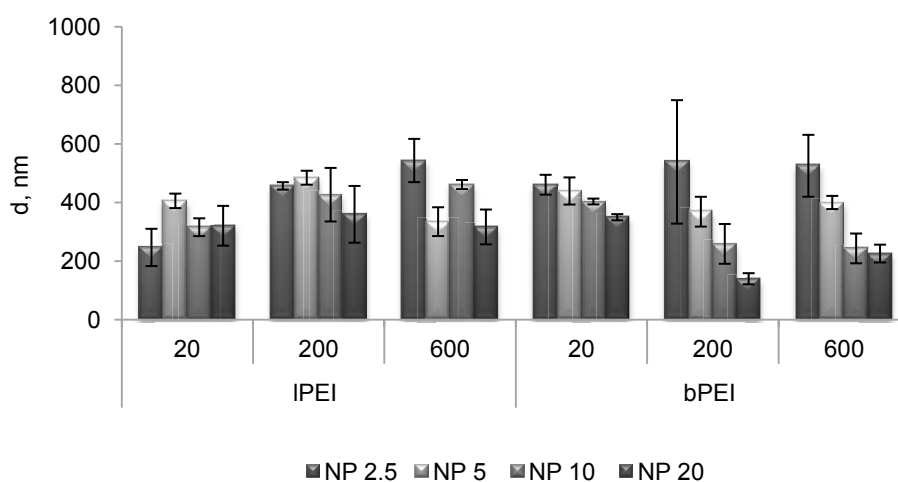


Figure 6.1 Hydrodynamic diameters of PEI/DNA complexes prepared by the pipetting robot. Values represent the mean, $n \geq 3$.

Cite this: DOI: 10.1039/c0xx00000x

www.rsc.org/xxxxxx

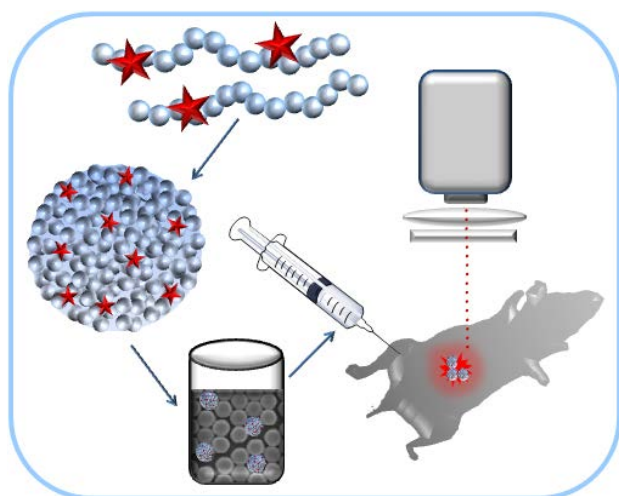
ARTICLE TYPE

Fluorescence imaging of cancer tissue based on metal-free polymeric nanoparticles - Review

Antje Vollrath,^a Stephanie Schubert,^{b,c} Ulrich S. Schubert^{a,b*}

5 Abstract

The utilization of fluorescent nanoparticles (FNPs), which consist of organic fluorophores embedded into a polymer matrix, seems to be a promising concept for *in vivo* cancer imaging showing good biocompatibility, biodegradability, and low toxicity of the agents. Polymeric nanoparticles as fluorescent nanocarriers can be systematically designed with regard to the requested task, *i.e.*, specific accumulation in the tumor tissue. Versatile organic fluorophores can be entrapped into polymers with fine-tuned properties, which were synthesized *via* polymerization techniques. Moreover, the formulation of the nanoparticles can be adjusted, and passive as well as active targeting strategies can be employed. Despite their evident benefits, fluorescent polymeric nanoparticles are still not in clinical application for cancer detection due to a still existing lack in the understanding of their *in vivo* interactions as well as their reproducible production. This review focuses on cancer imaging based on organic dyes and metal-free polymeric fluorescent nanoparticles highlighting recent interesting reports about their design and application as well as their limitations.



Notes and references

^a Laboratory of Organic and Macromolecular Chemistry (IOMC), Friedrich Schiller University Jena, Humboldtstrasse 10, 07743 Jena, Germany;

^b Jena Center for Soft Matter (JCSM), Friedrich Schiller University Jena, Philosophenweg 7, 07743 Jena, Germany

^c Institute of Pharmacy, Department of Pharmaceutical Technology, Friedrich Schiller University Jena, Otto-Schott-Str. 41, 07745 Jena, Germany

E-mail: ulrich.schubert@uni-jena.de

30 Keywords

Nanoparticle, polymers, fluorescence imaging, diagnostic, targeting



Antje Vollrath was born in 1984 in Weimar (Germany) and studied chemistry at the Friedrich-Schiller-University Jena (Germany; 2004–2009) She accomplished the master thesis in 2009 under the supervision of Prof. Ulrich S. Schubert and continued as a PhD student in Jena in the Organic and Macromolecular Chemistry Department. In her PhD studies she focussed on the synthesis of tailor-made

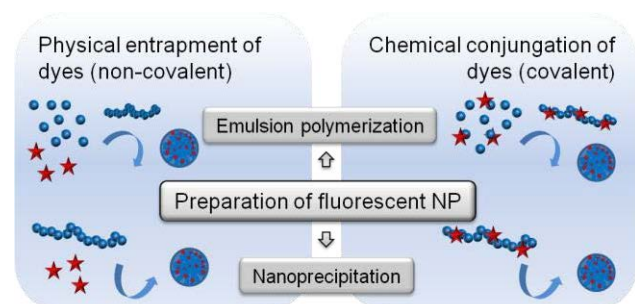
nanoparticles based on synthetic polymers for diagnostic and drug delivery.



Stephanie Schubert (née Hornig) was born in 1981 in Zwickau (Germany). She obtained her MS in chemistry at the Friedrich-Schiller-University of Jena (Germany) in 2005. After research activities at Virginia Tech (Blacksburg, USA), she finished her PhD studies in 2008 in the field of polysaccharide chemistry. During a postdoctoral training with J.M.J. Freché at Berkeley UC (USA), she gained further experiences in polymers as gene delivery

devices. She is currently working on projects related to nanoparticles for drug delivery and sensor applications in the Pharmaceutical Department at the University in Jena.

emerging matrix. The covalent attachment can be realized by copolymerization of original and dye-functionalized monomers.



5 **Figure 1.** Common preparation techniques of polymeric FNPs.

To obtain FNPs *via* the single emulsion technique, the labeled polymer units (covalent method) or a mixture of the polymer and the hydrophobic dye molecules (non-covalent method) are dissolved in a water-immiscible organic solvent (e.g. ethyl acetate, dichloromethane). Subsequently, the organic phase is emulsified in water with usage of appropriate surfactants (poly(vinylalcohol), polysorbate 20) to stabilize the particles, following the evaporation of the organic solvent. Hydrophilic dyes can be encapsulated by the double emulsion process.^[101,102] In this approach, the dye is dissolved in a small volume of an aqueous phase and emulsified in an organic phase that contains the polymer. The mixture is emulsified again in a larger amount of aqueous media. Comparable to emulsion polymerization, the particle size and degree of dye loading can be influenced by the type of polymer and solvents, concentrations, surfactants, emulsification time, and other formulation conditions.

Polymeric NPs are further produced by the nanoprecipitation method (also called solvent displacement) (**Figure 1**).^[97,103-105]

This method presents an alternative, easy, low cost as well as time efficient way to produce polymeric NPs and can be realized in a high-throughput manner.^[106,107] Thereby, particles are readily constructed by exposure of a polymer solution (organic phase) to a non-solvent (water). The major advantages of the nanoprecipitation process over the emulsification procedures are the non-requirement of surfactants and that no additional energy for sonification is required. Moreover, by variation of the initial conditions, such as the solvent/non-solvent ratio and the concentration of the polymer solution, the NP sizes can be tuned from a few nanometers up to 1 μm .^[106] For the dye labeling, the dye molecules are mixed with the polymer in the organic phase prior precipitation, and the dyes are encapsulated during the collapse or arrangement of the polymer molecules; not included dyes can be removed by washing procedures.

To achieve FNPs *via* a covalent procedure, active groups, such as carboxylic groups, amine functionalities or entities that may perform click reactions, are introduced into the polymer backbone for reaction with the dye molecules. Likewise, the dyes also have to provide at least one functionality that can react with the polymer without changing the fluorescence properties. By usage of coupling agents, high conversions can be reached,

though very often a low degree of dye substitution (e.g. few dye molecules per polymer chain) is sufficient as the particles contain multitudes of polymer molecules.

3.4 Design of smart NPs

Manifold biophysicochemical parameters are the key for NPs fate *in vivo*, which emphasizes that NP characteristics, such as size, shape, surface properties, and target unit, should be adjusted very carefully with regard to the final application of the nanocarriers.^[108-111] By implementation of targeting concepts, NPs can be directed to desired active sites (tumors) without adverse effects such as fast clearance by the macrophagocytotic system (MPS) or accumulation in healthy tissue. For improved diagnostic it is essential that the FNPs accumulate, but to a great extend, only in the target site to avoid interferences and to achieve high signal-to-background ratios for refined tumor detection.

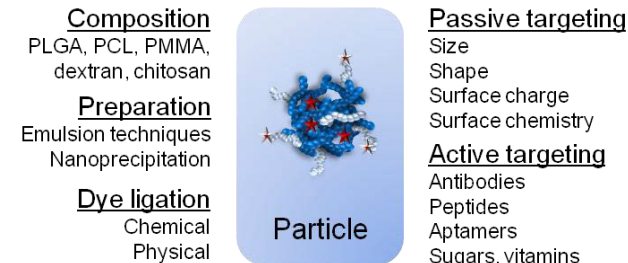


Figure 2. Important parameters for the design of polymeric NPs.

3.4.1 Passive targeting

Size

One of the most important parameters in the NP design is the size. It is evident that particles aimed for intravenous injection should be in a size range not larger than 1 μm in order to ensure long-term *in vivo* circulation without causing any thrombolytic reactions.^[1] In contrast, particles administered to the lung by aspiration of an aerosol can be in the range of several micrometers, and for GI tract imaging the particle size is supposed to be even less important.^[112] In literature, controversial size specifications are found for NPs to be used for *in vitro* and *in vivo* applications.^[107,110-114] The data range thereby from small particles below 10 nm up to 500 nm sized NPs. While NP with a diameter approximately below 30 nm show an efficient cell uptake, they are also rapidly cleared by glomerular filtration in the kidney. Contrary, larger NPs (> 200 nm) show a decreased internalization into cells and increased accumulation in spleen and liver.^[110] The optimal NP diameter is expected to be in the range of 30 to 200 nm, since NPs in that size range benefit from the enhanced permeation and retention (EPR) effect.^[115] The EPR effect exploits that the tumor tissue exhibits different structural features compared to normal cells, such as leaky vessels with enlarged gap functions

Electronic supplementary information

Instrumentation

Sedimentation velocity experiments.

The raw sedimentation data were evaluated by the program Sedfit using continuous $c(s)$, which is based on the numerical resolution of the Lamm equation. It allows the least-squares boundary modeling $ls - g^*(s)$, which describes sedimentation of a non-diffusing species, and to determine the average frictional ratio (f/f_{sph}) of the particles.^{1,2} The partial specific volume v was determined by the density variation method, *i.e.*, by sedimentation velocity experiments on the nanoparticle suspensions, using in parallel H₂O and D₂O. The partial specific volume was found to be $v = (0.78 \pm 0.01) \text{ cm}^3 \cdot \text{g}^{-1}$. Molar masses of the particles were estimated applying the modified Svedberg equation:

$$10 M_s = 9\pi\sqrt{2}N_A\sqrt{[s]^3v}$$

where N_A is the Avogadro's number, v the partial specific volume and $[s]$ is the intrinsic sedimentation coefficient which is defined as:

$$[s] = \frac{s_0\eta_0}{(1-v\rho_0)}$$

where s_0 is the sedimentation coefficient at zero concentration, η_0 the dynamic viscosity of the solvent, and ρ_0 the density of the solvent. The diameters were calculated from the Stokes approximation for a sphere:

$$d = 3\sqrt{2}\sqrt{[s]v}$$

Notes and references

1. P. Schuck, *Biophys. J.*, 2000, **78**, 1606-1619.
2. P. Schuck, P. Rossmannith, *Biopol.*, 2000, **54**, 328-341.
- 20 3. W. G. Martin, W. H. Cook, C. A. Winkler, *Can. J. Chem.*, 1956, **34**, 809-814.
4. W. Maechtle, *Makromolekulare Chemie-Macromolecular Chemistry and Physics*, 1984, **185**, 1025-1039.

25

30

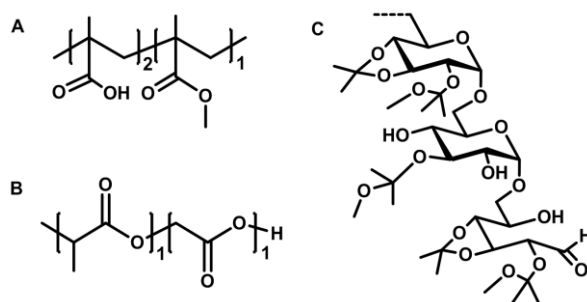


Fig. 1 Chemical structure of the polymers. A - p(MMA-*stat*-MAA)_{2:1}, B - poly(lactic-*co*-glycolic acid) (50:50), C - dextran acetal (DS = 2.17).

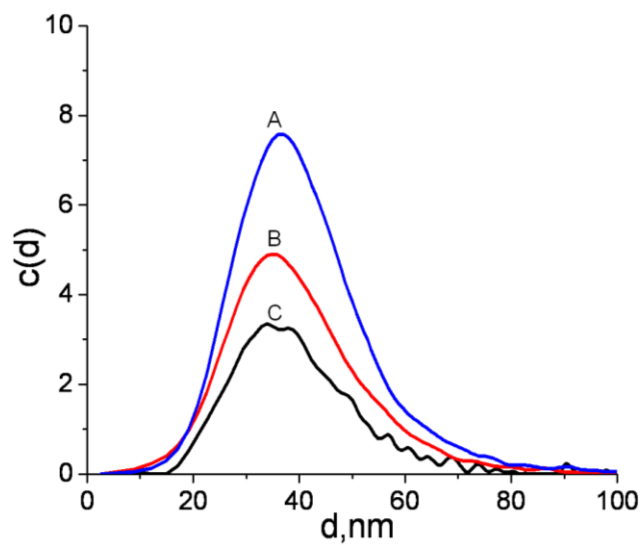


Fig. 2 Size distributions of the nanoparticles at different solvent/non-solvent ratios. The distributions were obtained by sedimentation velocity analysis. The values of the solvent/non-solvent ratio were 0.280 (A), 0.157 (B), and 0.099 (C). The polymer concentration was $3.57 \text{ mg} \cdot \text{mL}^{-1}$. The particles were prepared by dropping the polymer solution into water.

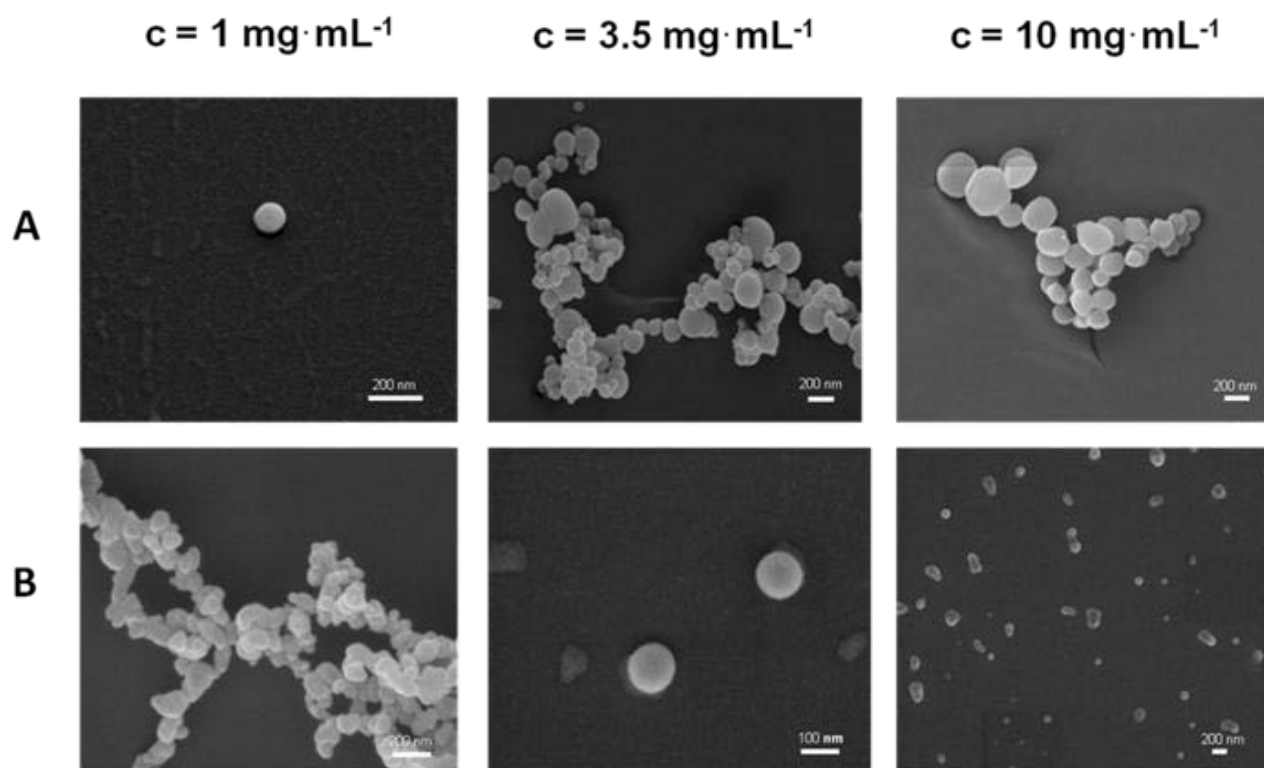


Fig. 3 SEM images of nanoparticles prepared from A) ac-dex and B) PLGA at different polymer concentrations. The particles were prepared by dropping the polymer solution into water.

5

10

15

20

25

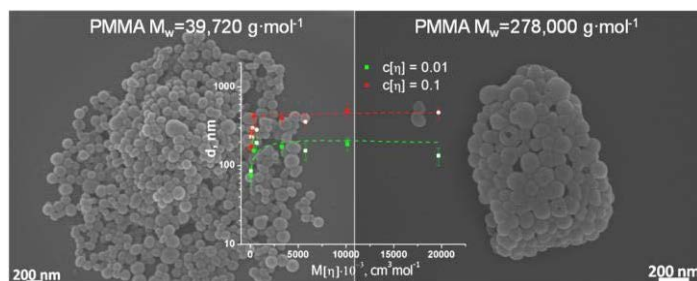
30

Publication 4

"Nanoprecipitation of poly(methyl methacrylate)-based nanoparticles: Effect of the molar mass and polymer behavior"

Igor Y. Perevyazko, Antje Vollrath, Christian Pietsch,
Stephanie Schubert, George M. Pavlov, Ulrich S. Schubert

J. Polym. Sci., Part A: Polym. Chem. **2012**, *50*, 2906–2913.

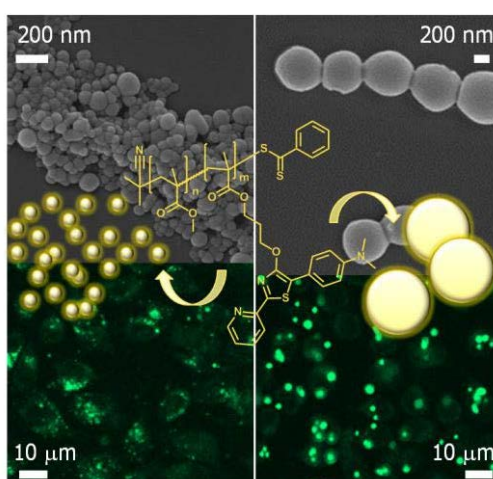


Publication 5

"Preparation, cellular internalization, and biocompatibility of highly fluorescent PMMA nanoparticles"

Antje Vollrath, David Pretzel, Christian Pietsch, Igor Y. Perevyazko,
Roberto Menzel, Stephanie Schubert, George M. Pavlov,
Dieter Weiß, Rainer Beckert, Ulrich S. Schubert

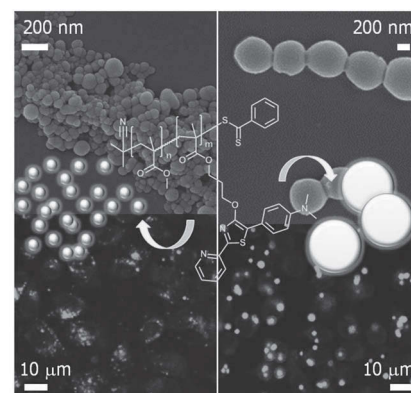
Macromol. Rapid Commun. **2012**, *33*, 1791–1797.



Preparation, Cellular Internalization, and Biocompatibility of Highly Fluorescent PMMA Nanoparticles

Antje Vollrath, David Pretzel, Christian Pietsch, Igor Perevyazko, Stephanie Schubert, George M. Pavlov, Ulrich S. Schubert*

Methacrylate monomers were functionalized with a 4-hydroxythiazole chromophore and copolymerized with methyl methacrylate via RAFT. Nanoparticles of 120 and 500 nm in size were prepared without using stabilizers/surfactants. For comparative studies, preparative ultracentrifugation was applied for the separation into small and large particle fractions. All suspensions were characterized by DLS, AUC, and SEM and tested regarding their stability during centrifugation and re-suspension, autoclavation, and incubation in cell culture media. In vitro studies with mouse fibroblast cell line and differently sized NP showed a particle uptake into cells. Biocompatibility, non-toxicity, and hemocompatibility were demonstrated using a XTT assay, a live/dead staining, and an erythrocyte aggregation and hemolysis assay.



1. Introduction

Recent progress in the area of nanosciences enabled the development of various nanoparticle (NP) devices as powerful tools in the pharmaceutical area for drug delivery

systems, but also in other scientific fields, for example, chemistry, biology, and electronics.^[1–3] In particular for diagnostic applications, like live cell imaging, the investigation of labeled nanosystems (1 to 1000 nm) is rapidly expanding.^[4–8] Such nanodevices can consist of various materials, such as silica, carbon, metal oxides, pure metals, and polymers.^[6,9,10] In particular, quantum dots have revolutionized the biological research with their fascinating light-emitting properties, though still having safety issues due to the liberation of heavy metals.^[2,11] The use of fluorescent polymeric NP represents a suitable alternative to avoid the obstacle of the potential toxicity of metal-based NP. A diversity of biocompatible polymers, such as poly(lactide-*co*-glycolide) and poly(ϵ -caprolactone), are used for formulation.^[12–14] The incorporation of dyes into the polymer shell during NP preparation or the use of labeled polymer systems provides a protection against external influences while keeping their spectral properties, which are essential for the subsequent analysis of particle–cell interactions via confocal laser scanning microscopy.^[7,13,15] A further benefit of polymeric NP is the variety of formulation techniques such as emulsification–solvent diffusion,

A. Vollrath, D. Pretzel, C. Pietsch, I. Perevyazko, G. M. Pavlov, U. S. Schubert

Laboratory of Organic and Macromolecular Chemistry,
Friedrich-Schiller-University Jena,
Humboldtstr. 10, 07743 Jena, Germany
E-mail: ulrich.schubert@uni-jena.de

C. Pietsch, U. S. Schubert

Dutch Polymer Institute (DPI), Post Office Box 902,
Eindhoven 5600 AX, the Netherlands
S. Schubert, U. S. Schubert

Jena Center for Soft Matter (JCMS),
Friedrich-Schiller-University Jena,
Humboldtstr. 10, 07743 Jena, Germany
S. Schubert

Institute of Pharmacy, Department of Pharmaceutical
Technology Friedrich-Schiller-University Jena,
Otto-Schott-Str. 41, 07745 Jena, Germany

nanoprecipitation, spray drying, salting out, and milling processes.^[16–18] By using the appropriate conditions for formulation, specific drugs can be encapsulated resulting in labeled drug carriers of desired sizes and with suitable charges.^[16,18,19]

In the herein presented study, polymethylmethacrylate (PMMA) copolymers were chosen as a model system to demonstrate that functional PMMA-based nanoparticles are well suitable for diagnostic applications such as the imaging of cells. The biocompatibility of PMMA microspheres enables their use in many biomedical applications, for example, as injectable dermal fillers, as PMMA-based NPs for in vitro gene delivery approaches, and also for orthopedic bone reconstruction.^[20–28] For the design of labeled nanosystems, a luciferin-based 4-hydroxythiazole derivative was incorporated into the PMMA polymer backbone, showing benefits as high fluorescence at room temperature with high quantum yields, easy adjustment of the fluorescent properties, and excellent stability.^[29,30] For this purpose, methacrylates were functionalized with the thiazole chromophore (MA^y) and then copolymerized with methyl methacrylate (MMA) using the reversible addition–fragmentation chain transfer (RAFT) polymerization technique.^[29,31–33] For the NP preparation, nanoprecipitation (solvent-evaporation) was chosen as a simple, fast, reliable, and cost-effective method.^[34–36] Different particle sizes were obtained by varying the initial conditions of the formulation. Additionally, preparative ultracentrifugation (pUC) was utilized for the fractionation of particles into discretely sized NP suspensions. It provides another dimension of physical control of the size distribution of particles on the nanoscale.^[14,37–39]

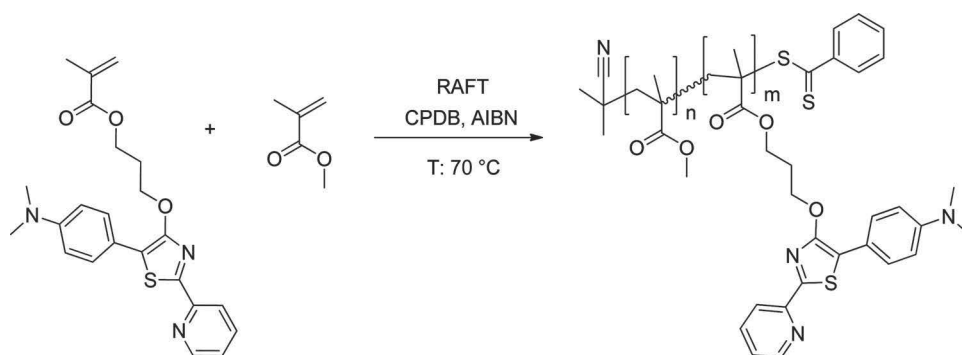
Since the size strongly influences the biodistribution of NPs and the way of internalization into target cells, it is imperative to have well-defined particles with narrow size distributions. Unfortunately, it is a matter of fact that in literature the accuracy of particle size determination is disputable.^[40–42] Consequently, in this distribution,

all suspensions were characterized comprehensively by dynamic light scattering (DLS), scanning electron microscopy (SEM), and analytical ultracentrifugation (AUC) to allow a detailed characterization of the NPs.^[43] The stability of the resulting nanosuspensions after long-time storage, autoclavation, and incubation in cell culture media was studied by measurements of size and zeta potential. The internalization of the differently sized nanoparticles into adherent cells was monitored by confocal laser scanning microscopy (CLSM). The biocompatibility of the particle suspensions in terms of their non-toxicity was proven by XTT cytotoxicity assay and microscopic evaluation of viability after a live/dead staining. Compatibility with blood was analyzed by checking the induction of hemolysis and aggregation of erythrocytes.

2. Results and Discussion

2.1 Synthesis of P(MMA-*stat*-MA^y)

The yellow light-emitting thiazole-dye 3-((5-(4-(dimethylamino)phenyl)-2-(pyridin-3-yl)thiazol-4-yl)oxy)propan-1-ol was attached to the methacrylate monomer by an esterification reaction. The non-classical 4-hydroxy-1,3-thiazole chromophore structure is similar to the luciferin dye of fireflies and shows excellent fluorescent properties.^[44] The resulting dye-functionalized methacrylate MA^y was copolymerized statistically with MMAs using the RAFT polymerization methodology (Scheme 1).^[31–33] The reaction was carried out using AIBN as a radical initiator, toluene as a solvent, and 2-cyano-2-propyl dithiobenzoate (CPDB) as a chain transfer agent. The ratio of MMA to the dye-functionalized monomers was 69:1, leading to a final conversion rate of 70% of the copolymers with a DP of 100. The dye-functionalized methacrylates were statistically distributed in the polymer backbone due to the same reactivity of both monomers.^[29] The low degree of labeling (1 to 3%) ensured the preservation of the properties of the PMMA



■ Scheme 1. Schematic representation of the synthesis of p(MMA-*stat*-MA^y).

Table 1. Summary of the size distributions of the nanoparticles based on p(MMA-*stat*-MA^y).

Sample	d_{DLS} [nm]	$\text{PDI}_{\text{particle}}$	d_{SEM} [nm]	d_{AUC} [nm]	ζ [mV]
S1	118	0.10	111	120	-36
L1	488	0.03	696	503	-35
S2	120	0.26	131	97	-32
L2	597	0.19	502	381	-33

homopolymer. As determined by SEC, the final p(MMA-*stat*-MA^y) revealed a molar mass (\bar{M}_n) of 8500 g mol⁻¹ with a polydispersity index value of 1.19 (Table S1, Supporting Information). Similar molar mass distributions recorded by both RI and UV detector clearly demonstrate that the thiazole dye was incorporated into the copolymer. The ratio of the MMA units and the thiazole dye in the copolymer was determined to be 2.9 mol% by ¹H NMR spectroscopy. The final copolymer showed the same absorbance and emission behavior like the monomeric thiazole chromophore (solvent acetonitrile; $\lambda_{\text{Abs}} = 413$ nm, $\lambda_{\text{Em}} = 557$ nm, Stokes-shift 6259 cm⁻¹, Figure S1, Supporting Information) with a quantum yield of $\Phi_{\text{PL}} = 0.29$.

2. 2 Nanoparticle Preparation and Characterization

The so-called nanoprecipitation or solvent evaporation process was found to be a suitable method for the preparation of differently sized NPs. Therefore, this simple, fast, and cost effective technique was applied for the preparation of p(MMA-*stat*-MA^y) NPs.^[34,45] The final particle size was tuned by variation of the initial polymer concentration in the organic phase and/or by changing the dropping method (polymer solution into water or water into polymer solution).^[46] In order to obtain small particles (**S1**), a polymer solution with a concentration of 4 mg mL⁻¹ was dropped into water. For larger particles (**L1**), water was dropped into the polymer solution with a concentration of 3 mg mL⁻¹. In general, a solvent/non-solvent ratio of 0.25 was used and continuous stirring was applied. After evaporation of the acetone, the particle sizes were examined by DLS. The Z-average diameter for the nanoparticles suspensions **S1** and **L1** was determined to be $d_{\text{S1}} = 118$ nm ($\text{PDI}_{\text{P}} = 0.10$) and $d_{\text{L1}} = 488$ nm ($\text{PDI}_{\text{P}} = 0.03$), respectively (Table 1). The resulting size distributions were monomodal (Figure 1). In addition to nanoprecipitation, preparative ultracentrifugation (pUC)^[47] in a density gradient was used for the separation of defined NP. For pUC, a thin layer of a particle suspension to be fractionated is layered on the top of a solution containing the density gradient. When a centrifugal field is applied, the various components move through the gradient at different rates depending on their sizes, densities, and shapes.^[37–39,48] In this respect, a particle

suspension with a broad size distribution was separated by pUC into fractions **S2** and **L2**. DLS and AUC measurements indicated particle sizes of $d_{\text{S2}} = 120$ nm ($\text{PDI}_{\text{P}} = 0.29$) and $d_{\text{L2}} = 600$ nm ($\text{PDI}_{\text{P}} = 0.19$, Table 1). The small increase of the PDI_{P} values of **S2** and **L2** compared with **S1** and **L1** might be caused by a slight agglomeration of the NP during the pUC treatment. The zeta potential of all suspensions were in the same range ($\zeta = -32$ to -36 mV) and thereby testified a good stability of the NP in suspension. SEM investigations were performed to obtain further information about the size and shape of the particles (Figure 1). The small particles **S1** and **S2** revealed more irregular shapes than the larger ones (**L1** and **L2**), which might be caused by the preparation technique, that is, dropping acetone in water, which is characterized by the fast exchange of the solvent against the non-solvent environment.^[34,35] For the small particles, the calculated diameters were in good agreement with the DLS results ($d_{\text{S1}} = 111$ nm, $d_{\text{S2}} = 131$ nm), whereas the large particle samples were characterized by slightly increased sizes in the particle fractions ($d_{\text{L1}} = 696$ nm, $d_{\text{L2}} = 502$ nm, Table 1). Complementary, the analysis of the samples by AUC revealed diameters of $d_{\text{S1}} = 120$ nm and $d_{\text{L1}} = 503$ nm as well as $d_{\text{S2}} = 97$ nm and $d_{\text{L2}} = 381$ nm, respectively. In order to exclude the occurrence of bulk precipitation and Ostwald ripening even over a long period of time, the nanosuspensions were stored at 5 °C for 6 months and examined again regarding their zeta potential and size distribution. No signs of instability of the initial nanosuspensions were found in terms of agglomeration or creaming up. It should be mentioned that no surfactants were added to inhibit particle aggregation. In addition, samples of the initial NP suspension were analyzed by DLS and SEM after centrifugation at 24.650 g for 20 min, autoclavation, lyophilization, and subsequent resuspension. Neither the size distributions nor the zeta potential values changed, which ensured the high stability of the p(MMA-*stat*-MA^y) nanoparticles. The absorption and emission spectra of the nanosuspensions in comparison to the monomer were equal within the range of the measurement errors (± 5 nm). This implies that the fluorescence properties of the monomers were unaffected by polymerization and NP formation.

2. 3 Biological Experiments

In order to prove the efficient internalization of the particles into cells, mouse fibroblasts L929 were incubated with 120 and 500 nm sized nanosuspensions prepared by nanoprecipitation and pUC separation, respectively. The internalization of the NP into the cells was monitored by CLSM (representative micrographs are shown in Figure 2). On the basis of the relative size distribution of their corresponding fluorescence signal, a clear discrimination of small and large particles was possible. Furthermore, a concentration-dependent internalization of all

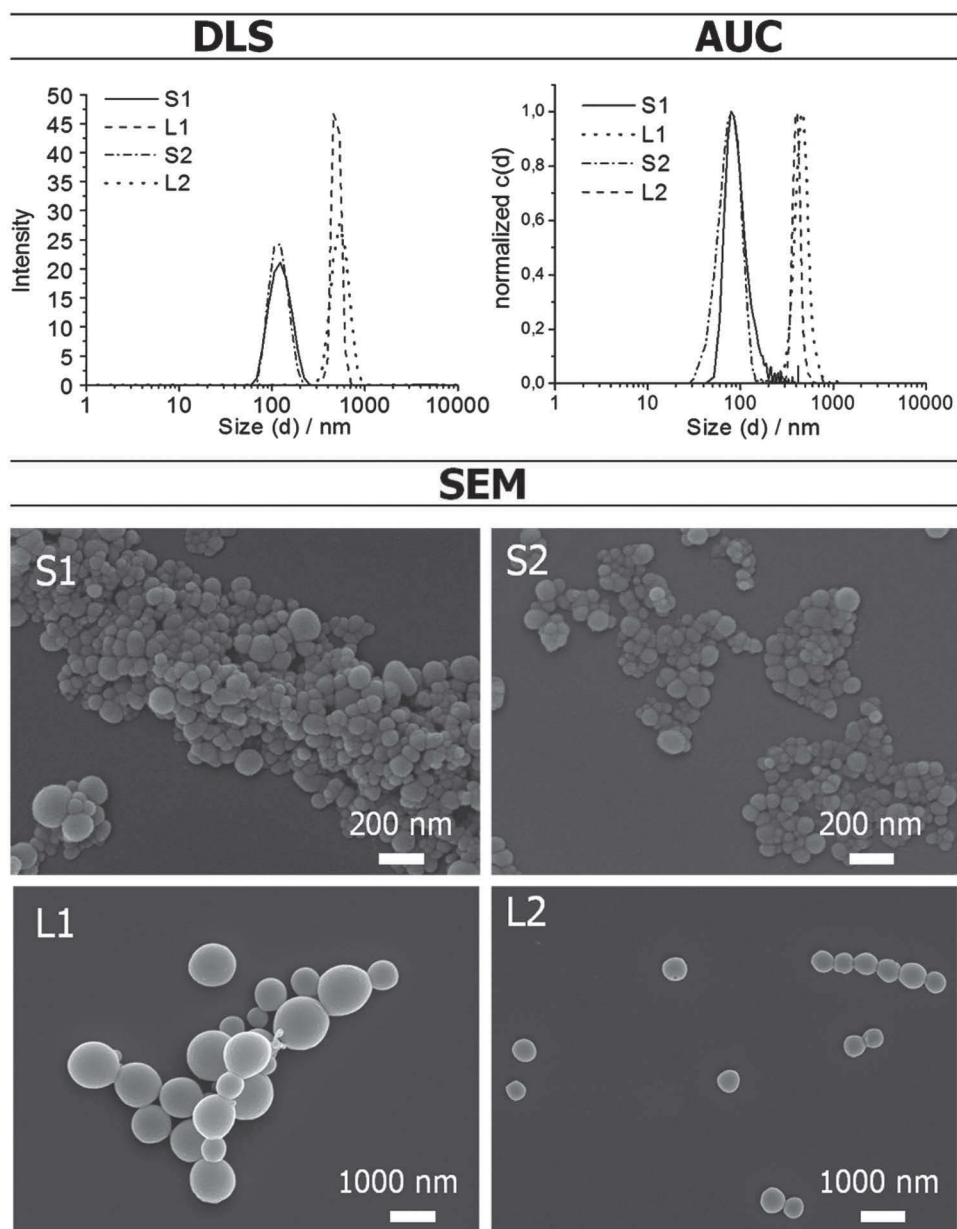


Figure 1. Size distributions of the particles in water ($c = 0.5 \text{ mg mL}^{-1}$) obtained by DLS and AUC as well as SEM images of the particle suspensions.

fluorescent NP into the cytoplasm in the range of $c = 0.1$ to $10 \text{ } \mu\text{g mL}^{-1}$ was observed. The more particles added for incubation with adherent cells, the more particles were consequently found in the cytoplasm. It was further obvious that the pUC prepared samples **S2** and **L2** were internalized to a higher degree than the particles **S1** and **L1**. This might be due to traces of sucrose attached to the particle surface. As described in literature, carbohydrate moieties can act as ligands for diverse receptors. Hence, their appearance on the particle surface could lead to an enhanced cellular recognition and internalization of the particle **S2** and **L2**.^[49–51]

It is known that PMMA particles are phagocytosable and it can be assumed that the cellular uptake of PMMA particles in the size range studied is presumable mediated in a similar fashion via an endocytotic pathway.^[27] The negative surface charge of the PMMA NP does not alter the cellular uptake and most probably yields to a reduction of the non specific binding of anionic proteins present in the cell culture medium and also in the body fluid, for example, in the blood, thus rendering opportunities for in vivo administration of NP.^[26]

For diagnostic applications, the biocompatibility and non-toxicity of the nanosuspensions are important

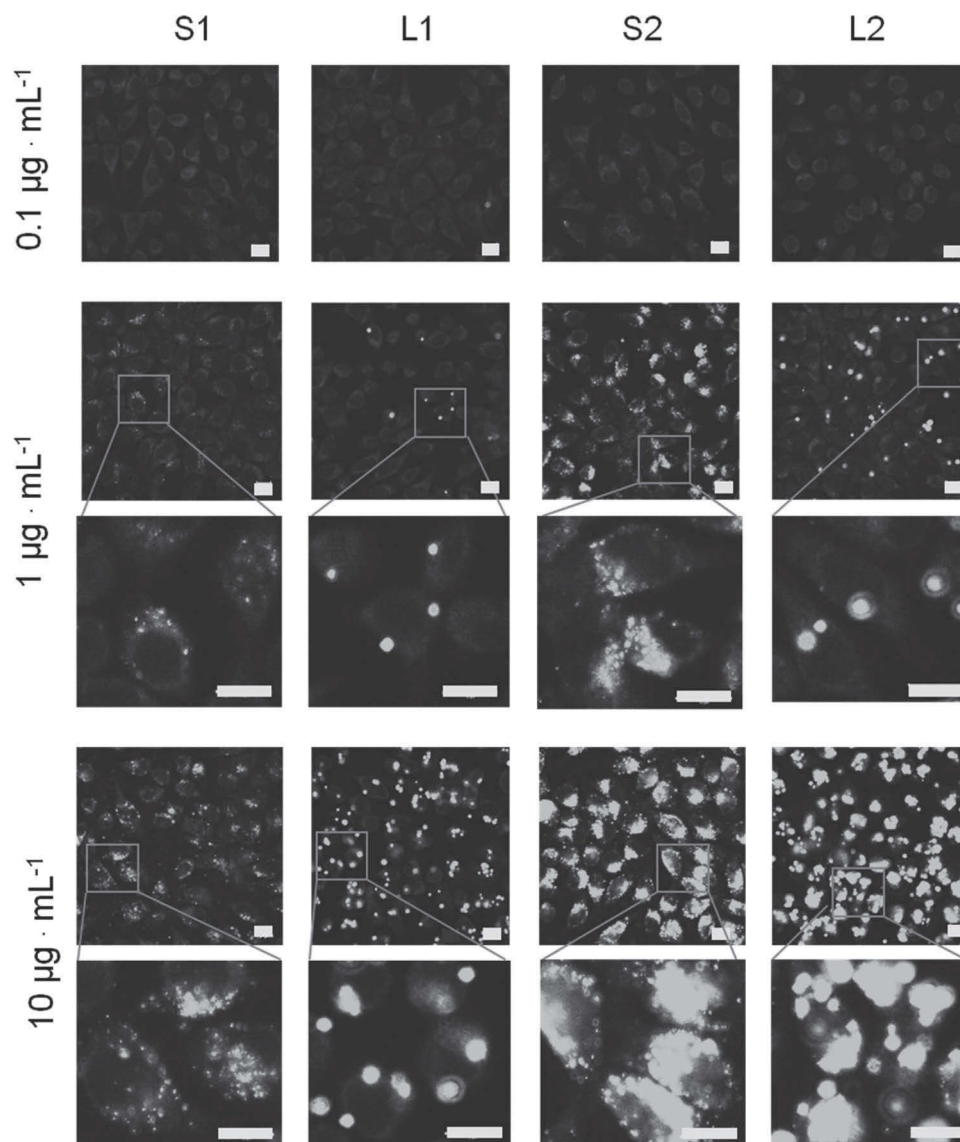


Figure 2. Confocal fluorescence images of L929 cells after 24 h incubation with polymeric p(MMA-*st-d*-MAV) nanoparticles. Cells incubated with polymer free culture medium served as control (not shown). All images were obtained with identical instrument settings (scale bars 10 μm).

prerequisites. The *in vitro* cytotoxicity experiment was performed on the basis of the XTT assay using L929 mouse fibroblasts, according to the German standard institution guideline DIN ISO 10993-5 as a reference for biomaterial testing. After 24 h of incubation with different NP concentrations ($c = 0.1\text{--}10\ \mu\text{g mL}^{-1}$), the metabolic activity of cells treated with test-samples was found to be on the level of untreated controls, which proves the absence of a toxic effect mediated by the NPs (Figure S2, Supporting Information). A detailed live/dead microscopy study of cells that were treated with NP confirmed the cell-membrane integrity (exclusion of red fluorescent PI from cell nuclei) and their excellent viability (strong green fluorescence

of FDA in cytoplasm) (Figure S3, Supporting Information). In addition, the interaction of NP suspensions with blood cells was investigated in terms of their potential to induce hemolysis (membrane damage and cell disruption) and/or aggregation of erythrocytes, one of the major cellular blood components. Whereas the treatment of erythrocytes with 1% Triton X-100 as positive control led to a complete disruption of the erythrocytes and subsequent release of the incorporated hemoglobin, none of the NP suspensions nor the PBS-treated negative control showed any hemolytic activity, indicating the absence of any harmful effect on the erythrocyte membrane integrity (Figure S4, Supporting Information). Furthermore,

the capability of NP suspensions to induce a formation of erythrocyte aggregates as an unwanted sign of blood incompatibility was studied microscopically and photometrically. None of the NP suspensions induced any red blood cell aggregation, even at the highest concentration of $10 \mu\text{g mL}^{-1}$ (Figure S5 and S6, Supporting Information). In contrast, the treatment with 25 kDa bPEI as positive control caused the clear formation of aggregates, whereas PBS-treated samples used as negative control did not yield in any aggregate formation. This observed absence of any nanoparticle-mediated blood incompatibility is in line with clinical evaluations of PMMA membranes dedicated for the use in blood dialysis.^[26] It is reported that due to their relatively hydrophobic and anionic surface PMMA particles show less nonspecific protein and peptide binding, and, thereby reduce the initial steps of opsonization leading to cell recognition/binding and possible immunological reactions.^[52] It is known that PMMA NP may be ingested and most probably can pass through the epithelial barrier and will likely end up in the bloodstream. Large particles are usually trapped by the liver,^[53] while smaller pass on and are captured by the kidneys.^[54] However, because of the very low toxicity documented for PMMA NPs, even in view of a chronic/continuous disease treatment in vivo, the possibility of obtaining sustainable effects by using PMMA NPs is presumably realistic. In addition, the good stability of the nanoparticles during autoclavation, centrifugation, and lyophilization/resuspension is basic requirements for the possible administration of lyophilized, resuspended/reconstituted, and autoclaved particles.

3. Conclusion

Consequently, the 4-hydroxythiazole-functionalized PMMA NPs are suitable for fluorescence-based long-term studies of biological processes at the molecular level. On the contrary to traditional fluorophores, the PMMA NPs combine small size and high photostability, and, in contrast to widely used quantum dots, they do not contain hazardous components, which need to be shielded by protective layers. The bio-analytical applications based on functionalized polymeric PMMA NPs are of emerging interest and provide opportunities like minimal-invasive intracellular monitoring of key components like pH value and oxygen content as well as ions like calcium, potassium or sodium. They can be combined with state-of-the-art imaging techniques like flow cytometry, fluorescence microscopy, and sophisticated imaging approaches, such as confocal imaging providing the opportunity for 3D analysis. In combination with dyes emitting in the near-infrared wavelength range, it offers an optical window for in vivo tissue imaging into several mm depth. By the immobilization of ligands to the

PMMA particles surface, also a specific binding to biomolecules can be mediated, thereby enabling approaches like specific cell targeting.^[55]

Supporting Information

Supporting Information is available from the Wiley Online Library or from the author.

Acknowledgements: The Thüringer Ministerium für Bildung, Wissenschaft und Kultur (TMBWK, ProExzellenz-Programm NanoConSens) is acknowledged for financial support. We gratefully thank Roberto Menzel and Prof. Dr. Rainer Beckert, Friedrich-Schiller-University of Jena, for providing the 4-hydroxyl thiazole dye and Steffi Stumpf and Dr. Frank Steininger, EMZ Jena, for assistance in the SEM investigations.

Received: May 13, 2012; Revised: June 28, 2012; Published online: August 7, 2012; DOI: 10.1002/marc.201200329

Keywords: fluorescent nanoparticles; 4-hydroxythiazoles; nanoprecipitation; particle size distribution; preparative ultracentrifugation; analytical ultracentrifugation; poly(methyl methacrylate); size-dependent cell uptake; solvent-evaporation technique

- [1] D. F. Emerich, C. G. Thanos, *J. Drug Targeting* **2007**, *15*, 163.
- [2] W. J. Stark, *Angew. Chem. Int. Ed.* **2011**, *50*, 1242.
- [3] N. Sanvicens, M. P. Marco, *Trends Biotechnol.* **2008**, *26*, 425.
- [4] A. Merkoci, *Biosens. Bioelectron.* **2010**, *26*, 1164.
- [5] C. J. Xu, L. Y. Mu, I. Roes, D. Miranda-Nieves, M. Nahrendorf, J. A. Ankrum, W. A. Zhao, J. M. Karp, *Nanotechnology* **2011**, *22*, 1.
- [6] K. H. Chung, M. Y. Cho, M. H. Sung, H. Poo, Y. T. Lim, *Chem. Commun.* **2011**, *47*, 8889.
- [7] G. Tosi, L. Bondioli, B. Ruozi, L. Badiali, G. M. Severini, S. Biffi, A. De Vita, B. Bortot, D. Dolcetta, F. Forni, M. A. Vandelli, *J. Neural Transm.* **2011**, *118*, 145.
- [8] M. Mahmoudi, V. Serpooshan, S. Laurent, *Nanoscale* **2011**, *3*, 3007.
- [9] A. H. Faraj i P. Wipf, *Biorg. Med. Chem.* **2009**, *17*, 2950.
- [10] H. S. Cho, Z. Dong, G. M. Pauletti, J. Zhang, H. Xu, H. Gu, L. Wang, R. C. Ewing, C. Huth, F. Wang, D. Shi, *ACS Nano* **2010**, *4*, 5398.
- [11] K. H. Lee, *J. Nucl. Med.* **2007**, *48*, 1408.
- [12] Z. Zili, S. Sfar, H. Fessi, *Int. J. Pharm.* **2005**, *294*, 261.
- [13] G. Tosi, F. Rivasi, F. Gandolfi, L. Costantino, M. A. Vandelli, F. Forni, *Biomaterials* **2005**, *26*, 4189.
- [14] M. Gaumet, R. Gurny, F. Delie, *Int. J. Pharm.* **2007**, *342*, 222.
- [15] A. E. Nel, L. Maedler, D. Velegol, T. Xia, E. M. V. Hoek, P. Somasundaran, F. Klaessig, V. Castranova, M. Thompson, *Nat. Mater.* **2009**, *8*, 543.
- [16] C. Vauthier, K. Bouchemal, *Pharm. Res.* **2009**, *26*, 1025.
- [17] R. A. Jain, *Biomaterials* **2000**, *21*, 2475.
- [18] J. P. Rao, K. E. Geckeler, *Prog. Polym. Sci.* **2011**, *36*, 887.
- [19] C. Pinto Reis, R. J. Neufeld, A. J. Ribeiro, F. Veiga, *Nanomed. Nanotechnol. Biol. Med.* **2006**, *1*, 8.

- [20] C. H. Lohmann, D. D. Dean, G. Koster, D. Casasola, G. H. Buchhorn, U. Fink, Z. Schwartz, B. D. Boyan, *Biomaterials* **2002**, *23*, 1855.
- [21] L. Araujo M. Sheppard, R. Lobenberg, J. Kreuter, *Int. J. Pharm.* **1999**, *176*, 209.
- [22] I. Perevyazko, A. Vollrath, S. Hornig, G. M. Pavlov, U. S. Schubert, *J. Polym. Sci., Part A: Polym. Chem.* **2010**, *48*, 3924.
- [23] A. Vollrath, S. Schubert, N. Windhab, C. Biskup, U. S. Schubert, *Macromol. Rapid Commun.* **2010**, *31*, 2053.
- [24] J. W. Yoo, N. Giri, C. H. Lee, *Int. J. Pharm.* **2011**, *403*, 262.
- [25] R. Q. Frazer, R. T. Byron, P. B. Osborne, K. P. West, *J. Long. Term Eff. Med. Implants* **2005**, *15*, 629.
- [26] H. Horikawa, H. Naitoh, M. Agatsuma, S. Hashimoto, T. Miyazaki, H. Nagasaka, A. Fujimori, *Kidney Dial.* **1994**, *94*.
- [27] A. Bettencourt, A. J. Almeida, *J. Microencapsul.* **2012**, *29*, 353.
- [28] M. L. W. Knetsch, N. Olthof, L. H. Koole, *J. Biomed. Mater. Res., Part A* **2007**, *82A*, 947.
- [29] R. Menzel, A. Breul, C. Pietsch, J. Schaefer, C. Friebe, E. Tauscher, D. Weiss, B. Dietzek, J. Popp, R. Beckert, U. S. Schubert, *Macromol. Chem. Phys.* **2011**, *212*, 840.
- [30] D. Weiss, R. Menzel, E. Tauscher, R. Beckert, H. Goerls, *Z. Anorg. Allg. Chem.* **2010**, *636*, 1380.
- [31] G. Moad, S. H. Thang, *Aust. J. Chem.* **2009**, *62*, 1379.
- [32] R. Hoogenboom, C. Pietsch, U. S. Schubert, *Polym. Chem.* **2010**, *1*, 1005.
- [33] J. Chiefari, Y. K. Chong, F. Ercole, J. Krstina, J. Jeffery, T. P. T. Le, R. T. A. Mayadunne, G. F. Meijer, C. L. Moad, G. Moad, E. Rizzardo, S. H. Thang, *Macromolecules* **1998**, *31*, 5559.
- [34] H. Fessi, F. Puisieux, J. P. Devissaguet, N. Ammoury, S. Benita, *Int. J. Pharm.* **1989**, *55*, R1.
- [35] S. Schubert, J. T. Delaney, U. S. Schubert, *Soft Matter* **2011**, *7*, 1581.
- [36] U. Bilati, E. Allemann, E. Doelker, *Eur. J. Pharm. Sci.* **2005**, *24*, 67.
- [37] F. Bonaccorso, T. Hasan, P. H. Tan, C. Sciascia, G. Privitera, G. Di Marco, P. G. Gucciardi, A. C. Ferrari, *J. Phys. Chem. C* **2010**, *114*, 17267.
- [38] V. Vogel, K. Langer, S. Balthasar, P. Schuck, W. Maechtle, W. Haase, J. van den Broek, C. Tziatzios, D. Schubert, *Prog. Colloid Polym. Sci.* **2002**, *119*, 31.
- [39] H. Pertoft, *J. Biochem. Bioph. Methods* **2000**, *44*, 1.
- [40] M. Gaumet, A. Vargas, R. Gurny, F. Delie, *Eur. J. Pharm. Biopharm.* **2008**, *69*, 1.
- [41] M. Gaumet, R. Gurny, F. Delie, *Eur. J. Pharm. Sci.* **2009**, *36*, 465.
- [42] C. He, Y. Hu, L. Yin, C. Tang, C. Yin, *Biomaterials* **2010**, *31*, 3657.
- [43] J. C. Giddings, *Science* **1993**, *260*, 1456.
- [44] E. Tauscher, D. Weiss, R. Beckert, J. Fabian, A. Assumpcao, H. Goerls, *Tetrahedron Lett.* **2011**, *52*, 2292.
- [45] S. Hornig, T. Heinze, C. R. Becer, U. S. Schubert, *J. Mater. Chem.* **2009**, *19*, 3838.
- [46] I. Y. Perevyazko, J. T. Delaney, Jr., A. Vollrath, G. M. Pavlov, S. Schubert, U. S. Schubert, *Soft Matter* **2011**, *7*, 5030.
- [47] M. K. Brakke, *J. Am. Chem. Soc.* **1951**, *73*, 1847.
- [48] X. Sun, S. M. Tabakman, W. S. Seo, L. Zhang, G. Zhang, S. Sherlock, L. Bai, H. Dai, *Angew. Chem. Int. Ed.* **2009**, *48*, 939.
- [49] S. R. S. Ting, G. Chen, M. H. Stenzel, *Polym. Chem.* **2010**, *1*, 1392.
- [50] J. J. Lundquist, E. J. Toone, *Chem. Rev.* **2002**, *102*, 555.
- [51] C. R. Becer, M. I. Gibson, J. Geng, R. Ilyas, R. Wallis, D. A. Mitchell, D. M. Haddleton, *J. Am. Chem. Soc.* **2010**, *132*, 15130.
- [52] D. H. Sun, M. C. D. Trindade, Y. Nakashima, W. J. Maloney, S. B. Goodman, D. J. Schurman, R. L. Smith, *J. Biomed. Mater. Res., Part A* **2003**, *65A*, 290.
- [53] G. Borchard, J. Kreuter, *Pharm. Res.* **1996**, *13*, 1055.
- [54] A. M. Gatti, F. Rivasi, *Biomaterials* **2002**, *23*, 2381.
- [55] Y. K. Gong, F. M. Winnik, *Nanoscale* **2012**, *4*, 360.

Polymer characterization

Table S1. Characterization data of the copolymer p(MMA-*stat*-MA^y).

[MMA]: [dye]	[M]: [CTA]: [AIBN]	Conv. MMA ^a (%)	$M_{n, \text{theo}}$ (g/mol)	$M_{n, \text{SEC}}$ (RI) ^b (g/mol)	PDI _{SEC} (RI) ^b	DP _{SEC} (RI) ^b	Dye content (NMR) ^c (%)
138:2	140:1:0.25	68	9,900	8,500	1.19	81	2.9

a) Calculated from vinyl integrals of ¹H NMR spectra using anisole as internal standard.

b) Calculated from SEC (CHCl₃), PMMA calibration.

c) Calculated from integrated areas of aromatic dye signals and the methyl signals of MMA.

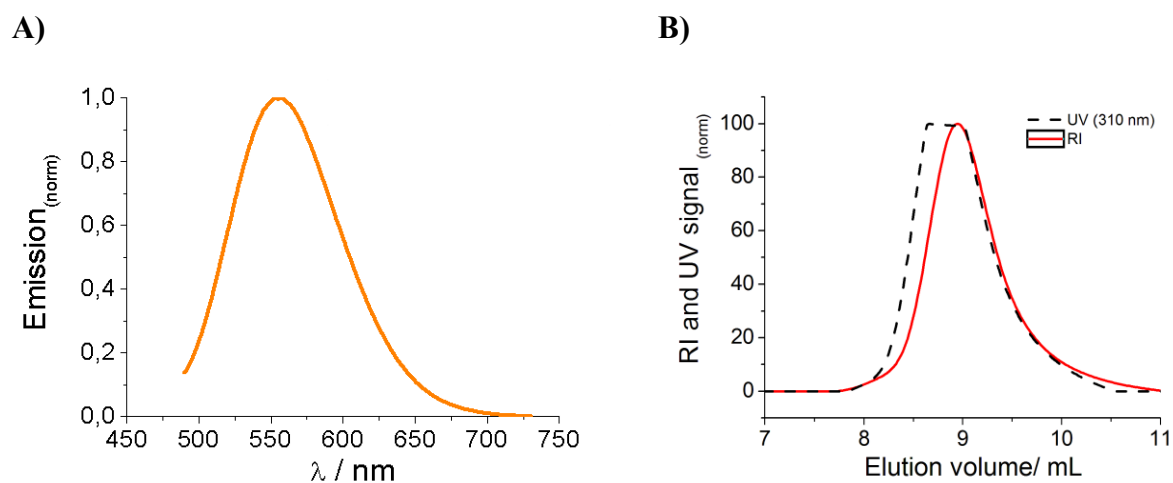


Figure S1. A) Fluorescence emission spectra of p(MMA-*stat*-MA^y) in acetonitrile (excited at $\lambda = 418$ nm). B) SEC measurements (CHCl₃) of p(MMA-*stat*-MA^y). The refractive index trace (--) and the UV trace at 310 nm (-) of the labeled polymer occur at the same retention time confirming the covalent attachment.

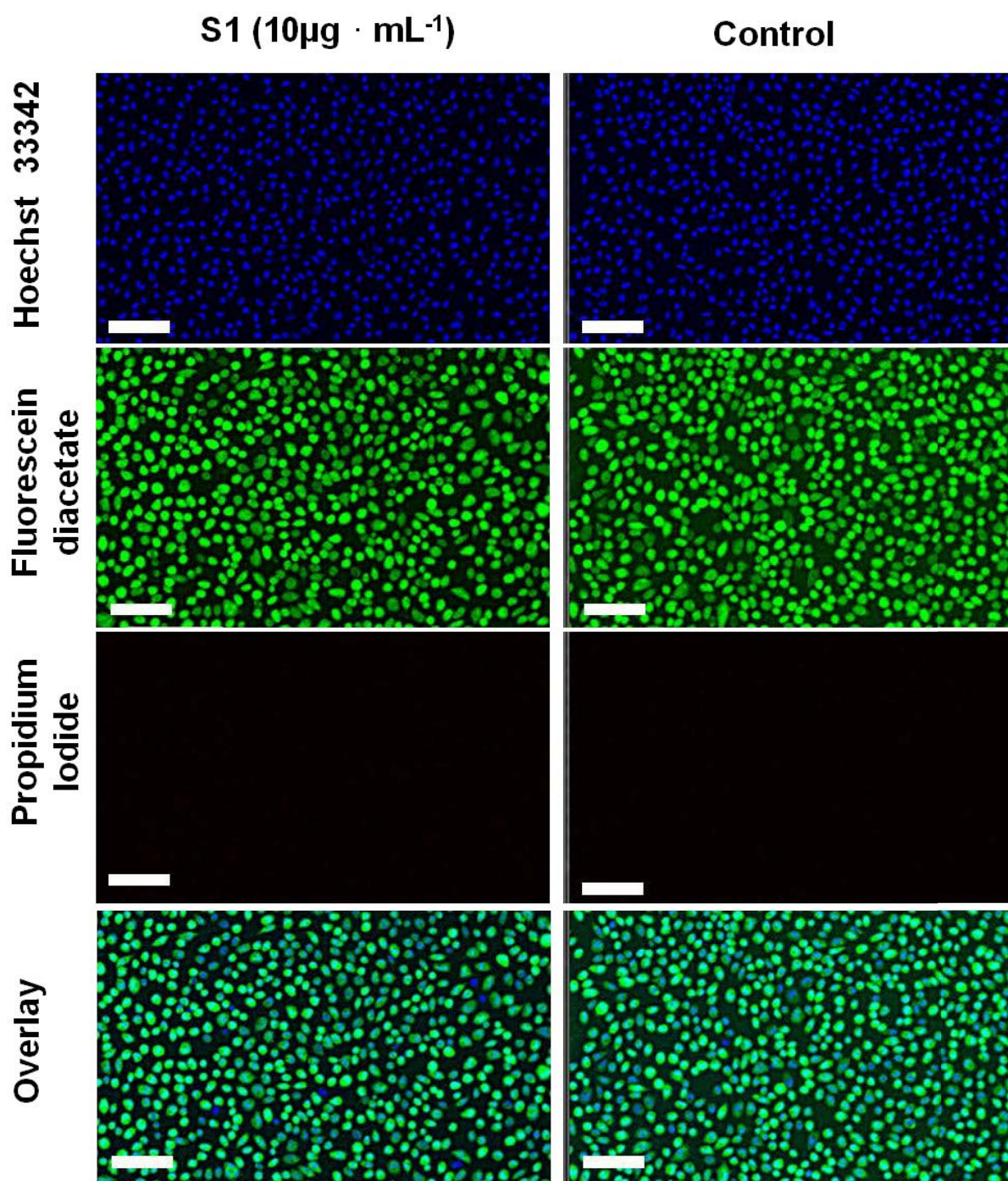


Figure S3. Representative fluorescence microscopy micrographs of Hoechst 33342/FDA/PI stained L929 mouse fibroblast cells cultured for 24 hours in the presence of the small (**S1/S2**) and large (**L1/L2**) polymeric p(MMA-*stat*-MA^y) nanoparticles up to 10 $\mu\text{g} \cdot \text{mL}^{-1}$ for 24 hours. Blue fluorescent Hoechst dye labels nuclei of all cells present, green fluorescent FDA dye indicates cytoplasm of vital cells, red fluorescent PI signals tag nuclei of dead cells. Left: 10 $\mu\text{g} \cdot \text{mL}^{-1}$ particle suspension added (small (**S1**); same results for small (**S2**) and large (**L1/L2**) particle suspensions), right: control culture without particles.

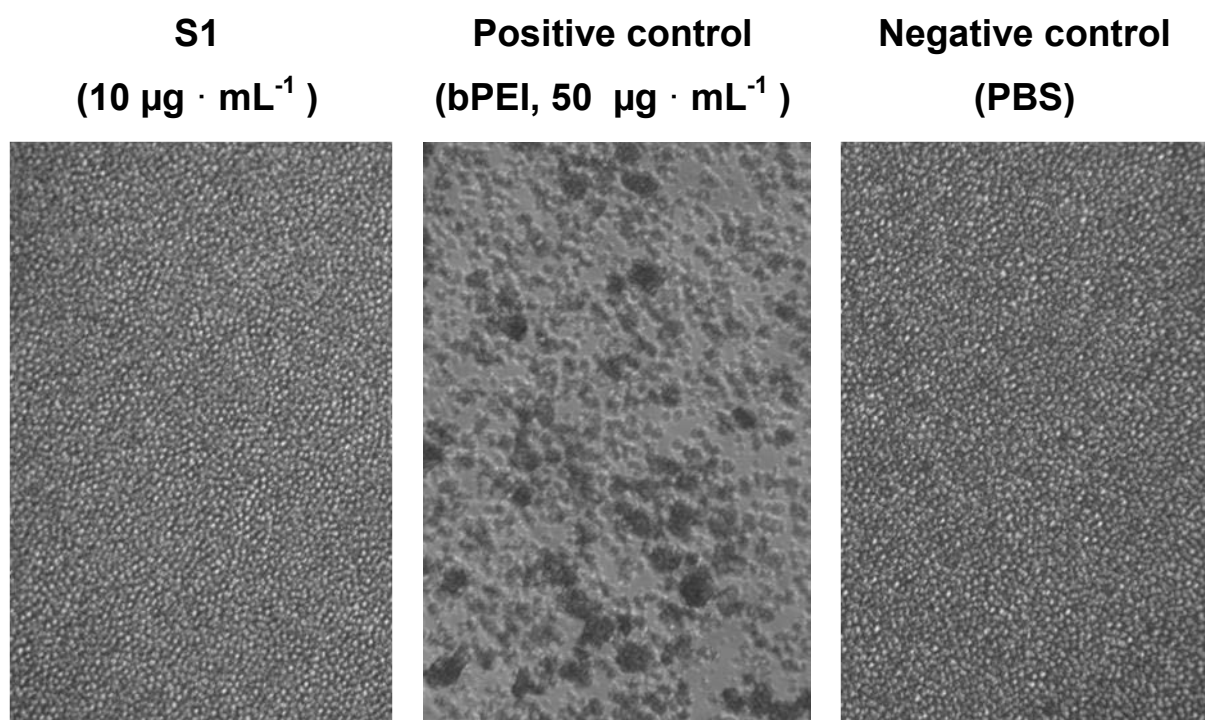


Figure S4. Representative micrographs of red blood cell aggregation after 2 h incubation at 37 °C with small polymeric p(MMA-*stat*-MA^y) nanoparticles (**S1**, 10 $\mu\text{g} \cdot \text{mL}^{-1}$). Same results as for **S1** were obtained for **S2/L1/L2**. 25 kDa bPEI (50 $\mu\text{g} \cdot \text{mL}^{-1}$) served as positive and PBS as negative control. Magnification 320 \times .

Preparation, Cellular Internalization, and Biocompatibility of Highly Fluorescent PMMA Nanoparticles

Antje Vollrath, David Pretzel, Christian Pietsch, Igor Perevyazko, Stephanie Schubert, George M. Pavlov, Ulrich S. Schubert*

DOI: 10.1002/marc.201200329

The authors regret that there were important omissions in the above article. The synthesis of the yellow light-emitting thiazole-dye 3-((5-(4-(dimethylamino)phenyl)-2-(pyridin-3-yl)thiazol-4-yl)oxy)propan-1-ol as well as the corresponding methacrylate monomer was not described in reference 29 of the manuscript or in reference 1 of the Supporting Information (in this publication only the related blue emitting monomer is described). The resulting yellow and blue polymers were both investigated – however, due to the non-visibility of the blue polymer only the yellow one was continued in the published study. In order to allow an exact reproduction of the monomer synthesis, a detailed description has been added as Supporting Information of this Correction.

In the original version of the above article, three co-authors' names (Roberto Menzel, Dieter Weiß, and Rainer Beckert) were missing from the byline and affiliation. The correct author byline is as follows:

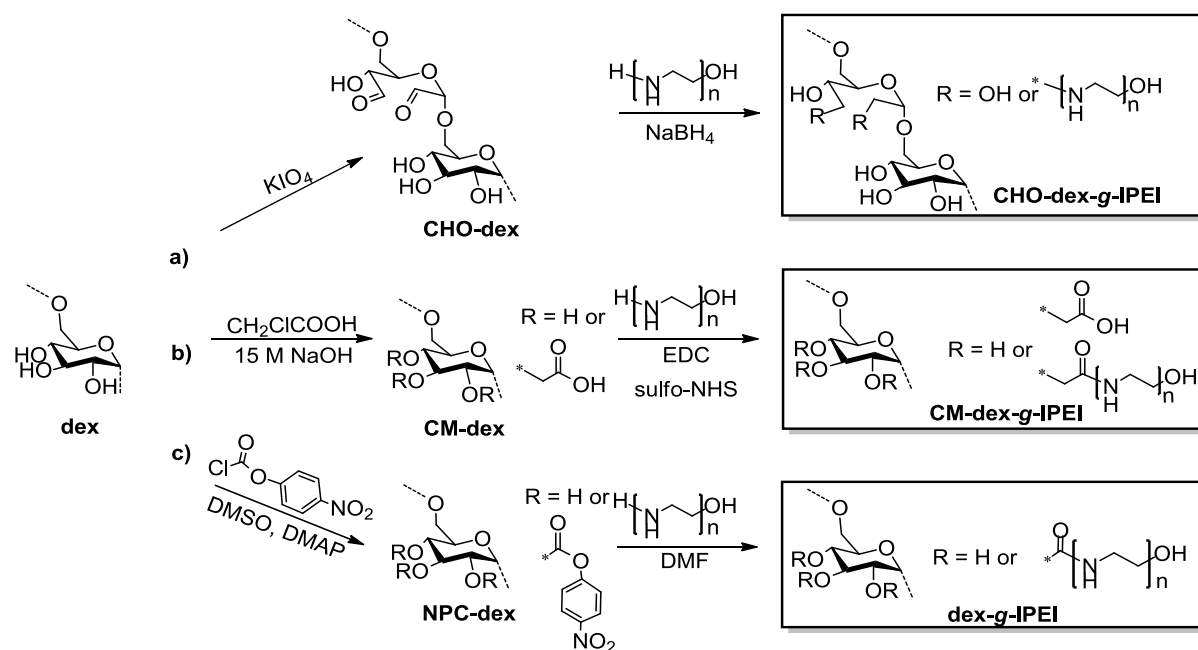
Antje Vollrath, David Pretzel, Christian Pietsch, Igor Perevyazko, Roberto Menzel, Stephanie Schubert, George M. Pavlov, Dieter Weiß, Rainer Beckert, Ulrich S. Schubert*

Finally, the Acknowledgments section in the above article should be replaced with the following paragraph.

The Thüringer Ministerium für Bildung, Wissenschaft und Kultur (TMBWK, ProExzellenz-Programm NanoConSens) is acknowledged for financial support. We gratefully thank Steffi Stumpf and Dr. Frank Steininger, EMZ Jena, for assistance in the SEM investigations.

A. Vollrath, D. Pretzel, C. Pietsch, I. Perevyazko, R. Menzel,
G. M. Pavlov, D. Weiß, R. Beckert, U. S. Schubert
Laboratory of Organic and Macromolecular Chemistry (IOMC),
Friedrich-Schiller-University Jena, Humboldtstr. 10,
07743 Jena, Germany
E-mail: ulrich.schubert@uni-jena.de
C. Pietsch, I. Perevyazko, G. M. Pavlov, U. S. Schubert
Dutch Polymer Institute (DPI), Post Office Box 902,
Eindhoven 5600 AX, The Netherlands
S. Schubert, R. Beckert, U. S. Schubert
Jena Center for Soft Matter (JCMS), Friedrich-Schiller-
University Jena, Humboldtstr. 10, 07743 Jena, Germany
Stephanie Schubert
Institute of Pharmacy, Department of Pharmaceutical
Technology Friedrich-Schiller-University Jena,
Otto-Schott-Str. 41, 07745 Jena, Germany

Figures and Tables



Scheme 1. Schematic representation of the functionalization of dextran by (a) oxidation, (b) carboxymethylation and (c) 4-nitrophenyl carbonate-activation with subsequent reaction with IPEIs *via* (a) reductive amination, (b) EDC coupling and (c) carbamate formation.

Table 1. Overview about the DS and nitrogen content of all synthesized dex-g-IPEI samples.

P	dex-g-IPEIs	CHO/ COOH: NH ₂ [mol]	DS [IPEI/ AGU]	N [%]	Cationic charge/M _{Monomer} ^a	Anionic charge/M _{Monomer} ^b
A	Reductive amination					
A1	CHO _{DS=0.5} -dex-g-IPEI ₂₀	1:0.5	0.18	15.78	0.0114	-
A2	CHO _{DS=0.5} -dex-g-IPEI ₄₀	1:0.5	0.13	19.12	0.0135	-
A3	CHO _{DS=1.0} -dex-g-IPEI ₂₀	1:0.5	0.38	21.45	0.0156	-
A4	CHO _{DS=1.0} -dex-g-IPEI ₄₀	1:0.5	0.19	21.73	0.0156	-
B	EDC coupling					
B1	CM _{DS=0.3} -dex-g-IPEI ₂₀	1:1.2	0.06	6.73	0.0052	0.0013
B2	CM _{DS=0.3} -dex-g-IPEI ₄₀	1:1.2	0.07	12.80	0.0093	0.0010
B3	CM _{DS=0.5} -dex-g-IPEI ₂₀	1:1.2	0.07	7.96	0.0056	0.0020
B4	CM _{DS=0.5} -dex-g-IPEI ₄₀	1:1.2	0.1	14.83	0.0110	0.0014
B5	CM _{DS=1.6} -dex-g-IPEI ₂₀	3:1	0.11	8.16	0.0063	0.0046
B6	CM _{DS=1.6} -dex-g-IPEI ₄₀	3:1	0.18	18.38	0.0127	0.0028

a) Calculated cationic charge/molar mass of monomer unit

b) Calculated anionic charge/molar mass of monomer unit

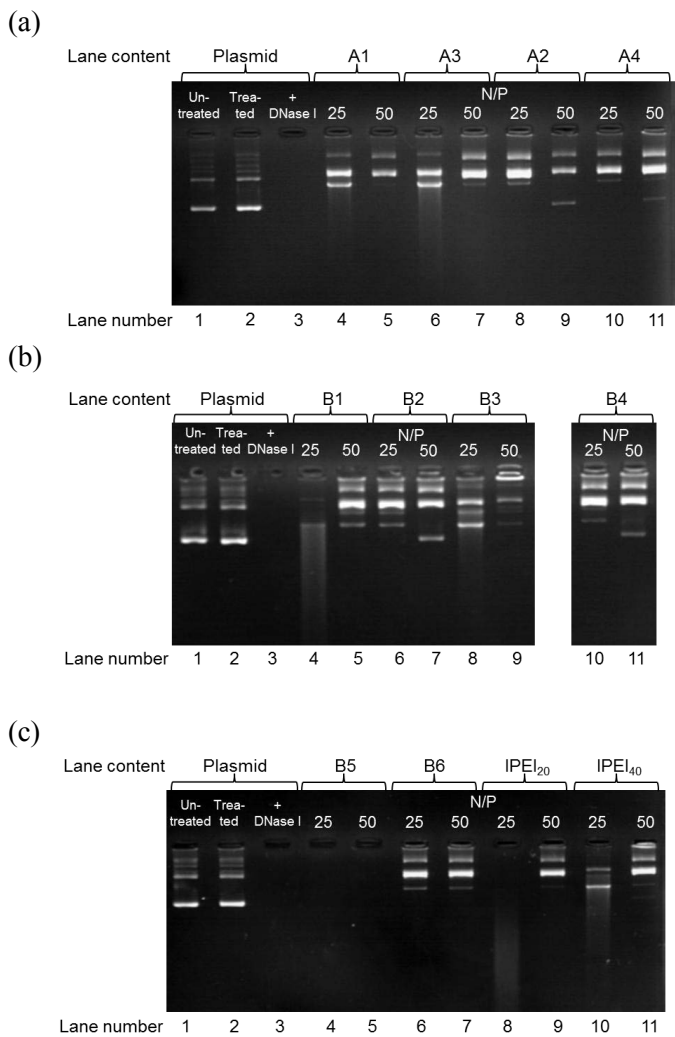


Figure 1: Stability of dex-g-IPEI/plasmid complexes against enzymatic degradation (DNase I, 37 °C, 45 minutes) at N/P ratio 25 and 50: (a) dex-g-IPEIs by reductive amination; (b + c) dex-g-IPEIs by EDC-coupling, (c) IPEIs. Controls: lane 1: untreated free plasmid; lane 2: free plasmid treated in the same way as complexes but without enzyme; lane 3: free plasmid treated with enzyme.

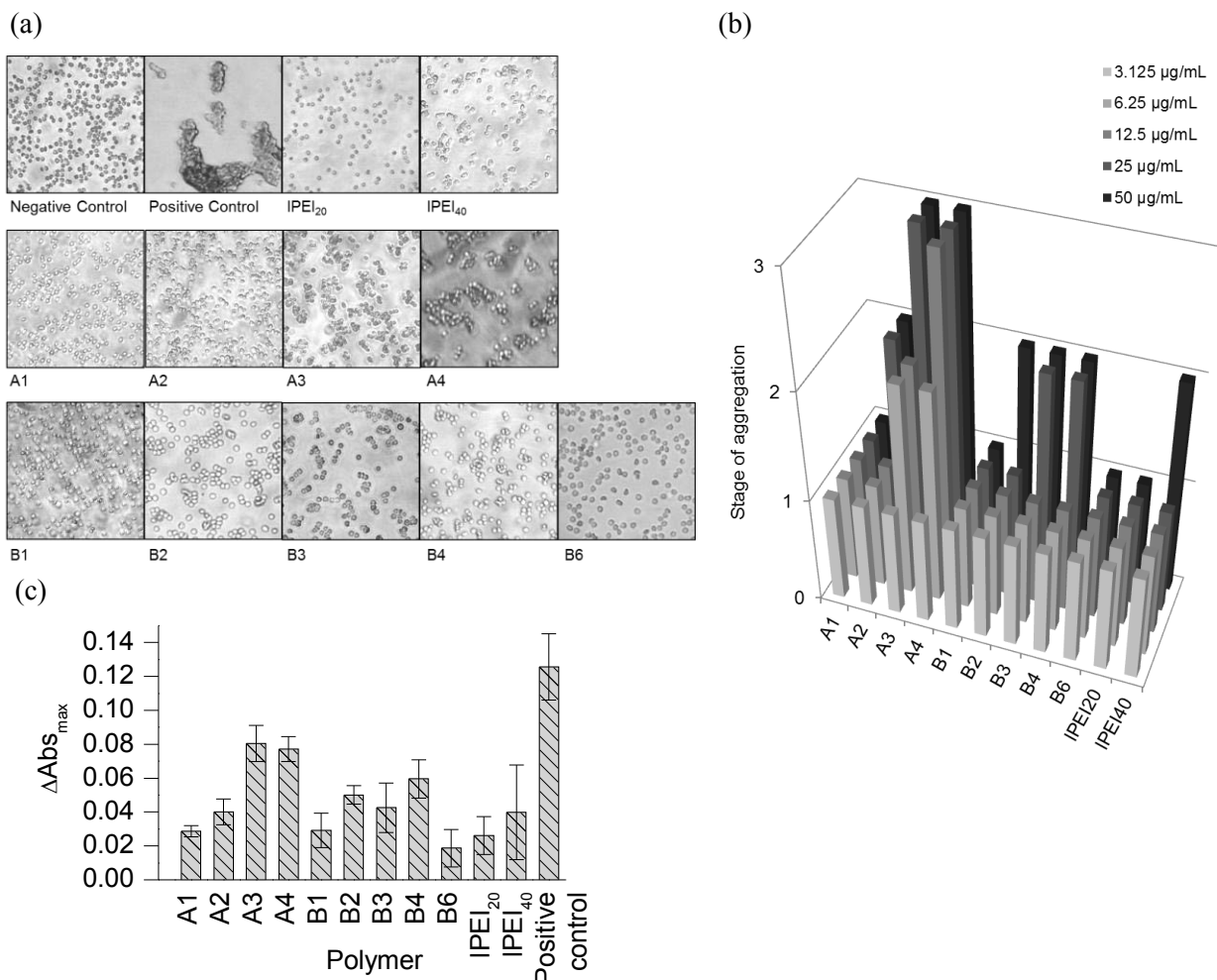


Figure 5: Aggregation of sheep red blood cells after treatment with free dex-g-IPEI and IPEI polymers incubated at 37 °C for 2 h. (a) Representative pictures of microscopic observation at 50 $\mu\text{g} \cdot \text{mL}^{-1}$ (negative control = PBS; positive control = 15 $\mu\text{g} \cdot \text{mL}^{-1}$ bPEI 25,000 $\text{g} \cdot \text{mol}^{-1}$) with magnification 200 \times . (b) Stages of sheep blood erythrocyte aggregation of dex-g-IPEIs and IPEIs at concentrations up to 50 $\mu\text{g} \cdot \text{mL}^{-1}$. Classification: 1 = no aggregation of erythrocytes, 2 = moderate aggregation with rouleau formation, 3 = strong aggregation with cluster formation. (c) ΔAbs_{max} of polymers. The RBC aggregation experiments were performed with $n = 2$ and repeated once (mean \pm SD).

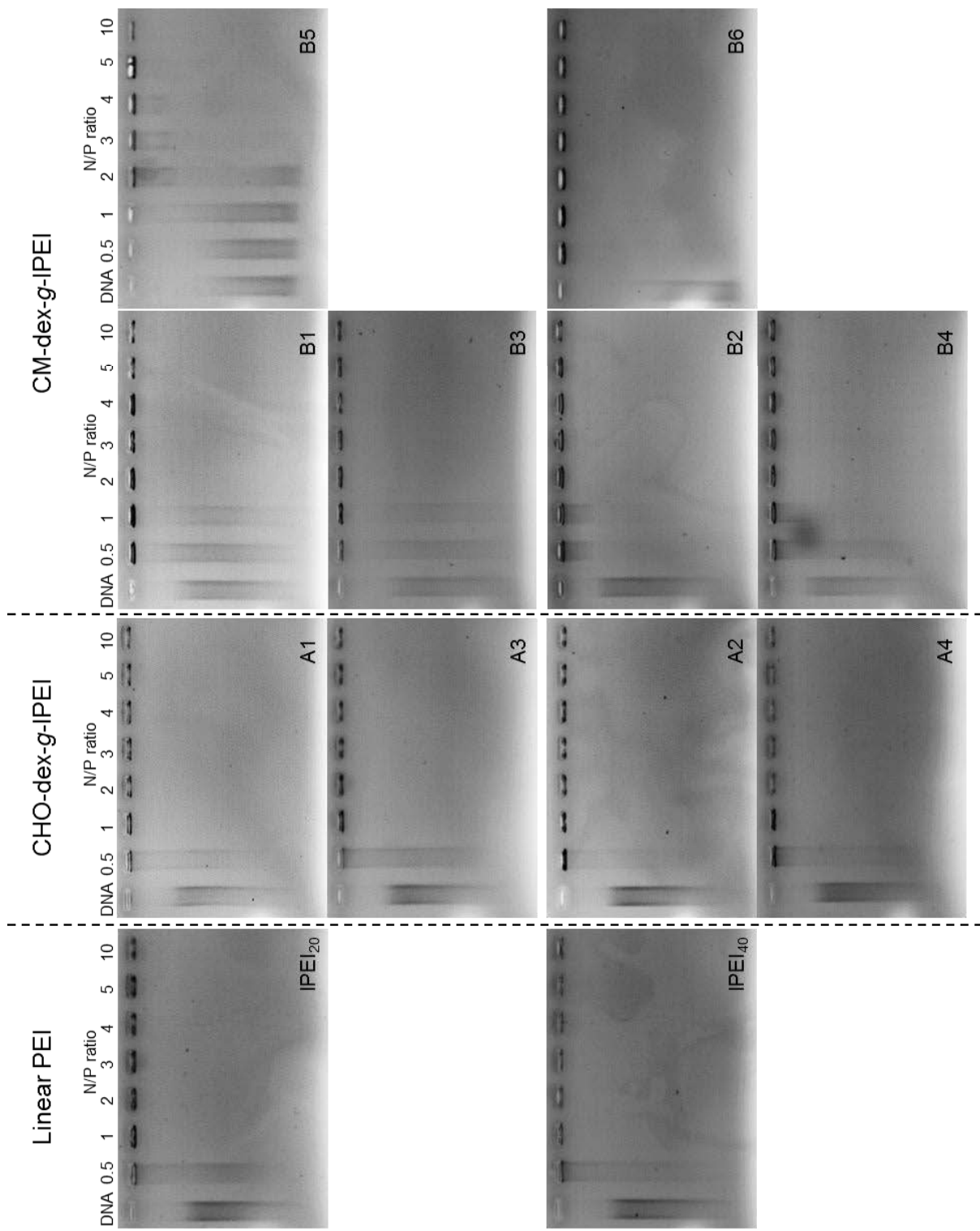


Figure S7. DNA binding capacity of IPEI_{20/40} and dex-g-IPEIs at different N/P ratios in comparison to free DNA, determined by agarose gel electrophoresis.

$$\text{RFU} [\%] = \frac{F_{\text{sample}}}{F_{\text{pDNA}}} \quad (1)$$

Here, RFU is the relative fluorescence. F_{sample} and F_{siRNA} are the fluorescence intensities of a given sample and the EB intercalated into pDNA alone.

DNA release by heparin

To investigate the release of pDNA from polyplexes, the heparin dissociation assay was used. For this purpose, 100 μL of polyplex solution were incubated for 10 min with EB ($0.4 \mu\text{g mL}^{-1}$) in a black 96-well plate. After transferring into the Tecan Genios Pro fluorescence microplate reader, heparin solutions were automatically added at the indicated concentrations. Therefore, 20 cycles of the following procedure were used: 5 μL of heparin stock solutions (10 U mL^{-1} or 200 U mL^{-1}) were dropped to each well. Afterwards the plate was shaken (orbital, 10 sec, 2 mm) and incubated for 5 min at $37 \text{ }^\circ\text{C}$. After each cycle, the fluorescence of EB was measured, and the percentage of intercalated EB was calculated as described before (1).

Cell Culture

HEK-293 (CRL-1573, ATCC) cells were maintained in RPMI 1640 culture medium, L929 (CCL-1, ATCC) in DMEM culture medium. Both media were supplemented with 10% fetal calf serum (FCS), 100 $\mu\text{g/mL}$ streptomycin, 100 IU mL^{-1} penicillin, and 2 mM L-glutamine. Cells were cultivated at $37 \text{ }^\circ\text{C}$ in a humidified 5% CO_2 atmosphere.

The cytotoxicity of the single polymers was tested with L929 cells, as this cell line is recommended by ISO10993-5. In detail, cells were seeded at 10^4 cells per well in a 96-well plate and incubated for 24 h. No cells were seeded in the outer wells. Afterwards, polymers at the indicated concentrations were added, the plates were slued, and incubated at $37 \text{ }^\circ\text{C}$ for further 24 h. Subsequently, the medium was replaced by PBS and AlamarBlue as recommended by the supplier. After incubation for 4 h, the fluorescence was measured at Ex 570 / Em 610 nm, with untreated cells on the same well plate serving as controls (2).

$$\text{viability} [\%] = \frac{F_{\text{sample}} - F_0}{F_{\text{control}} - F_0} \quad (2)$$

Here, viability is the relative fluorescence and F_{sample} , F_0 , and F_{control} are the fluorescence intensities of a given sample, the blank wells without cells, and the control cells without polymer treatment.

For transfection experiments, HEK cells were seeded at a density of 10^4 cells per well in 96-well plates 24 h before transfection. In order to avoid any misleading measurement results and to prevent a systematic mistake, the polyplexes were always placed and measured at different positions in the 96-well plate to avoid alterations due to differences in the gas exchange between outer and inner wells and 25 measuring points per well were taken. One hour prior transfection, cells were washed with PBS and supplemented with 100 μL OptiMEM (Life Technologies). Polyplex solutions were added (10 μL) to the cells and the plates were slued and incubated for 4

h at 37 °C. Afterwards, the supernatant was replaced by 100 µL of fresh growth medium (RPMI1640 based), and the cells were further incubated for 20 h. Before analysis, the cells were incubated with 1 µg mL⁻¹ Hoechst 33324 for 10 min at 37 °C, washed twice with PBS, and the plates were transferred to the plate reader. The expression of EGFP fluorescence (Ex 475 nm / Em 509 nm) and viability (Hoechst, Em 350 nm / Ex 461 nm) was quantified by using the fluorescence measured from the bottom of the plates. The transfection efficiency was calculated relative to cell number and control cells using the following equation (3), where EGFP_{sample}, EGFP_{control}, Hoechst_{sample}, Hoechst_{control} are the fluorescence signal of EGFP and Hoechst of treated (sample) and non treated (control) cells, respectively. Experiments were repeated 3 times independently.

$$\text{transfection efficiency [\%]} = \frac{\text{EGFP}_{\text{sample}} - \text{EGFP}_{\text{control}}}{\text{Hoechst}_{\text{sample}} / \text{Hoechst}_{\text{control}}} \quad (3)$$

Acknowledgment

The financial support from the Thuringian Ministry for Education, Science and Culture (grant #B514-09051, NanoConSens), the Dutch Polymer Institute (DPI, technology area HTE, project #729) and the Carl-Zeiss Foundation (JCSM Struktur Antrag) are gratefully acknowledged. We express our gratitude to Caroline Fritzsche for assistance in the cell culture, Dr. David Pretzel for assistance at the microscope as well as Michael Wagner for helpful discussions.

References

- [1] F. Schlenk, S. Grund, D. Fischer, *Ther. Delivery* **2013**, *4*, 95-113. doi: 110.4155/tde.4112.4128.
- [2] D. Pezzoli, R. Chiesa, L. De Nardo, G. Candiani, *J. Appl. Biomater. Function. Mater.* **2012**, *10*, e82-91. doi: 10.5301/JABFM.2012.9707.
- [3] M. Breunig, U. Lungwitz, R. Liebl, A. Goepferich, *Proc. Natl. Acad. Sci. U. S. A.* **2007**, *104*, 14454-14459.
- [4] K. Kunath, A. von Harpe, D. Fischer, H. Petersen, U. Bickel, K. Voigt, T. Kissel, *J. Control. Release* **2003**, *89*, 113-125.
- [5] P. Pereira, A. F. Jorge, R. Martins, A. A. Pais, F. Sousa, A. Figueiras, *J. Colloid Interface Sci.* **2012**, *387*, 84-94.
- [6] Z. Dai, C. Wu, *Macromolecules* **2012**, *45*, 4346-4353.
- [7] K. Itaka, A. Harada, Y. Yamasaki, K. Nakamura, H. Kawaguchi, K. Kataoka, *J. Gene Med.* **2004**, *6*, 76-84.
- [8] M. Neu, D. Fischer, T. Kissel, *J. Gene Med.* **2005**, *7*, 992-1009.
- [9] S. D. Patil, D. G. Rhodes, D. J. Burgess, *AAPS J.* **2005**, *7*, E61-77.
- [10] X. Jiang, W. Qu, D. Pan, Y. Ren, J. M. Williford, H. Cui, E. Luijten, H. Q. Mao, *Adv. Mater.* **2013**, *25*, 227-232.
- [11] R. Iwai, R. Haruki, Y. Nemoto, Y. Nakayama, *Bioconjugate Chem.* **2013**, *29*, 29.